Origins of Endothermy in the Mammalian Lineage

the Evolutionary Beginning of Fibro-lamellar Bone in the "Mammal-Like" Reptiles

Dissertation
zur
Erlangung des Doktorgrades (Dr. rer. nat.)
der
Mathematisch-Naturwissenschaftlichen Fakultät
der
Rheinischen Friedrich-Wilhelms-Universität Bonn

vorgelegt von
Christen Don Shelton
aus
Ardmore, Oklahoma,
USA

Bonn
December, 2014

Angefertigt mit Genehmigung der Mathematisch-Naturwissenschaftlichen Fakultät der Rheinischen Friedrich-Wilhelms-Universität Bonn

1. **Prof. Dr. P. Martin Sander**
2. **Prof. Dr. Thomas Martin**

Tag der Promotion: 23/3/2015

Erscheinungsjahr: 2015

Energy and persistence conquer all things

Benjamin Franklin ca. 1780

The fossils are there, I know they are. Go and find them.

Henry Fairfield Osborn 1922

Be kind to colleagues, ruthless with theories...

Robert T. Bakker 1986

Acknowledgements

Many people are thanked throughout this study, but I want to specifically say thank you to those individuals that had the most impact on this work.

I want to first and foremost thank Prof. Dr. Martin Sander who I first met in the Texas Red Beds and where I had my initial interview for this project. I wanted to study Dinosaurs and he persuaded me to study pelycosaurs by carrying on the knowledge passed down to him from Wann Langston Jr. I appreciate his patients and supervision. I was Martin's first, and I hope not the last, American PhD student. I want to also say thank you to my dear friend and colleague Dr. Koen Stein who was my field partner during all three excavations in Texas. I miss the comradery and our late night "brain storming" sessions in the office and at your apartment.

I also would like to thank the following technical staff at the Steinmann Institute: George Olechinski for his photography expertise. Peter Göddertz for helping out with computer problems and microscope software crises. Also, our former administrator Kay Heitplatz whose help was greatly appreciated especially with arranging the shipping of crated fossil material from Texas to Germany. I also want to recognize and thank Beate Mühlens for picking up where Kay left off. Most of all I want to recognize Olaf Dülfer and his technicians in the thin sectioning lab for whom none of this work would have been possible as all material and slides were processed there.

To all my coauthors I say thank you for your help and putting up with my stubbornness and for a wonderful research experience in Paris: Markus Lambertz, Dr. Steve Perry, Frederik Spindler.

I also need to recognize Herman Winkelhorst who is also thanked for his participation in the Texas 2010 dig and data collection at the AMNH and CFM. To Jack and Marie Loftin, we all appreciated your help with the local contacts taking us to the Briar Creek Bonebed during the 2010 and 2011 field season, and for allowing us to stay at your trailer in Archer City for the 3 field expeditions. Also thanked is David Williams of the DMNH for securing permission and assisting in the Rattlesnake Canyon dig of 2013. I can't express enough how thankful I am to have befriended Dr. Robert Bakker "a.k.a Dr. Bob" who has provided countless hours of intellectual discussions and exchange of ideas on topics of the Permian and numerous others subjects. I also want to thank him and Kathy Zoehfeld for allowing us to tour their site at the Craddok Bonebed and for loaning material for consumptive sampling.

Finally, I would like to thank my family back in America who have supported me before during and after this experience, especially my parents Brenda and Donald Shelton, my grandparents June and Doyle Riley, and my cousin Steven Tudor. Five years feels like an eternity when you are so far away from the ones you love. I tell my family to think of this as my "Voyage of the Beagle".

I want to dedicate this work to the memory of Wann Langston Jr. and Farish Jenkins Jr. who both passed away during the course of this study and helped to contribute to this research.

Table of Contents

Summary

This study reports on long bone histology of the pelycosaurs, and proposes the hypothesis that the presence of fibro-lamellar bone (FLB) and high growth rates were already present in the basal most synapsids during the Upper Carboniferous and Lower Permian which was due to the hyperoxic environment. This is contrary to the long held views that pelycosaurs were the plesiomorphic condition being poikilothermic sluggish reptiles and that mammalian endothermy originated within Therapsida. This was accomplished by the consumptive sampling of various pelycosaur taxa throughout the clade from every group, excluding eothyrids. evidence was taken from sphenacodontids, ophiacodontids, edaphosaurids, caseids, and varanopids. For the first time consumptive sampling and analysis of ontogenetic material was also made available from the following taxa: *Ophiacodon*, *Dimetrodon*, and *Cotylorhynchus.* Results show inter- and intra-specific histological variation among this clade. Basically, carnivores grew much faster than herbivorous pelycosaurs who appear to have secondarily reduced their growth rates during the Lower to Middle Permian despite having evolved to record sizes. Histological differences seem to be mostly due to diet and how it was acquired. Further consumptive sampling of the earliest insectivorous forms is required to fully understand this phenomenon and to finally resolve what the true plesiomorphic condition is for tetrapods. A complete list of all material sampled and measured for this research is given in the appendix. Unfortunately, there was not enough time to include all the material acquired over the last five years in this study.

Chapter 1: Pelycosaur, bone histology, thermoregulation

1. Introduction

The overall goal of this study was to improve our understanding of one of the major events in vertebrate evolution, mammalian endothermy, by studying the bone histology of the earliest representatives of the synapsids, the 'pelycosaur' grade mammal-like reptiles also known as the non-therapsid synapsids. This involved a representative sampling of the postcranial elements across pelycosaur diversity, revealing the presence of various bone tissue types, and a sampling of various growth series in common pelycosaur taxa: Chapter 3, *Dimetrodon* (sp); Chapter 4, *Ophiacodon* (sp); Chapter 5 and 6, various members of Caseidae; Chapter 7, myctosaurine-grade Varanopidae and Edaphosauridae (*Edaphosaurus* (sp) and *Lupeosaurus* (spp)).

However, time did not allow for all of the material that was acquisitioned and analyzed to be included in this write up. A complete list of all measured and consumptively sampled pelycosaur bones has been included in Chapter 2. Also, Chapter 2 gives a complete record of the fortuitist and fruitful field work undertaken in the Lower Permian Texas Red Beds during the course of this research. Also, this work gives us a better understanding of the metabolic status of some of the major groups of herbivores of the Lower Permian, such as Caseidae, shedding light on the evolution of herbivory in the Lower Permian, another major event in vertebrate evolution. A new hypothesis for the feeding ecology and respiratory physiology of large caseid taxa, in addition to an early model for the evolution of the mammalian diaphragm, are proposed in Chapter 5. The final chapter (Chapter 7) is provided as a synthesis of all histological work undertaken here and concludes with what implications these findings yield. This includes a new model for the timing and origin of endothermy in the mammalian lineage.

The current chapter provides an overview of the evolution and diversity of pelycosaurs, an summary of long bone formation and tissue organization, the property and principles of thermophysiology and how metabolic status is inferred from the fossil record, and a review of pelycosaur bone histology.

2. The evolution and diversity of 'Pelycosauria'

This section gives a brief over view of basal synapsid evolution with specific attention to the diversity and phylogenic position of Pelycosauria.

2.1 Background

The earliest representatives of the mammalian lineage are the non-therapsid synapsids. This paraphyletic group has traditionally been called 'Pelycosauria' (Fig. 1). In this study I will continue to use the term 'pelycosaur' but in an informal sense instead of the cumbersome "non-therapsid synapsids". From these basal amniotes arose the synapsid line which includes Therapsida, of which the mammals are a subgroup. Synapsida skull morphology is easily distinguished from those of Anapsida and Diapsida (as seen in the sauropsid line which birds, snakes, reptiles, turtles, and crocodilians have descended from) by the presence of a single opening behind the eyes known as temporal fenestra (Reisz 1986) (Fig. 2). During the inception of this study it was widely accepted that the long held view of cold-blooded sluggish ectothermic pelycosaurs were separated from the warm-blooded more active Therapsida by a time period estimated to be approximately two million years (Hotton et al. 1986). However, intermediate forms are few and controversial. This "missing time" was referred to as Olson's gap (Lucas 2004) (Fig. 1). It was during this supposed hiatus of fossilization that the transition from ectothermic synapsids evolved into the endothermic more mammal-like synapsids that we see today, must have occurred. It is noted here that this major evolutionary step, and the great morphological difference between the two groups, would be inconsistent in this time frame. This hypothesis is supported by Benton (2012) who has shown Olson's gap does not exist. With the exception of some recent finds in Russia, pelycosaurs and therapsid remains are not found within the same stratigraphic unit. It should be noted that the only evidence of therapsids in the Lower Permian of North America are a few fragmentary questionable fossils identified as *Tetraceratops insignis* Mathew, 1908 discovered in Texas (Laurin and Reisz 1990, 1996; Conrad and Sidor 2001; Amson and Laurin 2011).

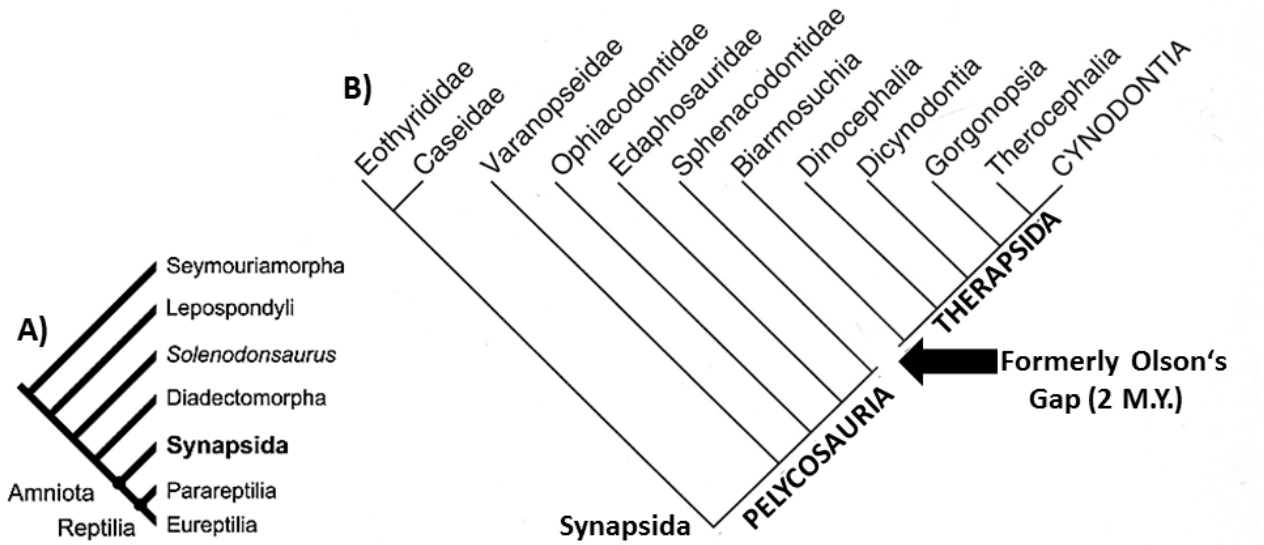

Figure 1. Phylogeny of A) basal tetrapods and B) basal synapsids. Note that the sister group to the synapsids is Diadectomorpha (Diadectidae). Also, a recent review by Benton (2012) has suggested Olson's Gap doesn't exist. A time period of approximately 2 M.Y. of "missing time" due to the lack of transitional fossils between the basal synapsid clades of Pelycosauria and Therapsida. It was during this time that many researchers believed endothermy began to evolve in the mammalian lineage. Adapted from Huttenlocker et al. (2011) and Benton (2005).

The synapsid lineage has its origins in the Late Carboniferous (Romer and Price 1940; Reisz 1986) based on ophiacodontid material identified as *Archaeothyris florensis* Reisz, 1972 and *Protoclepsydrops haplous* Carroll, 1964, which is older, but the synapsid affinity of the later is debatable. By this time, the sauropsid and synapsid lines had already deviated but the then contemporaneous amniotes are believed to share a common amphibian ancestor with the earliest known reptiles (*Hylonomus lyelli* Dawson, 1860 and *Paleothyris acadiana* Carroll, 1969 and *Petrolacosaurus kansensis* Lane, 1945). Also, it should be noted that the oldest amniotic eggs do not appear in the fossil record until the Triassic (Sander 2012). Fossilized amniote eggs have never been discovered in Paleozoic strata (Sumida and Martin 1997).

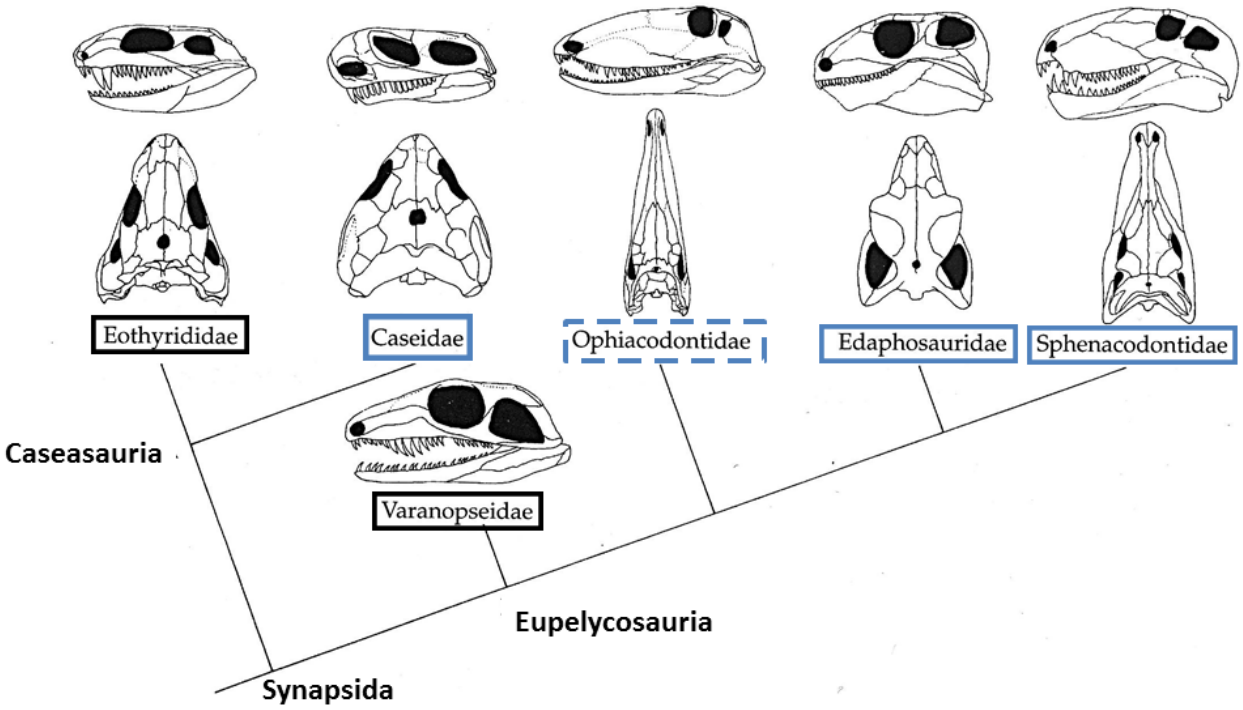

Figure 2. Phylogeny of Pelycosauria with published information on long bone histology indicated. Lamellar-zonal bone (LZB, blue box) is the plesiomorphic bone tissue and indicates low growth rates consistent with a low basal metabolic rate. The blue dotted box indicates that Ophiacodonitdae is also slow growing, but highly vascularized signifying what previous authors have generally concluded about the histology of this family. Black boxes indicate unknown or indeterminate bone histology. Data on bone tissue types were taken from the literature (Enlow 1969; de Ricqlès 1974a, b; Huttenlocker and Rega 2012). Note that basal pelycosaur long bone histology is poorly known. Modified after Kemp (2012).

2.2 Pelycosaur diversity

The pelycosaurs consist of two major clades, the Caseasauria and the Eupelycosauria. The Caseasauria lineage includes Eothyrididae and Caseidae, while the Eupelycosauria covers Varanopidae (also known as Varanopseidae), Ophiacodontidae, Edaphosauridae, and Sphenacodontidae (Kemp 2012) (Fig. 2). A major evolutionary innovation that arose at least twice among them (in Caseidae and Edaphosauridae) is herbivory. This happened in the Early Permian, but it first appears during the Carboniferous in the sister group to Amniota, Diadectomorpha (Diadectidae), and revolutionized terrestrial food webs (Sues 2000; Reisz and

Fröbisch 2014) (Fig. 1). There were other Lower Permian herbivores (bolosaurs and captorhinids), but these three groups dominated biomass-wise (Fig. 3) Reisz and Fröbisch 2014). A final caveat needs to be added: the alpha taxonomy in use today for pelycosaurs is still largely that proposed by Romer and Price (1940) as revised by Reisz (1986). Thus, a modern study and a computer-based phylogenetic analysis for pelycosaur species are lacking, although work on caseid, *Ophiacodon,* and *Dimetrodon* phylogeny has been in progress at the lab of Prof. Robert Reisz (Toronto, Canada) for several years. However, Benson (2012) has recently resolved the affinity of four previously indeterminate taxa; *Trichasaurus* (Caseidae), *Basicranodon* (Varanopidae), *Ruthiromia* (Varanopidae), and *Lupeosaurus* (Edaphosauridae).

2.2.1 Eothyrididae

Eothyrididae Romer and Price, 1940, is a family consists of only two genera; *Eothyris* and *Oedaleops* (Langston 1965; Sumida et al. 2014). Fossil material of this family is very rare, but eothyrids are considered the most primitive of the basal synapsids based on their skulls having teeth indicative of an insectivorous diet (Romer and Price 1940; Reisz 1986; Hotten et al. 1997). This hypothesis has support in that each family line has a basal member with an insectivorous diet. Postcranial material attributed to Eothyrididae has yet to be recovered and histologically investigated.

2.2.2 Caseidae

Caseidae Williston, 1912 is a herbivorous pelycosaur group that consists of many currently recognized species whose evolution briefly overlapped with the radiation of Therapsida. By the Middle Permian caseids were the largest tetrapods of their time (Olson 1968; Reisz 1986; Romano and Nicosia 2014). Members of this group are characterized by having a strikingly small head with large nasal openings, low jaw articulation (below the tooth row), heavy mandible with deep symphysis, loss of caniniform teeth, sulcated tooth rows, small cervical vertebrae, three sacral ribs and large iliac blade (Romer and Price 1940; Olson 1968; Reisz 1986; Huttenlocker and Rega 2012). These characteristics are believed to be derived traits and an adaption to herbivory, and due to an increase in size (Reisz 1986). However, Reisz and Fröbisch (2014) have recently described the oldest insectivorous caseid from Kansas, *Eocasea martini*, extending the line back into the Late Carboniferous. A similar trophic shift has been proposed for

Edaphosaurids. Caseidae persisted well into the Middle Permian (Reisz 1986; Maddin et al. 2008; Reisz et al. 2009). Members range in size from one to six meters in total length, and estimated to weigh between 300 - 500 kg (Romer and Price 1940). One of the largest genera of the Caseids, as well as the largest known pelycosaurs, until recently was *Cotylorhynchus* of Texas and Oklahoma. Fragmentary skeletal material from a slightly larger species has been recently discovered in Sardinia, Italy (Ronchi et al. 2011), and was described as *Alierasaurus ronchii* Romano and Nicosia 2014. The habitat of the larger species has been compared to that of sirenians and *Hippopotamus* (see chapter 5; Romer and Price 1940; Olson 1968). However, the consensus in the literature hypothesized a fossorial habitat. The limb length disparity (LLD) has been shown to vary in Caseidae as they are the only group in which some have longer humeri than femora (Olson 1968; Reisz et al. 2011; Felice and Angielczyk 2014). Reisz (1986) cites similarities (small head relative to body size, enlarged temporal fenestra, and the presence of a fully formed ectepicondyler foramen in the humerus) between the specialized features of the larger species of caseids and edaphosaurids as a sign of convergence.

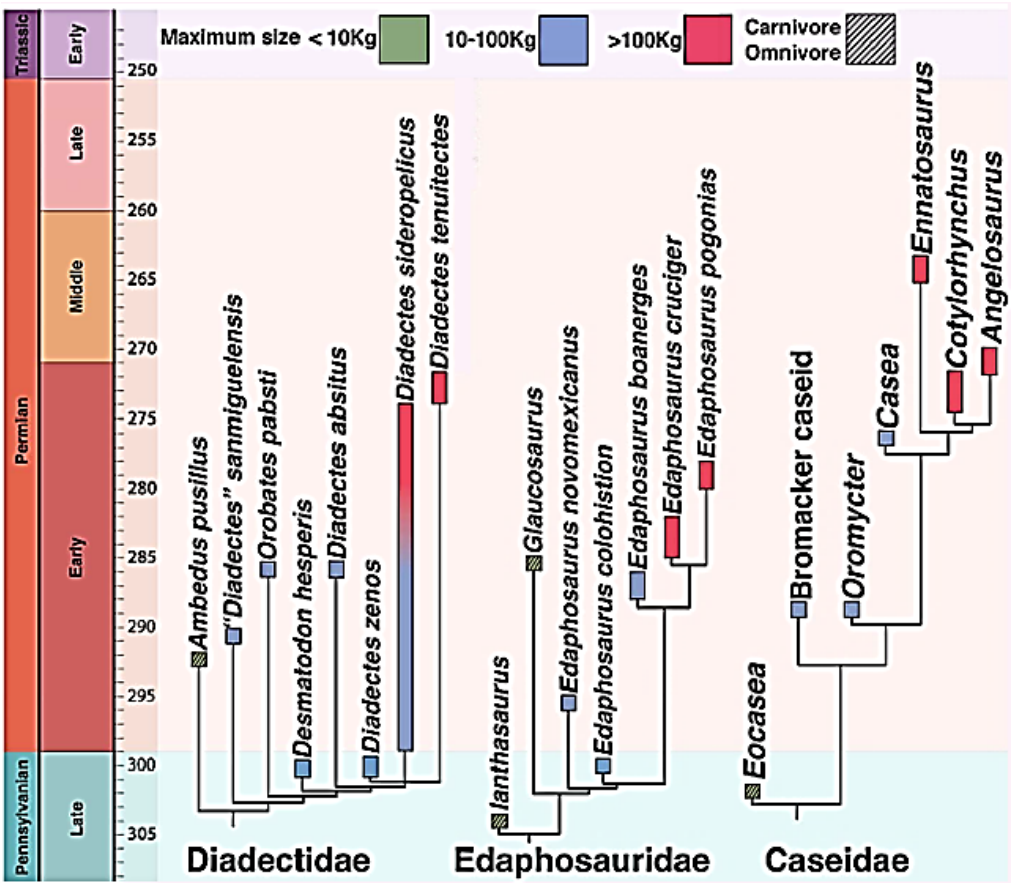

Figure 3. Time-calibrated phylogenies of the major lineages of early terrestrial tetrapod herbivores (Diadectidae, Caseidae, and Edaphosauridae). Herbivory first appears in the diadectids shortly before it appears in pelycosaurs. Estimates of maximum body size of included taxa are placed within three weight categories in order to indicate the general trends, less than 10 kg (green), 10–100 kg (blue), and more than 100 kg (red). The taxa shown as open, colored boxes of various shades of green are all considered to be herbivores. The taxa shown as crosshatched boxes are all considered to be either carnivorous or omnivorous (modified from Reisz and Fröbisch 2014).

2.2.3 Varanopidae

Varanopidae Romer and Price, 1940 is considered the least derived pelycosaur group (Reisz 1986). Skeletal morphology is closer related to sphenacodontids and modern varanids (hence their name), but Varanopidae is believed to have evolved from an early form related to *Archaeothyris*. Physical characteristics of these small (one to two meters in length) carnivorous eupelycosaurs include elongation of the limbs, lightening of the skeleton, and modifications to the skull and dentition. (Reisz 1986). Varanopids existed from the Late Carboniferous to the Middle Permian, and their bauplan remained similar to that of *Archaeothyris*, retaining the form of the earliest basal synapsids. Given their small size, the most parsimonious conclusion is that varanopids were insectivorous. Varanopids first show up in the Upper Carboniferous, and were the most successful pelycosaur line. Fossil material is cosmopolitan and has been found further from the paleoequator than any other pelycosaur.

2.2.4 Ophiacodontidae

Ophiacodontidae Nopcsa, 1923 is a eupelycosaur group that flourished throughout the Early Permian but originated in the Late Carboniferous. Even though they are considered primitive pelycosaurs by Romer and Price (1940) they have recently been shown to be more derived osteologically than varanopids, eothyrids, and caseids (Brinkman and Eberth 1983; Reisz 1986; Kemp 2007a, b). As previously mentioned, the earliest known synapsid fossils are assigned to this group dating back to the Carboniferous of Nova Scotia, the Czech Republic, and the USA (Reisz 1972, 1975). *Ophiacodon* (sp) is considered a more derived member of the family that existed between the Upper Carboniferous into the Lower Permian. Most of the fossil remains

have been found throughout the southwestern United States, specifically New Mexico, Kansas, Texas, and Oklahoma (Romer and Price 1940; Vaughn 1966, 1969; Reisz 1986). *Ophiacodon* possess autapomorphies that have been suggested as evidence for an amphibious or (semi-) aquatic lifestyle. These include, but are not limited to, an elongated narrow cranium suggestive of a piscivorous diet, poorly ossified endochondral skeleton, LLD between the humerus and femur, and a highly porous periosteal tissue in the long bones (to be discussed later) (Case 1915; Romer and Price 1940; de Ricqlès 1974a, b; Reisz 1986; Huttenlocker and Rega 2012; Felice and Angielczyk 2014).

2.2.5 Edaphosauridae

Edaphosauridae Cope, 1882 is the most abundant group of herbivorous pelycosaurs (Fig. 3), though they could have adapted an omnivorous diet based on the carnivorous dentition of the earlier forms (Hotton et al. 1997). This is not unusual as modern herbivores do incorporate some form of protein in their diet, meaning that strict herbivory is less common. Edaphosaurids existed between the Late Carboniferous and Early Permian, going extinct shortly after Ophiacodontidae and well before Sphenacodontidae and Caseidae. Edaphosaurids are found in Europe and North America, ranging in size from one to four meters in length. Their most distinguishing feature is the dorsal sail, similar to that of some sphenacodontids (see below), but they differ in that edaphosaurid neural spines contain lateral tubercles projecting out horizontally in all but the largest genera.

Four genera are currently recognized; *Ianthasaurus* (stratigraphically the oldest taxon), *Glaucosaurus, Edaphosaurus,* and, the largest edaphosaurid, *Lupeosaurus* (Berman 1979; Reisz and Berman 1986; Sumida 1989; Modesto and Reisz 1990; Benson 2012). It should be noted that juveniles are rarely found. Edaphosaurids are the earliest known tetrapods to display a dorsal sail. The earliest and smallest species, found in Kansas, is *Ianthasaurus hardestii* which was insectivorous (Reisz and Berman 1986; Modesto and Reisz 1992). Bennett's (1996) aerodynamic experiments on the edaphosaurid sail suggest the tubercles aided in airflow turbulence and in thermoregulation across the sail membrane surface (to be discussed later).

2.2.6 Sphenacodontidae

Sphenacodontidae Marsh, 1878, the dominant carnivore group appearing in the Upper Carboniferous of North America as well as some representatives from the Early Permian of Europe (Berman et al. 2001; Kemp 2007a, b; Fröbisch et al. 2011). They are believed to have given rise to Therapsida (Fig. 2) via sail-less sphenacodontoids such as *Haptodus* (Romer and Price 1940; Reisz 1986; Laurin and Reisz 1996). The most iconic and recognized pelycosaur is *Dimetrodon,* despite the fact that it is marketed and sold as a plastic dinosaur in museum gift shops and toy stores (Angielczyk 2009). This genus was the main sphenacodontid examined for this study (Chapter 3). As mentioned before, the neural spines of the *Dimetrodon* dorsal sail differ from those of edaphosaurids by lacking horizontal tubercles like those of *Lupeosaurus*. The main function of the dorsal sail is hypothesized to be a thermoregulatory organ to maintain a more efficient metabolism in addition to other functions such as sexual display (Bakker 1971; Bramwell and Fellgett 1973; Haack 1986; Turner and Tracey 1986; Tracey et al. 1986; Bennett 1996; Florides et al. 1999; Florides et al. 2001). It should be noted that allometric growth of the dorsal sail in this group is positive unlike in edaphosaurids which is negative (Romer and Price 1940). The largest of the pelycosaur predators are *D. grandis* and *D. giganhomogenes,* with body lengths of over three meters and weighing up to 250 kg. This is about half the size achieved by the largest herbivorous taxa. One of the smallest species of this genus is *D. teutonis* from the Lower Permian of Gotha, Germany (Berman et al. 2001, 2004), estimated to weigh 14 kg; only half the size of the previous "record holder" from North America, *D. natalis*. Sphenacodontidae goes extinct close to the same time as Caseidae.

3. Evolution of endothermy in the mammalian lineage

This section explains the basic principles of thermoregulation with regards to endothermy and homeothermy, and the different theories of how endothermy evolved in the mammalian lineage. Also, we show how physiological aspects of an extinct organism are in inferred in the fossil record.

3.1 Aspects of endothermy

Thermoregulation by definition is the ability of an organism to maintain its body temperature. This study will focus on two aspects of thermoregulation that are related to warm-

bloodedness; Endothermy, the metabolic generation and regulation of body temperature, the state of being warm-blooded, and homeothermy, the ability of an organism to maintain a stable body temperature regardless of external influences. The opposite of homeothermy is poikilothermy, the state in which an organism's body temperature varies considerably due to the environment. An organism is considered endothermic if its principle source of body heat is internal and ectothermic if its principle body heat is external (McNab 1978; Clarke and Pörtner 2010). Endothermy, is known to exist in nearly all forms of life including insects, fish, reptiles, specifically archosaurs, mammals, and even plants. Endothermy evolved at least twice in tetrapods, once in the lineage that led to birds via the dinosaurs and once in the lineage that led to modern mammals. This section will focus on the latter as the scope of the endothermy topic is too broad to be fully covered here. Exactly when the metabolic shift occurred has been highly debated in the literature (Hotton et al. 1986). Some authors believe that only the first small mammals of the Triassic were truly endothermic (Hopson 1973; McNab 1978). Others have stated that the metabolic shift first occurred during the Late Permian with endothermy originating in the therapsids which presumably where endothermic (Hillenius 1994). Regardless, everyone agrees that endothermy did not evolve among pelycosaurs which have been classically viewed as sluggish, cold-blooded, ectotherms. However, the universally accepted theory for the origin of Therapsida is that they evolved from the sail-less sphenacodontids (Olson 1986). This casts doubt on the pelycosaur dorsal sail functioning as a thermoregulatory organ. Several other lines of evidence exist supporting the evolution of high growth rates and endothermy in Therapsida during the Late Permian (see below).

3.2 Origins of mammalian endothermy

Even though endothermy is one of the major innovations in vertebrate evolution, there is no clear consensus of exactly how or why this came about. Various theories on the origins of mammalian endothermy now exist that either focus on an organism's thermoregulation or aerobic activity (for a more detailed review see Bennett and Ruben 1979, 1986; Kemp 2006a, b; Hayes and Garland 1995; Clarke and Pörtner 2010). The end result of either mechanism is believed to lead to some form of general homeothermy. Grigg et al. (2004) pointed out the often erroneous synonimization of these terms and states that endothermy proceeds homeothermy, but they

evolved independently of each other. Current studies (McKechnie and Mzilikazi 2011; Boyles et al. 2011) show that a majority of endotherms are in fact heterothermic meaning there incur daily variations in body temperature; examples include hibernation and torpor which may be the plesiomorphic reptilian condition (McKechnie and Lovegrove 2002; Geiser 2004; Grigg et al.2004).

There are basically two schools of thought on the origin and selective advantage of metabolic endothermy. The most accepted being the aerobic scope hypothesis first stated by Bennett and Ruben (1979): an increase in activity will increase oxygen intake and skeletal muscle production. Thus, the resting metabolic rate increases and prompts thermoregulation by initiating homeothermy (see below). An increase in the concentration of mitochondria is related to the production of ATP, mostly during activity of skeletal muscle, producing heat and energy. On the other hand, the thermoregulation hypothesis states that in order for any organism to accomplish aerobic activities, it must have already had a body temperature capable of allowing it to perform said activities that could be further sustained with the onset of fur of feathers as seen in derived Eutherians and birds (Pötner and Clarke 2010). However, Bennett et al.(2000) disproved the thermoregulation hypothesis by feeding lizards at rest large meals, and found that even though metabolic rate was quadrupled (35° C) the body temperature changed only slightly (0.5° C). Application of any endothermy model to an organism depends on the general size of the animal in question. It is understood that large animals, regardless of initial physiology, will also sustain some sort of prolonged homeothermy due to convection and radiation of heat from their large body mass and volume (Seebacher et al. 1999). This has been called inertial homeothermy (McNab 1978; Grigg et al. 2004). Kemp (2006) points out in his proposed correlated progression model that many of the previous hypotheses and variations thereof are only partially correct, but fail to take into account the complexity of an entire biological structure. Virtually everything in the biology and life of a mammal is either contributory to, or affected directly or indirectly by, endothermic temperature strategy. Kemp (2006) concludes by saying, “The exact pattern of small changes from the initial ancestral condition to the final derived condition will be below the resolution of any available evidence to illustrate, be it paleontological or neontological”. I would like to point out that an increase in oxygen intake can also increase an animal’s activity thus prompting heat or energy production. They increase in size, metabolism and food consumption. A good example of this is the giant insects found during the Carboniferous (Dudley 1998); a time

period that also coincides with an increase in atmospheric oxygen (35% more than today) and a decrease in carbon dioxide as is evident by the diversity and abundance of plants. This increase in oxygen also may account for the ability of insects to fly. Temnospondyls and early amniotes were the first vertebrates to be effected by this oxygen increase coupled with the transition to terrestriality, having to cope with gravity, breathing, and reproduction, but initially still keeping ties to the water. This would require an increase in skeletal muscle, and refinement of lungs.

3.3 Endothermy in the fossil record

Unfortunately, physiology of an extinct animal cannot be directly measured so it must be interpreted by fossil evidence and comparison with extant animals, observing the principle of uniformitarianism. Several lines of evidence exists which have been used for inferring warm-bloodedness in therapsids and non-avian dinosaurs. Some of these will be discussed here, listed in no particular order; predator-prey ratios (Bakker 1972, 1975; Hurlburt 1999; Cooper et al. 2008), latitudinal zonation (Lombard and Sumida 1992; Kemp 2006b), an upright stance (Bakker 1971, 1972; Pontzer et al. 2009), insulation using fur or feathers (Bennett and Ruben 1986; Ruben and Jones 2000; Hillenius and Ruben 2004; Clarke and Pörtner 2010), respiratory turbinates (Hillenius and Ruben 2004; Ruben 1995), Parental care (Farmer 2000), body size (McNab 1978; Turner and Tracey 1986; Klein et al. 2011) and of course the most important line of physical evidence that this study will focus on: bone histology (primarily that of long bones).

3.3.1 The predator-prey ratio

The predator-prey ratio is the relationship of the standing crop of a predator to that of its prey (Bakker 1972, 1975). Bakker (1975) states that this ratio, regardless of body size of the animals, is a constant measure of the metabolism of the predator. Benton (2005) notes that the ratio for large ectothermic predators is similar to that of endothermic predators, and size does play a role in the calculations. Regardless, Bakker (1975) has attempted to calculate the predator/prey ratio for large carnivores using members of Sphenacodontidae, more specifically *Dimetrodon*, as an example, by summing the calculated estimated live weight (Hurlburt 1999; Sander 2000; Packard et al. 2009) of each individual animal, and taking into account the number of individuals found together in the same sediment layer. Bakker (1975) concludes that "fin back" (*Dimetrodon*) communities had a predator-prey ratio range similar to that of extant

ectothermic spiders and lizards (35% to 60%). With regards to predator/prey interactions, Cooper et al. (2008) showed that prey dinosaurs like hadrosaurs did grow more rapidly and reached sexual maturity before their contemporaneous theropod predators. However, Bennett and Ruben (1986) have claimed that the predator/prey ratio method is unreliable. It is an excepted phenomenon in the fossil record that there is a higher carnivore to herbivore ratio during the Paleozoic and into the Mesozoic; slowly decreasing as evolution progresses to today where we find more herbivores to carnivores during the age of mammals. Also, it is observed today that carnivorous mammals produce larger litters than herbivores.

3.3.2 Latitudinal zonation

Latitudinal zonation has been utilized for deciphering areas of endothermic or ectothermic organisms. Berman et al. (1997) showed the movement of the paleoequator from the Devonian to the Early Permian of North America with marked Paleozoic tetrapod localities. This is possible to do by using paleomagnetic data to tract the movement of the tectonic plates (Lombard and Sumida 1992) Just before the Permian, glaciation in the Northern hemisphere was practically absent, however glaciations in the southern hemisphere had reached 30 degrees south latitude (Florides et al. 2001). Again, Bakker (1975) uses this approach, coupled with paleogeography, to show that pelycosaurs were exclusive to the paleoequator and did not exist in the glaciated Gondwana. According to Kemp (2006) pelycosaurs lived within 10 to 30 north and south latitude of Pangaea's paleoequator. During this time it is believed that the environment was becoming increasingly more arid and atmospheric oxygen levels began to decrease. This steep decline of oxygen drove the evolution of accessory organs such as nasal turbinates (to be explained later) in order to sustain the amount of blood the body had adapted to in previous hyperoxic conditions (Hillenius 1992, 1994; Hillenius and Ruben 2004; Hsia et al. 2013).

3.3.3 Gait

Today we see that mammals and birds in general have an upright stance or erect gait (Benton 2005) as opposed to a sprawling gait like that in modern alligators. Bakker (1971, 1972) suggests this is direct evidence of endothermy. However, de Ricqlès (1974a) believes that early archosaurs and primitive therapsids that had a sprawling gait were already endothermic. He also points to Monotremata, an examples of endothermic sprawlers. It is true there are no modern

parasagittal ectotherms, and terrestrial animals can only reach large size by having an upright stance in order to better support and distribute the weight, as seen in dinosaurs (Bakker 1971; de Ricqlès 1974a; Sander et al. 2011; Klein et al. 2011). Sprawlers who are amphibious or aquatic can also reach large size (de Ricqlès 1974a). It should be pointed out that this correlation of parasagittality and endothermy has been viewed as speculative or circumstantial lacking a functional correlation to endothermic processes (Ricqlès 1974a; Ruben 1995; Ruben and Jones 2000).

3.3.4 Pelage or plumage

The evolution of insulation (pelage or plumage) may have occurred as a direct result of the high metabolic rates like those hypothesized to have existed in therapsids (Ruben and Jones 2000) in order to sustain homeothermy (Clark and Pörtner 2010). The first hair is hypothesized to have served as a sensory organ, like vibrissae or whiskers, and it is believed that the infraorbital pits and ridges of some Triassic cynodonts are an indication of the presence of vibrissae (Ruben and Jones 2000). Thus, endothermy must have been present in basal Mammalia (Chinsamy and Hurum 2006; Chinsamy and Abdala 2008; Botha-Brink and Angielczyk 2010; Green et al. 2010; Chinsamy 2012). Only later is it hypothesized that a full pelage of fur or hair came about to help sustain homeothermy (Bennett and Ruben 1986; Ruben and Jones 2000; Hillenius and Ruben 2004). This happened sometime in the late Triassic when the first true mammals were seen as small, fossorial, and probably nocturnal.

3.3.5 Respiratory turbinates

Either as a direct connection with the development of vibrissae or not, respiratory turbinates are found in all modern mammals and birds. Romer and Price (1940) first described ridges in pelycosaurs suggesting evidence of possible turbinate attachments. Based on the position of these ridges, it is believed that these turbinates were only for olfactory use like those found in modern reptiles but they would not have preserved if they were not ossified. However, in therocephalians and cynodonts, we find respiratory turbinates similar to those of modern mammals. Due to the fact that bony turbinates are fragile or in the case of birds, the bony turbinates are only attached by cartilaginous ridges, they are rarely preserved in the fossil record. Turbinate evolution has been hypothesized to be linked to the drop in atmospheric oxygen at the

Permian/Triassic boundary, which may have prompted the need to increase oxygen intake for blood production in the tissue as well as account for the small body size of the therapsids and even smaller Mesozoic mammals (13% oxygen content) compared to their predecessors (Olson 1986; Hsia et al. 2013).

3.3.6 Bone histology

Bone histology, long bone histology in particular, is one of the few pieces of hard physical evidence that we have for attempting to analyze whether an extinct animal is endothermic or ectothermic (Bennett and Ruben 1986). While not directly indicating metabolic rate, long bone histology faithfully records patterns of bone deposition along with modification due to age (Schweitzer and Marshall 2001) and growth rate which in turn is closely tied to metabolic rate (Case 1978; Cubo et al. 2008, 2012; Montes et al. 2007, 2010). It needs to be understood, however, that the term "growth rate" can mean several things. For one, it is the rate of growth of the entire animal, in terms of linear size increase as well as body mass increase. Growth rate may also refer to the local bone apposition rate, which in the mid shaft of the long bones of the tetrapod skeleton (humerus and femur) is closely related to the growth rate of the animal (Sander 2000; Erickson and Tumanova 2000; Erickson et al. 2001; Bybee et al. 2006). Growth rate can be compared qualitatively, for example based on different bone tissue types or quantified as g/day or kg/year of mass gain of the entire animal. Based on the latter approach, Case (1978) in a seminal study found a close correlation between maximum growth rate and basal metabolic rate across a wide spectrum of vertebrates. Endothermic animals are able to sustain a maximum growth rate an order of magnitude higher than ectothermic animals (Werner and Griebeler 2014; Grady et al. 2014). The applications of such studies to fossil are possible because the microstructure of bone preserves well at the cellular level, and thus, fossilized bone a quarter of a billion years old can be directly compared qualitatively and quantitatively to recent bone under the microscope.

4. Bone Histology in general

In order to understand bone histology one must first learn how a typical long bone forms and grows. Bone tissue is made up of an inorganic mineral component that is preserved during fossilization and an organic collagen component that most often does not. A long bone consists of

two epiphyses, cones of endochondreal spongey bone, connected by a compact boney shaft called the diaphysis, and growth occurs in two directions. All bones start out as a cartilaginous precursor by which periosteal bone is deposited around a hyaline frame work by osteoblasts that travel through the blood vessels entering the bone via the nutrient canal, and embryonic tissue is resorbed to form the medullary cavity by chondroclasts. Simultaneously, chondrocytes in the epiphyses deposit cartilage thus increasing bone length. In life the epiphyseal articular surface is covered by a cap of cartilage that decomposes after death and does not preserve. The area where the nutrient canal penetrates the diaphysis often corresponds to the minimal diaphyseal circumference where the best record of bone growth is preserved. All histological analyses in this study will focus on this area (Fig. 4).

4.1 Physiological interpretation of bone tissue

Classical bone histology recognizes three basic bone tissue types, and follows the terminology set forth by Francillion-Vieillot et al. (1990). The first is known as fibro-lamellar bone (FLB) (de Ricqlès 1974a; de Ricqlès et al. 1991). It is informative with regard to physiology because it records bone apposition and thus overall growth at a rate only possible for a warm-blooded animal (Amprino 1947; Padian et al. 2001; Padian and Horner 2004; Montes et al. 2007, 2010; Cubo et al. 2008). This tissue is highly vascularized, and is made up of a framework of woven (WB) consisting of rapidly deposited randomly oriented collagen fibers (Francillion-Vieillot et al. 1990; Castanet et al. 2000). This framework is then later filled in by a slower growing bone lamellar bone (LB) matrix forming primary osteons and secondary trabecular bone (Fig. 4). Ectothermic animals such as lizard and crocodiles, on the other hand, have a histology known as lamellar-zonal bone (LZB) (de Ricqlès 1974a; Francillon-Vieillot et al. 1990; de Ricqlès et al. 1991; Chinsamy-Turan 2005; Castanet 2006) with much fewer blood vessels and a higher degree of fiber organization as indicated by a bone matrix of LB and parallel-fibered bone (PFB). In addition, LZB grows cyclically, resulting in regularly deposited growth marks in the bone wall such as lines of arrested growth (LAG). The third tissue type known as PFB tissue is comprised of a combination of WB and LB matrix. This is the name given to intermediate tissue types within the spectrum of FLB and LZB tissue.

Claims that the ectothermic American alligator, *Alligator mississippiensis*, lays down woven bone in the wild (Tumarkin-Deratzian 2007) have been shown to be unsubstantiated

(Woodward et al.2014). The reverse, that the lack of FLB indicates a low metabolic rate, does not universally apply either because many warm-blooded small mammals such as murine rodents do not show it. This is an effect of body size and does not apply to animals with a body mass above 10 kg, and the lack of FLB in larger mammals is strong evidence for low metabolic rates, even in mammals (Köhler and Moya-Sola 2009); the exception being *Myotragus*. Virtually all common pelycosaurs had body masses greater than 10 kg.

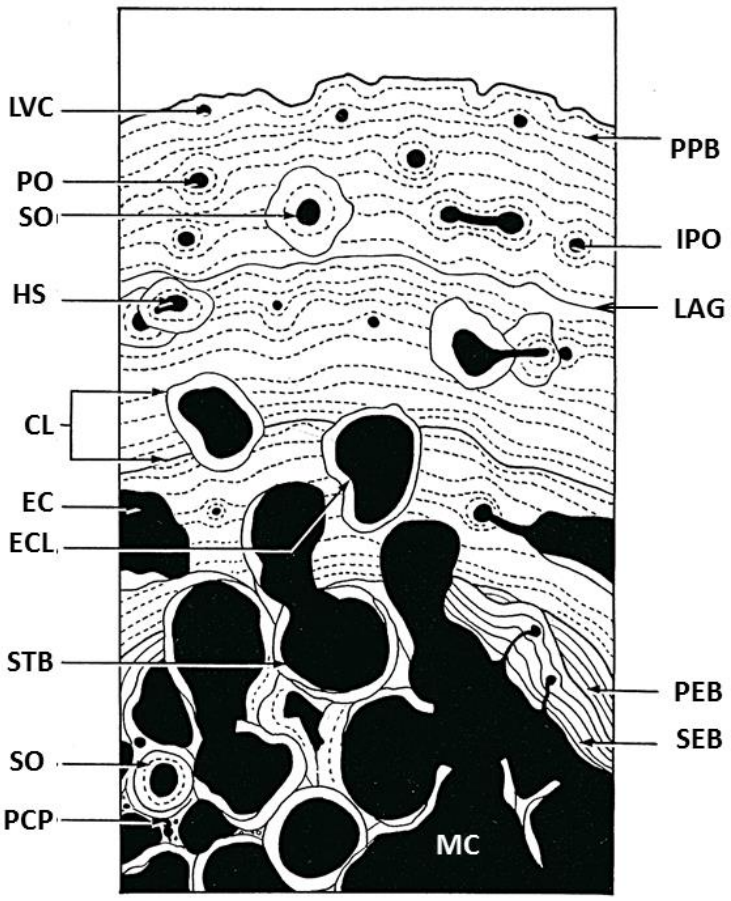

Figure 4. General histology of LZB described in transverse section representing primary and secondary bone formation. CL= cementing lines; EC= erosional cavity; ECL= erosional cavity with an inner single layer of lamellar bone; HS=Haversion system; IPO= incipient primary osteon; LAG= line of arrested growth; LVC= longitudinal vascular canal; MC= medullary cavity; PO=primary osteon; PCP= primary cortical periosteal bone patch; PEB= primary endosteal bone; PPB primary periosteal bone; SO= secondary osteon; SEB=secondary endosteal bone; STB= secondary trabecular bone. Modified from de Ricqlès 1975.

The cyclical (usually annual) growth marks preserved in the bone microstructure offer important insights into the thermophysiology of an extinct animal as well because they permit quantification of maximum growth rates which can then be linked to metabolic status (Case 1978; Montes et al. 2007, 2010; Cubo et al. 2008; Werner and Griebeler 2014; Grady et al. 2014) (Fig. 4). They also provide life history data that is not obtainable any other way (e.g. Erickson et al. 2006). Such growth marks are being extensively studied in dinosaurs (see Erickson 2005 for an excellent review) but are virtually unstudied in pelycosaurs. The annual nature of growth marks, in particular lines of arrested growth (LAG), in fossil bone tissue, is generally accepted (Chinsamy-Turan 2005) and has not been seriously questioned in the last few decades since Bennett and Ruben (1986) suggested cautionary use of bone histology for inferring an animal's metabolism. Evidence for annuality is provided by comparison with recent animals (Castanet et al. 1993) and by phylogenetic bracketing (Padian and Horner 2004) as well as by the fact, that growth models based on annual cyclicity can be applied to histological growth mark records

4.2 Previous work on non-mammalian synapsid bone histology

A sizeable body of current histologic work exists about non-mammalian therapsids from South Africa (Botha and Chinsamy 2000, 2004, 2005; Botha 2003; Ray and Chinsamy 2004; Ray et al. 2004, 2005, 2009; Chinsamy and Abdala 2008; Botha-Brink and Angielczyk 2010; Green et al. 2010). However, the metabolic status of the most basal synapsids of the Late Carboniferous and Early Permian (Figs. 1, 2) remains poorly understood. Mostly, because their long bone histology remains virtually unstudied at a modern level (see below), and we have a rather incomplete understanding of what the evolutionary point of departure on the road to endothermy was in the synapsid lineage. This issue has been the focus of much research in the archosauromorph lineage that leads to birds and is accordingly better understood (de Ricqlès et al. 2003, 2008; Cubo et al. 2012; Werning 2013; Stein and Werner 2013). Against the background of the comprehensive taxon sampling of particularly Triassic non-mammalian therapsids, it is striking how unstudied pelycosaurs are, and virtually all publications on the subject are older than 30 years and thus predate the establishment of paleohistology as a scientific field.

The first major work to address pelycosaur histology is the seminal three-part study by Enlow and Brown (1956, 1957, 1958). Here they included the examination and histological detail of selected bones from *Dimetrodon*, *Edaphosaurus*, and *Ophiacodon.* Their results showed that the bone tissue in these pelycosaurs appeared different from that found in mammals. Enlow and Brown (1957, 1958) concluded that the bone histology of pelycosaurs is similar to that of the "labyrinthodonts" and early groups of reptiles, dense heavily laminated bone with well-developed endosteal or irregular haversion patterns. Enlow (1969) re-examined *Ophiacodon* and observed that the porosity of the cortical bone indicated a high growth rate. However, In the same study he maintained his previous conclusion that pelycosaurian bone histology shows no indication of having mammalian traits.

Peabody (1961) examined ring structures in a sampling of cross sections through the maxillary bone of an indeterminate pelycosaur from the famous fissure fills near Fort Sill, Oklahoma. Peabody (1961), whose work was published posthumously, was one of the earliest studies to observe the “rings” in the bone represented growth marks, much like those of trees, and they were valuable for paleoclimate reconstructions.

Armand de Ricqlès (2007), who was inspired by the paleohistology work done by Donald Enlow, has contributed a great deal of his own work to the growing field of paleohistology starting with his dissertation that he published in part (de Ricqlès 1974a, 1975). It was in a seminal study that de Ricqlès (1974b) included his first descriptions of the types of bone tissue observed in thin sections sampled from selected pelycosaurs (caseids, varanopids, ophiacodontid, edaphosaurid, and sphenacodontid) including taxa previously studied by Enlow and Brown (1957) and Enlow (1969) (*Ophiacodon, Edaphosaurus, and Dimetrodon*). Of note, de Ricqlès (1974b) also made the first and to date only histological description of a caseid (*Ennatosaurus tecton*) femur from Russia noting lamellated LZB. In the same study he notes the observation of FLB tissue in the inner most cortex of an edaphosaur spine followed by an outer cortex of “nearly” avascular LZB. *Varanops brevirostris* material was also examined, but due to diagenetic recrystallization the preservation was not optimal and histology could not be determined (Huttenlocker and Rega 2012). De Ricqlès (1975) also gives the first and only account of calcified cartilage preserved on the articular surface of a *Dimetrodon* humerus. The material sampled by de Ricqlès (1974b) was reused in all his later histological papers dealing with pelycosaurs (de Ricqlès 1976a, b; 1977a, b; 1978a, b; de Ricqlès et al. 1991, 2004). Due to the

small sample base at the time, de Ricqlès reached his conclusions to encompass all pelycosaur species, based on evidence from as few as a single specimen.

However, despite the extensive mention in his papers, most material was fragmented and some of unknown species, sex, or relative age (Brinkman, 1988). Over all, from his work, de Ricqlès (1974b, 1976b) reached a similar conclusion to that of Enlow (1969), specifically *Edaphosaurus* and *Dimetrodon*, if not all non-ophiacodontid pelycosaurs, show a bone histology similar to that of "cotylosaurs" and "stegocephaleans" (LZB with low vascularization). Like Enlow (1969), de Ricqlès (1974a) noted that *Ophiacodon* differs from the other pelycosaurs in that its bone histology shows densely vascularized periosteal bone similar to basal Therapsida (Ray et al. 2004), but he concluded this only reflects an aquatic or amphibious habitat.

More recent work on pelycosaur bone histology has concentrated on the elongate neural spines of Sphenacodontidae and Edaphosauridae, more specifically on the reconstruction of the soft tissue covering the dorsal sail of *Dimetrodon* as well as on the variation in osteohistology and osteology within the neural spines of *Ianthasaurus, Edaphosaurus, Lupeosaurus, Sphenacodon* and various *Dimetrodon* species (Huttenlocker et al. 2006, 2010, 2011; Huttenlocker and Rega 2012). Some attention has also been given to the pathologies observed in sphenacodontid neural spines (Rega et al. 2002; Rega et al. 2005; Huttenlocker et al. 2010). For the most current review of all the previous histological studies on Pelycosauria see Huttenlocker and Rega (2012).

Focus has also been on cortical bone porosity because of the recent development of Bone Profiler by Girondot and Laurin (2003). Germain and Laurin (2005) examined the radius of an *Ophiacodon.* Even though their findings were inconclusive Germain and Laurin (2005) still state that *Ophiacodon* probably was aquatic, thus validating de Ricqlès's (1974a) earlier conclusion. Although, it should be noted Bone Profiler has limited use and is not the only means of quantifying bone porosity from a thin section. Lambert et al. (Chapter 5) used a standard stereological method of point counting established by Howard and Reed (2005).

Since the results of Armand de Ricqlès's pelycosaur work (see all cited studies) it has been assumed and unquestioned by the scientific community that pelycosaurs are all ectothermic, sluggish, and cold-blooded because the histology is similar to basal reptiles, and both share LZB with low vascularization (*Ophiacodon* being the exception to the latter) (Bakker 1975; Florides et al. 2001). These preliminary findings were based on a small sampling of mostly fragmented

specimens partly due to the fact pelycosaur finds were then mostly restricted to a single geographic region, North Texas, and that very little collecting activity has taken place in this region in the last 40 years.

5. References cited

Angielczyk, K. D. (2009) *Dimetrodon* is not a dinosaur: using tree thinking to understand the ancient relatives of mammals and their evolution. Evolution: Education and Outreach 2: 257-271.

Amprino, R. (1947) La structure du tissue osseux envisagée comme expression de différences dans la vitesse de l'accroissement. Archives de Biologie 58: 315-330.

Amson, E., Laurin, M. (2011) On the affinities of *Tetraceratops insignis*, an Early Permian synapsid. Acta Palaeontologica Polonica 56: 301-312.

Bakker, R. T. (1971) Dinosaur physiology and the origin of mammals. Evolution 25: 636-658.

Bakker, R. T. (1972) Anatomical and ecological evidence of endothermy in dinosaurs. Nature 238: 81-85.

Bakker, R. T. (1975) Chapter 21: Experimental and fossil evidence for the evolution of tetrapod bioenergetics. In Gates, D. M., Schmrel, R. B. (eds.) Perspectives of Biophysical Ecology: Ecological Studies 12. Springer, Berlin, 365-399 pp.

Bennett, A. F., Ruben, J. A. (1979) Endothermy and activity in vertebrates. Science 206: 649-654.

Bennett, A. F., Ruben, J. A. (1986) The metabolic and thermoregulatory status of therapsids. In Hotton, N.,

MacLean, P. D., Roth, J. J., Roth, E. C. (eds.) The Ecology and Biology of Mammal-like Reptiles. Smithsonian Institution, Washington D. C., 207-218 pp.

Bennett, A. F., Hicks, J. W., Cullum, A. J. (2000) An experimental test of the thermoregulatory hypothesis for the evolution of endothermy. Evolution 54: 1768-1773.

Bennett, S. C. (1996) Aerodynamics and thermoregulatory function of the dorsal sail of *Edaphosaurus*. Paleobiology 22: 496-506.

Benson, R. (2012) Interrelationships of basal synapsids: cranial and postcranial morphological partitions suggest different topologies. Journal of Systematic Palaeontology 10: 601-624.

Benton, M. J. (2005) Vertebrate Palaeontology. 3rd Edition. Blackwell Publishing, London, 455 p.

Benton, M. J. (2012) No gap in the Middle Permian record of terrestrial vertebrates. Geology 40: 339-342.

Berman, D. S. (1979) *Edaphosaurus* (Reptilia, Pelycosauria) from the Lower Permian of northeastern United States, with description of a new species. Annals of the Carnegie Museum of Natural History 48: 185-202.

Berman, D. S. Sumida, S., Lombard, R. E. (1997) Chapter2: Biogeography of primitive amniotes. In Sumida, S., Martin, K. L. (eds.) Amniote Origins: Completing the Transition to Land. Academic Press, London, 85- 140 pp.

Berman, D. S., Reisz, R., Martens, T., Henrici, A. C. (2001) A new species of *Dimetrodon* (Synapsida: Sphenacodontidae) from the Lower Permian of Germany records first occurrence of genus outside of North America. Canadian Journal of Earth Science 38: 803-812.

Berman, D. S., Henrici, A. C., Sumida, S., Martens, T. (2004) New materials of *Dimetrodon teutonis* (Synapsida: Sphenacodontidae) from the Lower Permian of Germany. Annals Carnegie Museum 73: 48-56.

Botha, J. (2003) Biological aspects of the Permian dicynodont *Oudenodon* (Therapsida: Dicynodontia) deduced from bone histology and cross-sectional geometry. Palaeontologica Africana 39:37-44.

Botha, J., Chinsamy, A. (2000) Growth patterns deduced from the bone histology of the cynodonts *Diademodon* and *Cynognathus*. Journal of Vertebrate Paleontology 20: 705-711.

Botha, J., Chinsamy, A. (2004) Growth and life habits of the Triassic cynodont *Triachodon* inferred from bone histology. Acta Palaeontologica Polonica 49: 619-627.

Botha, J., Chinsamy, A. (2005) Growth patterns of *Thrinaxodon liorhinus*, a non-mammalian cynodont from the Lower Triassic of South Africa. Palaeontology 48: 385-394.

Botha-Brink, J., Angielczyk, K. D. (2010) Do extraordinarily high growth rates in Permo-Triassic dicynodonts (Therapsida, Anomodontia) explain their success before and after the end-Permian extinction? Zoological Journal of the Linnean Society 160: 341-365.

Boyles, J. G., Smit, B., McKechnie, A. E. (2011) A new comparative metric for estimating heterothermy in endotherms. Physiological and Biochemical Zoology 84: 115-123.

Bramwell, C. D., Fellgett, P. B. (1973) Thermal regulation in sail lizards. Nature 242: 203-205.

Brinkman, D. (1988) Size-independent criteria for estimating relative age in *Ophiacodon* and *Dimetrodon (*Reptilia, Pelycosauria) from the Admiral and Lower Belle Plains formations of West-central Texas. Journal of Vertebrate Paleontology 8: 172-180.

Brinkman, D., Eberth, D. A. (1985) The interrelationships of pelycosaurs. Breviora 473:1-35.

Bybee, P. J., Lee, A. H., Lamm, E. T. (2006) Sizing the Jurassic theropod dinosaur *Allosaurus*: Assessing growth strategy and evolution of ontogenetic scaling of limbs. Journal of Morphology 267: 347-359.

Case, E. C. (1915) The Permo-Carboniferous Red Beds of North America and Their Vertebrate Fauna. The Carnegie Institution of Washington, Washington D. C., 176 p.

Case, T. J. (1978) On the evolution and adaptive significance of postnatal growth rates in the terrestrial vertebrates. The Quarterly Review of Biology 53: 243-282.

Castanet, J. (2006) Time recording in bone microstructure of endothermic animals; functional relationships. Comptes Rendus Palevol 5: 629-636.

Castanet, J., Francillon-Vieillot, H., Meunier F. J., Ricqlès A. d. (1993) Bone and individual aging. In Hall, B. K. (ed.) Bone. Volume 7: Bone Growth - B. CRC Press, Boca Raton, 245-283 pp.

Castanet, J., Rogers, K. C., Cubo, J., Boisard, J. J. (2000) Periosteal bone growth rates in extant ratites (ostrich and emu). Implications for assessing growth in dinosaurs. Comptes Rendus de l'Académie des sciences-Series III-Sciences de la Vie 323:543-550.

Carroll, R. L. (1964) The earliest reptiles. Zoological Journal of the Linnean Society 45: 61-83.

Chinsamy, A., Hurum, J. H. (2006) Bone microstructure and growth patterns of early mammals. Acta Palaeontologica Polonica 51: 325-338.

Chinsamy, A., Abdala, F. (2008) Palaeobiological implications of the bone microstructure of South American traversodontids (Therapsida: Cynodontia). South African journal of Science 104: 225-230.

Chinsamy-Turan, A. (2005) The Microstructure of Dinosaur Bone. Johns Hopkins University Press, Baltimore, 195 p.

Chinsamy-Turan, A. (2012) Forerunners of Mammals. Indiana University Press, Bloomington, 330 p.

Clarke, A., Pörtner, H. O. (2010) Temperature, metabolic power and the evolution of endothermy. Biological Reviews 85: 703-727.

Conrad, J., Sidor, C. A. (2001) Re-evaluation of *Tetraceratops insignis* (Synapsida: Sphenacodontia). Journal of Vertebrate Paleontology, 21: 42A.

Cooper, L. N., Lee, A. H., Taper, M. L., Horner, J. R. (2008) Relative growth rates of predator and prey dinosaurs reflect effects of predation. Proceedings of the Royal Society B: Biological Sciences 275: 2609-2615.

Cope, E. D. (1882) Third contribution to the history of the vertebrata of the Permian Formation of Texas. Proclamation of the American Philosophical Society 20: 447-461.

Cubo, J., Legendre, P., Ricqlès, A. d., Montes, L., Margerie, E. d., Castanet, J., and Desdevises, Y. (2008) Phylogenetic, functional, and structural components of variation in bone growth rate of amniotes. Evolution and Development 10: 217–227.

Cubo, J., Le Roy, N., Martinez-Maza, C., Montes, L. (2012) Paleohistological estimation of bone growth rate in extinct archosaurs. Paleobiology 38: 335-349.

Dawson, J. W. (1860) On a Terrestrial mollusk, a millipede, and new reptiles, from the Coal Formation of Nova Scotia. Quarterly Journal of the Geological Society of London 16: 268–277.

Dudley, R. (1998) Atmospheric oxygen, giant Paleozoic insects and the evolution of aerial locomotor performance. Journal of Experimental Biology 201: 1043-1050.

Enlow, D. H., Brown, S. O. (1956) A comparative histological study of fossil and recent bone tissues. Part I. The Texas Journal of Science 9: 405-439.

Enlow, D. H., Brown, S. O. (1957) A comparative histological study of fossil and recent bone tissues. Part II. The Texas Journal of Science 9: 186-214.

Enlow, D. H., Brown, S. O. (1958) A comparative histological study of fossil and recent bone tissues. Part III. The Texas Journal of Science 10: 187-230.

Enlow, D. H. (1969) The bone of reptiles. In C. Gans, ed. Biology of the Reptiles. Academic Press, London, 45-80 pp.

Erickson, G. (2005) Assessing dinosaur growth patterns: a microscopic revolution. Trends in Ecology and Evolution 20: 677-684.

Erickson, G. M., Tumanova, T. A. (2000) Growth curve of *Psittacosaurus mongoliensis* Osborn (Ceratopsia: Psittacosauridae) inferred from long bone histology. Zoological Journal of the Linnean Society 130: 551-566.

Erickson, G. M., Rogers, K. C. and Yerby, S. A. (2001) Dinosaurian growth patterns and rapid avian growth rates. Nature 412: 429-433.

Erickson, G., Mackovicky, P. J., Currie, P. J., Norell, M. A., Yerby, S. A., Brochu, C. A. (2006) Tyrannosaur life tables: An example of nonavian dinosaur population biology. Science 313: 213-217.

Farmer, C. G. (2000) Parental care: the key to understanding endothermy and other convergent features in birds and mammals. The American Naturalist 155: 326-334.

Felice, R. N., Angielczyk, K. D. (2014) Was *Ophiacodon* (Synapsida, Eupelycosauria) a swimmer? A test using vertebral dimensions. In Krammer, C. F., Angielczyk, K. D., Fröbisch J. (eds.) Early evolutionary history of the Synapsida. Springer, Netherlands, 25-51 pp.

Florides, G. A., Wrobel, L. C., Kalogirou, S. A., Tassou, S. A. (1999) A thermal model for reptiles and pelycosaurs. Journal of Thermal Biology 24: 1-13.

Florides, G. A., Kalogirou, S. A., Tassou, S. A., Wrobel L. C. (2001) Natural environment and thermal behavior of *Dimetrodon limbatus*. Journal of Thermal Biology 26: 15-20.

Francillon-Vieillot, H., Buffrénil, V. d., Castanet, J. Géraudie, J., Meunier, F. J., Sire, J. Y., Zylberberg, L., Ricqlès A. d. (1990) Microstructure and mineralization of vertebrate skeletal tissues. In Carter, G. J. (ed.) Skeletal Biomineralization: Patterns, Processes and Evolutionary Trends. Vol. 1. Van Nostrand Reinhold, New York, 471-530 pp.

Fröbisch, J., Schoch, R. R., Müller, J., Schindler, T., Schweiss, D. (2011) A new basal sphenacodontid synapsid from the Late Carboniferous of the Saar-Nahe Basin, Germany. Acta Palaeontologica Polonica 56: 113-120.

Geiser, F. (2004) Metabolic rate and body temperature reduction during hibernation and daily torpor. Annual Review of Physiology 66: 239-274.

Germain, D., Laurin, M. (2005) Microanatomy of the radius and lifestyle in amniotes (Vertebrata, Tetrapoda). Zoologica Scripta 34: 335-350.

Girondot, M., Laurin, M. (2003) Bone profiler: a tool to quantify, model, and statistically compare bone-section compactness profiles. Journal of Vertebrate Paleontology 23: 458-461.

Grady, J. M., Enquist, B. J., Dettweiler-Robinson, E., Wright, N. A., Smith, F. A. (2014) Evidence for mesothermy in dinosaurs. Science 344: 1268-1272.

Green, J. Schweitzer, M. H., Lamm, E. T. (2010) Limb bone histology and growth in *Placerias hesternus* (Therapsida: Anomodontia) from the Upper Triassic of North America. Palaeontology 53: 347-364.

Grigg, G. C., Beard, L. A., Augee, M. L. (2004) The evolution of endothermy and its diversity in mammals and birds. Physiological and Biochemical Zoology 77: 982-997.

Haack, S. C. (1986) A thermal model of the sailback pelycosaur. Paleobiology 12: 450-458.

Hayes, J. P. Garland, T. (1995) The evolution of endothermy: testing the aerobic capacity model. Evolution 49: 836-847.

Hillenius, W. J. (1992) The evolution of nasal turbinates and mammalian endothermy. Paleobiology 18: 17-29.

Hillenius, W. J. (1994) Turbinates in therapsids: evidence for Late Permian origins of mammalian endothermy. Evolution 48: 207-229.

Hillenius, W. J., Ruben, J. A. (2004) The evolution of endothermy in terrestrial vertebrates: Who? when? why? Physiological and Biochemical Zoology 77: 1019-1042.

Hopson, J. A. (1973) Endothermy, small size, and the origin of mammalian reproduction. American Naturalist 107: 446-452.

Hotton, N., Maclean, P. D., Roth, J. J., Roth E. C. (1986) The Ecology and Biology of Mammal-like Reptiles. Smithsonian Institution Press, Washington, 326 p.

Hotton, N., Olson, E. C., Beerbower, R. (1997) Chapter 7: The amniote transition and the discovery of herbivory. In Sumida, S., Martin, K. L. (eds.) Amniote Origins: Completing the Transition to Land. Academic Press, London, 207-264 pp.

Howard, C. V., Reed, M. G. (2005) Unbiased Stereology - Three-Dimensional Measurement in Microscopy, 2nd edition. Garland Science/BIOS Scientific Publishers, New York, 277 p.

Hsia, C. C., Schmitz, A., Lambertz, M., Perry, S. F., Maina, J. N. (2013) Evolution of air breathing: oxygen homeostasis and the transitions from water to land and sky. Comprehensive Physiology 3: 849-915.

Hurlburt, G. (1999) Comparison of body mass estimation techniques, using recent reptiles and the pelycosaur *Edaphosaurus boanerges*. Journal of Vertebrate Paleontology 19: 338-350.

Huttenlocker, A., Rega, E. (2012) Chapter 4: The paleobiology and bone microstructure of pelycosaurian-grade synapsids. In Chinsamy, A. (ed.) Forerunners of Mammals. Indiana University Press, Bloomington, 91-119 pp.

Huttenlocker, A., Angielczyk, K. D., Lee, A. (2006) Osteohistology of *Sphenacodon* (Synapsida: Sphenacodontidae) and the hidden diversity of growth patterns in basal synapsids. Journal of Vertebrate Paleontology 26: 79-80A.

Huttenlocker, A., Rega, E., Sumida, S. (2010) Comparative anatomy and osteohistology of hyperelongate neural spines in the sphenacodontids *Spenacodon* and *Dimetrodon* (Amniota: Synapsida). Journal of Morphology 271: 1407-1421.

Huttenlocker, A., Mazierski, D., Reisz. R. (2011) Comparative osteohistology of hyper elongate neural spines in Edaphosauridae (Amniota: Synapsida). Palaeontology 54: 573-590.

Kemp, T. S. (2006a) The origin and early radiation of the therapsid mammal-like reptiles: a palaeobiological hypothesis. Journal of Evolutionary Biology 19: 1231-1247.

Kemp, T. S. (2006b) The origin of mammalian endothermy: a paradigm for the evolution of complex biological structure. Zoological Journal of the Linnean Society 147: 479-488.

Kemp, T. S. (2007a) The Origin and Evolution of Mammals. Oxford University Press, Oxford, 342 p.

Kemp, T. S. (2007b) The origin of higher taxa: Macroevolutionary processes, and the case of the mammals. Acta Zoologica. 88:3-22.

Kemp, T. S. (2012) Chapter 1: The origin and radiation of Therapsids. In Chinsamy, A. (ed.) Forerunners of Mammals. Indiana University Press, Bloomington, 3-28 pp.

Klein, N., Remes, K., Gee, C. T., Sander, P. M. (2010) Biology of the Sauropod Dinosaurs: Understanding the Life of Giants. Indiana University Press, Bloomington, 344 p.

Köhler, M., Moya-Sola, S. (2009) Physiological and life history strategies of a fossil large mammal in a resource-limited environment. Proceedings of the National Academy of Science 106: 20354–20358.

Lane, H. H. (1945) New Mid-Pennsylvanian reptiles from Kansas: Transactions of the Kansas Academy of Science 47: 381-390

Langston, W. (1965) *Oedaleops campi* (Reptilia: Pelycosauria): new genus and species from the Lower Permian of New Mexico, and the family Eothyrididae. Bulletin of the Texas Memorial Museum 9: 5-47.

Laurin, M., Reisz, R. R. (1990) *Tetraceratops* is the oldest known therapsid. Nature 345: 249-250.

Laurin, M., Reisz, R. (1996) The osteology and relationships of *Tetraceratops insignis*, the oldest known therapsid Journal of Vertebrate Paleontology 16: 95-102.

Lombard, R. E., Sumida, S. (1992) Recent progress in understanding early tetrapods. American Zoologist 32: 609-622.

Lucas, S. G. (2004) A global hiatus in the middle Permian tetrapod fossil record. Stratigraphy 1: 47-64.

Maddin, H. C., Sidor, C. A., Reisz, R. R. (2008) Cranial anatomy of *Ennatosaurus tecton* (Synapsida: Caseidae) from the Middle Permian of Russia and the evolutionary relationships of Caseidae. Journal of Vertebrate Paleontology 28: 160-180.

Marsh, O. C. (1878) Notice of new fossil reptiles. American Journal of Science 89: 409-411.

Mathew, W. D. (1908) A four-horned pelycosaurian from the Permian of Texas. American Museum of Natural History Bulletin 24: 183-185.

McKechnie, A. E., Lovegrove, B. G. (2002) Avian facultative hypothermic responses: a review. The Condor 104: 705-724.

McKechnie, A. E., Mzilikazi, N. (2011) Heterothermy in Afrotropical mammals and birds: a review. Integrative and comparative biology 51: 349–363.

McNab, B. K. (1978) The evolution of endothermy in the phylogeny of mammals. American Naturalist 112: 1-21.

Modesto, S. P. Reisz, R. R. (1990) A new skeleton of *Ianthasaurus hardestii*, a primitive edaphosaur (Synapsida: Pelycosauria) from the Upper Pennsylvanian of Kansas. Canadian Journal of Earth Sciences 27: 834-844.

Modesto, S. P., Reisz, R. R. (1992) Restudy of Permo-Carboniferous synapsid *Edaphosaurus novomexicanus* Williston and Case, the oldest known herbivorous amniote. Canadian Journal of Earth Sciences 29: 2653-2662.

Montes, L., Le Roy, N., Perret, M., de Buffrénil, V. Castanet, J., Cubo, J. (2007) Relationship between bone growth rate, body mass, and resting metabolic rate in growing amniotes: a phylogenetic approach. Biological Journal of the Linnean Society 92: 63–76.

Montes, L., Castanet, J., Cubo, J. (2010) Relationship between bone growth rate and bone tissue organization in amniotes: first test of Amprino's rule in a phylogenetic context. Animal Biology 60: 25-41.

Nopcsa, F. (1923) Die Familien der Reptilien. Fortschritte der Geologie und Paläontologie 2: 1-210.

Olson, E. C. (1968) The family Caseidae. Fieldiana, Geology 17: 225-349.

Olson, E. C. (1986) Relationship and ecology of the early therapsids and their predecessors. In

Hotton, N., Maclean, P. D., Roth, J. J., Roth E. C. (1986) The Ecology and Biology of Mammal-like Reptiles. Smithsonian Institution Press, Washington, 47-60 pp.

Packard, G. C., Boardman, T. J., Birchard, G. F. (2009) Allometric equations for predicting body mass of dinosaurs. Journal of Zoology, 279: 102-110.

Padian, K., Ricqlès, A. d., Horner, J. R. (2001) Dinosaurian growth rates and bird origins. Nature 412: 405-408.

Padian, K., Horner, J. R. (2004) Dinosaur physiology; pp. In Weishampel, D. B., Dodson, P. and Osmólska, H. (eds.) The Dinosauria (Second Edition). University of California Press, Berkeley. 660-671 pp.

Peabody, F. E. (1961) Annual growth zones in living and fossil vertebrates. Journal of Morphology 108: 11-62.

Pontzer, H., Allen, V., Hutchinson, J. R. (2009) Biomechanics of running indicates endothermy in bipedal dinosaurs. Plos One 4: 1-9.

Ray, S., Chinsamy, A. (2004) *Diictodon feliceps* (Therapsida, Dicynodontia): bone histology, growth, and biomechanics. Journal of Vertebrate Paleontology 24: 180-194.

Ray, S., Botha, J., Chinsamy, A. (2004) Bone histology and growth patterns of some non-mammalian therapsids. Journal of Vertebrate Paleontology 24: 634-648.

Ray, S., Chinsamy, A., Bandyopadhyay, S. (2005) *Lystrosaurus murrayi* (Therapsida, Dicynodontia): bone histology, growth, and lifestyle adaptations. Palaeontology 48: 1169-1185.

Ray, S., Bandyopadhyay, S., Bhawal, D. (2009) Growth patterns as deduced from bone microstructure of some selected neotherapsids with special emphasis on dicynodonts: phylogenetic implications. Palaeoworld 18: 53-66.

Rega, E., Wideman, N. Brochu, C. (2002) Paleopathology of amniote specimens from the Late Paleozoic and Mesozoic of North America: Comparison of gross morphological and histological analyses. Journal of Vertebrate Paleontology 22: 98A.

Rega, E., Sumida, S., Noriega, K., Pell, C., Lee, A. (2005) Evidence-based paleopathology I: Ontogenetic and functional implications of dorsal sails in *Dimetrodon*. Journal of Vertebrate Paleontology 25: 103A.

Reisz, R. (1972) Pelycosaurian reptiles from the Middle Pennsylvanian of North America. Bulletin of the Museum of Comparative Zoology 144: 27-62.

Reisz, R. (1975) Pennsylvanian pelycosaurs from Linton, Ohio and Nýřany, Czechoslovakia. Journal of Paleontology 49: 522-527.

Reisz, R. R. (1986) Encyclopedia of paleoherpetology. Part 17A: Pelycosauria. Gustav Fischer Verlag, Stuttgart, 102 p.

Reisz, R. R., Berman, D. S. (1986) *Ianthasaurus hardestii* n. sp., a primitive edaphosaur (Reptilia, Pelycosauria) from the Upper Pennsylvanian Rock Lake Shale near Garnett, Kansas. Canadian Journal of Earth Sciences 23: 77-91.

Reisz, R. R., Fröbisch, J. (2014). The Oldest Caseid Synapsid from the Late Pennsylvanian of Kansas, and the Evolution of Herbivory in Terrestrial Vertebrates. PloS one, 9: e94518.

Reisz, R. R., Godfrey. S. J., Scott, D., (2009) *Eothyris* and *Oedaleops*: Do these early Permian synapsids from Texas and New Mexico form a clade? Journal of Vertebrate Paleontology 29: 39–47.

Ricqlès, A. d. (1974a) Evolution of endothermy: Histological evidence. Evolutionary Theory 1: 51- 80.

Ricqlès, A. d. (1974b) Recherches paléohistologiques sur les os longs des Tétrapodes IV: Eotheriodonts and pelycosaurs. Annales de Paléontologie 60: 3–39.

Ricqlès, A. d. (1975) Recherches paléohistologiques sur les os longs des tétrapodes VII. Sur la classification, la signification fontionnelle et l'histoire des tissus osseux des tètrapodes (Premiere partie). Annales de Paléontologie 61: 51-129.

Ricqlès, A. d. (1976a) Recherches paléohistologiques sur les os longs des tétrapodes VII. Sur la classification, la signification fonctionelle et l`histoire des tissus osseux des tétrapodes. Deuxième partie. Annales de Paléontologie 62: 71-126.

Ricqlès, A. d. (1976b) On the bone histology of fossil and living reptiles, with comments on its functional and evolutionary significance. In Bellairs, A. d. A., Cox, B. C. (eds.) Morphology and Biology of Reptiles. Academic Press, London, 123-150 pp.

Ricqlès, A. d. (1977a) Recherches paléohistologiques sur les os longs des tétrapodes VII. Sur la classification, la signification fonctionelle et l´histoire des tissus osseux des tétrapodes, (Deuxime partie, suite). Annales de Paléontologie 63: 33-56.

Ricqlès, A. d. (1977b) Recherches paléohistologiques sur les os longs des tétrapodes VII (Deuxieme partie, fin). Annales de Paléontologie 63: 133-160

Ricqlès , A. d. (1978a) Recherches paléohistologiques sur les os longs des tétrapodes VII. Sur la classification, la signification fonctionelle et l´histoire des tissus osseux des tétrapodes, Troisème partie. Annales de Paléontologie 64:85-111.

Ricqlès , A. d. (1978b) Recherches paléohistologiques sur les os longs des tétrapodes VII. Sur la classification, la signification fonctionelle et l´histoire des tissus osseux des tétrapodes, Troisème partie. Annales de Paléontologie 64:153-184.

Ricqlès, A. d. (2007) Fifty years after Enlow and Brown's comparative histological study of fossil and recent bone tissues (1956-1958): a review of Professor Donald H. Enlow's

contribution to palaeohistology and comparative histology of bone Comptes Rendus Palevol 6: 591-601.

Ricqlès, A. d., Meunier, F. J., Castanet, J., Francillon-Vieillot, H. (1991) Comparative microstructure of bone. In Hall, B. K. (ed.), Bone. Volume 3: Bone Matrix and Bone Specific Products. CRC Press, Boca Raton, 1-78 pp.

Ricqlès, A. d., Padian, K., Horner, J. R. (2003) On the bone histology of some Triassic pseudosuchian archosaurs and related taxa. Annales de Paléontologie 89:67-101.

Ricqlès, A. d., Castanet, J., Francillon- Vieillot, H. (2004) The 'message' of bone tissue in paleoherpetology. Italian Journal of Zoology 71: 3-12.

Ricqlès, A. d., Padian, K. Knoll, F. and Horner, J. R. (2008) On the origin of high growth rates in archosaurs: Complementary histological studies on Triassic archosauriforms and the problem of a "phylogenetic signal" in bone histology. Annales de Paléontologie 94: 57-76.

Romano, M., Nicosia, U. (2014) *Alierasaurus ronchii*, gen. et sp. nov., a caseid from the Permian of Sardinia, Italy. Journal of Vertebrate Paleontology 34: 900-913.

Romer, A. S., and Price, L. I. (1940) Review of the Pelycosaurs. Geological Society of America Special Papers 28: 1-538.

Ronchi, A., Sacchi, E., Romano, M., Nicosia, U., (2011) A huge caseid pelycosaur from north-western Sardinia and its bearing on European Permian stratigraphy and palaeobiogeography. Acta Palaeontologic Polonica 56: 723-738.

Ruben, J. A. (1995) The evolution of endothermy in mammals and birds: From physiology to fossils. Annual Review of Physiology. 57: 69-95.

Ruben, J. A., Jones, D. T. (2000) Selective factors associated with the origin of fur and feathers. American Zoologist 40: 585-596.

Sander, P. M. (2000) Long bone histology of the Tendaguru sauropods: Implications for growth and biology. Paleobiology 26: 466-488.

Sander, P. M. (2012) Reproduction in early amniotes. Science 337: 806-808.

Sander, P. M., Christian, A., Clauss, M., Fechner, R., Gee, C. T., Griebeler, E., Gunga, H., Hummel, J., Mallison, H., Perry, S., Preuschoft, H., Rauhut, O., Remes, K., Tütken, T., Wings, O., Witzel. U. (2011) Biology of the sauropod dinosaurs: the evolution of gigantism. Biological Reviews of the Cambridge Philosophical Society 86: 117-155.

Schweitzer, M. H., Marshall, C. L. (2001) A molecular model for the evolution of endothermy in the theropod-bird lineage. Journal of Experimental Zoology Part B: Molecular and Developmental Evolution 291: 317-338.

Seebacher, F., Grigg, G. C., Beard, L. A. (1999) Crocodiles as dinosaurs: behavioral thermoregulation in very large ectotherms leads to high and stable body temperatures. The Journal of Experimental Biology 202: 77–86.

Stein, K. W., Werner, J. (2013) Preliminary analysis of osteocyte lacunar density in long bones of tetrapods: all measures are bigger in sauropod dinosaurs. PloS one, 8: e77109.

Sues, H. D., (2000) Evolution of Herbivory in Terrestrial Vertebrates. Cambridge University Press, Cambridge, 268 p.

Sumida, S., Martin, K. L. (1997) Amniote Origins: Completing the Transition to Land. Academic Press, London, 510 p.

Sumida, S. S., Pelletier, V., Berman, D. S. (2014) New information on the basal pelycosaurian-grade synapsid *Oedaleops*. In Krammer, C. F., Angielczyk, K. D., Fröbisch J. (eds.) Early evolutionary history of the Synapsida Springer, Netherlands, 7-23 pp.

Tomkins, J. L., LeBas, N. R., Witton, M. P., Martill, D. M., Humphries, S. (2010) Positive allometry and the prehistory of sexual selection. American Naturalist 176: 141-148.

Tracey, R. C., Turner, J. S., Huey, R. B. (1986) A biophysical analysis of thermoregulatory adaptations in sailed pelycosaurs. Pp. 195-206. *In* N. Hotton, P. D. MacLean, J. J. Roth, and E. C. Roth, eds. The Ecology and Biology of Mammal-like Reptiles. Smithsonian Institute, Washington D.C., 195-206 pp.

Tumarkin-Deratzian, A. R. (2007) Fibrolamellar bone in wild adult *Alligator mississippiensis*. Journal of Herpetology 41: 341-345.

Turner, J. S., and C. R. Tracy. (1986) Body size, homeothermy and the control of heat exchange in mammal-like reptiles. In Hotton, N., MacLean, P. D., Roth, J. J., Roth, E. C. (eds.) The ecology and biology of mammal-like reptiles. Smithsonian Institution Press, Washington, D. C., 185-194 pp.

Vaughn, P. P. (1966) Comparison of the Early Permian vertebrate fauna of the Four Corners region and north-central Texas. Los Angeles County Museum of Natural History Contributions in Science 105: 1–13.

Vaughn, P. P. (1969) Early Permian vertebrates from southern New Mexico and their paleozoogeographic significance. Los Angeles County Museum of Natural History Contributions in Science 166: 1–22.

Werner, J., Griebeler, E. M. (2014) Allometries of Maximum Growth Rate versus Body Mass at Maximum Growth Indicate That Non-Avian Dinosaurs Had Growth Rates Typical of Fast Growing Ectothermic Sauropsids. PloS one, 9: e88834.

Werning, S., (2013) Evolution of bone histological characters in amniotes and the implications f or growth and metabolism. Department of Integrated Biology, University of Berkeley: Unpublished dissertation.

Williston, S. W. (1912) Primitive reptiles. Journal of Morphology 23: 637-666.

Woodward, H. N., Horner, J. R., Farlow, J. O. (2014) Quantification of intraskeletal histovariability in *Alligator mississippiensis* and implications for vertebrate osteohistology. PeerJ, 2: e422.

Chapter 2: Materials and Methods

1. Introduction

The purpose of this chapter is to give an account of how and where the material for this study was acquired and processed. This includes the logistics of the field work done in North Texas and collaborations made with institutions that currently hold the major collections of Lower Permian vertebrates in order to gain morphometric data and to secure various specimens for consumptive sampling.

Between the years 2010 and 2013 a collaborative effort was made to recover Lower Permian vertebrate material from the North Texas Red Beds. Specifically, we focused on predetermined sites in Archer County, Texas that are known to have yielded material for over a century beginning with the work of E. D. Cope. These are some of the richest Permian fossil deposits in the entire world equaled only by the Upper Permian deposits of the Karoo Basin of South Africa. In 2010 and 2011 excavations were carried out at the Briar Creek Bonebed (BCBB) and in 2013 at Rattlesnake Canyon (RSC) both of which are in the Nocona Formation (Artinskian) (Hentz 1988) (Fig. 1). In addition, we prospected briefly at other sites including Lake Kickapoo, the Loftin Bonebed (LBB), the Archer City Bonebeds (ACBB), and by invitation of the Houston Museum of Natural History (HMNH) under the supervision of Robert T. Bakker, the fossil deposits of the Craddock Ranch in Baylor County, North of Seymour, Texas located just south of Lake Kemp. The complete field notes (Appendix 1), field catalogues (Appendix 2), and field maps (Figs. 2-4) of all three campaigns are included as an intricate part of this chapter for the purposes of keeping a documented historical record of our work.

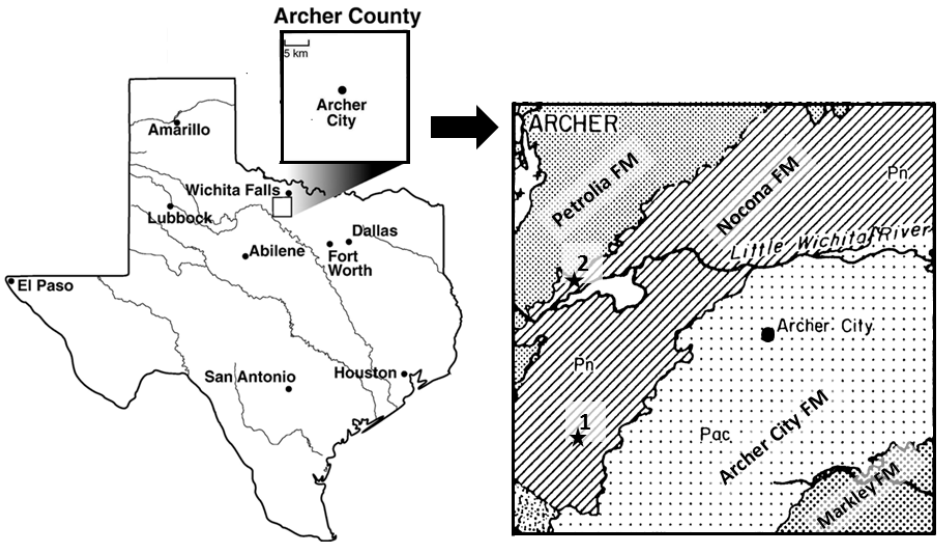

Figure 1 Location and geologic map of Archer County, Texas, USA. This map shows the location of the 1) Briar Creek Bonebed (BCBB) the site of the 2010 and 2011 excavations, and 2) Rattle snake Canyon (RSC) the site of the 2013 excavation. Both of these sites are of the Nocona Formation (Lower Permian, Artinskian). Modified from Hentz (1988) and Labandeira and Allen (2007).

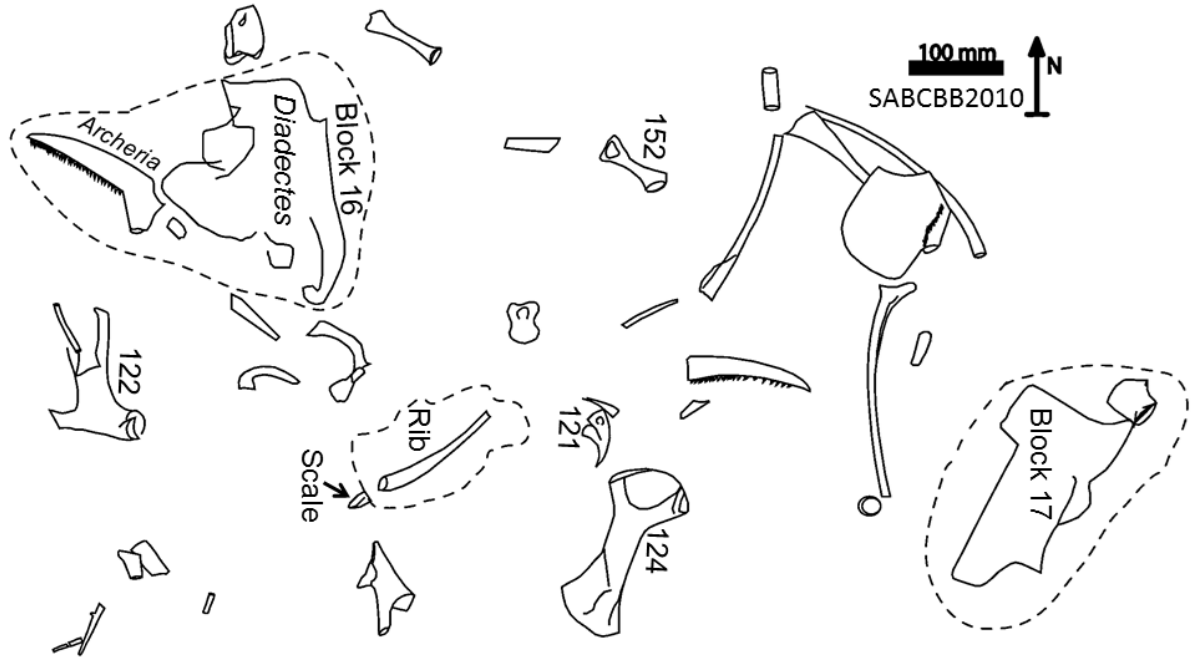

Figure 2 SABCBB2010 excavation field map of the bone spur at the Briar Creek Bonebed. Numbers correspond to the SABCBB2010 field catalogue (Appendix 2). Plaster jackets have been outlined. Drafted by K. Stein.

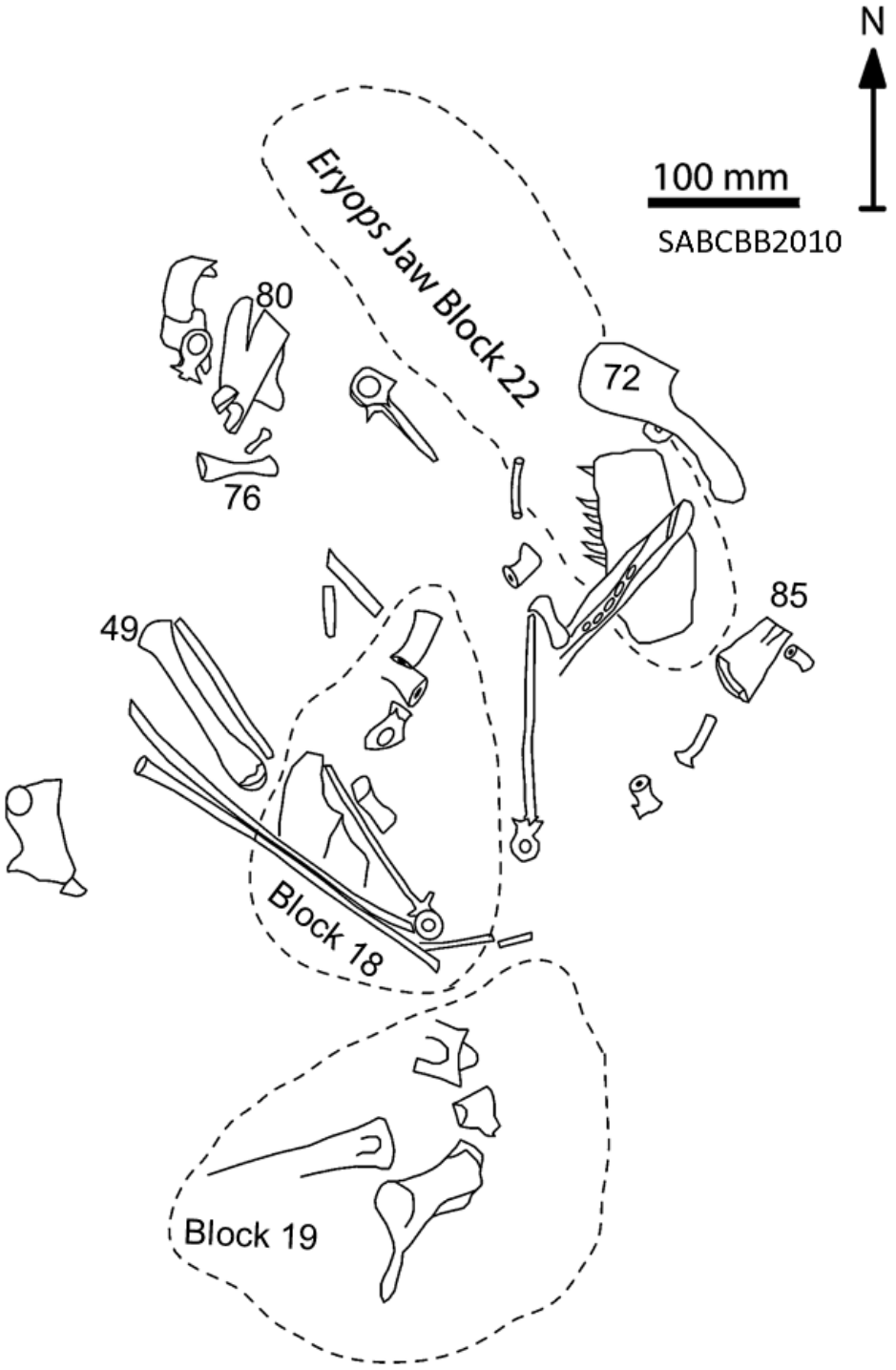

Figure 3 SABCBB2010 excavation field map of the bone spur at the Briar Creek Bonebed. Numbers correspond to the SABCBB2010 field catalogue (Appendix 2). Plaster jackets have been outlined. Drafted by K. Stein.

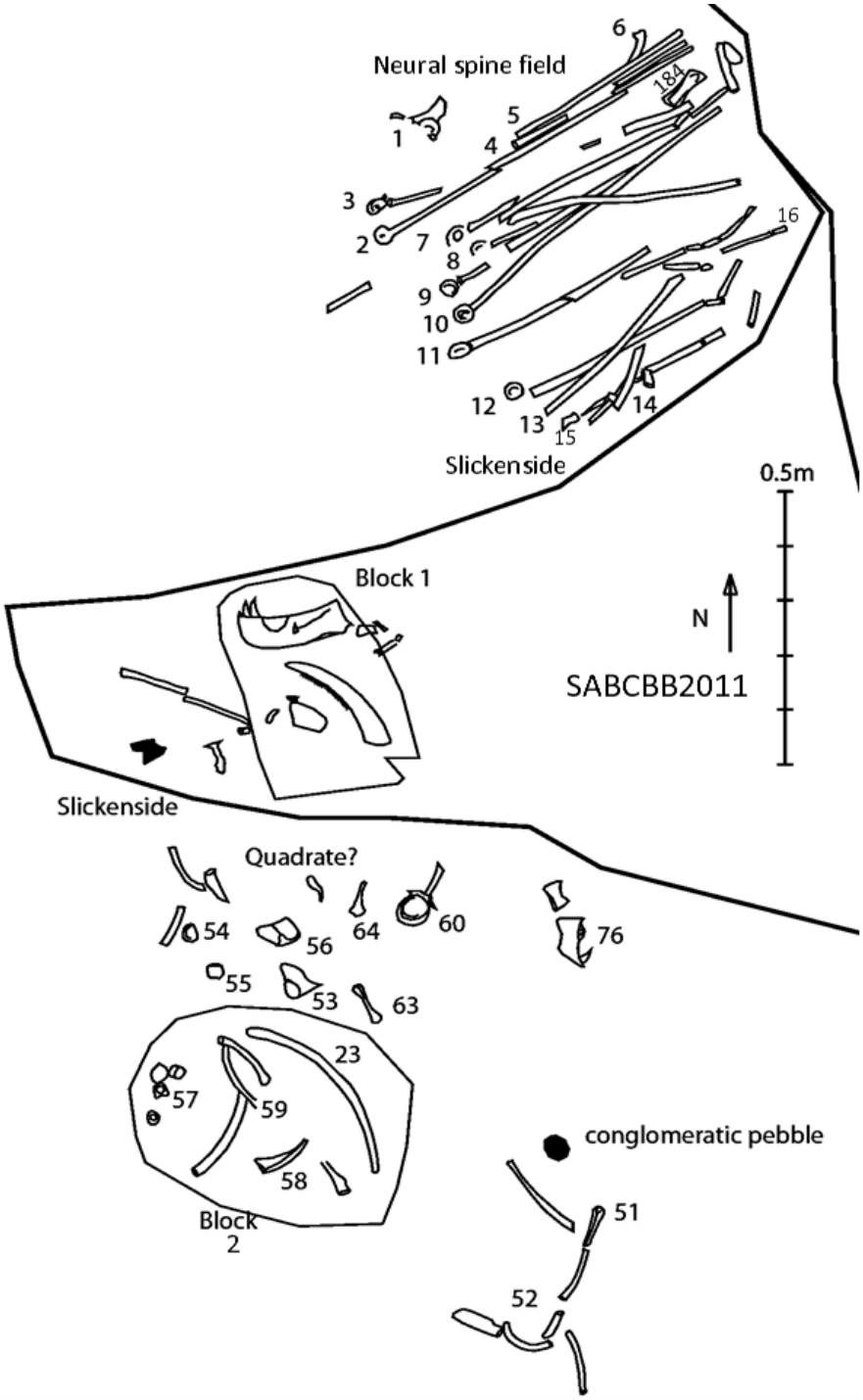

Figure 4 SABCBB2011 excavation field map of the bone spur at the Briar Creek Bonebed. Numbers correspond to the SABCBB2011 field catalogue (Appendix 2). However, SABCBB2011-89 is the *D. natalis* neural spine field and each spine has been numbered individually for reconstruction purposes (1-16). Drafted by K. Stein.

2. Nocona Formation (Artinskian) bonebeds

2.1 The Briar Creek Bonebed

The Briar Creek Bonebed (BCBB) was discovered by E. C. Case in 1912, and is well documented in the literature (Case 1915, spelled "Brier Creek") (Fig. 5). It was of great importance to the work of A. S. Romer of Harvard University who was the last to do an organized excavation at the site in 1972 (unpublished field notes) one year before his death. Since, amateur collectors have only picked over what debris washes out from the hillside. The bed contains an accumulation of unsorted, disarticulated, well preserved reptiles and amphibians in a grey mudstone. The BCBB taphonomy is unique in that some of the bones are considered to have rotted before preservations (Case 1915). Also, the influx of iron-bearing water has caused large iron stone concretions of bones. Case (1915) originally hypothesized that this area represented a pool or swamp that functioned as a macerating tank. This could also have been an oxbow lake or swamp formed by the meandering of a river similar to the hypothesized paleoenvironment described by Sander (1989) for the Geraldine Bonebed. Case (1915) further explains how bodies could have washed in and attracted scavengers that fed on and trampled the decomposing bodies, and then the scavengers themselves got trapped in the mud and joined those they fed on similar to the phenomena observed at the La Brea Tar Pits. Case (1915) stated that the bones themselves show no signs of being worn by water, but are crushed and badly fractured, possibly reflecting evidence of scavenging (Case 1915, Hutson et al. 2013). This same scavenging hypothesis is also reflected in bones from the Craddock Ranch (Bakker et al. 2013). The bonebed itself is estimated at 30 cm thick, and articulated material is very rare. Only two near complete pelycosaurs (*Edaphosaurus* and *Dimetrodon*) have been recovered from here during the entire history of the BCBB (Case 1915, Romer 1972 “unpublished field notes). Bones are either jumbled or associated. Case (1915) noted that fish remains are completely absent from the bed. Invertebrates are also absent but this is a general occurrence of all Lower Permian fossil sites in North Texas. It should also be noted that fossil plant material is very rare.

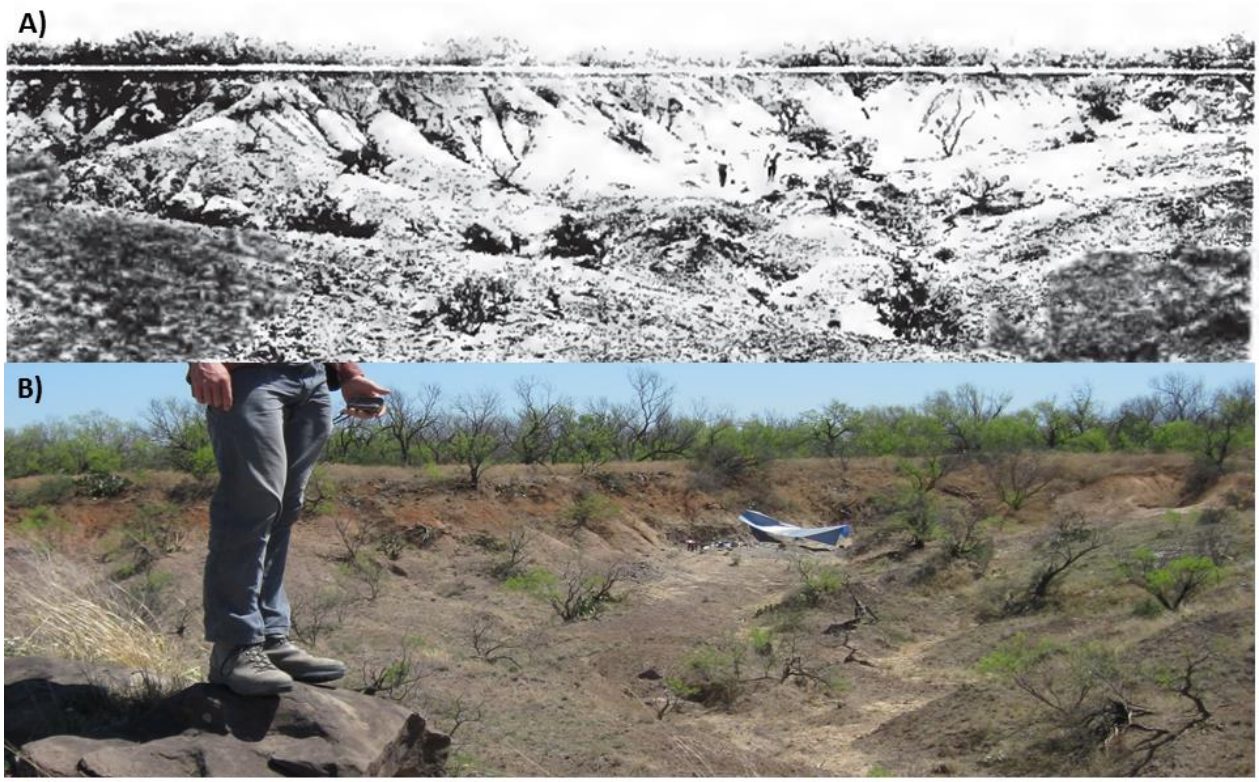

Figure 5 The Briar Creek Bonebed (BCBB) excavation site in Archer County, Texas. A) Photograph of the first excavations published by E. C. Case in 1915. B) BCBB photographed from a similar point of view in 2011. K. Stein in foreground.

2.2 Rattlesnake Canyon

Rattlesnake Canyon (RSC) is the same formation as the BCBB and located north of Lake Kickapoo (Fig. 1). However, it is hypothesized to have been and oxbow lake (pond) in filled by a crevasse splay surrounded by a forest (Sander 1987, Brinkman 1988). Sander (1987) noted the occurrence of the fusinite at the RSC derived from the charcoal of the conifer *Deadoxylon* sp. This is identical to the charcoal found at the Geraldine Bonebed (Artinskian), and it is most likely the same as that occurring in the BCBB (Sander 1989, Sander and Gee 1990). Fossilized flora is much more abundant here than what has been previously reported for the BCBB (Case 1915). The fauna is very similar to the BCBB, but there is more of an abundance of fish species (Sander 1987), Ophiacodon (bones and amphipolar coprolites) (C. D. Shelton personal observation), and

a *Trimerorachis* bone bed (A. S. Romer's unpublished field notes). However, the quality of the vertebrate material is much poorer than that found at the BCBB.

3. Field work

3.1 Briar Creek Bonebed

The majority of our field work was focused at the BCBB in 2010 & 2011 (Fig. 5, Appendix 1). Several hundred specimens were recovered during both campaigns totaling several kilograms of valuable research material (Appendix 2). In total, 25 plaster jackets were blocked out and shipped to the Museum für Naturkunde Berlin for preparation. Diagnostic vertebrate remains include several taxa previously reported in Case's and Romer's excavations; *Archeria* (Fig. 6), *Eryops* (Fig. 7), *Diadectes* (Fig. 8), *Araeoscelis* (Fig. 9C), *Bolosaurus* (9D), *Edaphosaurus* (9B), *Dimetrodon* (Fig. 10), and *Ophiacodon* (Fig. 11). Additionally, we discovered several isolated *Orthocanthus* shark teeth and large spiraled heteropolar bromalites (coprolite) (Fig. 9E, F) (Shelton 2013). Also, an unknown fossil plant bed and isolated bits of fusinite/charcoal were recovered (Sander and Gee 1990). However, much of this recovered material remains unidentified and unprepared as the main focus of this study was on postcranial material. Ontogenies of humeri and femora of *Dimetrodon* spp. material were most abundant (Brinkman 1988). The most common pelycosaur material encountered overall was *Edaphosaurus* and *Dimetrodon* neural spines, ribs and vertebrae. In the 2011 dig, sixteen associated *Dimetrodon* neural spines were recovered at the very bottom layer of the bone bed (Fig. 12). Also, from the plaster jackets, an associated *Ophiacodon uniformis* humerus and scapulae were prepared (Fig. 11). Some of the larger *in situ* material was mapped (Figs. 2-4)

Figure 6 Right mandible of *Archeria* prepared from plaster block 16 (SABCBB2010-136) (Fig. 3).

Figure 7 Left mandible of *Eryops* prepared from plaster block 22 (SABCBB2010-147) (Fig. 4).

Figure 8 Partial *Diadectes* skull and left mandible prepared from plaster block 16 (SABCBB2010-136) (Fig. 3).

Figure 9 An assortment of random specimens discovered during the SABCBB2010 excavation. A) A phalanx of an unknown large caseid prepared from plaster block 1 in dorsal and ventral view. Note the overlapping articulation (identified by R. Reisz). B) *Edaphosaurus* neural spine fragments are very common at the BCBB. C) Articulated aereoscalid vertebrae (Identified by R. Reisz). D) Bolosaurid jaw fragment (Identified by J. Müller). E) *Orthocanthus* tooth. D) SABCBB2011-80 a heteropolar spiral bromalite (coprolite) measuring 108.5 mm in length, 39 mm in width and 20 mm thick. Note that Case (1915) stated fish remains at the BCBB were absent do to the stagnant nature of the water. All scale bars are 1 mm.

Figure 10 Right mandible of *D. limbatus* prepared from plaster block 15 (SABCBB2010-120).

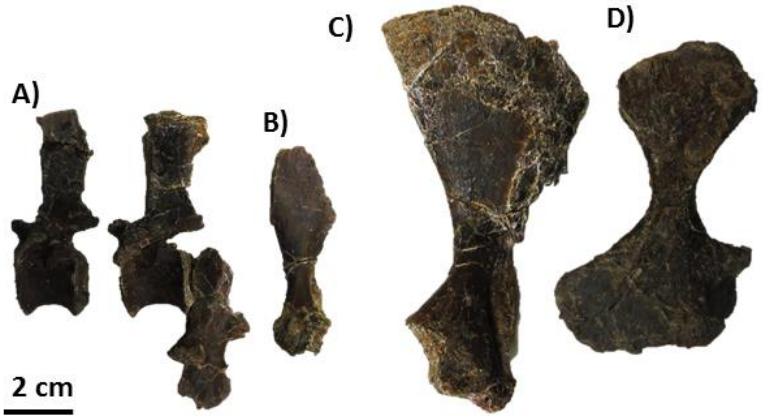

Figure 11 *Ophiacodon uniformis* remains prepared from plaster blocks 13 and 18 (SABCBB2010-102 and – 143) (Fig 4). This includes; A) three associated vertebrae, B) broken right scapula, and C) a complete left scapula with D) the corresponding left humerus (ventral view).

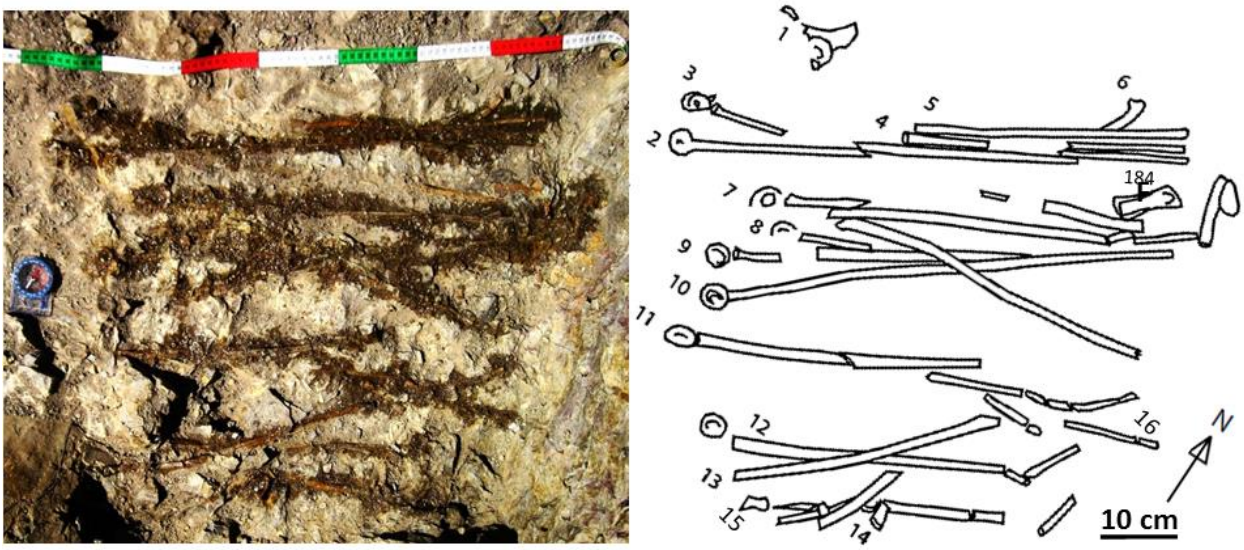

Figure 12 SABCBB2011-89 associated neural spines (1-16) from the dorsal sail of a *Dimetrodon natalis*. Also, SABCBB2011-184 is a juvenile *D. natalis* femur.

2.1 Rattlesnake Canyon

In 2013, the final field expedition in N. Texas took place (Appendix 1). The quality of the recovered pelycosaur material compared to BCBB was incomplete, weathered, or fragmented. Not a single complete pelycosaur long bone was recovered, only pieces (Appendix 2). Vertebrate taxa recovered include lung fish, *Orthocanthus, Ectosteorhachis, Trimerorachis, Eryops, Diadectes, Ophiacodon, Dimetrodon,* and *Ctenospondylus*. Invertebrates include a small *Pecten,* fusilinid tubes, a crinoid stem, and traces of arthropod activity in the form of mud balls formed by crustaceans (Appendix 2). Most notably, we discovered a small isolated bonebed of articulated mummified *Trimerorachis* remains with three partial skulls dubbed "Edina" (Fig. 13), "Fenne" and "Wann" (Appendix 1). Also, we note that an articulated *Ophiacodon* was discovered previously on the site by our guide David Williams, a volunteer for the Dallas Museum of Natural History, and is in the process of being fully excavated by him. We were restricted from collecting in this area.

Figure 13 A partial *Trimerorachis* skull and mandible dubbed "Edina" in A) dorsal and B) ventral view.

3.2 Other Lower Permian Bonebeds of North Texas

Other sites previously visited produced only novel, fragmentary remains (see field notes; Appendix 1). Nothing specific is worth noting with the exception to a visit made to the Craddock Ranch (Arroyo Formation) in Baylor County, TX in 2011. Dr. Robert Bakker gave us a tour of the "Wet Willey" site that contained several layers of articulated *Dimetrodon*, *Diplocalus*, and sharks. Also, at another site across the road christened "Area 51", we were allowed to collect several fully articulated aestivating *Lysorophus* skeletons for consumptive sampling to be used in a future research project (Fig. 14). The exact location of this area is here with held in order to maintain the integrity of this site. A new visitor center and museum founded by Dr. Robert

Bakker, highlighting the HMNS excavations of the last six years recently opened in Seymour, TX near the Craddock Ranch.

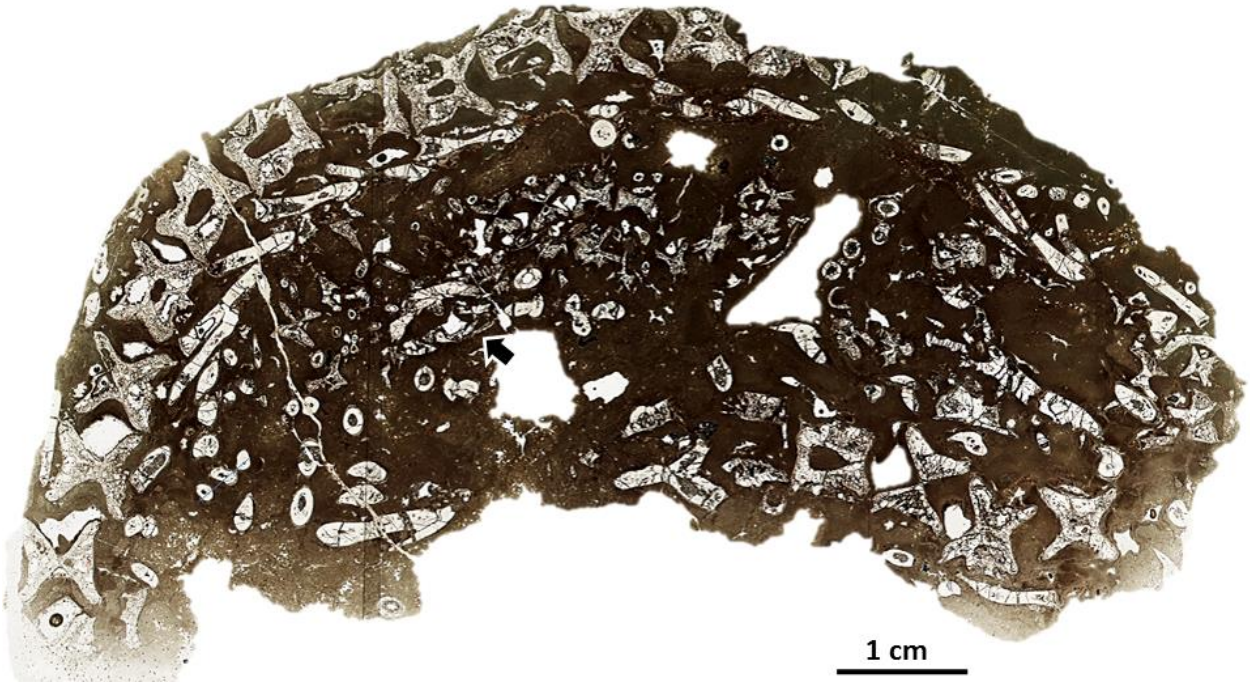

Figure 14 HMNS A51-2 is an adult *Lysorophus* skeleton in a limestone concretion that died during aestivation from the Craddock Bonebed in Baylor Co, Texas. The specimen has been sectioned longitudinally along the mid-sagittal plane. Arrow is pointing to the skull and lower jaw.

4. Archived material

Enough material was recovered to be ultimately accessioned in the collections of the Goldfuss Museum of the University of Bonn (ISPBH), the Museum für Naturkunde Berlin (in return for preparation services), the Texas Memorial Museum (Austin, Texas), and the Archer County Museum owned by county historians Jack and Marie Loftin. In addition to the current study, this material will form the basis for current and future work on taphonomy, histology, and evolution of lower Permian reptiles and amphibians, as well as paleobotany. We were thus very fortunate to have "partially circumvented" the difficult problem of obtaining permission to sample material already accessioned in scientific collections.

5. Morphometric data collection

At the conclusion of each field season time was set aside to visit vertebrate Permian collections and institutions in the United States including, the Dallas Museum of Natural History (DMNH) Museum of Comparative Zoology of Harvard University (MCZ), the Chicago Field Museum (FMNH), the Texas Memorial Museum (TMM) in Austin, TX, the Sam Noble Museum of Natural History at the University of Oklahoma in Norman, OK (OMNH), the American Museum of Natural History in New York City (AMNH), the University of Michigan (UMMP), and the Peabody Museum at Yale (YPM). All of the pelycosaur long bones (humerus, femur, radius, ulna, tibia, fibula) in each collection were measured for maximum bone length and minimal diaphysis circumference (Appendix 3). The area measured for minimal diaphysis also corresponds to the area of consumptive sampling (see below). Morphometric data was collected first before any destructive analysis was performed.

6. Consumptive sampling

Consumptive sampling of specimens was permitted from only a few of the more cooperative institutions (MCZ, OMNH, and TMM) and private collectors, including the initial collection at the University of Bonn started by Martin Sander. These have also been included here with the material that has thus been sectioned from the BCBB and RSC digs (Appendix 4). Bones were taken out on loan for consumptive sampling in the Institute of Paleontology, University of Bonn under the guidance of Prof. Sander and Mr. Olaf Dülfer, an experienced histology technician and magician of bone reconstruction.

Samples were taken from the long bones of the legs (humerus, femur, radius, ulna, tibia, fibula) at the minimal diaphysis (see above)where the bone tissue experiences the most periosteal bone apposition, and the resulting thin-sections were studied under a modern polarizing light microscope Leica DMLP with photographic facilities. Preferably bones are sectioned transversely across the mid shaft to obtain a histologic section (Chinsamy-Turan 2005), but less destructive method using a core drill can also be applied (Sander 2000, Stein and Sander 2009). For specific details on the process used to make these thin-sections please refer to the method sections of chapters 3, 4, and 6.

7. Acknowledgements

I would like to thank the following people and institutions who without their help this data and material would not have been available for study: Armand de Ricqlès, Jack & Marie Loftin, Ernst Lundelius, Lynn Murray, Georg Oleschinski, Kayleigh Wiersma, Katja Waskow, Rebecca Hofmann, Mark Nowak, Jessica Mitchell, Olaf Dülfer, Kay Heitplatz, Beate Müehlens, Koen Stein, Herman Winkelhorst, Robert Bakker, Kathy Zoehfeld, Don Brinkman, Farris Jenkins Jr., Jessica Cundiff, Jörg & Nadia Fröbisch, Robert Reisz, Rich Cifelli, Jennifer Larson, Kyle Davies, Doyle & June Riley, Donald & Brenda Shelton, Steven Tudor, Jocelyn Falconnet, R. Allain, Jeff Lindeman, David Williams, Dave Berman, Stuart Sumida, Thomas Martens, Steven Perry, Markus Lambertz, Fredrik Spindler , Jörg Schneider, Adam Huttenlocker, Sarah Werning, Bhart-Anjan Bhuller, William Simpson, Jeffery Wilson, Greg Gunnell, Mark Norell, Carl Mehling , Jack Horner, Carry Woodruff, Michel Laurin, Carol Gee, Winghart Von Königswald, Thomas Martin, John Kocurko. I want to recognize the following people for their specific contributions to this work: Herman Winkelhorst who participated in the 2010 excavation and assisted in the subsequent data collection at the AMNH and CFM. My field partner Koen Stein who participated in all three field excursions and was the field cartographer. Finally, I want to thank Martin Sander for leading the 2010 excavation and helping with data collection and thin-section analysis of material.

8. References

Bakker, R. T., Temple, D. P., Zoehfeld, K. (2013) Origin of mammalian efficiency: precise carcass dismemberment by the Texas finback, *Dimetrodon*, at the richest Early Permian tetrapod bone bed, Craddock Ranch, Arroyo Formation, Baylor County, Texas. Geological Society of America South-Central section Abstracts 45: 68.

Brinkman, D. (1988) Size-independent criteria for estimating relative age in *Ophiacodon* and *Dimetrodon* (Reptilia, Pelycosauria) from the Admiral and Lower Belle Plains formations Of West-central Texas. Journal of Vertebrate Paleontology 8: 172-180.

Case, E. C. 1915. The Permo-Carboniferous redbeds of North America and their vertebrate fauna. The Carnegie Institution of Washington 20: 1‑157.

Hutson, J. M., Burke, C. C., Haynes, G. (2013) Osteophagia and bone modifications by giraffe and other large ungulates. Journal of Archaeological Science 40: 4139-4149.

Olson, E. C., Mead, J. G. (1982) The Vale Formation (Lower Permian): its vertebrates and paleoecology. Texas Memorial Museum, University of Texas at Austin 29: 1-46

Reisz, R. R. (1986) Encyclopedia of paleoherpetology. Part 17A: Pelycosauria. Gustav Fischer Verlag, Stuttgart, 102 p.

Romer, A. S., Price, L. I. 1940. Review of the Pelycosaurs. Geological Society of America Special Papers 28: 1-538.

Sander, P. M. (1987) Taphonomy of the Lower Permian Geraldine Bonebed in Archer County, Texas. Palaeogeography, Palaeoclimatology, Palaeoecology 61: 221-236.

Sander, P. M. (1989) Early Permian depositional environments and pond bonebeds in central Archer County, Texas. Palaeogeography, Palaeoclimatology, Palaeoecology 69: 1-21.

Sander, P. M., Gee, C. (1990) Fossil charcoal: Techniques and applications. Review of Paleobotany and Palynology 63: 269-279.

Shelton, C. D. (2013) A new method to determine volume of bromalites: morphometrics of Lower Permian (Archer City Formation) heteropolar bromalites. Swiss Journal of Palaeontology 132: 221-238.

Chapter 3: Long bone histology indicates sympatric species of *Dimetrodon* (Lower Permian, Sphenacodontidae)

Published as: Shelton, C. D., Sander, P. M., Stein, K. and Winkelhorst, H. 2013 (for 2012). Long bone histology indicates sympatric species of Dimetrodon (Lower Permian, Sphenacodontidae). *Earth and Environmental Science Transactions of the Royal Society of Edinburgh.* 103:217-236.

ABSTRACT: ABSTRACT: The Briar Creek Bonebed (Artinskian, Nocona Formation) in Archer County is one of the richest sources of *Dimetrodon* bones in the Lower Permian of Texas, USA. Based on size, a small (*D. natalis*), an intermediate (*D. booneorum*), and a large species (*D. limbatus*) have been described from this locality. It has been proposed that these traditionally recognised species represent an ontogenetic series of only one species. However, the ontogenetic series hypothesis is inconsistent with the late ontogenetic state of the small bones, as suggested by their osteology and degree of ossification. Histological analysis of newly excavated material from the Briar Creek Bonebed has resolved some of the discretion between these two competing hypothesis, confirming the coexistence of a small (*D. natalis*) with at least one larger *Dimetrodon* species. An external fundamental system is present in the largest sampled long bones identified as *D. natalis*. The histology *of D. natalis* postcrania is described as incipient fibro-lamellar bone. This tissue is a combination of parallel-fibred and woven-fibred bone that is highly vascularised by incipient primary osteons. The species status of *D. booneorum* and *D. limbatus* remain unresolved.

KEY WORDS: Artinskian, Nocona Formation, Pelycosauria, *Secodontosaurus*

1. Introduction

Dimetrodon Cope, 1878, the dominant terrestrial predator of its time, has been studied for over a century resulting in the current recognition of twelve species (Romer & Price 1940; 1986; Berman *et al*. 2001). These iconic fossils are easily identified by the elongated vertebral spinous processes (or neural spines) forming a dorsal sail that ran the length of the vertebral column.

Although *Dimetrodon* remains and footprints have been discovered in Europe, specifically in Germany (Berman *et al.* 2001 & 2004), virtually all fossil *Dimetrodon* material comes from North America, including Utah, Arizona, New Mexico, Oklahoma, and primarily Texas (Romer & Price 1940; Berman 1977, 1993; Vaughn 1966, 1969; Reisz 1986;). *Dimetrodon* species varied in size (from an estimated 14 to 250 kg, Romer & Price 1940; Bakker 1975; Berman *et al.* 2001) and stratigraphic age (Romer & Price 1940; Reisz 1986). The most diverse *Dimetrodon* faunas are those from the Lower Permian redbeds of Texas, particularly of the Wichita Group (Romer & Price 1940; Reisz 1986) where three species are hypothesised to have co-occurred. This apparently high diversity has led to the hypothesis that at least some of the species may represent ontogenetic stages of a single species (Bakker 1982; Rushforth & Small 2003; Sumida *et al.* 2005), a hypothesis which is partly tested here for the first time using palaeohistological and skeletochronological methods.

Dimetrodon is a member of the basal synapsid clade Sphenacodontidae, which has traditionally been included within the 'Pelycosauria', now known to be paraphyletic (Kemp 2007). We continue to use the term 'pelycosaur' instead of the cumbersome 'non-therapsid synapsid', but in an informal sense.

1.1 Wichita Group Dimetrodon species diversity

The earliest bonebeds of rich vertebrate fauna come from the continental formations of the Wichita Group. In this work, we focus on the *Dimetrodon* species of the basal most Nocona Formation which is a consolidation of the Coleman Junction and Admiral formations as used by Romer (1974). Stratigraphy follows that of Hentz (1988).

Three species of *Dimetrodon* have been described from a number of localities within the Nocona Formation, including two mass assemblages: the Geraldine and Briar Creek bonebeds (Romer & Price 1940; Reisz 1986; Sander 1987). Both of these bonebeds have produced *Dimetrodon natalis* Romer, 1936. This species is the smallest known *Dimetrodon* species from North America, having an estimated maximum body mass of 28 kg and a total

length of 170 cm (Romer & Price 1940; Bakker 1975; Reisz 1986; Berman *et al*. 2001). *Dimetrodon booneorum* Romer, 1937 is "intermediate" in size (218 cm total length) between *D. natalis* and *Dimetrodon limbatus* Romer & Price, 1940 (270 cm total length), but it is osteologically more similar to *D. booneorum*. Stratigraphically, *D. natalis* is restricted to the Nocona Formation, whereas *D. booneorum* and *D. limbatus* also occur in the overlying Petrolia Formation (Fig. 1).

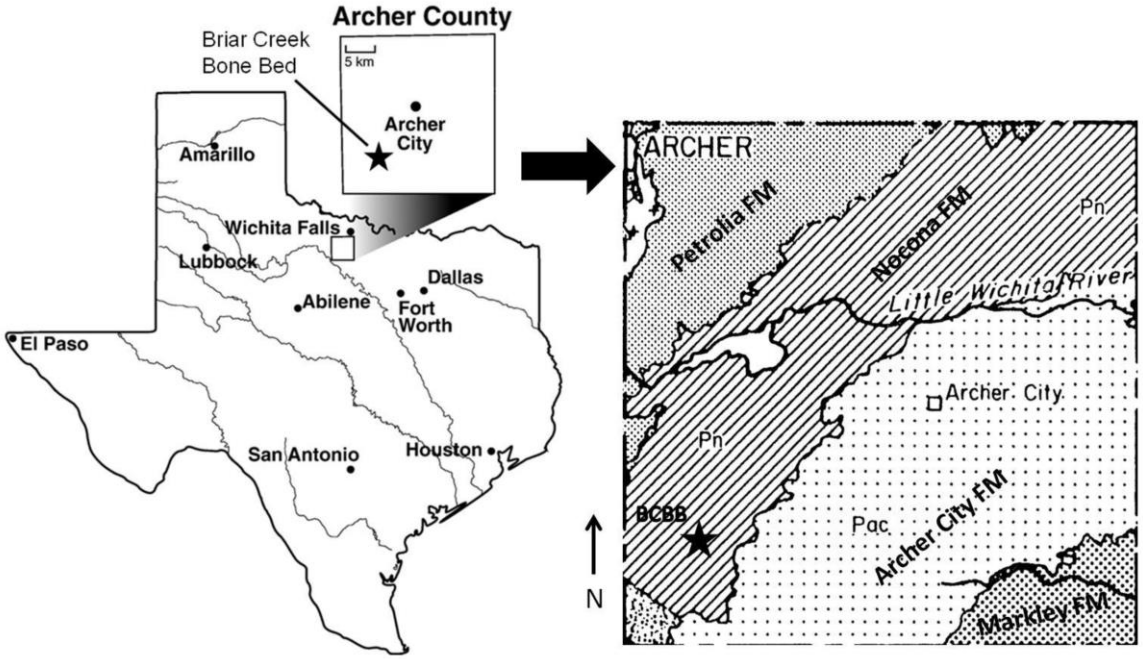

Figure 1 Location and geologic map of Archer County, Texas, USA. This map shows the location of the Briar Creek Bonebed within the Nocona Formation, coordinates are available on request at the JJ Pickle Laboratory at the University of Austin, Austin, TX (modified from Hentz 1988; Labandeira & Allen 2007).

Dimetrodon species were traditionally differentiated on the basis of size, stratigraphic distribution, and geographic range (Reisz 1986). Romer & Price (1940) thought that the taxa of this group followed two parallel lines of development. Those that were large, slow, and clumsy, and those that were smaller, faster, and more agile. They separated *Dimetrodon* species into two morphological categories based on skull shape, relative length of the vertebral column, and the length of distal segments in the limbs. Based on their criteria, *D. booneorum* and *D. limbatus* were placed in the same category because they are osteologically similar and differ only in size. *D. natalis* was placed in the other category for having a shorter skull, smaller temporal fenestra, a less convex maxillary margin, elongated cervical region in the vertebral column, and proportionally longer lower limb segments in comparison to the

Dimetrodon species assigned to the other category (Romer & Price 1940; Reisz 1986). Except for size difference, postcrania of *D. natalis* are almost indistinguishable from *D. booneorum* and *D. limbatus*.

Alternatively, it has been proposed that these traditionally recognized species represent an ontogenetic series of a single species (Bakker 1982). Bakker based this hypothesis on the observation (Romer & Price 1940; Reisz 1986) that many of the recognized *Dimetrodon* species are similar osteologically to a larger or smaller contemporaneous species, as is the case for *D. limbatus* and *D. booneorum* (Romer & Price 1940; Reisz 1986). *Dimetrodon loomisi* Romer, 1937 and *Dimetrodon gigahomogenes* Case, 1907 also are similar in this regard (Romer & Price 1940; Reisz 1986). Romer & Price (1940) also point out similarities between *D. limbatus* and *Dimetrodon milleri* Romer 1937, however they are not currently considered contemporaneous.

Bakker's (1982) ontogenetic series hypothesis, coupled with environmental interpretations of the localities the species were derived from, led him to suggest that adults and juveniles of *Dimetrodon* preferred different habitats. However, Brinkman (1988) noted that the ontogenetic series hypothesis is inconsistent with the late ontogenetic state of some of the small bones as evident in their external morphology.

Here we test the competing ontogenetic series (single species) hypothesis and the multiple species hypothesis for a single locality that has produced several nominal species, the classical Briar Creek Bonebed (BCBB) in the upper Nocona Formation of western Archer County, Texas. By examining *Dimetrodon* long bone histology across elements of increasing size, we can assess whether the largest specimens are also the oldest histologically (suggesting a single species), or whether an older histological profile occurs in both large and small individuals (suggesting more than one taxon). This approach is similar to recent histological studies of dinosaurs (Sander 2000; Klein & Sander 2008; Horner & Goodwin 2009, 2011; Stein *et al.* 2010).

1.2 Previous work on Dimetrodon long bone histology

Against the background of the comprehensive taxon sampling of particularly Triassic non-mammalian therapsids, it is striking how little we know about the histology of 'pelycosaurs.' The only recent works are the studies on the elongate neural spines of edaphosaurids and sphenacodontids by Huttenlocker and co-workers (Huttenlocker *et al.* 2006, 2010, 2011; Huttenlocker & Rega 2011; Rega *et al.* 2012). *Dimetrodon* limb bone

histology has remained virtually unstudied since the early work of Donald H. Enlow (Enlow & Brown 1956, 1957, 1958; Enlow 1969) and Armand de Ricqlès (de Ricqlès 1974a, b, 1976a, b, 1978). Huttenlocker and Rega (2011) have provided a synthesis of these early works. Since these preliminary studies, the scientific community has accepted the view that 'pelycosaurs' were in general slow-growing poikilothermic animals with cyclic growth patterns that were highly sensitive to environmental variation, and, by extension, had ectothermic physiology with low basal metabolic rates (Bakker 1975; Florides *et al*. 2001).

1.3 The Briar Creek Bonebed (BCBB)

The Briar Creek Bonebed (BCBB) (Case 1915, spelled "Brier Creek" by him) in the Artinskian, Nocona Formation of Archer County, Texas, USA, (Fig. 1) is one of the major Lower Permian bonebeds, and contains a large volume of material and variety of taxa (Case 1915). When E. C. Case, of the University of Michigan, originally found the BCBB in 1912, he hypothesised that this area represented a pool or swamp that functioned as a "macerating tank" in that some of the bones appear to have rotted before preservation. He hypothesised that carcasses may have been washed in by a stream or river, resulting in an accumulation of unsorted and disarticulated bones, pertaining to reptiles and amphibians as well as some fish remains (coprolites, teeth and cartilage). A. S. Romer, of Harvard University, began work at the BCBB in 1927, and he was the last to do an organised excavation at the site in 1972 (unpublished field notes), one year before his death. The bone-bearing layer is approximately 30 cm thick, and for nearly a century has produced large quantities of material held in the collections of the AMNH, FMNH, KUVP, MCZ, USNM, OMNH, UMMP, and TMM (explanation of institutional abbreviations is given below) (Romer & Price 1940, Reisz 1986).

The published literature (Romer & Price 1940, Reisz 1986) and records from museum collections suggest the presence of four *Dimetrodon* species (*D. milleri*, *D. natalis*, *D. booneorum*, and *D. limbatus*) in the BCBB. It should be noted that *D. milleri* cannot be substantiated as occurring in the upper Wichita Group until diagnostic skull material is found.

It should be noted that remains of another sphenacodontid, *Secodontosaurus obtusidens* Romer, 1936 (body size identical to *D. booneorum* and postcrania morphologically similar to *Dimetrodon* in general), have been rarely recovered from the BCBB as well (Romer & Price 1940). This means that intermediate-sized isolated sphenocodontid long bones from this locality may either pertain to *D. booneorum* or, less likely, to *Secodontosaurus*. However, species validation of the small *D. natalis* and large *D. limbatus* will not be obscured given the

known size range of *Secodontosaurus* (Romer & Price 1940). To test Bakker's (1982) ontogenetic series hypothesis, we collected a representative sample of disarticulated sphenacodontid limb bones (humeri and femora) of different size for histologic sectioning from the BCBB for this study.

Institutional abbreviations: AMNH, American Museum of Natural History, New York City, NY, USA; FMNH, The Field Museum, Chicago, IL, USA; KUVP, University of Kansas Museum of Natural History, Lawrence, KS, USA; MCZ, Museum of Comparative Zoology, Harvard University, Cambridge, MA, USA; IPBSH, Paleohistology collection, Steinmann Institute for Geology, Mineralogy, and Palaeontology, University of Bonn, Bonn, Germany; OMNH, Sam Noble Museum of Oklahoma Natural History, University of Oklahoma, Norman, OK, USA; UMMP, Museum of Paleontology, University of Michigan, Ann Arbor, MI, USA; USNM, United Stated National Museum, Washington D. C.; TMM, Texas Memorial Museum Vertebrate Paleontology Laboratory, Austin, TX, USA.

2. Materials and Methods

2.1 Material

Vertebrate postcranial material was excavated from the BCBB in 2010 and 2011 for the sole purpose of histological analysis. While we recovered numerous isolated bones of the zeugopodium as well, we base our study on two growth series made up of complete and partial sphencadontid humeri and femora (Figs. 2, 3). We identified this material as *Dimetrodon* sp. by comparison to identified specimens in museum collections and the literature, primarily Romer & Price (1940) and Reisz (1986). However, we cannot exclude the possibility that the material includes *Secodontosaurus* bones. Thirteen long bones were sectioned histologically (Figs. 2, 3; Table 1). The eight humeri studied ranged in size from 58 mm to 120 mm. Humeral epiphyses were damaged and incomplete. The five femora studied ranged in size from 98 mm to 137 mm. Two femora were crushed dorsoventrally.

Femur length was used as a proxy for body size (Carrano 2006). We constrained this by assuming the largest histologically sample sphenacodontid femur (IPBSH-2) represented maximum size (100%). We calculated the humerus/femur ratio (1.14) from combined measurements of three *D. booneorum* and seven *D. limbatus* specimens because there is insufficient articulated or associated *D. natalis* or *Secodontosaurus* material available from which to calculate a proper ratio(Table 2). This data was obtained from the literature (Romer & Price 1940) and combined with measurements taken from specimens of different localities

in the collections of the FMNH, MCZ, and OMNH (Appendix 5). The converted humerus lengths were taken as a percentage of maximum size based on the longest femur (IPBSH-2) (Fig. 3, Table 1). Humeral size ranged from 48 % to 100 % maximum size (Fig. 2, Table 1), a greater relative size range compared to the femora (72% to 100% maximum size) (Fig. 3, Table 1).

Table 2 Specimens used to calculate the femur to humerus ratio 1.14.

Specimen ID	Femur Length (mm)	Humerus Length (mm)	Ratio	*Dimetrodon*	Notes
MCZ-3176	100	99	1·01	*D. booneorum*	Measured by C. Shelton
MCZ-3176	100	90	1·11	*D. booneorum*	Measured by C. Shelton
MCZ-3176	100	95	1·05	*D. booneorum*	Measured by C. Shelton
MCZ-1123	205	195	1·05	*D. limbatus*	Measured by C. Shelton
MCZ-1123	205	160	1·28	*D. limbatus*	Measured by C. Shelton
UMMP-UC 1	223	174	1·28	*D. limbatus*	Measured by C. Shelton
OMNH Exhibits	225	200	1·13	*D. limbatus*	Measured by C. Shelton (Cast of original in Hayashibara Museum of Natural Science, Japan)
MCZ-1123	205	170	1·21	*D. limbatus*	Romer & Price 1940
MCZ-1347	190	168	1·13	*D. limbatus*	Romer & Price 1940
USNM-6723	190	164	1·16	*D. limbatus*	Romer & Price 1940

Brinkman's (1988) ontogenetic stages were not applied to the long bones because necessary landmarks were damaged or missing. Therefore, we used arbitrary size classes to organise and describe the specimens. Small bones are considered to be those at 55% maximum size or less, intermediate bones are those between 56% and 80%, and large bones are 81% or higher. The small humeri have a rough outer surface and unossified ends. The intermediate to larger humeri have a smooth surface with parallel micro-striations. All femora have a smooth outer surface. These size classes will be combined with the morphological information available to us and the histological data we find in an attempt to ontogenetically classify the long bones as juvenile, subadult or adult. All fossil material is reposited at the Steinmann Institute for Geology, Mineralogy, and Palaeontology, University of Bonn, Bonn, Germany.

Morphometric data (see below) was obtained from specimens excavated during the 2010 and 2011 campaigns and from BCBB material housed in the collections of the FMNH, MCZ, and UMMP (SI 2: BCBB material attributed to *D. milleri* has been stated here as *Dimetrodon* sp.).

Table 1 Physical dimensions and growth mark count of the sectioned small sphenacodontid long bones. Femur length for the humeri was calculated using the average length ratio (1.14)

of articulated and associated *D. limbatus* humeri and femora material from various museum collections Appendix 5. Abbreviations: C, circumference; EFS, external fundamental system; L, length; GC, growth cycles; LAG, line of arrested growth

Specimen Number	Bone	Length (mm)	Circumference (mm)	L/C ratio	Femur Length (mm)	% Maximum Size	Visible Growth Cycles	Visible LAGs	Maximally Missing Cycles
IPBSH-13	Left Humerus	58	28	2.1	66	48	1	1	2
IPBSH-25	Right Humerus	58	27	2.2	66	48	2	1	1
IPBSH-11	Left Humerus	63	29	2.2	72	53	2	1	3
IPBSH-14	Right Humerus	70	33	2.1	80	58	0	0	0
IPBSH-22	Left Humerus	81	42	1.9	92	67	6	5	6
IPBSH-5	Right Humerus	82	40	1.9	94	68	0	0	0
IPBSH-33	Right Humerus	114	54	2.1	130	94	3	1	6
IPBSH-4	Right Humerus	120	42	2.9	137	100	5	4 + EFS	6
IPBSH-19	Right Femur	98	38	2.6	/	72	4	4	4
IPBSH-6	Left Femur	107	50	2.1	/	78	5	4	5
IPBSH-31	Left Femur	108	45	2.4	/	79	4	3	6
IPBSH-29	Left Femur	131	45	2.9	/	96	5	4 + EFS	6
IPBSH-2	Right Femur	137	52	2.6	/	100	6	5 + EFS	11

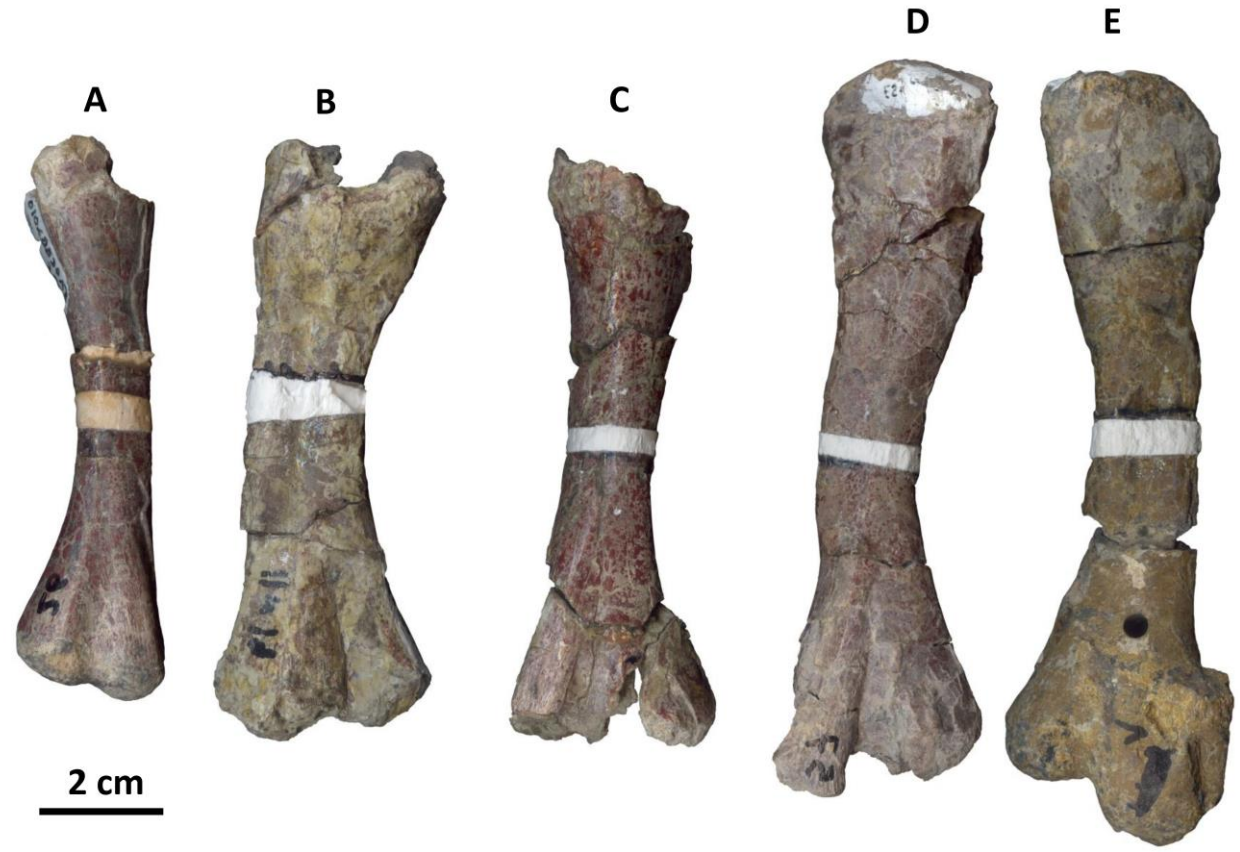

Figure 3 Ontogenetic series of *Dimetrodon natalis* femora**.** All femora were sectioned transversely at the mid-diaphysis. The sampled location was reconstructed with white plaster. Femora are arranged by increasing size: A) IPBSH-19 (72% maximum size); B) IPBSH-6 (78% maximum size); C) IPBSH-31 (79% maximum size); D) SABCBB2010-57 (96% maximum size); E) IPBSH-2 (100% maximum size). Dorsal side is facing up.

2.2. Methods

2.2.1. Morphometrics.

Morphometric analysis commonly needs to precede any histological work to procure the raw data before the bone is damaged in anyway (for example, Sander & Klein 2005; Sander *et al.* 2006; Klein & Sander 2007). In our case, simple morphometrics, i.e., plots of bone length vs. bone circumference, served two purposes. First, we wanted to detect size differences between the humeri and femora of BCBB sphenacodontid species (*Dimetrodon* spp. and *Secodontosaurus*) collected by us and earlier workers. Second, we wanted to detect possible species-specific clusters of length/circumference ratios. Thus, total length and minimal diaphysis circumference was recorded for each bone using standard analytical callipers and a metric measuring tape. Length was taken as the total distance between the termination of the proximal and distal ends. Circumference was taken at the mid-diaphysis (see Fig. 4).

Microsoft Excel 2010 was used to construct a scatter plot to understand how the mid-diaphysis circumference relates to the length of the long bone (Fig. 5). This relationship is of interests because, especially in femora, it is assumed that long bone appositional growth is isometric (Bonnan 2004; Lehman and Woodward 2008; Kilbourne and Makovicky 2010; Sander *et al*. 2011). As a long bone increases in length it also increases in shaft circumference, and if this relationship is linear, cortical thickness increase can also be used as a proxy for (increasing) body size. This permits construction of growth curves based on percentage of maximum estimated cortical thickness (e.g., Lehman & Woodward 2008). Only BCBB sphenacodontid (*Dimetrodon* spp. and *Secodontosaurus*) humeri and femora from the FMNH, MCZ, and UMMP collections were measured and included with the data from the bones we excavated Appendix 5. 110 humeri and 131 femora were measured (Fig. 5). This data was not log transformed.

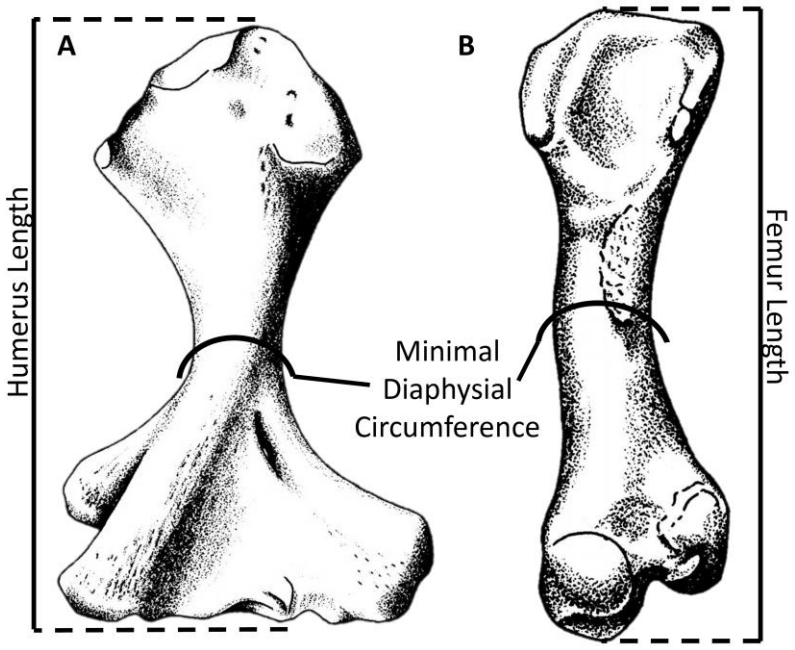

Figure 4 Illustration of a A) sphenacodontid humerus and a B) sphenacodontid femur with indication of how and where total length and the minimal diaphysis circumference were taken. The mid-diaphysis was sectioned in order to see the best preserved growth record. Note that the bones shown here are *D. limbatus* (modified from Reisz 1986).

2.2.2. Histological sampling, study, and imaging.

Silicon molds (Provil Novo putty regular) of all long bone diaphyseal areas were created before sectioning. The damaged areas are cast in plaster for purposes of reconstructing and preserving the morphological and anatomical features of the original material. Next, each long bone mid-diaphysis was encased in a green epoxy resin (Technovit Universalliquid and Technovit 5071 Pulver) before being sectioned transversely with a rock saw, equipped with a standard diamond tipped blade, to prevent splintering of the cortex. The mid-diaphysis of the long bone is the region of the bone where the most complete record of growth is preserved. It also corresponds to the area of the smallest shaft circumference (Francillon-Vieillot *et al.* 1990; Currey 2002). Humeral sections bisect the attachment of the coracobrachialis muscle, and the femoral sections bisect the area of the adductor muscle attachment (Romer & Price 1940; Romer 1969). After sawing, sections were ground to approximately 35 to 50 μm by hand on a glass plate with wet grit (600 and 800) and sealed with a cover slip using UV activated resin (Verifix LV 740). Sections were described, measured, and photographed under nonpolarised and polarised light using a Leica DM2500LP compound microscope and Leica DFC420 digital camera, both manufactured in Germany. Thin sections were imaged with an

EPSON V750 (manufactured in Japan) high-resolution transmitted light scanner in normal light (Figs 6, 7). Digital images were processed using the 2007 edition of Image Access Easy Lab7 software. Bone histological terminology follows Francillon-Vieillot *et al*. (1990).

High-resolution images of the transverse sections are digitally reposited online for scholarly use at MorphoBank (http://MorphoBank.org). The Project number is P845. All slides are reposited at the Steinmann Institute for Geology, Mineralogy, and Palaeontology, University of Bonn, Bonn, Germany.

2.2.3 Analysis of growth trajectory.

Growth marks within long bones can be used to establish a growth curve (Bybee *et al*. 2006; Klein & Sander 2007; Cooper *et al*. 2008; Lee & Werning 2008; Lehman & Woodward 2008; Sander *et al.* 2011) for studying aspects of life history. Growth marks develop annually (Kohler *et al.* 2012 , Castanet *et al.* 2004) and include lines of arrested growth (LAGs) and whole growth cycles divided into a fast growing zone and a slow growing annulus (when the latter is present at all). As an animal nears skeletal maturity, bone growth rates decrease. As a result of this slowed growth, the periosteum produces an external fundamental system (EFS) on the outermost circumference of the bone. The EFS is characterised by numerous rest lines laid down consecutively with very little space in between, and is composed of nearly avascular parallel-fibred or lamellar bone. Also, osteocyte lacunae are extremely flattened and oriented parallel to the bone surface. The amount of time represented by the EFS is often difficult to estimate (Erickson *et al*. 2004). As bones grow, expansion and remodelling of the medullary cavity destroys earlier growth marks, which must be determined to establish a reliable age. The missing growth cycles can be estimated by use of retrocalculation (e.g., Bybee *et al*. 2006; Klein & Sander 2007).

A growth trajectory for the sectioned sphenacodontid humeri and femora (Table 1) using Microsoft Excel 2010. We used bone length (Fig. 4) as proxy for body size and the number of growth cycles in each bone to determine the age of the individual at time of death (Fig. 10). We first counted each LAG visible in the cortex under regular transmitted light, each of which represents one year of growth. In some cases, a LAG was not visible, and we used the presence of corresponding zone and annulus (visible under crossed plane-polarised light) to infer one year. We report long bone lengths and age estimates in Table 1. The EFS represents an unknown amount of time (Erickson *et al.* 2004). They were noted (Table 1) if observed in the cortex, but were not used to calculate the growth trajectory (Fig. 10).

The number of missing cycles (Table 1) for each long bone was estimated by utilizing two methods of retrocalculation. The first method used was that of Klein & Sander (2007): the distance between the centre of the medullary cavity and the first visible LAG was measured and divided by the greatest distance between any two adjacent LAGs. This method will be referred to in the results section as RM1. It was used was applied to all humeri and to femora specimens that have little to no crushing (IPBSH-19, IPBSH-31, IPBSH-2) (Figs. 3, 7).

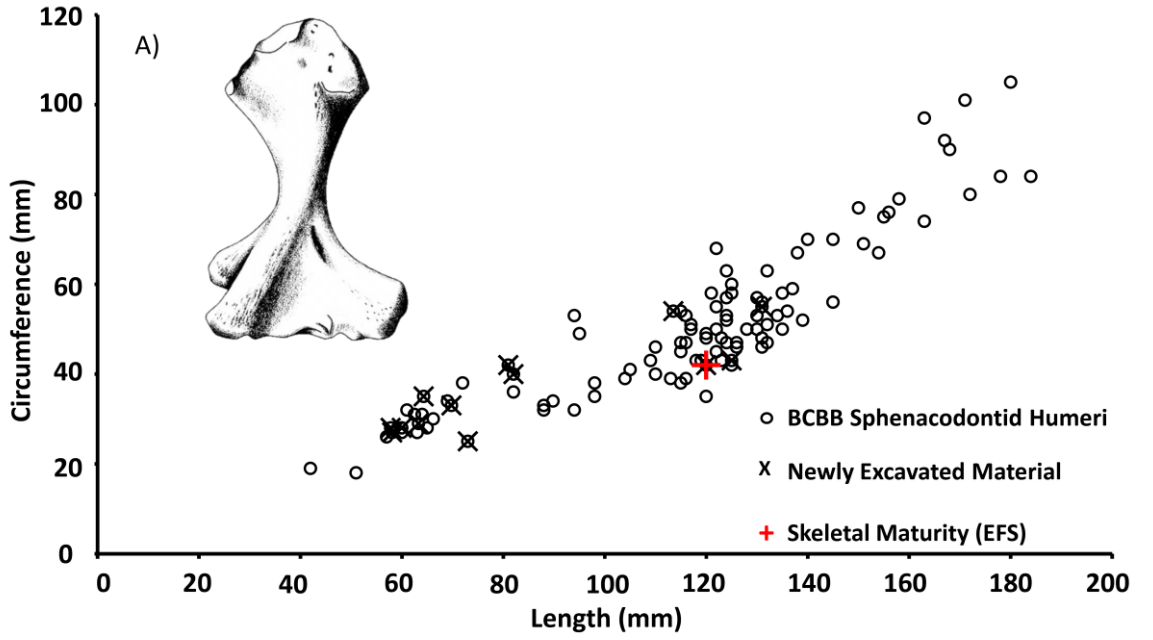

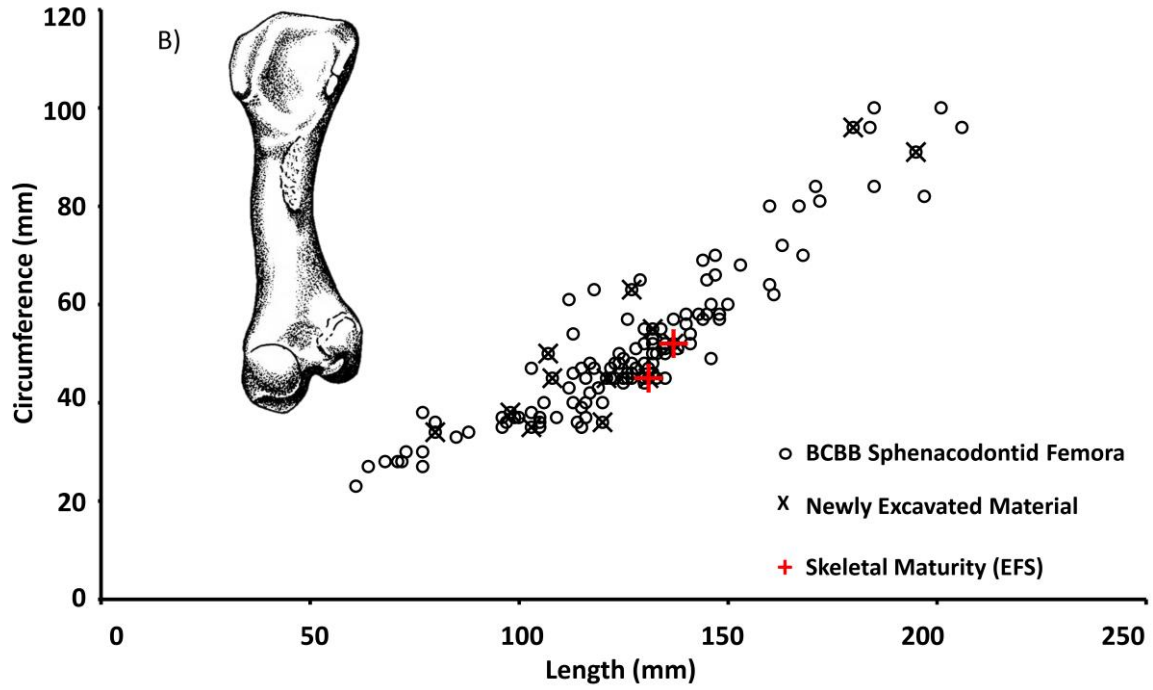

Figure 5 Minimal diaphysis circumference compared to length in the humerus and femur of Briar Creek Bonebed sphenacodontid species (*Dimetrodon* spp. and *Secodontosaurus*) A) humeri and B) femora. Sample is from historic museum collections (FMNH, MCZ, UMMP) and from new material excavated during the 2010 and 2011 field seasons (Appendix 5). Sectioned *Dimetrodon natalis* long bones that possess an EFS have been marked with a cross. No distinction was made between the different *Dimetrodon* species or *Secodontosaurus*.

The same retrocalculation method was used on femora that are dorsoventrally crushed (IPBSH-6 and IPBSH-29) (Figs 3, 7), but with a modification to first estimate the distance from the centre of the medullary cavity to the first LAG. Given the circumference (**c**) of the outer cortex (Table 1), diameter (**d**) was first calculated (**$d = c / \pi$**). The average thickness of the cortical bone (**ct**) was calculated, doubled, and subtracted from the diameter (**d**). The remaining number is the estimated diameter of the medullary cavity (**dmc**), (**dmc= d-(ct x 2)**). The **dmc** was then divided in half. This gives an approximation of the distance from the centre of the medullary cavity to its edge (also known as the approximated radius of the medullary cavity) (**rmc**) had the bone not been crushed (**rmc= dmc ÷ 2**). The distance from the edge of the medullary cavity to the first LAG was measured directly from the slide. This distance, when added to the approximated radius of the medullary cavity (rmc), gives you the best estimated measurement for the distance from the centre of the medullary cavity to the first LAG. As in the first method, final calculation is preceded by dividing this number by the greatest distance between any two adjacent LAGs. This method will be referred to in the results section as RM2.

In order to fully test our null hypothesis, an additional data point was added to the growth trajectory of the sectioned sphenacodontid femora. We assumed that the femur reached a total length of 60 mm within the first year of growth after hatching, as this is the smallest femur we have measured, but not sectioned, from the collections Appendix 5.

3. Results

3.1. Morphometrics

The scatter plots of the raw data of the minimal diaphysis circumference as a function of length of the humeri and femora, have two major results. First, all BCBB sphenacodontid material follows a similar growth trajectory (Fig. 5). This means the long bones are lengthening at a similar rate to the apposition of cortical bone in the diaphysis. Also, the

patterns produced by the scatter plots could be interpreted as resulting from the presence of a single species at the BCBB. Note, however, that this pattern does not exclude the presence of more than one species as multiple species could also exhibit similar growth trajectories. Small sized sphenacodontid long bones that possess an EFS have been specifically marked (Fig. 5).

Retrocalculation of missing growth cycles was performed using either RM1 or RM2 (see section 2.2.3) for all sectioned long bones (Table 1). Some of the humeri (IPBSH-14: 70 mm, and IPBSH-5: 82 mm) could not be retrocalculated due to the fact that visible growth cycles or LAGs are not preserved in the cortical bone. Humeri that do have growth marks were analysed using RM1. Humeri IPBSH-13 (58 mm) and IPBSH-25 (58 mm) both came from an individual estimated to have been three years old. Humerus IPBSH-11 (63 mm) was estimated to be five years old. IPBSH-22 (81 mm) was estimated to have belonged to an individual twelve years old. Humerus IPBSH-33 (114 mm) was estimated to have been nine years old. Finally, IPBSH-4 (120 mm) was determined to be approximately eleven years old, with six maximally missing annual growth cycles.

Femora crushed dorsoventrally were analysed using RM2 (IPBSH-6 and IPBSH-29) All other femora were analysed using RM1. Femur IPBSH-19 (98 mm) came from an individual estimated to have been about eight years old. Femora IPBSH-6 (107 mm) and IPBSH-31 (108 mm) were both estimated to have been approximately ten years old at time of death. Femur IPBSH-29 was estimated to be eleven years old. The largest femur IPBSH-2 was determined to be at least seventeen years old, with eleven maximally missing annual growth cycles.

The growth trajectory produced by plotting humerus length against total observed and estimated growth cycles (Fig. 10A; Table 1) revealed no obvious developmental pattern that would indicate the presence of a single species. However, there is an apparent variability in the sampled humeri with regards to size and age. This could be a reflection of developmental plasticity or sexual dimorpism, but most likely it is because some of these humeri are from juveniles or subadults of the larger BCBB sphenacodontids (Dimetrodon spp. and possibly *Secodontosaurus*).

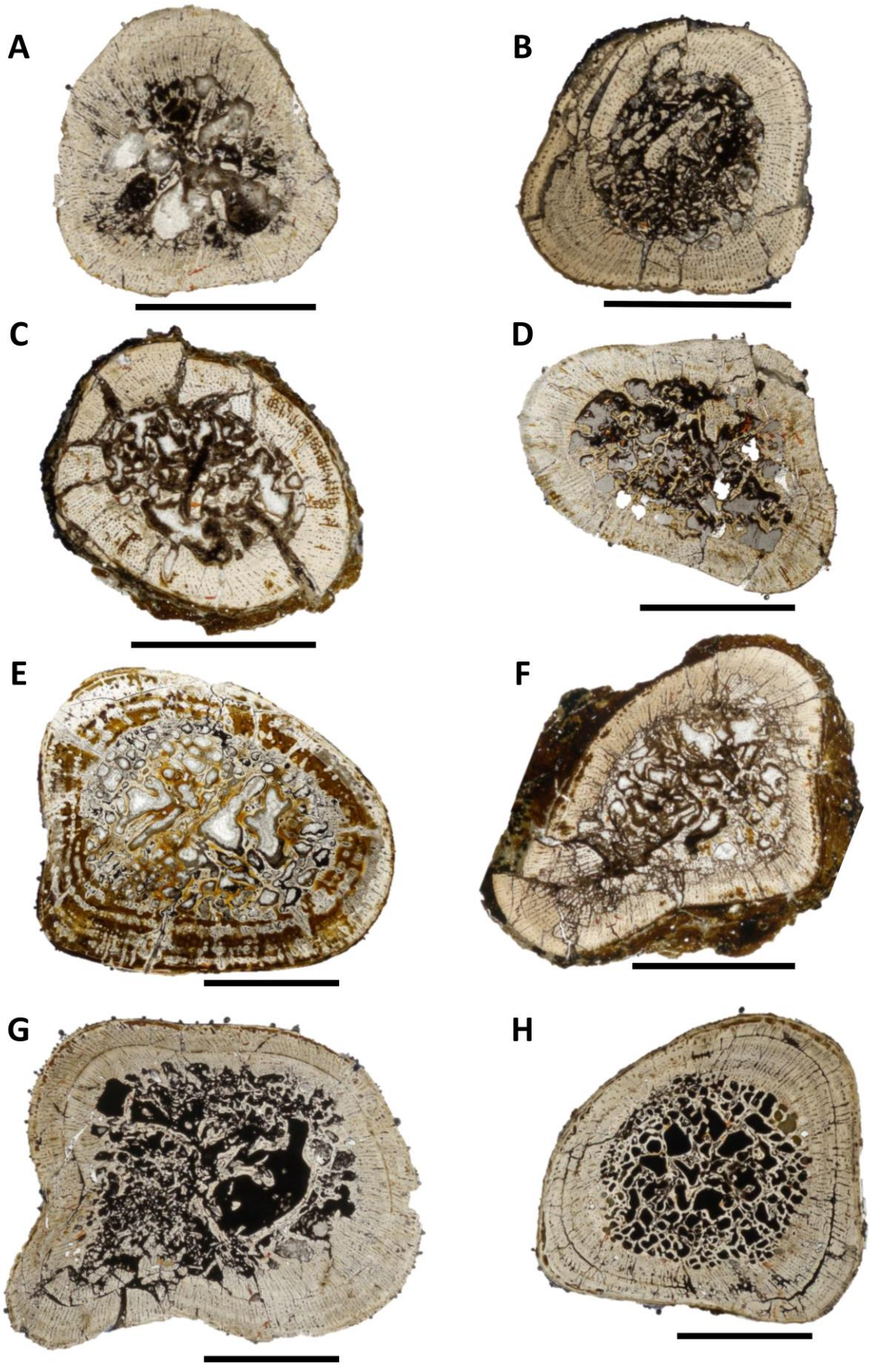
A
B
C
D
E
F
G
H

Figure 6 Ontogenetic series of BCBB *Dimetrodon natalis* humeri sectioned transversely at the mid-diaphysis. Images were captured with a high-resolution transmitted light scanner in normal light. The organisation of the vascular canals (radial and longitudinal) gives the cortical bone a "spoked bicycle wheel" appearance. The smaller humeri have more longitudinal canals, and the larger humeri have more radial canals. However, the density of vascularisation appears to decrease through ontogeny. The medullary cavity of the humerus is occupied by a lattice work of secondary trabecular bone. A) IPBSH-13 (48% maximum size); B) IPBSH-25 (48% maximum size); C) IPBSH-11 (53% maximum size); D) IPBSH-14 (58% maximum size); E) IPBSH-22 (67% maximum size) LAGs are visible in the cortex due to diagenetic staining. F) IPBSH-5 (68% maximum size) G) IPBSH-33 (94% maximum size) LAGs are visible in the cortex. H) IPBSH-4 (100% maximum size) LAGs are visible in the cortex. Letters correspond to the specimens featured in figure 2. Scale is 5 mm.

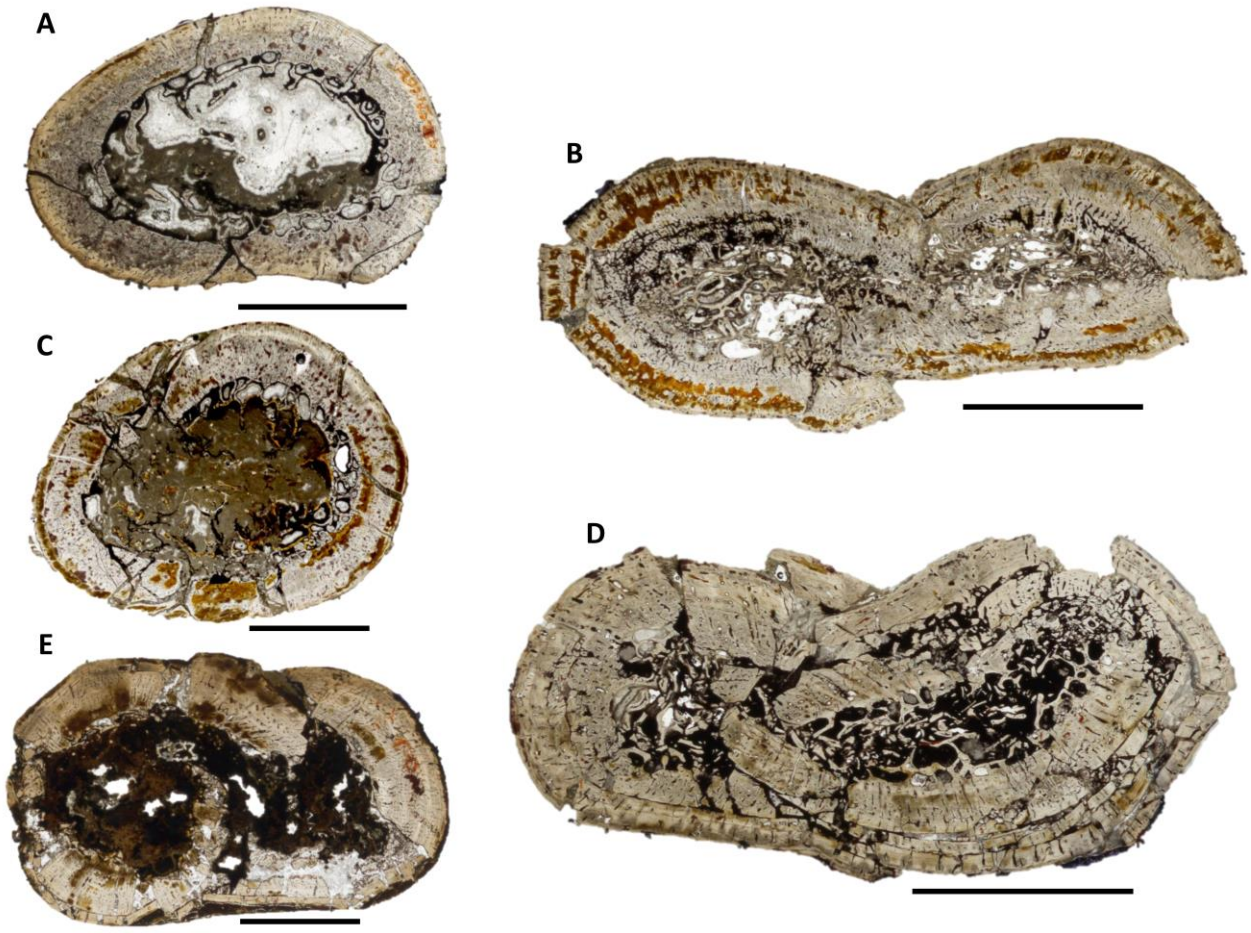

Figure 7 Ontogenetic series of BCBB *Dimetrodon natalis* femora sectioned transversely at the mid-diaphysis circumference. Images were captured with a high-resolution transmitted light scanner in normal light. The cortical bone of the femora is thin. Vascularization is similar to that seen in the humeri. Radial and longitudinal canals are organised such that they

form a “bicycle wheel” pattern. Smaller femora have more longitudinal canals, and the larger femora have more radial canals but with a higher degree of anastomosis. The medullary cavity is open, and secondary trabecular bone is exclusively found on the inner lining. A) IPBSH-19 (72% maximum size); B) IPBSH-6 (78% maximum size) dorsoventrally crushed. LAGs are visible in the outer cortex; C) IPBSH-31 (79% maximum size); D) IPBSH-29 (96% maximum size) dorsoventrally crushed. LAGs are visible in the cortex; E) IPBSH-2 (100% maximum size) slightly dorsoventrally crushed. LAGs and an EFS are visible in the cortex. Letters correspond to the specimens featured in figure 3. Scale is 5 mm.

The growth trajectory produced by plotting femur length against total observed and estimated growth cycles (Fig. 10B; Table 1) reveals growth in these specimens is levelling off. This does add further support to the notion that there is a small *Dimetrodon* species within the sample set.

3.2. Description of sphenacodontid humerus histology

The bone histology of the sampled sphenacodontid humeri (Figs 2, 6) is described below in order of increasing bone length. All histology is described from the mid-diaphysis (Fig. 4).

3.2.1. Small humeri.

Left humerus IPBSH-13 (58 mm, 48% maximum size), right humerus IPBSH-25 (58 mm, 48% maximum size) and left humerus IPBSH-11 (63 mm, 53% maximum size) all have a rough outer bone surface, and unossified epiphyses. IPBSH-25 is slightly crushed dorsoventrally. The cortices are relatively thick and consist of a combination of parallel-fibred and woven-fibred bone (Fig. 8) and are well vascularised by radially arranged longitudinal and radial canals. The radial organisation of the canals gives the cortical bone a “spoked bicycle wheel” appearance (Figs 6, 8). There is no further centripetal deposition of lamellar bone in the vascular canal. It is only surrounding the outer circumference of the canal. Thus, these are incipient primary osteons (Fig. 8). The woven bone is located in between the canals. These regions remain dark at low magnification under polarised light and do not appear to exhibit any birefringence (Fig. 8E). When the stage is rotated 90 degrees under polarised light and a lambda filter, again there appears to be no change in birefringence of the matrix, but a colour change in the osteonal bone can be seen (Fig. 8C, D).

One LAG is visible in IPBSH-13 just below the bone surface making the entire cortical area one growth cycle. IPBSH-25 has two growth cycles and one LAG mid-cortex. IPBSH-11 has two growth cycles and one LAG in the deep cortex near the resorption front. Vascularisation extends from the bone surface to the medullary region. The osteocyte lacuna shape is subangular to elliptical. Within the annuli osteocyte lacunae are flat and oriented parallel to the bone surface. Mineralised Sharpey's fibres (highly birefringent under polarised light) are visible in IPBSH-13 (like those in Fig. 9B) on the anterior side and in IPBSH-25 on the dorsal and ventral sides. They are situated in between the vascular canals and are perpendicular to the bone surface. Sharpey's fibres were not observed in IPBSH-11.

The medullary region, in general, is similar in all three specimens. The cortex is separated from the medullary region by large erosion cavities due to resorption activity, more so in IPBSH-13. Endosteal lamellar bone, in the process of forming secondary trabecular bone (as seen from cross-cutting relationships of cementing lines), is present around the periphery of the medullary cavity but in isolated areas. Secondary endosteal osteons are also visible in the medullary region, in general, is similar in all three specimens. The cortex is separated from the medullary region by large erosion cavities due to resorption activity, more so in IPBSH-13. Endosteal lamellar bone, in the process of forming secondary trabecular bone (as seen from cross-cutting relationships of cementing lines), is present around the periphery of the medullary cavity, but in isolated areas. Secondary endosteal osteons are also visible in the medullary margin (Fig. 8). The medullary cavity is filled with broken trabeculae that have been displaced due to diagenetic crushing of the bone.

3.2.2. Intermediate humeri.

Right humerus IPBSH-14 (70 mm, 58% maximum size), left humerus with broken epiphyses IPBSH-22 (81 mm, 67% maximum size), right humerus IPBSH-5 (82 mm, 68 % maximum size). The outer bone surface of these humeri is smooth with parallel micro-striations. The exception being IPBSH-5, which is slightly crushed dorsoventrally, and the outer surface is covered by a thin layer of iron stone. Only IPBSH-14, slightly crushed on the dorsal side, has unossified epiphyses in combination with a smooth surface and parallel micro-striations visible with the naked eye. The cortex of these humeri is thick, and consists of a combination of parallel-fibred and woven bone vascularised by longitudinal and radial canals. This gives the cortex a bicycle wheel pattern. There is no further centripetal deposition

of lamellar bone in the vascular canals compared to that seen in the smaller humeri. They remain incipient primary osteons (Fig. 8). The thinnest cortical region is on the ventral side.

Growth cycles were not observed in IPBSH-14 or IPBSH-5. IPBSH-22 had six growth cycles, and five LAGs with subcycles (lighter evenly spaced growth marks or rest lines in between adjacent LAGs) that are visible in the darker stained regions under nonpolarised light. All bones lack an external fundamental system (EFS). The vascular canals, of all three specimens, extend from the bone surface to the medullary region, with the exception of IPBSH-22 where vascularisation decreases after the fourth LAG. Osteocyte lacunae are subangular to elliptical and are randomly oriented, except for those in the annuli which are more flat and oriented parallel to the bone surface. A few mineralised Sharpey's fibres were only observed in IPBSH-14 under polarised light in the posterior dorsal region oriented perpendicular to the bone surface and extending to the medullary cavity parallel to the vascular canals. The medullary region of all three specimens contains a network of secondary trabecular bone as seen from cross-cutting relationships of cementing lines. Endosteal bone surrounds most of the medullar cavity. Large erosion cavities and secondary endosteal osteons are present throughout the medullary margin.

3.2.3. Large humeri.

Right humerus with crushed proximal end IPBSH-33 (114 mm, 94 % maximum size). This bone has an outer smooth surface with parallel micro-striations. Right humerus IPBSH-4 (120 mm, 100% maximum size). This bone has a rough surface due to weathering. The cortex of both bones consists of parallel-fibred and woven bone, and is well vascularised by radially arranged longitudinal and radial canals exhibiting the bicycle wheel pattern (Fig. 8B). There is no further centripetal deposition of lamellar bone in the vascular canals, which are incipient primary osteons (Fig. 8). Vascularisation remains constant throughout the cortex but appears to decrease just below the bone surface. A few mineralised Sharpey's fibres were observed in IPBSH-33 under polarised light in the posterior dorsal region oriented perpendicular to the bone surface and extending to the medullary cavity parallel to the vascular canals. Sharpey's fibres were not observed in IPBSH-4.

IPBSH-33 has only three growth cycles (zones and annuli visible under polarised light) but only one LAG is visible under nonpolarised light and correlates with the first annulus. The cortical bone of IPBSH-4 has five growth cycles and four LAGs (Fig. 8B). The beginning of an external fundamental system (EFS) is visible in the outer cortex. The EFS

confirms that this individual had reached skeletal maturity before death. It is unknown how much time is represented by the EFS (Erickson *et al*. 2004), but two rest lines with possible subcycles are visible. After the fourth growth cycle and first LAG, vascularisation decreases except between the dorsal and anterior side. In both humeri osteocyte lacunae are subangular to elliptical in shape. Within the EFS osteocyte lacunae are flattened.

For both humeri, the medullary region is separated from the cortex by lamellar endosteal bone, large erosion cavities, and secondary endosteal osteons. The medullary cavity is occupied by secondary trabecular bone.

3.3. Description of sphenacodontid femur histology

The bone histology of the sampled sphenacodontid femora (Figs 3, 7) is described below in order of increasing overall length (Table 1). All histology is described from a transverse section made at the mid-diaphysis (Fig. 4).

3.3.1. Intermediate femora.

Right femur IPBSH-19 (98 mm, 72% maximum size), left femur IPBSH-6 (107 mm, 78 % maximum size stage), and left femur IPBSH-31 (108 mm, 79 % maximum size) have ossified distal epiphyses, but the proximal ends are damaged. All bones have a smooth outer surface. IPBSH-6 is extremely crushed dorsoventrally. In all specimens the cortex is relatively thin and consists of parallel-fibred and woven-fibred bone and is well vascularised by radially arranged longitudinal canals exhibiting a high degree of anastomosis (Figs 7, 9). Radial canals are present but to a lesser degree than that seen in the humeri. Vascularisation is concentrated in the zones, where the woven bone is present (Fig. 9C, D). There is no further centripetal deposition of lamellar bone in the vascular canals, which remain as incipient primary osteons

(Fig. 9C, D).

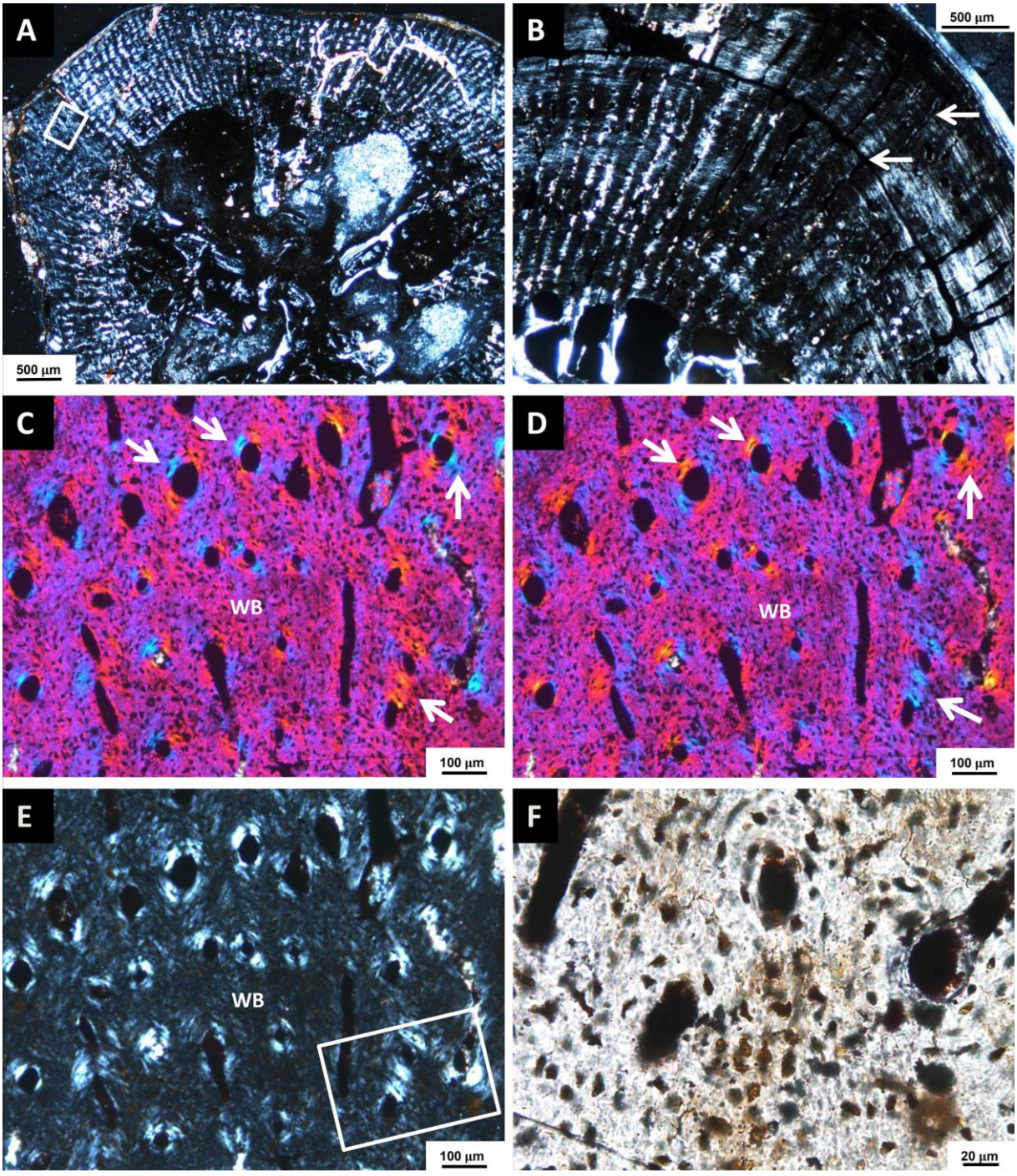

Figure 8 Histology of *Dimetrodon natalis* humeri from the Briar Creek Bonebed. A) Transvers section through the mid-diaphysis of juvenile humerus IPBSH-13 (48% maximum size) under polarised light. Radial and longitudinal canals extend from the medullary cavity to the outer cortex. Notice the "spoked bicycle wheel" pattern formed by the arrangement of the vascular canals. Incipient primary osteons are visible throughout the cortex. Large erosion cavities can be seen in the medullary region. Secondary trabecular bone is present in the medullary cavity. B) Transverse section through the mid-diaphysis of the adult humerus

IPBSH-4 (100% maximum size) under polarised light. Vascularisation of the cortex appears less dense when compared to the juvenile humerus in A. However, there are more radial canals than longitudinal canals in the adult humeri. The dark areas between the vascular canals consist of woven bone matrix; brighter areas are parallel-fibred and lamellar bone lining the medullary cavity and vascular canals. Arrows indicate LAGs. C) Magnification of ventral cortical region in proximity to the coracobrachialis muscle attachment, indicated by the white box in A. Cortex of IPBSH-13 viewed under polarised light and a lambda filter. Arrows indicate areas of colour change in the lamellar bone of the incipient primary osteons, from blue to yellow, when the light is rotated 90 degrees. Areas between the vascular canals are woven bone and remain pink when the stage is rotated. D) The same area pictured in C rotated 90 degrees. Note the colour change in the lamellar bone of the osteons and the areas of woven bone, indicated by the arrows, remain pink. E) Same view as in C but under polarised light without lambda filter. The crystallite orientation of the bone matrix is clearly visible. Woven bone between the vascular canals remains dark. Lamellar bone in the incipient primary osteons remains bright. F) Magnification of selected area in E. Incipient primary osteon viewed under normal light. These osteons are present in both humeri and femora and retain this immature appearance throughout ontogeny. Note the large size, shape, and orientation of the osteocyte lacunae within the lamellar bone. Abbreviations: WB, woven bone.

The cortex of IPBSH-19 contains four growth cycles and four LAGs. IPBSH-31 also contains four growth cycles but only 3 LAGs. IPBSH-6 contains five growth cycles and four LAGs. Osteocyte lacunae are shaped subangular to elliptical. Those within the annuli are flattened and oriented parallel to the bone surface. Under polarised light, mineralised Sharpey's fibres appear white and extend from the bone surface to the medullary cavity (Fig. 9B). Under normal light, black unmineralised Sharpey's fibres extend from the bone surface to the middle of the cortex (Fig. 9B).

The medullary region is separated from the cortex by lamellar endosteal bone forming secondary trabeculae as seen from cross-cutting relationships of the cementing lines. Large erosion cavities are present due to resorption activity of the osteoclasts. Secondary endosteal osteons are present in the medullary margin. The medullary cavity is open; trabecular bone is only present around the outer margins.

3.3.2. Large femora.

The material consists of a left femur IPBSH-29 (131 mm, 96% maximum size) that is extremely crushed dorsoventrally, and right femur IPBSH-2 (137 mm, 100% maximum) that is slightly crushed dorsoventrally. The cortex is relatively thin and consists of parallel-fibred and woven-fibred bone (Fig. 9) and is well vascularised by radially arranged longitudinal canals exhibiting a high degree of anastomosis. Vascularisation decreases just before reaching the bone surface where the EFS is located. There is no further centripetal deposition of lamellar bone in the vascular canals, which are incipient primary osteons (Fig. 9C, D).

The cortex of IPBSH-29 contains five growth cycles and four LAGs. IPBSH-2 contains six growth cycles and five LAGs, the deepest of which has almost been completely destroyed by expansion of the medullary cavity. The outermost cortex of both femora contains an EFS (Fig. 9E, F). The amount of time represented by the EFS is unknown (Erickson *et al.* 2004), however there are more visible rest lines in IPBSH-2 then in IPBSH-29. The distance between the LAGs decreases approaching the bone surface. The amount of vascularisation also decreases and is almost nonexistent in the EFS. In both specimens, osteocyte lacuna shape is subangular to elliptical and is extremely flat in the EFS. Mineralised and unmineralised Sharpey's fibres are visible throughout the cortex.

The medullary region is open and separated from the cortex by a thin layer of lamellar endosteal bone. Crushing has obscured much of this region in specimen IPBSH-29, but large erosion cavities and secondary endosteal osteons are still visible in the medullary margin. Secondary trabecular bone is present around the outer rim of the medullary cavity. IPBSH-2 has only a few small erosion cavities, and endosteal osteons are nonexistent in the medullary margin. Trabecular bone is not visible in the medullary cavity, which might be due to deformation of the diaphysis.

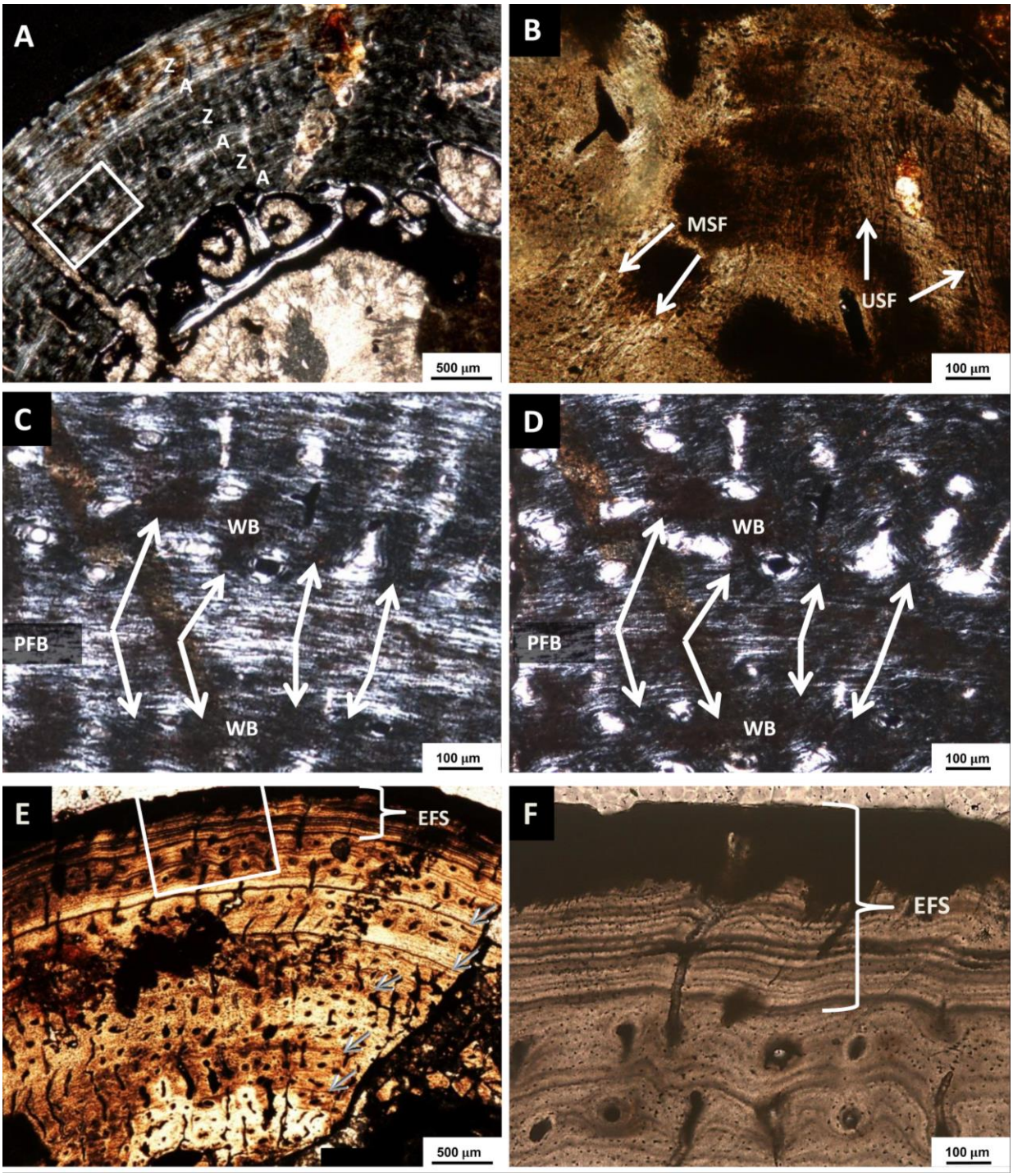

Figure 9 Histology of *Dimetrodon natalis* femora from the Briar Creek Bonebed. A) Transverse section through the mid-diaphysis of the smallest femur IPBSH-19 (72% maximum size). Note the thin cortex. Vascular canals are concentrated in the zones of woven-fibred bone that are bordered by annuli consisting of parallel-fibred bone. B) Cortical bone with mineralised (white) and unmineralised (black) Sharpey's fibres. These are found all femora specimens. C) Magnification of dorsal cortex, indicated by white box in A, viewed under polarised light. Bright areas are mostly crystallites extending parallel to the bone

surface (parallel fibred bone matrix), and the lamellar bone of the incipient primary osteons. Arrows indicate areas between the vascular canals that are woven bone. D) The same area pictured in C rotated 45 degrees to demonstrate extinction patterns exhibited by the crystallites oriented obliquely to the surface. The parallel crystallites exhibit extinction and are mostly dark. Also, areas indicated by the arrows appear to remain dark. This is the woven bone matrix. E) Transverse section through the mid-diaphysis of the largest femur (IPBSH-2) viewed under normal light. Note the EFS. Arrows indicate LAGs. F) Magnification of selected region in E (indicated by white box). Notice the closely spaced LAGs and reduction of vascularisation in the EFS. Diagenetic staining has obscured the view of the EFS in the outer most part of the cortex. Abbreviations: A, annulus; EFS, external fundamental system; MSF, mineralised Sharpey's fibres; PFB parallel fibred bone; USF, unmineralised Sharpey's fibres; WB, woven bone; Z, zone.

3.4. Summary and comparison of anatomy and histology of sphenacodontid humeri and femora

The mid-diaphysis of the humerus has a triangular to subtriangular cross section (Fig. 6), and femora are more round or oval (Fig. 7). Cortical bone in the humerus is relatively thick compared to that of the femora, both having the thinnest region of the cortex located on the ventral side. The cortex of the humeri and femora consists of a combination of two types of bone matrix: parallel-fibred bone and woven-fibred bone, either as annuli and zones or whole region of the bone (Figs 8, 9). In the humeri, vascularisation of the cortex consists of highly organised radially arranged longitudinal and radial canals extending from the medullary cavity to the bone surface. This gives the cortex a "spoked bicycle wheel" appearance (Figs 6, 8). The femora have a vascularisation consisting of radially arranged longitudinal canals with a higher degree of anastomosis (Figs 7, 9), but less organised and less dense than what is seen in the humeri. Density of the vascularisation appears to decrease from younger to older individuals, especially in humeri. There is no centripetal deposition of lamellar bone in the vascular canals, which are identified as incipient primary osteons (Figs 8, 9). This immature appearance does not change with ontogeny. Osteocyte lacunae are subangular or star-shaped to elliptical, especially those in the annuli that are flat and oriented parallel to the bone surface. They sometimes follow the direction of the vascular canals (Figs 8, 9). Osteocyte lacunae can be seen encircling the incipient primary osteons (Fig. 9F). LAGs were observed in all but three of the humeri (Table 1). LAGs were observed in all femora.

Superficially, this gives the cortical bone, laid out in the femora, a faux lamellar zonal pattern when viewed at low magnification (Fig. 9C, D). This is an artefact resulting from the fast and slow deposition of the bone tissue. The EFS is seen in the largest humerus (IPBSH-4) and the two largest femora (IPBSH-29 & IPBSH-2) (Fig. 9; Table 1). The amount of time represented by each EFS is unknown. Mineralised and unmineralised Sharpey's fibres are present in the cortex of both the humeri and femora, but more so in the femora (Fig. 9B).

In both humeri and femora, the medullary region is separated from the cortex by large erosion cavities due to resorption activity of the osteoclasts. Secondary endosteal osteons are also common in the medullary margin. Endosteal lamellar bone, in the form of secondary trabecular bone, as seen from cross-cutting relationships of cementing lines, is often present lining the medullary cavity. A network of secondary trabecular bone is found throughout the medullary cavity in the humeri. The medullary cavity in the femora appears to only have trabecular bone around the periphery. Most of the cavity is open.

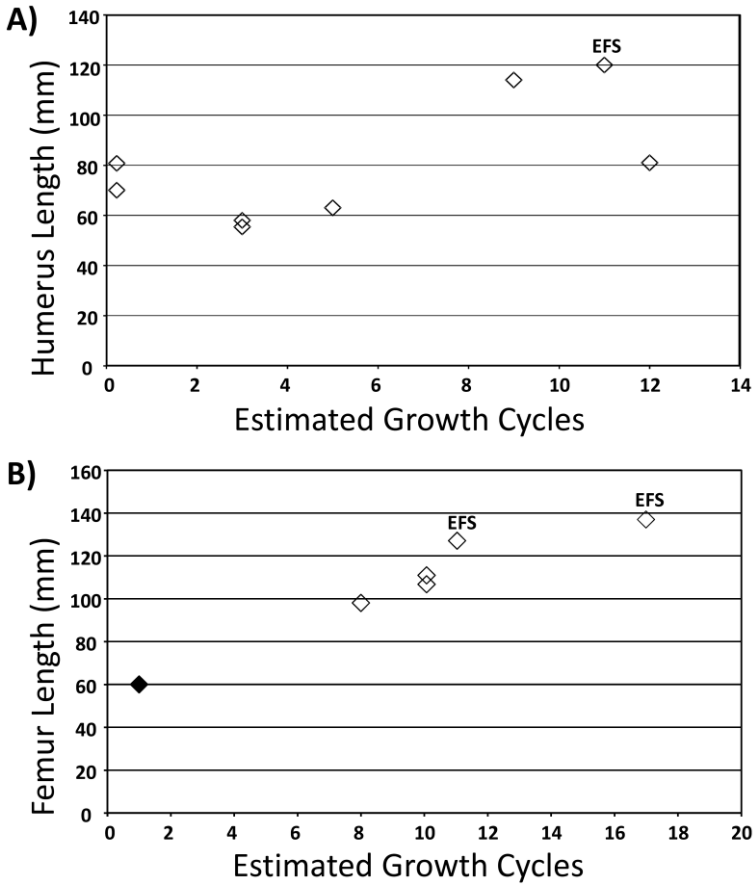

Figure 10 *Dimetrodon natalis* growth trajectory was visualised by plotting length and estimated number of growth cycles (both observed and calculated) for each humerus (A) and femur (B) listed in Table 1. With regards to the humeri, we see a high variability between size

and age. These discrepancies within the growth series can be explained by developmental plasticity or sexual dimorphism (Romer & Price 1940). However, the most parsimonious explanation is that the sampled humeri are a mix of early ontogenetic material from multiple sphenacodontid species (*Dimetrodon* spp. and the more rare *Secodontosaurus*). Note that IPBSH-13 (58 mm) and IPBSH-25 (58 mm) have the same number of growth cycles. Also, IPBSH-14 (70 mm) and IPBSH-5 (82 mm) have no growth marks preserved in the cortex which is necessary for retrocalculations. IPBSH-4 (120 mm) possesses an external fundamental system (EFS) and has been indicated on the graph. With regards to femora, in order to test the null hypothesis, we assumed that 60 mm was obtained within the first year of growth, after hatching, as this is the smallest *Dimetrodon* femur measured from the museum collections (indicated by the solid diamond) (see SI 2). Growth in these specimens is levelling off, adding further support to the notion that *D. natalis* is a small species. All other data points correspond to the femora listed in Table 1. Note that IPBSH-6 (107 mm) and IPHBSH-31(108 mm) have the same number of estimated growth cycles. Also, IPBSH-29 (131 mm) and IPBSH-2 (137 mm) both possess an EFS and have been labelled on the graph.

4. Discussion

4.1 Ontogeny of the sphenocodontid humeri and femora

The humeri growth series (Fig. 2) represents a time span of nine to twelve years (Fig. 10B; Table 1). IPBSH-13, IPBSH-25 (both are at 48% maximum size), and IPBSH- 11 (53% maximum size) have been classified as juvenile because of their size and morphology, which is evident of an early ontogenetic stage (Fig. 2). In addition, growth marks were not visible in the cortex of IPBSH-14 (58% maximum size) nor IPBSH-5 (68% maximum size), thus they are considered to be juveniles as well, possibly from a larger species. IPBSH-14 does have unossified epiphyses. However degree of ossification of the epiphyses of IPBSH-5 could not be observed due to an iron stone concretion encasing the entire bone (Fig. 2F).

Humeri with parallel micro-striations on the bone surface may indicate that these individuals reached a level of sexual maturity (Tumarkin-Deratzian *et al*. 2006; Bickelmann & Sander 2008; Klein 2010). IPBSH-22 is considered a subadult in addition to having parallel micro-striations on the bone surface (IPBSH-14 also has the same parallel surface micro-striations but we still consider it a juvenile). The number of growth marks and mid-diaphysis circumference is similar to that of the largest humerus measured (IPBSH-4), but an EFS is not

present in the cortex. Also, humerus IPBSH-22 has damaged and missing epiphyses, therefore the length of the bone is shorter than what it was in life (Table 1).

Although IPBSH-33 was 94% maximum size, we observed only one LAG and three growth cycles in the cortex, no sign of an EFS. Alternatively, this specimen could be an earlier ontogenetic stage (perhaps juvenile) of a larger sphenacodontid species. The shaft circumference is also larger than IPBSH-4 by a twelve millimetre difference, but IPBSH-33 is only six millimetres shorter than IPBSH-4. This could be due to the extreme crushing of the epiphyses in IPBSH-33, and this prevents us from properly ascertaining the extent of ossification of the epiphyses.

The presence of an external fundamental system (EFS) in the outer most layer of the cortex of the largest humerus (IPBSH-4: 100% maximum size) allows us to propose that this bone belonged to a fully grown adult of a small sphenacodontid species. Using retrocalculation to estimate the number of missing growth cycles, we have determined the age of this sphenacodontid, at time of death, to have been approximately eleven years old (Fig. 10a; Table 1). This individual could be even older than this, given the unknown amount of time represented by the EFS (Erikson et al 2004). Although the EFS indicates a slowdown in skeletal growth, this is not simply a thick annulus, after the deposition of which fast growth would resume. No such structure or condition has been observed in any of the large taxa that we have examined. This is the first time an EFS has been observed in pelycosaurs.

Due to discrepancies between size and histology of specimens within the humeri growth series, we have to consider the possibility that the variability we are observing could be due to several factors including developmental plasticity or sexual dimorphism (Romer & Price 1940). However, the most parsimonious explanation is that the sampled humeri are a mix of early ontogenetic material from multiple sphenacodontid species (*Dimetrodon* spp. and the more rare *Secodontosaurus*).

The femora growth series (Fig. 3) represents a time span of eleven years (Fig. 10A; Table 1). No identifiable juvenile femora were sampled. Although IPBSH-19 is the smallest femur sampled, we believe it is not a juvenile as the epiphyses are ossified and not unfinished. The smallest femur, IPBSH-19 (72 % maximum size), is from an individual at least eight years old based on visible growth cycles in the cortex and retrocalculation of maximally missing cycles (Fig. 10; Table 1). Subadult stage is also assigned to femora IPBSH-6 (78% maximum size) and IPBSH-31 (79% maximum size).

The EFSs observed in the two largest femora (IPBSH-29: 96% maximum size and IPBSH-2: 100% maximum size) allows us to propose that these bones belonged to fully grown adults of a small sphenacodontid species. Using retrocalculation to estimate the number of missing growth cycles, we have determined the age of these sphenacodontids, at time of death, to have been approximately eleven and seventeen years old respectively (Fig. 10b; Table 1). They could be even older than this, given the unknown amount of time represented by the EFS (Erikson et al 2004).

4.2 Multiple sphenacodontid species in the Briar Creek Bonebed

The information from the scatter plot (circumference vs. length) alone suggests that there are alternative interpretations of species composition. Either a single species of *Dimetrodon* occurs in this bonebed, possibly together with *Secodontosaurus,* or perhaps there were more than one species but with similar limb proportions (Bakker 1982) (Fig. 5). However, histological data (presence of the EFS) confirms at least two species of *Dimetrodon,* possibly with *Secodontosaurus,* present in the BCBB. The smallest sphenacodontid species we attribute to *D. natalis* whose body size compliments the small but fully grown long bones we studied histologically (IPBSH-4, IPBSH-29, IPBSH-2) (Figs. 2, 3, 8, 9), and the fact that this is the only named small species of *Dimetrodon* occurring in the North Texas Permian redbeds (Romer & Price 1940). We can exclude *Secodontosaurus* from consideration because of its larger body size (Romer & Price 1940). We are aware that a proper assignment of our material to *D. natalis* would require its comparison with the holotype from the Geraldine Bonebed locality and identification of autapomorphies, but this work is clearly beyond the scope of this study which was designed to test Bakker's (1982) ontogenetic series hypothesis.

These results thus partially refute Bakker's (1982) hypothesis, that the bones of *D. natalis, D. booneorum* and *D. limbatus* only represent an ontogenetic series of a single species, which may in turn reject the juvenile/adult habitat shift hypothesis. Juveniles and adults of *D. natalis* are found in the same bonebed. However, our findings are insufficient for fully testing the habitat shift hypothesis. Our results support Brinkman (1988) as well as the morphological classification used by Romer & Price (1940) discussed earlier (see section 1.1).

4.3. *Dimetrodon natalis* long bone histology and its implications for growth strategy

Incipient fibro-lamellar bone (IFLB) is present in the postcranial skeleton of *D. natalis* and remains so throughout ontogeny. Despite the appearance of the tissue at low magnification to have a superficially lamellar-zonal pattern, we choose to use the more descriptive IFLB because of the combination of incipient primary osteons and an interstitial matrix of highly vascularised woven-fibred bone. Enlow & Brown (1957) observed the same histology in an *Ophiacodon* long bone referring to it as "protohaversian-like". This is misleading, however, because it implies that the tissue in question is secondary whereas, in fact, there is no secondary tissue in the cortical bone of *Dimetrodon* at all.

The presence of IFLB in *D. natalis* suggests that it had a slightly faster metabolism than what is seen in modern reptiles. Many reptiles and amphibians possessing dorsal sails coexisted at this time. The main function of the dorsal sail is hypothesised to have been a thermoregulatory organ in addition to other functions such as sexual display (Hotton *et al*. 1986; Tracey *et al*. 1986; Florides *et al*. 1999, 2001; Tomkins *et al*. 2010). If this is true we would expect to find a similar tissue in edaphosaurids. In addition, as has been observed in modern mammals and sauropodomorphs (Bromage *et al*. 2009), osteocyte lacunae density OLD (Oc/mm^3) is higher in the youngest femur IPBSH-19 (47413 Oc/mm^3) than in the largest adult femur IPBSH-2 (34364 Oc/mm^3), suggesting a faster growth strategy in the younger *D. natalis* (OLD taken from Stein (2011), IPBSH-2 and IPBSH-19 are identified by their field numbers SABCBB2010-26 and SABCBB2010-1 respectively. For method of OLD calculations please refer to this study). Vascularisation appears to decrease through ontogeny but was not quantified (Figs. 6-9).

Our study of sphenacodontid long bones thus suggests that the early stages of evolution of the fibro-lamellar complex or fibro-lamellar bone (FLB) can be placed as far back as the Lower Permian. IFLB tissue existed in these mammal-like reptiles during a time soon after the reptile and mammal lines split. Further evidence of this is the existence of true FLB in the non-mammalian therapsids that appear during the Upper Permian, after the extinction of the sphenacodontid line of the pelycosaurs. IFLB is an intermediate between lamellar zonal bone (LZB) that is mostly found in modern reptiles and small (<10 kg) mammal species, and true FLB that exists in modern mammals (>10 kg) in addition to its occurrence in therapsids and many archosaurs (de Ricqlès 1974a; Francillon-Vieillot et al. 1990; de Ricqlès et al. 1991; Chinsamy-Turan 2005; Castanet 2006).

5. Conclusion

It has been shown through analysis of long bone histology that at least two species of *Dimetrodon* can be found in the Briar Creek Bonebed and by extension in the Nocona Formation. The smaller species we have attributed to *D. natalis.* The external fundamental systems observed in the largest humerus and the two largest femora confirm that *D. natalis* is not the juvenile of a larger species. The presence of the EFS in the cortex of their long bones unquestionably indicates that these animals had attained skeletal maturity. This is the first time an EFS has been reported for pelycosaurs. Validation of the sympatric *Dimetrodon* species *D. booneorum* and *D. limbatus* will require similar histologic work, in particular the identification of an ESF in significantly smaller specimens than the known maximum size of *D. limbatus*. Additionally, similar histological studies to determine the species validity of *D. booneorum* will be inconclusive without proper sampling of *Secodontosaurus* postcrania. We cannot ignore the presence of *Secodontosaurus* in the BCBB due to the similarities in size and morphology between these contemporaneous species (Romer & Price 1940).

Humeri were uninformative with regards to age approximation because not all specimens have distinguishable growth marks, and our sample set included ontogenetic material of more than one sphenacodontid species in addition to *D. natalis*. However, it did help to illustrate the variability we observed between bone size and histology. Histological analysis of additional humeri is required to better understand sphenacodontid species diversity in the BCBB.

According to the total number of missing and calculated growth cycles, the femora growth series represents a time frame of nine years. The smallest *D. natalis* femur (IPBSH-19) comes from an individual that was at least eight years old when it died. We have estimated the oldest adult *D. natalis,* represented by femur IPBSH-2, to have lived approximately seventeen years. This approximation may be more refined with additional analysis from juvenile femora that were not available for this study.

We found that incipient fibro-lamellar bone is present in the postcranial skeleton of *D. natalis* throughout ontogeny. We call this tissue incipient fibro-lamellar bone because of the combination of highly vascularised woven and parallel-fibred bone coupled with incipient primary osteons. According to Francillon-Vieillot et al. (1990), bone histology is a continuum of intermediate situations regarding bone matrix organisation and vascularity. IFLB tissue is between the end members of LZB tissue and FLB tissue. IFLB existed in these mammal-like reptiles during a time soon after the split of the reptiles and synapsids.

6. Acknowledgments

We would whole heartedly like to thank the following people: Jack and Marie Loftin of Archer City, Texas, for their help and hospitality. Without it this study would not have been possible. From the Texas Memorial Museum Vertebrate Paleontology Laboratory, Austin, TX, we especially would like to recognise and thank Wann Langston Jr. for his dedication to the science and his unyielding persistence to continue in the education of fledgling vertebrate palaeontologists. Also from the TMM, we thank Ernest Lundelius and Lyn Murray for their support and assistance with storage and shipping of fossil material. From the Steinmann Institute, University of Bonn, we would like to thank George Oleschinski for photography and figure preparation; Kayleigh Wiersma and Jessica Mitchell for helping with preparation; Katja Waskow and Olaf Dülfer for thin sectioning; Kay Heitplatz for administrative assistance. We thank Robert Bakker (Houston Museum of Natural History) for his personal communications and exchange of information. Also, we thank Don Brinkman (Tyrell Museum of Palaeontology) for his willingness to share data. We thank the following people for allowing access to their collections: Farish Jenkins Jr. and Jessica Cundiff (Museum of Comparative Zoology), William Simpson and Jörg and Nadia Frobisch (The Field Museum), Jeffrey Wilson and Gregg Gunnell (University of Michigan Museum of Paleontology), Richard Cifelli, Jennifer Larson, Brian Davis (Sam Noble Oklahoma Museum of Natural History) and Mark Norell and Carl Mehling (American Museum of Natural History). We thank Donald and Brenda Shelton of Iowa Park, TX, for their assistance and hospitality and Steven Tudor of the Sam Noble Foundation in Ardmore, OK, for his assistance. Finally we thank Jeff Lindeman for granting us permission to excavate on his land. This project was funded by DFG grant SA 469/34-1 and the University of Bonn.

7. References

Bakker, R. T. 1975. Dinosaur Renaissance. *Scientific America* **232**, 58-78.

Bakker, R. T. 1982. Juvenile-adult habitat shift in Permian fossil reptiles and amphibians. *Science* **217**, 53-55.

Berman, D. S. 1977. A new species of *Dimetrodon* (Reptilia, Pelycosauria) from a non-deltaic facies in the Lower Permian of north-central New Mexico. *Journal of Paleontology* **51,** 108-115.

Berman, D. S. 1993. Lower Permian vertebrate localities of New Mexico and their assemblages. Vertebrate Paleontology in New Mexico. *In* S. G. Lucas, S. G. & Zidek, J. (eds.) *New Mexico Museum of Natural History and Science Bulletin* **2**, 11-21.

Berman, D. S., Reisz, R., Martens, T. & Henrici, A. C. 2001. A new species of *Dimetrodon*

(Synapsida: Sphenacodontidae) from the Lower Permian of Germany records first occurrence of genus outside of North America. *Canadian Journal of Earth Science* **38**, 803-812.

Berman, D. S., Henrici, A. C., Sumida, S. & Martens, T. 2004. New materials of *Dimetrodon teutonis* (Synapsida: Sphenacodontidae) from the Lower Permian of Germany. *Annals of Carnegie Museum* **73**, 48-56.

Bickelmann, C. & Sander, M. 2008. A partial skeleton and isolated humeri of *Nothosaurus* (Reptilia: Eosauropterygia) from Wintersijk, The Netherlands. *Journal of Vertebrate Paleontology* **28**, 326-338.

Bonnan, M. F. 2004. Morphometric analysis of humerus and femur shape in Morrison sauropods: implications for functional morphology and paleobiology. *Paleobiology* **30**, 444-470.

Brinkman, D. 1988. Size-independent criteria for estimating relative age in *Ophiacodon* and *Dimetrodon* (Reptilia, Pelycosauria) from the Admiral and Lower Belle Plains formations of West-central Texas. *Journal of Vertebrate Paleontology* **8**, 172-180.

Bromage, T. G., R. S. Lacruz, R. S., Hogg, R., Goldman, S.C., McFarlin, S. C., Dirks, W., Perey-Ocha, I., Smolyar, D. H., Enlow, D. H. & Boyde, A. 2009. Lamellar bone is an incremental tissue reconciling enamel rhythems, body size, and organismal life history. *Calcified Tissue International* **84**, 388-404.

Bybee, P. J., Lee, A. H. & Lamm, E. T. 2006. Sizing the Jurassic theropod dinosaur *Allosaurus*: Assessing growth strategy and evolution of ontogenetic scaling of limbs. *Journal of Morphology* **267**, 347-359.

Carrano, M. T. 2006. Body-size evolution in the Dinosauria. *In* Carrano, M. T., Blob, R. W., Gaudin, T., & Wible, J. (eds.) Amniote Paleobiology: Perspectives on the Evolution of Mammals, Birds, and Reptiles, 225-256. Chicago: University of Chicago Press.

Case, E. C. 1907. Revision of the Pelycosauria of North America. *Carnegie Institution of Washington* **55**, 1-169.

Case, E. C. 1915. The Permo-Carboniferous redbeds of North America and their vertebrate fauna. The Carnegie Institution of Washington **20,** 1-157.

Castanet, J. 2006. Time recording in bone microstructure of endothermic animals; functional relationships. *Comptes Rendus Palevol* **5**, 629-636.

Castanet, J., Croci, S., Aujard, F., Perret, M., Cubo, J. & de Margerie, E. 2004. Lines of arrested growth in bone and age estimation in a small primate: *Microcebus murinus*. *Journal of Zoology* **263**, 31-39.

Chinsamy-Turan, A. 2005. The Microstructure of Dinosaur Bone. Baltimore, Johns Hopkins University Press. 216 pp.

Cooper, L. N., Lee, A. H., Taper, M. L. & Horner, J. R. 2008. Relative growth rates of predator and prey dinosaurs reflect effect of predation. *Proceedings of the Royal Society of London B* **275**, 2609-2615.

Cope, E. C. 1878. Descriptions of extinct Batrachia and Reptilia from the Permian of Texas. Proceedings of the American Philosophical Society **17**, 505-530.

Currey, J. D. 2002. *Bones. Structure and Mechanics*. Princeton: Princeton University Press. 436 pp.

Enlow, D. H. 1969. The bone of reptiles. *In* Gans, C. (ed.) *Biology of the Reptiles*, 45-80. London: Academic Press.

Enlow, D. H., & O. S. 1956. A comparative histological study of fossil and recent bone tissues. Part I. *Texas Journal of Science.* **9**, 405-439.

Enlow, D. H., & Brown, O. S. 1957. A comparative histological study of fossil and recent bone tissues. Part II. *Texas Journal of Science.* **9**, 186-214.

Enlow, D. H., & Brown, O. S. 1958. A comparative histological study of fossil and recent

bone tissues. Part III. *Texas Journal of Science.* **10**,187-230.
Erickson, G. M., Makovicky, P. J., Philip, J. C., Norell, M. A., Yerby, S. A. & Brochu, C. A. 2004. Gigantism and comparative life history parameters of tyrannosaurid dinosaurs. *Nature* **430**, 772-775.
Florides, G. A., Wrobel, L. C. & Kalogirou, S. A. 1999. A thermal model for reptiles and pelycosaurs. Journal of Thermal Biology **24**, 1-13.
Florides, G. A., Kalogirou, S. A., Tassou, S. A. & Wrobel, L. C. 2001. Natural environment and thermal behaviour of Dimetrodon limbatus. Journal of Thermal Biology **26**, 15-20.
Francillon-Vieillot, H., Buffrénil, V. d., Castenet, J., Géraudie, J., Meunier, F. J., Sire, J. Y., Zylbergberg, L. & Ricqlés, A. d. 1990. Microstructure and mineralization of vertebrate skeletal tissues. *In* Carter, J. G. (ed.) *Skeletal biomineralization: Patterns, processes and evolutionary trends*, Vol. **1**: 471-530. New York, Van Nostrand Reinhold.
Hentz, T. F. 1988. Lithostratigraphy and paleoenvironments of Upper Paleozoic continental red beds, north-central Texas: Bowie (new) and Wichita (revised) groups. *The* University of Texas at Austin, Bureau of Economic Geology Report of Investigations **170,** 1-55.
Horner, J. R. & Goodwin, B. 2009. Extreme cranial ontogeny in the Upper Cretaceous Dinosaur Pachycephalosaurus. PLoS One **4**, 1-11.
Horner, J. R. & Goodwin, B. 2011. Major cranial changes during *Triceratops* ontogeny. Proceedings of the Royal Society B **273**, 2757-2761.
Hotton, N., MacLean, P. D., Roth, J. J. & Roth, E. C. (eds). 1986. *The Evolution and Ecology of Mammal-Like Reptiles*. Washington, D.C.: Smithsonian Institution Press. 326 pp.
Huttenlocker, A. & Rega, E. 2011. The paleobiology and bone microstructure of pelycosaurian-grade synapsids. *In* Chinsamy, A. (ed.) *The Forerunners of Mammals-Radiation, Histology, Biology*, Indiana University Press. 352 pp.
Huttenlocker, A., Angielczyk, K. D. & Lee, A. 2006. Osteohistology of *Sphenacodon* (Synapsida: Sphenacodontidae) and the hidden diversity of growth patterns in basal synapsids. *Journal of Vertebrate Paleontology* **26**, 79-80A.
Huttenlocker, A., Rega, E. & Sumida, S. 2010. Comparative anatomy and osteohistology of hyperelongate neural spines in the sphenacodontids *Sphenacodon* and *Dimetrodon* (Amniota: Synapsida). *Journal of Morphology* **271**, 1407-1421.
Huttenlocker, A., Mazierski, D. & Reisz, R. 2011. Comparative osteohistology of hyperelongate neural spines in Edaphosauridae (Amniota: Synapsida). *Palaeontology* **54**, 573-590.
Kemp, T. S. 2007. *The Origin and Evolution of Mammals*. Oxford: Oxford University Press. 331 pp.
Kilbourne, B. M. & Makovicky, P. J. 2010. Limb bone allometry during postnatal ontogeny in non-avian dinosaurs. *Journal of Anatomy* **217** 135-152.
Klein, N. 2010. Long bone histology of Sauropterygia from the Lower Muschelkalk of the Germanic Basin provides unexpected implications for phylogeny. *PLoS One* **5**, 1-25.
Klein, N. & Sander, P. M. 2007. Bone histology and growth of the prosauropod *Plateosaurus engelhardti* MEYER, 1837 from the Norian bonebeds of Trossingen (Germany) and Frick (Switzerland). *Special Papers in Palaeontology*. **77**, 169-206.
Klein, N. & Sander, M. 2008. Ontogenetic stages in the long bone histology of sauropod dinosaurs. *Paleobiology* **34**, 247-263.
Kohler, M., Marín-Moratalla, N., Jordana, X. & Aanes, R. 2012. Seasonal bone growth and physiology in endotherms shed light on dinosaur physiology. *Nature* **487**, 358-361.
Labandeira, C. C. & Allen, E. G. 2007. Minimal insect herbivory for the Lower Permian

coprolite bone bed site of north-central Texas, USA, and comparison to other Late Paleozoic floras. *Palaeogeography Palaeoclimatology Palaeoecology* **247**, 197-219.
Lee, A. & Werning, S. 2008. Sexual maturity in growing dinosaurs does not fit reptilian growth models. *PNAS* **105**, 582-587.
Lehman, T. M. & Woodward, H. N., 2008. Modelling growth rates for sauropod dinosaurs. *Paleobiology* **34**, 264–281.
Rega, E. A., Noriega, K., Sumida, S. S., Huttenlocker, A., Lee, A. & Kennedy, B. 2012. Healed fractures in the neural spines of an associated skeleton of *Dimetrodon*: Implications for dorsal sail morphology and function. *Fieldiana Life and Earth Sciences* 5, 104-111.
Reisz, R. R. 1986. Encyclopedia of Paleoherpetology. 17A: Pelycosauria. Stuttgart: Fischer. 102 pp.
Ricqlès, A. d. 1974a. Evolution of endothermy: Histological evidence. *Evolutionary Theory* **1**, 51-80.
Ricqlès, A. d. 1974b. Recherches paléohistologiques sur les os longs des Tétrapodes IV : Eotheriodonts and pelycosaurs. *Annales de Paleontologie* **60**, 3-39.
Ricqlès, A. d. 1976a. Recherches paléohistologiques sur les os longs des tétrapodes VII. - Sur la classification, la signification fonctionnelle et l`histoire des tissus osseux des tétrapodes. Deuxième partie. *Annales de Paleontologie* **62**, 71-126.
Ricqlès, A. d. 1976b. On the bone histology of fossil and living reptiles, with comments on its functional and evolutionary significance. *In* Bellaris, A. d. A., & Cox, B. C. (eds.) *Morphology and Biology of Reptiles*, 123- 150. Dorchester: Dorset Press
Ricqlès, A. d. 1978. Recherches paléohistologiques sur les os longs des Tétrapodes VII. - Sur la classification, la signification fonctionnelle et l´histoire des tissus osseux des Tétrapodes, Troisième partie. *Annales de Paleontologie* **64**, 153-176.
Ricqlès, A. d., Meunier, F. J., Castanet, J. & Francillon-Viellot, H. 1991. Comparative microstructure of bone. In Hall, B. K (ed.) *Bone. Vol. 3: Bone Matrix and Bone specific Products*. Boca Raton, FL: CRC Press. 187 pp.
Romer, A. S. 1936. Studies on American Permo-Carboniferous tetrapods. *Problems of* Paleontology **1**, 85-96.
Romer, A. S. 1937. New genera and species of pelycosaurian reptiles. *New England Zoology* Club Proceedings **16**, 89-96.
Romer, A. S. 1974. The stratigraphy of the Permian Wichita redbeds of Texas. *Breviora* **427**, 1-28.
Romer, A. S. 1969. In *Osteology of the reptiles*. Chicago IL, University of Chicago Press. 800 pp.
Romer, A. S. & Price, L. W. 1940. Review of the Pelycosaurs. *Geological Society of America* Special Papers **28**, 1-538.
Rushforth, R. & Small, B. 2003. Analysis of Wichita Group (revised) "series A" *Dimetrodon* species using beta probability plots and Hotelling's T^2 statistic. *Journal of Vertebrate Paleontology* **23** (3, supplement), 91A.
Sander, P. M. 1987. Taphonomy of the Lower Permian Geraldine Bonebed in Archer County, Texas. Palaeogeography, Palaeoclimatology, Palaeoecology **61**, 221-236.
Sander, P. M. 2000. Long bone histology of the Tendaguru sauropods: Implications for growth and biology. *Paleobiology* **26**, 466-488.
Sander, M. & Klein, N. 2005. Developmental plasticity in the life history of a prosaruopod dinosaur. *Science* **310**, 1800-1802.
Sander, P. M., Mateus, O. Laven, T. & Knötschke, N. 2006. Bone histology indicates insular dwarfism in a new Late Jurassic sauropod dinosaur. *Nature* **441**, 739-741.
Sander, P. M., Klein, N., Stein, K. & Wings, O. 2011. Sauropod bone histology and

implications for sauropod biology. In Klein, N., Remes, K., Gee, C. T., & Sander, P. M. (eds.) *Understanding the Life of Giants: Biology of the Sauropod Dinosaurs*, 276-302. Bloomington: Indiana University Press. Stein, K. 2011. Osteocyte lacuna density in saurischian dinosaurs and the convergence of fibrolamellar bone in mammals and dinosaurs: different strategies to grow fast. *Journal of Vertebrate Paleontology* 31:133A.

Stein, K., Csiki, Z., Curry Rogers, K., Weishampel, D. B., Redelstorff, R., Carballido, J. L. & Sander, P. M. 2010. Small body size and extremem cortical remodeling indicate phyletic dwarfism in Magyarosaurus dacus (Sauropoda: Titanosauria). *Proceedings of the National Academy of Sciences of the United States of America* **107**, 9258-9263.

Sumida, S., Rega, E., & Noriega, K. 2005. Evidence-based paleopathology II: Impact on phylogenetic analysis of the genus *Dimetrodon*. *Journal of Vertebrate Paleontology* **25** (3, supplement), 120A.

Tomkins, J. L., LeBas, N. R., Witton, M. P., Martill, D. M. & Humphries, S. 2010. Positive allometry and the prehistory of sexual selection. *The American Naturalist* **176**, 141-148.

Tracey, R. C., Turner, J. S. & Huey, R. B. 1986. A biophysical analysis of thermoregulatory adaptations in sailed pelycosaurs. In Hotton III, N., MacLean, P. D., Roth, J. J., & Roth, E. C. (eds.) *The ecology and biology of mammal-like reptiles*, 195-206. Washington D.C.: Smithsonian Institute.

Tumarkin-Deratzian, A. R., Vann, D. R. & Dodson, P. 2006. Bone surface texture as an ontogentic indicator in long bones of the Canada goose *Branta canadensis* (Anseriformes: Anatidae). *Zoological Journal of the Linnean Society* **148**, 133-168.

Vaughn, P. P. 1966. Comparison of the Early Permian vertebrate fauna of the Four Corners region and north-central Texas. Los Angeles County Museum of natural History Contributions in Science **105**, 1-13.

Vaughn, P. P. 1969. Early Permian vertebrates from southern New Mexico and their paleozoogeographic significance. Los Angeles County Museum of natural History Contributions in Science **166**, 1-22.

Chapter 4: Ophiacodon long bone histology and ecology: discovering the roots of endothermy in the mammalian family tree

To be submitted as: Shelton, C. D. and Sander, P. M. (Submitted) *Ophiacodon* long bone histology: the earliest occurrence of FLB in the mammalian lineage. Peer J

Abstract: The origin of mammalian endothermy has long been held to reside within the early therapsid groups. However, shared histological characteristics have been observed in the bone matrix and vascularity between Ophiacodontidae and the later therapsids (Synapsida). Historically, this coincidence has been explained as simply a reflection of the presumed aquatic lifestyle of *Ophiacodon* or even a sign of immaturity. Here we show, by histologically sampling an ontogenetic series of *Ophiacodon* humeri, as well as additional material, the existence of true fibro-lamellar bone in the postcranial bones of a member of 'Pelycosauria'. Our findings have reaffirmed what previous studies first described as fast growing tissue, and by proxy, have disproven that the highly vascularized cortex is simply a reflection of young age. This tissue demonstrates the classic histological characteristics of true fibro-lamellar bone (FLB) with the exclusion of well-developed Haversian tissue. The cortex consists of primary osteons in a woven bone matrix and remains highly vascularized throughout ontogeny providing evidence to fast skeletal growth. Overall, the FLB tissue we have described in *Ophiacodon* is more derived or "mammal-like" in terms of the osteonal development, bone matrix, and skeletal growth then what has been described thus far for any other 'pelycosaur' taxa. With regards to the histological record, our results remain inconclusive as to the preferred ecology of *Ophiacodon,* but support the growing evidence for an aquatic lifestyle. Our findings have set the evolutionary origins of modern mammalian endothermy and high skeletal growth rates back approximately 20 M.Y. to the Lower Permian, and by extension perhaps the Upper Carboniferous.

Key words: Pelycosauria, Therapsida, Brinkman

1. Introduction

*Ophiacodon (*Marsh, 1878), which means "snake tooth", is a eupelycosaur that belongs to Ophiacodontidae (Nopcsa, 1923), considered a primitive 'pelycosaur' by Romer and Price (1940). However, it has shown to be more derived osteologically than varanopids, eothyridids, and caseids (Brinkman & Eberth, 1985; Reisz, 1986; Kemp, 2007a). The earliest known synapsid fossils, dating back to the Carboniferous and found in Nova Scotia, The Czech Republic, and the USA, are assigned to Ophiacodontidae (Reisz, 1972; Reisz 1975). *Ophiacodon* is considered a more derived member of the clade that existed between the Upper Carboniferous and the Lower Permian. Most of the fossil remains have been found throughout the Southwest of the United States, specifically New Mexico, Kansas, Texas, and Oklahoma (Romer & Price, 1940; Vaughn, 1966; Vaughn 1969, Reisz, 1986). Several gross- and micro-anatomical autapomorphies of *Ophiacodon* have been suggested as evidence for an amphibious or (semi-) aquatic lifestyle. These include an elongated narrow cranium, lack of a fully fused braincase, lack of claws, disparity in hind limb and fore limb lengths, a poorly ossified endochondral skeleton, and highly vascularized cortices in the long bones (Romer & Price, 1940; de Ricqlès, 1974a; de Ricqlès, 1974b; Reisz, 1986; Huttenlocker & Rega, 2012; Felice & Angielczyk, 2014). However, it should be noted that Romer and Price (1940) did observe well ossified epiphyses in a few large *Ophiacodon* specimens. Felice and Angielczyk (2014) suggested that further histologic analysis of the pelycosaur-grade synapsids is necessary to understand this delayed ossification phenomenon and how it could reflect the lifestyle of *Ophiacodon*.

The earliest histologic studies of *Ophiacodon* long bones all concur that the histology differs by sharp contrast in vascularity, matrix organization, and presence of growth marks from that observed in other 'pelycosaurs' (Enlow & Brown, 1957; Enlow & Brown, 1958; Enlow, 1969; de Ricqlès, 1974a; de Ricqlès, 1974b). The currently accepted hypothesis to explain this difference is their proposed aquatic or amphibious lifestyle (Romer & Price, 1940),supported by the histologic investigations of de Ricqlès (1974a; 1974b) despite noting similarities to some therapsids. Germain and Laurin (2005) addressed the ecology enigma by quantifying the cortical porosity and comparing it to extant animals. Their results were inconclusive. Enlow (1969), however, noted the characteristics of *Ophiacodon* bone tissue reflected fast skeletal growth, but

he suggested this could just be the juvenile condition as adequate detailed ontogenetic comparisons were lacking within the 'pelycosaur' group.

1.3 Brinkman's morphological stages of *Ophiacodon* humeral development.

Brinkman (1988) demonstrated that ontogenetic morphological stages in a taxon can be defined on the basis of degree of ossification of the limb bones. Size alone cannot be used as a proxy for reconstructing the age in taxa because individuals of the same size may represent more than one stage of development. However, because of the delayed ossification observed in the epiphysis of *Ophiacodon* (Romer & Price, 1940), Brinkman was restricted as to what elements to use to test his hypothesis. The humerus was chosen because the complex articulations in the epiphyses exhibited more than two stages of ontogeny.

Originally, Brinkman (1988) used 27 *Ophiacodon* humeri to denote five distinct morphological ontogenetic stages of development (MOS); bone length was used as a proxy for size. All material came from localities in the Nocona Formation (formerly the Admiral Formation), which includes Rattlesnake Canyon (RSC) and the Briar Creek Bonebed (BCBB), as well as various localities in the Petrolia Formation (formerly Belle Plains Formation) (Hentz, 1988). Here we summarize the criteria Brinkman (1988) used to develop his five MOS (Fig. 1): 1) Three specimens were scored as MOS I, where both proximal and distal ends of the humerus are concave, and the unfinished bone of the supinator process is confluent with the distal articular surface; 2) Five humeri were scored as MOS II, where finished bone separates the supinator process from the distal articular surface; 3) Eight humeri were scored as MOS III, where the radial-ulnar surface is convex, although the ectepicondyle and entepicondyle are concave; 4) Five humeri were scored as MOS IV, where the radial condyle is well formed, and the proximal articular surface, the ectepicondyle, and the entepicondyle are convex; 5) Six humeri were scored as MOS V, where it was observed that finished bone separates the radial condyle from the ectepicondyle, the ulnar surface from the entepicondyle, and the pectoralis process from the proximal articular surface (Fig. 1).

As noted earlier, Brinkman (1988) used humeri from both RSC and the BCBB. He noted that although both bonebeds are in the same geological formation (Nocona Formation: Artinskian), he observed most of the humeri from the BCBB are between MOS II and MOS V

and differ considerably in size from those of RSC (Fig. 2). This led Brinkman to note the presence of two sub assemblages of *Ophiacodon* in the same stratigraphic interval.

1.4 Purpose of this study

Huttenlocker and Rega (2012) have proposed that proper conclusions about the ecology and organismal dynamics might be derived from the micro-anatomical data obtained from a study of an ontogenetic *Ophiacodon* long bone series. In this study we have set out to obtain this data by sectioning Brinkman's (1988) figured *Ophiacodon* humeral growth series (Fig. 1) and comparing the results to material from BCBB, as well as material from various Oklahoma localities not previously examined by Brinkman (1988). Also, a growth model is extrapolated from the growth record retained in the cortex of these humeri. This will be a good test of Brinkman's (1988) morphologic stages of development that he assigned to these humeri to know if morphology and histology reflect the ontogenetic stage of the bone (Fig. 1).

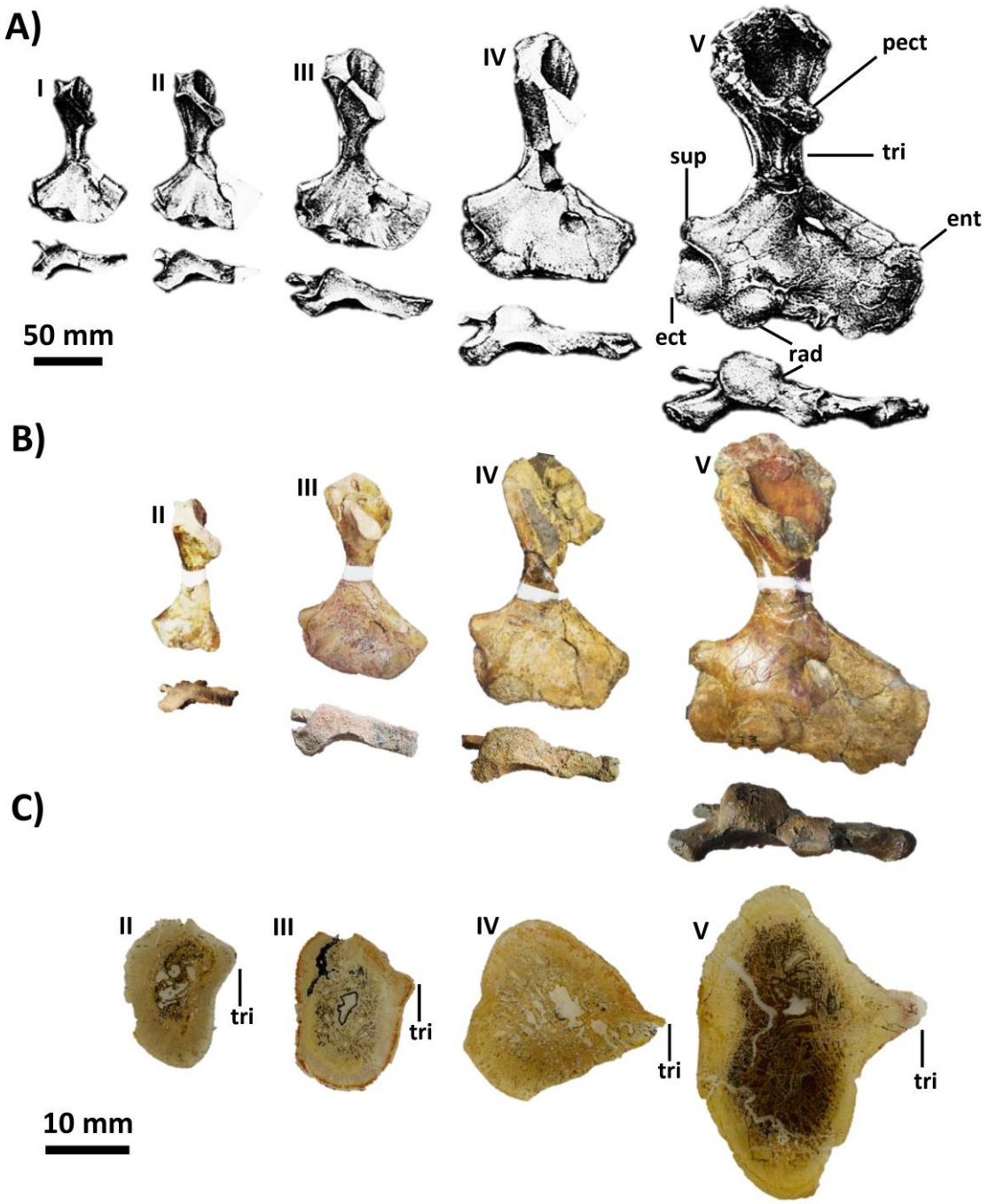

Figure 1 Brinkman (1988) showed that stages of development (MOS) in a taxon can be defined on the basis of morphology, specifically the degree of ossification. The humerus was chosen because the complex articulations in the epiphyses exhibited more than two stages of ontogeny. A) Illustrated *Ophiacodon* humeri from the Rattlesnake Canyon locality in Archer County, Texas. These were chosen by Brinkman to represent five distinct stages of

development distinguished by morphological features representing relative ages in an individual. MOS I- both proximal and distal ends of the humerus are concave and the unfinished bone of the supinator process is confluent with the distal articular surface. MOS II- finished bone separates the supinator process from the distal articular surface. MOS III- the radial-ulnar surface is convex, although the ectepicondyle and entepicondyle are concave. MOS IV- the radial condyle is well formed; the proximal articular surface, the ectepicondyle and the entepicondyle are convex. MOS V- finished bone separates the radial condyle from the ectepicondyle, the ulnar surface from the entepicondyle and the pectoralis process from the proximal articular surface (modified from Brinkman 1988, Fig. 1). The distal epiphysis is shown below each bone. B) Photographs of the actual bones that Brinkman used in his study with the exception of MOS I (MCZ-1435, length: 69 mm; circumference: 42 mm) as it was not available for this study. The white area in the mid-diaphysis corresponds to the area sectioned for histological analysis and was reconstructed with plaster. The distal epiphysis is shown below the bone. Stage II (MCZ-5926); Stage III (MCZ-2819, reversed); Stage IV (MCZ-4816, reversed); Stage V (MCZ-1486). C) Corresponding thin sections from the mid-diaphysis of the four humeri. Abbreviations: ect= ectepicondyle; ent= entepicondyle; pect= pectoralis crest; rad= radial articular surface; sup=supinator process; tri= triceps muscle insertion.

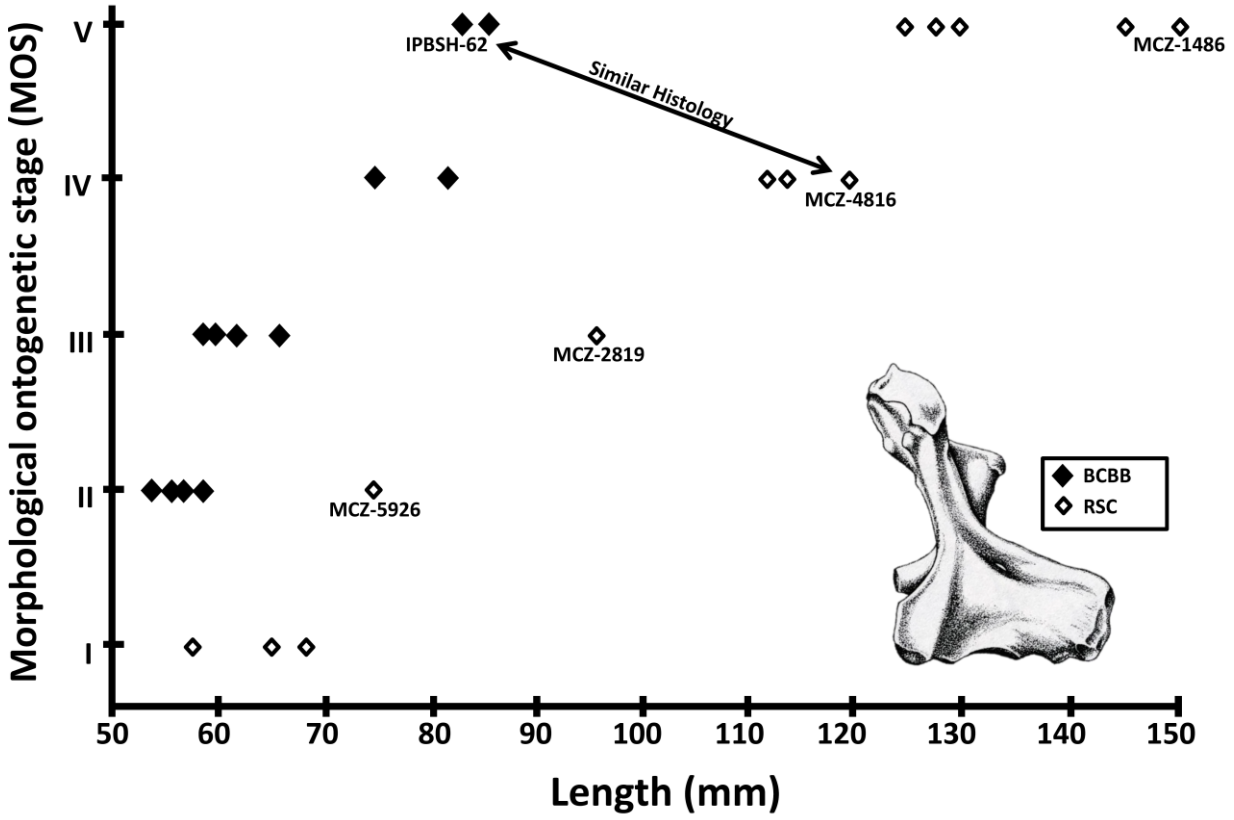

Figure 2 Graph showing the relationship between size and the morphological stage of development of Ophiacodon humeri from the Briar Creek Bonebed (BCBB: black diamonds) and other localities from the Petrolia and Nocona formations. The latter includes the sectioned Rattlesnake Canyon humeri (RSC: white diamonds). These humeri, as well as IPBSH-62, are marked on the graph. Note the arrow indicating IPBSH-62 (MOS V) and MCZ-4816 (MOS IV) both have a similar histology with the exception of better developed primary osteons in MCZ-4816. Graph inverted and modified from Brinkman (1988) figure 7.

Most importantly, we want to investigate what previous studies have called "fast growing" tissue (Enlow & Brown, 1957; Enlow 1969) as possibly an overlooked earliest occurrence of fibro-lamellar bone in the tetrapod skeleton of the mammalian lineage. Finally, the quantitative histologic results will be combined with the morphometric data in an attempt to ascertain any evidence for the preferred ecology of *Ophiacodon*.

Institutional Abbreviations: IPBSH, Palaeohistology collection, Steinmann Institute of Geology, Mineralogy, and Palaeontology, University of Bonn, Bonn, Germany; MCZ, Museum of Comparative Zoology, Harvard University, Cambridge, MA, USA; MSU, Midwestern State University Geology Department, Wichita Falls, TX, USA; OMNH, Sam Noble Museum of Oklahoma Natural History, University of Oklahoma, Norman, OK, USA.; UMMP, Museum of Paleontology, University of Michigan, Ann Arbor, MI, USA.

2. Materials

Carboniferous material comes from one of two localities in the Ada and Vamoosa Formations of Seminole County, Oklahoma, USA (Olson, 1977; Kissel & Lehman, 2002). Lower Permian localities of Oklahoma include the "Waurika Site" in the Wellington Formation of Jefferson County and the younger, less fossiliferous Garber Formation found in Tillman County (Olson 1967; Olson, 1977; Sander 1989). Texas localities include Rattlesnake Canyon (Sander, 1989) and the Briar Creek Bone Bed (Case, 1915), both of which are in the Nocona Formation (Lower Permian, Artinskian) (Hentz, 1988). The Wellington and Garber Formations of Southern Oklahoma are equivalent to Texas formations of the Upper Wichita and Lower Clear Fork Groups.

2.3 *Ophiacodon* Humeri

2.3.1 Rattlesnake Canyon Ophiacodon Humeri

Brinkman (1988) illustrated examples of the five stages of development seen in the *Ophiacodon* humeri from an ontogenetic sequence of bones collected from RSC (Lower Permian, Artinskian, Nocona Formation) that are housed in the MCZ collection (Fig. 1) (Hentz, 1988; Sander, 1989). We obtained permission for consumptive sampling of the specimens representing MOS II-V (MCZ-5926, MOS II; MCZ-2819, MOS III; MCZ-4816, MOS IV; MCZ-1486, MOS V) (Table 1; Fig. 1; S.I. 1A-E). Humerus MCZ-1435 (MOS I) (Fig. 1A) was measured (length 69 mm & circumference 42 mm), but permission was not granted for consumptive sampling. All material is of *O. retroversus*. Morphological terminology is based on Romer and Price (1940) and Brinkman (1988).

Table 1: Dimensions and growth mark count of the sectioned *Ophiacodon* long bones. Abbreviations: C=circumference; EFS= external fundamental system; HOS= histological ontogenetic stage; L= length; LAG= line of arrested growth; LLD= limb length discrepancy; NL= neonatal line; MOS= morphological ontogenetic stage.

Specimen Number	Species	Bone	MOS	Length (mm)	Circumference (mm)	LLD 1.20 (mm)	L/C ratio	Growth Cycles	Notes
MCZ-5926	*O. retroversus*	Right Humerus	2	76	44	91.20	1.73	1	NL
MCZ-2819	*O. retroversus*	Left Humerus	3	97	50	116.40	1.94	2	
MCZ-4816	*O. retroversus*	Left Humerus	4	122	69	146.40	1.77	2	Inc
MCZ-4816	*O. retroversus*	Right Humerus	4	125	71	150.00	1.76	2	Inc
MCZ-1486	*O. retroversus*	Right Humerus	5	152	83	182.40	1.83	4	EFS (+8GC)
OMNH-73698	*Ophiacodon* (sp)	Right Humerus	4-5	113	50	98.40	2.26	2	EFS
IPBSH-62	*O. uniformis*	Left Humerus	5	82	37	135.60	2.22	3	
IPBSH-46	*Ophiacodon* (sp)	Right Femur	NA	78	37	184.17	2.11	0	NL
OMNH-55234	*O. mirus*	Right Femur	NA	100	60	65.00	1.67	3	Inc
MSU Specimen	*O. uniformis*	Left Femur	NA	115	55	95.83	2.09	8	Inc
OMNH-35389	*O. retroversus*	Left Femur	NA	221	145	83.33	1.52	8	EFS

3.1.2 Briar Creek *Ophiacodon* humerus

IPBSH-62: This bone is identified as *O. uniform* (R. R. Reisz personal communication) and was obtained during a 2010 IPBSH excavation at the BCBB (Lower Permian, Artinskian, Nocona Formation) (Table 1; S.I. 1F) (Case, 1915; Hentz, 1988). A scapulocoracoid, believed to have originated from the same individual, was also associated with this humerus. Based on the criteria of Brinkman (1988), morphologically, this humerus is an early MOS V even though unfinished bone is still present on the edge of the entepicondyle, ectepicondyle, and the tip of the pectoralis process. The ulna and radial surfaces are both well ossified and finished bone separates the pectoralis process from the proximal articular surface (Brinkman 1988) (See for example Fig. 1).

2.3.2 OMNH humerus.

OMNH-73698: This specimen is housed in the collection of the OMNH at the University of Oklahoma in Norman, Oklahoma, USA. The humerus is of an *Ophiacodon* (sp) collected in Seminole, OK, from the Vamoose Formation (Pennsylvanian) (OMNH-V1518, the "Fixico Site") (Olson, 1977; Kissel & Lehman, 2002). It is difficult to assign a MOS based on the criteria set by Brinkman (1988) because the distal end is damaged; however, what remains of the entepicondyle

is highly rugose. The proximal end is convex and the pectoralis process is separated from the proximal articular surface by unfinished bone. Based on these observations we can label OMNH-73698 as a late MOS IV or early MOS V (Table 1; S.I. 1G).

2.4 *Ophiacodon* Femora

2.4.1 OMNH Femora

OMNH-55234: Is the distal fragment of a femur measuring 100 mm in length, but the assignment on the label to *O. mirus* is suspect due to the fragmentary nature of the bone. This specimen comes from the Upper Carboniferous Ada Formation in Seminole County OK, USA, (OMNH-V1005; Site 4) (Table 1; S.I. 2B) (Olson, 1977; Kissel & Lehman, 2002).

OMNH-35389: Is simply labeled as *Ophiacodon* (sp). in the OMNH collection and comes from the Lower Permian, Garber Formation in Tillman County OK, USA, (OMNH-V716; Site 6) (Olson, 1967; Olson, 1977; Sander, 1989). Total length measures 221 mm (Table 1; S.I. 2D). However, due to the size of this bone, it most likely belongs to *O. retroversus,* or a larger unknown species, and thus we identify it as the former.

2.4.2 MSU uncataloged Ophiacodon femur

This specimen has no catalog number. The only record for this specimen is "Waurika Site" Wellington Formation of Jefferson County (Olson, 1977). The overall length measures 115 mm and the mid-diaphysis circumference is 55 mm. The adductor crest is damaged; thus, the circumference would have been larger in life. We identified the specimen as *O. uniformis* based on Romer and Price (1940) and Reisz (1986) (Table 1; S.I. 2C).

2.4.3 Briar Creek Ophiacodon Femur

IPBSH-46: This femur was obtained during the 2011 IPBSH excavation at the BCBB (Lower Permian, Artinskian, Nocona Formation).The total length is 78 mm. Based on this criteria alone we would have identified this specimen as *O. uniformis* (Romer & Price, 1940; Brinkman 1988) (Table 1; S.I. 2A). However, the size of the specimen suggests that this femur belongs to a very immature individual of a larger species. The only other contemporaneous *Ophiacodon*

species was the larger *O. retroversus*, which is known from the area. For our purposes, we simply identify it as *Ophiacodon* (sp) due to the early ontogenetic development.

3. Method

3.3 The Full Mid-diaphysis Cross-sectioning Method

The mid-diaphysis is the region of the bone where the most complete record of growth is preserved. It also corresponds to the area of the smallest shaft circumference (Francillon-Vieillot et al., 1990; Currey, 2002). Silicon molds (Provil NovoTM putty, Heraeus Kulzer Technique; regular) of all long bone diaphyses were created before sectioning. Next, each long bone mid-diaphysis was encased in a green epoxy resin (Technovit Universal TM liquid and Technovit TM 5071 powder, Heraeus Kulzer Technique) before being sectioned transversely with a rock saw, equipped with a standard diamond-tipped blade, to prevent splintering of the outer cortex. The green epoxy resin is dissolved, and the damaged areas are cast in plaster for purposes of reconstructing and preserving the morphological and anatomical features of the original material. Humeral midshaft sections bisect the area where the medial head of the triceps muscle inserts, giving the cross section a distinct shape (Fig. 3A). And the femoral sections bisect the area of the adductor muscle attachment (Fig. 3B) (Romer & Price, 1940; Romer, 1969). After sawing, sections were ground to approximately 35 to 50 μm by hand on a glass plate with wet grit (600 and 800) and sealed with a cover slip using UV activated resin (Verifix TM LV 740 by Bohle). The following specimens were sectioned using this method: humeri, MCZ-5926, MCZ-2819, MCZ-4816, MCZ-1486, IPBSH-62 and femora, OMNH-55234, IPBSH-46, and the MSU specimen (Figs. 6-10, 12-14) .

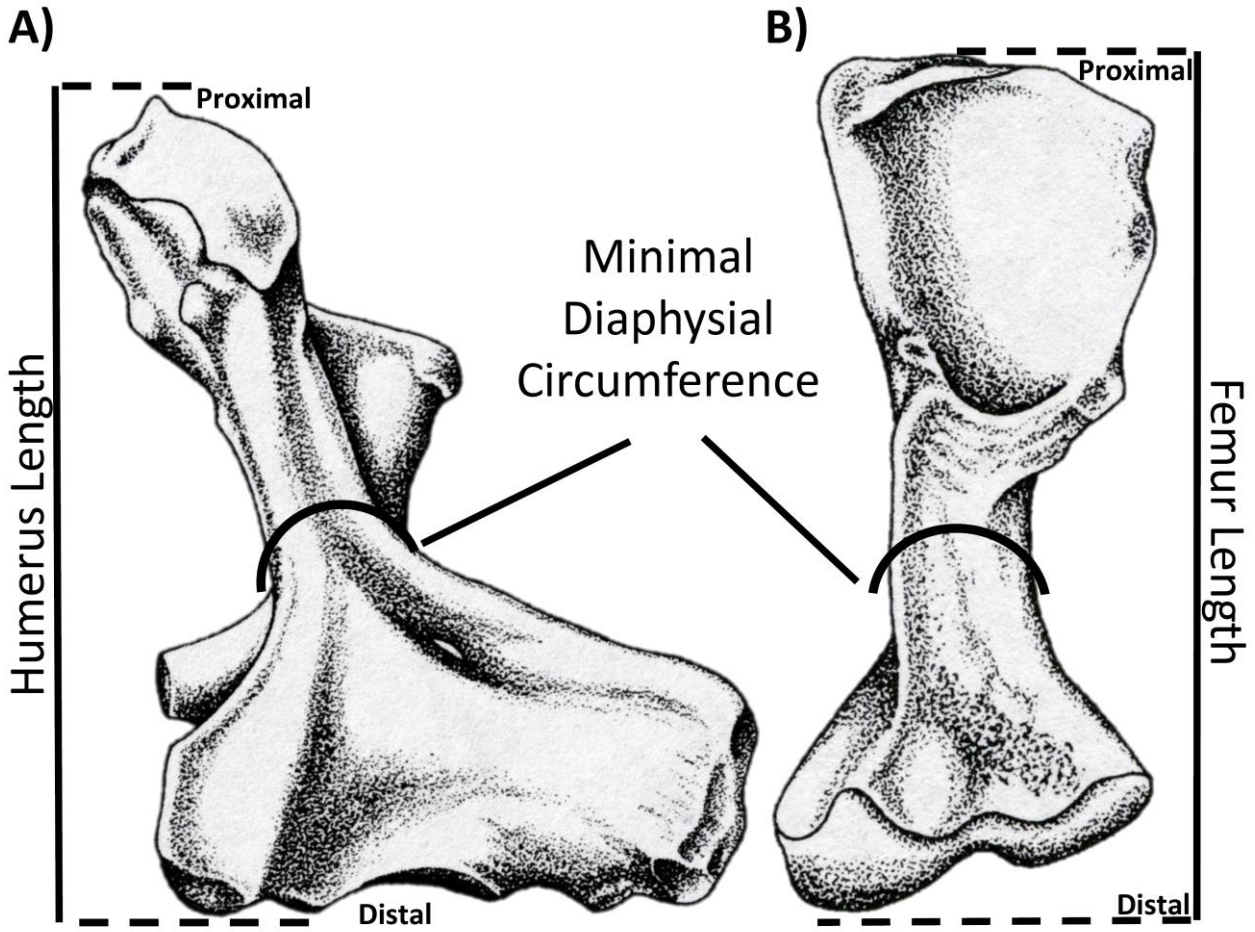

Figure 3 Illustration of an Ophiacodon humerus (A) and femur (B) with indications of how and where total length and the minimal diaphysis circumference were measured. The latter measurement also indicates the plane of section across the mid-diaphysis that contains the best preserved growth record. Note that the bones shown here belong to *O. retroversus* (modified from Reisz 1986).

3.4 The Miniaturized Coring Method

This method is a miniaturized version of that described by Stein and Sander (2009). While a full cross-section of the mid-diaphysis is preferred coring increases sample size and permits access to more valuable specimens and those encased in large aggregations of matrix. It is crucial for the coring method that homologous locations are sampled in the different bones (Stein and Sander 2009). Material available for sampling while onsite at the OMNH was core drilled dorsally at the mid-diaphysis allowing for minimal damage to the specimen (humerus OMNH-

73698 and femur OMNH-35389) (Figs. 11 & 17). The direction of the long bone axis was marked on the bone surface at the sample location by a line so that sample orientation could be maintained. Two sizes of diamond-tipped coring bits were used (3 mm and 5 mm), and attached to a Proxxon TM variable speed rotary tool mounted on a hand operated miniature drill press. Water was used to lubricate the drill bit to reduce friction and prevent damage of the outer periosteal tissue by building a small reservoir using plasticine (Fig. 4A). The core hole was later infilled with plasticine.

Cores were thin-sectioned in the Steinman Institute's paleohistology laboratory. Each core was imbedded in a translucent Araldite 2020 epoxy-resin (Bodo Möller Chemie) and allowed to harden for 24 hours before being sectioned by cutting the core perpendicular to the long axis of the original long bone orientation (Fig. 4), as indicated by the mark drawn prior to coring. The plane of section is thus the same as in the full transverse section of the mid-diaphysis. Thin-sectioning and slide preparation follow the same procedure as that described above for bones cut in full cross-section.

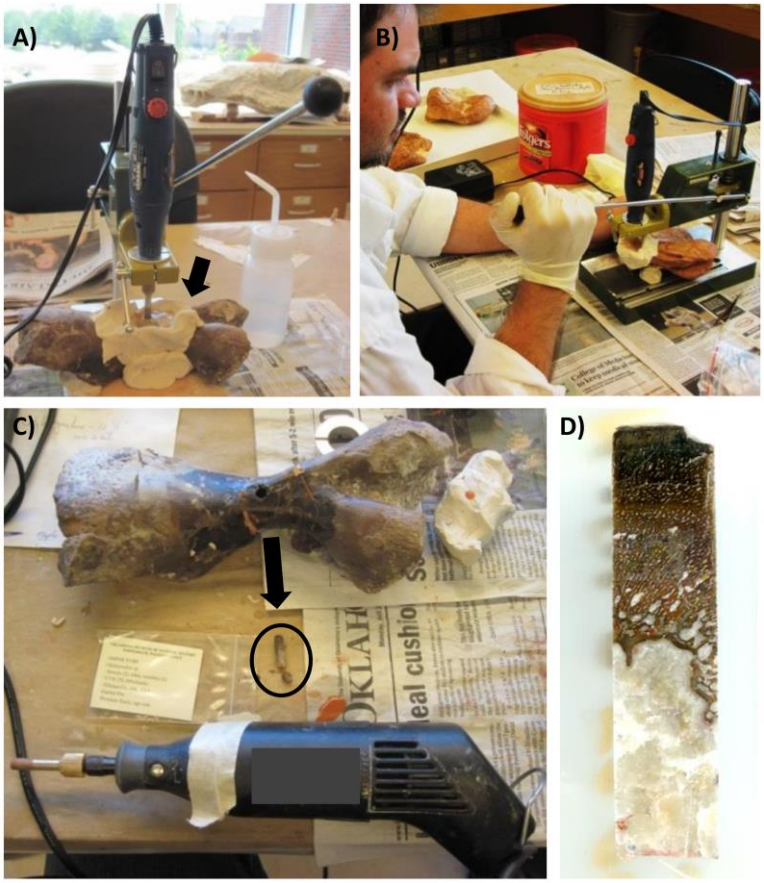

Figure 4 Miniaturization of the coring process. A) The miniature hand operated drill press is set up with a variable speed rotary tool. It is important to keep the core bit lubricated with water to prevent drill bit overheating. Arrow is pointing to a water bath constructed around the drilling site with plasticine. B) Operation of the drill press performed on a pelycosaur bone. Light pressure is applied to the drill while in operation to facilitate a slow, steady pace. It is important to drill into the cortex slowly because the outer cortex may be sheared off if drilled too quickly. C) The results of the coring operation on femur (OMNH-35389). The core was drilled on the dorsal side of the midshaft at the minimal diaphysis circumference. This core sample is further processed in the lab resulting in the next figure. Arrow indicates drill site, and the resulting core sample is indicated by the circle. D) The final core sectioned transversely after being embedded in a clear epoxy.

Thin sections were permanently cover slipped and imaged in conventional transmitted light and polarized transmitted light using a Leica DM2500LP Polarizing Microscope configured with a 360 degree rotating stage and polarized light lambda filters. Digital images were acquired with a Leica DFC420 color camera and produced using the 2007 Leica IMAGE ACCESS EASYLAB 7 software (Leica, Wetzlar, Germany) (See Petermann & Sander, 2013). Overview images of thin sections were obtained in normal light with an EPSON V750 (manufactured in Japan) and a high-resolution transmitted light scanner. Bone histological terminology follows Francillon-Vieillot et al. (1990) and Shelton et al. (2013).

Most slides are reposited at the IPBSH. Additionally, thin sections of all OMNH material are reposited at that institution.

3.5 Standard measurements

It is common practice to perform morphometric analysis of the individual bone being sampled preceding any histological work to procure the raw data before the bone is damaged in anyway (e.g., Sander & Klein, 2005; Sander et al., 2006; Klein & Sander, 2007). Total length and minimal diaphysis circumference was recorded for each bone using standard analytical calipers and a metric measuring tape (Table 1). Length was taken as the total distance between the

termination of the proximal and distal ends. Circumference was taken at the mid-diaphysis (see Fig. 3).

The limb length disparity (LLD) ratio (Kemp, 1987; Felice & Angielczyk, 2014), specifically femur length divided by humerus length (femur/humerus), was calculated from combined data measurements of *Ophiacodon.* These data were obtained from the literature (Romer & Price, 1940) and combined with measurements taken by the authors from specimens of different localities in the collections of the CFM, MCZ, and AMNH (Table 2).

We have reproduced and modified Brinkman's (1988) "Figure 7" (Fig. 2). The cut bones from RSC have been labeled, as well as a newly excavated BCBB humerus, ISBPH-62, were incorporated into the modified figure (Fig. 2). The remaining data points in figure 2 cannot be labeled because Brinkman (1988) does not identify the exact specimens used in the original study.

Table 2 Specimens used to calculate femur/humerus ratio 1.2

Specimen ID	Femur Length (mm)	Humerus Length (mm)	Ratio	*Ophiacodon* (sp)	Notes
WM-454	125	107	1.17	*Ophiacodon hilli*	Romer & Price 1940
WM-671	125	102	1.23	*Ophiacodon mirus*	Romer & Price 1940
UMMP-UC-241	102	84	1.21	*Ophiacodon mirus*	Measured by C. Shelton
UMMP-UC-241	106	84	1.26	*Ophiacodon mirus*	Measured by C. Shelton
UMMP-UC-671	117	111	1.05	*Ophiacodon mirus*	Measured by C. Shelton
UMMP-UC-671	122	108	1.13	*Ophiacodon mirus*	Measured by C. Shelton
UR-632	82	64	1.28	*Ophiacodon mirus*	Measured by C. Shelton
AM-4777	119	101	1.18	*Ophiacodon navajovicus*	Romer & Price 1940
WM-458	167	130	1.28	*Ophiacodon retroversus*	Romer & Price 1940
YP-1103	135	117	1.15	*Ophiacodon retroversus*	Measured by C. Shelton
MCZ-1121	149	130	1.15	*Ophiacodon retroversus*	Romer & Price 1940
MCZ-1121	149	120	1.24	*Ophiacodon retroversus*	Measured by C. Shelton
MCZ-1121	151	127	1.19	*Ophiacodon retroversus*	Measured by C. Shelton
MCZ-1121	144	127	1.13	*Ophiacodon retroversus*	Measured by C. Shelton
UMMP-UC-458	164	140	1.17	*Ophiacodon retroversus*	Measured by C. Shelton
WM-690	115	103	1.12	*Ophiacodon uniformis*	Romer & Price 1940
MCZ-1366	121	85	1.42	*Ophiacodon uniformis*	Romer & Price 1940
MCZ-1366	123	95	1.29	*Ophiacodon uniformis*	Measured by C. Shelton
MCZ-1366	119	95	1.25	*Ophiacodon uniformis*	Measured by C. Shelton

3.6 Growth Model

The Brinkman humeral growth series (Fig. 1) was subject to growth modeling. Each cross section was hand drawn with a camera Lucida and then traced onto clear translucent sheets. Subsequent overlays were correlated by matching cycle boundaries of successive MOS. This allowed for age estimates of the individual specimens at time of death, and the results are quantified by using a growth curve (Fig. 5). This method is similar to that figured by Bybee, Lee & Lamm (2006).

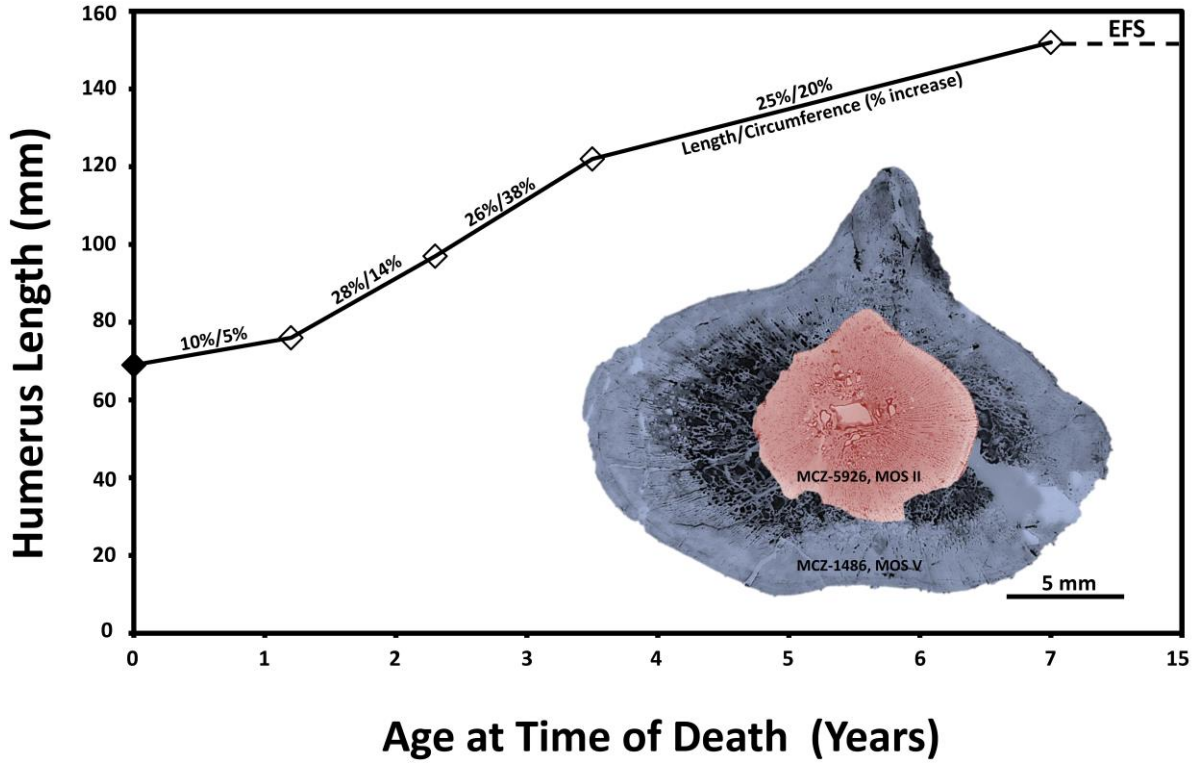

Figure 5 *Ophiacodon retroversus* growth curve, with specimens representing each MOS, was visualized by plotting overall bone length and individual age at time of death for each humerus. Age was calculated by correlating subsequent overlays of each MOS and matching successive cycle boundaries resulting in an asymptotic growth curve. MCZ-1435 (MOS I) was included as the earliest morphological stage of the ontogenetic series; however, it was not permitted for sectioning. This humerus is represented by a black diamond and assumed to be from a young organism that died shortly after hatching. All other humeri represented by white diamonds were sectioned and recorded in Table 1. Included here is the percentage increase of length and minimal diaphysis circumference between each successive MOS. Length seems to increase steadily throughout ontogeny, but circumference increases quite rapidly peaking at 38 percent between

MOS III and MOS IV. MCZ-2819 (MOS II) is a humerus from an individual that died shortly after completing its first life cycle marked by an annulus. The neonatal line (NL) is still visible in the deep cortex, but it is not present in any other MOS. MCZ-5926 (MOS V) contains many LAGs but no annuli, which correspond to the slowed growth. This is also evident by the reduction of vascularization and the presence of an external fundamental system (EFS) in the outermost cortex. The EFS indicates this individual had reached skeletal maturity and lived at least another eight years. Compared to *Dimetrodon* (See Shelton et al. 2013), *Ophiacodon* grew faster and reached skeletal maturity sooner, but had the same life expectancy.

4. Results

4.3 Morphometry

Length and circumference data for each bone used in this study is compiled in Table 1. The average length to circumference (L/C) ratio of the sampled *Ophiacodon* humeri was 1.96 and for the femora was 1.91 (Table 1). However, the stage five L/C ratio of humeri from RSC (MCZ-1486) is different from the L/C ratio of BCBB (IPBSH-62). MCZ-1486 is 152 mm in length and 83 mm in circumference with a ratio of 1.83 (Table 1). IPBSH-62 is 82 mm in length and 37 mm in circumference with a ratio of 2.22. The RSC humerus is 46% longer and the circumference is 55% larger than the BCBB humerus.

The average LLD ratio for *Ophiacodon* humeri and femora is 1.20 (Table 2). Estimated lengths for the missing partner limbs have been calculated by multiplying the humeri length by the LLD ratio, and dividing the femora length by the LLD ratio (Table 1). Most striking is the corresponding measurements of the smallest femur and humerus. However, with an increase in size comes an increase in error; corresponding sizes for the largest humerus and femur were off by at least four centimeters (see Table 1). It is unlikely the bones would have grown this much further in length after reaching skeletal maturity. Measurements of additional articulated specimens will better refine this ratio.

4.4 Growth model

Growth mark count and age estimate for each of the four *O. retroversus* humeri used by Brinkman (1988) have been recorded in Table 1. The first fully completed growth cycle is still visible in the smallest humerus sampled (MCZ-5926; MOS II) (Fig. 6C). This is the area between

the neonatal line (NL) and the first growth mark in the outermost cortex. We have estimated that this growth series represents seven years of growth between the time of hatching and the year skeletal maturity was achieved. At least another eight cycles were visible in the external fundamental system (EFS) of MCZ-1486 (See Fig. 9B). This means that *Ophiacodon* grew substantially for half of its life. The estimated total lifespan represented by this growth series is at least 16 years. However, due to preservation and shape discrepancies observed throughout humerus ontogeny, a proper figure using the Bybee, Lee & Lamm (2006) method to estimate age of the growth series was not possible. However, this method revealed a discrepancy between MOS IV (MCZ-4816) and MOS V (MCZ-1486) because of the uncertain matching of the fourth cycle in MOS IV, which had not yet been reached, and the third cycle boundary in MOS V, which is assumed to have been resorbed. This allows for at least a one year margin of error. The time represented by Brinkman's (1988) *O. retroversus* growth series (Fig. 1) correlates with the growth record preserved in some of the *Ophiacodon* femur (MSU specimen and OMNH-35389) (see Figs. 14 & 15).

4.5 *Ophiacodon* humerus histology

The histology of all transversely sectioned humeri (Table 1) is described below by increasing MOS. All histology is described from the mid-diaphysis bisecting the triceps muscle insertion, a prominent feature amongst *Ophiacodon* (Romer, 1969) (Figs. 1 & 3).

4.5.1 Brinkman's ontogenetic series of RSC O. retroversus

4.5.1.1 Morphological ontogenetic stage II

MCZ-5926 (MOS II; Fig. 2) is a right humerus, 76.23 mm in length (S.I. 1A) with unossified epiphyses exhibiting calcified matrix vesicles (Fig. 6B) that functioned to transport hydroxyapatite crystals to facilitate the ossification of the hypertrophic cartilage (Anderson, 1969; Hall, 2005; Nair & Jagannathan, 2013), and a smooth cortical surface. In thin section, the mid-shaft cortex is relatively thick and consists of parallel-fibered bone (PFB) and woven bone (WB), prevalent dorsally and ventrally. Vascularization in the cortex is dense and consists of longitudinal and radial canals. In the dorsal and ventral regions of the outermost cortex, anastomosis is strongest between the longitudinal canals making the vascularity more of a

reticular pattern in this area. The overall radial organization of the canals gives the cortical bone a "bicycle wheel" pattern (Fig. 6C & D). The vascular canals have varying degrees of lamellar bone (LB) infilling. Some have none while others are immature to fully formed primary osteons (Fig. 6E & F). Osteocyte lacunae (OL) are plump to sub-angular and appear to be randomly oriented in between the osteons, while others that follow the circumferential layering of the LB are flat.

The cortical bone contains a record of growth. Most notable is the division of the cortex by the neonatal line (NL) (Fig. 6A & C). This indicates the time when the animal hatched and appears as an annulus with three corresponding lines of arrested growth (LAGs), indicating a period where much energy was spent. In this specimen, we refer to the postnatal area beyond the NL as the outer cortex, and the prenatal area inside the NL towards the medullary margin, the innermost cortex (Fig. 6C). The width of the vascular canals below the NL appears to be slightly larger than most in the outer cortex. Two smaller lines of slowed growth can be seen within the prenatal area of embryonic bone in proximity to the boundary of the medullary cavity. This obviously formed while the animal was *in ovo* (Sander, 2012), but the significance of this growth mark is unknown. One true LAG appears near the outer bone surface approximately 3000 µm beyond the NL (Table 1). Sharpey's fibers (SF) were not observed. This animal died very shortly after completing its first life cycle (Fig. 5).

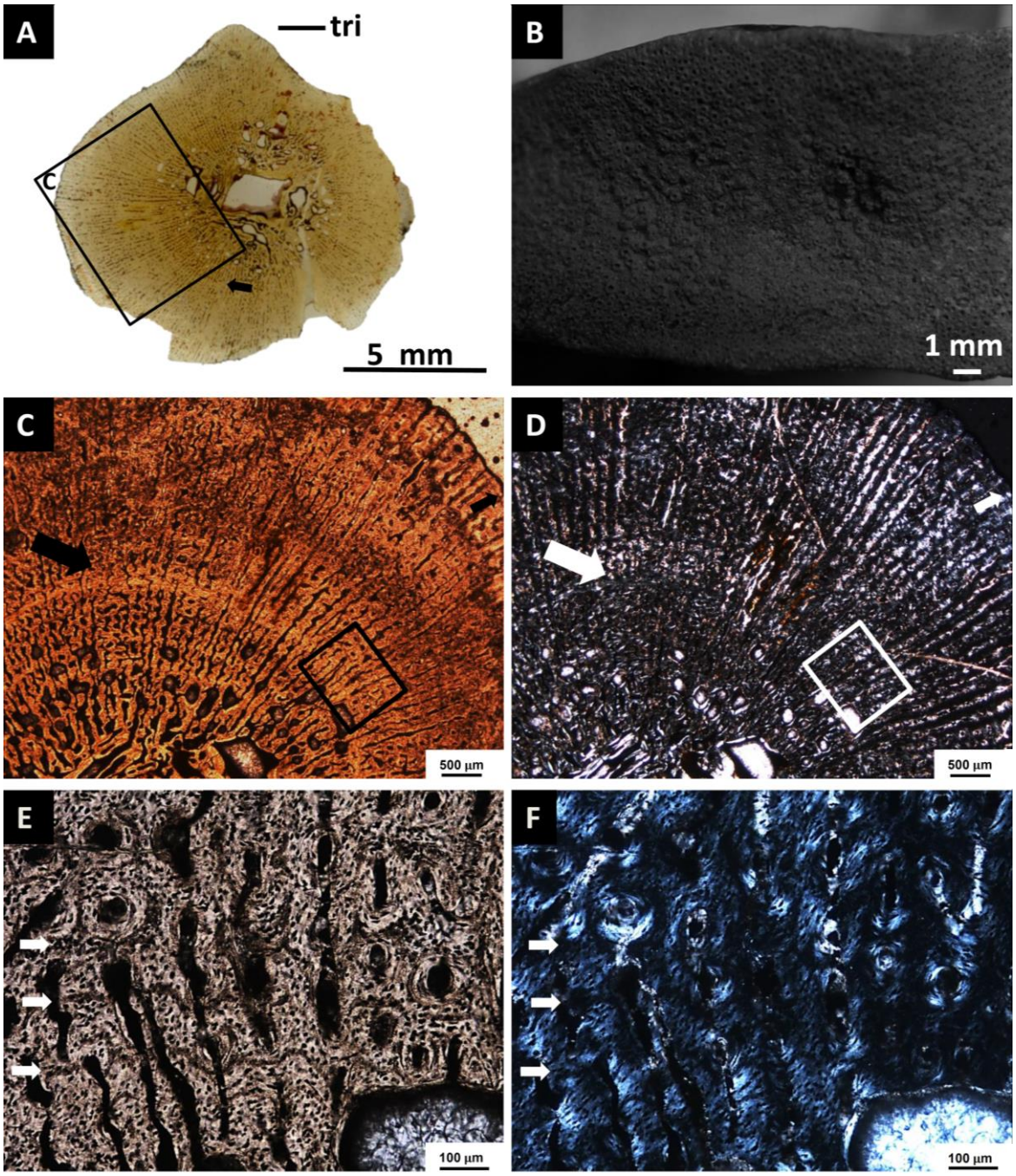

Figure 6 Humerus MCZ-5926, MOS II, *O. retroversus*. A) Scan of transverse section through the mid-diaphysis in normal light. Notice the "bicycle wheel" pattern formed by the radial arrangement of the vascular canals. Note that the radial canals are in the plane of section and extend from the medullary cavity to the outer cortex. The medullary cavity is occluded with mostly secondary (some primary) trabeculae, and erosional cavities (EC) are present in the medullary margin area. Note that EC do not extend past the neonatal line (NL) (indicated by

arrow), which is a line of slowed growth marking the time of hatching and is the boundary between the prenatal embryonic bone below, and the postnatal periosteal bone above. Also, the size of the vascular canals is larger in the prenatal area and smaller beyond the NL in the postnatal area. B) Close-up of the distal epiphysis with exposed calcified matrix vesicles. These allowed for the deposition of hydroxyapatite crystals during the ossification process of the hypertrophic cartilage. C) Microscopic image of the mid-diaphysis cortex viewed in conventional transmitted light magnified from an area marked by a box in (A). Arrow indicates the NL and associated growth marks. These smaller growth marks within the prenatal embryonic bone just beyond the medullary cavity. This line formed while the animal was *in ovo,* but the significance of this growth mark is unknown. D) Same view as (C) but in polarized transmitted light. Vascular canals can be viewed better in polarized light. Clearly the "bicycle wheel" pattern is very prominent given the extinction pattern of the lamellar bone infilling. Also, EC are clearly distinguishable. Parallel-fibered and woven-bone matrix are found throughout the cortex. The arrow indicates the position of the NL. E) Microscopic close-up of the NL indicated by the boxed area in (C) in conventional transmitted light. Notice the three parallel closely spaced growth marks within the NL (indicated by arrows). At MOS II, EC have not yet crossed the NL. Note the shape of the OL are large plump and very dense F) Same view as (E) but in polarized transmitted light. Notice the mix of incipient and fully primary osteons set in a woven-bone matrix is present in between the longitudinal vascular canals, thus forming fibro-lamellar bone. Abbreviation: tri= triceps muscle insertion.

The medullary region is distinguished from the cortex by small to medium-sized erosional cavities (EC), some of which are lined by a thin layer of lamellar bone (ECL) that extend into the inner cortex but do not go beyond the NL. Endosteal lamellar bone is present in the form of primary, but mostly secondary, trabecular bone in the medullary cavity. By definition (Francillon-Vieillot et al., 1990), the combination of primary osteons set in a woven bone matrix identifies this tissue as fibro-lamellar bone (FLB).

4.5.1.2 Morphological ontogenetic stage III

MCZ-2819 (MOS III; Fig. 2) is a left humerus, 97.22 mm in length with unossified epiphyses (S.I. 1B). The calcified matrix vesicles (first observed in MCZ-5926 MOS II) are only

visible as darkened rings on the proximal articular surface (not pictured). The outer surface of the bone is also smooth. In the transverse thin section, PFB is prevalent on the posterodorsal side, as well as in the outermost cortex at the triceps muscle attachment. WB is seen throughout the cortex, especially surrounding the vascular canals. Vascularity consists of small longitudinal canals from the mid to outer cortex and the "bicycle wheel" pattern persists. In the deeper cortex, vascularity is more radial and canals are more open (Fig. 7C). The vascular canals have varying degrees of LB infilling; they are immature to fully formed primary osteons (Fig. 7B). OL are plump to sub-angular as well as flat and oriented parallel to the bone surface in the "slower" growing areas.

The cortical bone contains two cycle boundaries (Table 1) marked by annuli and corresponding growth marks, and they are visible in the darkly stained areas of the outer cortex (Fig. 7A). The NL is no longer visible as it has been removed by the resorption front. SF are located mostly on the anterior side and visible at the triceps muscle attachment (Fig. 7B). By correlating the earliest annulus with the first life cycle boundary of MCZ-5926; this animal is estimated to have died shortly after completing its second life cycle (Fig. 5).

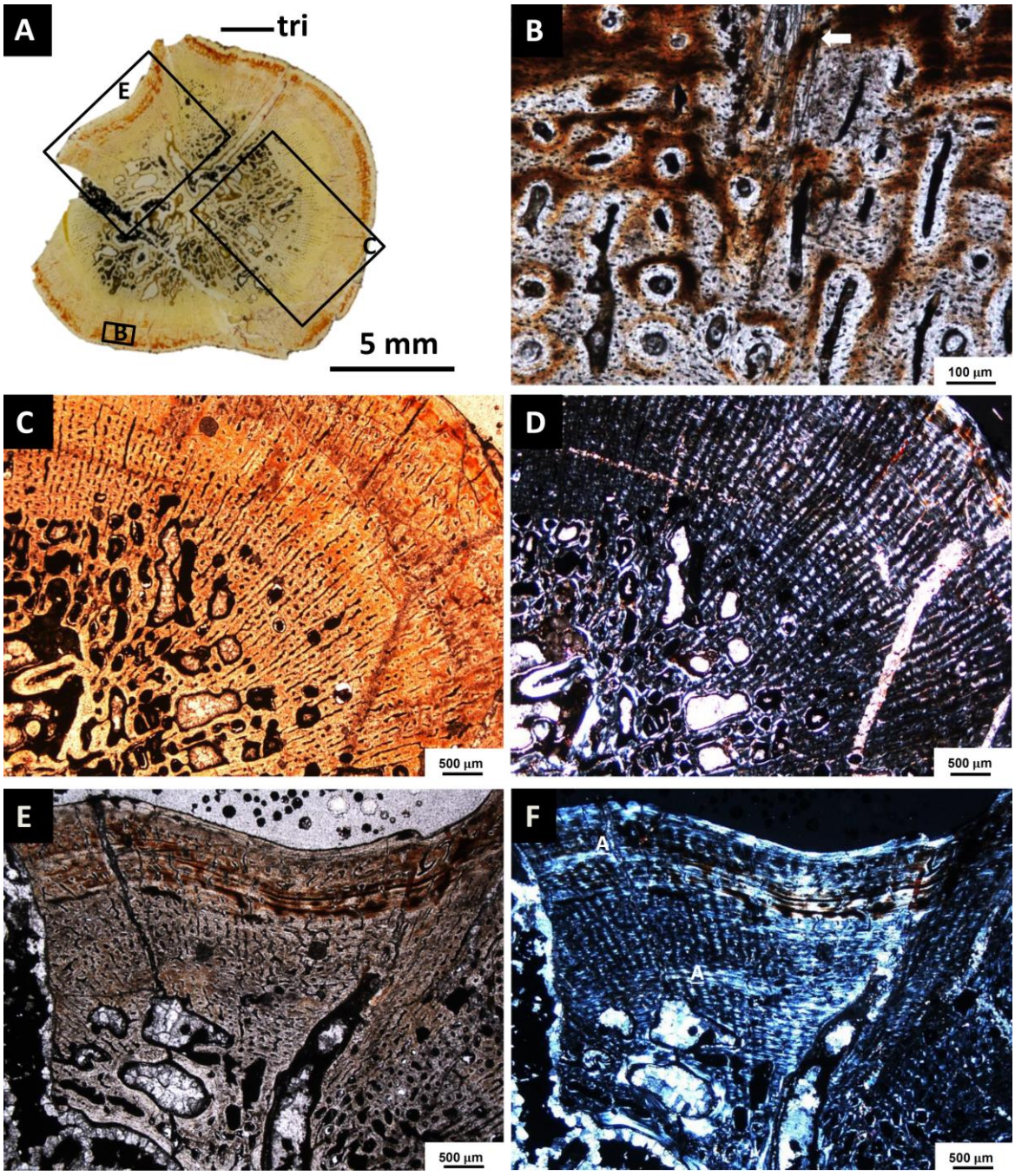

Figure 7 MCZ-2819, MOS III, *O. retroversus* humerus. A) Scan of transverse section through the mid-diaphysis in normal light. The NL has been completely resorbed as the medullary cavity has expanded. Radial and longitudinal vascular canals remain consistent with the "bicycle wheel" pattern. The EC have greatly increased throughout the medullary margin. Growth marks are preserved in the darkly iron-stained areas of the cortex. B) Magnified microscopic image of the outer cortex in conventional transmitted light. Arrow is pointing to Sharpey's fibers. These are

found in the cortex of the humeri from MOS III to MOS V. C) Microscopic view of the mid-diaphysis cortex in conventional transmitted light. Note the expansion of the medullary cavity has additionally erased all trace of the prenatal bone. Also, the vascular canals appear to decrease in size towards the outer cortex. D) Same view as (C) but in polarized transmitted light. The appearance the "bicycle wheel" pattern is better visible given the extinction pattern of the lamellar bone infilling in contrast to the WB matrix. E) Microscopic view of the outer cortex in conventional transmitted light. The darker iron-staining preserved growth marks just below the cortical surface marking the second growth cycle in the *Ophiacodon* humeral growth series. F) Same view as (E) in polarized transmitted light. Note the inner annulus of the first year growth cycle. Also the annulus corresponding with the visible growth marks in (E) marking the second year growth cycle. Abbreviations: A= annulus; tri= triceps muscle insertion.

The medullary cavity is occluded by a network of secondary trabeculae. ECL are abundant having formed by expansion of the medullary cavity by resorption activity of the osteoclasts, altering the pre- and neonatal areas observed in humerus MCZ-5926 (Fig. 6). Small to medium-sized ECs mark the outer most boundary of the medullary region (Fig. 7C & D).

4.5.1.3 Morphological ontogenetic stage IV

MCZ-4816 (MOS IV; Fig. 2) consists of a pair of associated humeri that presumably came from the same individual (S.I. 1C & D). Both are damaged at the mid-diaphysis and one is encrusted with a hematitic or limonitic matrix, which incorporates small bones from another animal (Fig. 8A & B). The two humeri themselves look yellowed and weathered with a worn surface. Epiphyses look roughened and black. The left humerus, which was figured by Brinkman (1988), has a length of 122.06 mm. The right humerus is 124.61 mm in length. Histology of the two humeri is identical and will be described together. Unfortunately, preservation of the histology is not optimal (Fig. 8C & E); most of this histological detail has been lost due to the effects of weathering and diagenesis. Diagenetic staining has darkened the tissue, making LAGs, OL, and even bone matrix nearly impossible to distinguish. LB can still be seen infilling some of the vascular canals. However, immature or fully formed primary osteons cannot be differentiated (Fig. 8E & F); the canals appear ragged and degraded due to their taphonomic situation (Fig. 8C).

The “bicycle wheel” vascularity pattern is still visible in the cortex (Fig. 8D). PFB is distinguishable in some patchy areas. WB could not be observed. Vascularity appears to consist of small densely concentrated radial and longitudinal canals. The outermost cortex has even thinner radial canals.

The preserved growth record consists of two cycle boundaries (Table 1) marked by annuli within the medullary region and inner cortex, mostly visible only in polarized light (Fig 8D). By correlating the earliest annulus with the second life cycle boundary of MCZ-2819, this animal is estimated to have died between the third and fourth life cycle (Fig. 5). Note that both humeri do share the same growth record reaffirming they are from the same organism.

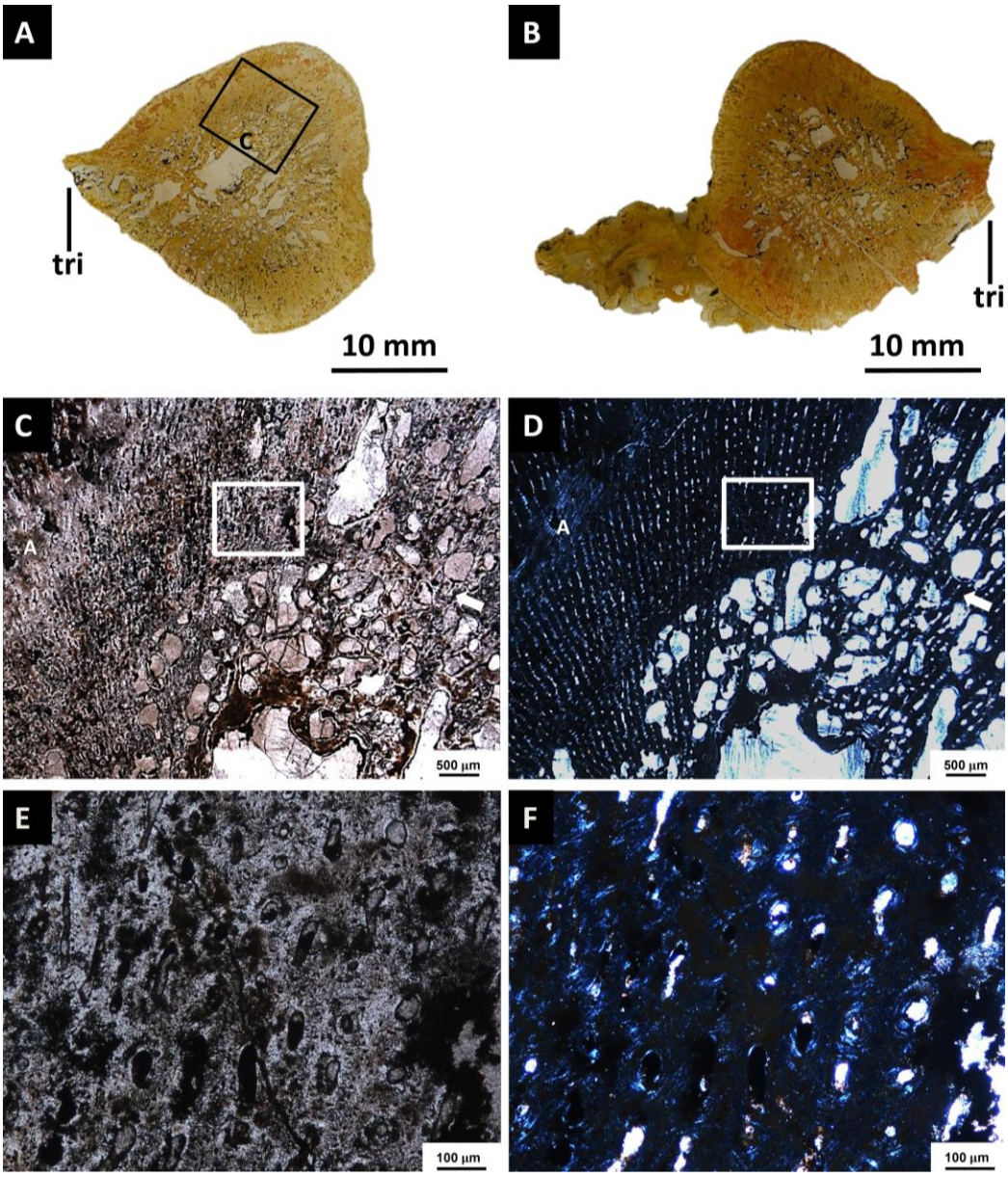

Figure 8 MCZ-4816, left and right humerus of a MOS IV *O. retroversus* individual. Both of these bones have been affected by physical and chemical weathering. A) Scan of the transverse section through the mid-diaphysis of the left humerus. Mid-shaft is damaged. The cortical bone is thinner and the EC are much larger, stretching across the cortex. The radial arrangement of vascular canals is seen even in the bone last deposited. B) Scan of the transverse section through the mid-diaphysis of the right humerus. This bone was also incrusted with hematitic or limonitic matrix that incorporated long thin bones from another animal (visible on the left). Mid-shaft is also damaged. C) Microscopic view of the mid-diaphysis cortex as indicated by the boxed area in

(A) in conventional transmitted light. The EC appear to be following the pattern of the vascular canals. As the EC develop, they isolate areas of primary cortex that are being incorporated as trabeculae in the medullary cavity and are bounded by LB. D) Same view as (C) but in polarized transmitted light. The interstitial cortical bone is better visible in polarized light. But because of the poor taphonomy, the polarized light gives a false positive for WB as most of the affected matrix remains dark due to the alteration of the crystallites. This has caused areas of PFB and most areas of LB to be obscured. Arrow marks the second year cycle boundary that was resistant to resorption. Also, the third year cycle is visible as a thick annulus in the middle cortex marked by "A". E) Magnified view of the cortex indicated by the boxed area (C), in conventional transmitted light. The bone matrix is obscured by taphonomic staining rendering proper identification of the specific type of bone matrix difficult; however, it is most likely WB and PFB. F) Same view as in (E) but in polarized transmitted light. Also, most of the LB seen in the primary osteons has been masked as the extinction pattern has been affected by the taphonomy. Abbreviations: A= annulus; tri= triceps muscle insertion.

The medullary margin consists mainly of large ECs stretching into the cortex as they appear to follow the orientation of the vascular network. Interstitial primary cortical bone is incorporated as trabeculae due to the formation of large and small ECL (Fig. 8C & D).

4.5.1.4 Morphological ontogenetic stage V

MCZ-1486 (MOS V; Fig. 2) is a right humerus 152 mm in length with fully ossified epiphyses (S.I. 1E). The outer surface is smooth with a high amount of rugosity in the epiphyses. In the midshaft thin section the cortical bone is very thin (Fig. 9A & C) and vascularized by radial and longitudinal canals radially arranged, again forming the "bicycle wheel" pattern in the cortex (Fig. 9C, D, E). WB is concentrated in the dorsal and posterior areas. PFB is seen throughout the cortex. Blackened SF appear in the anterior region. OL are smaller and more angular than in MCZ-2819. Primary and, rarely, secondary osteons are observed in the deep cortex (Fig. 9F)

The cortical bone contains a growth record consisting of four zones separated by four LAGs (Table 1), as well as an external fundamental system (EFS) in the outer cortex (Fig. 9B, C, D, E). The EFS itself represents at least eight years of growth and is clearly visible in this specimen (Fig. 9B). Correlating with the size and growth cycles of MCZ-4816, in addition to the

record contained in the EFS, this animal lived at least 16 years (Fig. 5). The reduction of vascularity in this region and the presence of the EFS unequivocally indicate that the animal was sexually mature and had begun to slow down in skeletal growth. The zones are heavily vascularized by small longitudinal canals that consist of primary osteons. The zone preceding the EFS has a reduced vascularity and consists of very thin radial canals with almost no LB infilling (Fig. 9D).

The medullary region has nearly reached the surface. ECs as well as ECL persist throughout most of the bone forming trabeculae of interstitial primary cortical bone (Fig. 9F).

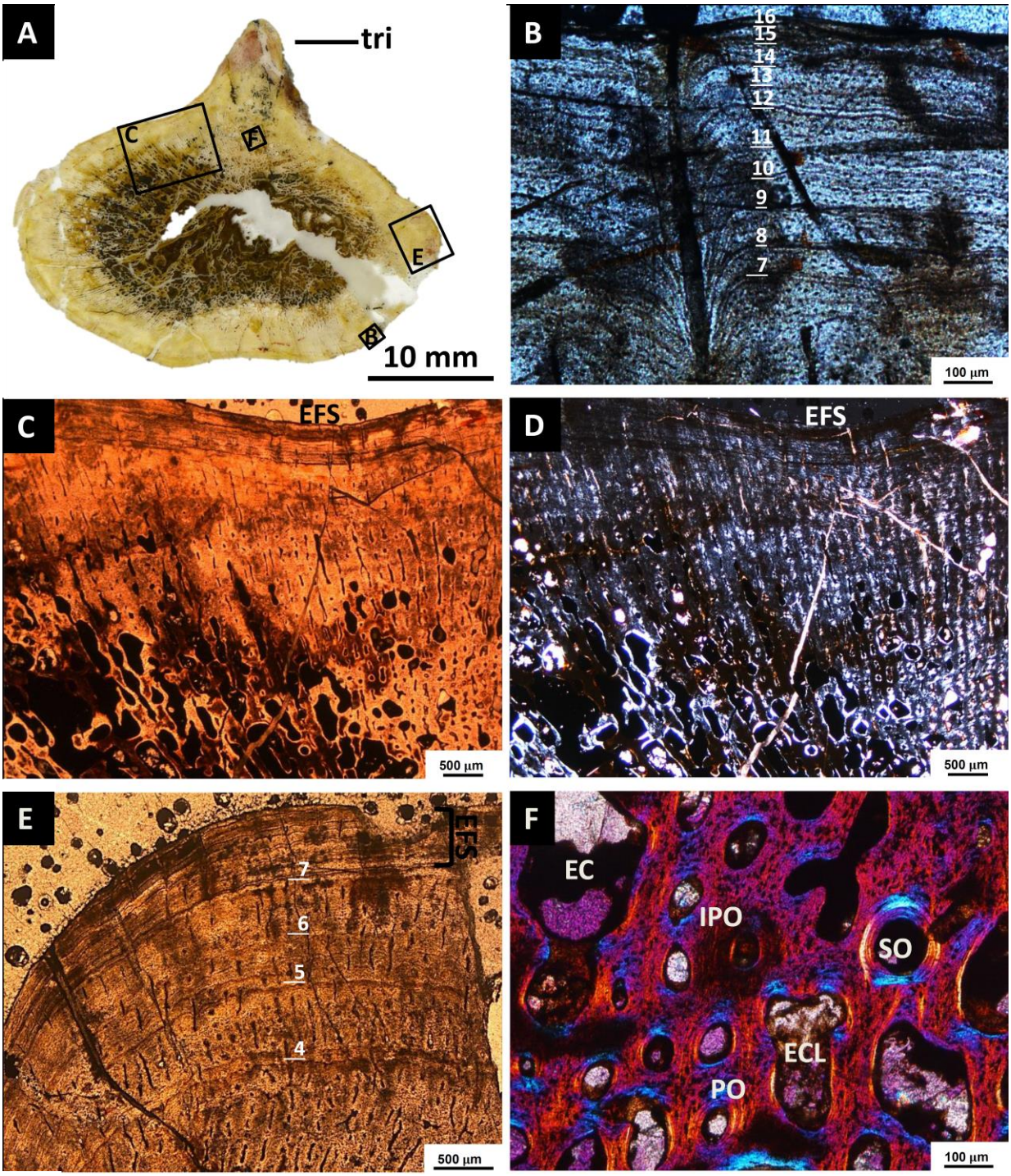

Figure 9 MCZ-1486, MOS V, *O. retroversus* humerus. A) Scan of the transverse section through the mid-diaphysis. Overall shape of this section is affected by the triceps muscle insertion, which is extremely exaggerated in growth indicating a very powerful muscle attachment point. Vascularity is highly reduced in the outer cortex but still maintains the "bicycle wheel" pattern of

longitudinal and radial canals. True LAGs are visible in the outer cortex. Skeletal maturity of this specimen has been reached as is indicated by the EFS. B) Magnified microscopic view of the boxed area in (A) of the EFS in conventional transmitted light. Vascularity is highly reduced. The bone matrix in this area is PFB. At least eight additional growth cycles are visible within the EFS itself. C) Microscopic view of the mid-diaphysis cortex in conventional transmitted light. While retaining a radial orientation, the vascularity diminishes from the medullary cavity to the outer cortex where it is almost nonexistent in the EFS. ECs have not yet reached the outer cortex, but they seem to be following the same pattern incorporating interstitial primary cortex as trabeculae. D) Same view as (C) in polarized transmitted light. The diminishing vascularity is better observed in this light. ECs are lined by a thin layer of LB. E) Microscopic view of the outer cortex as indicated by the boxed area in (A) in conventional transmitted light. The growth record preserved here consists of four LAGs. The oldest LAG matches with the fourth cycle boundary established in MCZ-4816, MOS IV. Note that most of these are double LAGs. Skeletal maturity was reached after the seventh life cycle. F) Magnified microscopic view of boxed area indicated in (A) in polarized transmitted light through a lambda filter. This area is just beneath the triceps muscle insertion. Primary woven cortex is still visible and OSL are large and densely concentrated. Abbreviations: EC= erosional cavity; EFS= external fundamental system; IPO= incipient primary osteons; PO= primary osteons; ECL= erosional cavity with a thin lining of lamellar bone; SO= secondary osteon; tri= triceps muscle insertion.

4.5.2 IPBSH-62, O. uniformis

IPBSH-62 (MOS V; Fig. 2) is a left humerus 82 mm in length (S.I. 1F). The cortex consists of WB and PFB. Vascularity consists of radial and longitudinal canals exhibiting anastomosis (Fig. 10E). Immature and fully formed primary osteons are present in the outer cortex (Fig. 10E & F). Primary osteons and the more rare secondary osteons are observed in the deeper cortex. Interstitial primary cortical bone remains in the medullary margin as secondary trabeculae similar to what is observed in MCZ-4816 (Fig. 10A & B). Vascularity is more radial in the deeper cortex whereas the vascular canals near the cortical surface are more longitudinal (Fig. 10C). OL are plump to sub-angular in the areas with WB and more flat and oriented parallel

to the cortical surface in the areas with PFB. There are very few SF, and those are only visible under polarized light (Fig. 10F).

Three annuli are visible in the mid to upper cortex (Fig. 10D). Two LAGs are visible and correspond with the two deepest annuli (Fig. 10C & D). The earliest LAG is essentially the boundary between the medullary region and the cortex (Fig. 10C & F) as ECs do not extend beyond this area. The other LAG is within the annulus that divides the outer cortex into two zones. Thick LB lines the largest ECs in the center of the bone. The histology described here is similar to that described in MCZ-4816 (MOS IV) (Fig. 2).

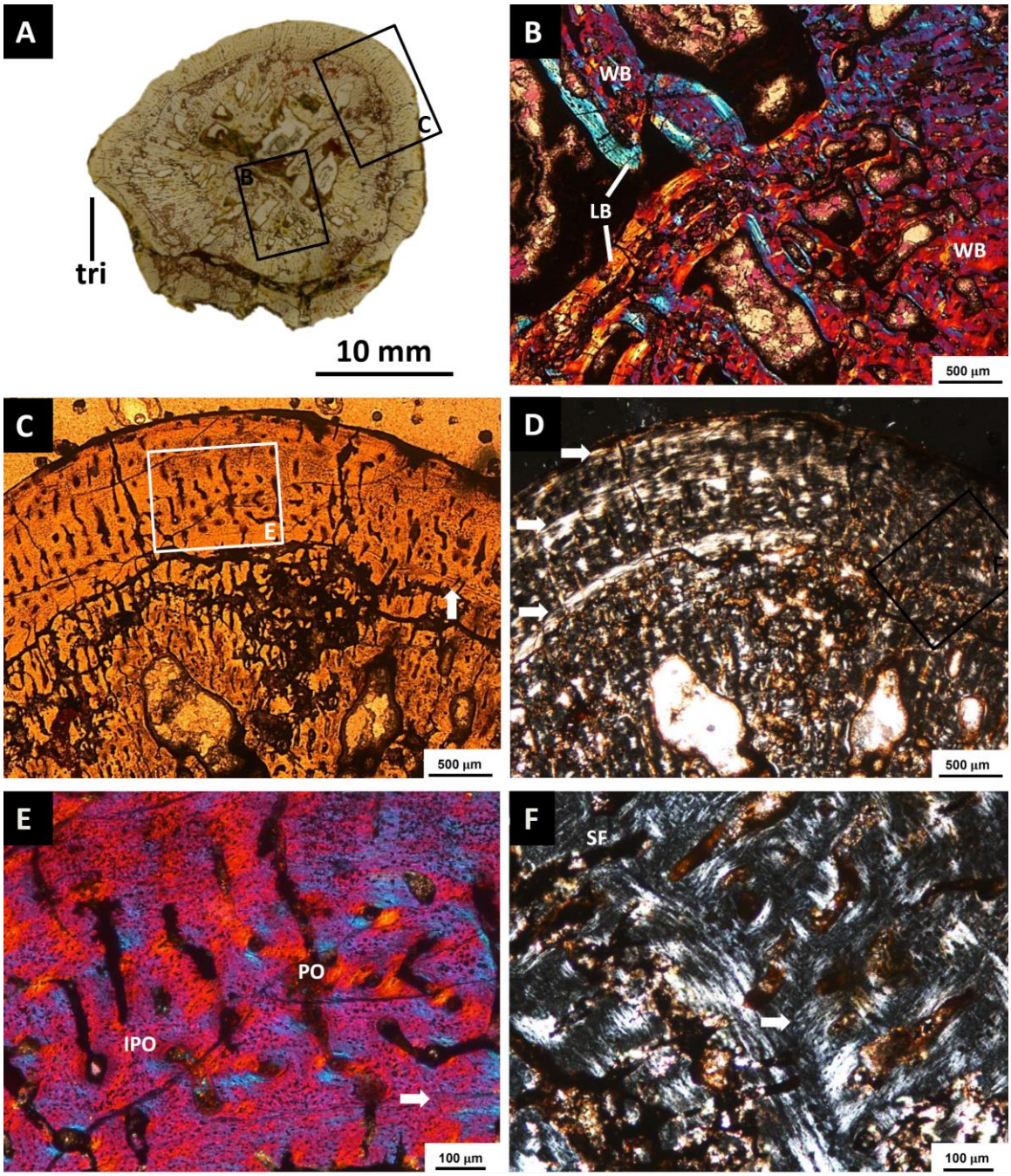

Figure 10 IPBSH-62 MOS V, *O. uniformis* humerus. A) Scan of the transverse section through the mid-diaphysis. The triceps muscle insertion is much smaller at this stage than what is seen in *O. retroversus*. ECs are in the mid to lower cortex but do not yet cross the LAG. Histology is similar to what was described in MCZ- 4816. This individual died before reaching skeletal maturity as the EFS is not present. B) Magnified microscopic view of boxed area indicated in (A) viewed through in polarized transmitted light through a lambda filter. Large areas of

interstitial primary cortex of WB are being incorporated as secondary trabecular bone bound by LB. Primary osteons are present here in the oldest areas of the cortex. C) Microscopic view of the boxed area in (A) in conventional transmitted light. The "bicycle wheel" pattern is present in the cortex, consisting of radial and longitudinal canals with a varying degree of anastomosis. Arrow is pointing to the LAG. D) Same view as (C) in polarized transmitted light. Arrows indicate the corresponding annuli. E) Magnified microscopic view of boxed area indicated in (C) viewed in polarized transmitted light through a lambda filter. Note the combination of both Incipient and primary osteons. Arrow is pointing to the LAG. F) Magnified microscopic view of boxed area in (C) in polarized transmitted light. Arrows indicates Sharpey's fibers and the LAG. Overall the cortical matrix consists of WB. Abbreviations: A= annulus; IPO=incipient primary osteon; PO= primary osteons; tri= triceps muscle insertion; Z= zone.

4.5.3 OMNH-73698 core Ophiacodon (sp)

OMNH-73698 (MOS V) is a right humerus 113 mm in length (S.I. 1G). The histology described here is from a core drilled through the dorsal and ventral sides of the midshaft closer to the proximal metaphysis (Fig. 11A).

The cortex is thin. Vascularity appears to be reduced consisting mainly of small primary osteons and thin radial canals. These are similar to what is seen in the outer cortex of MCZ-1486. The dorsal side is mostly PFB with flat OL oriented parallel to the bone surface and reduced vascularity (Fig. 11B). The ventral cortex is WB, and OL are large and round with a dense concentration of SF (Fig. 11C)

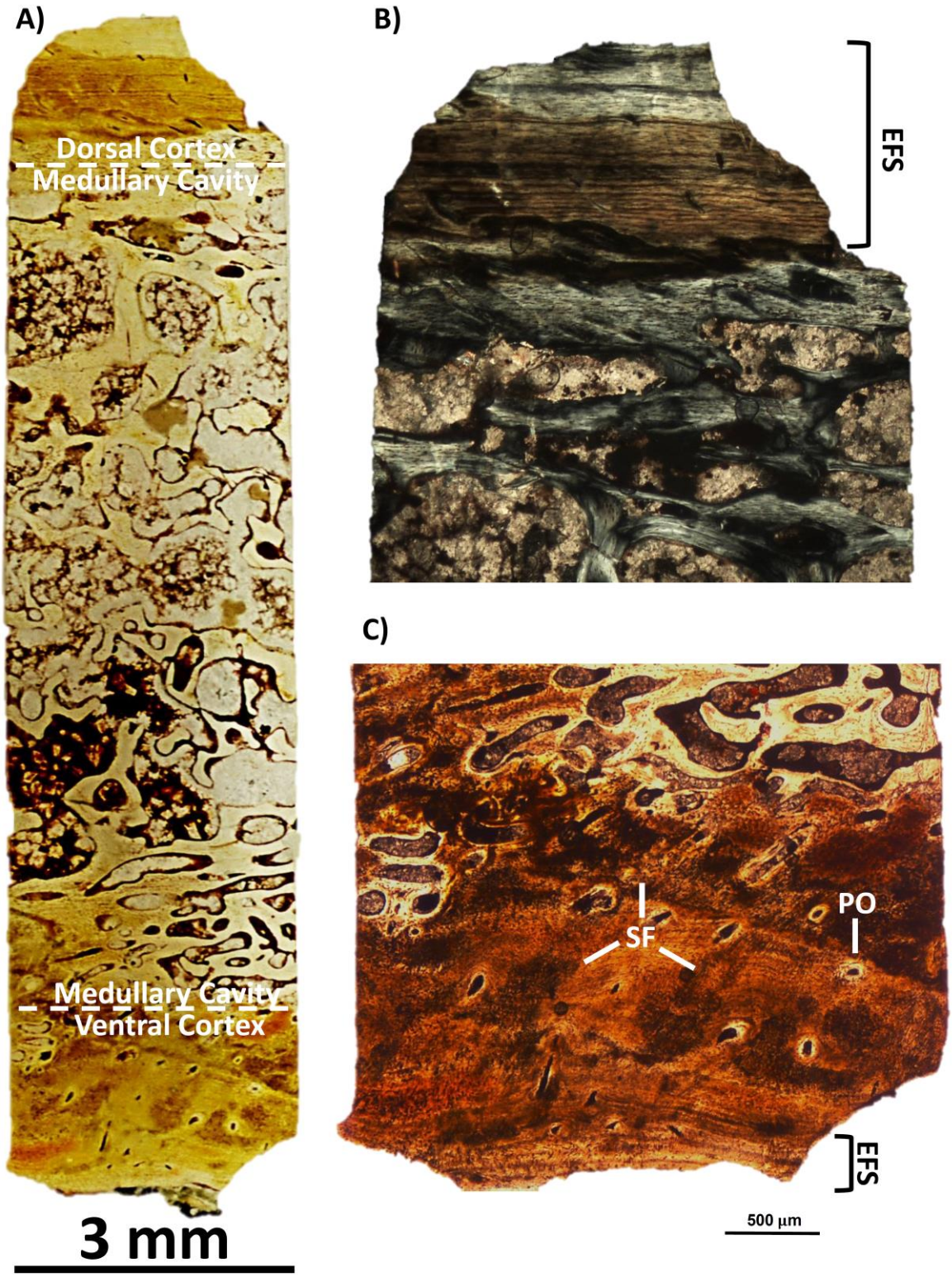

Figure 11 OMNH-73698, MOS V, *Ophiacodon* humerus. A) Scan of a transverse core section drilled through the dorsal and ventral sides of the diaphysis closer to the proximal metaphysis.

EFS can be seen in the cortex on the dorsal side. The cortex is thin and vascularity is highly reduced in the dorsal cortex. The ventral cortex contains small primary osteons and larger incipient osteons. Notice the vascular canals are smaller on the dorsal side and near the EFS. The resorption front is nearing the surface of the bone. The medullary cavity is highly occluded with secondary trabeculae. B) Microscopic view of the EFS in the dorsal cortex in polarized transmitted light. Osteocyte lacunae are flattened and oriented parallel to the cortical surface. The cortical bone matrix of the dorsal side is mostly PFB with a strong LB affinity. C) Magnified view of the ventral cortex in conventional transmitted light. This area is highly concentrated with Sharpey's fibers. Osteocyte lacunae are rounder and randomly oriented. The cortical bone matrix on the ventral side is WB. Abbreviations: EFS= external fundamental system; PO= primary osteon.

The cortical bone contains an EFS visible in the outermost cortex (Fig. 11B & C); no other growth marks are visible. The medullary cavity consists of secondary trabecular bone with very little interstitial primary cortical bone (Fig 11A). There are ECs and ECL in the medullary region that extend very close to the outer bone surface (Fig. 11B & C).

4.6 *Ophiacodon* femur histology

All *Ophiacodon* femora (Table 1) are described according to an increase in overall length of the specimens (Fig. 3). Overall shape of the cross section is affected by the development of the adductor crest.

4.6.1 IPBSH-46 Ophiacodon (sp)

IPBSH-46 is a right femur 78 mm in length with unossified epiphyses (S.I. 2A). This specimen is the smallest femur sampled. The outer surface is smooth. The bone is dorsoventrally crushed along the diaphysis (Fig. 12A) and distal end. Histology is similar to what is seen in MCZ-5926 (MOS II). The deep cortical bone consists of embryonic or prenatal bone that developed *in ovo* (Sander, 2012), which is mostly WB with large wide radial and longitudinal vascular canals (Fig. 12B & E). The onset of PFB in the midcortex marks the NL and is the boundary where the postnatal bone begins to develop (Fig. 12B & E). Just above this in the outermost cortex is the start of a zone of fast growth with a WB matrix and thin reticular vascular

canals. The nutrient canal is located in the dorsal region (Fig. 12A). It extends from the prenatal cortex and the MC to the outermost cortical layer (Fig. 12B). The periosteal bone is well vascularized in the outer cortex by longitudinal and reticular canals. The posterior region, where the adductor crest is located, consists mostly of radial canals (Fig. 12A & C). The vascular pattern is longitudinal and reticular in the postnatal area, but the vascularity of the prenatal area is more radial (Fig. 12E).

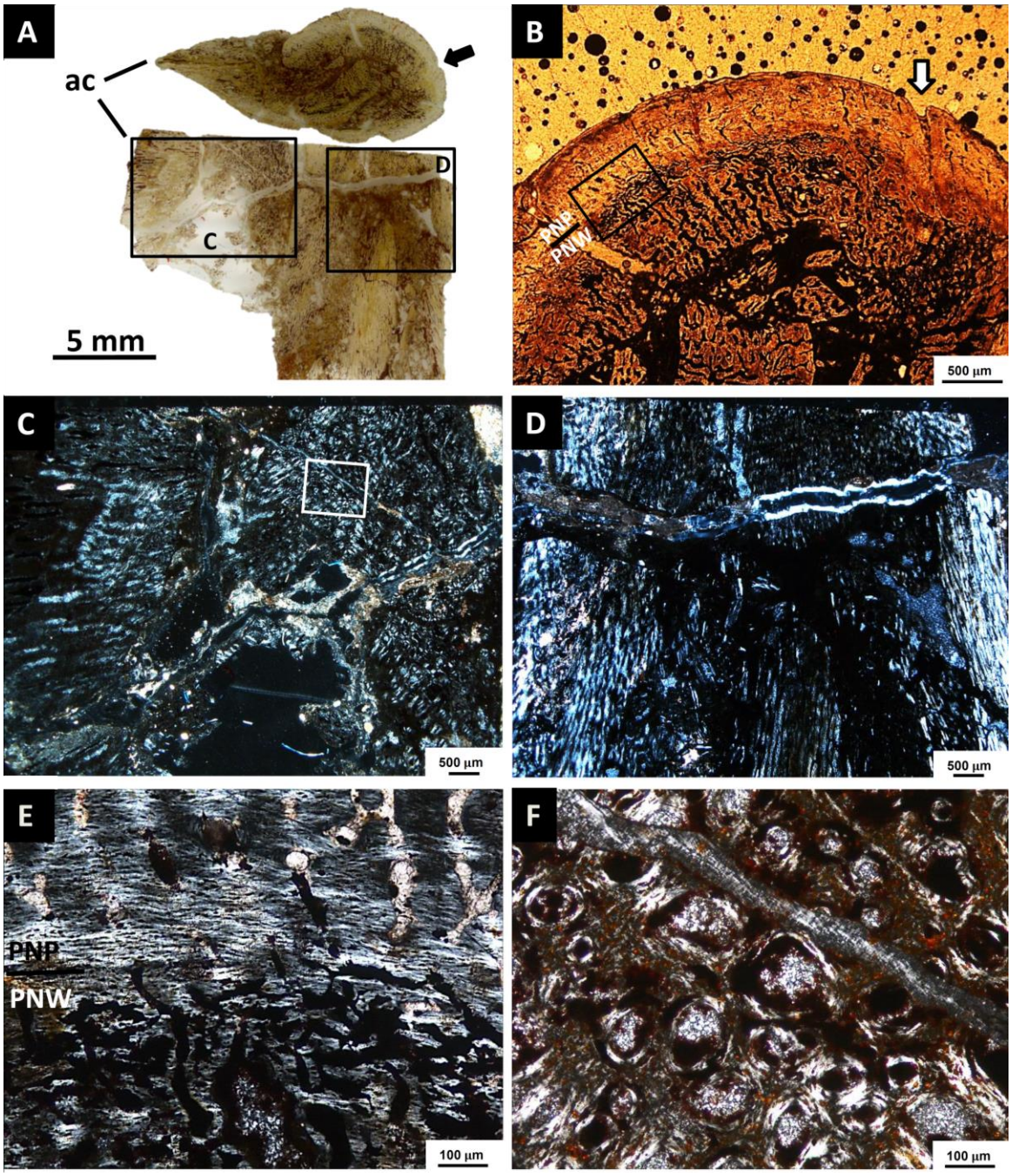

Figure 12 IPBSH-46 *Ophiacodon* femur 78 mm in length. A) Scan of the transverse (above) and longitudinal section (below) of the mid-diaphysis. Even though the mid-shaft is crushed, there is a marked distinction between the prenatal and postnatal cortex. Arrow indicates the nutrient canal on the dorsal side. B) Microscopic view of the dorsal cortex in conventional transmitted light. Arrow indicates the nutrient canal that extends into the prenatal cortex. Vascular canals in the prenatal bone are larger than those in the postnatal bone. Vascularity consists of longitudinal, radial and reticular canals. Vascularity in the deep prenatal cortex somewhat resembles the "bicycle wheel" pattern. However, this is not the case in the postnatal cortex as the vascularity is more reticular. This animal was within the first year of its life when it died. C) Microscopic view of boxed area in (A) of the longitudinally sectioned adductor crest in polarized transmitted light. Note the high concentrations of PO in the WB matrix. D) Microscopic view of boxed area in (A) of the longitudinally sectioned diaphysis in polarized transmitted light. E) Magnified microscopic view of boxed area in (B) in polarized transmitted light. Most striking is the sudden change from the PNW in the inner cortex and the PNP in the mid- to outer cortex. Incipient primary osteons are prevalent in the outer cortex. F) Magnified microscopic view of the boxed area in (C) in polarized transmitted light. Note the large primary osteons and OSL set within a WB matrix. This tissue is characteristic of embryonic fibro-lamellar bone. Abbreviations: ac= adductor crest; PNP= postnatal parallel-fibered bone; PNW= prenatal woven bone.

The vascular canals themselves have varying degrees of LB infilling in that most are incipient in the postnatal cortex, but there are many fully formed primary osteons in the prenatal areas (Fig. 12C & F). OL shape in postnatal WB are large and plump while those in the prenatal PFB are more flat and oriented parallel to the cortical surface. Overall tissue in the deep cortex reflects embryonic fibro-lamellar bone.

The growth record contained in the cortex indicates that the individual most likely died within the first year of its life, shortly after hatching (Fig. 12B). The MC is obscured due to deformation; trabecular bone is not evident, but a few small ECs appear around the medullary cavity (Fig. 12A).

4.6.2 OMNH-55234 O. mirus

OMNH-55234 is a broken right femur (100 mm in length) (S.I. 2B). The adductor crest is damaged (Fig. 13A). The cortical bone consists of WB and PFB alternating as zones and annuli (Fig. 13D). The vascularity is radially arranged, similar to what is observed in the humeri, forming an overall "bicycle wheel" pattern in the cortex (Fig. 13C & D). Vascularity remains radial until it reaches the first LAG and then it changes to a more reticular pattern (Fig. 13D & F). Primary osteons are present throughout the cortex (Fig. 13E & F). OL are large in the zones and more flat in the annuli (Fig. 13E).

The cortex contains a growth record of three zones separated by two LAGs corresponding with annuli (Fig. 13C & D). It is worth noting that WB decreases from the inner to the outer cortex (Fig. 13D). Also, in the dorsal region of the outer cortex, perpendicular to the bone surface, the remnants of the nutrient canal extend deep into the medullary region (Fig. 13B).

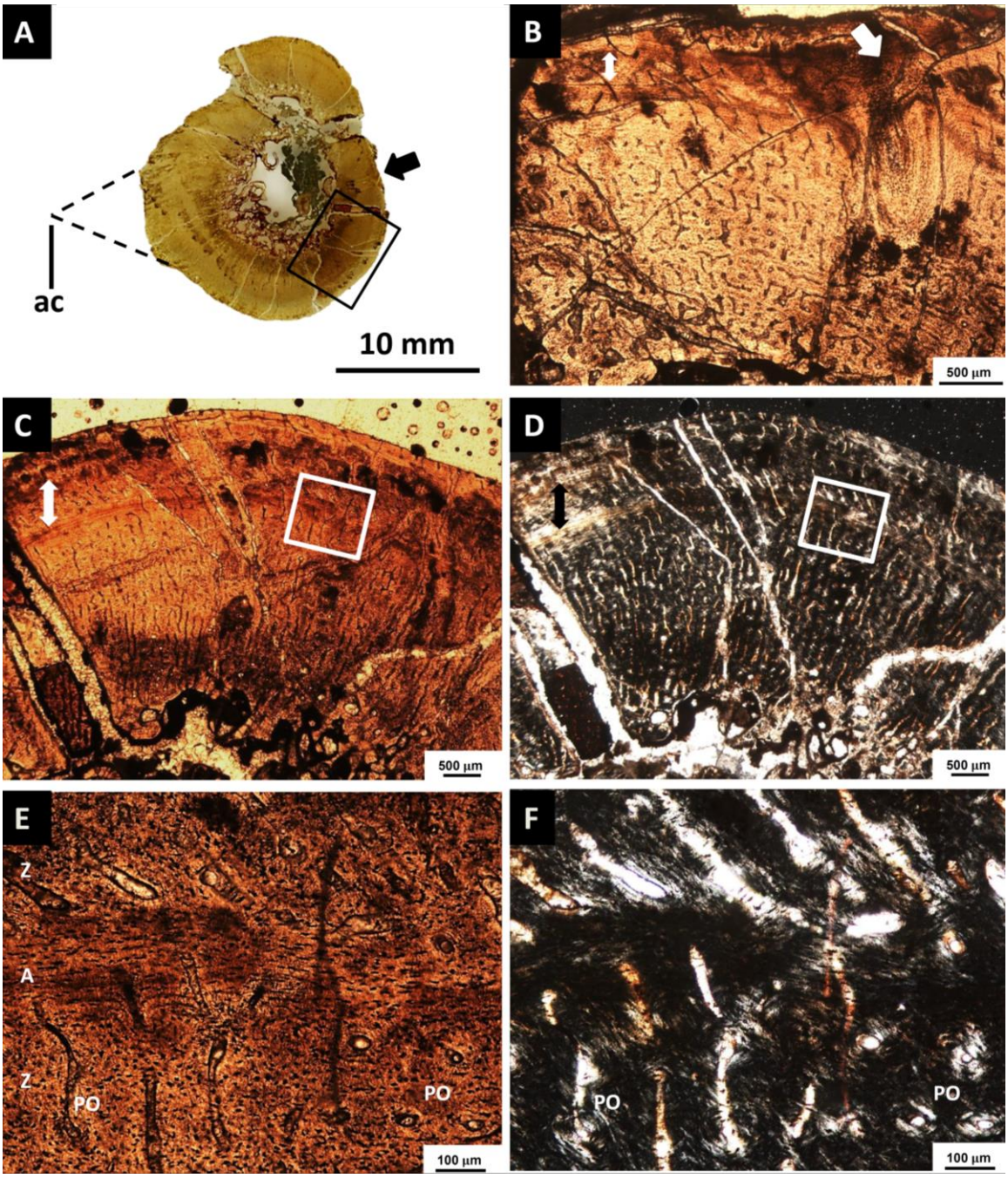

Figure 13 OMNH-55234 *O. mirus* femur 100 mm in length. A) Transverse section through the mid-diaphysis. The midshaft is damaged and the adductor crest is incomplete (reconstruction of the missing area is general and not an accurate morphological reconstruction). Arrow is pointing to the location of the nutrient canal. B) Magnified microscopic view of the dorsal cortex in conventional transmitted light. Arrow is pointing to the nutrient canal. Surrounding vascularity is reticular C) Microscopic view of the mid-diaphysis cortex in conventional transmitted light of the

boxed area in (A). Arrow is pointing to the LAG. D) Same view as in (C) but in polarized transmitted light. Note the radial and longitudinal canals form the same "bicycle wheel" pattern as that seen in the humeri below the LAG. Small reticular vascular canals are also present above the LAG. E) Magnified microscopic view of the boxed area in conventional transmitted light. OSL appear flat and generally oriented parallel to the cortical surface within the LAG. F) Same view as in (E) in polarized transmitted light. Note the primary osteons set in a WB matrix, i.e., fibro-lamellar bone. Abbreviation: ac= adductor crest.

The medullary region is occluded by secondary trabeculae and bound by large ECs in the process of complete resorption of the primary cortex and formation of secondary trabecular bone (Fig. 13A). A few ECs have appeared in the lower cortex. Endosteal resorption/redeposition is strongest in the posterior region. A true medullary cavity opening is present unlike what is observed in the humeri.

4.6.3 MSU uncatalogued Ophiacodon femur

The MSU specimen is a right femur, 115 mm in length (S.I. 2C) with a damaged adductor crest (Fig. 14A). In the transverse thin section, it can be seen that the cortical bone consists of WB and PFB alternating as zones and annuli (Fig. 14B). The vascularization is reticular and longitudinal with sparse thin radial canals (Fig. 14C & D). OL range in shape from round to flat (Fig 14B). Incipient and fully formed primary osteons are visible throughout the cortex, but secondary osteons are concentrated near the boarders of the medullary region (Fig. 14E & F).

A growth record is contained in the periosteal bone. At least eight growth cycle boundaries are marked by annuli and corresponding growth marks (Fig. 14C & D). The cortex contains one large annulus at the medullary boundary, but it's in the process of being resorbed. This could be the first complete cycle of growth; although previous growth marks would have been completely resorbed. ECs have already formed and extended to the fifth annulus. A nutrient canal in the dorsal region of the outer cortex is similar to OMNH-55234 and IPBSH-46 (Fig. 14A, C, D).

The medullary margin is bound by many ECL and ECs that extend to the mid cortex. The MC is mostly occluded by secondary trabecular bone and primary cortex is being completely

resorbed (Fig. 13A). The concentration of secondary and primary osteons at the border of the medullary region is considered here to be a poorly defined Haversian tissue (Fig. 14E & F).

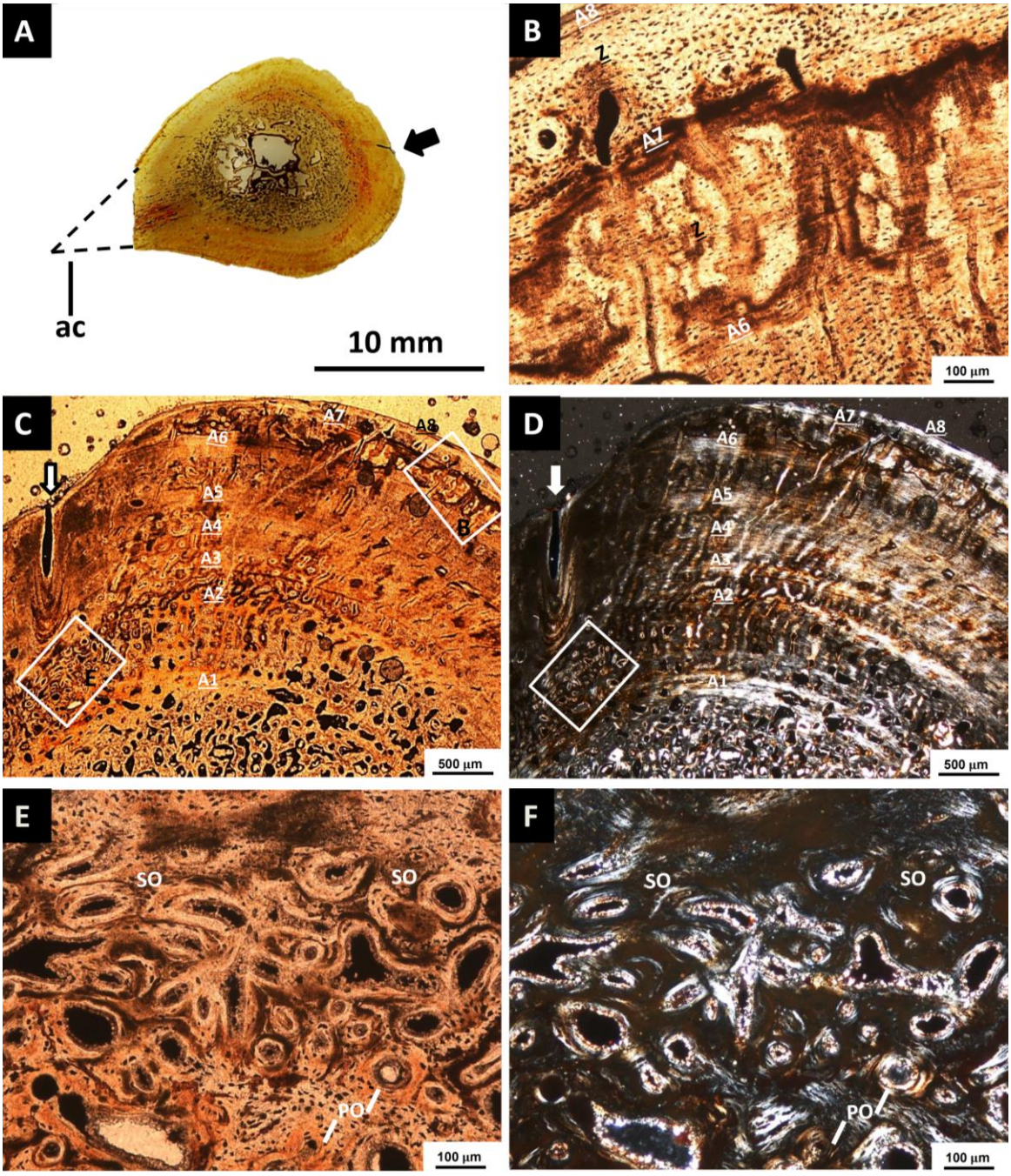

Figure 14 Uncatalogued MSU femur, *O. uniformis*, 115 mm in length. A) Scan of the transverse section of the mid-diaphysis. The midshaft is damaged and the adductor crest is incomplete (reconstruction of the missing area is general and not an accurate morphological reconstruction). Arrow indicates the nutrient canal. B) Magnified microscopic view of the boxed area in (C) in

normal transmitted light. Alternating zones and annuli can be observed. C) Magnified view of the dorsal cortex in conventional transmitted light. Arrow indicates the nutrient canal that extends into the deep cortex. Note how the cortex was affected during development to continually incorporate this permanent structure throughout the life of the animal. The growth record consists of eight annuli, some of which are associated with LAGs. The oldest annulus (A1) is the boundary between the cortex and the medullary region. The inner cortical vascularity is longitudinal. The mid cortex is a combination of longitudinal and reticular canals. In the outermost cortex, there are thin zones with one to two rows of longitudinal primary osteons. Secondary trabeculae occlude the medullary cavity. D) Same view as in C) but in polarized transmitted light. Annuli are better visible in polarized light. Notice the vascularization does not form the same "bicycle wheel" pattern as that seen in OMNH-55234 E) Magnified microscopic view of the boxed area in (C) in conventional transmitted light just below the nutrient canal. Here is the best example of Haversian tissue though poorly defined. Note the combination of primary and secondary osteons. F) Same view as in (E) in polarized transmitted light. Abbreviations: A= annulus; ac= adductor crest; Z= zone.

4.6.4 OMNH-35389, O. retroversus

OMNH-35389 is a left femur with a total length of 221 mm (S.I. 2D); this is the largest femur sampled. The histology described here is from a core drilled through the dorsal side of the midshaft. The cortical bone consists of WB and PFB with alternating zones and annuli (Fig. 15A & B). Vascularization is mainly restricted to the zones and is found in reticular, radial, and longitudinal patterns, decreasing in size from the deep inner cortex to the outer cortex (Fig. 15C). Vascular canals are more radial in the deeper primary cortex and become more reticular towards the outer surface (Fig. 15A). OL are plump in the deep cortex and in the zones, but they are flat in the annuli and EFS (Fig. 15C). Primary osteons are mostly incipient in the outer cortex, but fully formed osteons are observed in the deeper cortex.

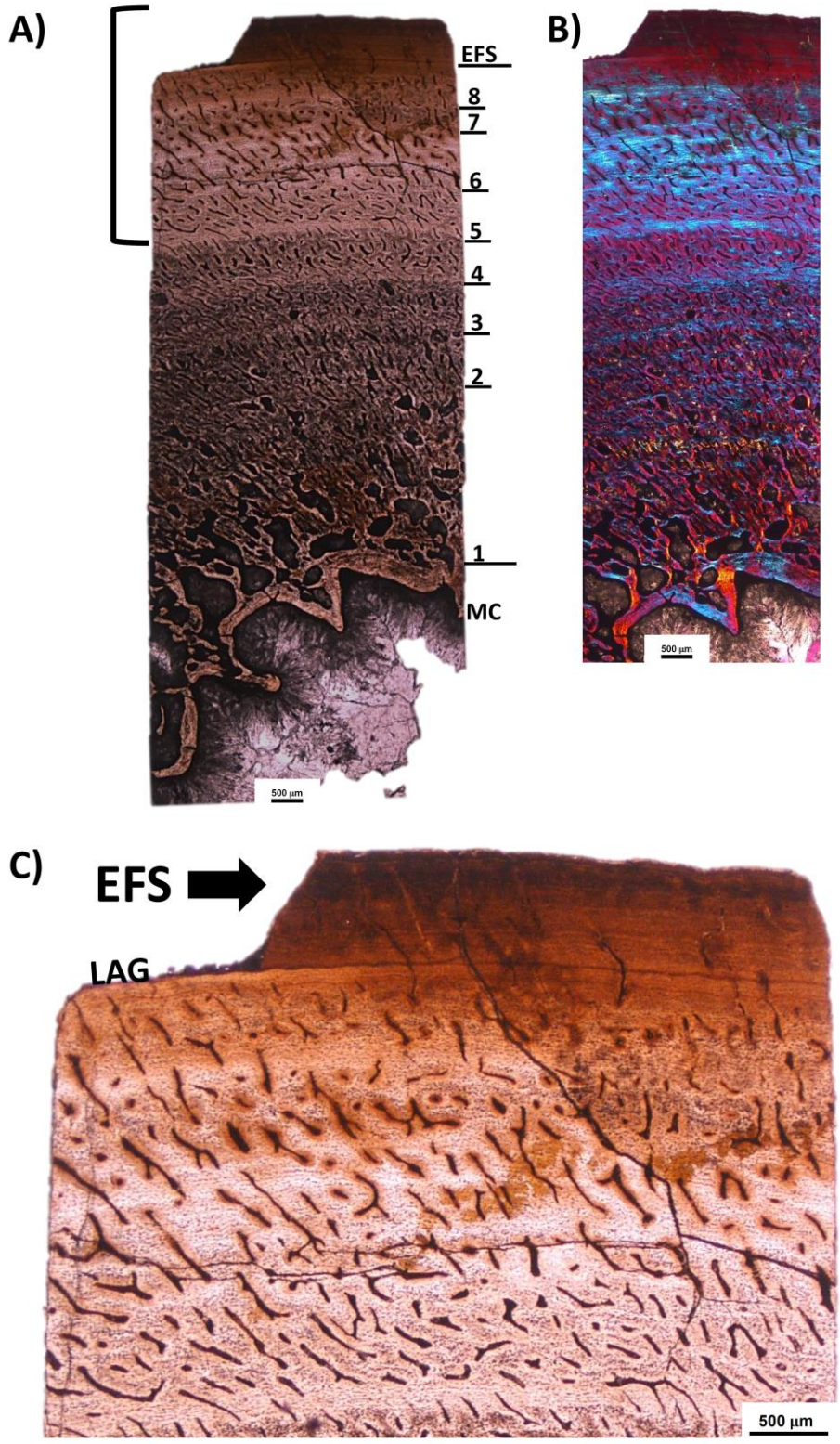
A)
EFS
8
7
6
5
4
3
2
1
MC
500 µm
B)
500 µm
C)
EFS
LAG
500 µm

Figure 15 OMNH-35389 *O. retroversus* femur 221 mm in length. A) Scan of a transverse core section drilled through the dorsal sides of the mid-diaphysis. EFS can be seen in the outer cortex. Vascularity consists of longitudinal and reticular canals. In addition to the EFS, eight growth cycles can be seen in the cortex. Earlier growth cycles may have been resorbed. ECs do not extend beyond the third cycle. B) Microscopic view of (A) in polarized transmitted light with a lambda filter. The annuli separating the zones are more distinctive. C) Magnified microscopic view of the outer cortex as indicated by bracket in (A). Vascularity has greatly decreased towards the EFS just below the LAG. Abbreviations: EFS = external fundamental system; LAG = line of arrested growth; MC = medullary cavity.

The cortical bone contains eight growth cycles separated by annuli (Fig. 15A) and one very prominent LAG marking the start of the EFS in the outermost cortex (Fig. 15C). Any earlier growth cycles have been resorbed (Fig. 15B). This is the only femur to exhibit an EFS; however, the exact number of growth cycles in the EFS remains unknown due to the diagenetic staining (Fig. 15C). This again means that the animal had reached skeletal maturity. The medullary cavity appears to be open with extensive ECs extending into the third growth cycle. Secondary trabeculae are present. There is much more endosteal resorption and redeposition of the primary cortex in contrast to what was observed in the humeri.

5. Discussion

In this study we set out to section *Ophiacodon* material from Texas and Oklahoma localities of various ages in order to investigate what previous studies have called “fast growing” tissue as a possibly overlooked earliest occurrence of fibro-lamellar bone in the mammalian lineage. Included in this sampling is Brinkman’s (1988) figured *Ophiacodon* humeral growth series from RSC. The sectioning of this ontogenetic series served two purposes: first, to answer the call for proper ontogenetic sampling of ‘pelycosaur’ material as to ascertain data relevant for explaining the dense vascularity of the cortical bone. Additionally, this sample set allowed us to test Brinkman’s (1988) hypothesis, to determine if histology correlates with the morphologic stages of development assigned to these bones (Figs. 1 & 2). Finally, an attempt was made to ascertain the preferred ecology of *Ophiacodon* by analyzing the quantitative morphometric and histologic results.

5.3 Synthesized histology

In general, the bone tissue of *Ophiacodon* is both a mixture of WB and PFB alternating as zones and annuli. LB is restricted to the osteons and trabecular bone. The cortical bone is well vascularized. All humeri, including the Carboniferous period femur OMNH-55234 and the prenatal cortex of IPBSH-46 consists of radially arranged longitudinal and radial canals. The organization of the canals gives the cortical bone a "bicycle wheel" pattern (See Figs. 6-10 & 14). The other femora sampled, including the postnatal cortex of IPBSH-46, consisted of longitudinal and reticular vascular canals with varying degrees of LB infilling. True primary osteons are prevalent in all bones. A few secondary osteons were only observed in the deep cortex of the largest sampled humerus (Fig. 9F), but they are not present in the largest femur. However, the best evidence of Haversian tissue was only seen in the uncataloged femur from MSU (Fig. 14E & F). Osteocyte lacunae are mostly plump while others that follow the circumferential layering of the LB are basically flat. The medullary cavity of the humeri is completely occluded with secondary trabeculae in contrast to the open MC of the femora. Mostly, the humeri and femora differ in resorption strategy, which affects the preserved growth record. In humeri, erosional cavities follow the radial organization of the vascular network and incorporate areas of primary cortical bone into the medullary region as trabeculae bound by lamellar bone. Femora completely resorb the primary cortex and develop a more open MC. Resorption and endosteal deposition seem to be occurring at a much slower rate than the periosteal deposition, resulting in a better preservation of the growth record in femora. In addition, as observed in humeri, primary and, more rarely, secondary osteons develop within the vascular canals in the deeper isolated parts of the primary cortex. One feature that seems unique for the *Ophiacodon* femora, regardless of geologic age or size, is the dorsal position of the nutrient canal (Figs. 12-14). This has not yet been consistently observed in the other 'pelycosaur' taxa and reaffirms the accuracy of our sampling technique with regards to the minimal diaphyseal circumference (Fig. 5).

Specifically, the histology of the *Ophiacodon* humeral growth series does indeed correlate with the MOS assigned by Brinkman (1988), and contains histological evidence of progressive growth from a juvenile stage to fully grown adult (Figs. 2 & 5). The smallest sampled humerus MCZ-5926 (MOS II) (Table 1, Fig. 1) contains a neonatal line denoting the time of hatching. All

humeri sampled, as noted earlier, contain a highly vascularized cortex of woven and parallel-fibered bone incorporating numerous primary osteons. Through the progressive stages of growth, the medullary region expands through resorption, and secondary trabeculae form from remodeling of primary cortex. The largest humerus MCZ-1486 (MOS V) (Fig. 2) contains an external fundamental system, as is expected, in the outermost cortex where a noticeable decrease in vascularity can be observed. These are signs that the animal reached skeletal maturity. Only a few secondary osteons were observed within the isolated patches of original cortex, but no sign of Haversian tissue.

The growth curve constructed from this data supports the theory that these animals grew fast (Fig. 5), which culminates in a life history for *Ophiacodon* revealing that they grew for half of their life before reaching skeletal maturity. This is also evident in the preserved growth record, which is mostly denoted by annuli as the animal is still growing at a rate too fast to produce true LAGs until the individual was well advanced in age.

5.4 Fibro-lamellar *Ophiacodon* bone.

Based on our sampling we can confirm that true fibro-lamellar bone does exist in Ophiacodon, the dense vascularized woven bone is not just a simple reflection of immaturity, but is present throughout life. Our results corroborate with the findings of Enlow and Brown (1957) and Enlow (1969) that the histologic detail observed in the long bones was indicative of rapid skeletal growth. Fibro-lamellar bone is defined as "Circumferential lamellae are poorly defined in the periosteum, highly vascularized compacta with woven or parallel-fibered matrix incorporating densely packed isometric osteocyte lacunae, lamellar bone was restricted to the primary osteons as well as endosteal bone only" (Francillon-Vieillot et al., 1990). Unfortunately, these and subsequent studies failed to identify it as such. Enlow (1969) concluded the specimen he analyzed must have been a juvenile because of the extreme difference from the other 'pelycosaurs'; however, at the time proper ontogenetic sampling of this group had not yet occurred in order to make a proper comparison. de Ricqlès (1974a, p. 63) makes a comparison to therapsids noting a similarity in the dense vascularization of the periosteal bone, but he concludes this must reflect the aquatic lifestyle of *Ophiacodon* further noting a similarity to crocodiles and plesiosaurs. This will be discussed later.

However, this is not the first claim of FLB occurring within 'pelycosaur' long bones. Huttenlocker, Angielczyk & Lee (2006) and Huttenlocker and Rega (2012) have made unsubstantiated claims that this same tissue exists in *Sphenacodon ferocior* (Synapsida: Sphenacodontidae). Shelton et al. (2013) have noted incipient FLB in *Dimetrodon natalis*. Further comparison to *D. natalis* will be discussed later. As a final note, FLB is believed to exist in the neural spines of sphenacodontids and edaphosaurids according to Huttenlocker and Rega (2012); Huttenlocker, Rega & Sumida (2010), and Huttenlocker, Mazierski & Reisz (2011).

Previously, the earliest occurrence of true FLB (with a well-developed Haversian tissue) in the mammalian lineage was found in Dinocephalia (Therpasida) (de Ricqlès, 1972; de Ricqlès, 1974a), one of the earliest therapsid groups preceded by Biarmosuchians (Therapsida), which itself is considered to be the intermediate group between the sphenacodontids and therapsids (Kemp, 1987; Kemp, 2007b; Kemp, 2012).

5.5 Comparison to *Dimetrodon natalis*

Ophiacodon is not as primitive as once thought (Romer & Price, 1940). Huttenlocker and Rega (2012) compare *Ophiacodon* to published data of the known sampled taxa noting varanopids, eothyridids, and caseids are less derived osteologically than *Ophiacodon* (Brinkman & Eberth, 1985; Reisz 1986). In addition, *Ophiacodon* is histologically more advanced than *Dimetrodon* in terms of osteonal development. We find in sphenacodonts an incipient form of FLB where osteons remain immature/incipient throughout ontogeny and the cortex contains more PFB than *Ophiacodon* (Shelton et al., 2013). Specifically, *Dimetrodon* and *Ophiacodon* humeri differ mainly by resorption and remodeling strategy. Also, this "bicycle wheel" vascular pattern has been described in both the humerus and femur of *Dimetrodon*, whereas, this occurs only in the *Ophiacodon* humerus, the femur from the Carboniferous period, and the embryonic tissue of IPBSH-46. In comparison to the growth trajectory of *D. natalis* (Shelton et al., 2013, Fig. 10), it is clear that *O. retroversus* reached skeletal maturity much earlier, but the life expectancy of both seems to be similar (Fig. 5).

With regards of the humerus to femur ratio (femur length divided by humerus length) for *D. natalis*, this ratio was reported as 1.14 with the use of larger *Dimetrodon* species because sufficient articulated *D. natalis* specimens were unavailable. The average ratio for *Ophiacodon*

was 1.20 (Table 2). However, the smaller species (*O.uniformis* and *O. mirus*) have a slightly larger ratio than the bigger species (*O. retroversus*). This may indicate the LLD ratio used for *D. natalis* is not accurate. Further evidence of a differing morphometry between large and small species is also reflected in the L/C ratio discussed earlier (Table 1)

5.6 *Ophiacodon* ecology: terrestrial, amphibious, or aquatic?

Due to the limitations of the data, we cannot infer an aquatic habitat for *Ophiacodon* based solely on histologic results. It has been assumed in previous studies that the dense vascularization of the periosteal bone is evidence of an amphibious lifestyle (de Ricqlés, 1974a; de Ricqlés, 1974b; de Ricqlés 1976; Germain & Laurin, 2005). However, the specific "bicycle wheel" pattern formed by the radially arranged longitudinal and radial vascular canals has been noted in the limb bones of both extinct and extant aquatic, semi-aquatic, and terrestrial organisms. These include but are not limited to the following taxa: Sphenacodontidae (Shelton et al., 2013), Varanopsidae (Huttenlocker & Rega, 2012), and *Notosllasia* and *Theriognathus* (Therapsida, Therocephalia) (de Ricqlès, 1975; Huttenlocker & Botha-Brink, 2014). Also, this pattern has been recognized in several aquatic sauropterygians of both the Placodontia and the Eusauropterygia groups, but this pattern is specific only to certain morphotypes (see Klein, 2010; Krahl, Klein & Sander, 2013). The vascular pattern is also prevalent in large modern varanids such as *Varanus komodoensis* (Reid, 1984) and the semi-aquatic Nile Monitor Lizard, *Varanus niloticus* (de Buffrénil & Francillon-Vieillot, 2001; de Ricqlès, Castanet & Francillon-Vieillot, 2004). The "bicycle wheel" pattern has also been unofficially observed by the authors in *Edaphosaurus* humeri; however, until sufficient edaphosaurid material can be sectioned and described, an adequate comparison to *Ophiacodon* histology remains to be officially reported. It should be noted that the partial *Ophiacodon* radius described by de Ricqlès (1974b, 1978) does not possess this "bicycle wheel" pattern; instead longitudinal primary osteons are randomly arranged within a PFB matrix.

However, one might draw a more thorough conclusion by synthesizing all the lines of evidence reviewed earlier. Huttenlocker and Rega (2012) lamented that the organization of *Ophiacodon* bone histology is most likely a reflection of both the growth pattern and lifestyle. We suggest additional geochemical and isotope analyses of *Ophiacodon* teeth to definitively resolve the preferred habitat enigma (for example see Fischer et al., 2013). de Margerie et al.

(2004) point out that radial vascularization is most resistant to shear forces. Perhaps this bicycle wheel vascular pattern is a response to specific biomechanical forces acting upon the stylopodium of *Ophiacodon* given that they have the largest muscle attachment points of any of the 'pelycosaurs', with exception to edaphosaurid femora, both of which share an extended adductor crest (Romer & Price, 1940). Further detailed analysis is required in order to make a proper assessment of this phenomena including further sectioning of the zeugopodium and autopodium as it appears to vary in vascularity from the "bicycle wheel" pattern found in the stylopodium.

6. Conclusion.

By sampling Brinkman's (1988) *Ophiacodon* ontogenetic series (Figs. 1 & 2), as well as additional material (S.I. 1 & 2), we have confirmed the presence of true fibro-lamellar bone in the postcrania of 'pelycosaurs'. Our findings here reaffirm what Enlow and Brown (1957, 1958) first described as fast growing tissue and by proxy have disproven that the highly vascularized cortex is simply a reflection of immaturity. The tissue we describe here demonstrates the classic histological characteristics of the text book definition of FLB (Francillon-Vieillot et al., 1990) with the exclusion of a well-developed Haversian system. In general, the compacta consists of primary osteons in a woven bone matrix. Overall, the FLB tissue we have described in *Ophiacodon* is more derived or "mammal-like" in terms of the osteonal development, bone matrix, and skeletal growth then what has been described thus far in any other 'pelycosaur' taxa. With regard to resolving the question of the (semi-) aquatic habitat of *Ophiacodon*, our results remain inconclusive but we can state our findings have set the evolutionary origins of modern mammalian enodthermy and high skeletal growth rates back approximately 20 M.Y.

7. Acknowledgments

We would wholeheartedly like to thank the following people: Jack and Marie Loftin of Archer City, Texas, for their help and hospitality. From the Texas Memorial Museum Vertebrate Paleontology Laboratory, Austin, TX, we would like to thank the late Wann Langston Jr., Ernest Lundelius, and Lyn Murray for their support and assistance with storage and shipping of fossil material. From the Berlin Museum für Naturkunde we thank Johannes Müller, Jörg Fröbisch, and Marten Schobben for receiving, transporting, and preparing jacketed fossil material from the

2010 BCBB excavation. From the Steinmann Institute, University of Bonn, we would like to thank Koen Stein for his assistance of three field seasons digging in in the Lower Permian; Rebecca Hofmann, Marlena Nowak, and Olaf Dülfer for thin sectioning; Yasuhisa Nakashima for discussion about nutrient canals; Aurore Canoville for help translating original French manuscripts to English; Jessica Mitchell for linguistic improvement; and Kay Heitplatz for administrative assistance. We thank Zhe-Xi Lou (University of Chicago) for his discussion and insights. From the University of Toronto we thank Jessica Hawthorn for general discussion about *O. major*, and Robert Reisz for preliminary identification of excavated Briar Creek material. We also would like to thank Herman Winklehorst of the Netherlands for his help on the 2010 BCBB excavation. We thank Don Brinkman (Tyrell Museum of Palaeontology) who did the initial study in 1988 for sharing his raw data. We would like to extend gratitude to the following people for allowing access to their collections and granting permission for consumptive sampling of specimens: Farish Jenkins Jr. and Jessica Cundiff (MCZ), Richard Cifelli, Jennifer Larson, and Kyle Davies (OMNH). Also, we thank Pamela Buzas-Stephens (MSU). Jeffrey Wilson, and Gregg Gunnell (UMMP). Finally, we thank the current land owner of the Briar Creek Bonebed Jeff Lindeman for granting permission to excavate in 2010 and 2011. This project was funded by DFG grant SA 469/34-1 and the University of Bonn.

8. References

Anderson HC. 1969. Vesicles associated with calcification in the matrix of epiphyseal cartilage. *Journal of Cell Biology* 41:59-72.

Bakker RT. 1982. Juvenile-adult habitat shift in Permian fossil reptiles and amphibians. *Science* 217:53-55.

Brinkman D. 1988. Size-independent criteria for estimating relative age in *Ophiacodon* and *Dimetrodon* (Reptilia, Pelycosauria) from the Admiral and Lower Belle Plains formations of West-central Texas. *Journal of Vertebrate Paleontology* 8:172-180.

Brinkman D, Eberth DA. 1985. The interrelationships of pelycosaurs. *Breviora* 473:1-35.

Buffrénil Vd, Francillon-Vieillot H. 2001. Ontogenetic changes in bone compactness in male and female Nile monitors (*Varanus niloticus*). *Journal of Zoology* 254:539-546.

Bybee PJ, Lee AH, Lamm ET. 2006. Sizing the Jurassic theropod dinosaur *Allosaurus*: Assessing growth strategy and evolution of ontogenetic scaling of limbs. *Journal of Morphology* 267:347-359.

Case EC. 1915. *The Permo-Carboniferous red beds of North America and their vertebrate fauna*. The Carnegie Institution of Washington: Washington D. C.

Currey JD. 2002. Bones. *Structure and mechanics*. Princeton: Princeton University Press.

Enlow DH, Brown SO. 1957. A comparative histological study of fossil and recent bone tissues. Part II. *The Texas Journal of Science* 9:186-214.

Enlow DH, Brown SO. 1958. A comparative histological study of fossil and recent bone tissues. Part III. *The Texas Journal of* 10:187-230.

Enlow DH. 1969. The bone of reptiles. In Gans C, ed. *Biology of the reptiles*. Academic Press: London, 45-80.

Felice R N, Angielczyk KD. 2014. Was *Ophiacodon* (Synapsida, Eupelycosauria) a swimmer? A test using vertebral dimensions. In Krammer CF, Angielczyk KD, Fröbisch J, eds. *Early evolutionary history of the Synapsida*. Springer: Netherlands, 25-51.

Fischer J, Schneider JW, Hodnett JPM, Elliott DK, Johnson GD, Voigt S, Joachimski MM, Marion Tichomirowa M, Götze J. & Götze, J. 2013. Stable and radiogenic isotope analyses on shark teeth from the Early to the Middle Permian (Sakmarian–Roadian) of the southwestern USA. *Historical Biology* 26:1-18.

Francillon-Vieillot H, Buffrénil Vd, Castanet J, Géraudie J, Meunier FJ, Sire JY, Zylberberg L, Ricqlès Ad. 1990. Microstructure and mineralization of vertebrate skeletal tissues. In Carter GJ, ed. *Skeletal biomineralization: Patterns, processes and evolutionary trends*. *Vol. 1*. Van Nostrand Reinhold: New York, 471-530.

Germain D, LaurinM. 2005 Microanatomy of the radius and lifestyle in amniotes (Vertebrata, Tetrapoda). *Zoologica Scripta* 34:335-350.

Hall BK. 2005. *Bones and cartilage: Developmental and evolutionary skeletal biology*. Elsevier: Academic Press.

Hentz TF. 1988. Lithostratigraphy and paleoenvironments of Upper Paleozoic continental red beds, north-central Texas: Bowie (new) and Wichita (revised) groups. *The University of Texas at Austin, Bureau of Economic Geology Report of Investigations* 170**:** 1-55.

Huttenlocker A., Rega E. 2012. Chapter 4: The paleobiology and bone microstructure of pelycosaurian-grade synapsids. In Chinsamy A, ed. *Forerunners of mammals*. Indiana University Press: Bloomington, 91-119.

Huttenlocker AK, Botha-Brink, J. 2014. Bone microstructure and the evolution of growth patterns in Permo-Triassic therocephalians (Amniota, Therapsida) of South Africa. *PeerJ*, *2*, e325.

Huttenlocker A, Angielczyk KD, Lee A. 2006. Osteohistology of *Sphenacodon* (Synapsida: Sphenacodontidae) and the hidden diversity of growth patterns in basal synapsids. *Journal of Vertebrate Paleontology* 26:79-80A.

Huttenlocker A, Rega E, Sumida S. 2010. Comparative anatomy and osteohistology of hyperelongate neural spines in the sphenacodontids *Spenacodon* and *Dimetrodon* (Amniota: Synapsida). *Journal of Morphology* 271:1407-1421.

Huttenlocker A, Mazierski D, Reisz R. 2011. Comparative osteohistology of hyper elongate neural spines in Edaphosauridae (Amniota: Synapsida). *Palaeontology* 54:573-590.

Kemp TS. 1987. *Mammal-like reptiles and the origin of mammals*. London: Academic Press.

Kemp TS. 2007a. *The origin and evolution of mammals*. Oxford University Press: Oxford.

Kemp TS. 2007b. The origin of higher taxa: Macroevolutionary processes, and the case of the mammals. *Acta Zoologica*. 88:3-22.

Kemp, TS. 2012. Chapter 1: The origin and radiation of Therapsids. In Chinsamy A, ed. *Forerunners of mammals*. Indiana University Press: Bloomington, 3-28.

Kissel RA, Lehman, TM. 2002. Upper Pennsylvanian tetrapods from the Ada Formation of Seminole County, Oklahoma. *Journal of Paleontology* 76:529-545.

Klein N. 2010. Long bone histology of Sauropterygia from the Lower Muschelkalk of the Germanic Basin provides unexpected implications for phylogeny. *PLoS One* 5:1-25.

Klein N, Sander PM. 2007. Bone histology and growth of the prosauropod *Plateosaurus engelhardti* MEYER, 1837 from the Norian bonebeds of Trossingen (Germany) and Frick (Switzerland*). Special Papers in Palaeontology*. 77:169-206.

Krahl A, Klein N, Sander PM. 2013. Evolutionary implications of the divergent long bone histologies of *Nothosaurus* and *Pistosaurus* (Sauropterygia, Triassic). *BMC evolutionary biology* 13: http://www.biomedcentral.com/1471-2148/13/123.

Marsh OC. 1878. Notice of new fossil reptiles. *American Journal of* Science 89:409-411.

Margerie Ed, Robin JP, Verrier D, Cubo J, Groscolas R, Castanet J. 2004. Assessing a relationship between bone microstructure and growth rate: a fluorescent labelling study in the king penguin chick (*Aptenodytes patagonicus*). *Journal of Experimental Biology* 207:869-879.

Nair A, Jagannathan N. 2013. The role of matrix vesicles in mineralization of bone. *Analele Societaii Nationale de Bilogie Celulara* 18:28-32.

Nopcsa F. 1923. Die Familien der Reptilien. *Fortschritte der Geologie und Paläontologie* 2:1-210.

Olson EC. 1977. Permian lake faunas: A study in community evolution. *Journal of the Palaeontoligcal Society of India* 20:146-163.

Olson EC. 1967. Early Permian vertebrates of Oklahoma. *Oklahoma Geological Society* 74: 1-107.

Petermann H, Sander PM. 2013. Histological evidence for muscle insertion in extant amniote femora: implications for muscle reconstruction in fossils. *Journal of Anatomy*, 222:419-436.

Reid, REH. 1984. Primary bone and dinosaur physiology. *Geological Magazine* 121:589-598.

Reisz RR. 1972. Pelycosaurian reptiles from the Middle Pennsylvanian of North America. 7 *Bulletin of the Museum of Comparative Zoology* 144:27-62.

Reisz RR. 1975. Pennsylvanian pelycosaurs from Linton, Ohio and Nýřany, Czechoslovakia. *Journal of Paleontology* 49:522-527.

Reisz RR. 1986. *Encyclopedia of paleoherpetology. Part 17A: Pelycosauria*. Gustav Fischer Verlag: Stuttgart.

Ricqlès Ad. 1972. Recherches paleohistologiques sur les os longs des tetrapodes, III. Titanosuchiens, Dinocéphales, et Dicynodontes. *Annales de Paléontologie* 58:15-78.

Ricqlès Ad. 1974a. Evolution of endothermy: Histological evidence. *Evolutionary Theory* 1:51-80.

Ricqlès Ad. 1974b. Recherches paléohistologiques sur les os longs des Tétrapodes IV: Eotheriodonts and pelycosaurs. *Annales de Paléontologie* 60:3–39.

Ricqlès Ad. 1975. Recherches paléohistologiques sur les os longs des tétrapodes VII. Sur la classification, la signification fontionnelle et l'histoire des tissus osseux des tètrapodes (Premiere partie). *Annales de Paléontologie* 61:51-129.

Ricqlès Ad. 1976b. On the bone histology of fossil and living reptiles, with comments on its functional and evolutionary significance. In Bellairs, AA, Cox BC, eds. *Morphology and biology of reptiles*. Academic Press: London, 123-150.

Ricqlès Ad. 1978. Recherches paléohistologiques sur les os longs des tétrapodes VII. Sur la classification, la signification fonctionelle et l´histoire des tissus osseux des tétrapodes, Troisème partie. *Annales de Paléontologie* 64:153-184.

Ricqlès Ad, Castanet J, Francillon-Vieillot H. 2004. The 'message' of bone tissue in paleoherpetology. *Italian Journal of Zoology* 71:3-12.

Romer AS. 1969. *Osteology of the reptiles*. Chicago IL, University of Chicago Press.

Romer AS, Price LI. 1940. Review of the Pelycosaurs. *Geological Society of America Special Papers* 28:1-538.

Sander PM. 1989. Early Permian depositional environments and pond bone beds in central Archer County, Texas. *Palaeogeography, Palaeoclimatology, Palaeoecology*. 69:1-21.

Sander PM. 2012. Reproduction in early amniotes. *Science* 337:806-808.

Sander PM Klein N. 2005. Developmental plasticity in the life history of a prosaruopod dinosaur. *Science* 310:1800–1802.

Sander PM, Mateus O, LavenT, Knötschke N. 2006. Bone histology indicates insular dwarfism in a new Late Jurassic sauropod dinosaur. *Nature* 441:739-741.

Shelton, C. D., Sander, P. M., Stein, K. and Winkelhorst, H. 2013. Long bone histology indicates sympatric species of Dimetrodon (Lower Permian, Sphenacodontidae). *Earth and Environmental Science Transactions of the Royal Society of Edinburgh.* 103:217-236.

Stein K, Sander, PM. 2009. Histological core drilling: A less destructive method for studying bone histology. Pp. 69-80. In Brown MA, Kane JF, Parker WG, eds. *Methods in fossil preparation: proceedings of the first annual fossil preparation and collections symposium*, 69-80.

Vaughn PP. 1966. Comparison of the Early Permian vertebrate fauna of the Four Corners region and north-central Texas. *Los Angeles County Museum of Natural History Contributions in Science* 105:1–13.

Vaughn PP. 1969. Early Permian vertebrates from southern New Mexico and their paleozoogeographic significance. *Los Angeles County Museum of Natural History Contributions in Science* 166:1–22.

Chapter 5: Palaeobiology among basal synapsids: A caseian point for the Palaeozoic evolution of the diaphragm

In review as: Lambertz, M., Shelton, C.D., Spindler, F. and Perry, S. F. Palaeobiology among basal synapsids: A caseian point for the Palaeozoic evolution of the Diaphragm. Nature (Chapter formatted for earlier submission to Nature Communications).

Abstract Caseids are very basal synapsids and peculiar, large Palaeozoic herbivorous pelycosaurs. While caseids generally are regarded to have been terrestrial grazers, we present evidence that clearly favours a predominantly aquatic biology. Quantitative limb-bone histology indicates a strongly osteoporotic-like morphology and therefore severely limited weight-bearing capacity. Reappraisal of the cervical and pectoral anatomy further reveals that the mouth could not reach the ground, making drinking almost impossible, and feeding severely restricted and costly on land. Our models further reveal that rib movement alone would result in insufficient ventilation during exercise and an auxiliary inspiratory mechanism must be postulated. Given the phylogenetic position of caseids, a homologue of the muscular diaphragm is the most parsimonious explanation and would provide an exaptation for the (semi-)aquatic lifestyle indicated above. Our data suggest that a diaphragm homologue evolved geological periods before the rise of mammals, possibly already in conjunction with the advent of the Synapsida.

1. Introduction

Amniotes are the primarily fully terrestrial vertebrates and they fall into two distinct lineages: sauropsids and synapsids. The former make up the "traditional reptiles" and the birds, while the latter eventually gave rise to mammals[1]. The origin of the Mammalia dates back to about the Middle Jurassic[2], or, depending on its phylogenetic definition, possibly to the Late Triassic[1], but definitely not before the Mesozoic. A problem with dating the origin of Mammalia is that not all traits arose simultaneously. The entire synapsid line, however, can be traced back into the Late Carboniferous and thus well into the Palaeozoic[3,4]. Approximately the first 100 million years of this radiation generally is characterized as the age of "mammal-like reptiles". These non-mammalian synapsids are evolutionarily of particular interest as they can help us to better understand how the mammalian *Bauplan* evolved. Whereas phylogenetically highly derived non-mammalian Synapsida can be helpful for understanding

complex transitions at a very detailed level, such as the evolution of the inner ear and its auditory performance[5], the more basal taxa can provide insights into fundamental deviations from the plesiomorphic amniote condition. One crucial and still unresolved mystery of mammalian evolution is the origin of the muscular diaphragm[6,7]: a unique characteristic of their respiratory apparatus that is pivotal to the success of this group as high-performance, endothermic animals[8].

The basal-most taxon of synapsids is the Caseasauria, which is composed of the two clades Eothyrididae and Caseidae[1]. Of these, the caseids make up the majority of known forms, both in terms of biodiversity and abundance of fossils[9,10]. The fossil record of caseids recently has been extended back to the Late Carboniferous[4], while the major radiation is recovered from the Permian. Caseids probably had a Laurussian-wide distribution, with present-day localities from modern North America[4,9,11-14], northwestern Russia[12,15], France[16,17], Italy (Sardinia)[18] and Germany[4,11]. With a body length usually well in excess of one metre, they are believed to have constituted the predominant terrestrial herbivore fauna of their time[9, 11-19]. Since several lines of evidence, however, appear to contradict this terrestrial hypothesis, we here re-evaluate the biology of these stem synapsids in light of a possible aquatic lifestyle and furthermore focus on information relevant to the evolution of the respiratory apparatus among synapsids.

2. Results

2.1 Anatomy of the cervical and appendicular skeleton

A trunk that is encased by long and directly laterally extending ribs creates the overall barrel-like physiognomy of caseids (Fig. 1a). The extremities have large, almost paddle-like autopodia (Fig. 1c-d). Also characteristic are the ponderous shoulder girdle and the extremely short neck and tiny head (Fig. 1a). The vertical height of the shoulder girdle serves as a minimum estimate of the dorso-ventral distance of the head from the ground in resting position. Even if it were assumed that the neck and head could have been lowered almost vertically (which probably would have been prevented by the long cervical ribs), *Cotylorhynchus* would not have been able to reach the ground with its mouth (Fig. 1b).

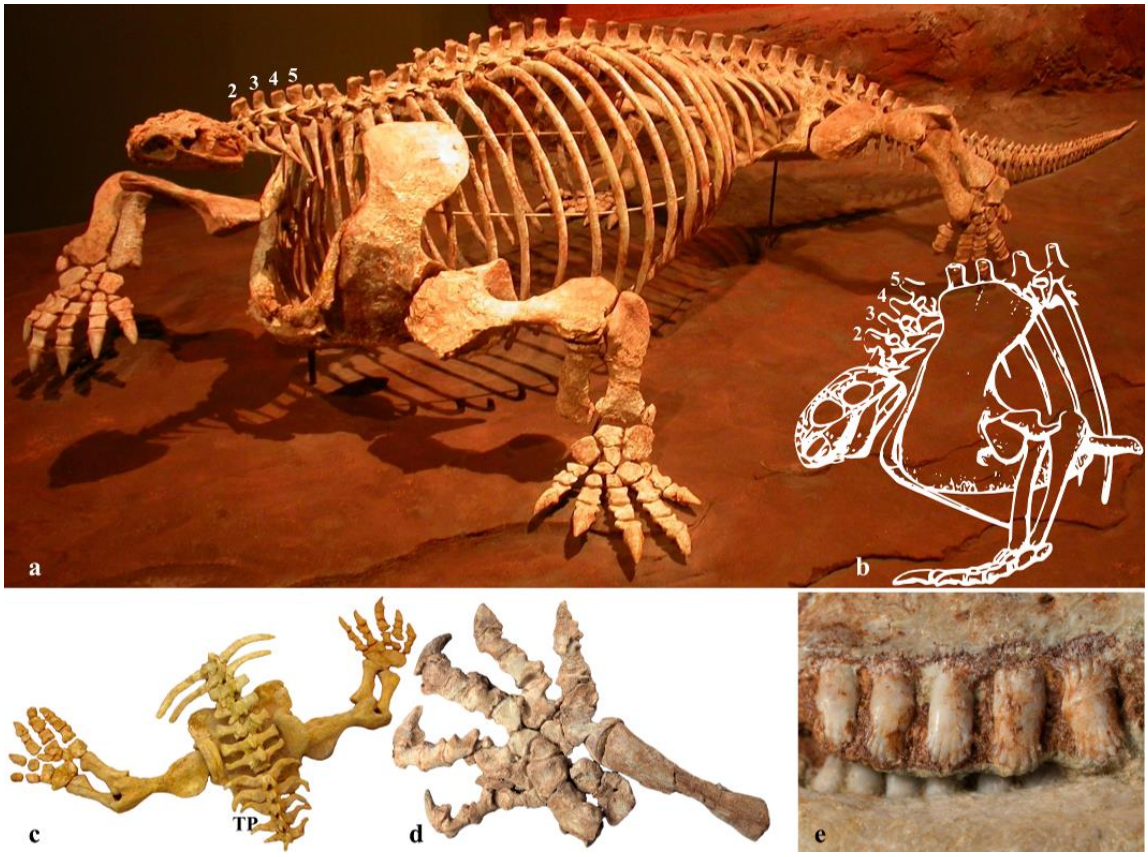

Figure 1 General appearance of caseids. (**a**) Photograph of a mounted *Cotylorhynchus romeri* at OMNH (courtesy M. Wedel). (**b**) The tiny head with its short neck could not have reached past the shoulder girdle (redrawn after Stovall *et al.*[28]). Numbers above the vertebrae correspond to those in (**a**). (**c**) Pelvic region of *C. romeri* in dorsal view showing the dorsoventrally flattened posterior extremities and broadened transverse processes (TP) of the caudal vertebrae. (**d**) Flattened left distal anterior extremity of *Euromycter rutenus*. (**e**) Sulcated teeth of *E. rutenus*.

2.2 Histology and compactness of the limb bones

The histology of the limb bones (humerus, femur and ulna) of adult North American *Cotylorhynchus romeri*, as well as that of juvenile conspecifics (humerus and femur) consistently revealed an extremely cancellous, osteoporotic-like condition at mid-diaphysis (Fig. 2). This low-density architecture is accompanied by an extremely thin cortex of nearly avascular lamellar bone (Fig. 2f-g). No qualitative ontogenetic structural changes between young and adult animals were evident, and the interior of the adult bone strongly resembles the microskeletomorphology of the juveniles (compare Fig. 2b and 2d, 2c and 2e). Even in the much larger bones of the adults, the outer portion is only slightly denser than the central

region. Quantitative analysis of the compactness of these bones revealed that only 32% of the entire cross-sectional area of the adult humerus actually is made up of bony tissue. In the adult femur, the compactness could not be quantified, because it was largely reconstructed with plaster (white) and several additional large holes (black) were scattered throughout the cross-section. The overall appearance, however, is very similar to that of the humerus, although the femur appears to be slightly more compact than the former. Values for the juveniles indicate that 18% of the humerus and 12% of the femur cross-sections consist of bony tissue: even less compact bone than for the adult humerus.

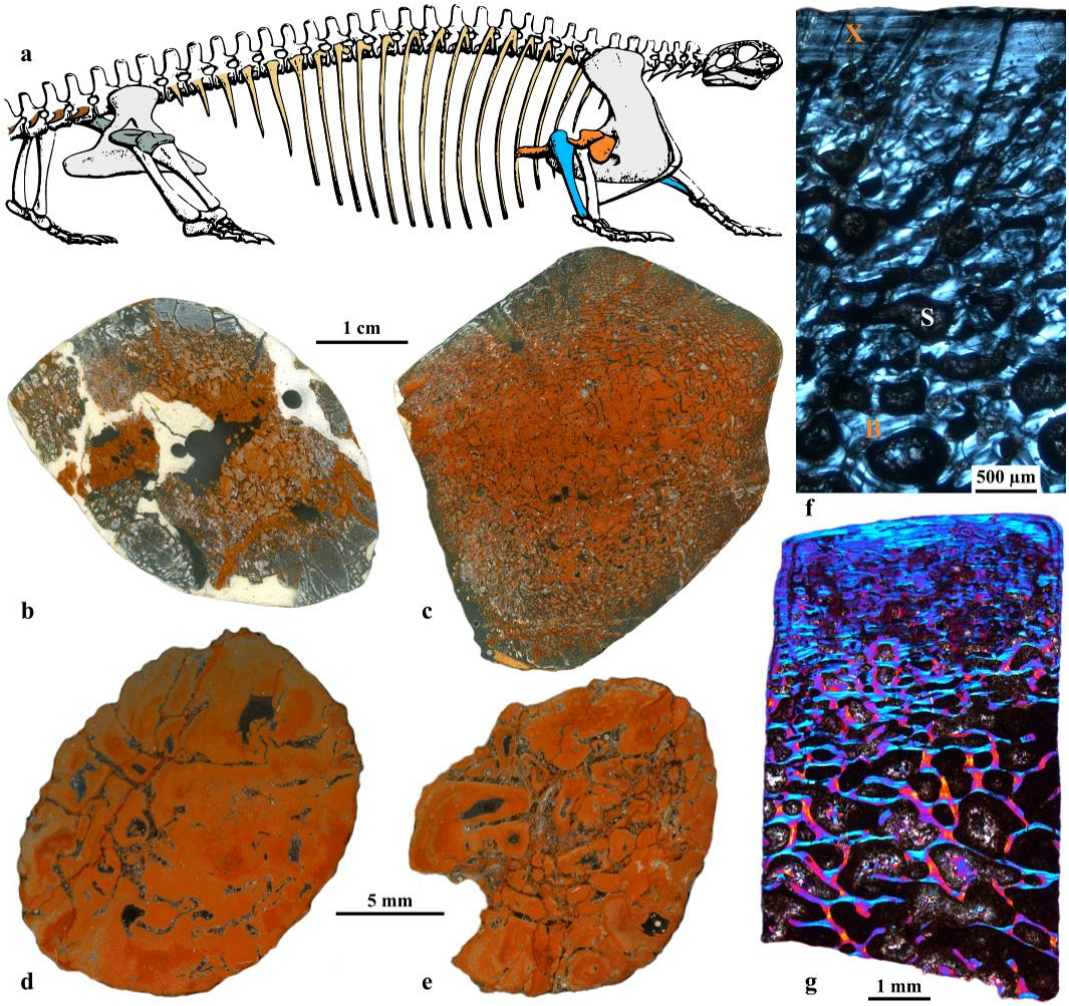

Figure 2 Histology of caseian limb bones. (**a**) Overview of the skeleton of *Cotylorhynchus romeri* (redrawn after Stovall *et al.*[28]) highlighting the bones discussed in the present study. Scans of cross sections through the mid-diaphysis of an adult femur 27.2 cm in length (**b**) and humerus (26.8 cm) (**c**), and of a juvenile femur (7.5 cm) (**d**) and humerus (7.6 cm) (**e**). (**f**) Photomicrographic detail of the adult humerus under polarized light showing an extremely thin cortex (X). (**g**) Photomicrograph of a cored adult ulna (15.5 cm in length) under polarized

light with lambda filter showing the same osteoporotic-like bone histology as in the other long bones. Note that each bone cut for this study is most likely from a separate organism. B: bone; S: interstitial space.

2.3 Rib articulation in caseids

The ribs in caseids articulate at two points with the vertebral column, the proximal capitulum and the distal tuberculum. The capitulum articulates with the vertebral column at the centrum and the tuberculum articulates dorsally with the transverse process. Throughout the entire vertebral column, the tuberculum articulates almost directly dorsal to the capitulum, which results in a virtually perpendicular orientation of the ribs (Fig. 3). This pattern is generally designated as “bucket-handle” articulation. From this position, the maximal caudad inclination that the ribs potentially could exhibit (maximum swing angle) was determined to be 15°

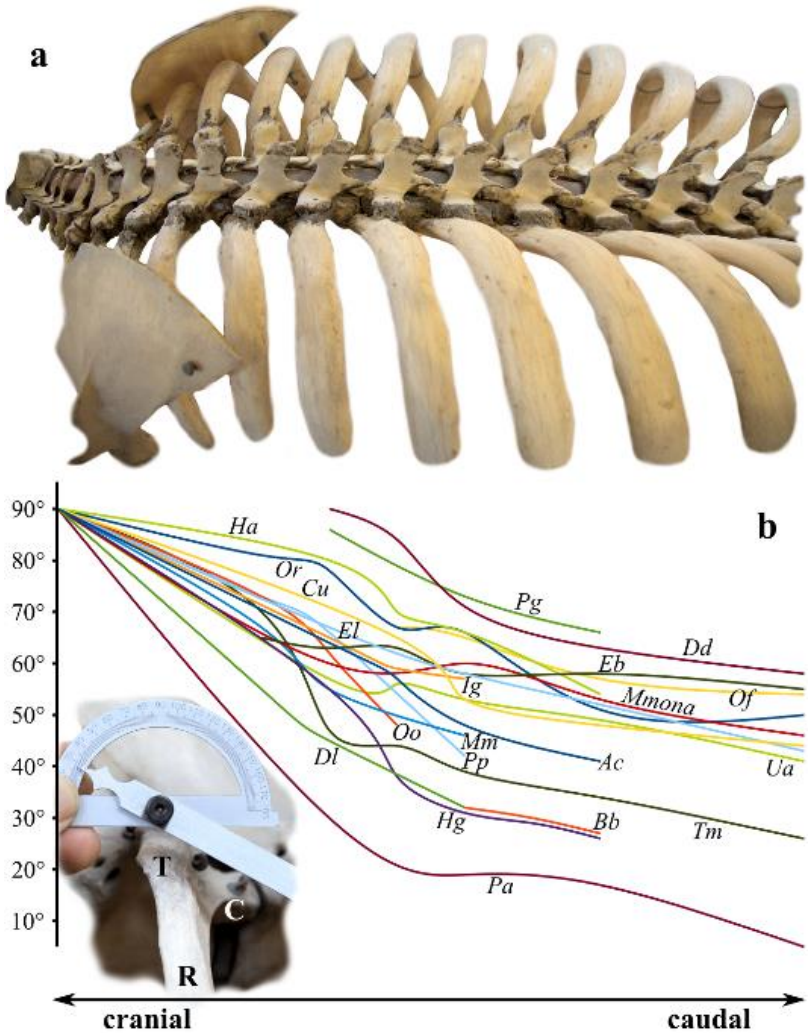

Figure 3 Rib articulation in mammals. (**a**) Dorsolateral view of the trunk of a West Indian

manatee (*Trichechus manatus*) on display at MNHN. (**b**) Diagram showing the measured angles for various post-cervical ribs and species. Inset shows how the angles of rib (R) articulation were measured. C: capitulum; T: tuberculum. Lettering in the diagram corresponds to the abbreviated species names, which can be found in the Methods.

2.4 Histology of caseian ribs

The micromorphology of the ribs exhibits a thin cortex and a well-defined medullary cavity filled with a network of secondary trabeculae (Fig. 3d). The cortical tissue is composed of dense, slow-growing lamellar bone with well-defined primary and secondary osteons. The bone matrix appears almost acellular due to the extremely small size of the osteocyte lacunae, a characteristic that seems to be unique to Caseidae. Dense concentrations of Sharpey's fibres are found both on the cranial and the caudal side of the ribs, and extend through the entire cortex (Fig. 3d-e).

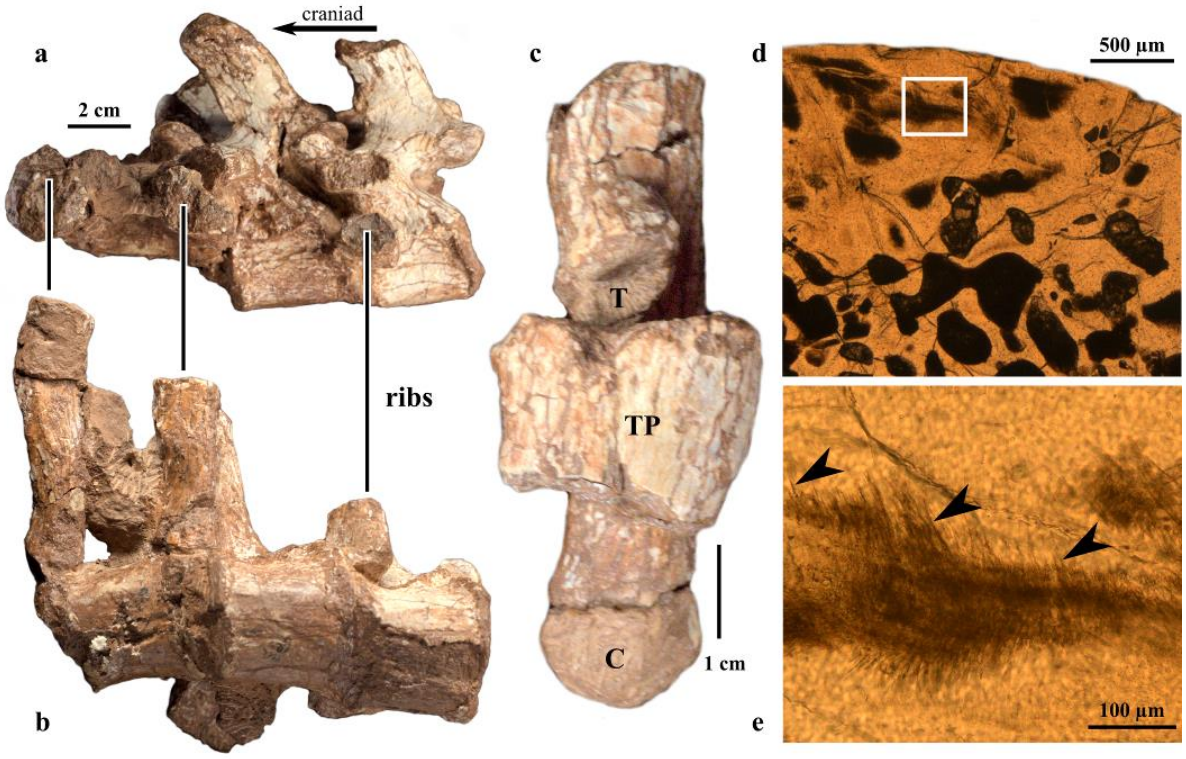

Figure 4 Rib articulation and histology in caseids. Three partial "thoracic" vertebrae with articulated ribs of *Ruthenosaurus russellorum* in left lateral (**a**) and ventral (**b**) view. (**c**) Dorsal view of an isolated proximal rib fragment showing the capitulum (C), tuberculum (T) and rest of the distal transverse process (TP). (**d**) Photomicrograph of a partial cross section of a rib from *Cotylorhynchus romeri* under normal light. (**e**) Detail of the content of the white frame in (d), showing densely packed Sharpey's fibres oriented towards the edge of the rib

(arrowheads).

2.5 Rib angles in mammals

Mammalian ribs also exhibit two articulations with the vertebral column, but show a position-specific angle between the articulation points of the capitulum and tuberculum. This angle on the first rib in all mammalian species examined was at about 90°. These first ribs consequently are oriented perpendicularly to the axis of the vertebral column as in caseids. Unlike caseids, however, in mammals the angle between the two articulations decreases gradually as one proceeds caudad (Fig. 4). Already at rib number 6, the average angle has changed from 90° to 60°. Thus, the more caudal ribs become progressively angled.

2.6 Costal ventilation in caseids

If the ribs were oriented perpendicularly in resting position as seen in the fossils, any costal movements would have resulted in a decrease in trunk volume. We consequently define this position as maximum inspiration. Maximum resting expiratory position is set at 15° inclination (compare above). Beginning in this assumed position, maximal costal movements would increase trunk volume from 427.65 litres to 441.79 litres in our assumed ellipsoid model *Cotylorhynchus* trunk (Fig. 5). This equals an increase in volume of 3.3%, or a potential vital capacity of 14.14 litres. Using a more realistic degree of excursion for the ribs during normal ventilation (10°), trunk volume would increase from 435.90 litres to 441.79 litres. This represents a gain in volume of roughly 1.4% or an assumed tidal volume (the volume of air inspired or expired during habitual breathing) of 5.89 litres (Fig. 5).

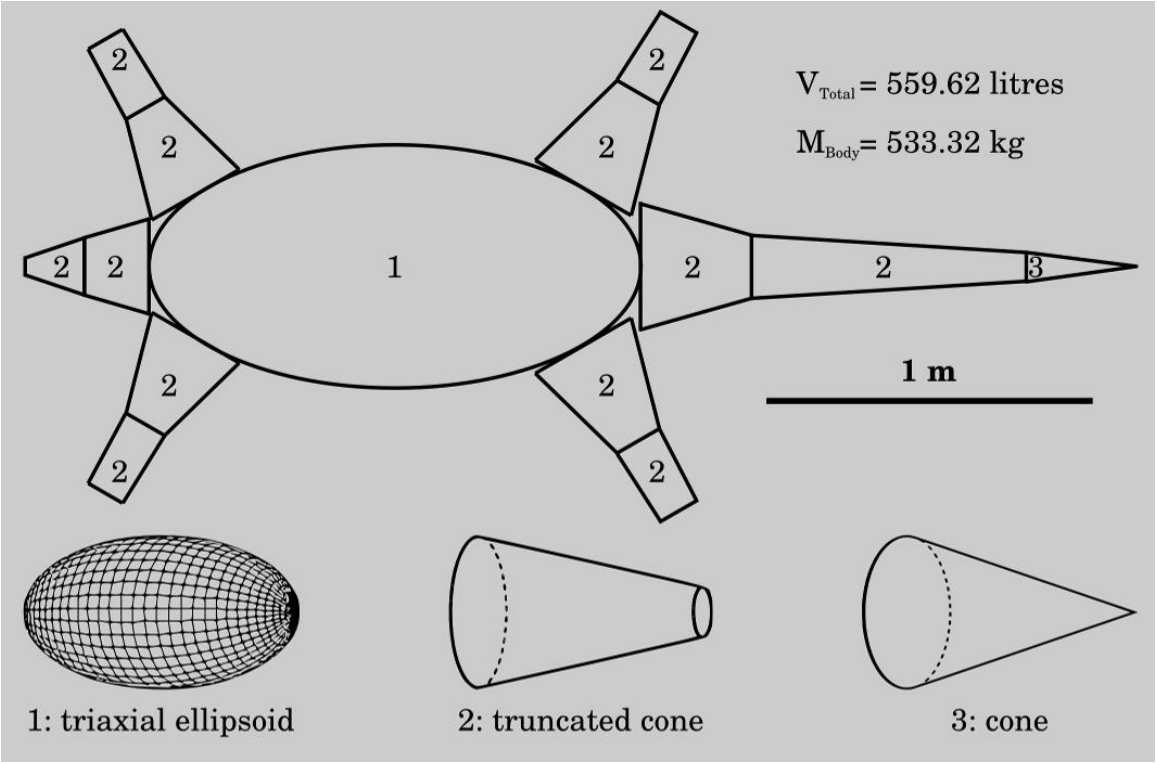

Figure 5 Geometrical model used for body mass estimation. The entire animal, except for the autopodia, which are left out of the reconstruction, is composed of a triaxial ellipsoid for the trunk, and truncated cones and a cone for the appendages.

2.7 Pulmonary parameters and body mass in *Cotylorhynchus*

Based on the geometrical model (Fig. 6), we estimate body mass in *Cotylorhynchus* to be approximately 533 kg. Using the allometric relationship between body mass and lung volume developed for marine turtles[20], such a specimen accordingly would have had a pulmonary volume of 37.36 litres, of which approximately 1.92 litres are dead space. Combining these data with our analyses on costal ventilation given above, the maximal possible volumetric change (14.14 litres), would account for a vital capacity of about 37.84% of total lung volume. Subtracting the dead space, we arrive at a maximum of 32.70% of total pulmonary volume that can be replaced by a single, deep breath, based on the maximal possible excursion of the ribs of 15°. Using the more conservative estimate of rib excursion for regular tidal ventilation (10°), this would result in 15.77% of total pulmonary volume, or 10.63% taking dead space into account.

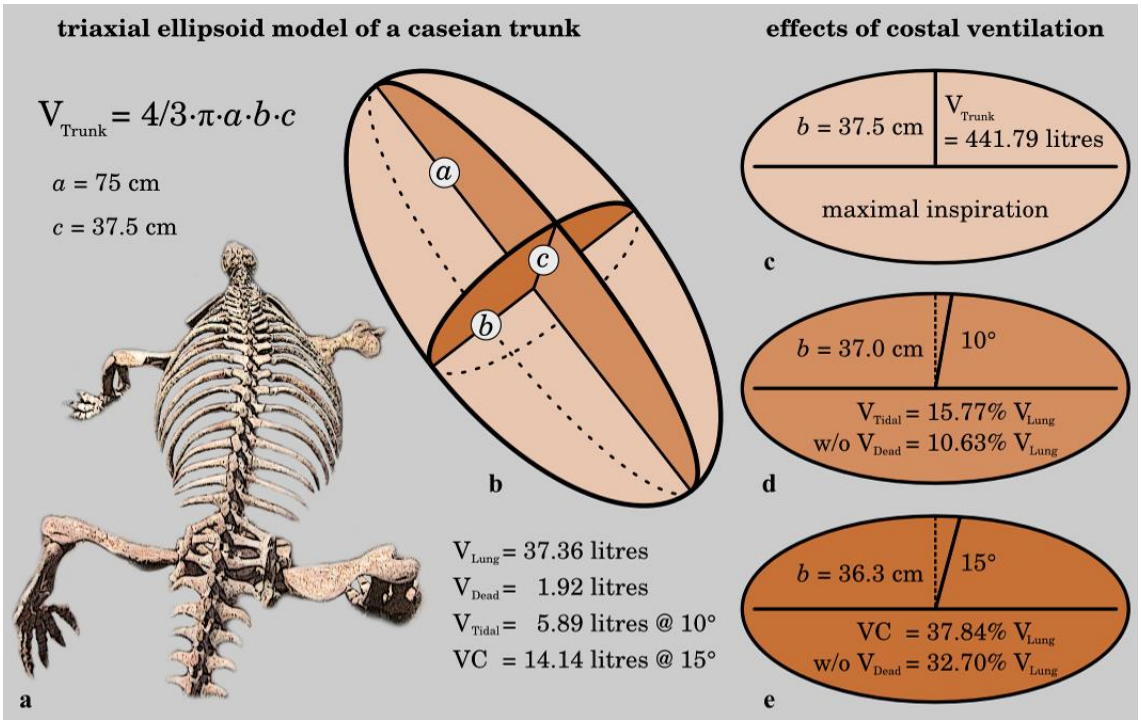

Figure 6 Simulated breathing mechanics in *Cotylorhynchus*. (**a**) Mounted specimen on display (OMNH), illustrating the ellipsoid shape of the trunk. (**b**) Triaxial ellipsoid as used for the modelling. (**c-e**) Frontal sections through the ellipsoid at various stages of rib movement. (**c**) maximal inspiration. (**d**) normal resting position, ribs inclined at 10°. (**e**) maximal expiratory position, ribs inclined at 15°

3. Discussion

The goal of the present paper is to evaluate aspects of caseian anatomy that can provide insight into whether the animals were strictly terrestrial or whether they might have had a predominantly aquatic biology, including underwater foraging. Since the latter would place constraints on the respiratory system, both with regards to breath holding and rapid replenishing of air upon resurfacing, we also examined osteological indicators of breathing mechanics. Evidence for terrestrial versus aquatic biology is juxtapositioned and summarized in Table 1.

Table 1. Comparison of a terrestrial vs. (semi-)aquatic lifestyle for caseids. Implications that provide a significant conflict with a hypothesis are indicated in red.

	implications for … lifestyle	
"character complex"	terrestrial	(semi-)aquatic
sedimentary deposits	intuitive explanation	draughts as a common cause of death
paddle-like autopodia	digging behaviour	swimming (paddling!) and (submerged) digging behaviour
short neck and tiny head	drinking virtually impossible, feeding severely restricted	cost-effective underwater foraging in 3D
limb bone histology	low strength and stiffness, limited weight bearing capacity	indicative of aquatic adaptation
costal ventilation	marginally sufficient for ventilation at rest, but insufficient during exercise	too small volumetric changes for sufficient ventilation after diving

The localities in which caseids are found have been characterized as outcrops of sediments that indicate relatively dry to arid environments. Although this argument is usually used as evidence that the animals actually inhabited such terrestrial environments[9,11-18], it is also possible that that they were fossilized under conditions different from those that represent their favoured habitat. The sandstone layers that indicate dry conditions alternate with mudstone layers, which unambiguously indicate that water was periodically present to a large extent in the same localities[13,15,16,18]. The relatively large number of specimens recovered, frequently in groups[12,14], may indicate that they died due to environmental factors that caused them to congregate. The hippopotamus (*Hippopotamus amphibius*) represents a modern analogue for such a phenomenon. It is well known that these animals are aquatic and in times of drought gather in the remaining water holes. Once these pools also dry up, the population could become extinct, numerous dead specimens eventually becoming preserved surrounded by sediments indicative of arid regions[21] in spite of the known lifestyle of this species. If such a sequence of events led to the observed excellent preservation of numerous individuals, (semi-)aquatic caseids are perfectly consistent with the hypothesis that the initial herbivory was acquired in dry upland environments from which they eventually moved to the wetter lowlands[4].

With the possible exception of the recently described Late Carboniferous stem representative *Eocasea martini*, there is no doubt that caseids were herbivorous[4]. The heavy mandible, long pedicelate homodont teeth with apical sulcations (Fig. 1e), and the lack of canine teeth all indicate herbivory.[22] The teeth are usually compared with the tricuspid ones of iguanids[23], among which particularly the marine iguana, *Amblyrhynchus cristatus*, exhibits similar apical sulcations that are lacking in the terrestrial species. Another characteristic of the skull remains enigmatic: the very large nasal openings. These have also been compared with those of the marine iguana[24] and could possibly have housed a mechanism for nasal closure. The barrel-like body with its long ribs and massive shoulder girdle effectively prevents dorso-ventral compression of the trunk, and combined with the tiny head and short neck means that the animal could not have reached the ground with its mouth (Fig. 1b). In the absence of any indication of a proboscis or specialisations of the tongue, one must assume that the animal had to enter the water in order to drink unless it were able to satisfy its needs from moist vegetation. Given the large size of caseids (*Cotylorhynhus*, for example, reaching 4 m in length and a presumed body mass in excess of 500 kg), however, the latter seems highly unlikely. In addition, the short neck and small head restrict the fraction of food resources that could be gleaned in a three-dimensional terrestrial environment without energy-consuming locomotion[25]. The large size and simple dentition, which was not suitable for mastication, indicate that the amount of vegetation consumed must have been considerable[26]. The osteoporotic-like histological structure of the long bones (see also below), however, does not indicate an animal that is well suited for constant locomotion or indeed migration, typical of many similar-sized extant mammalian herbivores. Romer and Price[11] compared caseids with sauropod dinosaurs because of the “curiously small head” in relation to body size. The long necks of sauropods, however, allowed them to maximize their feeding envelope and consume large amounts of vegetation with a minimum of locomotion, resulting in a highly efficient terrestrial herbivorous feeding strategy[27]. Taken together, the above-mentioned anatomical data indicate that it is unlikely that caseids foraged on land. Foraging in the water, however, where the animal can move with little energetic effort in three-dimensional space would correlate well with the caseian *Bauplan* (Fig. 7). The flattened, paddle like extremities (especially the autopodia) and the massive shoulder girdle as well as prominent transverse processes or fused ribs at the base of tail would have been instrumental as muscle attachments not only in terrestrial locomotion, but also in underwater foraging. We assume that the flattened autopodia are real, as it seems unlikely that the anterior and posterior autopodia on

both sides of the body would be diagenetically flattened[28] while the rest of the postcranial skeleton is not.

In a recent study of vertebral dimensions and their relationship to aquatic adaptations, it was found that caseids, and indeed all basal synapsids, cluster close to a variety of aquatic species[19]. The conclusion that caseids might have been aquatic, however, was rejected by the authors because it contradicted previous interpretations. In the seminal monograph by Romer and Price[11], terrestriality was the concluded habitat for caseids, but the authors did not rule out aquatic affinities: "To think of these barrel like creatures as swimming types seems absurd; but one may call to mind the case of the hippopotamus." Furthermore, ichnological support for at least a semi-aquatic environment for caseids comes from the Lower Permian of France, where swimming tracks ascribed to members of this group were found[29,30].

The osteoporotic-like appearance of the limb bones (Fig. 2), which may consist of as little as 12% bony tissue, while not excluding the possibility that caseids spent some time on dry land for thermoregulating, mating, oviposition or the like, are highly inconsistent with the hypothesis that these massive animals were predominantly terrestrial. Osteoporotic-like bone exhibits very low strength and stiffness and has very limited weight-bearing capacity[31,32]. Such bones, on the other hand, are characteristic of highly aquatic species[33,34] such as the elephant seals (Pinnepedia: *Mirounga* spp.). Not only the bone histology[35] but also the size and physiogomy of these animals, including paddle-like extremities, barrel-like trunk and short neck make them at least in part a good model for (limnic) caseids as a marine counterpart.

If one assumes that the main predators were terrestrial pelycosaurs, it appears curious that caseids – in particular the young – with their tiny heads and bulky bodies would have no possibility of defending themselves on land. Retreat to the water and submersion would seem an effective behavioural mechanism. Although this same argument could be applied to sauropod dinosaurs, which are presumed not to be aquatic, it is now assumed that these animals were r-strategists, producing large numbers of offspring[27]. Little is known about the reproductive biology of caseids, but if their terrestrial motility was as limited as their bone histology indicates, it is likely that they remained near their breeding grounds, and retreat to the water would have been their best means of escaping predation.

Since lungs, as gas filled organs, must act as flotation devices when animals are in the water, the respiratory system is integrally incorporated in the locomotor system of aquatic animals. In addition, if these animals forage underwater, it is expedient for them to empty and

fill the lungs in a single breath while surfacing in order to get back to the business of foraging. Indeed, both sea turtles and diving mammals are able to exchange nearly the entire pulmonary volume on surfacing[36,37], and the ribs of diving birds exhibit very long uncinate processes, which are instrumental in rapid and powerful inspiration[38].

The vertical orientation of the two costal articulation points (capitulum and tuberculum) results in a "bucket-handle" movement, with a frontal swing plane (Fig. 3). This pattern of articulation is more typical of ribs that have a supportive or postural rather than respiratory function (Holger Preuschoft pers. comm.). It is well suited to protect the trunk from compression during dives and in concert with action of the intercostal muscles, as indicated by the presence of Sharpey's fibres on both sides of the ribs, to dynamically provide stabilisation during locomotion. Despite the presence of a diaphragm, all extant mammals show a transition to an articulation in which the capitulum lies progressively more anterior to the tuberculum as one moves along the vertebral column (Fig 4). This allows the ribs to swing outward in a more "pump-handle" fashion, which increases volumetric changes of the trunk. Nevertheless, even the bucket handle configuration permits a certain amount of costal ventilation, and we were interested in testing the hypothesis that these ribs alone are sufficient to satisfy the respiratory needs of caseids. To this end, we created a three-dimensional ellipsoid model of the caseid trunk that allowed us to simulate costal ventilation. Since ribs with a vertical bucket-handle articulation swing only back and forth (that is, towards the head or tail but not diagonally), the length and height of the model remain constant and only the width changes. This allows us, knowing the changes in the width of the model, to calculate volumetric changes caused by the movement of the ribs (Fig. 5). A maximal excursion of 15° between maximal expiration and inspiration would result in a respiratory vital capacity (defined as the maximum amount of air that can be inspired or expired in a single breath) of 14.14 litres. Based on the osteological evidence, this is a liberal estimate as it suggests that the rib would articulate at the posterior-most point of the transverse process. Such a forced inspiration would result in a maximum replacement of 37.84% of the air within the lungs; 32.70% if we take into account the constant-volume dead space in the incompressible airways. These values appear very small compared with a vital capacity of around 75% of total pulmonary volume in man[39], for example. Vital capacity should not be confused with tidal volume (i.e. the amount of air inspired or expired with each breath during regular ventilation). In extant mammals for instance, tidal volume typically accounts for approximately 10% of vital capacity[40]. Our simulated tidal volume for caseids is 5.89 litres

and accounts for about 42% of vital capacity. Since most animals have considerable safety factors regarding vital functions, it appears strange that resting tidal volume in a caseid would be close to half of its vital capacity. At a more reasonable swing angle of 10°, slightly more than 10% of pulmonary volume can be replaced. These data suggest that caseids would be marginally capable of supplying the resting animal with fresh air by costal ventilation alone. For exercising animals, the situation would rapidly become critical, and becomes unrealistic if one takes a foraging (either terrestrial or aquatic), courting, mating, defending or otherwise active animal into account. Terrestrial foraging would require satisfying a high cost of transport accompanied by increased tidal volume and breathing frequency, while underwater foraging requires a tidal volume approaching total lung volume on surfacing. Neither of these alternatives could be satisfied by bucket-handle costal ventilation alone. An accessory breathing mechanism must be postulated in any case. We hypothesise that this mechanism was a diaphragm-homologue that arose in the upland ancestors of caseids and served as an exaptation allowing this group to arrive at a more aquatic lifestyle. Other possibilities for accessory breathing mechanisms are also known among tetrapods. These include buccal ventilation in amphibians and varanid lizards, the hepatic piston in crocodilians, and oblique abdominal muscles in chelonians[8]. Buccal pumping would be ineffective in caseids due to the tiny head[9], and the hepatic piston requires a kinetic pubis[41], lacking in caseids. This leaves the oblique abdominal muscle, a diaphragm-homologue or some unknown caseid-specific structure that could supplement rib breathing. The latter possibility is purely speculative and will not be further discussed. Given the phylogenetic proximity to mammals as opposed to the phylogenetic distance from turtles, a diaphragm-homologue is the most parsimonious possibility to circumvent this severe respiratory constraint.

The presence of a rib-free lumbar region in non-mammalian cynodonts has been taken to indicate the origin of the diaphragm[42,43], but this remains entirely speculative[44] as there are no direct, unambiguous osteological indicators for the diaphragm. The absence of a rib-free lumbar region does not necessarily indicate the lack of a muscular diaphragm. Diaphragm structure and function have been studied in the Florida manatee (*Trichechus manatus latirostris*)[45], an animal with upward arching ribs, a barrel-like trunk and a highly reduced lumbar region (Fig. 4a), all of which are reminiscent of caseids. The diaphragm serves the manatee not only in respiration but also in dynamic buoyancy control through separate adjustment of the volume of left and right lungs under water. While we do not suspect this refined mechanism in caseids, the manatee demonstrates that a highly functional diaphragm

can be present in an animal that virtually lacks a lumbar region. Also as in the manatee, the lungs could have been displaced dorsally under the arch of the ribs, thus providing optimal aquatic righting and buoyancy control. We propose that a diaphragm-homologue, already present in basal pelycosaurs, could have relieved the ribs and intercostal muscles of their respiratory function and made possible the observed bucket-handle rib articulation. This, in turn, provided stability for underwater foraging, coinciding with compelling indicators of an aquatic biology. A similar division of labour is also assumed for the evolution of the chelonian ventilatory apparatus, where the ribs took over an exclusively supportive function[46]. If a diaphragm-homologue were present in the basal synapsid lineages, it also must be assumed to have been present in the earliest cynodont therapsids. This could help explain how these animals may have coped with falling environmental temperatures and oxygen concentrations during the Permian mass extinction, through evolution of the highly efficient bronchioalveolar lung, endothermy and high-performance physiology.

In summary, we find that many anatomical characteristics of caseids are more indicative of an aquatic biology than a terrestrial one (Fig. 7). No trait actually would prevent an aquatic biology, while several appear to strongly contradict the purely terrestrial hypothesis (Table 1, see comments on ventilation below). The osteoporotic-like bone histology in particular unambiguously indicates unsuitability for habitual weight support and extensive terrestrial locomotion. Also the neck constraint presents problems, which remain difficult to circumvent in a strictly terrestrial environment. The perpendicular bucket-handle rib articulation is self-limiting for costal breathing (even on land), and at the same time provides a stable configuration for stiffening the trunk during diving and locomotion in general, whereas the presence of a diaphragm-like breathing muscle relieves the ribs of their respiratory function. A diaphragm-homologue consequently appears to have been present in basal synapsids and may even represent an autapomorphy of this taxon.

Figure 7 Life reconstruction of a large caseid such as *Cotylorhynchus*. Hypothesized underwater foraging is shown in the foreground, while adults and young are shown resting on land.

4. Methods

4.1 Species and specimens studied

Three species of caseids, with a focus on the well-documented giant North American *Cotylorhynchus romeri*, were compared to 29 species of extinct and extant crown synapsids (mammals) and three species of sauropsids. The specimens are deposited at MNHN (Muséum national d'Histoire naturelle, Paris, France), OMNH (Sam Noble Oklahoma Museum of Natural History, Norman, OK, USA), STIPB (Steinmann-Institut für Geologie, Mineralogie

und Paläontologie, Goldfuß Museum, Bonn, Germany), and ZFMK (Zoologisches Forschungsmuseum Alexander Koenig, Bonn, Germany). Extinct taxa are marked with a dagger (†).

Synapsida
Caseasauria: Caseidae
†*Cotylorhynchus romeri* Stovall, 1937: OMNH 631, OMNH 627, OMNH 655, OMNH 1673, OMNH 1728, OMNH 4329
†*Euromycter rutenus* (Sigogneau-Russell & Russell, 1974): MNHN.F.MCL-2 (holotype), STIPB R 639 "Gilbert" (cast)
†*Ruthenosaurus russellorum* Reisz *et al.*, 2011: MNHN.F.MCL-1 (holotype)

Monotremata: Ornithorhynchidae
Ornithorhynchus anatinus (Shaw, 1799): MNHN.A.3316

Monotremata: Tachyglossidae
Zaglossus bruijni Peters & Doria, 1876: MNHN.A.3318

Placentalia: Bovidae
Bison bison (Linnaeus, 1758): MNHN.A.10618
Bos mutus (Przewalski, 1883): MNHN.1864-15

Placentalia: Cetacea
Balaenoptera physalus Linnaeus, 1758: MNHN.1894-36
†*Cynthiacetus peruvianus* Martínez-Cáceres & Muizon, 2011: MNHN.F.PRU10 (holotype)
Delphinapterus leucas (Pallas, 1776): MNHN.A.3246
Inia geoffrensis Blainville, 1817: MNHN.A.61
Megaptera novaeangliae (Borowski, 1781): MNHN.A.2931
Monodon monoceros Linnaeus, 1758: MNHN.A.3235
Orcinus orca (Linnaeus, 1758): MNHN.A.3231
Phocoena phocoena (Linnaeus, 1758): MNHN.1983-31

Placentalia: Hippopotamidae

Hippopotamus amphibius Linnaeus, 1758: MNHN.A.7986

Placentalia: Mustelidae
Aonyx capensis (Schinz, 1821): MNHN.A.3388
Enhydra lutris (Linnaeus, 1758): MNHN.A.10951

Placentalia: Pinnipedia
Callorhinus ursinus (Linnaeus, 1758): MNHN.A.11972
Erignathus barbatus (Erxleben, 1777): MNHN.A.7949
Monachus monachus Hermann, 1779: MNHN.A
Odobenus rosmarus (Linnaeus, 1758): MNHN.A.14015
Otaria flavescens Shaw, 1800: MNHN.A.7958
Pagophilus groenlandicus (Erxleben, 1777). MNHN.A.7955

Placentalia: Sirenia
Dugong dugon (Müller, 1776): MNHN.A.14515
†*Halitherium schinzii* (Kaup, 1838): MNHN.Cat6.1884
†*Hydrodamalis gigas* (Zimmermann, 1780): MNHN.A.14516
†*Metaxytherium cuvieri* de Christol, 1832: MNHN.F.1921-10
Trichechus manatus Linnaeus, 1758: MNHN.A.14514
Trichechus senegalensis Link, 1795: MNHN.A.14399

Placentalia: Suidae
Phacochoerus aethiopicus (Pallas, 1766): MNHN.A.14037

Placentalia: Ursidae
Ursus americanus Pallas, 1780: MNHN.A.3503

Sauropsida
Lepidosauria: Iguania
Amblyrhynchus cristatus Bell, 1825: ZFMK 84167
Ctenosaura pectinata (Wiegmann, 1834): ZFMK 59067
Iguana iguana (Linnaeus, 1758): ZFMK 14843

4.2 Bone histology

Humerus, femur and ribs of adult and humerus and femur of juvenile *Cotylorhynchus romeri* were embedded in resin, cut at mid-diaphysis (humeri and femora) or distal to the rib head (ribs), and processed according to standard procedures[47]. One ulna of an adult from the same species was core-drilled at mid-diaphysis and processed according to standard procedures as well[48]. Mounted thin sections were cover-slipped and analysed with a Leica DM2500LP Polarizing Microscope configured with a 360° rotating stage under normal, polarized, and lambda filtered, polarized light. Photomicrographs were taken with a Leica DFC420 color camera and processed using the Leica ImageAccess easyLab 7 software (Leica, Wetzlar, Germany). Entire cross sections of bones were scanned against a black background using an Epson Perfection V750 Pro high-resolution transmitted light scanner (Epson, Japan), yielding bone in grey tones, sediment in red tones, plaster for reconstruction in white, and holes in the bone in black. The images were edited and compiled into figures using GIMP 2.8 (www.gimp.org) and Inkscape 0.48.4. (www.inkscape.org).

4.3 Morphometry of bone compactness

Bone compactness (ratio of bone tissue area to total cross-sectional area) was calculated according to standard stereological point counting methods[49]. To this end, a grid was digitally superimposed on the cross sections using Inkscape. The mesh size of the grid was chosen such that a minimum of 200 points over tissue were obtained, and the grid was placed at random. The computer programme Bone Profiler[50], which is routinely used in such quantitative palaeohistological analyses, could not be employed here, because the delicate trabeculae of the exceptionally osteoporotic-like bone did not allow high-contrast images of sufficient quality for automated analysis. Since stereological methods have been used to quantify medically relevant osteoporotic changes[51], we feel that its application is justified also in the present case.

4.4 Measurement of rib angles

Rib angles were measured to the nearest degree with a hand-held, contact goniometer. The reference plane was aligned to the horizontal vertebral axis and the angle between tuberculum and capitulum of selected ribs between numbers 1 and 12 was determined (see Fig. 4b, inset). Measurements were plotted and the values connected using LibreOffice Calc

4.1.3.2 (www.libreoffice.org) and the resulting diagram was imported to Inkscape to finalize Fig. 4b. To assess the range of motility for caseian ribs, we determined the maximal inclination relative to the sagittal vertebral axis that the ribs can exhibit, such that the tuberculum would still be able to articulate with the posterior margin of the transverse process.

4.5 Rib movements and volumetric changes in *Cotylorhynchus*

Based on the anatomical parameters of the ribcage as determined by the methods explained above, we calculated the possible volumetric changes for caseids, which allows us to estimate vital capacity and tidal volume (see below). For practical purposes, we approximated the entire trunk region as a triaxial ellipsoid (Fig. 5). We assumed the trunk length for *Cotylorhynchus* to be 1.5 m and the height and maximum width both to be 0.75 m, in order to approximate the restoration by Stovall *et al.*[28]. The mechanical restriction to bucket-handle movements that is caused by the vertical alignment of the rib articulations allowed us to use a two-dimensional (2D) approach to determine the changes in trunk volume that could be caused by costal ventilation. Since the height and length of the trunk (representing the first two axes of the ellipsoid) are not affected by bucket-handle costal movements, only the width is changed. We generated an elliptical approximation of a frontal section through a model caseid in Inkscape, to which "ribs" that reach to the margin of the approximated frontal section were added in the form of straight lines. The centre of rotation for these ribs was placed at the "vertebral column". The orientation with the ribs set at an angle of 90° represents the state of maximal inspiration. We used the determined maximal inclination of the ribs (see above) as the hypothetical resting position at maximum expiration. The width of the 2D frontal section was fitted to this resting position so that its outline again touched the distal-most points of the "ribs". The same procedure was applied for an inclination of 10° deviant from the maximal inspiratory position to simulate a "normal" resting position. We determined the change in width of the ellipses between these two inclined positions and the perpendicular orientation of the ribs in the maximal inspiratory position. All three values accordingly were used to calculate the different volumes of the ellipsoid using the appropriate formula ($V_{Trunk}= 4/3*\pi*a*b*c$), whereby *a*, *b* and *c* represent the three semi-axes of length (0.75 m), height (0.375 m) and width (0.375 m at maximal inspiration or the calculated values, see above), respectively (Fig. 5b). The difference in volume between the maximal expiratory and maximal inspiratory position is defined as the vital capacity of the

lung (VC): the maximum amount of air that can be inspired or expired. The difference in volume between the inclination at 10° and maximal inspiratory position represents the assumed tidal volume (V_{Tidal}): the amount of air that is moved during a normal inspiration or expiration.

4.6 Reconstruction of lung volume, pulmonary dead space and body mass of *Cotylorhynchus*

In order to test the hypothesis that costal ventilation alone would be sufficient for caseids, lung volume and pulmonary dead space had to be approximated. Our current understanding of the amniote respiratory system suggests for caseids a multichambered lung structure similar to that of a sea turtle[52-54]. We used the allometric relationship between total pulmonary volume (V_{Lung}) and body mass (M_{Body}) developed by Hochscheid *et al.*[20]: V_{Lung} [l] = 0.1136 * $M_{Body}^{0.923}$. Although this scaling exponent is higher than that previously determined for reptiles in general (i.e. 0.75[55]), we agree with Hochscheid *et al.*[20] that, due to the relatively small lungs of the largest reptiles measured (sea turtles) in comparison to lizards, and the enormous variation in pulmonary structure among reptiles, an exclusively sea turtle-based exponent of 0.923 appears more realistic than the "global" reptilian one. There are unfortunately no data on an allometric relationship of dead space (V_{Dead}) in marine turtles, but Gatz *et al.*[56] have determined that the dead space in the green turtle (*Chelonia mydas*) is 3.6 ml/kg, and we use this value as the closest approximation available.

A requirement for all these approximations is a reliable estimate of body mass. Stovall *et al.*[28] estimated body mass in their *Cotylorhynchus* to be 331 kg based on the orthometric linear unit approach using vertebral dimensions[11,57], and subsequent authors usually cite this estimate[4]. We developed a volume-based approach similar to that used for marine mammals[58]. To this end, a caseid was approximated as the sum of simple geometrical elements (triaxial ellipsoid, truncated cone, cone) (Fig. 6). The autopodia were excluded, and the attachment points of the neck, extremities and tail with the trunk result in empty spaces that do not enter into the calculated volume and thus lead to a conservative estimate. The trunk volume was determined at maximal expiration (see above) to reduce air content. Body mass was estimated by assuming a mean density of 0.953 kg/litre[59].

5. References

1. Kemp, T. S. *The Origin and Evolution of Mammals* (Oxford University Press, 2005).

2. Rowe, T. Definitions, Diagnosis, and Origin of Mammalia. *J. Vertebr. Paleontol.* **8,** 241-264 (1988).

3. Brocklehurst, N., Kammerer, C. F, & Fröbisch, J. The early evolution of synapsids, and the influnce of sampling on their fossil record. *Paleobiology* **39,** 470-490 (2013).

4. Reisz, R. R. & Fröbisch, J. The oldest Caseid Synapsid from the Late Pennsylvanian of Kansas and the evolution of herbivory in terrestrial vertebrates. *PLoS ONE* **9,** e94518 (2014).

5. Rodrigues, P. G., Ruf, I. & Schultz, C. L. Digital Reconstruction of the Otic Region and Inner Ear of the Non-Mammalian Cynodont *Brasilitherium riograndensis* (Late Triassic, Brazil) and Its Relevance to the Evolution of the Mammalian Ear. *J. Mamm. Evol.* **20,** 291-307 (2013).

6. Perry, S. F, Similowski, T., Klein, W. & Codd, J. R. The evolutionary origin of the mammalian diaphragm. *Respir. Physiol. Neurobiol.* **171,** 1-16 (2010).

7. Hirasawa, T. & Kuratani, S. A new scenario of the evolutionary derivation of the mammalian diaphragm from shoulder muscles. *J. Anat.* **222,** 504-517 (2013).

8. Hsia, C. C. W, Schmitz, A., Lambertz, M., Perry, S. F. & Maina, J. N. Evolution of Air Breathing: Oxygen Homeostasis and the Transitions from Water to Land and Sky. *Compr. Physiol.* **3,** 849-915 (2013).

9. Reisz, R. R. in *Handbuch der Paläoherpetologie, Teil 17A*. (ed Wellnhofer, P.) 1-102 (Gustav Fischer Verlag, 1986).

10. Reisz, R. R., Godfrey, S. J. & Scott, D. *Eothyris* and *Oedaleops*: Do These Early Permian Synapsids from Texas and New Mexico form a Clade?. *J. Vertebr. Paleontol.* **29,** 39-47 (2009).

11. Romer, A. S & Price, L. I. Review of the Pelycosauria. *Geol. Soc. Am. Spec. Pap.* **28,** 1-

534 (1940).

12. Olson, E. C. Late Permian terrestrial vertebrates, U.S.A. and U.S.S.R. *Trans. Am. Philos. Soc., N. S.* **52,** 1-224 (1962).

13. Olson, E. C. Early Permian vertebrates of Oklahoma. *Okla. Geol. Surv. Circ.* **74,** 1-111 (1967).

14. Olson, E. C. The family Caseidae. *Fieldiana, Geol.* **17,** 225-349 (1968).

15. Maddin, H. C., Sidor, C. A. & Reisz, R. R. Cranial anatomy of *Ennatosaurus tecton* (Synapsida: Caseidae) from the Middle Permian of Russia and the evolutionary relationships of Caseidae. *J. Vertebr. Paleontol.* **28,** 160-180 (2008).

16. Reisz, R. R., Maddin, H. C., Fröbisch, J. & Falconnet, J. A new large caseid (Synapsida, caseasauria) from the Permian of Rodez (France), including a reappraisal of "*Casea*" *rutena* Sigogneau-Russell & Russell, 1974. *Geodiversitas* **33,** 227-246 (2011).

17. Sigogneau-Russell, D. & Russell, D. E. Étude du premier Caséidé (Reptilia, Pelycosauria) d'Europe occidentale. *Bull. Mus. Natl. Hist. Nat. (3^{e} série)* **230,** 145-215 (1974).

18. Ronchi, A., Sacchi, E., Romano, M. & Nicosia, U. A huge caseid pelycosaur from north-western Sardinia and its bearing on European Permian stratigarphy and palaeobiogeography. *Acta Palaeontol. Pol.* **56,** 723-738 (2011).

19. Felice, R. N. & Angielczyk, K. D. in *Early Evolutionary History of the Synapsida* (eds Kammerer, C. F., Angielczyk, K. D. & Fröbisch, J.) 25-51 (Springer Verlag, 2014).

20. Hochscheid, S. *et al*. Allometric scaling of lung volume and its performance for marine turtle diving performance. *Comp. Biochem. Physiol. A* **148,** 360-367 (2007).

21. Jernvall, J., Wright, P. C., Ravoavy, F. L. & Simons, E. L. Report on Findings of Subfossils at Ampoza and Ampanihy in Southwestern Madagascar. *Lemur News* **8,** 21-23

(2003).

22. King, G. *Reptiles and Herbivory* (Chapman & Hall, 1996).

23. Sues, H.-D. & Reisz, R. R. Origins and early evolution of herbivory in tetrapods. *Trends Ecol. Evol*. **13,** 141-145 (1998).

24. Williston, S. W. *American Permian Vertebrates* (University of Chicago Press, 1911).

25. Preuschoft, H. Hohn, B., Stoinski, S. & Witzel, U. in *Biology of the Sauropod Dinosaurs - Understanding the Life of Giants* (eds Klein, N., Remes, K., Gee, C. T. & Sander, P. M.) 197-218 (Indiana University Press, 2011).

26. Schmidt-Nielsen, K. *Scaling - Why is Animal Size so Important?*. (Cambridge University Press, 1984).

27. Sander, P. M. *et al*. Biology of the sauropod dinosaurs: the evolution of gigantism. *Biol. Rev. Camb. Philos. Soc.* **86,** 117-155 (2011).

28. Stovall, J. W., Price, L. I. & Romer, A. S. The Postcranial Skeleton of the Giant Permian Pelycosaur *Cotylorhynchus romeri*. *Bull. Mus. Comp. Zool. Harv. Univ.* **135,** 1-30 (1966).

29. Gand, G. Interprétations paléontologique et paléoécologique de quatre niveauxà traces de vertébrés observes dans l'Autunien du Lodévois (Hérault). *Géologie de la France* **2,** 155-176 (1986).

30. Gand, G. Essai de reconstitution paléoenvironnementale et paléoécologique d'un partie du nord du bassin de Lodève (Hérault) au Permien inférieur. *Géologie de la France* **4,** 17-30 (1989).

31. Dickenson, R. P., Hutton, W. C. & Stott, J. R. The mechanical properties of bone in osteoporosis. *J. Bone Joint Surg. Br.* **63-B,** 233-238 (1981).

32. Oxnard, C. E. Bone and bones, architecture and stress, fossils and osteoporosis. *J. Biomech.* **26(Suppl. 1),** 63-79 (1993).

33. Laurin, M., Canoville, A. & Germain, D. Bone microanatomy and lifestyle: A descriptive approach. *CR Palevol* **10,** 381–402 (2011).

34. Houssaye, A. Bone histology of aquatic reptiles: what does it tell us about secondary adaptation to an aquatic life? *Biol. J. Linn. Soc.* **108,** 3-21 (2013).

35. Hayashi, S. *et al*. Bone Inner Structure Suggests Increasing Aquatic Adaptations in Desmostylia (Mammalia, Afrotheria). *PLoS ONE* **8**, e59146 (2013).

36. Lutcavage, M. E. & Lutz, P. L. in *The Biology of Sea Turtles* (eds Lutz, P. L. & Musick, J. A.) 277-296 (CRC Press, 1997).

37. Wartzok, D. in *Encyclopedia of Marine Mammals*, 2nd edition (eds Perrin, W. F., Würsig, B. & Thewissen, J. G. M.) 152-156 (Academic Press, 2008).

38. Tickle, P. G., Ennos, A. R., Lennox, L. E., Perry, S. F. & Codd, J. R. Functional significance of the uncinate processes in birds. *J. Exp. Biol.* **210,** 3955-3961 (2007).

39. Thews, G. in *Physiologie des Menschen*, 28th edn (eds Schmidt, R. F., Thews, G. & Lang, F.) 565-591 (Springer Verlag, 2000).

40. Gleysteen, J. J. & Stroud, R. C. in *Respiration and Circulation* (eds Altman, P. L. & Dittmer, D. S.) 56-59 (Federation of American Societies for Experimental Biology, 1971).

41. Farmer, C. G. & Carrier, D. R. Pelvic aspiration in the American alligator (*Alligator mississipiensis*). *J. Exp. Biol.* **203,** 1679-1687 (2000).

42. Parrington, F. R. On the Cynodont Genus *Galesaurus*, with a Note on the Functional Significance of the Changes in the Evolution of the Theriodont Skull. *Ann. Mag. Nat. Hist. (Series 10)* **13(73),** 38-67 (1934).

43. Brink, A. S. Speculations on some advanced mammalian characteristics in the higher mammal-like reptiles. *Palaeontol. Afr.* **4,** 77-96 (1956).

44. Crompton, A. W. & Jenkins, F. A. Jr. Mammals from Reptiles: A Review of Mammalian Origins. *Annu. Rev. Earth Planet. Sci.* **1,** 131-155 (1973).

45. Rommel, S. & Reynolds, J. E. III. Diaphragm Structure and Function in the Florida Manatee (*Trichechus manatus latirostris*). *Anat. Rec.* **259,** 41-51 (2000).

46. Lyson, T. R. *et al*. Origin of the unique ventilatory apparatus of turtles. *Nature Commun.* (in press).

47. Shelton, C. D., Sander, P. M., Stein, K. & Winkelhorst, H. Long bone histology indicates sympatric species of *Dimetrodon* (Lower Permian, Sphenacodontidae). *Trans. R. Soc. Edinb. Earth Sci.* **103,** 1-20 (2013, "2012").

48. Stein, K. & Sander, P. M. in *Methods in Fossil Preparation: Proceedings of the First Annual Fossil Preparation and Collections Symposium* (eds Brown, M. A., Kane, J. F. & Parker, W. G.) 69-80 (Petrified Forest, 2009).

49. Howard, C. V. & Reed, M. G. *Unbiased Stereology - Three-Dimensional Measurement in Microscopy*, 2nd edn (Garland Science/BIOS Scientific Publishers, 2005).

50. Girondot, M. & Laurin, M. Bone Profiler: A tool to quantify, model, and statistically compare bone-section compactness profiles. *J. Vertebr. Paleontol.* **23,** 458-461 (2003).

51. Melsen, F., Melsen, B., Mosekilde, L. & Bergmann, S. Histomorphometric Analysis of Normal Bone From the Iliac Crest. *Acta Pathol. Microbiol. Scand., Sect. A Pathol.* **86,** 70-81 (1978).

52. Perry, S. F., Darian-Smith, C., Alston, J., Limpus, C. J. & Maloney, J. E. Histological Structure of the Lungs of the Loggerhead Turtle, *Caretta caretta*, Before and After Hatching.

Copeia **1989(4),** 1000-1010 (1989).

53. Lambertz, M., Böhme, W. & Perry, S. F. The anatomy of the respiratory system in *Platysternon megacephalum* Gray, 1831 (Testudines: Cryptodira) and related species, and its phylogenetic implications. *Comp. Biochem. Physiol. A* **156,** 330-336 (2010).

54. Lambertz, M., Grommes, K., Kohlsdorf, T. & Perry, S. F. Lung structure in the first amniotes: why simple if it can be complex?. *Nature* (under review).

55. Tenney, S. M. & Tenney, J. B. Quantitative morphology of cold-blooded lungs: Amphibia and Reptilia. *Respir. Physiol.* **9,** 197-215 (1970).

56. Gatz, R. N., Glass, M. L. & Wood, S. C. Pulmonary function of the green sea turtle, *Chelonia mydas*. *J. Appl. Physiol.* **62,** 459-463 (1987).

57. Currie, P. J. The orthometric linear unit. *J. Paleontol.* **52,** 964-971 (1978).

58. Bell, C. M., Hindell, M. A. & Burton, H. R. Estimation of body mass in the southern elephant seal, *Mirounga leonina*, by photogrammetry and morphometrics. *Marine Mammal Science* **13,** 669-682 (1997).

59. Henderson, D. M. Tipsy punters: sauropod dinosaur pneumaticity, buoyancy and aquatic habits. *Proc. R. Soc. Lond. B (Suppl.)* **271,** S180-S183 (2004).

6. Acknowledgements

Ronan Allain (MNHN), Wolfgang Böhme (ZFMK), Richard Cifelli (OMNH), Béatrice Coursier (MNHN), Kyle Davies (OMNH), Jocelyn Falconnet (MNHN), Jennifer Larson (OMNH), Jean-Sébastien Steyer (MNHN), Renaud Vacant (MNHN) and Luc Vivès (MNHN) are thanked for access to/support with specimens in collections and/or for permission to cut material for histology. Martin Sander (STIPB), Alexandra Houssaye (STIPB), Yasuhisa Nakajima (STIPB), Georges Gand (Université de Bourgogne) and Robert Bakker (Houston Museum of Natural History) are thanked for general discussion and debate. Katja Waskow (STIPB), Rebecca Hofmann (STIPB) and Olaf Dülfer (STIPB) are thanked for bone-

histological laboratory work. Mathew Wedel (Western University of Health Sciences) kindly gave permission to use his photograph. M.L., C.D.S. and S.F.P. would further like to thank Heather MacLeod and family for their hospitality while work was performed at MNHN. Parts of this study were funded by a grant from the Deutsche Forschungsgemeinschaft (Sa 469/34-1) to Martin Sander (STIPB).

Author contributions:

M.L., C.D.S. and S.F.P. conceived the study and collected the data. M.L. and C.D.S. analysed the data. M.L. and S.F.P. drafted the manuscript. F.S. contributed the artistic life reconstruction. All authors contributed to and approved the final version of the manuscript

Chapter 6: Comparative long bone histology of Caseidae

Submitted as: Shelton, C. D. (2014) Comparative bone histology of Caseida. Comptes Rendus Palevol.

Abstract: The evolution of basal metabolic rates is best understood through the study of bone microstructure, because bone histology faithfully records growth rates which is closely tied to metabolic rate. Here are described histological variations among five different sampled caseid taxa including a redescription of *Ennatosaurus tecton*. The dominant periosteal tissue in all specimens is predominantly avascular lamellar bone. Occurrence of vascularized woven bone was only observed in immature specimens. Caseids grew slower and lived longer than the contemporaneous carnivorous forms. Despite having reached record body sizes, caseids possessed the smallest osteocyte lacunae of any known pelycosaur. These results demonstrate an osteoporotic-like condition in the largest caseid taxa that was maintained throughout ontogeny. Inter- and intraspecific variation of pelycosaur bone histology is a result of the individual organism's trophic level, and how sustenance was acquired. Thus, we conclude that amongst the pelycosaur-grade synapsids endothermy was not perpetuated through cellulose herbivory.

1. Introduction

Caseidae Williston, 1912 is a nearly exclusive herbivorous pelycosaur (non-therapsid synapsid) group that persisted from the Late Carboniferous well into Middle Permian (Gaudalupian 30-40 MY) encompassing the radiation of the therapsids (Maddin et al. 2008; Reisz, 1986; Reisz and Fröbisch, 2014; Reisz et al., 2009). The exception being the recently described taxon *Eocasea martini* (Reisz and Fröbisch, 2014), currently the most basal caseid believed to be insectivorous. Members of this group are characterized by having a small head, low jaw articulation (below the tooth row), heavy mandible with a deep symphysis, sulcated teeth, small cervical vertebrae, three sacral ribs and a large iliac blade (Huttenlocker and Rega, 2012; Olson, 1968; Reisz, 1986; Romer and Price, 1940). These characteristics are believed to be derived traits due to an increase in size as an adaption to herbivory (Reisz, 1986). One of the peculiarities often observed amongst some caseid taxa is that they have longer humeri than femora, if not almost equal in length (See Olson, 1968; Stovall et al., 1966). This is the only pelycosaur family where this is a fact, and the phenomenon has been noted in recent studies

without an explanation of why this occurs (Felice and Angielczyk, 2014; Reisz et al., 2011). Members range in size from one to at least five and a half meters long, and reached a conservative maximum weight of between 330 kg and one ton or more in the larger taxa (Olson, 1968; Reisz, 1986; M. Romano pers. comm., 2014; Romer and Price, 1940). Caseids dominated the biomass making them not only the largest pelycosaur but also the largest tetrapods of their time. Until recently, the record holder for the largest known species was *Cotylorhynchus hancocki* Olson and Beerbower, 1953, but new finds from Sardinia, Italy have revealed a caseid species that was slightly larger (Ronchi et al., 2011), recently named *Alierasaurus ronchii* Romano and Nicosia, 2014. A study is currently underway to determine the exact biometrics of *A. ronchii* (M. Romano pers. comm., 2014). Classically, members of this family have been considered terrestrial. Reisz and Fröbisch (2014) have shown that their evolution in size correlates to a migration of more lowland habitats increasing in proximity to water. A new theory has been proposed that accounts for this dramatic size increase in relation to their feeding ecology: an adaptation to an aquatic lifestyle similar to that of modern hippos or manatees (Romer and Price, 1940). Olson (1968) speculated on the large caseid's preferred habitats as being somewhat fossorial living in shallow swamps. Unfortunately, he relied only on geology and ignored particular anatomical feature of the skeleton.

All pelycosaur groups have basal members that flourished on a primarily insect diet (Sues, 2000). At this time, insects were large and abundant because of the hypoxic atmosphere oxygen levels that reached their peak at 35% before dramatically dropping to their lowest at 15% by the Early Triassic (Dudley, 1998; Graham et al., 1997; Hsia et al., 2013). Throughout the Late Paleozoic, carnivorous tetrapods were more abundant than the herbivores (Bakker, 1975; Zimmerman and Tracey, 1989). But the pelycosaur groups had diversified diets by the Early Permian with piscivorous ophiacodontids and carnivorous sphenacodontids, as well as insectivorous eothyrids and varanopids and, omnivorous edaphosaurids (Hotton et al., 1997). All Permian caseids were unquestionably herbivorous. Pough (1973) has shown that the young of herbivorous lizard species will feed on insects until reaching a certain size, whereby dietary requirements for calorie intake are supplemented by a trophic level shift towards herbivory. This has also been hypothesized by Berman et al. (1998) to have occurred in the first known herbivorous tetrapod group, the large bodied Diadectidae, as is evident by their deciduous occlusal dentary that changes from the omnivorous juvenile form to the herbivorous adult. In order to digest cellulose, herbivores have developed a symbiotic relationship with microbes,

which breakdown plant matter because animals, including insects, cannot digest plant matter on their own (Sues and Reisz, 1998). Modern juvenile lizards acquire these microbes by ingesting insects as they too require symbiotic microbial fermentation (Gow, 1978; Sues, 2000). This is a likely model for the acquisition of herbivory among the pelycosaur-grade basal synapsids (Bakker, 1975). Coprophagy (ingestion of the parent's fecal matter already rich in cellulose digesting microbes) is also plausible (Troyer, 1982).

2. Historical background

De Ricqlès (1974a) published the first detailed histological study of a caseid when he described the serially sectioned femur of an immature *Ennatosaurus tecton* Efremov, 1956 (MNHN- 142.1) found in Russia (Late Guadalupian or Kazanian) (Table 1). This is one the latest surviving caseid taxon (Maddin et al., 2008; Reisz and Fröbisch, 2014) appearing in the Late Middle Permian overlapping, shortly before their extinction, with Therapsida. Only one micrograph image (142.1.2.T) was ever published from the four original sections, and it was again republished in a later study (de Ricqlès et al., 2004) (Figs. 1 and 2). De Ricqlès (1974a) found that the cortical vascularity consisted of only a few primary longitudinal vascular canals in a lamellar bone matrix, complete with Sharpey's fibers. Growth marks were already present in the cortex grading into endosteal trabecular bone. This indicated to de Ricqlès (1974a) an overall low growth rate that seemed inconsistent with what had been observed for other juvenile tetrapods which exhibited fast growing highly vascularized woven bone. De Ricqlès (1974a) concluded from his sample that this clade was exhibiting the plesiomorphic condition.

Table 1. Morphometrics and cortical thickness

Specimen Number	Caseid Taxa	Bone	Length (mm)	Circumference (mm)	Avg. Cortical Thickness (µm)	LAGs Count	Locality
MPUR 151	*Alierasaurus ronchii*	Rib Shaft	N/A	98	377	12	Italy
OMNH 00627	*Cotylorhynchus romeri*	Rib Head	N/A	56	1345.26	9	USA
OMNH 00627	*Cotylorhynchus romeri*	Rib Head	N/A	46	1439.7	9	USA
MNHN.F.MCL-1	*Ruthenosaurus russellorum*	Rib Shaft	N/A	44	1497.75	11	France
MNHN.F.MCL-1	*Ruthenosaurus russellorum*	Radius left	100+	58	3658.18	13	France
OMNH 00631	*Cotylorhynchus romeri*	Humerus	268	135	686.42	6	USA
OMNH 00631	*Cotylorhynchus romeri*	Femur	272	119	2514.37	11	USA
OMNH 00627	*Cotylorhynchus romeri*	Ulna	155	79	356.82	1	USA
OMNH 01728a	*Cotylorhynchus romeri*	Humerus	78	64	297.19	1	USA
OMNH 01728b	*Cotylorhynchus romeri*	Humerus	76	58	0	0	USA
OMNH 01728d	*Cotylorhynchus romeri*	Femur	75	60	0	0	USA
OMNH 01728c	*Cotylorhynchus romeri*	Femur	75	60	0	0	USA
MNG 10552	Undescribed Taxon	Radius	64	17	755.49	15	Germany
MNG 10552	Undescribed Taxon	Ulna	82	18	812.76	15	Germany
MNHN 142.1 ?	*Ennatosaurus tecton*	Femur	67	52	2000	3	Russia

2.1 Goals

In this study, we have followed the suggestion of Huttenlocker and Rega (2012) that further histologic investigation of additional caseid taxa may reveal variations in histology. Here we want to test the hypothesis that this shift in size correlates with the evolution of fibro-lamellar bone tissue by examining the long bone histology, which is a proxy for metabolic rates. In addition to the various caseid taxa, we will reexamine and redescribe (Table 1), the original *E. tecton* femur sections described by de Ricqlès (1974a) (Figs. 1 and 2). Finally, we will investigate

the limb length disparity (LLD) phenomenon (longer humerus than femur) that occurs in Caseidae (Felice and Angielczyk, 2014; Reisz et al., 2011).

2.2 Institutional abbreviations

IPBSH, Paleohistology collection, Steinmann Institute of Geology, Mineralogy and Palaeontology,
University of Bonn, Bonn, Germany; FMNH (CNHM), The Field Museum, Chicago, IL, USA ; MCZ, Museum of Comparative Zoology, Harvard University, Cambridge, MA, USA; MNHN, Muséum National d'Histoire Naturelle, Paris, France; MNG, Museum der Natur Gotha, Gotha, Germany; MPUR, Museum of "La Sapienza" Univeristy of Rome, Rome, Italy. OMNH, Sam Noble Oklahoma Museum of Natural History, University of Oklahoma, Norman, OK, USA; USNM, United States National Museum of Natural History, Washington DC, USA.

3. Materials

Various caseid specimens were available for consumptive sampling from France, Germany, Italy, and North America. These are described below in a constrained geologic context. Russian material was previously prepared by de Ricqlès (1974a).

3.1 MNG 10552 undescribed caseid specimens

MNG-10552 consist of an associated radius and ulna from the largest known specimen of an undescribed Lower Permian (Tambach Formation; earliest Wolfcampian) caseid species discovered at the famous Bromacker Quarry in the Thuringian Forest of Gotha, Germany (Table 1) (Berman et al., 2004; Reisz et al, 2011; Maddin et al., 2008). Paleoecology has been interpreted as an upland terrestrial ecosystem (Berman et al., 2000; Eberth et al., 2000; Martens et al., 2009). These bones are from the largest caseid skeleton recovered from the site (D. Berman Per. Comm. 2013). A formal description is currently being written at the University of Toronto in Canada by Robert Reisz and his colleagues of the Carnegie Institute in Pittsburg, PA, USA.

3.2 MNHN.F.MCL-1 Ruthenosaurus russellorum

MNHN.F.MCL-1 consist of a rib shaft section and a mid-shaft section from the incomplete right radius from the holotype skeleton of *Ruthenosaurus russellorum* Reisz et al., 2011 from the Early to Late Permian Grès Rouge Group of the Rodez Basin (Upper Sakmarian to

Lower Lopingian) (Lopez et al., 2008) (Table 1). The paleoenvironment and ecosystem has been interpreted to be that of a playa lake with a semi-arid to hot climate (Gand et al., 2008; Hübner et al., 2011; Lopez et al., 2008; Schneider et al., 2006). This site is in proximity to the Lodève basin where possible swimming tracks of caseids have been described (Gand, 1986, 1989).

3.3 OMNH Cotylorhynchus romeri

Cotylorhynchus (sp) is divided into three species based on size and stratigraphic position much like the way the three species of *Dimetrodon* were distinguished at the Briar Creek Bonebed (Reisz, 1986; Romer and Price, 1940; Shelton et al., 2013). All sampled material (OMNH-00627, two rib heads and an ulna; OMNH-01728a-d, two immature humeri and femora designated by the lower case letters; OMNH-00631 humerus and femur) (Table 1) is of the intermediate sized species *C. romeri* Stovall, 1937 from the red Hennessey shale of the Hennessey Formation (Early Leonardian) of central Oklahoma, USA (Olson, 1968; Reisz, 1986; Romer and Price, 1940; Stovall, 1937; Stovall et al., 1966). We are fortunate enough to have discovered previously unidentified immature *C. romeri* long bones in the vertebrate paleontology collection of the SNMONH (APPENDIX 8), and even more fortunate to be granted permission for their consumptive sampling (APPENDIX 9) given the rarity of juvenile caseid material. Records from the collection identified them simply as ‘Pelycosauria’ of Cleveland Co, Oklahoma, USA, from site V381 (see collection records held at the SNMONH). It is unknown whether or not these bones all belong to the same individual. The humeri differ slightly in size, but the femora are equal in length and circumference (Table 1; S.F. 1).

3.4 MPUR-151 Alierasaurus ronchii

MPUR-151 is a random fragment of the rib shaft from *Alierasaurus ronchii*; the newly discovered largest caseid skeleton from the Italian island of Sardinia (Romano unpublished thesis, 2014; Romano and Nicosia, 2014; Ronchi et al., 2011). Material comes from the Early to Middle Permian Cala del Vino Formation (Anisian) 30 meters below the local Triassic contact (Romano and Nicosia, 2014). Lithostratigraphy consists of poorly consolidated silty mudstone and sandstone units. The circumference of the size of the rib rivals that of any sectioned caseid rib in this study (Table 1).

3.5 Ennatosaurus tecton femur 142.1

The Russian *Ennatosaurus tecton* femur (MNHN-142.1) was previously sectioned and prepared by de Ricqlès (1974a) (Table 1). Sections 142.1.2.T and 142.1.3.T will be reexamined and redescribed using modern analytical techniques and the results will be compared to the histology of the other caseid taxa examined in this study. Both sections are from the proximal epiphysis (Fig. 1). Two additional sections were originally prepared from this femur, but these have been lost. Length of the uncut femur was reported at 67 mm, and the average cortical thickness (ACT) was estimated to be 2 000 µm (de Ricqlès, 1974a). Based on the scale drawing published of section 142.1.4.T taken at the minimal diaphysis, the circumference was estimated to be 52 mm (Table 1).

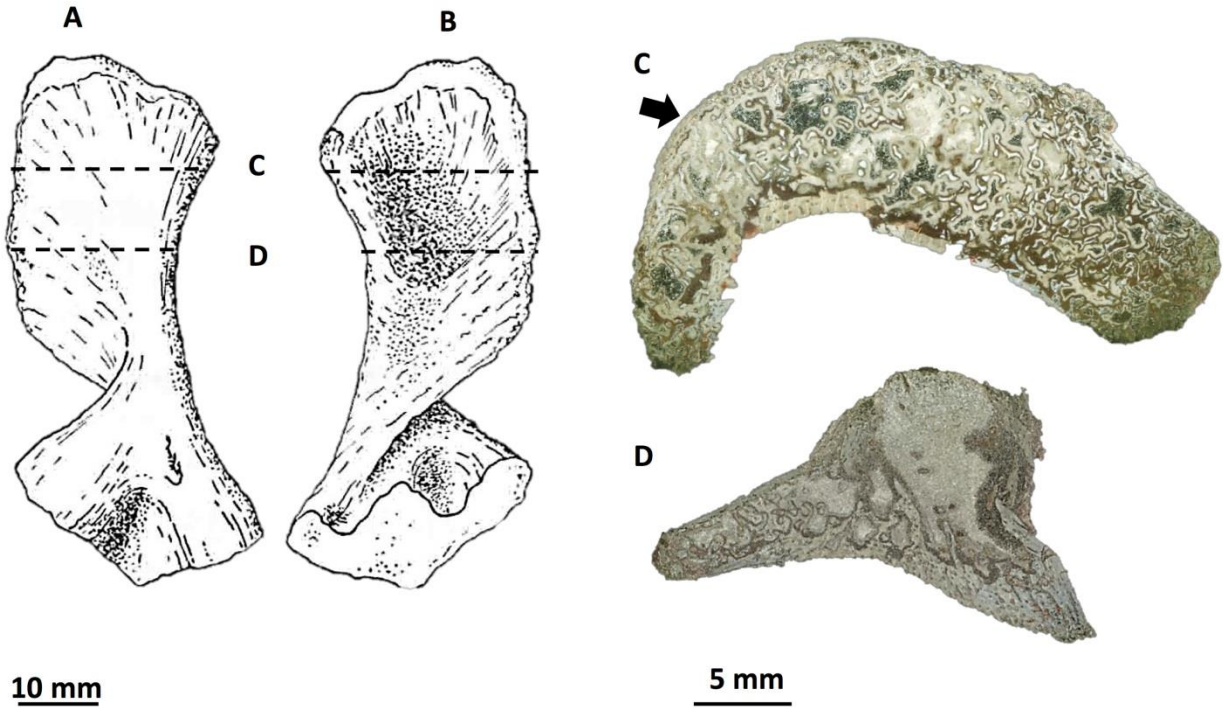

Figure 1. Armand de Ricqlès (1974a) serial sectioned an immature femur of *Ennatosaurus tecton* (preparation number 142.1) originally found in Russia (Lower Permian, Kazanian). As of to date, this has been the only published caseid specimen to be histologically described. Here we show the original drawing made of the A) dorsal and B) ventral sides. Lines C and D correspond to the transverse sections from the proximal epiphysis that is C) more proximal (142.1.2.T) and D) nearer to the midshaft (142.1.3.T). Thin sections 142.1.2.T (C) and 142.1.3.T (D) were scanned in normal light. Two additional sections were originally described by de Ricqlès (1974a) at

midshaft and more towards the articulation surface of the proximal epiphysis, but these have been lost. Periosteal cortex was originally estimated at 2000 µm. The medullary cavity seems somewhat open in section D but moving towards the direction of the proximal epiphysis it becomes occluded with trabecular bone. The arrow in (C) is pointing to the region originally published as a micrograph in de Ricqlès (1974a) and de Ricqlès et al. (2004) (See A; Fig. 2).

4. Methods

4.1 Morphometrics

4.1.1 Standard measurements

It is common practice to perform morphometric analysis of the individual bone being sampled preceding any histological work in order to procure the raw data before the bone is damaged in anyway (for example, Klein and Sander, 2007; Sander and Klein, 2005; Sander et al., 2006). Total length and minimal diaphysis circumference was recorded for each complete long bone using standard analytical calipers and a metric measuring tape (Table 1). Length was taken as the total distance between the termination of the proximal and distal epiphyses and, circumference was taken at the minimal-diaphysis corresponding to the area sectioned preserving the best record of growth (see Fig. 3). Rib circumference was measured at the sectioned area.

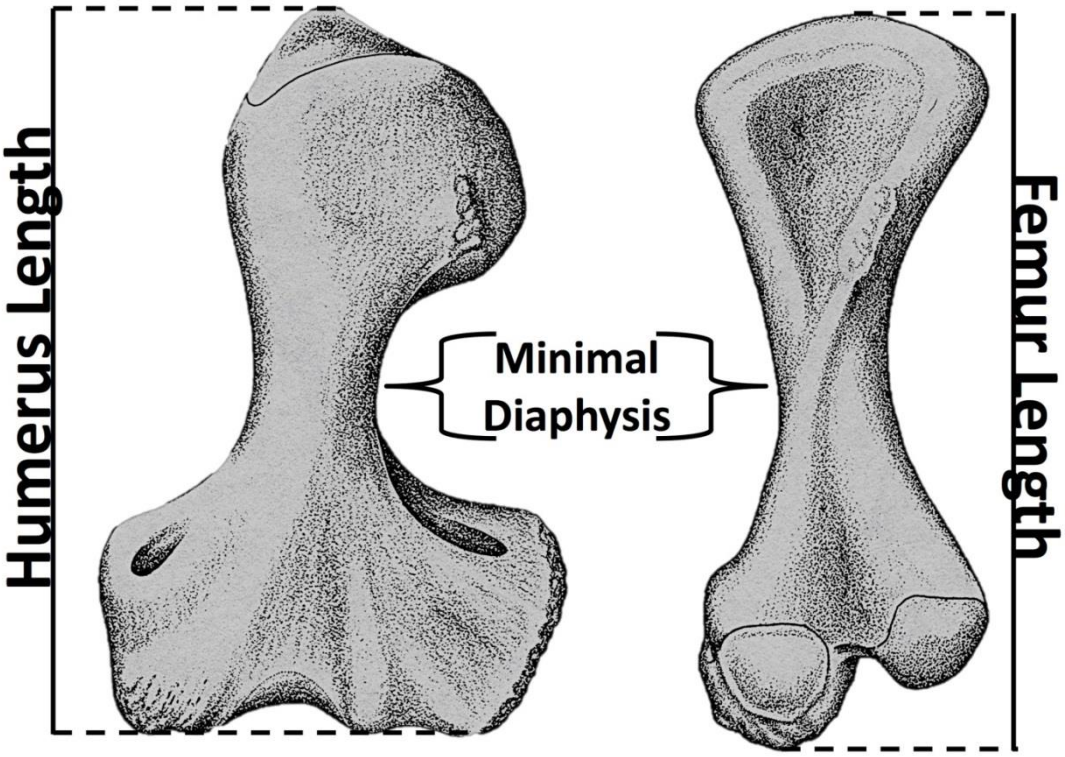

Figure 3. Illustration of a caseid humerus (A) and femur (B) with indications of how and where total length and the minimal diaphysis circumference were measured. The latter line of measurement also indicates the plane of section across the mid-diaphysis that contains the best preserved growth record. Note that the bones shown here are of *Cotylorhynchus romeri* (modified from Reisz 1986 after Stovall et al. 1966).

4.1.2 Limb length disparity between caseid humeri and femora

It has been observed that Caseidae is the only pelycosaur group in which the humerus can grow larger than the femur in an individual (Felice and Angielczyk, 2014; Reisz et al., 2011). Reisz et al. (2011) were the first to point out the occurrence of the limb length disparity (LLD) phenomenon in the holotype skeleton of *R. russellorum* (MNHN.F.MCL-1). In order to understand this LLD phenomenon, we have compiled measurements from individuals that display this characteristic (Table 2) from the literature and from specimens of various vertebrate paleontology collections measured specifically for this study (MNHNF, MCZ, FMNH, OMNH) (Olson, 1968; Stovall et al., 1966). The LLD ratios were calculated by dividing the femur length by the corresponding humerus length (F/H ratio) resulting in values less than one, and by dividing the humerus length by the corresponding femur length (H/F ratio) resulting in values equal to or greater than one (Table 2).

Table 2. Caseid specimens with longer humeri than femora

Specimen Number	Caseid Taxa	Humerus Length (mm)	Femur Length (mm)	Absolute Difference (mm)	F/H Ratio	H/F Ratio	Source
FMNH UC 656 (left)	*Casea broilii*	81	74	7	0.914	1.095	Measured by C. D. Shelton
FMNH UC 656 (right)	*Casea broilii*	81	68	13	0.840	1.191	Measured by C. D. Shelton
FMNH UC 656	*Casea broilii*	86	76	10	0.884	1.132	Olson 1968 Table 3a
FMNH UR 151	*Caseoides sanangeloensis*	157	145	12	0.924	1.083	Olson 1968 Table 3a
FMNH UR 581	*Cotylorhynchus hancocki*	405	400	5	0.988	1.013	Olson 1968 Table 3a
OMNH 4-0-S13	*Cotylorhynchus romeri*	196	195	1	0.995	1.005	Olson 1968 Table 3a
MCZ 3416	*Cotylorhynchus romeri*	246	239	7	0.972	1.029	Olson 1968 Table 3a
OMNH 4-0-S16	*Cotylorhynchus romeri*	260	260	0	1.000	1.000	Olson 1968 Table 3a
USNM	*Cotylorhynchus romeri*	263	251	12	0.954	1.048	Stovall et al. 1966 Table 1
FMNH PR 272 (left)	*Cotylorhynchus romeri*	324	308	16	0.951	1.052	Measured by C. D. Shelton
FMNH PR 272 (right)	*Cotylorhynchus romeri*	324	312	12	0.963	1.038	Measured by C. D. Shelton
FMNH PR 272	*Cotylorhynchus romeri*	327	305	22	0.933	1.072	Olson 1968 Table 3a
CNHM 272	*Cotylorhynchus romeri*	327	308	19	0.942	1.062	Stovall et al. 1966 Table 1
OMNH 4-0-S4	*Cotylorhynchus romeri*	338	308	30	0.911	1.097	Olson 1968 Table 3a
OMNH 4-0-4	*Cotylorhynchus romeri*	343	305	38	0.889	1.125	Stovall et al. 1966 Table 1
OMNH 4-0-S6	*Cotylorhynchus romeri*	348	313	35	0.899	1.112	Olson 1968 Table 3a
OMNH 4-0-6	*Cotylorhynchus romeri*	352	311	41	0.884	1.132	Stovall et al. 1966 Table 1
MNHN.F.MCL.1	*Ruthenosaurus russellorum*	245	225	20	0.918	1.089	Measured by C. D. Shelton

4.2 Consumptive sampling Methods

Prior to transverse and longitudinal sectioning, silicon molds (Provil Novo™ putty, Heraeus Kulzer Technique, regular) of all long bone diaphyses were produced for purposes of reconstruction. Next, each long bone mid-diaphysis was encased in a green epoxy resin (Technovit Universal™ liquid and Technovit™ 5071 powder, Heraeus Kulzer Technique) before being sectioned transversely with a rock saw, equipped with a standard diamond tipped blade, to prevent splintering of the outer cortex. The green epoxy resin was then dissolved, and the damaged areas were cast in plaster for purposes of reconstructing and preserving the morphological and anatomical features of the original material. After sawing, sections were ground to approximately 35 to 50 μm by hand on a glass plate with wet grit (600 and 800) and sealed with a cover slip using UV activated resin (Verifix™ LV 740 by Bohle).

All rib specimens were transversely sectioned. The two OMNH-00627 rib heads were sectioned at the neck just beyond the tubercle. This area of the rib contains the best preserved growth record as suggested by Waskow and Sander (2014).

All long bones were sectioned at the minimal diaphysis, with exception to the previously prepared *E. tecton* (see above). This region of the bone is where the most complete record of growth is preserved. It also corresponds to the area of the smallest shaft circumference (Currey, 2002; Francillon-Vieillot et al., 1990) (Fig. 3). Humeral midshaft sections bisect the area where the medial head of the triceps muscle inserts, and the femoral sections bisect the area of the adductor muscle attachment (Romer, 1969; Romer and Price, 1940).

Longitudinal sectioning is important to consider when examining bone tissue organization in three dimensions if consumptive sampling is allowed (Prondvai et al., 2014; Stein and Prondvai, 2013). A small area of the MNHN.F.MCL-1 radius shaft of *R. russellorum* was longitudinally sectioned perpendicular to the transverse plane of section.

Cotylorhynchus romeri ulna OMNH-00627 was sampled by a miniaturized version of the coring technique described by Stein and Sander (2009). This sample was taken from the anterior region of the minimal diaphysis. The direction of the ulna long axis was first marked on the bone surface with a permanent marker to maintain sample orientation. A diamond tipped coring bit measuring 5 mm in diameter was utilized and attached to a Proxxon^{TM} variable speed rotary tool mounted on a hand operated miniature drill press. Water, in a small plasticine reservoir, was used to lubricate the drill site to reduce friction and prevent damage of the outer periosteal. The core was imbedded in a translucent Araldite 2020 epoxy-resin (Bodo Möller Chemie), and allowed to set for 24 hours before being sectioned perpendicular to the long axis of the original long bone orientation. The transverse section was then prepared by following the same procedure as that described above for bones cut in full cross-section. Note that due to the osteoporotic-like condition of *Cotylorhynchus* (sp) bones, a full cross-section is recommended.

Histological slides are reposited at the IPBSH. Additionally, thin sections of all OMNH material are reposited in their vertebrate paleontology collection. Original *E. tecton* sections (142.1.2.T and 142.1.3.T) are housed in the research collection of the Centre de Recherche sur la Paléobiodiversité et les Paléoenvironnements (CR2P-MNHN) in Paris, France, managed by Vivian de Buffrénil.

4.3 Imaging

After thin sections were permanently cover slipped, they were then imaged in conventional transmitted light and polarized transmitted light, with or without a lambda filter,

using a Leica DM2500LP Polarizing Microscope configured with a 360 rotating stage. Digital images were acquired with a Leica DFC420 color camera and produced using the 2007 Leica IMAGE ACCESS EASYLAB 7 software (Leica, Wetzlar, Germany) (see Petermann and Sander, 2013). Overview images of thin sections were obtained in normal light with an EPSON PERFECTION V750 PRO high-resolution transmitted light scanner (manufactured in Japan) with a black background in order to better view microanatomical structures due to the white color of the preserved bone. Histological terminology follows Francillon-Vieillot et al. (1990) and Shelton et al. (2013).

4.4 Age estimation for *Cotylorhynchus romeri* humeri and femora

Age at time of death was estimated for both the adult *C. romeri* humerus and femur (OMNH-00631). Growth marks develop annually (Castanet, 2006; Castanet et al., 2004; Kohler et al., 2012) and include lines of arrested growth (LAGs). As an animal nears skeletal maturity, bone growth rates decrease. As bones grow, expansion and remodeling of the medullary cavity destroys earlier growth marks, which must be determined to establish a reliable age. The missing growth cycles can be estimated by use of retrocalculation (e.g., Bybee et al., 2006; Klein and Sander 2007). We assume the juvenile bones represent at least one year of growth based on an isolated patch of unresorbed cortex just below the surface of humerus OMNH-01728a that contains growth marks. However, it should be noted that there is no significant unaltered outer cortex preserved with growth marks of any other specimen indicating otherwise. Thus, each juvenile section was conservatively estimated to represent at least one year of growth, but they lack periosteal tissue and a well-defined cortical boundary (explained below). So, this conservative estimate of one year might be under estimated, and we allow for an error of at least two or three years. Actual retrocalculations of the maximum missing growth cycles will pertain to the area between that occupied by the juvenile sections and the earliest LAG of each adult specimen following a technique similar to that of Shelton et al. (2013).

First, each LAG, which represents one year of growth, was counted under polarized light (Table 1). The LAGs can be seen well in polarized light than in normal transmitted light. The retrocalculation method used here was modified from that of Shelton et al. (2013). First juvenile sections were superimposed onto the center of the corresponding adult sections, and then the distance between the outer surface of the juvenile bone and the first visible LAG of the adult specimen was measured and divided by the greatest distance between any two adjacent LAGs.

5. Results

5.1 Limb length disparity (LLD) ratio

Here we show the LLD ratio for known Caseidae specimens, either previously published (Olson, 1968; Stovall et al., 1966) or measured by the author, which have longer or equal length humeri compared to the corresponding femora (Table 2). The average femur to humerus ratio of the five different taxa was 0.941 and the average humerus to femur ratio was 1.0643 (Table 2). However, these results are due to a sampling bias of specimens with intact articulated humeri and femora.

5.2 Age estimation for *Cotylorhynchus romeri* humerus and femur

The age estimated from the resulting retrocalculations of the *C. romeri* long bones are highly controversial. Note juvenile bones represented a minimum of one year of growth give or take a few years. The adult humerus was estimated to be 79 years old with a maximum of 72 missing growth cycles, whereas the femur was only 30 years old at time of death with a maximum of 21 missing growth cycles, which is more plausible. The discrepancy in age between the two bones is due to the lack of a cortex in the juvenile specimens, which would render any illustrated growth trajectory to be purely speculative. Significant differences between the thicknesses of the cortex preserved in the adult specimens only reinforce the fact that these bones are not from a single individual. The close spacing of the LAGs attests to the slow periosteal deposition and bone growth. The only aspect we can be sure of is the average percentage increase of length and circumference between the immature long bones and the adults, but not the amount of time it took. The humerus increased by 248 % in length and 121 % in circumference, and the femur grew 263 % in length and 98 % in circumference.

5.3 Histology

5.3.1 Ribs

4.2.1.1 Cotylorhynchus romeri

OMNH-00627 is two rib heads sectioned at the neck with circumferences of 46 and 56 mm (Table 1; Fig. 4A). Their average cortical thicknesses (ACT) are 1440 and 1350 µm, respectively (Table 1). The histology of the cortex consisted entirely of lamellar bone (LB) (Fig. 5A). The periosteal bone is mostly avascular in the upper cortex and contains a few longitudinal

vascular canals in the middle and lower cortex; most of which are secondary osteons (SO), but some primary osteons (PO) are present (Fig. 5B). The SO are infilled with lamellar bone (LB), but exhibit a different extinction pattern than that of the LB matrix in the surrounding cortex indicating the orientation of the crystallites change from the primary to the secondary deposition period. Osteocyte lacunae (OL) are very small and are almost indistinguishable.

The cortical bone contains a growth record with growth marks (GM) visible at low magnification under polarized light and more so in transmitted light under a higher magnification (Fig. 5A and B). Nine lines of arrested growth (LAGs) can be seen throughout the entire cortex. Spacing between LAGs is slightly greater in the lower cortex. Sharpey's fibers (SF) are also present.

The medullary cavity (MC) is very distinct, and is occluded with secondary trabeculae formed of LB surrounding isolated patches of the primary cortex.

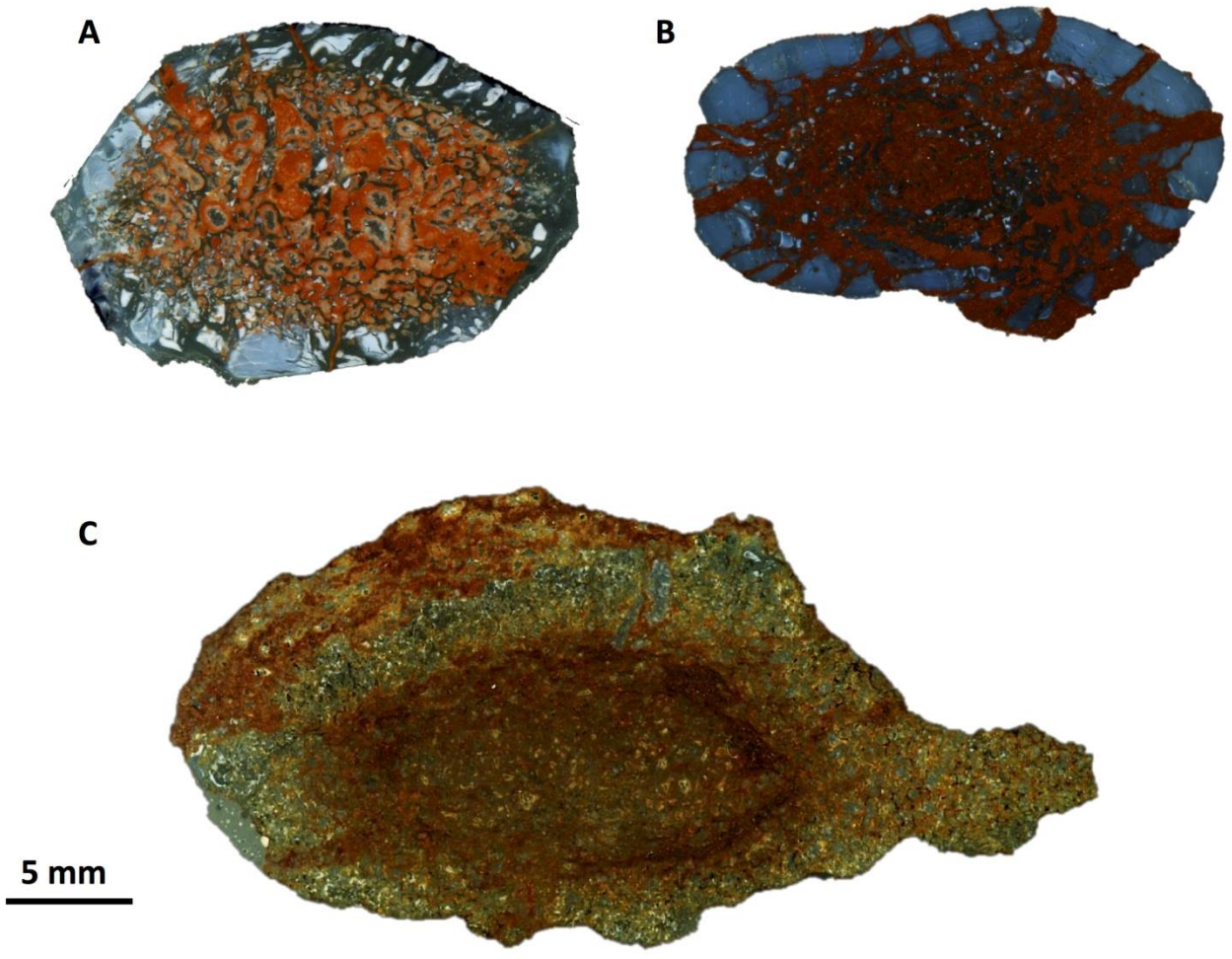

Figure 4. Scans of transverse rib sections in normal light with a black background for purposes of imaging. Original periosteal bone color is white. A) OMNH-00627, *Cotylorhynchus romeri*,

circumference is 46 mm and the average cortical thickness (ACT) is 1440 µm. B) MNHN.F.MCL-1, *Ruthenosaurus russellorum*, circumference is 44 mm and ACT is 1500 µm. C) MPUR-151, *Alierasaurus ronchii*, circumference is 98 mm and the ACT is 300 µm, but this number can vary as most of the periosteal bone has been altered by diagenesis as well as the outer cortical surface has been eroded away.

4.2.1.2 Ruthenosaurus russellorum

MNHN.F.MCL-1 is a transverse section of a rib from an unknown area of the shaft (Fig. 4B). Circumference is 44 mm and ACT is 1500 µm similar in dimension to that of rib heads OMNH-00627, but in this section, the OL are better visible and are round to angular in shape with accompanying canaliculi (Table 1; Fig. 5D). Histology is very similar to OMNH-00627, but there is less remodeling at the cortical medullary boundary (Fig. 5C). Eleven LAGs are visible (Table 1). SF are present, and PO are located in the lower cortex (Fig. 4D)

4.2.1.3 Alierasaurus ronchii

MPUR-151 is the largest rib sampled with an estimated circumference of at least 98 mm, which is nearly twice the size of the other sampled ribs. The ACT was measured as 377 µm (Table 1; Fig. 4C), but the actual ACT is unknown due to the degradation of the bone matrix (Figs. 4C and 5E) and would be a much lower value. The outer cortex is taphonomically altered, and the internal structure has been recrystallized and altered by diagenesis. Only isolated patches of bone matrix are left (Fig. 5E and F). The outer cortex is LB (Fig. 5F). The unaltered areas are identical to what has been described above but on a more extensive scale. LAGs are very close together and number at least twelve, with half of them being resorbed (Fig 5F). OSL and primary osteons are not visible. Traces of the medullary region are still visible (Figs 4C and 5E). Erosion cavities (EC) are circular to oval in shape throughout the rest of the bone, from relatively small cavities just below the cortex and increasing in size towards the center of the medullary region. The center of the rib is almost devoid of recognizable bone tissue, but small remnant patches of trabeculae are still visible indicating the possibility of an occluded MC like those described in the other rib specimens (Fig. 4A and B). Sharpey's fibers are present. The thin cortex lends to the bone compactness appearing osteoporotic like (de Buffrénil and Schoevaert, 1988; Hayashi et al., 2013; de Ricqlès and Buffrénil, 2001).

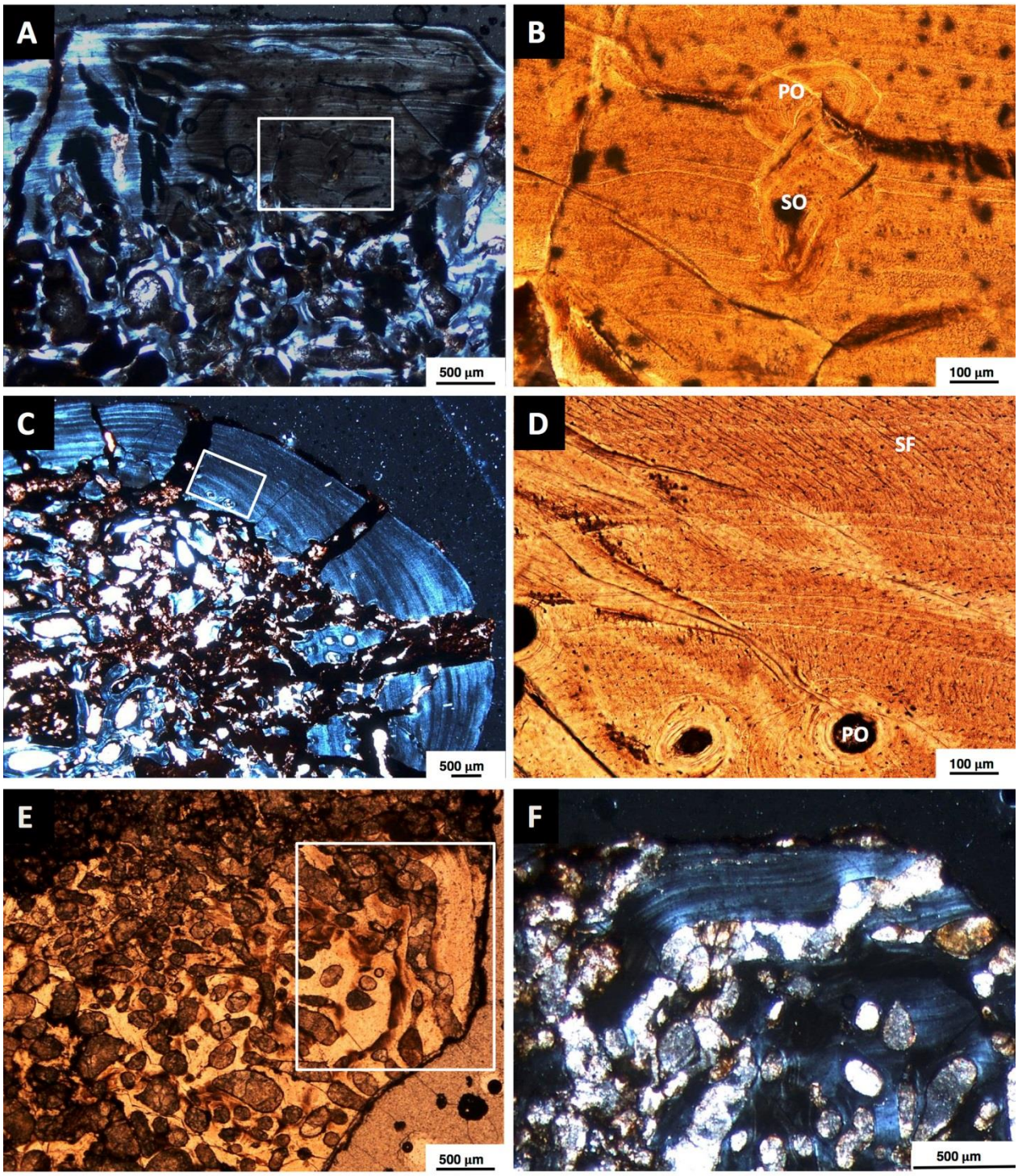

Figure 5. Microscopic view of the various transverse rib sections from Figure 3. A) OMNH-00627 *Cotylorhynchus romeri* (A; Fig. 3) imaged in polarized light. Nine regular closely spaced growth marks are visible in the cortex. The medullary region is occluded with a trabecular network. B) Microscopic view of the primary cortex as indicated by the boxed area in (A), imaged in conventional transmitted light. Two generations of osteons are visible in the center as

an irregular SO cross cutting a PO. C) MNHN.F.MCL-1 *Ruthenosaurus russellorum* (B; Fig. 3) imaged in polarized light. Histology is identical to the previously described *C. romeri* rib section. Thin cortex, eleven closely spaced growth marks, and an occluded medullary region. D) Microscopic view of the primary cortex as indicated by the boxed area in (A), imaged in conventional transmitted light. Growth marks are very thin but clearly visible. Primary osteons can be seen in the lower cortex near the MC boundary. Sharpey's fibers are also very visible extending into the mid-cortex perpendicular to the surface. E) MPUR-151 *Alierasaurus ronchii* (C; Fig. 3) imaged in conventional transmitted light. Resorption of the periosteal bone is very prevalent as is indicated by the many erosional cavities. Redepostion of LB has not yet occurred nor have any osteons formed. Exact location of the medullary cavity is unknown as this tissue is damaged. Unaltered primary cortical bone is only visible in a few isolated patches. F) Microscopic view of the primary cortex as indicated by the boxed area in (E) imaged in polarized light. Cortical histology is similar to the previously described sectioned ribs. Matrix consists of LB and growth marks are closely spaced together. Abbreviations: PO= primary osteon; SF= Sharpey's fibers; SO= secondary osteon.

5.3.2 Radii

4.2.2.1 Undescribed caseid taxon

MNG-10552 is a radius (64 mm in length) of the undescribed Bromacker Quarry caseid species from Germany (Table 1). The transverse section is taken from the minimal diaphysis, and is somewhat square in shape (Fig. 6). The cortex is relatively thick (ACT is 756 µm) compared to the circumference (17 mm) (Table 1), and consists of avascular lamellar bone with small OL (Fig. 8A and B). SF are visible in the cortex. The preserved growth record consists of at least fifteen very closely spaced LAGs. This is the best record of growth cycles preserved in any of the caseid bones sampled in this study. The same number of LAGs is found in the associated ulna described later. There is only a minor occurrence of secondary trabecular bone. Minimal remodeling has occurred in this bone. Scalloping of the MC periphery is visible due to osteoclast activity forming small EC at the medullary border (Fig. 6).

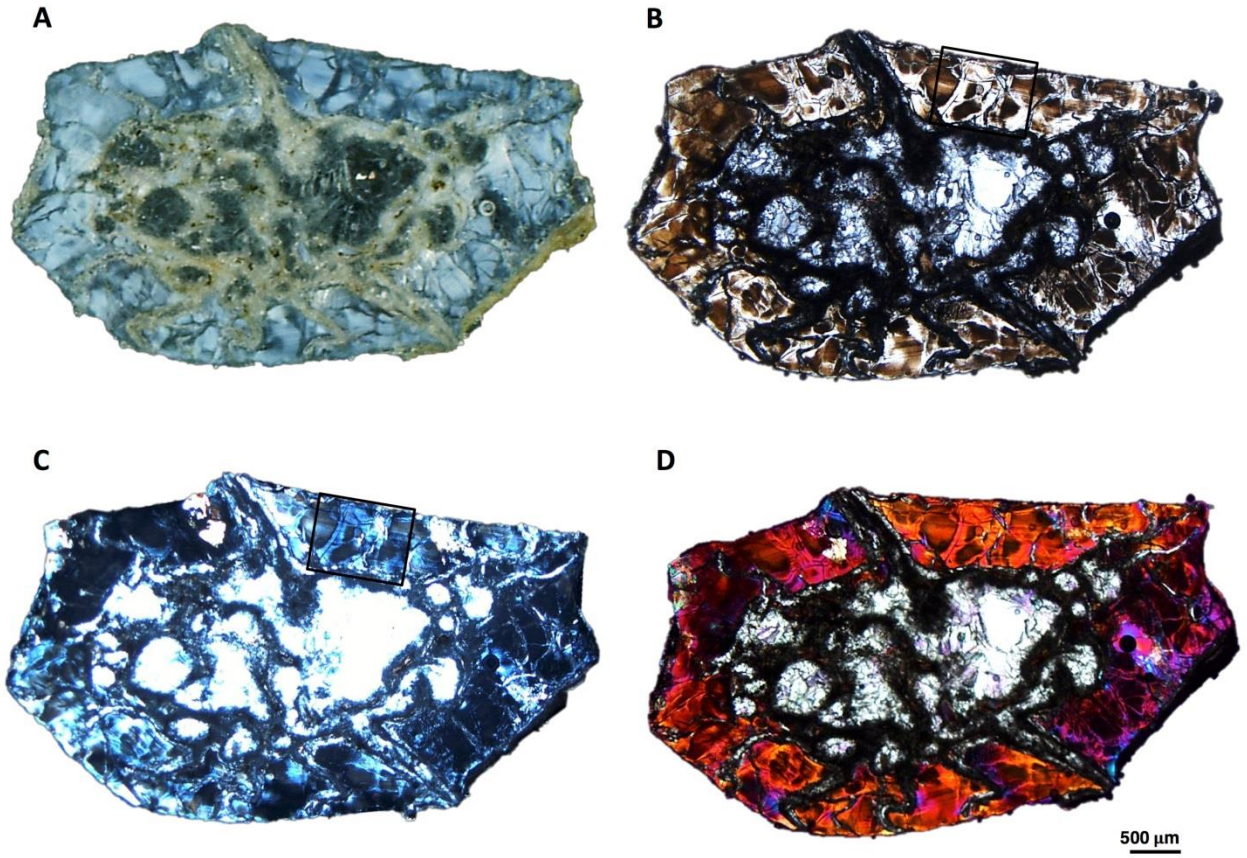

Figure 6. MNG-10552; Transvers section through the minimal diaphysis of a radius from the unnamed caseid taxa of Gotha Germany. Circumference is 17 mm and the average cortical thickness is 756 µm. A) Scan of the transverse radius section in normal light with a black background for purposes of imaging. Medullary region is distinct from the cortex. The MC is occluded with a few widely spaced trabecular lattices. Resorption is minimal. The cortex itself is much fractured but it is avascular. Osteocyte lacunae are very difficult to see. B) Micrograph of the transverse radius section imaged under conventional transmitted light. The brown areas are diagenetically stained and help to preserve histologic structures such as the growth record. C) Micrograph of the same section imaged under polarized light. Here the growth marks are more visible in the unstained areas. D) Micrograph of the same section imaged under polarized transmitted light through a lambda filter. The bone matrix is entirely LB. The histology is identical to that described in the associated ulna (MNG-10552) (see figs. 9 and 10). The boxed areas in (B) and (C) are magnified in Figure 7A and B.

4.2.2.2 Ruthenosaurus russellorum

MNHN.F.MCL-1 is a partial radius from the holotype of *R. russellorum* (Reisz et al. 2011). The transverse section was cut near the mid-diaphysis and is square in shape with a circumference of 58 mm and an ACT of 3658 µm (thickest cortex of all the sampled bones) (Table 1; Fig. 8). The cortex consists of LB and a minor occurrence of parallel-fibered bone (PFB) (Figs. 8B and 7C-H). PFB is located only in the region with a few small longitudinal vascular canals (Figs. 8A and 7C -F). SF and small round OL are densely concentrated throughout the cortex (Fig. 7E-H). The vascularized area was longitudinally sectioned (Fig. 7C and G) and found to contain SF extending from the mid to outer cortex, as well as flat OL oriented parallel to the cortical surface (Fig. 7G and H). Here vascularity consists of radial canals oriented perpendicular to the LAGs (Fig. 7G). The growth record consists of thirteen closely spaced LAGs. The MC is occluded with trabecular bone (Fig 8).

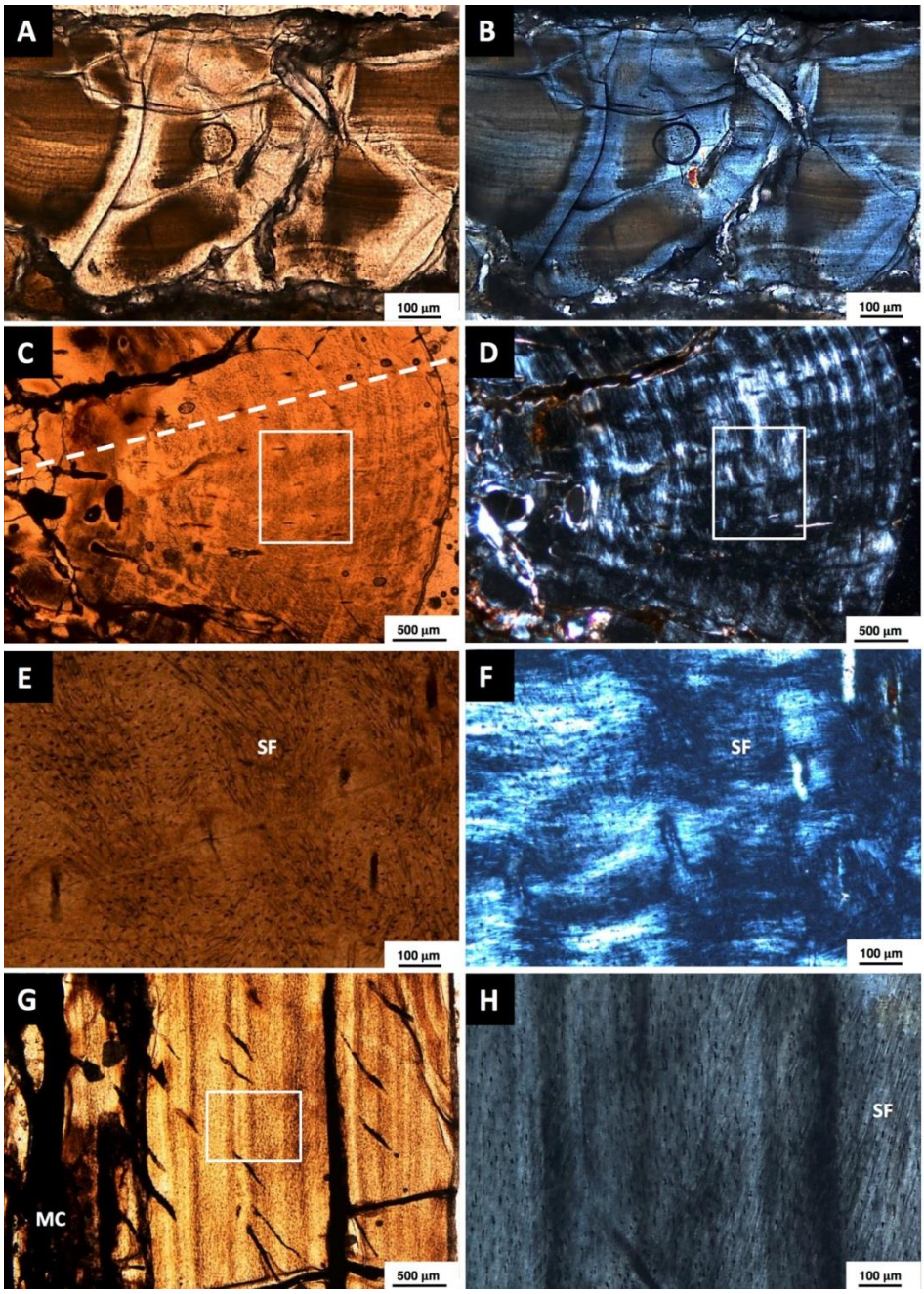

Figure 7. Micrograph images of caseid radii, the unnamed Bromacker Quarry specimen (A and B) from Fig. 6, and the partial right radius of MNHN.F.MCL-1, *R. russellorum* (C-H) from figure 8, A. A) Micrograph of MNG-5001 radius cortex magnified from boxed area indicated in Figure 6 (B), and imaged in transmitted conventional light. At least fifteen LAGs are present. This is the most extensive growth cycle record of all the sampled caseid taxa from this study. Cortex is avascular lamellar bone with minimal resorption and redepostion. B) Same area as (A) magnified from boxed area in figure 6 (C) imaged in polarized light. Note the structure in the center of the image is an air bubble. C) Micrograph imaged in conventional transmitted light of boxed area in

Figure 8A. Note the longitudinal vascular canals. White dotted line indicates area of the cortex sectioned longitudinally. D) The same area pictured in (C) imaged in polarized light. Notice the regularly spaced growth marks. E) Micrograph imaged in transmitted conventional light of boxed area in (C). This area contains a dense concentration of Sharpey's fibers. Notice the small osteocyte lacunae F) The same area pictured in (E) imaged in polarized light. The dense concentration of Sharpey's fibers makes the lamellar bone matrix appear more parallel-fibered. G) Longitudinal section of cortex indicated by the dotted line in (C). Micrograph imaged in conventional transmitted light. Growth marks are very visible. Note the radial canals oriented at an angle to the surface. H) Micrograph imaged in conventional transmitted light of boxed area in (G). Sharpey's fibers are densely concentrated from the mid to outer cortex. Osteocyte lacunae are very dense and flat, oriented parallel to the cortical surface. Abbreviations: MC= Medullary Cavity; SF= Sharpey's fibers.

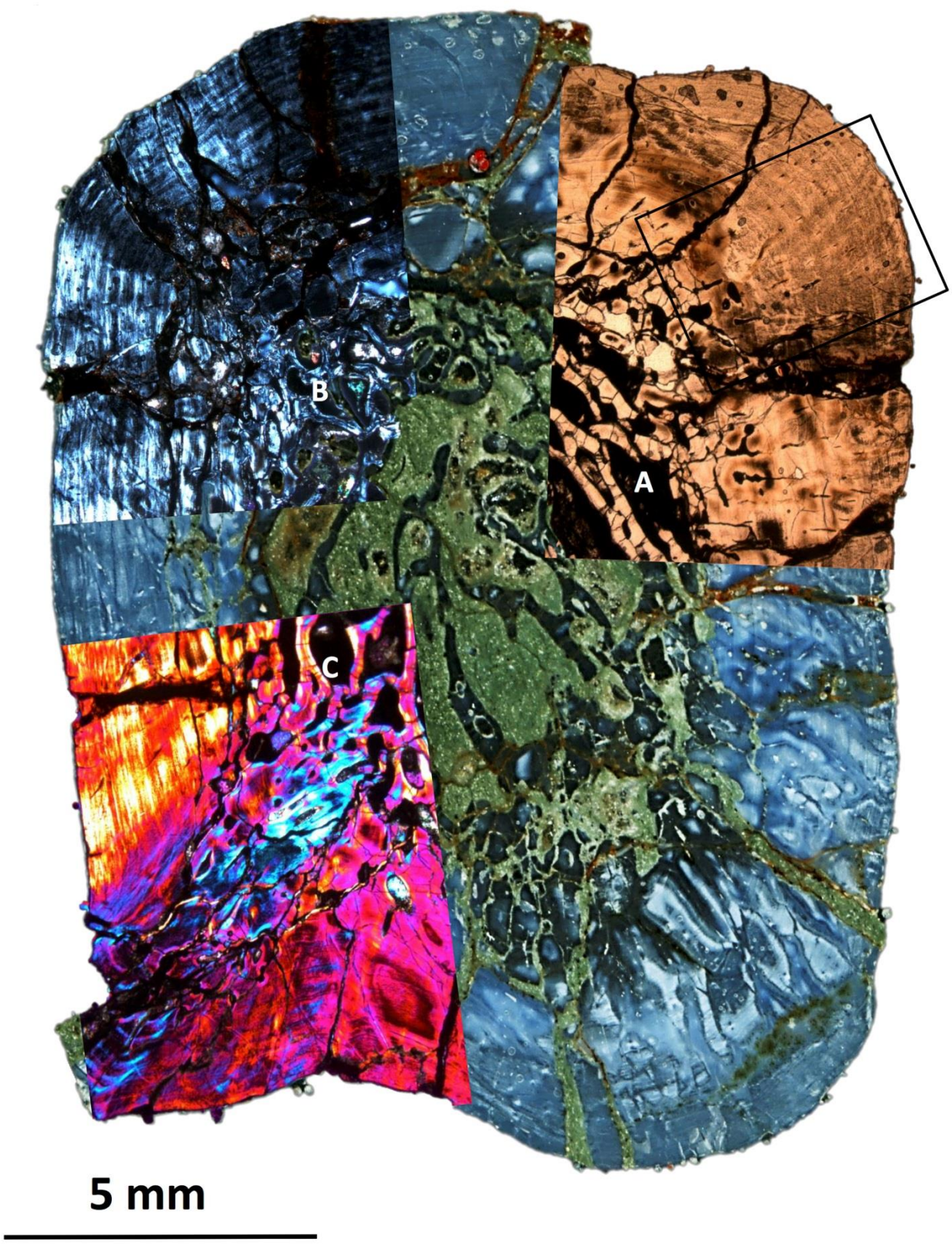
B
A
C
5 mm

Figure 8. MNHN.F.MCL-1, transverse section through the mid-diaphysis of a *Ruthenosaurus russellorum* radius scanned in normal light with superimposed micrograph images. Circumference is 58 mm and has the highest average cortical thickness (3658 µm) of any sampled bone in this study. The cortex is extremely lamellar except for the vascularized region (A) which appears slightly more parallel fibered due to the dense concentration of Sharpey's fibers. Note the medullary cavity is occluded with a trabecular network. A) Superimposed micrograph imaged in transmitted conventional light. This is the only vascularized region of the cortex (longitudinal canals). The remaining cortical regions appear avascular. The boxed area is further analyzed in Fig. 8. B) Superimposed micrograph imaged in polarized light which allows better imaging of the regularly spaced growth marks. C) Superimposed micrograph imaged in polarized transmitted light through a lambda filter. This region is the site of a major muscle attachment.

5.3.3 Ulnae

4.2.3.1 Undescribed caseid taxon

MNG-10552 is an ulna (82 mm in length) of an undescribed Bromacker Quarry caseid species from Germany. The transverse section is elliptical in shape (Fig 9). Like the associated radius, the cortex is relatively thick (813 µm) compared to the circumference (18 mm), and consists of avascular LB with small OL (Table 1; Fig. 10D and E). SF are present and the growth record is the same as radius MNG-10552 consisting of at least fifteen LAGs. The MC is occluded but with only a few trabeculae. Scalloping is evident at the periphery of the MC (Fig. 9).

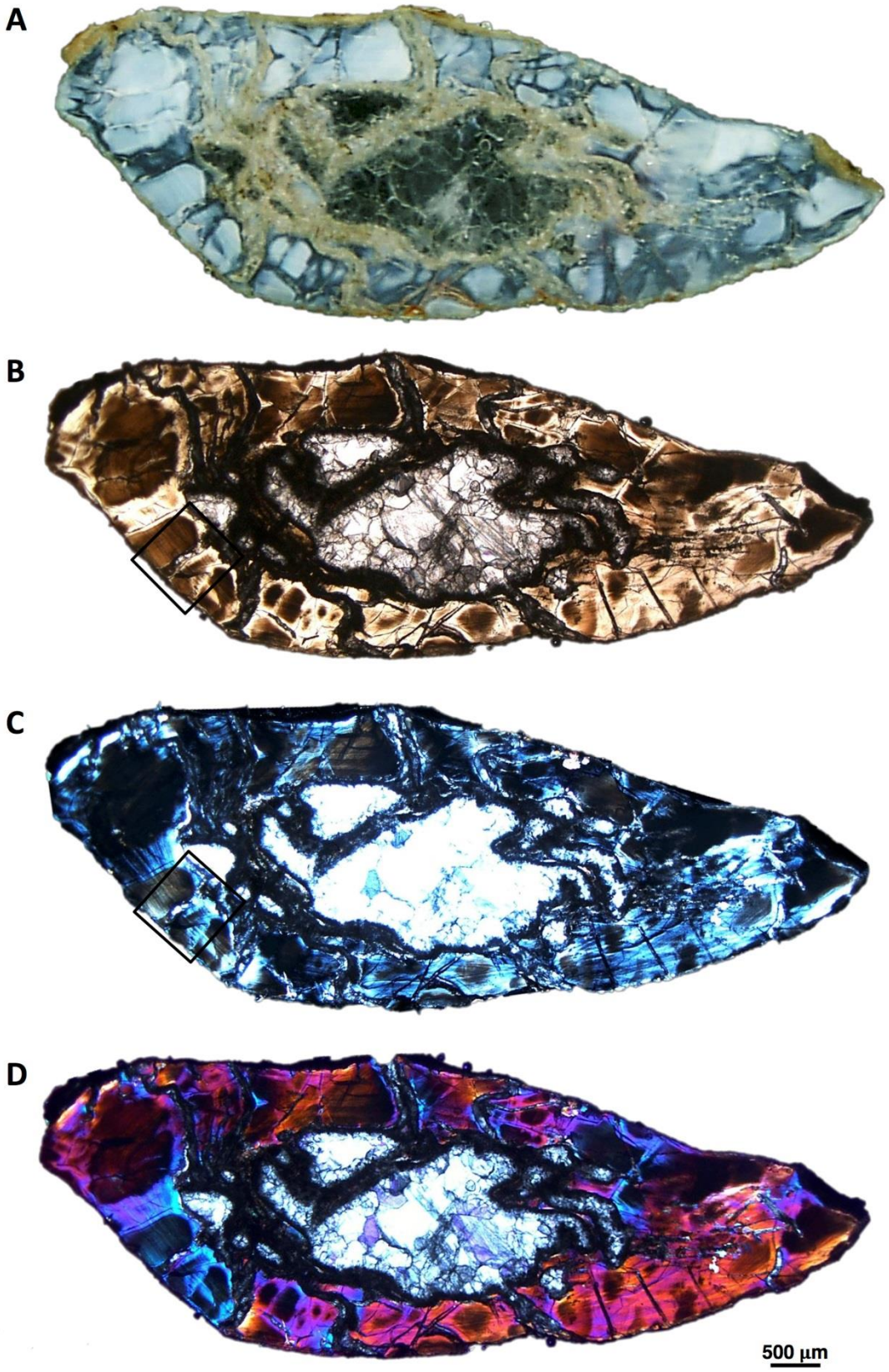
A
B
C
D
500 µm

Figure 9. MNG-10552, Transverse section through the minimal diaphysis of an ulna from the unnamed caseid taxa of Gotha Germany. Circumference is 18 mm and the average cortical thickness is 813 μm. A) Scan of the transverse radius section in normal light with a black background for purposes of imaging. Medullary region is distinct from the cortex. The MC is more open with only a few lattices near the peripheries. Resorption is minimal. The cortex itself is much fractured but it is avascular. Osteocyte lacunae are very difficult to see. B) Micrograph of the transverse radius section imaged under conventional transmitted light. The brown areas are diagenetically stained and help to preserve histologic structures such as the growth record. C) Micrograph of the same section imaged under polarized light. Here the growth marks are more visible in the unstained areas. D) Micrograph of the same section imaged under polarized transmitted light through a lambda filter. The bone matrix is entirely LB. The histology is identical to that described in the associated radius (MNG-10552) (see figs. 6 and 8). The boxed areas in (B) and (C) are magnified in Figure 10.

4.2.3.2 Cotylorhynchus romeri

OMNH-00627 is a *C. romeri* ulna 155 mm in length and cored at the minimal diaphysis (circumference 79 mm) with a 5 mm bit (Table 1; Fig. 10A). The transverse section reveals an extremely thin area of unremodeled LB in the outer cortex (Fig. 10B and C). OL are not visible in this section, but SF are visible along with a few longitudinal vascular canals (Fig. 10B and C). Perhaps, one LAG is visible. The deeper cortex is remodeled, and consists of many small secondary osteons resembling Haversian bone, which also marks the boundary of the medullary region. The MC is occluded with secondary trabeculae (Fig. 10A). This bone is most likely exhibiting an overall osteoporotic like state similar to that observed in the other *C. romeri* long bones described below (Fig. 10C).

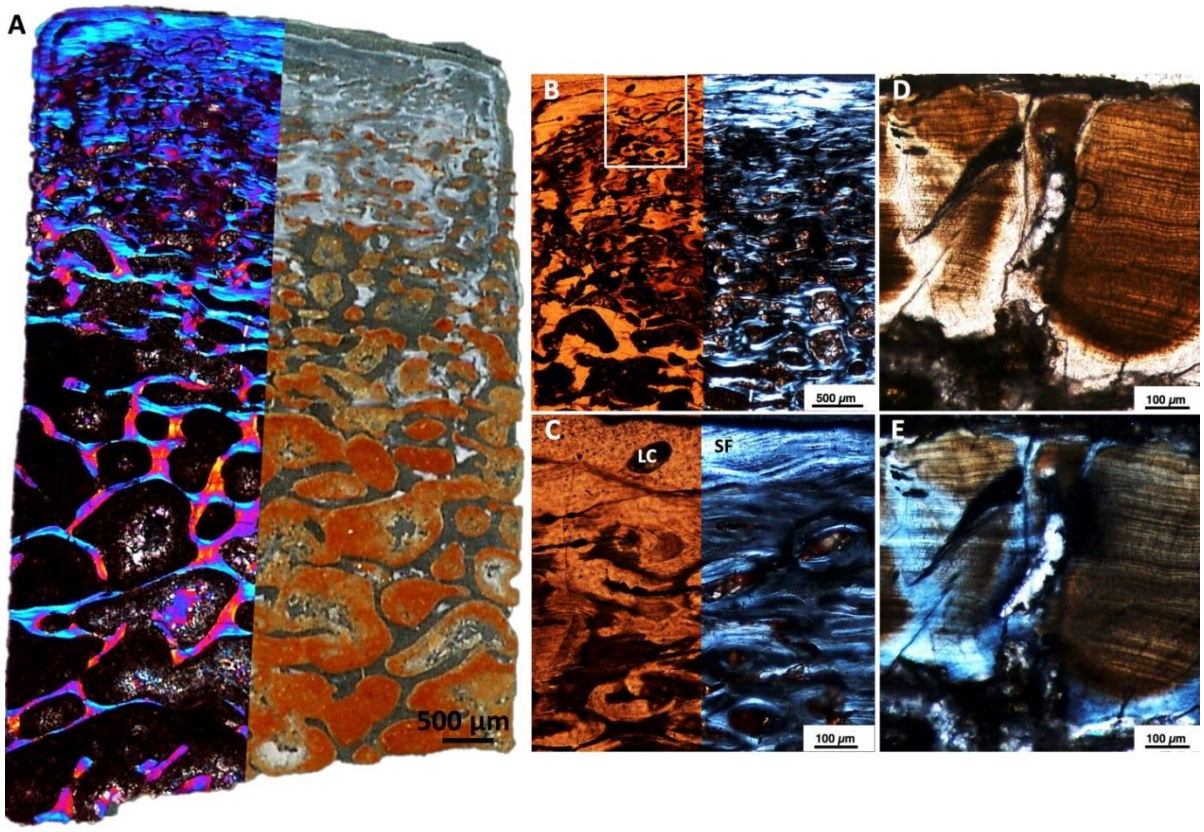

Figure 10. Micrograph images of caseid ulnae, OMNH-00627 *Cotylorhynchus romeri* (A-C), and MNG-10552 unnamed Bromacker specimen (D and E) from Figure 9. A) *C. romeri* ulna core transversely sectioned and scanned in normal light partially superimposed with a micrograph imaged in polarized transmitted light through a lambda filter. Overall bone matrix is lamellar. Notice the cortex has almost been completely resorbed reflecting an overall osteoporotic-like condition. B) A split micrograph of the outer cortical region of the core in (A) imaged in conventional transmitted light (left) and polarized light (right). C) Magnified view of the boxed area in (B) of the thin outer cortex. Split micrograph imaged in conventional transmitted light (left) and polarized light (right). Notice the solitary longitudinal vascular canal. Sharpey's fibers are also visible. D) Micrograph of MNG-5001 ulna cortex magnified from the boxed area indicated in Figure 9 (B), and imaged in transmitted conventional light. At least fifteen LAGs are present. This is the most extensive growth cycle record of all the sampled caseid taxa from this study. Cortex is avascular lamellar bone with minimal resorption and redepostion. Note the structure in the center of the image is an air bubble E) Same area as (D) magnified from boxed area in Figure 9 (C) imaged in polarized light. Abbreviations: LC= longitudinal canals; SF= Sharpey's fibers.

5.3.4 Cotylorhynchus romeri humeri and femora

4.2.4.1 Juveniles long bones

OMNH-01728a-d consists of many of immature long bones of juvenile *C. romeri*, and will first be described synthetically (APPENDIX 8). Transverse sections are of the minimal diaphysis (Fig. 11; S.F. 2). OMNH-01728a is a right humerus 78 mm in length and 64 mm in circumference; OMNH-01728b is a left humerus 76 mm in length and 58 mm in circumference; OMNH-01728c and d are a left and right femur respectively, equal in length (75 mm) and circumference (60 mm) (Table 1; Fig. 11; APPENDIX 8). The only significant cortical bone to speak of is a small isolated patch of LB from the right humerus (ACT is 297 µm) just below the outer surface, heavily scalloped by resorption activity from osteoclasts (Fig. 12A). Longitudinal vascular canals and a single LAG are present here (Fig. 12C and D). In all juvenile sections the outer cortex is absent either because of non-deposition or weathering. The overall bone structure indicates an osteoporotic-like condition in that they are essentially just a network of secondary trabeculae; some of which are composed of primary woven periosteal tissue with large longitudinal canals bounded by LB (Fig. 12B) (de Buffrénil and Schoevaert, 1988; Hayashi et al., 2013; de Ricqlès and de Buffrénil, 2001). These trabecular lattices are surrounded by large spaces that were open cavities in life are now infilled with red iron stained sediment (Fig. 11). A majority of the trabeculae are degraded and have undergone recrystallization (Fig. 12E and F).

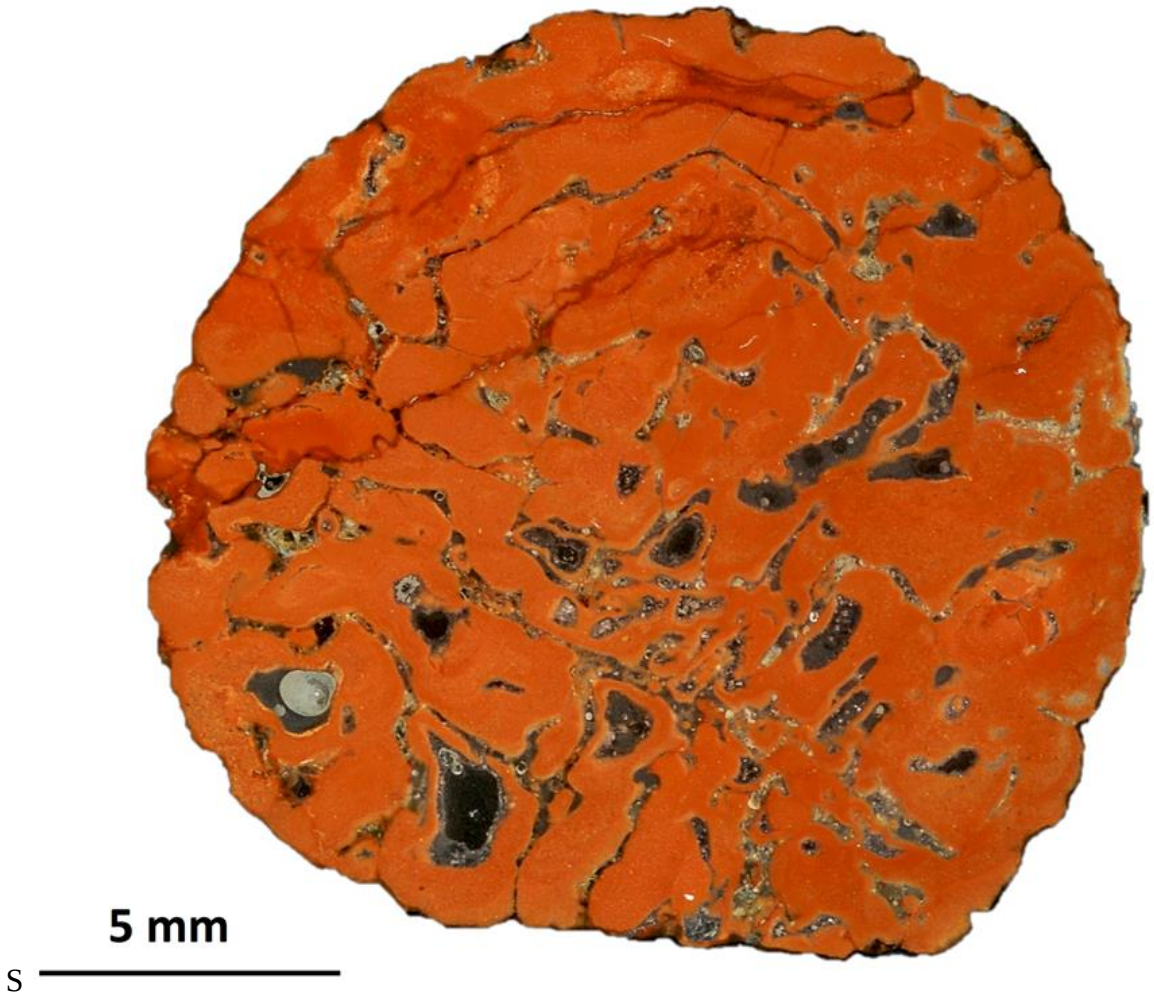

Figure 11. OMNH-01728C juvenile *Cotylorhynchus romeri* femur transversely section at the minimal diaphysis scanned in normal light with a black background for purposes of imaging. Note the red areas were open spaces during the life of the animal. The overall bone is osteoporotic-like and without a cortex. See micrograph images in Figure 11.

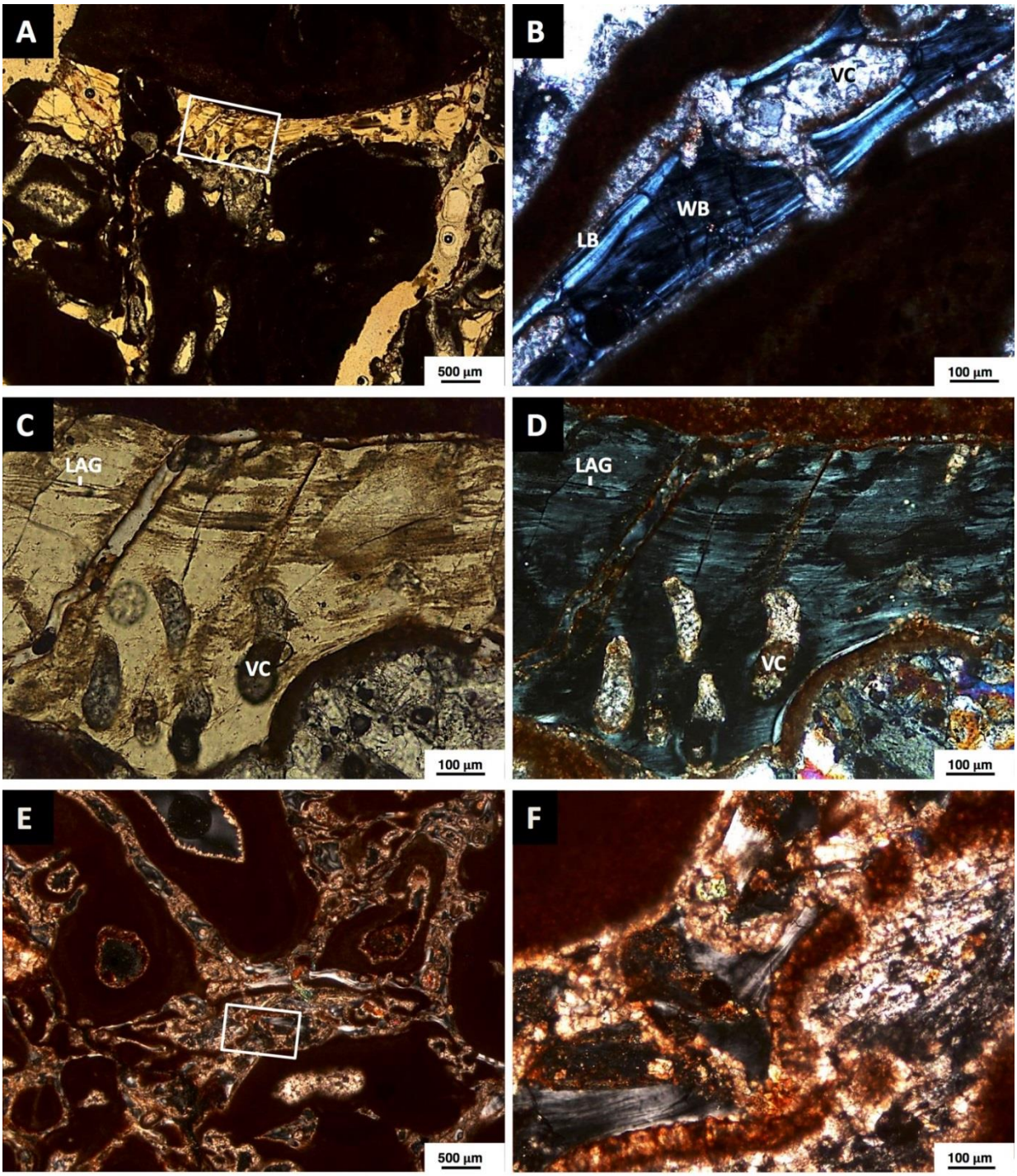

Figure 12. Synthesized micrograph images of the juvenile *Cotylorhynchus romeri* humeri and femora (Appendices 8 and 9) transversely sectioned at the minimal diaphysis. Histology is identical in all bones and has been synthesized. A) Micrograph of trabecular bone in conventional transmitted light. B) Micrograph of trabecular bone at higher magnification. Note the primary woven bone bond by secondary lamellar bone. Vascular canals are also present in the woven bone. C) Micrograph imaged in conventional transmitted light of boxed area in (A). This appears

to be unaltered primary bone with irregularly shaped erosion cavities. The bone matrix is lamellar and contains growth marks. D) Same area as in (C) imaged in polarized light. Growth marks are better visible. Note that there is no lamellar bone infilling the erosional cavities. At least one LAG is visible. E) Micrograph imaged in polarized light from the middle region of a humerus section. F) Micrograph imaged in polarized light of the boxed area in (E). Notice the bone tissue is undergoing diagenetic alteration. Abbreviations: EC= erosional cavity; LAG= line of arrested growth; LB= lamellar bone; VC= vascular canal; WB= woven bone.

4.2.4.2 Adult Humerus

OMNH-00631 is a transverse section of the minimal diaphysis of an adult *C. romeri* humerus with a length of 268 mm and a circumference of 135 mm; ACT is 686 µm (Table 1). Like the juvenile specimens described above, the humerus is also osteoporotic-like (Fig. 13A). Unremodeled primary cortical bone is only present in a small area of the dorsal region (Fig. 14A-D). This thin cortical layer is composed of avascular lamellar bone. OL are very small but better visible at higher magnification (Fig. 14C). SF are present. Six LAGs are visible in polarized light gradually decreasing in distance by a few micrometers towards the outer cortex (Fig. 14D). Primary and secondary osteons appear at the border of the medullary region (Fig. 14C and D). The remainder of the tissue is remodeled secondary trabecular bone and erosional cavities lined with LB (Fig. 14A and B). The center of the section, although lacking a distinct MC, is similar to the histomorphology of the juvenile OMNH-01728 *C. romeri* sections (Fig. 11; S.F. 2).

4.2.4.3 Adult femora

OMNH-00631 is a transverse section of the minimal diaphysis of an adult *C. romeri* femur with a length of 272 mm, a circumference of 119 mm, and an ACT of 2514 µm (Table 1; Fig. 13B). Histology is the same as that described for the *C. romeri* humerus (OMNH-00631), but this specimen has a greater amount of primary cortex (Fig 14E-H). This specimen is not as osteoporotic like as the other *C. romeri* bones, but some regions have been fully resorbed up to the bone surface. Overall cortical tissue is avascular and consists of lamellar bone. OL are visible in some of the darker stained areas (Fig. 14G). SF extend into the deep cortex and medullary region. Because of the thicker cortex, a more extensive growth record has been preserved. Eleven LAGs are present including double LAGs (Fig. 14H) better visible in polarized light. The white areas in (Fig. 13B) are plaster.

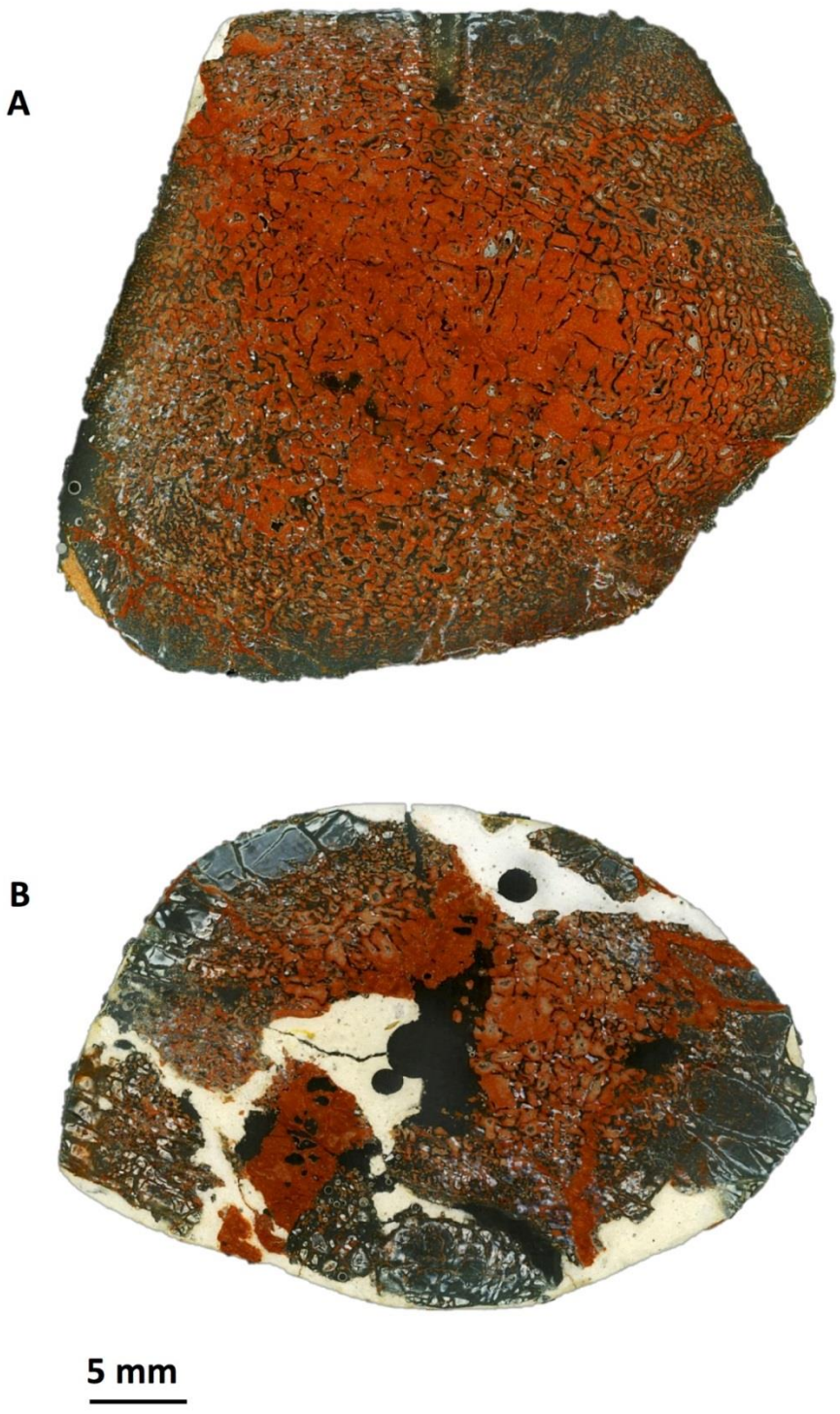

Figure 13. OMNH-00631, scanned transverse sections of an adult *Cotylorhynchus romeri* associated humerus and femur in normal light with a black background for purposes of imaging. Note that these are most likely not from the same individual. Like the juveniles (Fig. 11, Appendix 8), the red areas were open spaces during the life of the animal similar to the juveniles. A) Humerus with a circumference of 135 mm, and the average cortical thickness (ACT) is 686

µm. The cortical layer is almost completely resorbed and has an osteoporotic-like condition. B) Femur with a circumference of 119 mm and the ACT is 2514 µm. The white areas were previously reconstructed with plaster.

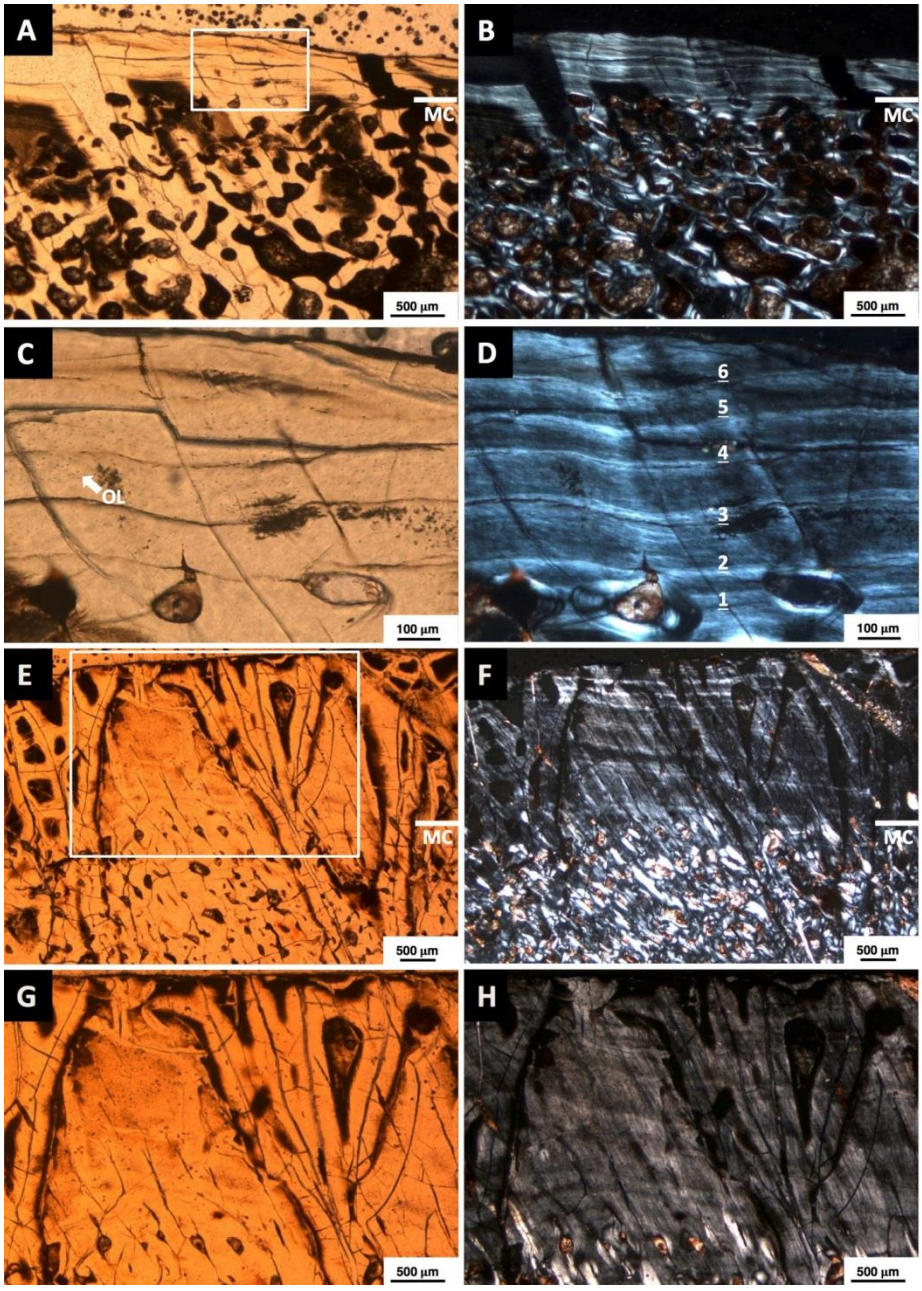

Figure 14. OMNH-00631; Micrograph images of the adult *Cotylorhynchus romeri* humerus (A-D) and femur (E-H). A) Humerus micrograph imaged in conventional transmitted light of the cortex and medullary region separated by the extent of the erosional cavities in the lower cortex. Cortex is avascular. Line denotes the boundary between the cortex above and the medullary

region. B) Same area in (A) imaged in polarized light. Growth marks are better visible. Note the abrupt change between the medullar region and cortex. C) Micrograph imaged in conventional transmitted light of the boxed area in (A). Arrow is pointing to a cluster of very small osteocyte lacunae. D) Micrograph of the same area in (C) imaged in polarized light. Six LAGs are visible in the cortex of which the earliest one is almost completely resorbed. Primary osteons are visible in the lower cortex. E) Femur micrograph imaged in conventional transmitted light of the cortex and medullary region separated by the extent of the erosional cavities in the lower cortex. Line denotes the boundary between the cortex above and the medullary region. F) Same area in (E) imaged in polarized light. Growth marks are better visible. Note the abrupt change between the medullary region and cortex. G) Micrograph imaged in conventional transmitted light of the boxed area in (E). H) Micrograph of the same area in (G) imaged in polarized light. Growth marks are better visible. Abbreviations: MR= medullary region, OL= osteocyte lacunae.

5.3.5 Ennatosaurus tecton femur

Sections 142.1.2.T and 142.1.3.T are transverse cuts through the proximal epiphysis of the immature *Ennatosaurus tecton* femur (MNHN-142.1) described from slides previously prepared by de Ricqlès (1974a) (Fig. 1), and a summary of the initial description has been given in the Introduction (see section 1.2 State of the art). The only micrograph image published from the original studied is from section 142.1.2.T (Fig. 2A and B). Overall cortical tissue is lamellar bone (Fig. 2A and B). Extensive resorption and remodeling has already occurred here as evident by the multiple generations of LB cross cutting each other in the open medullary cavity (Fig. 2F). OL are small, and a few longitudinal canals are visible.

Section 142.1.3.T was cut more distally towards the mid-diaphysis, and differs from the previous section. The cortex is mostly primary woven bone vascularized by large longitudinal vascular canals (Fig. 2C-E). Fully formed primary osteons are also visible in the deeper cortex, and OL are large and plump (Fig. 2E). Three LAGs are also visible in this primary woven cortex (Fig. 2D). Large EC have formed throughout the periosteum from resorption activity by the osteoclasts. Secondary trabeculae consisting of primary woven bone bound by endosteal lamellar bone have started to form partially occluding the MC in the adductor crest region. (Fig. 2E). These structures are similar to that observed in the juvenile *C. romeri* sections (Fig. 12B).

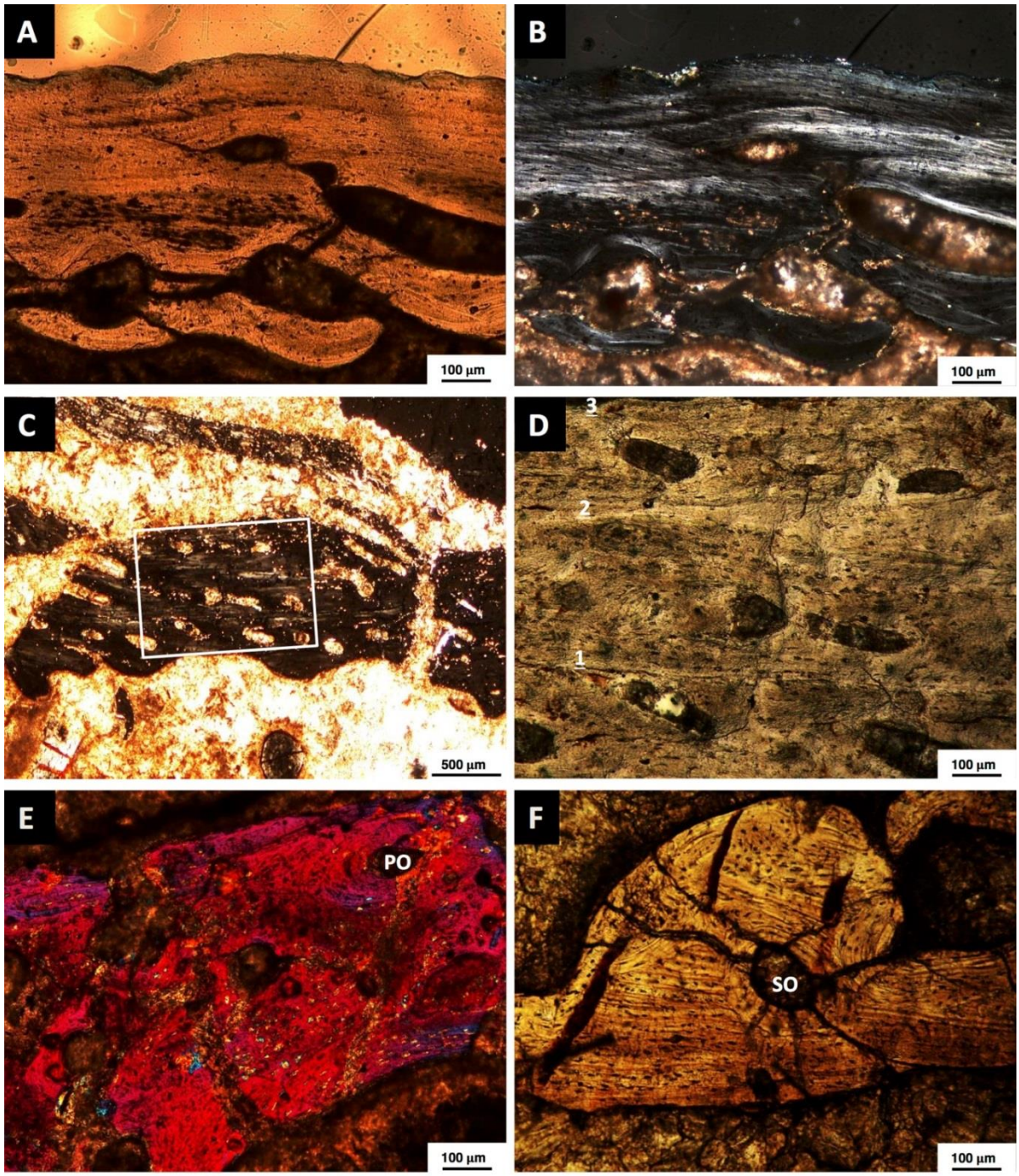

Figure 2. Microscopic re-examination of original thin sections made by de Ricqlès (1974a) of a left femur from an immature *Ennatosaurus tecton*. This specimen is most likely in the transition phase from postnatal hatchling to adolescent. Also, this is the time period hypothesized for offspring to transition from insectivores to herbivores while acquiring their symbiotic microbes for cellulose digestion (Ref). A) Microscopic view of the transverse section of the cortex imaged in conventional transmitted light (Arrow in C; Fig. 1). This is the same and only area of the

cortex that was published in a micrograph (de Ricqlès, 1974a; de Ricqlès et al. 2004). Cortex is thin and the bone matrix consists of a mixture of PFB and LB. Longitudinal vascular canals are large and sparse in the upper cortex as was noted by de Ricqlès (1974a) as being unusual for a juvenile specimen. Growth marks are visible as well as very small osteocyte lacunae. Resorption of the periosteal bone is occurring, greatly expanding the medullary cavity as secondary trabeculae begins to form and lamellar bone is deposited around these erosional cavities. B) Same view as in (A) but imaged in polarized light. Lamellae are distinguishable in the cortex as is the LB surrounding the erosion cavities at the medullary margin. C) An isolated detached fragment of primary cortical bone that has not yet been resorbed. Imaged in polarized light. Notice vascularity is much denser than that observed in the younger outer cortex in (A). D) Microscopic view of the primary cortex as indicated by the boxed area in (C) imaged in conventional transmitted light. Three growth marks are visible. Notice the large osteocyte lacunae surrounding the vascular canals that are restricted to these patches of fast growing WB. This is more typical of the very young juvenile cortical tissue overlooked by de Ricqlès (1974a) in his original description. The WB is stratified by LAGs on either side in PFB. The longitudinal vascular canals are restricted to these zones and do not cross the LAG. E) Microscopic view of the secondary trabecular bone from the more distal section towards the center of the medullary cavity (C; Fig. 1), imaged in polarized transmitted light through a lambda filter. Original primary cortex bordered on either side by lamellar bone. Notice the large vascular canals, isolated primary osteon, and osteocyte lacunae. F) Microscopic view of the trabecular bone just below the cortex imaged in conventional transmitted light. Notice the secondary osteon in the center and the multiple generations of secondarily deposited PFB marked by cementing lines. Abbreviations: PO= primary osteon; SO= secondary osteon.

6. Discussion

In this study we set out to histologically analyze a variety of caseid taxa in order to reveal any variations in histology (Huttenlocker and Rega, 2012) and compare these results to a re-examination of the original *Ennatosaurus tecton* specimen originally described by de Ricqlès (1974a) (Table 1, Fig. 1). In addition, we wanted to test the theory that an elevated basal metabolic rate (BMR) together with an increase in body temperature would have furthered the evolution of herbivory and large body size in pelycosaur-grade basal synapsids because a high BMR would have allowed fast growth as well as improved fermentation efficiency. The

evolution of BMR and thermoregulation is best understood through the study of bone microstructure, because bone histology, while not directly indicating metabolic rate, faithfully records growth rate and faster and slower growing tissue types.

6.1 Synthesized histology and the absence of FLB

Our results have revealed that the dominant periosteal tissue in all specimens is avascular lamellar bone. The only notable exceptions are the localized vascularization in MNHN.F.MCL-1 *R. russellorum* radius and the minor occurrences of longitudinally vascularized woven bone observed in the immature specimens (OMNH-01728a-d and the *E. tecton* femur) discussed in more detail later. Also, caseids possess the smallest osteocyte lacunae of any known pelycosaur, but this is not unusual given their slow growing periosteal tissue, which is also evident by the closely spaced LAGs denoting the growth cycles; annuli and zones do not appear in any sample. MNG-10552 radius and ulna contain the most extensive growth record of any specimen examined (Table 1). The overall differences in this sample set are size and ACT, the thickest being MNHN.F.MCL-1 *R. russellorum* radius. Members of Caseidae shared an ecological commonality, like habitat and diet, which is reflected not only in the similar bone tissue but also in the taphonomy, a universal whitening of all fossilized skeletal remains regardless of geographical occurrence.

After a re-examination of *E. tecton,* we find our results to be in line with those originally reported by de Ricqlès (1974a) with the exception of *C. romeri,* which is discussed later. Basically, there is an overall slow growing lamellar cortex with very little vascularization. In section 142.1.3.T (Fig. 2C) detached unaltered isolated patches of highly vascularized primary woven bone is present just beneath this lamellar layer. However, we believe this tissue in the outer cortex formed during the beginning of the sub-adult stage. Hypothetically, this animal died during the period shortly after the transition between trophic levels from the insectivory period into herbivory. This has been shown to happen in the juveniles of modern herbivorous lizards that start out as insectivores (Pough, 1973), but this has not yet been correlated with changes in histology. Berman et al. (1998) made the same hypothesis for diadectids showing the transformation of the occlusal tooth surface from the juveniles to the adults indicating a change in diet from omnivorous to herbivorous. However, this has not been observed in caseids as juvenile material is very rare. It should be noted that diadectid postcranial histology is highly

vascularized, similar to that observed in sphenacodontids (de Ricqlès, 1974b). This is unusual given their assumed herbivorous diet.

6.2 Specialized microanatomy and histology of *Cotylorhynchus romeri*

Cotylorhynchus romeri histology is an example of paedomorphosis in that both the juvenile and the adult forms demonstrate an osteoporotic-like condition; these sections appear to consist almost entirely of trabeculae with exception of the adult femur (Figs. 11 and 13; S. F. 2). This is very similar to the bone compactness profile observed in ichthyosaurs and dolphins (de Buffrénil and Schoevaert, 1988; Hayashi et al., 2013; de Ricqlès and de Buffrénil, 2001). The osteoporotic-like condition could be explained as an effect of Wolf's law produced by displacing the load on bones in a hypothetical aquatic environment. This would also allow for their large size as well. Reisz and Fröbisch (2014) have also noted a correlation between a size increase in caseid taxa and a habitat migration towards more lowland environments, and Olson (1968) noted the sedimentology of a *Cotylorhynchus* locality reflected a paludal environment. There is no visible distinct medullary cavity in *C. romeri*, nor is there any periosteum in the juveniles as the bone remained open and highly porous throughout life (Fig.11). However, there is a thin outer cortex of lamellar bone preserved only in one region of the OMNH-00631 humerus adjacent to the dorsal side. The OMNH-00631 femur has a lamellar cortex at least three times the thickness of the humerus (Table 1). As noted earlier it is unlikely that these bones are from the same individual. In the juvenile specimens (OMNH-01728), a primary woven cortex with longitudinal vascular canals is still visible between the lamellar bone of the trabeculae (Fig. 11). In the adult specimens this primary cortex has been resorbed and replaced with lamellar bone. A similar osteoporotic-like state possibly exists in the sampled *Alierasaurus ronchii* rib (MPUR-151). This species is much larger than *C. romeri* and could indicate that this osteoporotic-like condition is somehow related to the large size of these animals, perhaps to reduce mass, like the spongy bone found in elephant skulls. However, if the actual preferred habitat of these large caseids is terrestrial they are the largest osteoporotic-like organisms to have ever walked on land. Further ontogenetic consumptive sampling is required of the postcranial material of *A. ronchii* and *C. hancocki*.

The age estimations calculated for *C. romeri* remain speculative. Errors are most likely to have occurred because of the lack of preserved growth marks in the juveniles and the osteoporotic-like nature of the bones in general. The LAGs preserved in the adult specimens do

decrease in thickness beyond the deep cortex, but they are spaced further apart in the femur than in the humerus. It is unclear whether or not skeletal senescence has occurred in the adult material. An external fundamental system might be the only evidence of growth preserved in the outer cortex, but with resorption of the earlier growth marks this is a possibility.

6.3 A comparison to other pelycosaurs

In comparison to what is known of the other herbivorous pelycosaur family, Edaphosauridae (Huttenlocker and Rega, 2012; de Ricqlès, 1976), caseids are less vascularized but seem to possess a similar bone matrix. This may be due to the fact that edaphosaurids were not strictly herbivorous but were omnivorous, capable of feeding on both insects and plants (Hotton et al., 1997). These results are in stark contrast to the histology of the sampled carnivorous pelycosaur families Sphenacodontidae and Ophiacodontidae (Huttenlocker and Rega, 2012; Shelton et al., 2013), which possess highly vascularized fibro-lamellar cortical tissue. They grew much quicker than the herbivorous pelycosaurs. The difference in tissue types among the basal synapsid groups could be an indication of diet and how feeding was achieved. More active hunters grew faster due to higher metabolic requirements, whereas herbivores were less active because of foraging or browsing. Omnivores fall somewhere in between. However, further testing of edaphosaurids at a modern level is required in order to reconstruct a proper comparable growth trajectory, as well as a histological analysis of the largest edaphosaurid taxa, *Lupeosaurus* (spp).

6.4 Limb length disparity phenomenon

With regards to morphometrics, it is interesting to note that some taxa of Caseidae have longer humeri than femora, if not almost equal in length (See Olson, 1968). This is the only pelycosaur group where this is true, and the phenomenon has been noted recent studies without an explanation of why this occurs (Felice and Angielczyk, 2014; Reisz et al., 2011). It is also interesting to note that the mid-diaphysis circumference of the humerus is larger than the accompanying femur regardless which one is longer. In addition, they also possess massive shoulder girdles; this could mean that more weight is placed on the front limbs. This could also be related to locomotion or feeding. This adaption is often seen in modern marine mammals such as pinnipeds where the hind limbs are reduced, and the majority of their body mass is supported by the front limbs when on land. This same LLD phenomenon is also evident in both extinct and

extant species of sea turtles. De Ricqlès (1974c) did make the statement that a sprawling animal has the potential to grow large if it is amphibious or aquatic.

7. Conclusions

These findings have confirmed that Caseidae grew slowly as revealed by an overwhelming presence of avascular, extremely lamellar periosteal bone. One of the benefits of herbivory is that it allows animals to consume large amounts of food with minimal locomotion, thereby presenting a very effective and energy-efficient solution to daily physiological demands. Also, this permits larger body size because energy is not lost to trophic level effects. This explains the presence of lamellar bone because of the lower energy required to forage than it does to hunt if the results are compared to *Dimetrodon* (sp) and *Ophiacodon* (sp) histology (Huttenlocker and Rega, 2012; Shelton et al., 2013). Woven bone is only preserved in the primary cortex during the juvenile stages. Hypothetically, growth may have slowed after the trophic level shift from insectivorous feeding to a primary herbivore diet (Plough, 1973; Sues, 2000) as observed in the *E. tecton* femur (MNHN-142.1) described above. In order to expand on this hypothesis, further consumptive sampling of the illusive juvenile caseids is required as well as a histological analysis of bone tissue from the recently described Carboniferous insectivore taxon, *Eocasea martini* (Reisz and Fröbisch, 2014). These preliminary results are the first step in rejecting the hypothesis that endothermy furthered the evolution of cellulose herbivory in pelycosaur-grade basal synapsids via a high metabolic rate and large body size. The osteoporotic-like condition observed throughout the *Cotylorhynchus romeri* ontogeny has revealed an alternative mechanism to reaching the record body sizes achieved by these later species. Perhaps by utilizing Wolff's Law in displacing mass in a gravity reduced environment. A final comparison to common edaphosaurid taxa such as *Edaphosaurus* (sp) and *Lupeosaurus* (spp), as well as ontogenies of the other caseid taxa, is required in order to fully test this theory

8. Acknowledgements:

I would like to thank the following people for loaning research material and for lively discussions on this topic: Jennifer Larson, Rich Cefelli, and Kyle Davies of the Sam Noble Oklahoma Museum of Natural History. Umberto Nicosia and Marco Romano of the Museum of "La Sapienza" Univeristy of Rome and the Soprintendenza per i Beni Archeologici per le Province di Sassari e Nuoro. Vivian de Buffrénil, Jocelyn Falconnet, Ronan Allain, Armand de Ricqlès of

Muséum National d'Histoire Naturelle Paris. Thomas Martens of the Museum der Natur Gotha. Markus Lambertz, Steven Perry, and Aurore Canoville Olaf Dullfer, Katja Waskow, Rebecca Hoffman, Yasuhisa Nakajima, Jessica Mitchell, Martin Sander of the University of Bonn. Robert Bakker of the Houston Museum of Natural Science. This project was funded by DFG grant SA 469/34-1.

9. References cited

Bakker, R. T., 1975. Experimental and Fossil Evidence for the Evolution of Tetrapod Bioenergetics. In: Gates D. and Schmerl R. (Eds.) Perspectives of biophysical ecology. Springer-Verlag, New York, pp. 365- 399.

Berman, D. S., Henrici, A. C., Sumida, S. S., 1998. Taxonomic status of the Early Permian *Helodectes paridens* Cope (Diadectidae) with discussion of occlusion of diadectid marginal dentitions. Carnegie Mus. Nat. Hist. 67, 181-196.

Berman, D. S., Henrici, A. C., Kissel, R. A., Sumida, S. S., Martens, T., 2004. A new diadectid (Diadectomorpha) *Orobates pabsti* from the Early Permian of Central Germany. Bull. Carnegie Mus. Nat. Hist. 35, 1-36.

Berman, D. S., Henrici, A. C., Sumida, S. S., Martens, T., 2000. Redescription of *Seymouria sanjuanensis* (Seymouriamorpha) from the Lower Permian of Germany based on complete, mature specimens with a discussion of paleoecology of the Bromacker locality assemblage. J. Vert. Paleontol. 20, 253-268.

Buffrénil, V. d., Schoevaert, D., 1988. On how the periosteal bone of the delphinid humerus becomes cancellous: ontogeny of a histological specialization. J. Morph 198, 149-164.

Bybee, P. J., Lee, A. H., Lamm, E. T., 2006. Sizing the Jurassic theropod dinosaur *Allosaurus*: Assessing growth strategy and evolution of ontogenetic scaling of limbs. J. Morph. 267, 347–59.

Castanet, J., 2006. Time recording in bone microstructure of endothermic animals; functional relationships. C. R. Palevol 5, 629–36.

Castanet, J., Croci, S., Aujard, F., Perret, M., Cubo, J., Margerie, E. d., 2004. Lines of arrested growth in bone and age estimation in a small primate: *Microcebus murinus*. J. Zool. 263, 31–39.

Currey, J. D., 2002. Bones. Structure and Mechanics. Princeton University Press, Princeton . 436 p.

Dudley, R., 1998. Atmospheric oxygen, giant Paleozoic insects and the evolution of aerial locomotor performance. J. Exp. Biol. 201, 1043-1050.

Eberth, D. A., Berman, D. S., Sumida, S. S., Hopf, H., 2000. Lower Permian terrestrial paleoenvironments and vertebrate paleoecology of the Tambach Basin (Thuringia, Central Germany): the upland Holy Grail. Palaios 15, 293–313.

Efremov, J. A., 1956. American elements in the fauna of Permian reptiles of the USSR. Doklady Akademii Nauk SSSR 111, 1091–1094.

Felice, R. N., Angielczyk, K. D., 2014. Was Ophiacodon (Synapsida, Eupelycosauria) a Swimmer? A test using vertebral dimensions. In: Kramerer, C. F., Angielczyk, K. D., Fröbisch, J. (Eds.) Early evolutionary history of the Synapsida. Springer, New York, pp. 25-51.

Francillon-Vieillot, H., Buffrénil, V. de., Castenet, J., Gèraudie, J., Meunier, F. J., Sire, J. Y., Zylbergberg, L. & Ricqlès, A. de., 1990. Microstructure and mineralization of vertebrate skeletal tissues. In Carter, J. G. (ed.) Skeletal biomineralization: Patterns, processes and evolutionary trends. Van Nostrand Reinhold., New York, pp. 471-530.

Gand, G., 1986. Interprétations paléontologique et paléoécologique de quatre niveauxà traces de vertébrés observes dans l'Autunien du Lodévois (Hérault). Géol. Fr. 2, 155-176.

Gand, G., 1989. Essai de reconstitution paléoenvironnementale et paléoécologique d'un partie du nord du bassin de Lodève (Hérault) au Permien inférieur. Géol. Fr. 4**,** 17-30.

Gand, G., Garric, J., Schnieder, J., Walter, H., Lapeyrie, J., Martin, C., Thiery, A., 2008. Notostraca trackways in Permian playa environments of the Lodève basin (France) J. Iberian Geol. 34, 73-108.

Gow, C. E., 1978. The advent of herbivory in vertain reptilian lineages during the Triassic. Paleontol. Afr. 21. 133-141.

Graham, J. B., Aguilar, N., Dudely, R., Gans, C., 1997. The Late Paleozoic atmosphere and the ecological and evolutionary physiology of tetrapods. In: Sumida, S., Martin, K. L. M. (Eds.) Amniote origins: completing the transition to land. Academic Press, New York, pp. 141-168.

Hayashi, S., Houssaye, A., Nakajima, Y., Chiba, K., Ando, T., Sawamura, H., Osaki, T., 2013. Bone inner structure suggests increasing aquatic adaptations in Desmostylia (Mammalia, Afrotheria). PloS one, 8.e59146.

Hotton, N., Olson, E. C., Beerbower, R., 1997. Amniote origins and the discovery of herbivory. In: Sumida, S., Martin, K. L. M. (Eds.) Amniote origins: completing the transition to land. Academic Press, New York, pp. 207-264.

Hsia, C. C., Schmitz, A., Lambertz, M., Perry, S. F., Maina, J. N., 2013. Evolution of air breathing: oxygen homeostasis and the transitions from water to land and sky. Comp. Physiol. 3, 849-915.

Huttenlocker, A., Rega, E., 2012. The paleobiology and bone microstructure of pelycosaurian-grade synapsids. In: Chinsamy, A. (ed.) The forerunners of mammals- radiation, histology, biology. Indiana University Press, Bloomington, pp. 91-120.

Hübner, N., Körner, F., Schneider, J., 2011. Tectonics, climate and facies of the Saint Affrique Basin and correlation with the Lodève Basin (Permian, Southern France). Z. dt. Ges. Geowiss. 162, 157-170.

Klein, N., Sander, P. M., 2007. Bone histology and growth of the prosauropod Plateosaurus engelhardti MEYER, 1837 from the Norian bonebeds of Trossingen (Germany) and Frick (Switzerland). Spec. Pap. Palaeontol. 77, 169–206.

Kohler, M., Marín-Moratalla, N., Jordana, X., Aanes, R., 2012. Seasonal bone growth and physiology in endotherms shed light on dinosaur physiology. Nature 487, 358–61.

Lopez, Gand, G., Garric, J., Körner, F., Schnieder, J., 2008. The playa environments of the Lodève Permian basin (Languedoc-France): Los ambientes de playa de la Cuenca de Lòdeve (Languedoc-Francia). J. Iberian Geol. 34, 29-56.

Maddin, H. C., Sidor, C. A., Reisz, R. R., 2008. Cranial anatomy of Ennatosaurus tecton (Synapsida: Caseidae) from the Middle Permian of Russia and the evolutionary relationships of Caseidae. J. Vert. Paleontol. 28, 160-180.

Martens, T., Hahne, K., Naumann, R., 2009. Lithostratigraphie, Taphofazies und Geochemie des Tambach-Sandsteins im Typusgebiet der Tambach-Formation (Thüringer Wald, Oberrot-liegend, Unteres Perm). Z. Geol. Wiss, 37, 81-119.

Olson, E. C., 1968. The family Caseidae. Fieldiana: Geol. 17, 223-349.

Olson, E. C., Beerbower, J. R. 1953. The San Angelo Formation, Permian of Texas and its vertebrates. J. Geol. 61, 389-423.

Petermann, H., Sander, M., 2013. Histological evidence for muscle insertion in extant amniote femora: implications for muscle reconstruction in fossils. J. Anat. 222, 419-436.

Pough, F. H., 1973. Lizard energetics and diet. Ecology, 54, 837-844.

Prondvai, E., Stein, K. H., Ricqlès, A. d., Cubo, J., 2014. Development-based revision of bone tissue classification: the importance of semantics for science. Biol. J. Linn. Soc. 112, 799-816.

Reisz, R. R., 1986. Encyclopedia of Paleoherpetology. 17A: Pelycosauria. Fischer, Stuttgart, 102 p.

Reisz, R. R., & Fröbisch, J., 2014. The Oldest Caseid Synapsid from the Late Pennsylvanian of Kansas, and the Evolution of Herbivory in Terrestrial Vertebrates. PloS one, 9(4), e94518.

Reisz, R. R., Godfrey. S. J., Scott, D., 2009. *Eothyris* and *Oedaleops*: Do these early Permian synapsids from Texas and New Mexico form a clade? J. Vert. Paleont. 29, 39–47.

Reisz, R. R., Maddin, H. C., Fröbisch, J., Falconnet, J., 2011. A new large caseid (Synapsida, Caseasauria) from the Permian of Rodez (France), including a reappraisal of "*Casea*" *rutena* Sigogneau-Russell & Russell, 1974. Geodiversitas, 33, 227-246.

Ricqlès, A. d., 1974a. Recherches pale´ohistologiques sur les os longs des Te´trapodes IV: Eotheriodonts and pelycosaurs. Annls. Paléont. 60, 3–39.

Ricqlés, A. d., 1974b. Recherches pale´ohistologiques sur les os longs des Te´trapodes V: Cotylosaures et Mésosaurs. Annls. Paléont. 60, 171–231.

Ricqlès, A. d., 1974c. Evolution of endothermy: Histological evidence. Evol. Theory 1, 51–80.

Ricqlès, A. d., Buffrénil, V. d., 2001. Bone histology, heterochronies and the return of Tetrapods to life in water: where are we? In: Mazin, J. M., Buffrénil, V., (Eds.), Secondary adaptation of tetrapods to life in water. Verlag, München, pp. 289–310.

Ricqlès, A. d., Castanet, J., Francillon-Vieillot, H., 2004. The 'message'of bone tissue in paleoherpetology. It. J. Zool. 71, 3-12.

Romano, M., Nicosia, U., 2014. *Alierasaurus ronchii*, gen. et sp. nov., a caseid from the Permian of Sardinia, Italy. J. Vert. Paleont. 34, 900-913.

Romer, A. S., Price, L. I. 1940. Review of the Pelycosaurs. Geol. Soc. Am. Spec. Pap. 28, 1-538.

Romer, A. S., 1969. Osteology of the reptiles. Chicago Illinois: University of Chicago Press, Chicago, 800 p.

Ronchi, A., Sacchi, E., Romano, M., Nicosia, U., 2011. A huge caseid pelycosaur from north-western Sardinia and its bearing on European Permian stratigraphy and palaeobiogeography. Acta Palaeont. Pol. 56, 723- 738.

Sander, M., Klein, N., 2005. Developmental plasticity in the life history of a prosaruopod dinosaur. Science 310, 1800–1802.

Sander, P. M., Mateus, O. Laven, T., Knötschke, N., 2006. Bone histology indicates insular dwarfism in a new Late Jurassic sauropod dinosaur. Nature 441, 739–41.

Schneider, J. W., Körner, F., Roscher, M., Kroner, U., 2006. Permian climate development in the northern peri-Tethys area-the Lodève basin, French Massif Central, compared in a European and global context. Palaeogeog., Palaeoclimatol., Palaeoecol., 240, 161-183.

Shelton, C. D., Sander, P. M., Stein, K., & Winkelhorst, H., (2013). Long bone histology indicates sympatric species of Dimetrodon (Lower Permian, Sphenacodontidae). Earth Env. Sci. Trans. Royal Soc. Edinburgh, 103, 217-236.

Stein, K., Prondvai, E., 2014. Rethinking the nature of fibrolamellar bone: an integrative biological revision of sauropod plexiform bone formation. Biol. Rev., 89, 24-47.

Stein, K., Sander, M., 2009. Histological core drilling: a less destructive method for studying bone histology. Methods in fossil preparation: proceedings of the first annual Fossil Preparation and Collections Symposium 1, 69-80.

Stovall, J. W., 1937. *Cotylorhynchus romeri*, a new genus and species of pelycosaurian reptile from Oklahoma. Am. J. Sci. 34, 308-313.

Stovall, J. W., Price, L. I., and Romer, A. S., 1966. The postcranial skeleton of the giant Permian pelycosaur *Cotylorhynchus romeri.* Bull. Mus. Comp. Zool. Harv. 135, 1–30.

Sues, H. D., 2005. Evolution of herbivory in terrestrial vertebrates: perspectives from the fossil record. Cambridge University Press, 256 p.

Sues, H. D., Reisz, R. R., 1998. Origins and early evolution of herbivory in tetrapods. Trends Ecol. Evol. 13, 141-145.

Troyer, K., 1982. Transfer of fermentative microbes between generations in a herbivorous lizard. Science 216, 540-542.

Waskow, K., Sander, P. M., 2014. Growth record and histological variation in the dorsal ribs of *Camarasaurus* sp.(Sauropoda). J. Vert. Paleontol. 34, 852-869.

Williston, S. W., 1912. Primitive reptiles. J. Morphol. 23, 637-666.

Zimmerman, L. C., Tracy, C. R., 1989. Interactions between the environment and ectothermy and herbivory in reptiles. Physiol. Zool. 62, 374-409.

Chapter 7: State of the art Pelycosaur bone histology and the Carboniferous origins of fibro-lamellar bone in the basal synapsids

1. Introduction

Studying the inter- and intraspecific bone histology of the earliest representatives of the mammal lineage, the pelycosaurs, has improved our understanding of one of the major events in vertebrate evolution, mammalian endothermy, as well as the overall metabolism and physiology of these early synapsids. Ectothermy and endothermy cannot be detected directly in extinct animals. Instead a proxy is used: bone tissue types, which indicate bone growth rates.

In order to have a complete picture of the different pelycosaur groups, a detailed histological description of postcrania from Varanopidae and Edaphosauridae is needed and therefore included here as time did not allow for separate chapters of these two groups. Pelycosaur groups analyzed in the previous chapters will be summarized and compared to captorhinids (formerly, cotylosaur) and diadectid bone histology. Eothyrididae material was not available for consumptive analysis and is therefore excluded from this summary. Later, the implications of these histological findings are discussed with regard to pelycosaur evolution, physiology, and ecology.

2. Phylogenetic comparison

2.1 Basal reptiles

2.1.1 Background

Reptiles first appear during the Carboniferous and are represented by such animals as *Hylonomus*, considered the earliest member of the group. Reptiles have always been viewed as poikilothermic sluggish tail draggers. And this has been the consensus for the pelycosaur grade mammal-like reptiles. Unfortunately, not much is known about the histology of these early synapsids. The anapsid reptiles from the captorhinid group represent some of the earliest known histologically studied amniotes. (Enlow and Brown 1957; Peabody 1961; de Ricqlès 1974a). They first appear during the Carboniferous and go extinct during the Permian. *Captorhinus agouti* is a larger form believed to be herbivorous (Reisz and Fröbisch 2014). *Labidosaurus* is an

omnivorous captorhinid that coexisted with *Captorhinus*, both of which are found in the Texas Red Beds.

2.1.2 Published histology.

Captorhinidae is one of the most abundant reptile forms and has been well studied histologically. Enlow and Brown (1957) described the tissue in *Captorhinus* and *Labidosaurus* as being similar to that observed in the 'labyrinthodont' amphibians as having lamellar bone with small longitudinal vascular canals, being devoid of trabecular bone, and secondary structures in the medullary region. Peabody (1961) sectioned a *Captorhinus* humerus from Richard Spur, Oklahoma, and noted a lamellar tissue with areas of slow and fast growth corresponding to annuli and zones, respectively. He interpreted this as perhaps seasonal changes that left a record in the bone. Resorption activity in the medullary region is clearly visible in the sections Peabody (1961) examined. De Ricqlès (1974a) made similar findings to those observed by previous researchers by noting the same lamellar tissue and vascularity.

2.2 Sister taxa, *Diadectes* (sp)

2.2.1 Background

A proper phylogenetic comparison needs to be made regarding the postcranial histology of the reptiliomorph *Diadectes* Cope 1878. Most common in North America and Germany, this group was prevalent from the Late Carboniferous to the Early Permian. Diadectids are considered the sister group to Amniota (Chapter 1). Not only are they the first tetrapod group to have achieved herbivory, they are also the only non-amniote herbivore. As shown by Pough (1973), juveniles of herbivorous squamates start out as insectivores and eventually a trophic shift occurs, whereby physiological requirements force a dietary change to plants. This transition is rarely observed in the fossil record, and was described for the first time in pelycosaur bone tissue in Chapter 6. However, dental material from a juvenile diadectid has been found that shows a difference in occlusion compared to the adult form, indicating a trophic shift from possibly omnivory to high-fiber herbivory (Berman et al. 1998)

2.2.2 Published histology:

Ricqlès (1974a) (Fig. 1A) previously described diadectid histology of the femoral diaphysis. His findings showed that the cortex consisted of a lamellar bone matrix with dense

longitudinal vascular canals. However, compared to the consumptive sampling of femur ISPBH-77, collected in the Briar Creek Bonebed (BCBB) by P. M. Sander in 1999, the published specimen described by Ricqlès (1974a) is a younger individual (Fig. 1B).

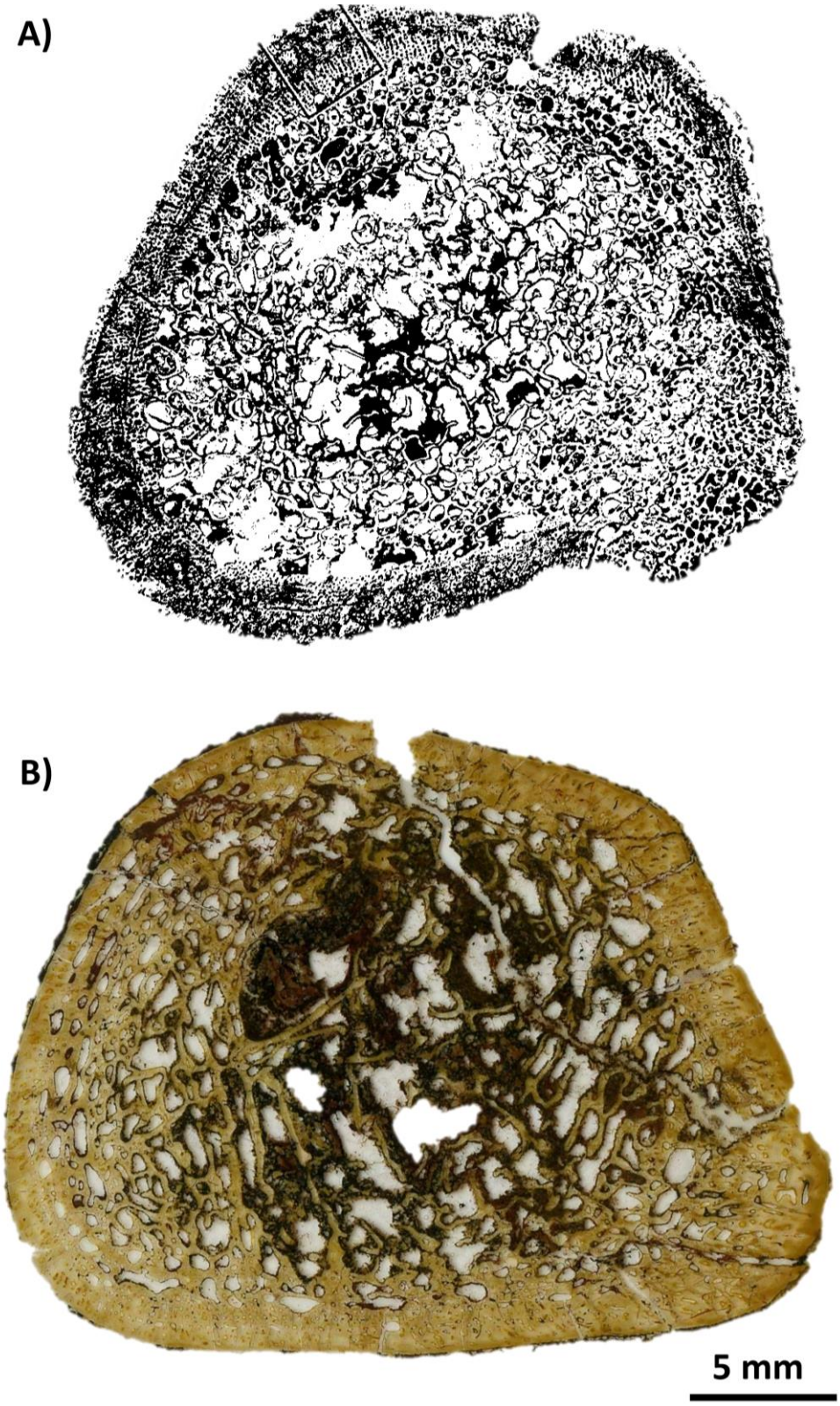

Figure 1. Diadectes (sp) mid-diaphysial transverse femoral sections. A) Transverse femoral section prepared and described by de Ricqlès (1974a). Cortex is thin and densely vascularized.

One LAG is visible at mid cortex. Vascular canals in the lower cortex are radially arranged longitudinal canals. Beyond this LAG, the vascular pattern is more random and the canals remains longitudinal. Medullary cavity is occluded. B) Scan of IPBSH-77 Diadectes femur, minimal diaphysis transverse section (length 138 mm and circumference is 87 mm) in normal light. This specimen appears to be older than that pictured in (A) described by de Ricqlès (1974a). Cortex remains thin (average thickness is 1225 μm) and consists of PFB. Vascular canals are longitudinal, and expansion of the MC occurs circumferentially.

2.2.3 Histological description of Diadectes femur IPBSH-77:

Histology was described from a transverse section of the minimal diaphysis for the Diadectes specimen, IPBSH-77, of a femur, in the Nocona Formation of the BCBB (Lower Permian, Artinskian) (Fig. 1B). This femur has a length of 138 mm and a circumference of 87 mm (Table 1). The cortex consists of parallel-fibered bone (PFB) and woven bone (WB) matrix. Vascularity consists of small and large longitudinal canals arranged in circumferential layers (Fig. 2A, B). Most canals have a single layer of lamellar bone (LB), but some of the smallest canals are fully formed primary osteons (Fig. 2C, D). Osteocyte lacunae (OL) are round, medium-sized and disorganized. The cortex contains a growth record of five growth cycles visible in polarized light. Three cycle boundaries are visible in the darker stained area in the adductor region. Sharpey's fibers are visible on the adductor crest of the ventral region as expected (Fig. 2E, F). The medullary region is marked by erosional cavities (EC) that seem to follow the direction of vascularity. The medullary cavity (MC) is occluded with trabecular bone.

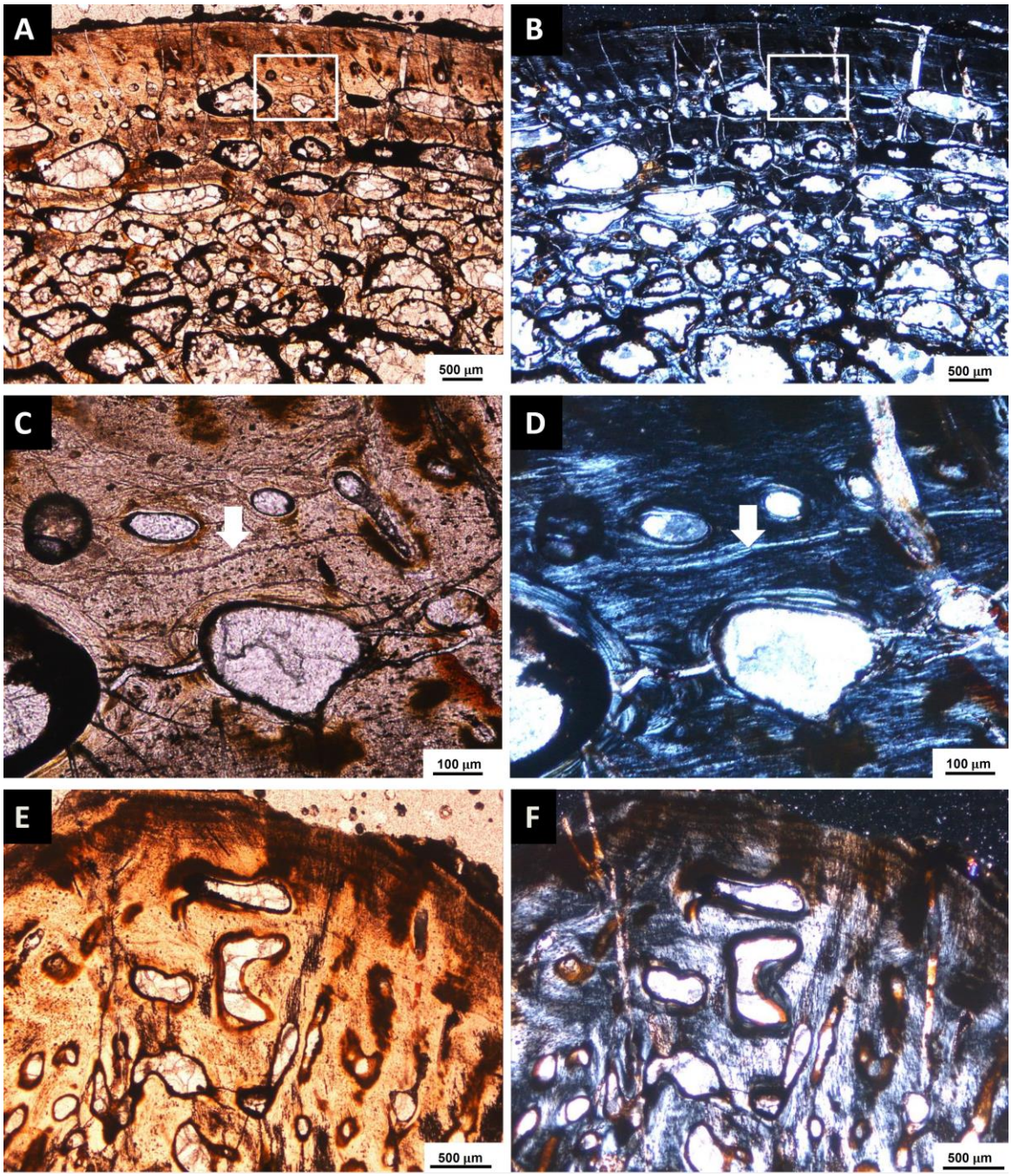

Figure 2. Microscopic view of *Diadectes* IPBSH-77 femoral section from (Fig. 1B). A) The primary cortex imaged in conventional transmitted light (CTL). Note the organization of the primary canals is similar to those in Figure 1A. B) The same area as in (A) imaged in polarized transmitted light (PTL). Five LAGs are visible. The MC is marked by the boundary of the EC. C) Microscopic view of the primary cortex as indicated by the boxed area in (A) imaged in CTL. Arrow is pointing to a LAG. D) Same are as in (C) imaged in PTL. Arrow is pointing to a LAG. Note the difference between the smaller primary vascular canals and the larger secondary canals.

E) Adductor region imaged in CTL. Notice the large Sharpey's fibers. F) Same area as (E) imaged in PTL. Abbreviations: SF= Sharpey's fibers.

Table 1. Diadectid, varanopid, and edaphosaurid morphometrics and average cortical thickness. All Texas material is from various Lower Permian sites in Archer County. All varanopid material is from the Dolesese Quarry of Richard Spur, Oklahoma.

Specimen Number	Bone	Name	Length (mm)	Circumference (mm)	Avg. Cortical Thickness (µm)	LAGs	Locality
IPBSH-77	Femur	*Diadectes* (sp)	138	87	1224.81	5	BCBB-TX
OMNH-52543	Humerus	*Mycterosaurus longiceps*	30	7	676.45	3	Richard Spur, OK
OMNH-73750C	Femur	Varanopidae: Mycterosaurine	49	17	1122.6	4	Richard Spur, OK
OMNH-73354	Femur	Varanopidae: Mycterosaurine	50	17	1564.94	3	Richard Spur, OK
OMNH-73750B	Femur	Varanopidae: Mycterosaurine	51	18	1292.3	4	Richard Spur, OK
OMNH-73750A	Femur	Varanopidae: Mycterosaurine	57	22	1404.61	4	Richard Spur, OK
OMNH-73758	Femur	*Varanops brevirostris*	88	37	2214.81	6	Richard Spur, OK
TMM 3125-71	Humerus	*Edaphosaurus boanerges*	120*	60	2732.23	4	GBB-TX
TMM 31255-70	Humerus	*Edaphosaurus boanerges*	151	61	2501.37	6	GBB-TX
TMM 31255-2	Humerus	*Edaphosaurus boanerges*	174	76	2160.08	4	GBB-TX
MCZ VPRA 3412	Tibia	*Lupeosaurus kayi*	140	81	970.42	6 + EFS (5)	Near GBB-TX
MCZ VPRA 3412	Femur	*Lupeosaurus kayi*	230	109	797.21	3 + EFS (4)	Near GBB-TX
MCZ VPRA 1368	Humerus	*Lupeosaurus kayi*	212	110	1706.73	4 + EFS (5)	Black Flat-TX
IPBSH-84	Femur	*Edaphosaurus* (sp)	118*	87	2153.64	9 + EFS (10)	BCBB-TX
TMM 31255-20	Femur	*Edaphosaurus boanerges*	159	72	2162.44	7	GBB-TX
TMM 31255-6.1	Femur	*Edaphosaurus boanerges*	180	76	2590.35	4 + EFS (13)	GBB-TX

2.3 Histological comparison to Pelycosauria

2.3.1 Basal reptiles:

In comparison to the sampled pelycosaur taxa summarized below, basal reptiles and herbivorous pelycosaurs are more similar to each other. Both grow slowly and produce lines of arrested growth (LAGs) set in a lamellar matrix. Vascularity is reduced.

2.3.2 Diadectes:

Diadectes has a dense postcranial bone tissue similar to that of sphenacodontids. *Diadectes* differs considerably from the histology of other herbivorous amniotes and is more like that of *Dimetrodon*, highly vascularized PFB with large incipient osteons in a radial pattern early in ontogeny. Later in ontogeny vascularity is more amphibian like with a plexiform pattern. The similarities to the sphenacodontid bone tissue pattern is better seen in de Ricqlès' (1974a) specimen (Fig. 1A) because the vascular pattern is the same bicycle wheel pattern of radially arranged longitudinal canals. The longitudinal vascular canals are wider in ISPBH-77 being

larger in the medullary region and deep cortex and reducing in size towards the outer cortex. In contrast, the vascular pattern in the sample from the Briar Creek Bonebed (BCBB) has more similarities to *Eryops* and *Metoposaurus* (Klein and Konietzko-Meier 2013; Shelton and Konietzko-Meier et al. *in progress*), but centripetal layering of lamellar zonal bone (LZB) is less developed in *Diadectes.* The histological similarity to the carnivorous pelycosaurs is unusual as it is perceived to be a herbivore but histology and growth rate reflects otherwise.

2.3.3 Plesiomorphic condition

Given that the available histological material of the captorhinids and diadectids are from possible herbivorous and omnivorous forms, it is still unclear what the plesiomorphic condition is. Consumptive sampling of the earlier tetrapods is required, specifically, the basal Carboniferous pelycosaurs, as well as earlier basal carnivorous amniotes. As of now, slow growing lamellar bone is considered the plesiomorphic histological condition, but this is still just an assumption until further data is collected.

3. Pelycosaur long bone histology summary

3.1 Caseidae

3.1.1 Summarized bone histology:

Based on the findings from Chapters 6, all caseid material examined in this study, regardless of taxa or bone, varied only by size, porosity, and cortical thickness. All cortical bone tissue was found to be almost completely avascular, lamellar bone and contained the smallest osteocyte lacunae of any pelycosaur. Caseids have the slowest growth rate, but achieved record sizes for any known tetrapod at that time. Currently, the largest known caseid taxon is the recently described *Alierasaurus ronchii* discovered in Sardinia, Italy (Romano and Nicosia 2014; Ronchi et al. 2011). The former record holder was *Cotylorhynchus* (sp) from North America.

3.1.2 Bone compactness:

In contrast to the smaller caseid taxa examined in this study (*Ruthenosaurus russellorum,* and the undescribed Bromacker caseid species), the larger taxa, such as *A. ronchii* and *C. romeri*, have an osteoporotic-like condition that persisted throughout ontogeny. Based on the findings in

Chapter 5, a more aquatic habitat could explain this osteoporotic-like condition. The aquatic habitat hypothesis explains how caseids could minimize energy loss when feeding and how these animals could have avoided predation as juveniles.

3.1.3 Trophic shift:

Finally, in regards to the redescribed *Ennatosaurus tecton* sections produced by de Ricqlès (1974b), one can observe the phenomena studied by Pough (1973) in which juvenile herbivorous squamates experience a necessary trophic level shift from insectivory to herbivory. This specimen appears to have perished shortly after making this transition given the sequential evidence of slow and fast growth in the periosteum. The inner primary cortex is highly vascularized woven bone, which is indicative of fast growing juvenile tissue, and the outermost cortex is slow growing lamellar bone as is evident by the close proximity of the growth marks and the smaller osteocyte lacunae. This shows that pelycosaur growth rates are secondarily reduced in Caseidae.

3.2 Varanopidae

Varonopids are small to moderate sized carnivorous, agile pelycosaurs and have shown to display parental care (Botha-Brink 2007). Material described here consists of five femora and one humerus all of which are from the Richard Spur locality in Ft. Sill Oklahoma (Table 1). Hutttenlocker and Rega (2012) point out the postcrania of two varanopids that occur here as *Varanops brevirostris* and a small indeterminate mycterosaurine. The second most common vertebrate at Richard Spur is *Mycterosaurus longiceps* (Reisz et al. 1997).

3.2.1 Published bone histology:

The histology described in Enlow and Brown (1957) and Enlow (1969) deviated from the earlier preconceived notions of pelycosaur limb construction (cortex appears more compact/dense, and well defined medullary cavity). De Ricqlès (1974b) serial sectioned a radius and fibula, but the bones had poor preservation. The radius has a 1 mm cortex and a well-defined medullary cavity. However, de Ricqlès (1976a) studied *Watongia* Olson, 1974, which was recently reassigned to Varanopidae (Reisz and Laurin 2004; Maddin et al. 2006), only noting

non-specific histological similarities to pelycosaurs. Additionally, Huttenlocker and Rega (2012) described material from Richard Spur, Oklahoma (Kungurian, Lower Permian), identical to material described below (Table 1). Their findings showed the cortex consisted of unorganized small primary longitudinal canals set in a lamellar matrix lacking LAGs and an open medullary cavity with smooth endosteal bone deposited around the edges. Erosion cavities and trabeculae were absent. Also, Huttenlocker and Rega (2012) used Bone Profiler to compare the bone compactness of a mycterosaurine varanopid femur to the Ophiacodon radius analyzed by Germain and Laurin (2005), and found a more compact bone in the latter.

3.2.2 Descriptive bone histology

3.2.1.1 Mycterosaurus longiceps humerus

OMNH-52543 is a *Mycterosaurus longiceps* left humerus 30 mm in length and 7 mm in circumference (Table 1; Figs. 3A, 4A). The bone itself has been carbonized and is very light as is common for material from the Richard Spur locality. The outer surface of the bone is smooth and black. In the transverse thin section, it can be seen that lamellated PFB is prevalent throughout the cortex (Fig. 4D). Vascularity consists of a few longitudinal canals with no apparent LB deposition. Some small primary osteons are present. OL are dense and become increasingly flattened towards the outer cortex. The cortical bone contains eight or nine growth cycles visible in polarized light. Three LAGs are visible in conventional transmitted light (Fig. 4C). Sharpey's fibers are also present. The medullary region is sharply marked by an inner circumferential layer (ICL) of lamellar bone (Fig. 4B, D), and it is open, lacking trabecular occlusions with no signs of resorption or remodeling. This is unusual as it has not been observed in other pelycosaur taxa.

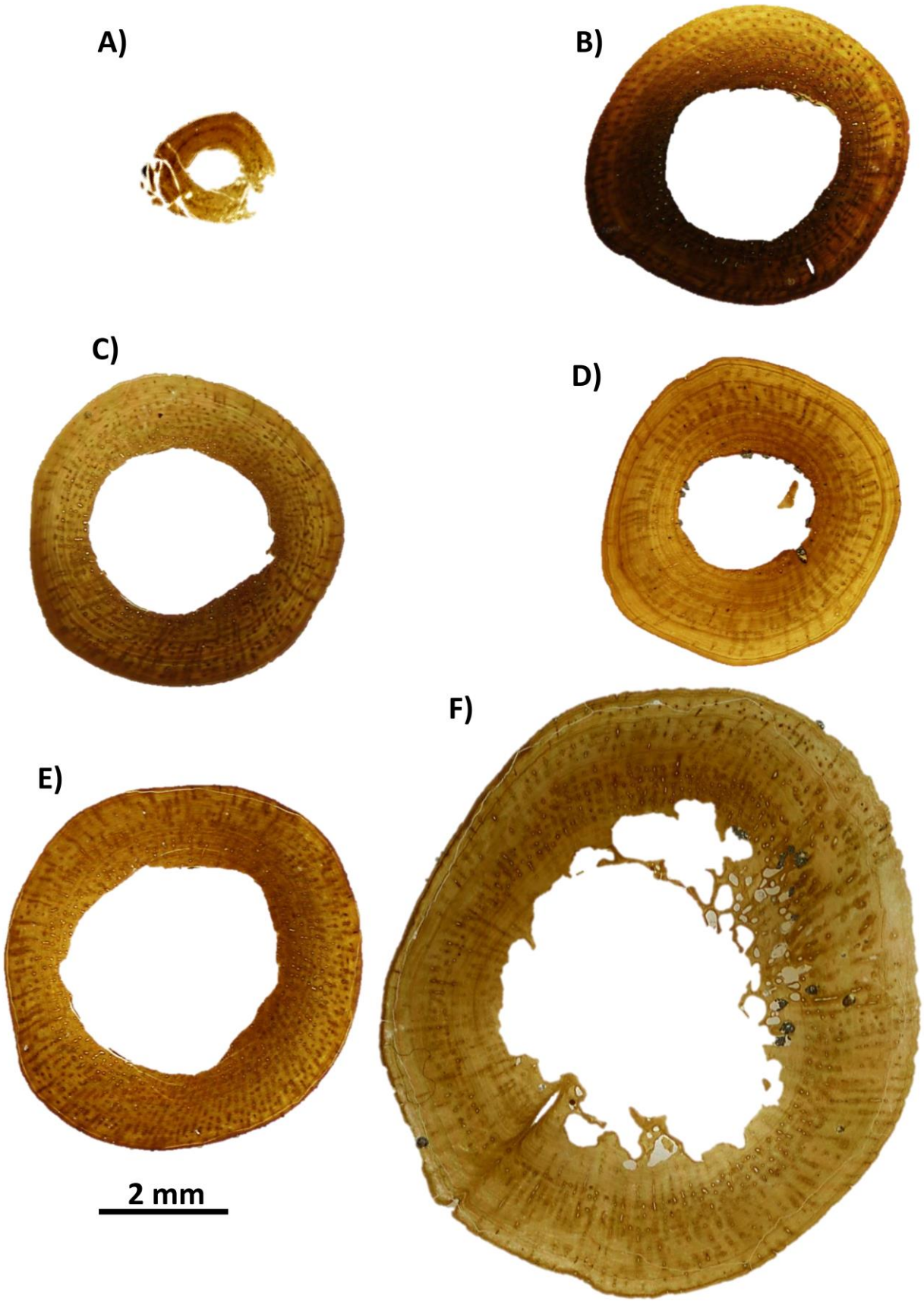
A)
B)
C)
D)
E)
F)
2 mm

Figure 3. Scanned transverse sections of Varanopidae ordered by length (Table 1). A) Humerus OMNH-52543 *Mycterosaurus longiceps*; average cortical thickness (ACT) 676 µm. B) Femur OMNH-73750C Mycterosaurine; ACT 1123 µm. C) Femur OMNH-73354 Mycertosaurine; ACT 1565 µm. D) Femur OMNH-73750B Mycterosaurine; 1292 µm. E) Femur OMNH-73750A Mycterosaurine; ACT 1405 µm. F) Femur OMNH-73758 *Varanops brevirostris*; ACT 2215 µm.

3.2.2.2 Mycterosaurine-grade femora

The following four femora will be described synthetically: OMNH-73750A-C, OMNH-73354 (Fig. 3B, E). These have been simply identified as Varanopidae, possibly mycterosaurine. Length of the bones ranged from 49 - 57 mm and the circumference ranged from 17 – 22 mm (Table 1). The bones themselves have been carbonized like the previously mentioned specimens. The outer surface of the bone is smooth and black, which interferes with the polarizing optics. In the transverse thin section, it can be seen that PFB and LB is prevalent throughout the cortex. The vascular canals are mainly small longitudinal canals and thin radial canals, radially arranged from the inner to outer cortex in the radial "bicycle wheel" pattern observed in all other carnivorous pelycosaurs (Fig. 4E, F). The cortex has densely packed, randomly oriented OL with a flat to oval shape. The cortical bone contains a growth record of three to four LAGs visible in conventional light. Sharpey's fibers are not present. Again, an ICL of LB is visible in polarized light around the MC. The MC is open, lacking trabeculae with signs of resorption indicated by the scalloped edges by osteoclasts. Fully formed EC are not visible.

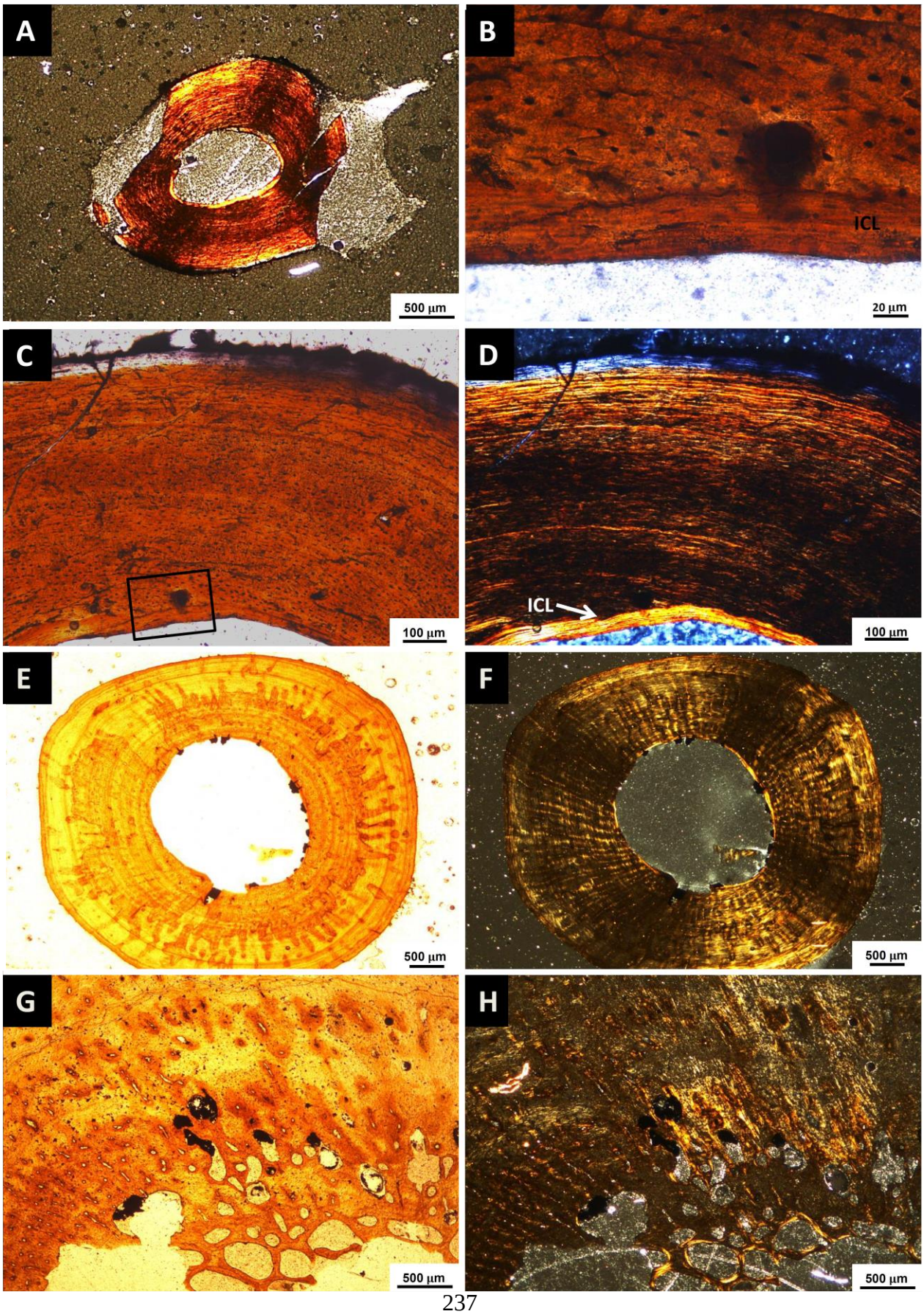
A
500 µm
B
ICL
20 µm
C
100 µm
D
ICL
100 µm
E
500 µm
F
500 µm
G
500 µm
H
500 µm

Figure 4. Micrograph images of varanopid sections. A) Humerus OMNH-52543 imaged in polarized transmitted light B) Magnified view of boxed area in (C) imaged in conventional transmitted light (CTL). Note the region of the inner circumferential layer (ICL). C) Magnified view of the cortex of OMNH-52543. Vascularity is extremely low. D) Same section as (D) imaged in polarized transmitted light. The ICL is better imaged here. E) Mycterosaurine femur OMNH-73750C imaged in CTL. F) Same section as in (E) imaged in polarized light. Note the vascular pattern is radially arranged longitudinal canals, typical of carnivorous pelycosaurs. G) Femur OMNH-73758 *Varanops brevirostris* imaged in CTL. Resorption of the medullary cavity occurs late in ontogeny. H) Same section as in (G) imaged in polarized transmitted light. Abbreviations: ICL= inner circumferential layer.

3.2.2.3 Varanops brevirostris

OMNH-73758 is a *Varanops brevirostris* femur 88 mm in length 37 mm in circumference (Table 1; Fig. 3F). The bone itself has been carbonized and is very light as is common for material from the Richard Spur locality. The outer surface of the bone is smooth and black, which interferes with the polarizing optics. In the transverse thin section, it can be seen that mostly LB, and some PFB, is prevalent throughout the cortex. The vascular canals form the same "bicycle wheel" pattern observed in the previous specimens (Fig. 4G, H). Small primary osteons are present. The OL are densely packed and randomly oriented similar to the other described varanopids. The cortical bone contains a growth record of six LAGs (some double) visible in conventional light. Sharpey's fibers are present, visible only in polarized light. A partial ICL is visible in polarized light around the lining of the medullary cavity. A few secondary trabeculae have formed in the MC, but it is mostly open (Fig. 4G, H).

3.2.3 Growth Dynamics:

The growth model (Fig. 5), similar to the method used in Chapter 4 (Bybee et al. 2006) has revealed ten total growth marks with a conservative estimate of two missing growth marks; thus, assuming each growth mark equates to a year, the *Varanops brevirostris* femur (OMNH-73758) belonged to an individual that is estimated to have died between the 12^{th} and 13^{th} life cycle (Fig. 5). It should be noted that determinate growth has yet to be observed in this pelycosaur group (no EFS was detected).

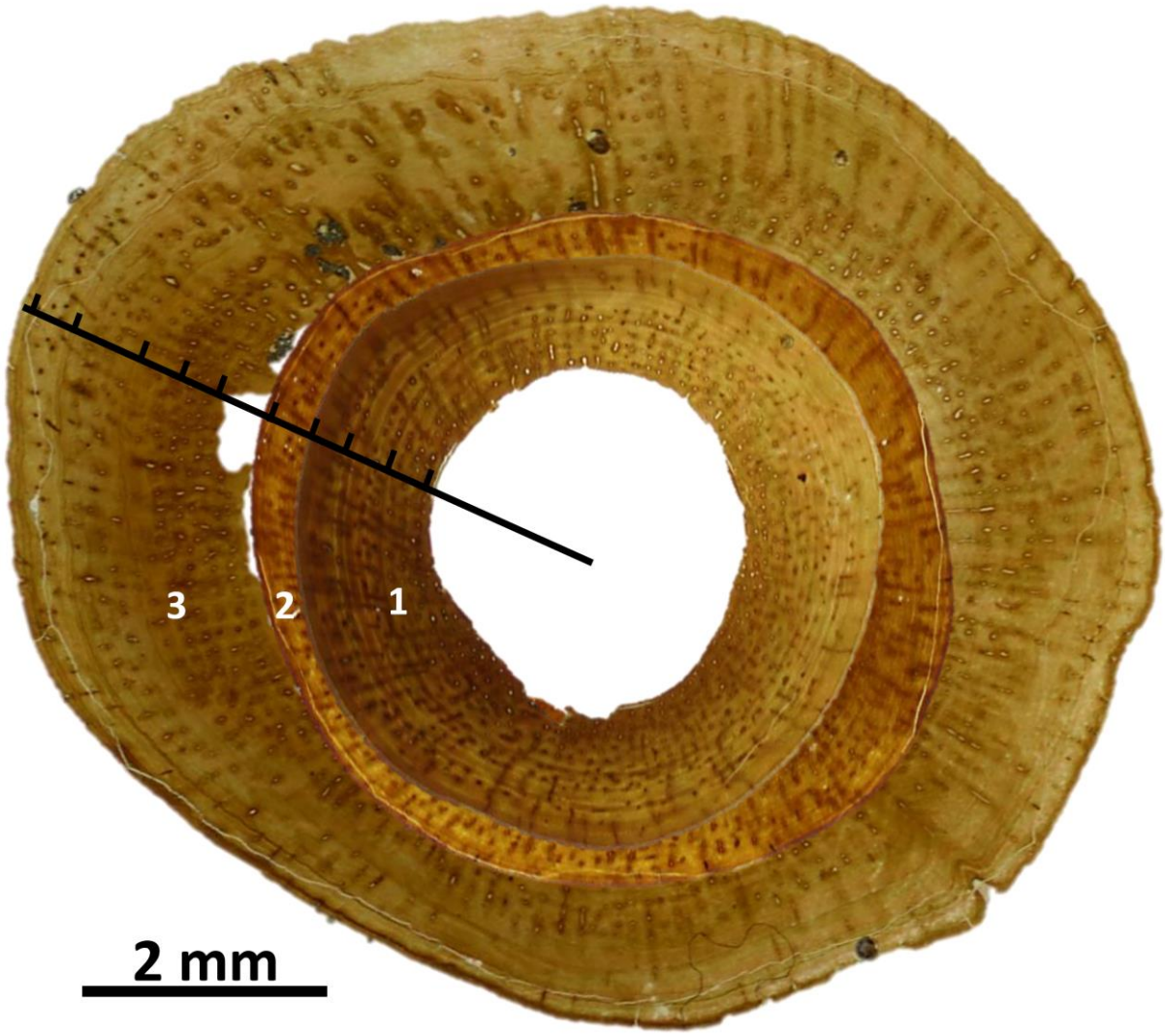

Figure 5. Bybee et al. (2006) method with scanned varanopid femur sections (Fig. 3). Total amount of time recorded in the cortex was 10 years with two to three maximal missing years. This would mean the largest femur sampled to be from an individual that is estimated to have died after reaching the 12th life cycle. Section 1) OMNH-73750C; section 2) OMNH-73750A; section 3) OMNH-73758.

3.3 Ophiacodontidae

3.3.1 Summarized bone histology:

Based on the results from chapter 4, *Ophiacodon* bone tissue was found to be mostly fast growing fibro-lamellar bone (FLB) tissue consisting of a woven and parallel-fibered bone matrix. The matrix contained large round OL, and LAGs were only present in the oldest more mature specimens. The cortex was extremely vascularized. All sampled humeri, as well as a

Carboniferous age femur and the prenatal cortex of an immature specimen (IPBS-46), consisted of radially arranged longitudinal and radial canals. The organization of the canals gave the cortical bone a “bicycle wheel” pattern. All other sampled femora, including the postnatal cortex of the previously mentioned immature specimen, consisted of longitudinal and reticular vascular canals. Primary osteons are prevalent in many samples and secondary osteons are less common as is Haversian bone. The humeri and femora differed mainly in their resorption strategies. In humeri, erosional cavities followed the radial organization of the vascular network and incorporate areas of the primary cortical bone into the medullary region as trabeculae bounded by lamellar bone. However, in the femora, the primary cortex was completely resorbed forming a more open MC.

This tissue pattern was largely ignored and assumed to reflect a juvenile condition or related to an aquatic/amphibious habitat, even though it was noted to be similar to the more derived therapsids (Enlow 1969; de Ricqlès 1974c). The results in Chapter 4 supported the original findings of Enlow and Brown (1957) in which they concluded that the highly vascularized periosteum reflected a high growth rate. These findings (Chapter 4) suggest the evolution of mammalian endothermy must be traced back to the Carboniferous, prior to the evolution of sailed-back pelycosaurs in the basal synapsid line.

3.3.2 Growth Dynamics:

Consumptive sampling of Brinkman’s ontogenetic *O. retroversus* humeral growth series (see Fig. 1 in Brinkman 1988) revealed that *Ophiacodon* grew fast throughout its life, so much so that LAGs are rare and only present well into advanced age. A growth curve was reconstructed by using the Bybee et al. (2006) method of superposition of sections by correlating the annuli as the animal was still growing at a rate too fast to produce proper growth marks. The estimated life span of *Ophiacodon* is 16 years; they grew faster than any of the other pelycosaur.

3.4 Edaphosauridae

Edaphosauridae Cope 1882, varied in body size, but had a small skull with a large inferior temporal fenestra. Edaphosaurs possessed a dorsal sail similar to that of sphenacodontids with greatly elongated neural spines, which are more round in cross-section with tubercles on the presacral neural spines. There are four currently recognized genera: the insectivorous *Ianthasaurus*, the small *Glaucosaurus*, the largest genus, *Lupeosaurus*, and the most common

with eight currently recognized species, *Edaphosaurus* from North America and Europe (Romer and Price 1940; Reisz 1986; Reisz and Berman 1986; Benson 2012). *Lupeosaurus* is monophyletic and differs from the others in size, lack of lateral tubercles on the neural spines, and lack of an ectepicondylar foramen, but most skeletal remains are fragmentary and incomplete. Also, Edaphosaurids were the first herbivorous pelycosaurs to appear, slightly preceding the caseids (Reisz and Fröbisch 2014).

3.4.1 Published bone histology:

Enlow (1969) and Enlow and Brown (1957) examined *Edaphosaurus* bone fragments. Except for ribs, which are more porous, the other elements consist of compact lamellar bone with low vascularity. De Ricqlès (1974b, 1976b) had similar findings. Huttenlocker et al. (2011) examined the histology of *Ianthasaurus*, *Lupeosaurus*, and *Edaphosaurus* neural spines. Results were the same for each species: an almost avascular lamellar matrix with a well-defined MC. Also, Huttenlocker et al. (2011) note that the lateral tubercles, which are lacking in *Lupeosaurus*, grow faster in *Edaphosaurus* than in *Ianthasaurus* and the central canal is lined by endosteal bone similar to modern amniote bone.

3.4.2 Descriptive bone histology:

Material sampled belongs to a humerus, femur and tibia of *Lupeosaurus kayi* discovered by A. S. Romer one mile east of the Geraldine bone beds (Nocona Formation, Lower Permian) in Archer County, Texas (Fig. 6). Also, humeri and femora of *Edaphosaurus boanerges* from Geraldine Bonebed (GBB) and an *Edaphosaurus* (sp) femur from Briar Creek Bonebed (BCBB) (Nocona Formation, Lower Permian) are described (Fig. 7).

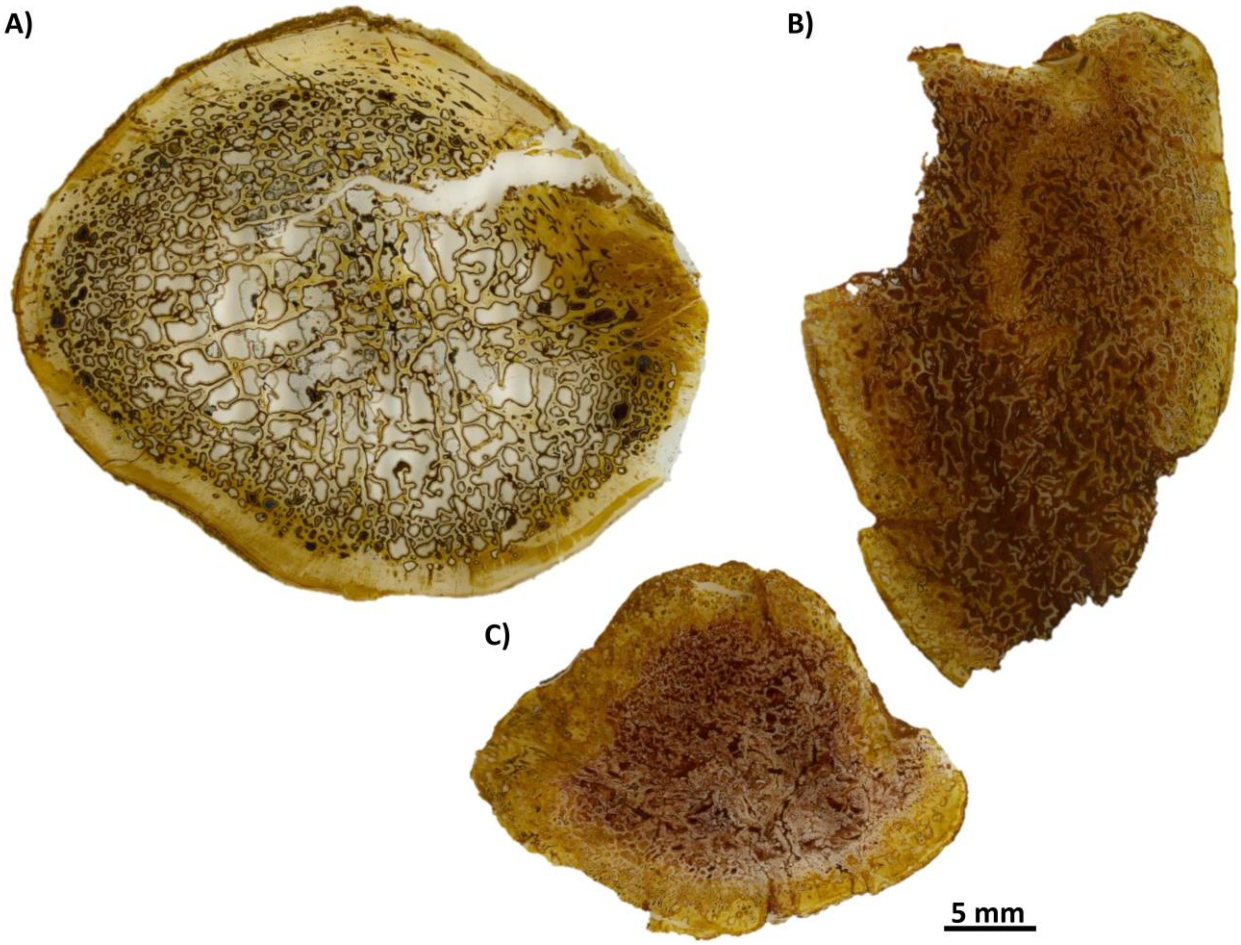

Figure 6. Scanned transverse sections of *Lupeosaurus kayi*. A) Humerus MCZ VPRA-1368; average cortical thickness (ACT) µm 1707. B) Femur MCZ VPRA-3412; ACT 797 µm. C) Tibia MCZ VPRA-3412; ACT 970 µm.

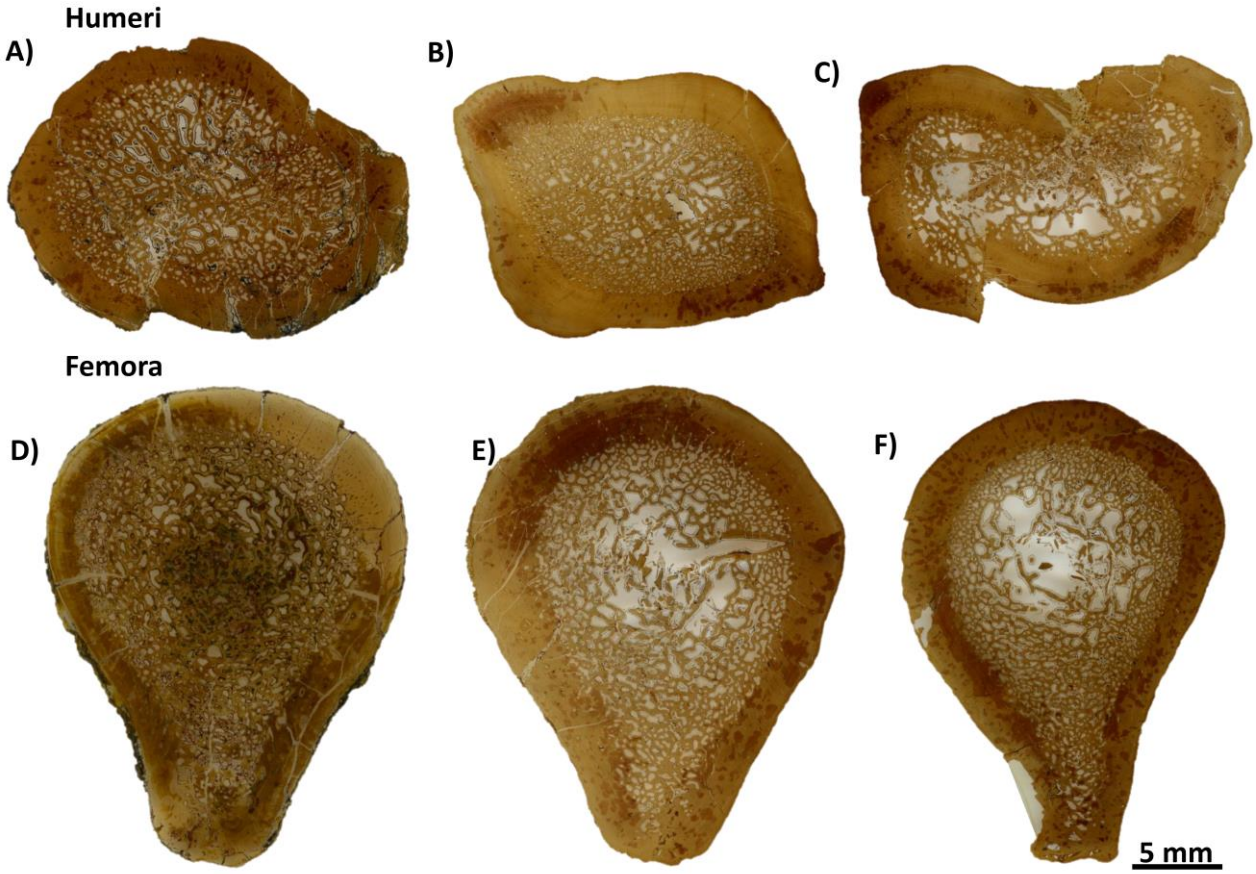

Figure 7. Scanned transvers sections of *Edaphosaurus* (sp). A) Humerus TMM-31255-2 *Edaphosaurus boanerges*; average cortical thickness (ACT) is 2160 µm. B) Humerus TMM 31255-70 *E. boanerges*, ACT is 2501 µm. C) Humerus TMM 31255-71 *E. boanerges*, ACT is 2732 µm. D) Femur IPBSH-84 *Edaphosaurus* (sp); ACT is 2154 µm. E) Femur TMM 31255-6.1 *E. boanerges*; ACT is 2590 µm. F) Femur TMM 31255-20 *E. boanerges*; ACT is 2162 µm.

3.4.2.1 Lupeosaurus kayi humerus

MCZ-VPRA-1368, *Lupeosaurus kayi*, is a right humerus, 212 mm in length, and 110 mm in circumference (Table 1; Fig. 6A). From the transverse section of the minimal diaphysis, the cortical tissue consists of thin lamellar bone (Fig. 8A, B). Vascularity consists of randomly oriented, large, longitudinal canals. Primary and very large secondary osteons are present (Fig. 8C, D). OL are dense. There is a growth record present in the cortex. Six LAGs are visible in conventional visible light; the earliest few are nearly resorbed. Additionally, an EFS is present in the outermost cortex, consisting of five LAGs (Fig. 8A). Sharpey's fibers are present. The

medullary region is very distinct and the MC is occluded with secondary trabeculae and patches of primary cortex.

3.4.2.2 Edaphosaurus boanerges humeri

Edaphosaurus boanerges humeri TMM-31255-71, 31255-70, 31255-2 will be described synthetically (Fig. 7A-C). The length of the humeri ranged from 120-174 mm, and the circumference ranged from 60 – 76 mm (Table 1). The cortex consists of PFB. Vascularity is reduced compared to other pelycosaurs; the canals are small and longitudinal, and most are fully developed primary osteons, which are concentrated at the boundary of the medullary region (Fig. 9A, B). Also, smaller less developed canals are present in the mid to outer cortex. The vascular arrangement is somewhat radial like the bicycle wheel pattern observed in the carnivorous pelycosaurs but to a lesser degree. OL are dense and round. Diagenetic staining has revealed the density and abundance of the canaliculi that, in life, connected the individual osteocytes (Fig. 9C, D). Four to six growth marks are present in the cortex. Sharpey's fibers are present. The medullary region is marked by a layer of vascular canals in the inner cortex. The MC is occluded with secondary trabeculae and isolated patches of primary cortex like that observed in *Ophiacodon*.

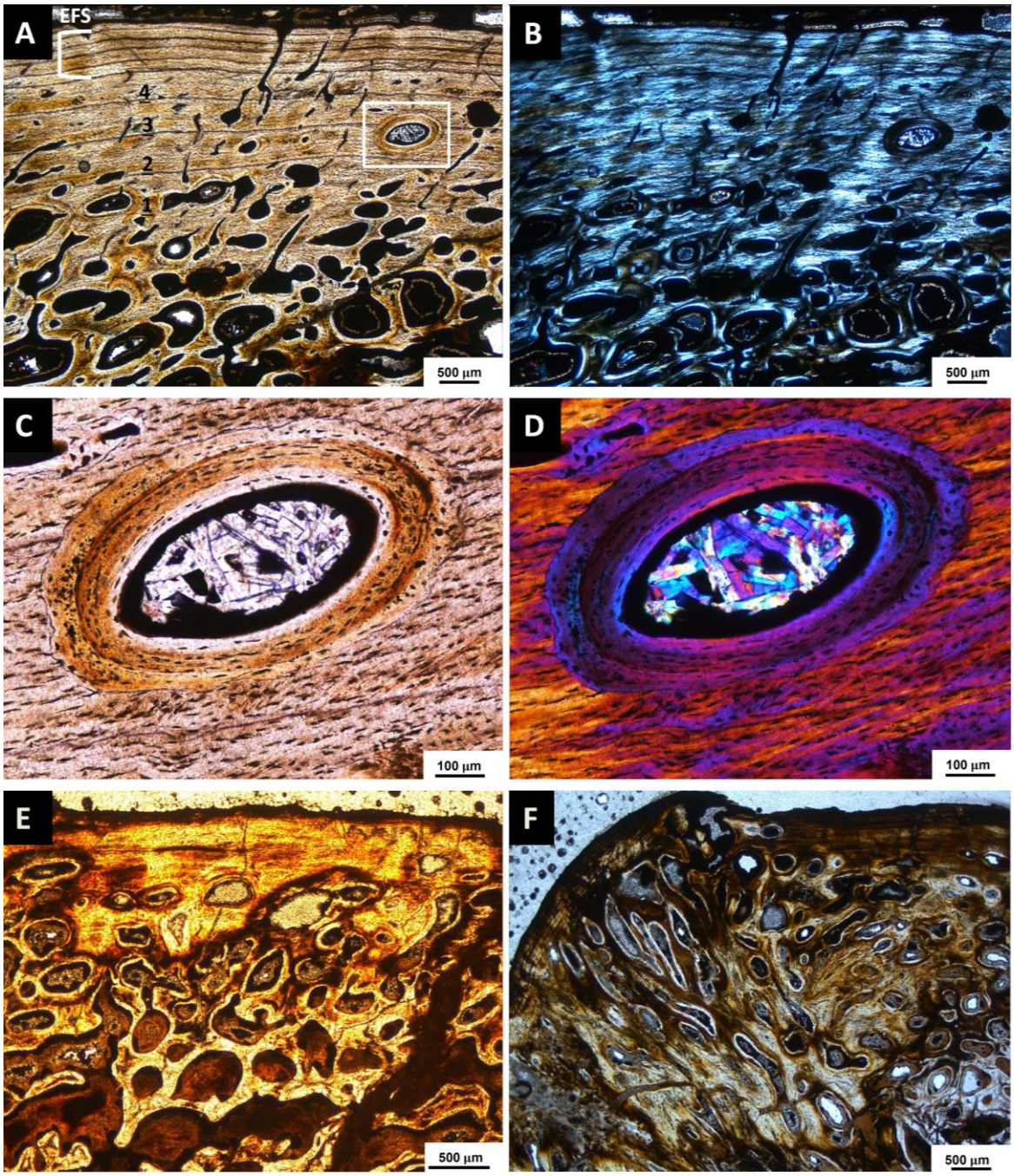

Figure 8. Micrograph images of *Lupeosaurus kayi* postcrania. A) Humerus MCZ VPRA-1368 imaged in conventional transmitted light (CTL). Note the four LAGs, the earliest of which is being resorbed. An EFS is present in the outer most cortex representing at least five years of slowed growth. B) Same area as in (A) imaged in polarized transmitted light. The periosteum is lamellar bone. C) magnified view of the boxed area in (A) imaged in CTL. This is a very large secondary osteon crosscutting one of the LAGs. Note the multiple layers of centripetal lamellar bone deposition. D) Same area as in (C) imaged in polarized transmitted light with a lambda

filter. E) Micrograph images of femur MCZ VPRA imaged in CTL. Resorption has nearly reached the cortical surface giving this bone an osteopenia condition. LAGs are present but poorly preserved in this section. F) Micrograph image of tibia MCZ VPRA- imaged in CTL. Note the EFS in the outer cortex. Abbreviations: EFS= external fundamental system

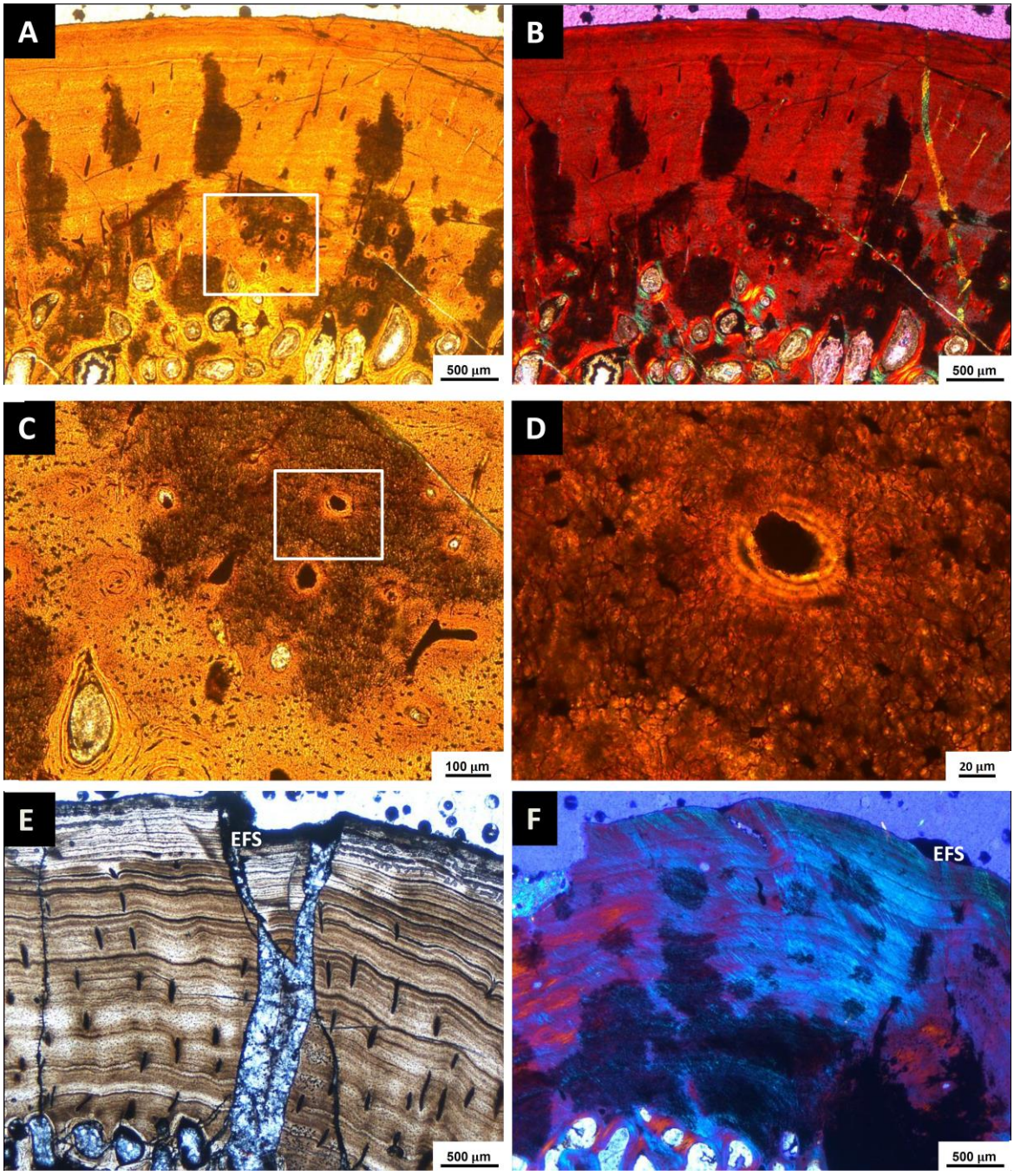

Figure 9. Micrograph images of *Edaphosaurus* (sp) humeri and femora. A) Humerus TMM 31255-2 imaged in conventional transmitted light (CTL). The darkened stained areas of the cortex are preserved canaliculi. Note the reduction of vascularity in the cortex. Growth marks are

present but poorly preserved. B) Same area as in (A) imaged in polarized light with a lambda filter. Vascular pattern and growth marks in the outer cortex are better visible. Note the small primary osteons separating the medullary regions from the outer cortex. C) Magnified image of the boxed area in (A) in CTL. Note the details of the canaliculi surrounding the primary osteons. D) Magnified image of boxed area in (C) imaged in CTL. E) Femur IPBSH-84 imaged in CTL. Growth marks are better preserved in the Briar Creek specimen when compared to those from the Geraldine Bone bed. Nine LAGs are visible in the cortex followed by an EFS in the outer most layer. F) Femur adductor crest region imaged in polarized light with a lambda filter. Growth marks are concentrated in this area indicating less deposition of the periosteum than in any other region of the diaphysis. Sharpey's fibers are present. Abbreviations: EFS= external fundamental system.

3.4.2.3 Lupeosarus kayi Femur

MCZ-VPRA-3412A *Lupeosaurus kayi* is a femur 140 mm in length and 81 mm in circumference (Table 1; Fig. 6B). Weathering has degraded preservation of the tissue. This specimen is from the same location as the tibia MCZ-VPRA-3412B. From the transverse section of the minimal diaphysis the cortical tissue is thin LB to slightly PFB. Vascularity consists of randomly oriented large longitudinal canals. Primary osteons and very large secondary osteons are present. OL are dense and oval to flat in shape. There is a growth record present in the cortex. Seven LAGs are visible in conventional visible light; resorption has begun to erode the earliest LAGs closest to the medullary region (Fig. 8E). Sharpey's fibers are present. The medullary region is very distinct and the MC is occluded with secondary trabeculae and patches of primary cortex. The resorption/remodeling front has nearly reached the cortical surface in some areas (Fig. 8E).

3.4.2.4 Edaphosaurid femora

Edaphosaurid femora will be described together: IPBSH-84 *Edaphosaurus* (sp) and *Edaphosaurus boanerges* 31255-20, 31255-6.1 (Fig. 7D-F). The femora range from 118 to 180 mm in length and 72 – 87 mm in circumference (Table 1). From the transverse section of the minimal diaphysis, the cortical tissue is thin LB. Vascular canals are small and longitudinal or thin and radial, similar to the humeri, but the radial pattern is not as prominent (Fig. 9A, E).

Small primary osteons are present. OL are dense and oval to flat. The best record of growth is preserved in the femora (Table 1). LAGs are visible in conventional visible light, and an EFS is present in the two larger specimens (Fig. 9E). Sharpey's fibers are present (Fig. 9F). The medullary region is very distinct, and the MC is occluded with secondary trabeculae and patches of primary cortex.

3.4.2.5 Lupeosaurus kayi Tibia

MCZ-VPRA-3412B, *Lupeosaurus kayi,* is a right tibia 140 mm in length and 81 mm in circumference (Fig. 6C). Weathering has degraded the preservation of the tissue. From the transverse section of the minimal diaphysis the cortical tissue is thin LB. Vascular canals are randomly oriented, large longitudinal canals. Primary osteons and very large secondary osteons are present. OL are dense and oval. Five LAGs are visible in conventional visible light, but the ones closest to the inner cortex are beginning to be resorbed (Fig. 8F). Sharpey's fibers are present. The medullary region is very distinct, and the MC is occluded with secondary trabeculae and patches of primary cortex. The resorption/remodeling front has nearly reached the cortical surface in some areas.

3.4.3 Age estimation

The material available for consumptive sampling did not include an ontogenetic series, so a growth curve could not be reconstructed. However, the age of specimens with the best growth records were calculated using the retrocalculation method (for method see Chapter 3; Shelton et al. 2013). The *Edaphosaurus* (sp) femur, IPBSH-84, found at the BCBB was estimated to have died during the 42nd growth cycle (maximum 23 missing years) at time of death. The *E. boanerges* femur, TMM-31255-6.1, from the GBB was conservatively estimated to have died during the 30th growth cycle (maximum 13 missing years). LAGs in femur ISPBH-84 are more defined and are more closely spaced together than those of TMM-31255-6.1. However, a very diagnostic external fundamental system was present in both of these specimens (Table 1).

3.5 Sphenacodontidae

3.5.1 Summarized bone histology:

Based on the findings in Chapter 3 (Shelton et al. 2013) as well as the current work by Knaus et al. (2014), sampled ontogenies of small and large *Dimetrodon* species have revealed a consistent histologic pattern. The tissue was christened incipient fibro-lamellar bone (IFLB) and is present in the postcranial skeleton of all *Dimetrodon* species sampled during this study, and remains so throughout ontogeny. We chose to use the more descriptive term IFLB because of the combination of incipient primary osteons and an interstitial matrix of highly vascularized woven and parallel-fibered bone. There was an absence of secondary tissue in the cortical bone of *Dimetrodon* (sp) and only a minor occurrence of fully formed primary osteons in some of the larger species later in ontogeny. Histology of the larger species (*D. limbatus* and *D. giganhomogenes*) was described from material initially acquired for this study (Chapter 2; Knaus et al. 2014), and is identical to the IFLB described in the smaller *D. natalis* (Chapter 3; Shelton et al. 2013).

3.5.2 Growth Dynamics:

Material described in Chapter 3 was excavated from the Briar Creek Bonebed (Lower Permian, Artinskian), which yielded an ontogenetic series of *D. natalis* humeri and femora (Chapter 2); the latter of which preserved the better growth record. It should be noted that an EFS was described for the largest humerus and the two largest femora specimens of *D. natalis,* and this is the first published account of an EFS occurring in a pelycosaur (Shelton et al. 2013). The EFS confirmed that *D. natalis* was a valid species and it proved pelycosaurs have a determinate growth pattern.

Two retrocalculation methods were developed to estimate age of the individual femora depending on the deformation of the midshaft (see Chapter 3 for details). These results were put into a growth trajectory, and the estimated maximum age reached was at least 17 years. The amount of time represented by the EFS is indeterminate.

3.6 Inter- and intraspecific pelycosaur bone histological variation

Pelycosauria has a varied bone histology. Overall, the histological differences follow a general pattern; herbivorous and omnivorous pelycosaurs (caseids and edaphosaurids) are less

vascularized, with LB and PFB matrix , and therefore utilized a slower growth strategy than the carnivorous groups (sphenacodontids, ophiacodontids, varanopids) which show a highly vascularized WB and PFB matrix (Fig. 10). The histology of juvenile specimens is similar in all groups with highly vascularized woven bone and longitudinal vascular canals. The variations that occur within families tend to be based on the difference in species size, specifically those that are herbivorous. Histological profiles of carnivorous species tend to remain the same regardless of species size. In Caseidae, the periosteum consists of avascular slow growing lamellar bone, and the larger species display an osteoporotic-like condition. In Varanopidae the cortex is highly vascularized fast growing parallel-fibered bone with small longitudinal primary osteons in a radial pattern. In Ophiacodontidae, the cortical tissue is extremely vascularized, fast growing WB and PFB matrix with longitudinal primary osteons, which is essentially fibro-lamellar bone. The edaphosaurids are moderately vascularized, slow growing PFB and LB with small longitudinal primary osteons; the larger species *Lupeosaurus kayi* has mainly lamellar bone and demonstrates more of an osteopenia condition probably due to age. In Sphenacodontidae, bone tissue is highly vascularized, fast growing WB and PFB matrix with incipient longitudinal primary osteons canals in a radial pattern, IFLB. This group had a lower growth rate than Ophiacodontidae, which appears to be the fastest growing pelycosaur group. All carnivorous pelycosaur taxa have a dense vascularized cortex. In general, herbivores grow much slower.

The pelycosaurs had a diversified diet by the Late Permian: piscivorous ophiacodontids, carnivorous sphenacodontids, Insectivorous varanopids, possibly omnivorous edaphosaurids, and undoubtedly herbivorous caseids (Hotton et al. 1997).The general difference in growth mark record between the herbivores, which show more closely spaced regular lines, and the carnivores, which have irregular widely spaced or even double LAGs(Werner and Griebeler 2014; Grady et al. 2014), I hypothesize to be a reflection of diet and the means in which they procure it. Herbivores could eat constantly not needing to actively hunt down or search for food; carnivores, on the other hand, would need to hunt or scavenge, the implications of which will be further discussed later.

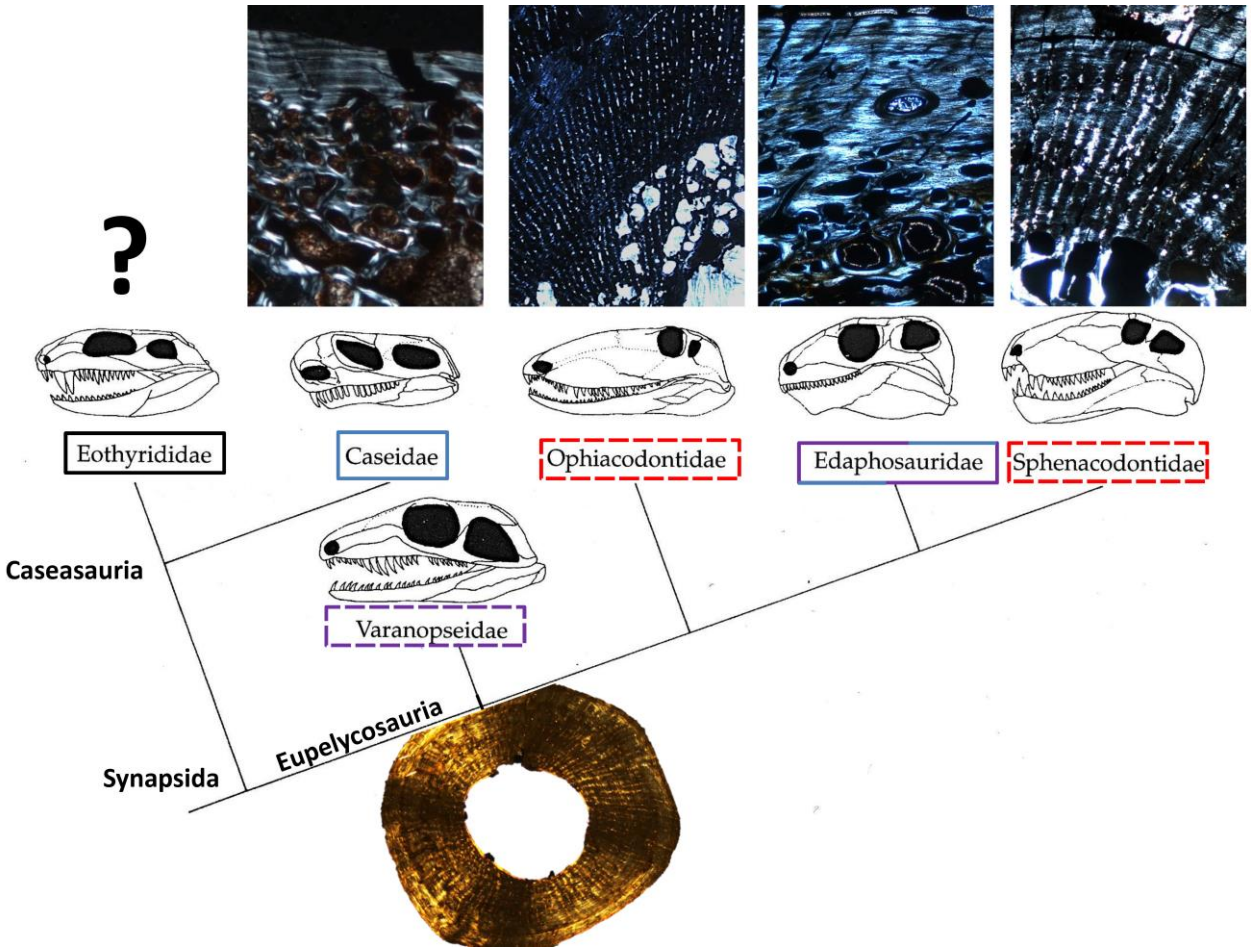

4. Implications

4.1 Origins of high growth rates and fibro-lamellar bone in the mammalian lineage

As mentioned above, bone histology of the pelycosaurs can be divided based on their trophic level and how they acquired food. In general, carnivorous groups (Varanopidae, Ophiacodontidae, and Sphenacodontidae) were growing at a magnitude faster than those of the more herbivorous groups (Caseidae and Edaphosauridae), but had a much shorter life span (Werner and Griebeler 2014; Grady et al. 2014). All postcranial tissue of the carnivores is composed of a mixture of WB and PFB matrix, forming either IFLB tissue, described, for example, in *Dimetrodon* (sp), and more developed FLB tissue, described, for example, in *Ophiacodon* (sp), which is similar to the FLB observed in Therapsida and Mammalia (Fig. 10). The bone tissue is highly vascularized, often by radially arranged pattern of longitudinal and radial canals with varying degrees of osteonal development (incipient, primary, and more rarely, secondary). By proxy, this highly vascularized bone tissue indicates the animal had a high

metabolic rate. This implies that Ophiacodontidae had achieved a form of endothermy, which can be traced back to their origins in the Carboniferous.

4.1.1 The Carboniferous period

The earliest representative of the pelycosaurs originated during the Upper Carboniferous (chapter 1). The earliest undisputed taxon *Archeothyris florensis*, one of the largest amniotes of its time (estimated length 50 cm), belongs to Ophiacodontidae (Benson 2012). Ophiacodontids are the fastest growing pelycosaur group and histologically the most mammal-like (see above; Chapter 4). Later discoveries from Pennsylvanian aged localities in Kansas revealed the simultaneous appearance of the ancestral pelycosaurs, represented by small insectivorous forms (Romer and Price 1940; Reisz 1986; Reisz and Berman 1986; Reisz and Sues 2000; Reisz and Fröbisch 2014).

The most notable and possibly the most significant event affecting the evolution of endothermy in tetrapods is the dramatic fluctuations of atmospheric oxygen levels beginning with the initial spike during the Carboniferous to the steep decline over the next 20-40MY. The Carboniferous period flourished because of a sudden 35% increase in the atmospheric oxygen content, which accounts for the dramatic evolutionary changes that took place diversifying the Paleozoic biota. This is evident by the appearance of large, flying insects, diverse plant species, a size increase in temnospondyls, and the tetrapod exploitation of land (Bakker 1975; Graham et al. 1997, Dudley 1998; Hsia et al. 2013).

4.1.2 Endothermy hypothesis

The hyperoxic atmospheric conditions of the Carboniferous allowed for an increase in mitochondria and ATP production raising metabolic rates and aerobic activities with adaptations for terrestrial niches such as an increase in skeletal muscle production by which the majority of the oxygen is used here by the body (West et al. 2002; Hsia et al. 2013). This increase in oxygen drove the evolution of endothermy in the basal synapsids allowing them to exploit the land (Bakker 1975; Hsia et al. 2013). It is well documented that physiology, metabolism, and aerobic performance improves with oxygen consumption (Hsia et al. 2013). Ophiacodontids were capable of regulating their body temperature through active muscle movement. This is reflected by the

most defined, well developed muscle attachment sites in the midshaft of the femora and humerus of *Ophiacodon* (Chapter 4; Romer and Price 1940; Reisz 1986).

These findings reinforce the aerobic scope hypothesis first proposed by Bennett and Ruben (1979, 1986) and later modified by Kemp (2006) in the correlated progression model (Fig. 11). Combined, these hypotheses explain how endothermy evolved, as a result of increased aerobic activity and mitochondrial development affecting all the organ systems of the body, independently of thermoreguation, proceeding homeothermy (Bennett and Ruben 1979, 1986; Bennett et al. 2000; Grigg et al. 2004; Kemp 2006, Hsia et al. 2013). Therefore, a rise in atmospheric oxygen allowed for a wider aerobic scope, increased physical activity, and allowed for an increased metabolism which was sustained by active predation on fish, smaller vertebrates or insects (Fig. 11). For the most up-to-date reviews on endothermy and effects of oxygen levels throughout time see Nespolo et al. (2011) and Hasia et al. (2013).

Further evidence of increased aerobic activity was reported by Hunt and Lucas (1998) who published pelycosaur tracks of the ichnogenus *Dimetropus*, from New Mexico noting that they are narrow and are not associated with either belly or tail drag marks that are often associated with reptile tracks. In fact, tail drag marks have never been found in association with *Dimetropus* or any known pelycosaur tracks; a key piece of evidence used to defend the theory of warm-blooded dinosaurs (Bakker 1972; Benton 1979; Fichter and Kowalczyk 1983; Gand 1986, 1989; Padian and Horner 2004).

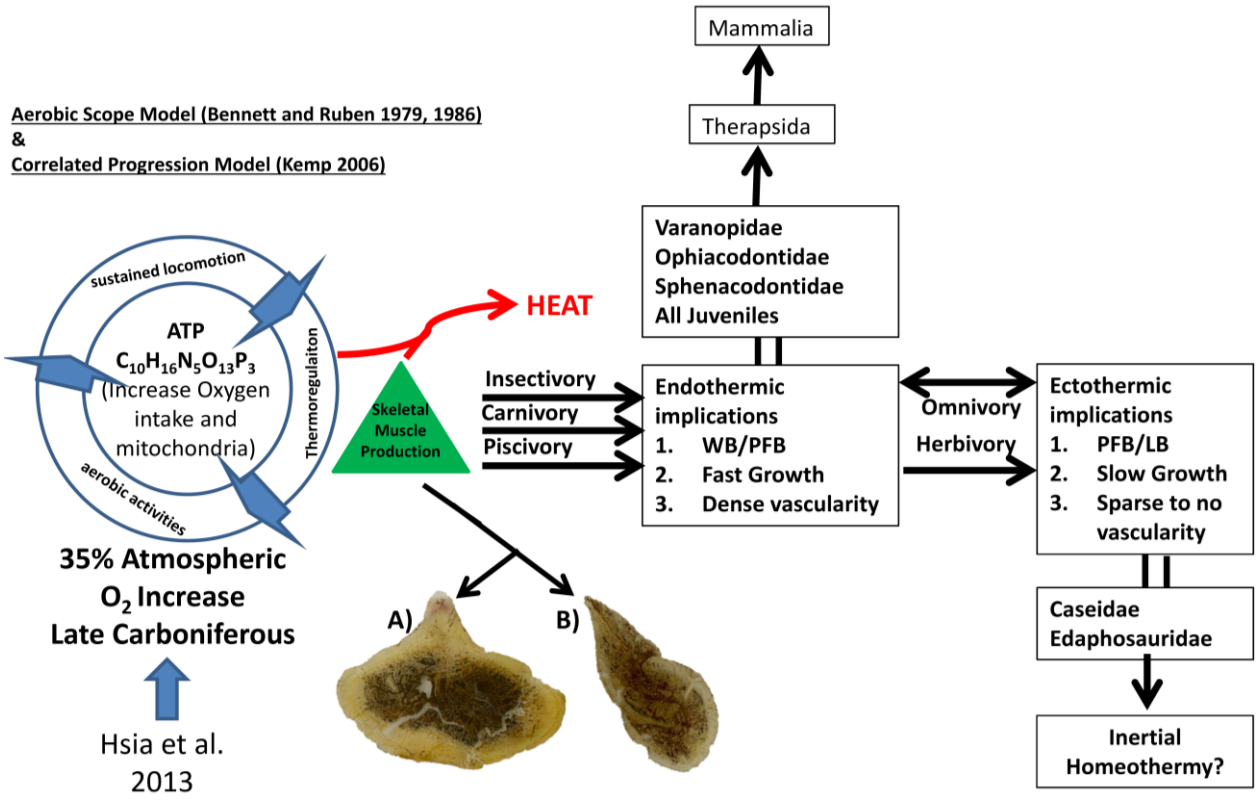

Figure 11. A Model explaining the origins of endothermy in the mammalian line and how this effected basal synapsid evolution which is tied to their feeding ecology and the atmospheric oxygen content. The hyperoxic atmospheric conditions of the Carboniferous allowed for an increase in mitochondria and ATP production simultaneously affecting all organ systems of the body and increased metabolic rates, aerobic activities, and thermoregulation. Hyperoxia allowed for increased skeletal muscle production and opened up knew terrestrial niches. It is well documented that physiology, metabolism, and aerobic performance improves with oxygen consumption (Hsia et al. 2013). Note that ophiacodontids were capable of regulating their body temperature through active muscle movement. This is reflected by the most defined, well developed muscle attachment sites in the midshaft in their femora and humerus. Note the A) arrows pointing to the triceps muscle insertion of the *Ophiacodon* A) humerus and the adductor crest of the *Ophiacodon* B) femur (histological sections were taken at the minimal diaphysis; Chapter 4). Throughout the Permian, oxygen levels steeply decreased and caused a body size increase of herbivorous taxa proceeding the evolutionary shift from insectivory to herbivory. This reinforces the aerobic scope hypothesis first proposed by Bennett and Ruben (1979, 1986) and later modified by Kemp (2006) in the correlated progression model.

4.1.3 Effects of atmospheric oxygen decrease in the Permian

After oxygen levels peaked at the end of the Carboniferous, they sharply decreased throughout the Permian. Ophiacodontids and edaphosaurids become extinct simultaneously during the Early to Middle Permian. However, this drop in oxygen content also coincided with a general body mass increase in pelycosaurs (typical as seen in Cope's rules). The low oxygen conditions forced adaptions to maintain the oxygen levels required by the brain and other tissues established earlier to function, thus increasing thermoregulation and homeothermy by adapting a much broader aerobic scope, driving the need for more activity and more oxygen consumption (Crompton et al. 1978). This is evident in the change of a parasagittal gait and adaption of nasal turbinates in amniotes (Clarke and Pörtner 2010). Homeothermy was maintained and adapted for use over a broad range of environments as is evident today by the evolutionary diversity of mammals and birds. However, Between approximately 240 and 200 M. Y. atmospheric oxygen concentration dropped between 10% and 13% coinciding with the largest extinction event to occur on the planet (93% marine life, 70% terrestrial life, 83% insect species) and the only one to affect insects (Labandeira and Sepkoski 1993; Sahney and Benton 2008; Hsia et al. 2013).

4.1.4 Further testing

A possible modern day analog for comparing the aerobic scope of *Ophiacodon* is the varanid lizard *Varanus komodensis* (Bakker 1975). They can elevate their body temperature and sustain heat throughout the night in a burrow or thick brush. The bone tissue vascularity of large varanids and *Ophiacodon* were compared in Chapter 4 and found to be similar, both having a highly vascularized periosteum with a radially arranged longitudinal canals.

Furthermore, consumptive sampling of both the earliest synapsid fossils and other contemporaneous insectivorous pelycosaur taxa from the Carboniferous deposits of Kansas and the fossil beds of Florence, Nova Scotia is required to further test these results.

4.2 Cellulose Herbivory in basal synapsids is not linked to high growth rates

One benefit of herbivory is that it allows animals to consume large amounts of food with minimal locomotion, thereby presenting a very effective and energy-efficient solution to daily physiological demands. Also, herbivores can obtain larger body sizes than carnivores because no energy is lost to trophic level effects. It has been hypothesized (M. Sander Pers. Comm. 2013)

that an elevated basal metabolic rate (BMR) together with an increase in body temperature in basal Synapsida would have furthered the evolution of herbivory and large body size because a high BMR would have allowed fast growth as well as improved fermentation efficiency (to our knowledge this hypothesis has not yet appeared in print). The evolution of increased BMR and thermoregulation is again best understood through the study of bone microstructure. Here, the hypothesis that endothermy furthered the evolution of cellulose herbivory in pelycosaur-grade basal synapsids is rejected because histological analysis of the long bones of Edaphosauridae and Caseidae reveals mostly slow-growing lamellar or parallel-fibered bone. Vascularity is highly reduced or absent. This suggests that the pelycosaur-grade herbivores grew a magnitude slower than the contemporaneous carnivores, despite attaining considerably larger body size (Bakker 1975; Werner and Griebeler 2014; Grady et al. 2014). They secondarily reduced their growth rate. However, the sizes they could reach imply the possibility of inertial homeothermy as seen in large modern lizards (Pough 1973; McNab 1978; Zimmerman and Tracey 1989; Hawkins 1995; Legard et al. 2003).

Further testing of ontogenetic series of *Ianthasaurus* as well as juvenile material of herbivorous pelycosaurs, which is extremely rare, is required. Also, consumptive sampling of *Eocasea martini* would be beneficial in understanding the transition from insectivory to herbivory in Pough's (1973) model, ingesting herbivorous insects to acquire the necessary symbiotic microbes for cellulose digestion or by coprophagy of herbivore feces (Bakker 1975; Troyer 1982; Hotton et al. 1997; Sues and Reisz 1998).

A final caveat; without the consumptive sampling of Eothyrididae the complete histological spectrum of the pelycosaurs and the evolution of amniote ecology will never be fully resolved.

4.2 What was the dorsal sail good for?

The dorsal sail, formed by hyper-elongated neural spines, arose independently in two clades, Edaphosauridae (omnivorous) and Sphenacodontidae (carnivorous). Sail allometry (compared to body size), although positive in *Dimetrodon* (sp), is negative in Edaphosauridae (Romer and Price 1940). The exact function of the iconic dorsal sail is still highly debated and must be addressed when discussing pelycosaur physiology. Over the past few decades, a growing amount of morphological and histological evidence has been put forward to suggest that the dorsal sail did not serve as a thermoregulatory organ (Baker 1971; Bailey 1997; Huttenlocker et

al 2010, 2011, Tomkins et al. 2010; Huttenlocker and Rega 2012). It has been pointed out that the earliest sailed back pelycosaurs were small and the size would have been inefficient for heating or cooling (Bailey 1997; Tomkins et al. 2010). The small insectivorous edaphosaurid species *Ianthasaurus* was the first to possess such a hyper-elongated dorsal sail (Reisz 1986) .If cooling was required then all the animal had to do was stand in water as this would provide a much more effective means of cooling than air (Ruxton 2001). Even though they are generally thought of as strictly terrestrial, Olson (1986) noted that pelycosaurs lived around water to obtain food be it either animal or plant. They probably still relied on water for protection, and heat radiation.

The results of the current study add further histological evidence to the dorsal sail was not a thermoregulatory organ. By comparing the results in Chapter 3 of *Dimetrodon natalis* histology, including the larger *Dimetrodon* species examined by Knaus et al. (2014), with those of the sampled edaphosaurids summarized above, postcranial histology differs despite the presence of a dorsal sail. This is clear evidence that the dorsal sail had no effect on growth patterns, remember these are affected by diet and food acquirement (see above). Perhaps the dorsal sail was just for display purposes or sexual selection as previously suggested by other studies (Bakker 1971; Angielczyk and Schmiz 2014).

5. Conclusion

The origin of mammalian endothermy has its start as far back as the Carboniferous due to a record content in atmospheric oxygen that allowed for a wider aerobic scope, increased physical activity that allowed for higher growth rates, and increased metabolism sustained by active predation on either fish, smaller vertebrates or giant insects (Fig. 11). The hyperoxic conditions allowed for an increase in ATP and energy production raising metabolic rates and aerobic activity. Over the next 20 to 40 M.Y. oxygen levels steeply declined causing hypoxia forcing an adaption to maintain the oxygen levels required by the brain and other tissues established earlier to function. These findings are in contrast to the long held view that mammalian endothermy had its start in the upper Permian amid the therapsids.

I have shown that, especially in the *Ophiacodon*, this highly vascular fibro-lamellar bone is similar to the fast growing tissue later recognized in some therapsids (de Ricqlès 1974c). During the Lower Permian, synapsid trophic levels shifted allowing for cellulose herbivory to evolve, possibly as a direct result of insectivory. This was accompanied by an extreme increase in

body size but secondarily reduced growth rates. Also, these findings lend more evidence to the school of thought that the dorsal sail of eadaphosaurids and sphenacodontids was not used for thermoregulation.

The bone tissue of the pelycosaur is closely tied to ontogeny, but mostly, it is associated with their diet and how it was acquired. These findings should signify the importance of, and the necessity for, consumptive sampling not just for topologic, but also phylogenetic purposes. I have demonstrated here the importance of paleohistology as an indispensable field of research, and the continued allowance of consumptive sampling of not only multiple species by ontogeny, as well as individual type specimens, is necessary for the growth of vertebrate paleontological research and fully understanding the development of individual clades.

6 Acknowledgements:

I would like to recognize everyone that helped bring this final chapter to a close especially Martin Sander for his insights and discussion and for letting me bend the deadlines a little. For help with thin-sectioning, I whole heartedly thank Olaf Dülfer and Rebecca Hoffman. I want to also thank Philipp Knaus who has continued studying the sphenacodontid thin sections I was not permitted to fully include in this write up due to time and amount of material readily available in the Texas Redbeds. Also, Jessica Mitchell for editing an early draft of the manuscript. Rich Cifelli, Jennifer and Kyle Davies for loan of the varanopid material and permission for consumptive sampling. Jack Loftin of Archer City, TX for excavating the Briar Creek *Edaphosaurus* femur. From the Texas Memorial Museum Vertebrate Paleontology Laboratory, Austin, TX, I especially would like to recognize and thank Wann Langston Jr. and Ernst Lundelius for giving their permission to consumptively sample the Geraldine material. I would also like to also thank Thomas Martens of Die Gotha Museum Natur for giving permission to sample the undescribed Bromacker Caseid taxa and Dave Berman of the Carnegie Institute for sending the specimen. Finally I would like to recognize my coconspirators whom helped to conceive the possibility of an aquatic caseid; Steve Perry and Markus Lambertz of the University of Bonn and Frederik Spindler of Freiberg University. This research made possible by the DFG (SA 469/34-1).

7 References

Angielczyk, K. D., Schmitz, L. (2014) Nocturnality in synapsids predates the origin of mammals by over 100 million years. Proceedings of the Royal Society B: Biological Sciences 281: 20141642.

Bakker, R. T. (1971) Dinosaur physiology and the origin of mammals. Evolution 25: 636-658.

Bakker, R. T. (1972) Anatomical and ecological evidence of endothermy in dinosaurs. Nature 238: 81-85.

Bakker, R. T. (1975) Chapter 21: Experimental and fossil evidence for the evolution of tetrapod bioenergetics. In Gates, D. M., Schmrel, R. B. (eds.) Perspectives of Biophysical Ecology: Ecological Studies 12. Springer, Berlin, 365-399 pp.

Bennett, A. F., Ruben, J. A. (1979) Endothermy and activity in vertebrates. Science 206: 649-654.

Bennett, A. F., Ruben, J. A. (1986) The metabolic and thermoregulatory status of therapsids. In Hotton, N., MacLean, P. D., Roth, J. J., Roth, E. C. (eds.) The Ecology and Biology of Mammal-like Reptiles. Smithsonian Institution, Washington D. C., 207-218 pp.

Bennett, A. F., Hicks, J. W., Cullum, A. J. (2000) An experimental test of the thermoregulatory hypothesis for the evolution of endothermy. Evolution 54: 1768-1773.

Benson, R. (2012) Interrelationships of basal synapsids: cranial and postcranial morphological partitions suggest different topologies. Journal of Systematic Palaeontology 10: 601-624.

Benton, M. (1979) Discussion of evidence for dinosaur endothermy. Evolution: 983-997.

Berman, D. S., Henrici, A. C., Sumida, S. S. (1998) Taxonomic status of the Early Permian *Helodectes paridens* Cope (Diadectidae) with discussion of occlusion of diadectid marginal dentitions. Annals of the Carnegie Museum of Natural History 67: 181-196.

Botha-Brink, J., Modesto, S. P. (2007) A mixed-age classed 'pelycosaur'aggregation from South Africa: earliest evidence of parental care in amniotes? Proceedings of the Royal Society B: Biological Sciences 274: 2829-2834.

Brinkman, D. (1988) Size-independent criteria for estimating relative age in *Ophiacodon* and *Dimetrodon* (Reptilia, Pelycosauria) from the Admiral and Lower Belle Plains formations of West-central Texas. Journal of Vertebrate Paleontology 8: 172-180.

Bybee, P. J., Lee, A. H., Lamm, E. T. (2006) Sizing the Jurassic theropod dinosaur *Allosaurus*: Assessing growth strategy and evolution of ontogenetic scaling of limbs. Journal of Morphology 267: 347-359.

Clarke, A., Pörtner, H. O. (2010) Temperature, metabolic power and the evolution of endothermy. Biological Reviews 85: 703-727.

Cope, E. D. (1882) Third contribution to the history of the vertebrata of the Permian Formation of Texas. Proclamation of the American Philosophical Society 20: 447-461.

Cope, E. D. (1878) Description of extinct Batrachia and Reptiles from the Permian formation of Texas. Proceedings of the American Philosophical Society, Philadelphia 17: 505-530.

Crompton, A. W., Taylor, C. R., Jagger, J. A. (1978) Evolution of homeothermy in mammals. Nature 272: 333-336.

Dudley, R. (1998) Atmospheric oxygen, giant Paleozoic insects and the evolution of aerial locomotor performance. Journal of Experimental Biology 201: 1043-1050.

Enlow, D. H., Brown, S. O. (1957) A comparative histological study of fossil and recent bone tissues. Part II. The Texas Journal of Science 9: 186-214.

Enlow, D. H. (1969) The bone of reptiles. In C. Gans, ed. Biology of the Reptiles. Academic Press, London, 45-80 pp.

Fichter, J., Kowalczyk, G. (1983) Tetrapodenfährten aus dem Rotleigenden der Wetterau und ihre stratigraphishe Auswertung. Mainzer Geowissenschaftlishe Mitteilungen 12: 123-158.

Gand, G. (1986) Interprétations paléontologique et paléoécologique de quatre niveauxà traces de vertébrés observes dans l'Autunien du Lodévois (Hérault). Bulletin de la Société Géologique de France 2: 155-176.

Gand, G. (1989) Essai de reconstitution paléoenvironnementale et paléoécologique d'un partie du nord du bassin de Lodève (Hérault) au Permien inférieur. Bulletin de la Société Géologique de France 4**:** 17-30.

Germain, D., Laurin, M. (2005) Microanatomy of the radius and lifestyle in amniotes (Vertebrata, Tetrapoda). Zoologica Scripta 34: 335-350.

Grady, J. M., Enquist, B. J., Dettweiler-Robinson, E., Wright, N. A., Smith, F. A. (2014) Evidence for mesothermy in dinosaurs. Science 344: 1268-1272.

Graham, J. B., Aguilar, N., Dudely, R., Gans, C. (1997) The Late Paleozoic atmosphere and the ecological and evolutionary physiology of tetrapods. In: Sumida, S., Martin, K. L. M. (Eds.) Amniote origins: completing the transition to land. Academic Press, New York, pp. 141-168.

Grigg, G. C., Beard, L. A., Augee, M. L. (2004) The evolution of endothermy and its diversity in mammals and birds. Physiological and Biochemical Zoology 77: 982-997.

Hawkins, A. J. (1995) Effects of temperature change on ectotherm metabolism and evolution: metabolic and physiological interrelations underlying the superiority of multi-locus heterozygotes in heterogeneous environments. Journal of Thermal Biology 20: 23-33.

Hotton, N., Olson, E. C., Beerbower, R. (1997) Chapter 7: The amniote transition and the discovery of herbivory. In Sumida, S., Martin, K. L. (eds.) Amniote Origins: Completing the Transition to Land. Academic Press, London, 207-264 pp.

Hsia, C. C., Schmitz, A., Lambertz, M., Perry, S. F., Maina, J. N. (2013) Evolution of air breathing:oxygen homeostasis and the transitions from water to land and sky. Comprehensive Physiology 3: 849-915.

Hunt, A. P., Lucas, S. G. (1998). Vertebrate tracks and the myth of the belly-dragging, tail-dragging tetrapods of the late Paleozoic. Bulletin of the New Mexico Museum of Natural History and Science 12: 67-70.

Huttenlocker, A., Rega, E. (2012) Chapter 4: The paleobiology and bone microstructure of pelycosaurian-grade synapsids. In Chinsamy, A. (ed.) The Biology of Non-mammalian Therapsids: Insights from Bone Microstructure. Indiana University Press, Bloomington, 91-119 pp.

Huttenlocker, A., Mazierski, D., Reisz. R. (2011) Comparative osteohistology of hyperelongate neural spines in Edaphosauridae (Amniota: Synapsida). Palaeontology 54: 573-590.

Huttenlocker, A., Rega, E., Sumida, S. (2010) Comparative anatomy and osteohistology of hyperelongate neural spines in the sphenacodontids *Spenacodon* and *Dimetrodon* (Amniota: Synapsida). Journal of Morphology 271: 1407-1421.

Kemp, T. S. (2006) The origin of mammalian endothermy: a paradigm for the evolution of complex biological structure. Zoological Journal of the Linnean Society 147: 479-488.

Kemp, T. S. (2012) Chapter 1: The origin and radiation of Therapsids. In Chinsamy, A. (ed.) The Biology of Non-mammalian Therapsids: Insights from Bone Microstructure. Indiana University Press, Bloomington, 3-28 pp.

Knaus, P. Shelton, C. D., Sander, P. M., (2014) Ontogenetic stages in the long bone histology of Dimetrodon (Lower Permian, Sphenacodontidae). Journal of Vertebrate Paleontology: 34: 160A

Konietzko-Meier, D., Klein, N. (2013) Unique growth pattern of *Metoposaurus diagnosticus krasiejowensis* (Amphibia, Temnospondyli) from the Upper Triassic of Krasiejów, Poland. Palaeogeography, Palaeoclimatology, Palaeoecology, 370, 145-157.

Konietzko-Meier, D., Shelton, C. D., Sander, P. M. (in progress) How did the *Eryops* live? - The problematic histological framework of not-amniotes long bones from Early Permian of Briar Creek (Texas).

Labandeira, C. C., Sepkoski, J. J. (1993) Insect diversity in the fossil record. Science 261: 310-315.

Lagarde, F., Bonnet, X., Corbin, J., Henen, B., Nagy, K., Mardonov, B., Naulleau, G. (2003) Foraging behaviour and diet of an ectothermic herbivore: *Testudo horsfieldi*. Ecography, 26: 236-242.

Maddin, H. C., Evans, D. C., Reisz, R. R. (2006) An Early Permian Varanodontine varanopid (Synapsida: Eupelycosauria) from the Richards Spur locality, Oklahoma. Journal of Vertebrate Paleontology 26: 957-966.

Nespolo, R. F., Bacigalupe, L. D., Figueroa, C. C., Koteja, P., Opazo, J. C. (2011) Using new tools to solve an old problem: the evolution of endothermy in vertebrates. Trends in Ecology and Evolution 26: 414-423.

Olson, E. C. (1974) On the Source of Therapsids. Annals of the South African Museum 64: 27-46. Olson, E. C. (1986) Relationship and ecology of the early therapsids and their predecessors. In

Hotton, N., Maclean, P. D., Roth, J. J., Roth E. C. (1986) The Ecology and Biology of Mammal-like Reptiles. Smithsonian Institution Press, Washington, 47-60 pp.

Padian, K., Horner, J. R. (2004) Dinosaur physiology; pp. In Weishampel, D. B., Dodson, P. and Osmólska, H. (eds.) The Dinosauria (Second Edition). University of California Press, Berkeley. 660-671 pp.

Peabody, F. E. (1961) Annual growth zones in living and fossil vertebrates. Journal of Morphology 108: 11-62.

Pough, F. H. (1973) Lizard energetics and diet. Ecology 54: 837-844.

Reisz, R. R. (1986) Encyclopedia of paleoherpetology. Part 17A: Pelycosauria. Gustav Fischer Verlag, Stuttgart, 102 p.

Reisz, R. R., Berman, D. S. (1986) *Ianthasaurus hardestii* n. sp., a primitive edaphosaur (Reptilia, Pelycosauria) from the Upper Pennsylvanian Rock Lake Shale near Garnett, Kansas. Canadian Journal of Earth Sciences 23: 77-91.

Reisz, R. R., Fröbisch, J. (2014). The Oldest Caseid Synapsid from the Late Pennsylvanian of Kansas, and the Evolution of Herbivory in Terrestrial Vertebrates. PloS one, 9: e94518.

Reisz, R. R., Laurin, M. (2004) A reevaluation of the enigmatic Permian synapsid Watongia and of its stratigraphic significance. Canadian Journal of Earth Science 41: 377-386.

Reisz, R. R., Sues, H. D. (2000) Herbivory in late Paleozoic and Triassic terrestrial vertebrates. In Sues, H. D., (ed.) Evolution of Herbivory in Terrestrial Vertebrates. Cambridge University Press, New York, 9-41.

Reisz, R.R., Wilson, H., Scott, D. (1997) Varanopseid synapsid skeletal elements from Richards Spur, a Lower Permian fissure fill near Fort Sill, Oklahoma. Oklahoma Geology Notes 57: 160–170.

Ricqlés, A. d. (1974a) Recherches pale´ohistologiques sur les os longs des Te´trapodes V: Cotylosaures et Mésosaurs. Annales de Paleontologie 60: 171–231.

Ricqlès, A. d. (1974b) Recherches paléohistologiques sur les os longs des Tétrapodes IV: Eotheriodonts and pelycosaurs. Annales de Paléontologie 60: 3–39.

Ricqlès, A. d. (1974c) Evolution of endothermy: Histological evidence. Evolutionary Theory 1: 51- 80.

Ricqlès, A. d. (1976a) On the bone histology of fossil and living reptiles, with comments on its functional and evolutionary significance. In Bellairs, A. d. A., Cox, B. C. (eds.) Morphology and Biology of Reptiles. Academic Press, London, 123-150 pp.

Ricqlès, A. d. (1976b) Recherches paléohistologiques sur les os longs des tétrapodes VII. Sur la classification, la signification fonctionelle et l`histoire des tissus osseux des tétrapodes. Deuxième partie. Annales de Paléontologie 62: 71-126.

Romano, M., Nicosia, U. (2014) *Alierasaurus ronchii*, gen. et sp. nov., a caseid from the Permian of Sardinia, Italy. Journal of Vertebrate Paleontology 34: 900-913.

Romer, A. S., and Price, L. I. (1940) Review of the Pelycosaurs. Geological Society of America Special Papers 28: 1-538.

Ronchi, A., Sacchi, E., Romano, M., Nicosia, U., (2011) A huge caseid pelycosaur from north-western Sardinia and its bearing on European Permian stratigraphy and palaeobiogeography. Acta Palaeontologica Polonica 56: 723-738.

Ruxton, G. D. (2001) Heat loss from giant extinct reptiles. Proceedings of the Royal Society of London. Series B: Biological Sciences 268: 1921-1924.

Sahney, S., Benton, M. J. (2008) Recovery from the most profound mass extinction of all time. Proceedings of the Royal Society B: Biological Sciences 275: 759-765.

Shelton, C. D., Sander, P. M., Stein, K., Winkelhorst, H. (2013) Long bone histology indicates sympatric species of Dimetrodon (Lower Permian, Sphenacodontidae). Earth Env. Sci. Trans. Royal Soc. Edinburgh 103: 217-236.

Sues, H. D., Reisz, R. R. (1998) Origins and early evolution of herbivory in tetrapods. Trends in Ecology and Evolution 13: 141-145.

Troyer, K., (1982) Transfer of fermentative microbes between generations in a herbivorous lizard. Science 216: 540-542.

Werner, J., Griebeler, E. M. (2014) Allometries of Maximum Growth Rate versus Body Mass at Maximum Growth Indicate That Non-Avian Dinosaurs Had Growth Rates Typical of Fast Growing Ectothermic Sauropsids. PloS one 9: e88834.

West, G. B., Woodruff, W. H., Brown, J. H. (2002) Allometric scaling of metabolic rate from molecules and mitochondria to cells and mammals. Proceedings of the National Academy of Sciences of the United States of America 99: 2473-2478.

Zimmerman, L. C., Tracy, C. R. (1989) Interactions between the environment and ectothermy and herbivory in reptiles. Physiological Zoology 62: 374-409.

APPENDECIES

Appendix 1 (Chapter 2):

Notes taken during fieldwork in the Lower Permian of Archer County, Texas and visit to AMNH, DMNH, FMNH, MCZ, OMNH, TMM, UMMP (2010-2013). Note that phone numbers have been removed to protect the privacy of the individual.

Part I. September 6 - September 26, 2010

Written by: P. Martin Sander and edited by Christen D. Shelton
Participants:Martin Sander, Chris Shelton, Koen Stein, Herman Winkelhorst

Monday, September 6, 2010: flew Germany –Austin, TX

06.09.10 Dusseldorf - Atlanta 09:20 - 13:15
06.09.10 Atlanta - Austin 16:10 - 17:32

- stayed at La Quinta Inn Downtown Austin
- had dinner with Judy and Ernie Lundelius at Serrano's at Red River and 11th Street. They are doing great.

Tuesday, September 7, 2010: Austin – Iowa Park, TX

- Were picked up by driver from Longhorn Rentals
- rented from them Ford F 150 crew cab pickup estimated to cost us a total of about 1400 $ for two weeks. This includes collision damage waiver, liability insurance, and a fee of 2.50 $ per extra driver per day. Vehicle had worn tires and not enough oil, we should have checked this.
- visited VP Lab and studied Texas Lower Permian collections. In particular, the Sid McAdams locality in Taylor County was of interest here because it represents an excellent sample of the latest and largest species of *Dimetrodon*, *D. giganhomogenes*. The material was collected by WPA crews and described in a thesis by James G. Mead supervised by Wann Langston Jr. The thesis was later published by Olson and Mead (1982). The material consists of partial skeletons and isolated bones representing an excellent growth series from very small to very large individuals. The Mead thesis contains an excellent graph plotting humerus length against width. This sample would be of great interest for Chris' dissertation. At least, it will be great for morphometrics if we do not get access for sampling. I discussed with Chris the measuring procedure and also gave the three of them (HW, KS, CS) a crash course in pelycosaur and other Lower Permian tetrapod anatomy. So now they are ready to identify the bones in the field.
- drove up to Wichita Falls via Hwy 183 and 281. It is incredible to see how Austin has expanded along Hwy 183. We stopped at Stephenville to eat dinner at a new but very good BBQ place called "Hard 8" which is right on Hwy 281. Rained all the way. Not good truck has worn tires.
- we stayed at Chris' parents, Brenda and Don, in Iowa Park west of Wichita Falls, TX.

Wednesday, September ***8, 2010:*** Archer County- Iowa Park, TX

- we met up with Jack Loftin at his ranch in the morning, saw his collections at his house and in the yard, and then went to the Archer City Museum joined by Chris's dad Don.
- In addition to the beautiful *Dimetrodon*, the great *Diadectes*, the encrusted *Edaphosaurus*, and the *Eryops* skull, he now has created a mount by incorporating the latter that consists of bones he and Steve dug out from the Briar Creek bonebed (BCBB) in May of this year. This indicated to me that there would be plenty to collect there.
- Jack also secured permission for us to excavate in the BCBB from the land owner, a Jeff Lindeman, who also is a junior partner in the prosperous looking Lindemann drilling company of Archer City.
- Marie Loftin has offered us the use of her trailer home in Archer City, right on Texas HWY 25 west of the town center. We inspected it and found it to be great, albeit in need of a bit of cleaning.
- After a lunch at the Dairy Queen (DQ), we drove out to the BCBB. Turning off from the Archer City-Seymour road, we had to navigate the dirt road leading to the bonebed. At first, I proposed to walk into the locality but Jack decided to give it a try with his Ford sedan. We followed suit in the truck, tearing up the road some more, but fortunately it has a gravel base. The road was well travelled, anyway, because of a drilling rig a few miles down the road.
- The BCBB looks good and ready to dig in, with the back wall not being too high yet and plenty of isolated bones weathering out in the S part of the bed. I picked up a complete *Archeria* humerus, as well as a number

of other partial and complete pelycosaur long bones. So it is clear that it is a go. We were also told by Jack where he and Steve had been digging in May.

- Accordingly, after parting with Jack, we went to Chris' parents to get our equipment together. Apart from two shovels, we had to buy pretty much everything from a local hardware store on US HWY 287 (Atwoods) and from a Walmart in the W of W' Falls. This included a pick, a wheelbarrow, a set of screw drivers and small awls, four steak knives, and some hand brooms. Traditional whiskbrooms and awls were not available, though.
- Stayed at Chris's parent's house again.

Thursday, September 9, 2010: Archer City, TX

- today, We moved to Marie's trailer in the morning and we started the dig by cleaning out Jack's excavations and taking the back wall down as well as removing the lower overburden on the spur S of the quarry where I had picked up the long bones yesterday. It was hot (around 96 deg.) and humid, and the crew did not do too well, all of them overheating to varying degrees. But we got all the loose dirt out and most of the back wall of the quarry taken back about 40 cm. Since it was clear that we would not get all the necessary heavy digging done today, we started exploring the bonebed in the middle of the excavation and encountered good bone soon.
- upon digging a drainage ditch at the S end of the main quarry, Koen ran into a plant layer, as evidenced by a bit of horsetail and some other scraps.
- at night, I took a drive into W'Falls to the Walmart on the S edge of town to by parts for a canopy over the quarry. This consisted of a 10' by 20' tarp blue on one side and silver on the other, three shepherds hooks about 9 feet long, and rope.
- stayed at Marie's trailer for the first night.

Friday, September 10, 2010: Archer City, TX

- continued to take down the back wall and removed the overburden from the spur
- before noon, we put up the canopy too good effect, it was pretty pleasant to work under.
- we started digging in earnest into the bonebed, me starting in the middle of the quarry, soon encountering bone about 30 cm above the layer that Jack had indicated his finds to have come from.
- at night, we also discussed the numbering system for the finds.

Saturday, September 11, 2010: Archer city-Wichita Falls, TX

- The numbering system of this dig is as follows: Finds are labelled SA BCBB 2010 (for Sander Briar Creek bonebed 2010), followed by a running number. Plaster jackets also get the running numbers and are sequentially numbered as block 1 to block n in addition. Numbers were assigned to long bones, jaws, other distinctive or unique fossils; less important finds such as isolated vertebrae were only packaged in a "day bag" for the specific day. Non-jacket specimens were generally packaged in heavy-duty aluminum foil after having been treated with Paleobond Stabilizer while still in the rock (upper surface) and after taking out (underside).
- We kept a find catalog, first in Chris' small notebook and then in my larger format notebook. In addition to the numbers we also recorded the elevation of the individual bones in the bonebed, distinguishing between lower, middle, and upper layers. The thickness of the bonebed is up to 35 cm, but the highest bones are very widely spaced, and sometimes they are thickly encrusted with ironstone.
- That Paleobond stuff works wonders! We had bought about 300 ml of stabilizer, and a 2-ounce bottle of 40, 100, and 1500 viscosity glue each, plus a spray can of activator, and had all the stuff shipped to Chris' parents.
- were joined by Jack in the morning who showed us his technique of excavating bone which consists of scratching along the bone layer with his home-made excavating tool, a small but heavy pickaxe with a car spring welded to it that he dubbed his "Mexican backhoe". This rather crude method only recovered the larger bones, of course. The area he excavated was the far left (i.e. N) of the quarry.
- despite being tempted to proceed the same way, I made everybody dig down carefully in layers from the top of the exposed area so as to get a complete overview of the bone occurrences. We all got bone soon, but at different levels and in different quantities. We were lined up as follows from left (N) to right (S) along the exposed bonebed: Koen, Chris, me, Herman. Chris initially did not find much. Koen kept running into jaw bones and found a small jumbled skeleton, so did I pretty high up in the section. My area was later designated "Martin's bone field in the middle of quarry" (MBFMQ).
- Chris' father had found out where to get surgical plaster bandages, at a hobby stores in Wichita Falls, so Chris got a first bunch. In the end, he had to go three times, and we bought about 15 rolls, both 4" and 8" wide.

- at night, we went with Chris' parents to the drag races in Wichita Falls. Amazing!

Sunday, September 12, 2010: Archer City, TX

- We continued to dig into the bonebed under the tarp canopy. Because Chris wasn't having much luck in his original position he switched spots with where Jack had dug yesterday encountering a couple *Eryops* Femurs. Chris named this spot "Jack's Hole." This order pretty much stayed intact throughout the dig and can be used to roughly localize the finds based on their collector (Chris, Koen, Me, Herman).
- In addition, I opened up the spur area to the S of the area covered by the canopy where I had picked up the long bones on Wednesday. I wanted to check what the bone density was in this area to help in planning the excavation strategy. I pretty quickly encountered bone, including a large *Eryops* (Later ID as *Dimetrodon*) femur, but the bone is largely in a single layer and more widely spaced than under the canopy. There are very few bone higher up, including a rib that I exposed and left on a pedestal to show this. It soon got too hot, though, and I decided to continue in the morning.

Monday, September 13, 2010: Archer City, TX

- Koen started drawing the MBFMQ of which I had exposed an area of about 40 by 80 cm. We marked out a grid of 10 cm squares, initially with mesquite spines and then with tooth picks that Chris' father had in his truck. The tooth picks only stuck after we had wetted down the sediment some, which we mainly did to get the dust off and bring out the bones for photography. Koen kept extensive photographic records of how the bones occur in the rock but the bone-rock contrast is always poor.
- At first I had thought that there were mainly small bones higher up in the bone layer and bigger ones lower down but that does not seem to hold up because the biggest bone we found was a complete *Eryops* jaw high up, the tip of which was covered up by a partial *Dimetrodon* jaw. At the same height level, I had found a very small skeleton of a fish or reptile. We collected half of it. Koen found a similar small specimen, but with jaw which indicated it to be a reptile. So it is worth digging very carefully for these things. The size of these skeletons is the same as the material coming from the Fort Sill (Richard's Spur) localities.

Tuesday, September 14, 2010: Archer City, TX

- We continued the excavation, but it is becoming clear that a) Thursday will be our
- last full day in the field and that b) we will not be able to properly excavate the entire area of the bonebed we had exposed to a few inches above the bone level.
- We continue to take out individual bones and blocks.
- In the morning, I finished exposing the bone field S of the canopy so that Koen could start drawing it. In the end, the best finds from this bone field were: the *Eryops* femur, a flat shoulder girdle bone, two flattened fragmentary or partial skulls of *Dimetrodon*, a nice ?*Archeria* interclavicle, an exceedingly large *Dimetrodon* claw, a rather complete lower jaw of *Archeria*, and a partial disarticulated skeleton of a small reptile (pelvis less than one inch but apparently fully ossified). This actually was the only hint of associated material we saw at the bonebed.

Wednesday, September 15, 2010: Archer City, TX

- We continued the work, exposing bone, taking it out individually, and blocking it out if it is too thick. But we are running out of Paleobond stabilizer! We will have to use the glues as last resort but they are not nearly as good for the purpose.
- The same picture remains, bones are thickest in the area I am digging in and where Herman is. Again, there is no apparent order, with big and small bones intermingled, no sorting by size or taxon.
- Koen drew the bone field on the spur after he and I again put up a grid defined by toothpicks. We had to use the ice pick, though, make holes for the tooth picks because the sediment had hardened so much.
- Koen and Herman took the two fragmentary skulls in the spur bone field out as blocks.

Thursday, September 16, 2010: Archer City, TX

- A number of blocks are coming out of the MDFMQ after Koen had finished drawing the upper layer. Below that, there is poorly defined middle layer which we did not draw but only photographed. I did collect the material from the upper and the middle layer separately, however. Once through the middle layer, the lower layer contained a lot less bone in this area, unlike the areas where the others were digging.
- We pretty much finished digging today and took out all blocks except for a few that needed to set. We also left a small area of MDFMQ for the writer whom Jack is bringing tomorrow.

Friday, September 17, 2010: Archer City - Iowa Park, TX

- To visualize the base of the bonebed in our quarry, Herman had the good idea of marking it with salt that we had bought for speeding up the setting of the plaster but had not used. So we did this for both the S spur

and the main quarry, and Koen took good pics. In the pic of the main quarry, I marked the upper limit of the bonebed with steak knives stuck into the wall, two of which point to actual bones in the sediment.

- Jack came with his writer friend, a member of the North Texas U writing class that meets in Archer City every year. Her name is Elizabeth (Beth) Langton, and she wants to write about our work for her class. We had a good chat with her (http://centerandmain.org/fossils/)
- Jack also brought a massive, five-foot rattler he had killed that morning near his house. Now we have seen almost all the Texas-specific wildlife, alive or dead: dead rattler, scorpions, black widows, a beautiful tarantula, dead armadillos, jackrabbit etc The boys are satisfied.
- Herman dug into the plant layer, which is 25 cm below the base of the bone layer. Herman found more calamites, a few fern pinules, some nice *Walachia* sprigs, and long, strap-shaped fossil that I think are cordaite leafs. These were all collected, including a part of a cordaite leave in a small block (block 23). Pretty neat!
- Chris had finished excavating "Jack's Hole" and continued with his original position in the bone bed which was to the immediate left of MDFMQ. He left a few cm unexposed as time and glue had run out.
- After lunch we covered up the S spur and the main quarry with a layer of debris to slow down weathering and preserve the exposed bonebed for future excavation campaigns. We then took up the tarp, took some group photos and that was the end of the SABCBB 2010 campaign.
- In the afternoon, Chris typed up the field catalog (which was a good idea, considering the scribbling abounding in the catalog). We collected over 150 numbered bones, a lot of unnumbered bones, and 23 plaster jackets! Herman and I properly labelled all the blocks, and Koen sorted and edited his photographs. Herman packed up the specimen into plastic bins we had bought, and I cleaned the truck. He and I also cleaned the trailer, while first Chris and then Koen drove to Iowa Park, Chris to pack up and Koen to tell them that Herman and I would stay the last night in the trailer.

Saturday, September 18, 2010: Archer City - Austin, TX

- Chris's parents came to the trailer in Archer City in the morning to see us off.
- went to say good-bye to Jack and Marie at their ranch. Koen transferred his pictures of the dig to their computer. Chris picked up two large *Eryops* long bones (one later ID by histology as *Edaphosaurus* (spp)) that Jack had collected when he visited us at the dig. These still need numbers, they are from the far left of the main quarry, lower level ("Jacks Hole").
- then visited Adam Armstrong in Keene, TX to see his collections. He has a very nice and pretty diverse vertebrate collections but says his main interest these days is fossil crabs on which he collaborates and publishes on with different scientists.
- He lives in Keene, (SW of Dallas, of HWY 67) and his phone number is _____ at home or _____at work. In terms of North Texas Lower Permian, he did not have too much, but what he really excelled in is Richard's Spur stuff that he shares freely with professional paleontologists, including Robert Reisz, Jason Anderson, and us. He let Chris pick up a possible growth series of femora and various other bones to cut up.
- not far from Keene to the SW is Glen Rose and Dinosaur Valley State Park along the Paluxy River. We paid it a short visit but the tracks in the river bed were pretty much under water, unusual for September but still a result of tropical storm Hermine. Only one are of newly exposed tracks was good.
- drove to Austin, got their by 8 pm and were treated to dinner by Wann Langston Jr. at the County Line at the Lake. Good BBQ (had been here before), and Herman and Koen were very convinced by the beef ribs.
- stayed at La Quinta downtown again

Sunday, September 19, 2010: Austin, TX – Chicago, IL

- met Wann at the VP Lab at 8 am to drop off the blocks from the excavation for storage and future shipping to Germany. I also showed him some pictures and reported on what we did. He will ask the collections manager Lyn Murray to look into shipping companies for surface shipping to Bonn. I labelled everything in great detail and will get back to them from Bonn. We also checked out the BCBB stuff in the TMM collections, it's pretty similar in preservation (dark, with ironstone incrustations) to what we got. The TMM material was collected by E.C. Case together with Jack Wilson (or the other way around).
- - dropped the Longhorn Rentals truck off at the Austin airport and flew to Chicago
  Austin - Chicago 12:26 - 17:48
- with Koen being with us on the first leg to Detroit and from there travelled on, back Germany.

Monday, September 20 and 21, 2010: Chicago, IL

- Field Museum: worked with Nadia and Jörg on "Jim" and with Chris and Herman on pelycosaur morphometrics. For progress on the ichthyosaur, see separate notes.

Wednesday, September 22, 2010: Chicago, IL – New York City, NY

- Field Museum: continued work, got news that Lars and I got the NGS grant to dig up the *Omphalosaurus* next fall. September seems to be the time to go, possibly right before SVP which is also being held in Nevada (Las Vegas), after all. Work on "Jim" is progressing well but the complete preparation will draw on because of the budget cuts at the museum. The upshot of this is that it is unlikely that Olivier can have our *Omphalosaurus* prepared there. Accordingly, we took the specimen from its basement repository, and Jörg and Nadia will move it to Germany together with their household. We are on the lookout for a federal repository for the fossil, since we do not feel that the FMNH should get a specimen that it refused to prepare!
- we decided to have a first draft of the paper, figures and all, finished by the end of the year.
- - evening: flew to NYC Chicago - New York 18:05 - 21:30
- came in late because La Guardia had been shut down due to Pres. Barak Obama flying in.

Thursday, September 23, 2010: New York City, NY

AMNH closed because of UN reception in planetarium, including Obama and 120 other heads of state. Went site seeing in NYC, empire state building, 911 site, Broadway, downtown

Friday, September 24, 2010: New York City, NY

- American Museum met Mark Norell and Carl Mehling
- Herman helped Chris measure pelycosaur long bones in the collection as I worked on the new upcoming Sauropod exhibit.

Saturday, September 25, 2010: New York City, NY – Düsseldorf Germany

- see AMNH
- - leave for Germany 25.09.10 New York – Paris 19:05 - 08:35
- 26.09.10 Paris – Düsseldorf 09:45 - 10:55

Sunday, September 26, 2010: Germany

- arrived in Düsseldorf, Germany

Part II. March 31 to May 12, 2011

Written by Christen D. Shelton
Participants: Chris Shelton and Koen Stein

Thursday, March. 31, 2011: flew Germany - Dallas

Friday, April 1, 2011*:* Landed in Dallas at 2:15 pm and drove to Iowa Park, TX

- Steven Tudor and Koen were already at DFW, Koen flew from Florida after doing research in Greg Erikson's lab and landed 30 minutes earlier. Steven was there to drive us to Iowa Park, TX.
- Stopped at a Cretaceous site on the way through Decatur, TX for about an hour to show Koen. Found ammonites, echinoids, coral, worm tubes, various bivalves and gastropods.
- Had dinner in Wichita Falls at Samurai of Tokyo. Koen had Calamari, me and Steven had the chicken.
- Got to Iowa Park around 8 pm. Spent the night at my parent's house in. 1600 Karen Ln Iowa Park, TX 76367.
- 9:00 am Met Jack Loftin at the Mobile home we used on the SABCBB2010 campaign with Koen and Steven to get the keys, and then went with Jack out to the BCBB. Looked around for about 45 minutes and picked up some float. Jack tried to dig but he had a fall trying to feed cattle breaking some ribs and it hurt to swing his "Mexican bulldozer".
- JACK'S COMBO LOCK ON GATE**: 3013**
- Returned to Iowa Park around lunch time. Steven returned to Dallas, Koen took a nap, I called Dr. Robert Bakker (Dr. B) to arrange our meeting with he and Kathy Zoehfeld tomorrow morning in Seymour, Texas to see their dig site. **7:30am breakfast at the Maverick.**
- Bob and Kathy are in Seymour until Monday and will return April 11-17th to do some work on the "Wet Willy" *Dimetrodon* skeleton.

Sunday, April 3, 2011: Seymour – Iowa Park, TX

- Made it to Seymour by7:30am
  7:30 -9:30 am Koen and I had breakfast with Bob and Kathy and discussed paleontology at the Maverick

Saturday, April 2, 2011: Archer City-Iowa Park, TX

- before heading out to the Craddock Ranch. My first time to talk to Dr. B in person, and it was Koen's first time meeting and getting to know him, as well. First thing Bob said to me was what day is it? To test my jet lag.
- Dr. B called me and Koen, Williston and Sternberg. I was whoever had the mustache.
- Bob paid for our breakfast. (me-Big Breakfast, Koen- waffles) I didn't finish my omelet it was too big, Bob commented we should have brought it with us for later.
- We went to their HQ first to see some lysorophid fossils. Koen and I also got shots holding a replica of the skull of *Dracorex hogwartsia* and Dr. B told us about it. KP and JH think it's not a valid taxon and it's just an ontogenetic stage in the development of *Pachycephalosaurus.*
- Stopped at Allsup's on the way to the site. Kathy and Koen went in to get supplies. Dr. B told me an anecdote about using Paleobond. He said, "be careful in the morning if you have the glue on your fingers and you have to pee not to glue yourself to yourself. If somebody hollers about it everybody comes running with their cameras to catch your embarrassment." Haha.
- Went to the new lysorophid site "**Area 51"** first. Just found a few weeks ago while they lead a group of school children out on a field trip, the whole hill side is nothing but thousands of lysorophid skeletal concretions preserved during aestivation. Dr. B gave us ten to cut up for fun to see what we can do with them. Could see skull and jaw impressions on surface of a few. (late Mississippian, first found in Illinois, Vermillion Creek), "The Sleeping Serpents of Seymour".
- Dr. B commented that the US philosophy on the war in Vietnam is the same for bone histologists, "We destroyed it to preserve it."
- Then to the Wet Willy (WW) site, my old site where I found a complete *Dimetrodon* spine and vertebrae some years earlier with Lisa Black, and Mike Miller. But we left it in the ground. John Wayne wanted it excavated commercially for the town to benefit from it. (see unpublished newspaper article)
- SS and conglomerate are the floor of the Craddock BB, *Dimetrodon* occurs in 3 layers.
- *D. grandis* (not a figure 8 X-sec neural spine), *D. loomisi*, *Secodontosaurus*, *D. giganhomogenes*?
- Koen sang happy Birthday in Dutch to Bob and Kathy's colleague David Temple in Houston.
- Dr. B showed us how to use a straw to direct the flow of air when clearing a fossil from the ground. Also, that Decay bubbles can manipulate the position of bones.
- Dr B suggested we check the Eh-pH of the BCBB site.
- Koen found a sharp slender fang like tooth at the site near the WW skeleton. Kathy found a shed *Trimerorhachis* tooth (Enzymes had etched the base).
- The aestivating *Diplocalus* or "Mud Kitten" as Dr. B calls them, was covered so we couldn't see it
- The Craddock BB has a 7°N dip to the bones bone (need digital inclinometers)
- Also near WW was a concentration of 30 *Ctenacanthus* dorsal spines, teeth and cartilage as well as *Dimetrodon* and *Eryops* teeth.
- Mud Kitten level: 800mm
- Wet Willie level: 300mm also occurring here, *Seymouria*, *Diplocalus*, *Trimerorhachis*.
- *Secodontosaurus* is everywhere
- Amphibian to *Dimetrodon* ratio decreases to the north and then no more amphibians. (I think it is Marine Permian up north "lake Kemp")
- Romer was a sweetie, but not a good field person. Always losing his hammer. Favorite site was Tit Mountain. His office was just down the hall from Dr. B's graduate office at Harvard.
- At CBB they found a 9 ton block of *Trimerorhachis* skeletons and under estimated the weight braking the axial on trailer it was being loaded on.
- We finished our outing with lunch at Subway continuing with stories, questions, general musings, jokes, and laughter. I think I had the meatball sub. We parted after a group photo. Koen and I agreed that was a pretty awesome experience!

Monday, April 4, 2011: Archer City, TX

- Started our excavation (SABCBB2011).
- Began by removing overburden from the top of the old bone spur until lunch.
- Found the first bones (Proximal humerus)
- Explored a little down the wash and found more fragments
- Koen found a particularly nice daffy NS frag with long yardarms. Largest I have seen from the site. Koen marked the site with GPS as **Ä1** (see Koen's notes for coordinates). These sites are marked on a rough map in my field note book as a triangle with a number in it. Also, **Ä1, Ä2**, & **Ä3** is a clay pebble conglomerate.

Ä4 fossil in SS top of north canyon wall. See Koen's field notes for GPS coordinates. Bone frag Ä3&Ä2 must originate from the BCBB. Channel detritus SS follows stream flow. S curve. Sand, clay, conglomerate, clay. Was flow west to east or east to west?

Tuesday, April 5, 2011: Archer City, TX – Iowa Park, TX

- Began on the spur finding broken fragments of amphibian bone like on day 1, maybe the other half.
- 5:18 pm I found an amphibian long bone maybe and iron incased femur and jaw
- Koen found rib 110mm long
- Worked west side of bone spur, found many isolated long bones. Looked like it could have 3 femora (later to be Tibia) in it.
- Email from Bakker - told me that his size estimates for the pelycosaurs that he used in his paper "dinosaur renaissance" differed from Romer's by 5 to 10 %

Wednesday, April 6, 2011: Archer City, TX

- Replied to Bakker's last email, sent him a PPT of the lysorophid fossils with the collection numbers A51-1 to A51-10 as he instructed. Also, a monkey picture, Koen suggested the caption, " Hasta la victoria siempre!"
- Found fibula and Koen hit upon a nice *Archeria* jaw.
- Stopped a t 3:30 because of heat.
- Koen shot his first gun today. (my .22 cal revolver with rat shot) The victim was a cactus.

Thursday, April 7, 2011: Archer City, TX

- 2:48 pm Pimp battle text from Bakker, Monkey and a caveman toy.
- I found another small field of long bones today, Koen didn't find much but he hangs a good tarp.

Friday, April 8, 2011: Archer City, TX

- Took the day off from digging today
- Went with Dad to the Burk gun range to let Koen shoot some bigger calibers (22, 44 mag, 9mm, 45…ect) (9 guns, 6 callibers). He was excited but growing up with it Its boring to me.
- Went to MSU and picked up a Brunton compass from the Geology department. Introduced Koen to Pam Stephens and some of my biology professors, Dr. Fred Stangl and Dr. Mike Shipley. Pam gave Koen a plush Trilobite and I got to look through what was left of the Permian bones in the MSU collection. I will pick some later to cut. We got some reprints and copies of Walter Dalquest's Festschrift from Dr. Stangl . Also saw Drs. Mills, Rincon, Votsberger, Cook, and Scales.
- Tried to Catch Dr. Kocurko at home but he was gone so left a note.
- Ate dinner at DQ in Archer City, Aubrey came by to see us at the trailer from 7:00 – 10:30.
- Noticed that one of the lysorophid fossils Dr. B gave us had a skull impression on the surface. Koen thought it was the one I found but Dr. B kept it.

Sunday, April 10, 2011: Wichita Falls – Archer City, TX

- Not a lot to note today, Adam Armstrong was going to join us but never showed up. Jack may come out tomorrow.
- Koen found a good femur, looks like *D. natalis*
- I found an amphibian long bone (*Eryops* Tibia/ulna?)
- Found another long bone behind the block of 3 (radius) will try to plaster out tomorrow, vertebrae sits in front of it, calling it (4LB).
- As we were leaving a found a rib in the layer below the 4LB block, (*Edaphosaurus*?) black and dark blue. Extends under lock 4LB.
- Ate dinner at Pioneer 3 and going to take in some local entertainment. (no Beef ribs, Koen had Brisket I had Chicken)
- Had to skip the evening plans, went out to the site at 11:00 pm to secure it and the tarps, storm was coming with 65 to 70 mph winds.

Monday, April 11, 2011: Archer City, TX

- Found an *Eryops* femur today and hit a bone field, Found 9 or 8 ribs and 8 *Archeria*? Vertebrae
- Koen has had bad luck for the last couple days, he has been in a "gap" of no bones. He finally hit some bone today at the end of the gap.
- While trying to clean a bone from matrix, Koen stabbed his finger with the ice pick screwdriver. He bled a little put his hand in the ice chest and then passed out followed by a seizure that lasted a few seconds. I jumped over and tried to hold his head down to prevent him from hurting himself. He then lay at the spot and took a nap for an hour. I continued to check on his breathing. Koen said it's a condition called

Vasovagal Syncope. Condition in which fainting is triggered by a stimulus resulting in loss of blood pressure.

- Ate dinner at DQ, we had grilled chicken burgers and I had a snickers blizzard.
- Went to bed early tonight, around 9:00 pm (kinda bad day for Koen).

Tuesday, April 12, 2011: Archer City, TX

- Uncovered more of the bone field today, Wind was bad, big storm last night.
- Koen found *D. natalis* neural spines and misc. bones.
- I found a lot of longbones more of the rib field and a large vertebra in the bone field (SABCBB2011-19) 7 cm long vertebral process. Also, a large *D. limbatus*? Jaw under fibula 8.
- Dr. B texted me after I sent him a pic of the D'don Phoenix, he replied: Sunday Sermon, was Lazerus a zombie?
- I replied, IDK? Was Jesus? Zombie begot Zombie.
- 11:22 am got a text from Dr. B, "want to cut up 3 D'don species, *D. loomisi, D. grandis, and D. giganhomogenes.*
- I replied, Hell yeah!
- Had Idea to email pic of Easter basket with D'don and Easter eggs, "*Dimetrodon* nest" to Martin, hahaha.

Wednesday, April 13, 2011: Archer City, TX

- 1:38 Jack Loftin Came out and told us stories about Romer. Said he died at 72, Argie Lewis was his field Partner.
- Found many *Dimetrodon* vert with attached neural spines at the lowest level of the bed on the north west side of the spur.
- Decided to plaster out the big *Dimetrodon* jaw with the *Archeria* jaw above it the Koen found.
- Ray or Roy Russel stopped by as he was hauling Salt water to the oil rig to see what we were finding.
- Uncovered 650 mm long D'don NS in the Neural Spine Field.
- Had to tear down the wall and dig fast, lost some good longbones on the way. I was digging a bit frantically due to time. Also, found a humerus just below the spine.
- Dad came out too.

Thursday, April 14, 2011: Archer City, TX

- Drove to town to get more plaster 30.00 dollars
- Stopped at the Rattlesnake Canyon site and the Loftin Bonebed. Found some long bone pieces and coprolites.
- Went to gas station Stop n Go at Lakeside City and car broke down. Had to wait for dad to come fix it.
- Got to site late but managed to plaster out block 1 and flip it.
- Koen mapped Block 2 with the ribs and vertebrae.
- Ate dinner at sub & pizza shop at gas station
- Aubrey came by the trailer to hang out with us from 8:30 to midnight.

Friday, April 15, 2011: Archer City, TX

- Continued extracting the neural spine field and began removing bones from rock.
- Koen plastered out block 2.

Saturday, April 16, 2011: Archer City and Wichita Falls, TX

- Went out to the Loftin's house to visit with Jack and Marie
- Gave Marie 40 dollars for staying in the trailer and using the utilities. Tried to give her 100 but she said it was too much.
- Koen and I bought a copy of Jack's map for 5 dollars and had it signed by he and Marie.
- Jack gave me some of his coprolites and a small vertebrae he found on our first day there.
- Got to the site at noon, was very hot.
- Found more bone on the upper bone field and East wall where the NSF is.
- Took the wall down more and broke the handle on the pick, found 9 or 10 complete spines
- Koen finished plastering block 2. However it will require an additional layer of plaster later. Too thin on the back, no more plaster
- This means that then I will have to take the NSF out in pieces and wrap it in foil.
- Jack had a copy of Romer's map with sites pointed out on it. I took photos of it.
- Spent the evening making up for the lost one the night of the storm.

Sunday, April 17, 2011: Archer City, TX

- Slept in till 9:00am

- Went to my Plateau site at Lake Kickapoo.
- Found an ulna head the size of your fist.
- Started cleaning, mapping and removing the *Dimetrodon* neural spine field.
- We had to wait until 12:00 to buy beer because it was Sunday. Bought Land Shark Beer.
- Got gas at Allsup's $3.79/gal. it was $3.46/gal when we landed.
- Pulled half the NSF after Koen drew it but I ran out of foil before I could finish it.
- Will have to finish it up on Tuesday.
- Took pictures of the fake D'don nest and made one with a pterosaur for Edina. Sent pics to Martin, Bob, and Robert Reisz. Dr. B said it wasn't good enough; we have to trick RR with a mummified *Tetraceratops*. Hahaha.

Monday, April 18, 2011: Archer City, TX and Dallas, TX

- 1:30 am, Koen is taking a shower, got all the # bones and NSF packed up in a suitcase from Wal-mart, 100 Kilos. Used the tarp and Styrofoam ice chest to pack rocks in. Koen is also taking the lysorophids with him. Dad will arrive at 7:00am to drive us to Dallas by 10:00 to check in Koen's luggage.
- I'm blistered sun burned, and my hands hurt. Hate to see Koen go, it was fun.
- Koen flies back to Germany 12:00pm
- Specimen numbering got off a little bit. Will have to fix that later. (see notes)
- Koen lost his hammer, probably buried at the site.
- Bag weighed 98 lbs, $205.00 for extra bag and overweight charges.
- Stayed at Aubrey's tonight in Electra.

Tuesday, April 19, 2011: Archer City, TX

- Finished up the dig and took out the rest of the NSF.
- Still found longbones coming out of the top of the spur.
- Had a last beer and searched the "false float"
- Found 5 large heteropolar coprolites, one was 108.5mm long. "Scheizen Stein"
- Last night in the Loftin trailer

Wednesday, April 20, 2011: Iowa Park, TX

- Cleaned up the trailer and moved out to Mom and Dad's in Iowa Park.
- Went to MSU to return the Compass to the Geology department. Never used it. Had an electronic GPS instead.
- Stayed to hear Dr. Stangl's student Will Wiggin have his thesis defense. He started when I left MSU.
- Had a steak dinner with Will and Profs Shipley and Stangl.

Thursday, April 21 - 24, 2011: Falconhead, OK

- Went to Oklahoma to see my grandparents and stay a few day for Easter holiday.
- Finished plastering the blocks and weighed them. Will not mail back. Will leave with my parents to pick up later in Texas.
  (jaw block = 36.5lbs) (Rib block = 44.5lbs)
- My two bags are 41.5lbs. and = 27.5lbs

Monday, April 25, 2011*:* Archer City – Iowa Park, TX

- Returned to the BCBB with a metal detector and found Koen's hammer he had lost (J'ai trouvé votre marteau sacré). It was buried on the south edge of the bone spur.
- Leaving tomorrow to go to University of Oklahoma to research their pelycosaur collection. Harvard and Michigan after that before returning to Germany.

Tuesday April 26 thru Thursday April 28, 2011: Norman, OK

- Met, Jennifer Larsen, Kyle Davies, and Dr. Rich Cifelli. Also, Dr. Nic Czaplewski
- Cored several bones (*Dimetrodon, Cotylorhynchus, Ophiacodon*) before the bearings burned out. No more core drilling for the rest of the trip, had to borrow one from OMNH prep lab to finish.
- *Cotylorhynchus* cores are unusable, fall apart like sugar.
- Borrowed a small collection to cut back in Bonn (varanopsid, *Mycterosaurus longiceps*, *Ophiacodon*, 4 unidentified juvenile *Cotylorhynchus romeri* long bones)
- Saw a crushed *Diadectes* ulna that was carbonized like the Richard spur material with tar on it.

Friday April 29, 2011

- Returned to Iowa Park, TX and stayed at Mom and Dad's place

Saturday April 30, 2011

- Returned to OKC with mom and dad to fly to Boston tomorrow

Sunday May 1 thru Saturday May 7, 2011: Boston, MA

- Arrived in Boston, staying in a half way type hostel in the theater district. Have to take the sub way to get to Harvard
- Was assisted by curator Jessica Cundiff
- Arrived at MCZ 2 hours late. Measured skeletons on exhibit in the Museum of Comparative Zoology (MCZ)
- Met Dr. Farish Jenkins Jr. briefly, He said I could have one of each of the left over reprints from Romer's publications. Also met L. Laszlo Meszoly an illustrator that knew Dr. B when he was a student. Said he used to borrow his pencils and not give them back.
- Was given and access card and keys to come and go as I wish, worked till very late in the mornings.
- Spent the night in the collection twice and once in Alfred Sherwood Romer's old office.
- Also, met Bhart-Anjan Bhullar my last day, said I can crash with him next time im there.
- No time for sightseeing but did have a beer at the bar used in the TV show Cheers!
- In 5 days I measured and photographed 635 pelycosaur long bones, missed some *Edaphosaurus* material
- Marked 80 bones I wished to thinsection, have to be approved by Dr. Jenkins first.
- First consignment will be mailed to me in Germany.
- Found a drawer of old letters to and from Romer dealing with Texas field work in the 1940's, photographed all of these (100 pages)
- I liked Boston!

Sunday May 8 thru Wednesday May 11, 2011: Ann Arbor, MI

- Arrived in Ann Arbor Michigan to study the pelycosaur collection at the University of Michigan Museum of Paleontology (UMMP) hosted by Dr. Greg Gunnell
- Missed seeing Phillip Gingerich
- Computer power chord shorted out and had to buy new one at Circuit City (75$)
- Was not allowed access to the archives to study E.C. Cases's original field notes, they said I would need to hire an archivist to handle the documents or pay them 40$ per hour to do it, outrageous!
- Most of the collection is by Case, original finds from the BCBB during the early 1900's expeditions. Measured and photographed all bones, lots of *Ophiacodon* material.
- Measured a *Dimetrodon* and *Edaphosaurus* skeleton in the exhibits
- Set aside 40 bones and a few coprolites to sample, has to be approved by Dr. Jeffery Wilson. He will email me later.

Thursday May 12 and Friday May 13, 2011: Germany

- Returned to Germany Via Frankfurt from Ann Arbor, Michigan

Part III. March 28 to April 23, 2013

Written by: Christen D. Shelton
Participants: Chris Shelton & Koen Stein

March 28 to April 2, 2013***:*** This time was my Easter holiday, back with my family that I have not seen since the second field excursion in 2011.

Wednesday April 3 to Saturday April 6, 2013***:*** Iowa Park, Austin, Dallas, Wichita Falls, TX

- Hitched a ride with Dr. Robert Bakker (Dr. B) from Iowa Park, TX to Austin, TX to attend the South-Central Division of the 47th GSA meeting. Stayed at same hotel from 2010, La Quinta Inn.
- Presented my *Ophiacodon* work in the session honoring Dr. Wann Langston Jr.
- Rode back with Dr. B and Kathy Zoehfeld to Iowa Park, TX via Dallas, TX from Austin, TX for the GSA field trip to the Cretaceous of Dallas led by Louis Jacobs,
- Had Dinner at Pasquel's with everybody and met Dr. B's student Kim Beck who is a grad student at MSU in Biology doing research on growth marks in Paleozoic animals.

Sunday April 7, 2013: Seymour, TX

- Met Dr. B and Kathy in Seymour, TX to have breakfast and go prospect for new vertebrate sites on the Craddock Ranch.
- I found a rattlesnake and a new site with a shed pelycosaur tooth and a coprolite (Carter Site).

- Kathy found an arrowhead and a new site with diadectid, *Dimetrodon* and unknown amphibian fragments, near "Area 51", the Lysorophid site we visited in 2011. She named it the "Mayo Site".

Monday April 8, 2013: Archer County, TX

- Met our contact for the Rattlesnake Canyon site David Williams, volunteer for the Dallas Museum of Natural History, the Perot Museum, and first chair harpist for the Dallas Symphony Orchestra.
- Land owner of RSC is John Holly
- Found *Ophiacodon* coprolites, broken flanged bone and a *Diadectese* vertebrae
- Wann Langston Jr. passed away Sunday.

Tuesday April 9, 2013: Iowa Park, TX

- Picked up Koen from the Wichita Falls Municipal airport at 7:00pm.

Wednesday April 10, 2013: Wichita Falls, TX

- Took the day off to let Koen settle in and buy proper funeral attire to attend Wann's burial in Oklahoma on Friday.

Thursday April 11, 2013: Archer County, TX

- We met Dr. B, Kathy, and Dave Temple (a curator from the HMNH) for breakfast at the Wildcat Cafe in Archer City, TX.
- Took them out to RSC for the day, they helped us get started by locating several potential excavation sites and we discussed paleoenvironment of RSC.
- Dr. B said, "Not a lake unless in the flood season maybe, large paleosols. Bird egg size carbonate nodules. Saw no varves. Mudstone grades from yellow, grey, red digging down (O^2 increases, formed by plants). Might be 2 taphonomic scenarios."
- Started a site list by first bone found and GPS coordinates.
- Site 1: Pig Bush (33° 40' 43"N, 98° 48' 48" W)
- Site 2: Hungary (33° 40' 43"N, 98° 48' 48" W)
- Site 3: Lester (33° 40' 43"N, 98° 48' 48" W)
- Site 4: Braincase (33° 40' 43"N, 98° 48' 48" W)
- Site 5: Scorpion (33° 40' 43"N, 98° 48' 48" W)
- Site 6: Beck (33° 40' 43"N, 98° 48' 48" W)
- Site 7: Black Jack (33° 40' 43"N, 98° 48' 48" W)
- Site 8: Worm Hill (33° 40' 43"N, 98° 48' 48" W)

Friday April 12, 2013: Lawton, Purdy, OK

- Koen and I drove to Purdy, OK for Wann's funeral service and burial. We were asked to be pallbearers along with Kyle Davies from the University of Oklahoma in Norman, OK. The other 3 pallbearers were cemetery grounds keepers.
- Small graveside service attended by about 10 people including Wann's 2 daughters and grandson (Sandra-Archaeologist in Italy). Wann was laid to rest dressed in his field boots, hat, kakis, and his pick
- Kyle had a 3D printed juvenile *Apatosaurus* skull with him. He invited Koen and I to visit the Sam Noble Museum of Natural History if we had time
- Lunch was provided by the church and funeral home
- Truck did fine on the drive but AC is out
- Bought supplies and food for our HQ in Archer City, TX ($150 USD). We were again generously allowed to have full use of the Loftin's mobile home. Water pressure is low and we can still smell gas. Kitchen sink no longer works.

Saturday April 13, 2013: Archer County, TX

- David Williams met us at the site in the morning and we located 2 more sites.
- Site 9: Crab Ninja(33° 40' 43"N, 98° 48' 48" W)
- Site 10: Fenne(33° 40' 43"N, 98° 48' 48" W)
- Site 11: Man Bear Big (See KS's field notes)
- Went back to trailer, David stayed the night and brought us material to look at
- RSC left femur *Lupeosaurus?* RSC L/200 mm & C/136 mm"Grey"
- Belle Plains left femur edaphosaurid L/188 mm & C/130 mm "Black"
- Gave us several casts of skulls and limb bones to take back to Martin and showed us his notes and maps from his work on RSC over the years. I photographed most of it.

Sunday April 14, 2013: Archer County, TX

- Found a new site south of MBB (site 11) going towards the Lake Kickapoo: Lots of rolled weathered bone. Koen found a huge heterpolar spiraled bromalite and a large *Dimetrodon* Ulna head.
- Site 12: Faux (see KS's field notes)
- I slipped on the rocks walking up hill, fell and almost broke my left pinky
- David slipped at a different area and landed on his back
- He showed us a *Trimerorachis* site to try later, known for producing skulls
- Koen placed a dead bird on an red harvest ant hill to be cleaned
- Went to Jason Gilmore's for BBQ dinner that evening in Iowa Park, TX
- Made plans to go to OMNH on Thursday

Monday April 15, 2013: Norman, Davis, Ardmore, OK

- Called up Kyle Davies on our way into OK in the morning to let him know we were coming, went via Ardmore on I 35 and ate breakfast at Wataburger in Burkburnett, TX. Changed plans to visit OMNH today instead because my injured finger prevented me from digging. It was swollen and a little bit purple in colour, stiff to move.
- Met Kyle at McAllister's Deli for lunch in Norman, OK. Koen treated
- Went to the OMNH and saw the collection (Sauroposiden, Caseids)
- I asked permission to do a full crossection on an adult femur and humerus (attempted to drill before) of *Cotylorhynchus romeri*
- Saw the exhibits, "Pentaceratops" or "Titanoceratops"
- Left at 6:00pm and drove to Turner Falls to look for arrowheads
- I found 2 broken tips and a damaged diamond shaped one, gave them to Koen for a souvenir
- Drove back to Wichita Falls, TX and ate dinner at IHOP at 11:30 pm

Tuesday April 16, 2013: Archer County, TX

- Searched an area on David's map called site "0" (DW Site 0)
- Found a hand size piece of "Sharkilage" (Dr. B term for shark cartilage). Also, small edaphosaur spines and Diadectese vert. Lots of fish and *Trimerorachis* bones. Eryops intracentrum, coprolites
- Lungfish tooth
- White sandstone layer with malachite inclusion
- Dug a little bit into the *Trimerorachis* site David showed us a few days earlier, found some skull bone in place, will have to plaster out
- Went into to WF to buy plaster at Hobby Lobby and eat dinner at Red Lobster
- Stayed at Mom and Dad's house in IP

Wednesday April 17, 2013: Archer County, TX

- Visited Jack and Marie today and their son Craig
- Jack is not doing too good after his stroke, but somewhat coherent
- He remembered me but not Koen or Martin's name. Couldn't remember certain fossils anymore. Jack didn't have the full use of his left side.
- He did tell us stories though, did talk to us a bit but got confused often
- Gave Marie $40 ($20/each) for using their trailer, she only wanted $20 total!
- Ate dinner at Quiznos
- Stayed in AC, storms possible tonight

Thursday April 18, 2013: Archer County, TX

- Woke up to near freezing temperatures, had to figure out the heater. Hope Koen is not sick he is often cold.
- Windy! Dug in Davids *Trimerorachis* site, found a few bits of bone, nothing major or worth plastering.
- I found a conglomerate layer on an adjunct hill with broken up bones of an animal (toe, radius, humerus) and small *Trimerorachis* long bones
- Koen stopped to have a piss actually and found a bed of "mummified" *Trimerorachis* remains dubbed "Koen's piss site" (KPS)
- 3 partial skulls and a body fossil with multiple articulated vertebrae running through it, looks like skin dried and is stretched over it. Tibia and pelvic girdle on one part.
- We had a small party to celebrate the find

Friday April 19, 2013: Archer County, TX

- Woke up with slight hangover (7:30 am) from too much celebrating with Koen. Eating a big hot breakfast at Wildcat café and then continuing the dig at KPS for more of the *Trimerorachis* mummy material
- RSC is a delta, found one dipping bed of white sandstone with 2 varves and no bones north of KPS
- Found several more pieces of the mummified material, no new skulls

- Material is split on the south and west face on 3 sides of a slope, could not locate the layer.
- Went to Lake Kickapoo south plateau site as well, found fragments and large vertebrae of an *Ophiacodon?*

Saturday April 20, 2013*:* Archer County, Iowa Park, TX

- David met us at the trailer and we bought sub sandwiches for lunch to eat later
- Stopped at the Circle A ranch to search the ACBB first.
- Land caretaker told us to hunt as much fossils as we want so we did, lots of *Orthacanthus* shark teeth and spiraled bromalites.
- David then drove us around for about 2 hours trying to find Cottonwood Creek Site but couldn't remember how to get to it
- Next we stopped at the Loftin bone bed: Lots of material (Diadectese jaw fragment, large *Eryops* bone large shark teeth and *Edaphosaurus* spines.
- Spent the night at Mom and Dad's in IP

Sunday April 21, 2013*:* Iowa Park, Archer County, TX

- Koen did a protestant radio show interview for an Amsterdam station in the Netherlands during the morning Via skype. It was about the new article he did with Reisz in Nature. Only lasted 5 minutes after Koen blasted nonbelievers over the bird/dinosaur evolutionary connection.
- Spent the day packing and numbering fossils. Went to bed at midnight in AC

Monday April 22, 2013*:* Dallas, Little Elm, TX

- Drove to Dallas and met David at 2 to see the Dallas Museum collection
- Measured their pelycosaur material from RSC (22 long bones)
- Saw a new near complete articulated *Ophiacodon* skeleton from RSC
- Drove to Little Elm, TX and stayed the night with my cousin Steven Tudor and his family

Tuesday April 23, 2013*:* Dallas, Archer County, TX

- Put my European brother on the plane to Germany at 1:15 ($120 USD for luggage)
- Stayed in AC, near freezing again tonight

Wednesday April 24, 2013: Wichita Falls, TX

- Invited speaker at MSU, Dr. Mike Shipley's class on Bone Histology
- Met Kim Beck, Dr. B's biology grad student

Thursday April 25, 2013: Archer County, TX

- Got permission from Dr. Ciffeli to cut the *Cotylorhynchus* bones from OMNH, Will drive up and pick up the femur and humerus on Monday
- Giving a poster at ISPH

Friday April 26, 2013: Iowa Park, TX

- Cleaned up the trailer and moved back to mom and dad's in IP

Monday April 29, 2013: Norman, Falconhead, OK

- Drove up to OMNH and picked up *Cotylorhynchus* humerus and femur
- Also re-examined OMNH 73698 *Ophiacodon* humerus to determine SOD- Entepicondyle looks rugose, Proximal end with unfinished surface. SOD-III?

Friday May 3, 2013: Boston, MA

- Arrived in Boston MA to do research at the MCZ
- I am being hosted by Bhart-Anjan Bhuller 1679 Massachusetts Ave, Cambridge

May 4- May 7: Boston, MA

- Worked in the collections to examine and measure various Briar Creek long bones (reptile/amphibian) for comparative purposes and the remaining *Edaphosaurus* bones I missed last time including the *Trimerorachis* long bones measured for Koen Stein (190),

Wednesday May 8, 2013: Hartford, CT

- I arrived at Yale by train
- Im being hosted by Holger Peterman (PhD student under Jacques Gauthier who is a former student of Kevin Padian)
- Holger showed me a park near campus that was an old Colonial church yard, they removed the headstones but not the graves, a recent blizzard had saturated the ground and human skulls had floated to the surface shortly after.

Thursday May 9 to Saturday May 11, 2013: Hartford, CT

- Worked in the collections of the Peabody Museum measuring the Permian collection, small compared to Harvard's.
- Anjan is also interviewing for a faculty position in the Geology department.
- Discussed my thesis briefly in a session with Jacques, his advice is to do phylogenetics and try to figure out why the vascular pattern is the way it is and try to compare what I'm finding to extant species. Maybe varanids? He asked me if Pelycosaurs had scales and about their common ancestor. Jacques was intrigued by my work and wished we had more time to discuss it. Also, I put a word in with Jacques that he should hire Anjan. I think he has a very good shot at getting the position.
- Visited the Yale cemetery where O. C. Marsh, Eli Whitney, and Noah Webster is buried
- Just down the road is the Skull and Bones secret society
- Met Holger's friends Rachel Racicot and her boyfriend Simon Darroch
- Went to the Aquarium with Rachel
- Holger said he thinks I made a very good impression overall. He seems to be adjusting well to American life.

Sunday May 12, and Monday May 13, 2013: Germany

Returned to Germany via Frankfurt from Newark, New Jersey

Appendix 2 (Chapter 2):

Field catalogs corresponding with field notes.

Field ID	#	Bone	Organism	Notes
SABCBB2010	1	Left Femur	Dimetrodon	
SABCBB2010	2	Left Femur	Dimetrodon	
SABCBB2010	3	vertebrae		
SABCBB2010	4	Long Bone Fragment	Pelycosaur	
SABCBB2010	5	Jaw, NS\phalynx	Dimetrodon & Caseid	Block 1
SABCBB2010	6	Fibula?	Pelycosaur	
SABCBB2010	7	tibia	Pelycosaur	
SABCBB2010	8	braincase		
SABCBB2010	9	Atlas vertebrae		
SABCBB2010	10	tooth	Dimetrodon	
SABCBB2010	11	Small Femur	Pelycosaur ?	
SABCBB2010	12	small Humerus		
SABCBB2010	13	Small jaw	Bolosaurus	
SABCBB2010	14	Small jaw	Bolosaurus	
SABCBB2010	15	Small Tibia		
SABCBB2010	16	Interclavicle		
SABCBB2010	17	Pelvis, LBs, vert, misc frags\femur	Dimetrodon & ?	Block 2
SABCBB2010	19	Femur		
SABCBB2010	20	Small jaw	Reptile	
SABCBB2010	21	Quadrate		
SABCBB2010	22	Strange humerus		
SABCBB2010	23	Dense Bone		Block 3
SABCBB2010	24	Flat Long Bone		
SABCBB2010	25	jaw	Dimetrodon	Block 4a
SABCBB2010	26	Right Femur	Pelycosaur	
SABCBB2010	27	Biggest Radius	Pelycosaur	
SABCBB2010	28	Femur with keel		
SABCBB2010	29	Dermal Scale	Eryops?	
SABCBB2010	30	Jaw		
SABCBB2010	31	Humerus/ Partial		
SABCBB2010	32	3 large skull fragments	Edaphosaurus	
SABCBB2010	33	Humerus	Archeria	
SABCBB2010	34	radius	Pelycosaur	
SABCBB2010	35	Cervical rib	amphibian	
SABCBB2010	36	Humerus	Archeria	
SABCBB2010	37	Fibula?		
SABCBB2010	38	Scapula?		

SABCBB2010	39	Ulna		
SABCBB2010	40	Skull bone		
SABCBB2010	41	radius	Pelycosaur	
SABCBB2010	42	broken longbone		
SABCBB2010	43	Misc bones/ Shark tooth	Dimetrodon	Block 4b
SABCBB2010	44	Round bone-jaw?		
SABCBB2010	45	Round bone-jaw?		
SABCBB2010	46	Femur	Eryops	
SABCBB2010	47	Rib	Edaphosaurus	
SABCBB2010	48	Pelvis fragment		
SABCBB2010	49	small long bone		
SABCBB2010	50	Right Pelvis	Eryops	
SABCBB2010	51	Proximal humerus, pelvis	reptile	
SABCBB2010	52	Vertebrae weathered pre-burial	pelycosaur	
SABCBB2010	53	Jaw + 3 Longbones	Dimetrodon	Block 5
SABCBB2010	54	small jaw	Dimetrodon	
SABCBB2010	55a	small right ulna	Dimetrodon	
SABCBB2010	56a	Jaw	Dimetrodon	
SABCBB2010	55b	adult vertebrae	Dimetrodon	
SABCBB2010	56b	large flat bone, vert	Dimetrodon?	Block 6
SABCBB2010	57	Femur	Dimetrodon	
SABCBB2010	58	Interclavicle	Dimetrodon	
SABCBB2010	59	jaw		
SABCBB2010	60	Longbone		
SABCBB2010	61	large longbone?		
SABCBB2010	62	neural arch & spine	Edaphosaurus	
SABCBB2010	63	jaw	Eryops	
SABCBB2010	64	WS Skull ?	Eryops	Block 7
SABCBB2010	65	small tibia	Dimetrodon	
SABCBB2010	66	Femur	Dimetrodon	
SABCBB2010	67	radius	Dimetrodon	
SABCBB2010	68	Fibula & Humerus	Dimetrodon	
SABCBB2010	69	Vertebrae	Edaphosaurus	
SABCBB2010	70	adult vertebra	Dimetrodon	
SABCBB2010	71	rib	Eryops	
SABCBB2010	72	left humerus	Dimetrodon	
SABCBB2010	73	interclavicle, NS	Dimetrodon & Edaphosaurus	Block 8
SABCBB2010	74	Interclavicle	Dimetrodon	Block 9
SABCBB2010	75	vertebrae with spine	Dimetrodon	
SABCBB2010	76	small long bone		
SABCBB2010	77	ulna head		

SABCBB2010	78	radius, jaws, vert	Dimetrodon & Bolosaur	Block 10
SABCBB2010	79	Right Femur	Dimetrodon	
SABCBB2010	80	vertebrae?		
SABCBB2010	81	fibula	Eryops	
SABCBB2010	82	small long bone	Archeria?	
SABCBB2010	83	small long bone	Eryops	
SABCBB2010	84	vertebrae	Archeria	
SABCBB2010	85	humerus small	Archeria	
SABCBB2010	86	jaw part	Eryops?	
SABCBB2010	87	jaw	Dimetrodon	
SABCBB2010	88	long bones & little bones		
SABCBB2010	89	jaw, radius, vert and NS, interclavival	Dimetrodon	Block 11
SABCBB2010	90	Pelvis, rib, jaw	Dimetrodon	Block 12
SABCBB2010	91	Femur	Dimetrodon	
SABCBB2010	92	tibia		
SABCBB2010	93	sacral rib & vertebrae		
SABCBB2010	94	Dermal Scale	Eryops	
SABCBB2010	95	Skull part	Eryops	
SABCBB2010	96	ankle bone	Eryops	
SABCBB2010	97	ankle bone	Dimetrodon	
SABCBB2010	98	tibia weathered	Dimetrodon	
SABCBB2010	99	NO SPECIMEN		
SABCBB2010	100	Not USED		
SABCBB2010	101	welded bone mass	Dimetrodon	Block 14
SABCBB2010	102	humerus, scapula, vert misc. Bones	Ophiacodon & Dimetrodon	block 13
SABCBB2010	103	Ulna	Eryops	
SABCBB2010	104	scapula corocoid	amphibian	
SABCBB2010	105	small long bone	amphibian	
SABCBB2010	106	Fibula?	Dimetrodon	
SABCBB2010	107	Humerus	Dimetrodon	
SABCBB2010	108	Femur and tail vertebrae	Dimetrodon?	
SABCBB2010	109	Humerus	?	
SABCBB2010	110	rear end of jaw	Eryops	
SABCBB2010	111	small femur	Eryops	
SABCBB2010	112	jaw	Eryops	
SABCBB2010	113	jaw		
SABCBB2010	114	small long bone		
SABCBB2010	115	4 piece Radius?	amphibian	
SABCBB2010	116	radius	Dimetrodon	
SABCBB2010	117	tibia or Fibula	amphibian	

SABCBB2010	118	Toe bone	amphibian	
SABCBB2010	119	small tibia		
SABCBB2010	120	humerus, radius, large jaw	Dimetrodon	Block 15
SABCBB2010	121	claw	Dimetrodon	
SABCBB2010	122	quadrate	Dimetrodon	
SABCBB2010	123	little skeleton		
SABCBB2010	124	femur	Dimetrodon or Lupeosaurus	
SABCBB2010	125	vertebrae	Archeria	
SABCBB2010	126	phalanx big	Caseid	ID R. Reisz
SABCBB2010	127	Mystery bone		
SABCBB2010	128	snout	Edaphosaurus	
SABCBB2010	129	skull bone	Dimetrodon	
SABCBB2010	130	small pelvis		
SABCBB2010	131	very small fibula	Dimetrodon	
SABCBB2010	152	small humerus	Dimetrodon	
SABCBB2010	133	Interclavicle	Archeria	
SABCBB2010	134	jaw	Archeria	
SABCBB2010	135	pelvis	Archeria	
SABCBB2010	136	Jaws and skull	Archeria & Diadectes	block 16
SABCBB2010	137	Flat bone pelvis?		block 17
SABCBB2010	138	Small radius 3 pieces		
SABCBB2010	139	small humerus	Dimetrodon	
SABCBB2010	140	fibula?		
SABCBB2010	141	femur?		
SABCBB2010	142	spine & 2 limb bones	Edaphosaurus & Eryops	
SABCBB2010	143	Vert. Interclavical, claw	Ophiacodon &Edaphosaurus?	Block 18
SABCBB2010	144	Vert, fibulae	Dimetrodon & Eryops	block 19
SABCBB2010	145	jaw & skull frag	Eryops	block 20
SABCBB2010	146	skull roof, jaw segment/ Jaw	Dimetrodon & Archeria	block 21 -w/block 22?
SABCBB2010	147	left lower jaw, fragmented jaw	Eryops & Dimetrodon	block 22
SABCBB2010	148	small femur, shaft	Dimetrodon	
SABCBB2010	149a	femur ironstone		
SABCBB2010	149b	jaw (toothless?) ironstone		
SABCBB2010	150	bone ironstone concreation 1/2		
SABCBB2010	151	bone ironstone concreation 2/2		
SABCBB2010	132	pelvis, Skull bone, humerus	Dimetrodon	
SABCBB2010	153	Plant material	Plants	block 23 not preped

SABCBB2010	154	Humerus right	Archeria	
SABCBB2010	155	tibia	Dimetrodon	
SABCBB2010	156	femur proximal	Dimetrodon	
SABCBB2010	157	femur right	Eryops	
SABCBB2010	158	femur right	Eryops	
SABCBB2010	159	quadrate		
SABCBB2010	160	jaw	Dimetrodon	5 pieces
SABCBB2010	161	ankle bone		
SABCBB2010	162	vertebrae	Eryops	
SABCBB2010	163	humerus	Amphibian?	
SABCBB2010	164	Plant material		
SABCBB2010	165	tibia		
SABCBB2010	166	toe bone ?	Amphibian	
SABCBB2010	167	fibula		
SABCBB2010	168	vertebrae	Dimetrodon?	
SABCBB2010	169	rib bifurcated		
SABCBB2010	170	toe bone		
SABCBB2010	171	toe bone		
SABCBB2010	172	toe bone		
SABCBB2010	173	toe bone broken		
SABCBB2010	174	humerus 2 frag		
SABCBB2010	175	small toe bone		
SABCBB2010	176	femur proximal	Dimetrodon?	
SABCBB2010	177	humerus distal left frag	Dimetrodon?	
SABCBB2010	178	humerus proximal	Dimetrodon?	
SABCBB2010	179	ischium	Eryops	ID Dorota
SABCBB2010	180	Tusk	Eryops	ID Dorota
SABCBB2010	181	osteoderm	amphibian-*Archeria?*	ID Dorota
SABCBB2010	182	manus/pes	amphibian	ID Dorota
SABCBB2010	183	Femur, radius, Ulna?	amphibian	
SABCBB2010	184	Femur	Dimetrodon	Chris
SABCBB2010	185	Femur right	Dimetrodon	
SABCBB2010	186	jaw frag immerging tooth	Dimetrodon	ID & loaned: R. Reisz
SABCBB2010	187	jaw frag	Dimetrodon	ID & loaned: R. Reisz
SABCBB2010	188	jaw frag	Eryops	ID & loaned: R. Reisz
SABCBB2010	189	jaw frag	Dimetrodon	ID & loaned: R. Reisz
SABCBB2010	190	jaw frag 5 teeth	Diadectes	ID & loaned: R. Reisz
SABCBB2010	191	Neural Spine terminal	Edaphosaurus	
SABCBB2010	192	Neural Spine terminal	Edaphosaurus	
SABCBB2010	193	Nerual spine frag	Edaphosaurus	
SABCBB2010	194	bone	amphibian	
SABCBB2010	195	humerus midshaft	Dimetrodon?	

SABCBB2010	195 A	rib	Amphibian	
SABCBB2010	195B	Long bone	Amphibian	
SABCBB2011	1	femur	Amphibian	5.2cm lng
SABCBB2011	2	Jaw		160 mm iron stone
SABCBB2011	3	Femur	Pelyc	
SABCBB2011	4	femur?		85 mm Iron
SABCBB2011	5	Femur		end broke
SABCBB2011	6	Mystery		w/ small piece
SABCBB2011	7	Jaw	Archeria	195mm, Block 1
SABCBB2011	8	Fibula	Pelyc	2 piece 100mm
SABCBB2011	9	Femur	Eryops	90mm
SABCBB2011	10	Femur	Dimetrodon	65mm, LB4
SABCBB2011	11	Femur		small, LB4
SABCBB2011	12	Iron bone		w/ small LB
SABCBB2011	13	weathered Femur		Large 130mm
SABCBB2011	14	rib		Biforcated
SABCBB2011	15	Charcoal	plant	
SABCBB2011	17	humerus		
SABCBB2011	18	Charcoal		
SABCBB2011	19	tibia		LB4 back, 80mm
SABCBB2011	20	femur		70, small mystery bone
SABCBB2011	21	bone?		81mm, Below Femur 20
SABCBB2011	22	weathered longbone		w/pieces
SABCBB2011	23	Rib	Edaphosaurus	Block 2
SABCBB2011	24	hatchet head LB		65mm, 2 piece
SABCBB2011	25	weathered Femur		33mm?, S of LB 90 mm
SABCBB2011	26	rib		small, W/ condyles
SABCBB2011	27	femur		78mm
SABCBB2011	28	tibia		85mm
SABCBB2011	29	Femur		75mm
SABCBB2011	30	triangle bone		
SABCBB2011	31	neural spine	Eryops	
SABCBB2011	32	Rib/LB Frag?		
SABCBB2011	33	Spine	Edaphosaurus	
SABCBB2011	34	Humerus		Distal
SABCBB2011	35	Scapula/fibula		95mm
SABCBB2011	36	Femur	Edaphosaurus	juvenile
SABCBB2011	37	Ulna&vert		M. cent spur
SABCBB2011	38	tibia		
SABCBB2011	39	Prox femur/humerus?		
SABCBB2011	40	jaw		small

SABCBB2011	41	femur		small
SABCBB2011	42	Femur		
SABCBB2011	43	femur		small
SABCBB2011	44	Long bone	Amphibian	
SABCBB2011	45	Flat		
SABCBB2011	46	LB		small
SABCBB2011	47	NS/centrum	Secodont. or *Ophiacodon*	
SABCBB2011	48	Mystery		
SABCBB2011	49	Humerus		
SABCBB2011	50	Femur end		Prox
SABCBB2011	51	LB	Amphibian	Block 2
SABCBB2011	52	rib		Block 2
SABCBB2011	53	vert		Block 2
SABCBB2011	54	vert		Block 2
SABCBB2011	55	vert		Block 2
SABCBB2011	56	humerus	Archeria	Block 2
SABCBB2011	57	Vertebrate		Block 2
SABCBB2011	58	2 Ribs		Block 2
SABCBB2011	59	3 ribs		1 long 2 small
SABCBB2011	60	Vert		Large
SABCBB2011	61	Vert		big triangle
SABCBB2011	62	NS		Juvenile
SABCBB2011	63	LB	Edaphosaurus	small
SABCBB2011	64	Humerus	Pelyc	prox point north
SABCBB2011	65	tibia		
SABCBB2011	66	humerus	Archeria	
SABCBB2011	67	tibia		
SABCBB2011	68	humerus		
SABCBB2011	69	NS	Edaphosaurus?	
SABCBB2011	71	femur		
SABCBB2011	77	big rib		
SABCBB2011	76	2X?		
SABCBB2011	80	heteropolar Coprolite	Shark	108.5mmX39mmX20mm
SABCBB2011	73	LB		
SABCBB2011	74	Bunch O Bones		
SABCBB2011	81	tibia	Dimetrodon natalis	
SABCBB2011	82	toe bone	Caseid	overhanging articulation
SABCBB2011	83	Tibia	Dimetrodon	
SABCBB2011	84	Tibia	Dimetrodon	
SABCBB2011	85	rib frag		Float
SABCBB2011	86	rib frag		Float

SABCBB2011	87	NS	Edaphosaurus	
SABCBB2011	88	prox humerus	Ophiacodon?	
SABCBB2011	89	NS field (16 total)	Dimetrodon natalis	
SABCBB2011	184	Small femur in NS field	Dimetrodon?	looks immature
RSC3-2013	1	Radius or Scapula	pelycosaur	
RSC3-2013	2	Vertebrae	Diadectes	
RSC3-2013	3	Scapula	Eryops	quadrate, rib, misc bones assc.
RSC3-2013	4	Vertebrae	Ophiacodon	
RSC3-2013	5	Stem, echinoderm	Crinoid	
RSC3-2013	6	small mollusc shell	Pecten	
RSC3-2013	7	Ulna head	Ophiacodon?	
RSC3-2013	8	skull roof	Ectosteorhachis	
RSC3-2013	9	Skull?	?	mashed together; powder blue
RSC3-2013	10	jaw	Amph	
RSC3-2013	11	Dorsal fin spine	Ctenacanth shark	
RSC3-2013	12	large Vert.	Ophiacodon	
RSC3-2013	13	Seds	Caliche balls	"Easter Eggs"
RSC3-2013	14	Seds	mudstone	Limy with Charcoal and bone
RSC3-2013	15	Plant	Calamites	
RSC3-2013	16	Scapula	Eryops?	
RSC3-2013	17	Prox Femur	Eryops	
RSC3-2013	18	Ulna head	Dimetrodon?	
RSC3-2013	19	Ulna head	Dimetrodon	
RSC3-2013	20	coprolite	Shark	Heteropolar
RSC3-2013	21	Large skull	Trimerorachis	"Wann"
RSC3-2013	22	Medium Skull	Trimerorachis	"Fenne"
RSC3-2013	23	Small Skull	Trimerorachis	"Edina" w/ small pieces
RSC3-2013	24	Jaws	Trimerorachis	Assc. w/ Edina skull
RSC3-2013	25	Dermal, rib, IC	Trimerorachis	
RSC3-2013	26	Axial Skelton, pieces	Trimerorachis	"Toet" mummified
RSC3-2013	27	pelvis, IC	Trimerorachis	
RSC3-2013	28	Dermal, rib, IC	Trimerorachis	
RSC3-2013	29	Dermal, Femur	Trimerorachis	
RSC3-2013	30	small Dermal, IC	Trimerorachis	
RSC3-2013	31	ribs, IC	Trimerorachis	
RSC3-2013	32	Ribs, IC, Small pieces	Trimerorachis	Lot 32
RSC3-2013	33	9 broken LBs	Trimerorachis	Lot 33
RSC3-2013	34	3 scapula	Trimerorachis	Lot 34
RSC3-2013	35	Dermal	Trimerorachis	Lot 35, mummified
RSC3-2013	36	Skeleton	Fish?	A, B, and C

RSC3-2013	37	Tooth plate	Sagenodus periprion	
RSC3-2013	38	Misc Bones	Amphibian	
RSC3-2013	39	Cartilage	Shark	Sharkilage
RSC3-2013	40	Brain Case	Dimetrodon	ID by RB
RSC3-2013	41	frags	Trimerorachis insignis	Lot 41
RSC3-2013	42	zygopophysis	Diadectes	
RSC3-2013	43	Distal Humerus	Dimetrodon	
RSC3-2013	44	Misc Bones	Amphibian	day bag
RSC3-2013	45	Coporlite	shark	Heteropolar
RSC3-2013	46	Misc Bones		day bag
RSC3-2013	47	LB, Toe Bone	?	
RSC3-2013	48	Coprolite and Bone	Ophiacodon	day bag
RSC3-2013	49	Misc bones & coprolites	Eryops	
RSC3-2013	50	Misc bones & coprolites	Amph, rep, fish, Pelyc	Combined day bags, HS
RSC3-2013	51	Misc bones & coprolites	Amph, rep, fish, Pelyc	Combined day bags, PBS
RSC3-2013	52	Misc bones & coprolites	Amph, rep, fish, Pelyc	DAY 1 bag
RSC3-2013	53	Misc bones & coprolites	Amph, rep, fish, Pelyc	Combined day bags, LS
RSC3-2013	54	Misc bones & coprolites	Amph, rep, fish, Pelyc	Combined day bags, WHS
RSC3-2013	55	Misc bones & coprolites	Amph, rep, fish, Pelyc	Combined day bags, FS
RSC3-2013	56	Misc bones & coprolites	Amph, rep, fish, Pelyc	Combined day bags, FS
RSC3-2013	57	Misc bones & coprolites	Amph, rep, fish, Pelyc	Combined day bags, NTS
RSC3-2013	58	Misc bones & coprolites	Amph, rep, fish, Pelyc	Loftin BB
RSC3-2013	59	Misc bones & coprolites	Amph, rep, fish, Pelyc	Combined day bags, NTS
RSC3-2013	60	Misc bones & coprolites	Amph, rep, fish, Pelyc	Archer City BB
RSC3-2013	61	bones	Fish	KPS
RSC3-2013	62	Misc bones & coprolites	Amphibian	Combined day bags, AHS
RSC3-2013	63	Misc bones & coprolites	Misc	Combined day bags,MBB
RSC3-2013	64	Misc bones & coprolites	Misc	Combined day bags, CNS
RSC3-2013	65	Misc bones & coprolites	Misc	Combined day bags, SS
RSC3-2013	66	Misc bones & coprolites	Misc	Combined day bags

Appendix 3 (Chapter 2):
Measurements collected from all pelycosaur postcrania during this study. Morphometric data is arranged by taxon and bone.

Institution	Specimen	*Taxon*	Bone	Length	Shaft Circ.
	Number			(mm)	(mm)
FMNH	UR149	*Angelosaurus dolani*	Femur	211	133
FMNH	UR149	*Angelosaurus dolani*	Femur	213	129
FMNH	UR149	*Angelosaurus dolani*	Humerus	198	209
FMNH	UR149	*Angelosaurus dolani*	Radius	138	83
FMNH	UR149	*Angelosaurus dolani*	Tibia	150	85
FMNH	UR149	*Angelosaurus dolani*	Ulna	164	69
FMNH	UR 257	*Angelosaurus greeni*	Femur	258	128
FMNH	UR 977	*Angelosaurus romeri*	Femur	137	112
FMNH	UR 827	*Angelosaurus romeri*	Femur	163	92
FMNH	UR 904	*Angelosaurus romeri*	Femur	174	104
FMNH	UR 917	*Angelosaurus romeri*	Femur	220	117
FMNH	UR 911	*Angelosaurus romeri*	Tibia	140	80
FMNH	UC 1092	*Brachycnemus dolichomerus*	Femur	203	100
FMNH	UC 1092	*Brachycnemus dolichomerus*	Fibula	138	60
FMNH	UC 1092	*Brachycnemus dolichomerus*	Tibia	126	77
MNHN	AUT 490	*Callibrachion gaudryi*	Humerus	69	13
MNHN	AUT 490	*Callibrachion gaudryi*	Humerus	73	18
MNHN	AUT 490	*Callibrachion gaudryi*	Radius	64	10
FMNH	UC 656	*Casea broilii*	Femur	68	28
FMNH	UC 656	*Casea broilii*	Femur	74	31
FMNH	UC 656	*Casea broilii*	Fibula	65	19
FMNH	UC 656	*Casea broilii*	Humerus	81	41
FMNH	UC 656	*Casea broilii*	Radius	59	21
FMNH	UC 656	*Casea broilii*	Tibia	58	25
FMNH	UC 656	*Casea broilii*	Ulna	72	21
MNG	10552	Caseidae	Radius	64	17
MNG	10552	Caseidae	Ulna	82	18
FMNH	UR152	*Caseoides sanangerloensis*	Femur	134	100
FMNH	UR 151	*Caseoides sanangeloensis*	Humerus	154	82
FMNH	UR 151	*Caseoides sanangeloensis*	Tibia	94	54
FMNH	UR152	*Caseoides sanangerloensis*	Tibia	129	85
FMNH	UR 151	*Caseoides sanangeloensis*	Ulna	102	39
FMNH	UR 253	*Caseopsis agilis*	Femur	234	99
FMNH	UR 255	*Caseopsis agilis*	Fibula	144	55
FMNH	UR 253	*Caseopsis agilis*	Radius	116	74
FMNH	UR 255	*Caseopsis agilis*	Tibia	133	70

FMNH	UR 253	*Caseopsis agilis*	Ulna	120	66
FMNH	UC 6548	*Clepsydrops*	Femur	76	33
FMNH	UR 466	*Clepsydrops*	Fibula	51	20
UMMP	3380	*Clepsydrops*	Tibia	85	25
FMNH	UC 6551	*Clepsydrops collettii*	Femur	108	40
FMNH	UC 6575	*Clepsydrops collettii*	Humerus	92	32
FMNH	UC 6555	*Clepsydrops collettii*	Tibia	59	25
FMNH	UC 6545	*Clepsydrops vinslovii*	Humerus	38	18
FMNH	UC 6549	*Clepsydrops vinslovii*	Femur	64	27
FMNH	UR 970	*Cotylorhychus/Angelosaurus*	Fibula	168	68
FMNH	UR 835	*Cotylorhynchus bransoni*	Femur	256	116
FMNH	UR 836	*Cotylorhynchus bransoni*	Fibula	169	61
FMNH	UR 919	*Cotylorhynchus bransoni*	Humerus	237	124
FMNH	UR 837	*Cotylorhynchus bransoni*	Radius	127	72
FMNH	UR 839	*Cotylorhynchus bransoni*	Tibia	123	72
FMNH	UR 836	*Cotylorhynchus bransoni*	Tibia	155	86
FMNH	UR 1182	*Cotylorhynchus bransoni*	Tibia	158	95
FMNH	UR 881	*Cotylorhynchus bransoni*	Tibia	234	161
FMNH	UR 840	*Cotylorhynchus bransoni*	Ulna	134	56
FMNH	UR 837	*Cotylorhynchus bransoni*	Ulna	160	81
FMNH	UR 581	*Cotylorhynchus hancocki*	Femur	372	220
FMNH	UR 878	*Cotylorhynchus hancocki*	Femur	374	222
FMNH	UR 703	*Cotylorhynchus hancocki*	Femur	406	234
FMNH	UR 581	*Cotylorhynchus hancocki*	Fibula	208	110?
FMNH	UR 621	*Cotylorhynchus hancocki*	Fibula	232	115
FMNH	UR 249	*Cotylorhynchus hancocki*	Fibula	258	156
FMNH	UR 878	*Cotylorhynchus hancocki*	Fibula	265	110
FMNH	UR 571	*Cotylorhynchus hancocki*	Fibula	270	113
FMNH	UR 622	*Cotylorhynchus hancocki*	Fibula	274	104
FMNH	UR 823	*Cotylorhynchus hancocki*	Humerus	49.1	22
FMNH	UR 879	*Cotylorhynchus hancocki*	Humerus	380	193
FMNH	UR 822	*Cotylorhynchus hancocki*	Humerus	386	201
FMNH	UR 488	*Cotylorhynchus hancocki*	Humerus	403	194
FMNH	UR 622	*Cotylorhynchus hancocki*	Humerus	408	176
FMNH	UR 581	*Cotylorhynchus hancocki*	Humerus	441	216
FMNH	UR 488	*Cotylorhynchus hancocki*	Humerus	450	205
FMNH	UR 488	*Cotylorhynchus hancocki*	Humerus	450	195
FMNH	UR 154	*Cotylorhynchus hancocki*	Radius	148	136
FMNH	PR 272	*Cotylorhynchus hancocki*	Radius	163	96
FMNH	UR 585	*Cotylorhynchus hancocki*	Radius	212	144
FMNH	UR 879	*Cotylorhynchus hancocki*	Radius	227	142
FMNH	UR 571	*Cotylorhynchus hancocki*	Tibia	226	141

FMNH	UR 707	*Cotylorhynchus hancocki*	Tibia	229	135
FMNH	UR 581	*Cotylorhynchus hancocki*	Tibia	234	134
FMNH	UR 893	*Cotylorhynchus hancocki*	Tibia	244	168
FMNH	UR 622	*Cotylorhynchus hancocki*	Tibia	250	138
FMNH	UR 586	*Cotylorhynchus hancocki*	Tibia	251	141
FMNH	UR 703	*Cotylorhynchus hancocki*	Tibia	251	166
FMNH	UR 622?	*Cotylorhynchus hancocki*	Tibia	256	145
FMNH	UR 581	*Cotylorhynchus hancocki*	Tibia	309	180?
FMNH	UR 581	*Cotylorhynchus hancocki*	Ulna	230	120
FMNH	UR 581	*Cotylorhynchus hancocki*	Ulna	282	150
FMNH	UR 567	*Cotylorhynchus hancocki*	Ulna	304	148.5
FMNH	UR 623	*Cotylorhynchus hancocki*	Ulna	309	130
FMNH	UR 703	*Cotylorhynchus hancocki*	Ulna	312	157
OMNH	655	*Cotylorhynchus romeri*	Femur	350	151
OMNH	655	*Cotylorhynchus romeri*	Femur	350	145
OMNH	1728	*Cotylorhynchus romeri*	Femur	75	60
OMNH	1728	*Cotylorhynchus romeri*	Femur	75	59
OMNH	631	*Cotylorhynchus romeri*	Femur	272	119
FMNH	PR 272	*Cotylorhynchus romeri*	Femur	308	140
FMNH	PR 272	*Cotylorhynchus romeri*	Femur	312	130
FMNH	PR 272	*Cotylorhynchus romeri*	Fibula	157	68
FMNH	PR 272	*Cotylorhynchus romeri*	Fibula	178	72
OMNH	631	*Cotylorhynchus romeri*	Fibula	183	58
OMNH	655	*Cotylorhynchus romeri*	Humerus	345	N/A
OMNH	655	*Cotylorhynchus romeri*	Humerus	355	N/A
OMNH	655	*Cotylorhynchus romeri*	Humerus	320	153
OMNH	1728	*Cotylorhynchus romeri*	Humerus	76	58
OMNH	1728	*Cotylorhynchus romeri*	Humerus	78	64
MCZ	3416	*Cotylorhynchus romeri*	Humerus	210	125
OMNH	631	*Cotylorhynchus romeri*	Humerus	265	135
FMNH	PR 272	*Cotylorhynchus romeri*	Humerus	324	144
FMNH	PR 272	*Cotylorhynchus romeri*	Humerus	324	148
OMNH	631	*Cotylorhynchus romeri*	Humerus	268+	135
OMNH	655	*Cotylorhynchus romeri*	Radius	180	N/A
OMNH	655	*Cotylorhynchus romeri*	Radius	180	N/A
OMNH	655	*Cotylorhynchus romeri*	Radius	150	115
OMNH	627	*Cotylorhynchus romeri*	Radius	124	89
OMNH	627	*Cotylorhynchus romeri*	Radius	133	75
OMNH	631	*Cotylorhynchus romeri*	Radius	142	74
FMNH	PR 272	*Cotylorhynchus romeri*	Radius	142	98
FMNH	PR 272	*Cotylorhynchus romeri*	Tibia	111	115
FMNH	PR 272	*Cotylorhynchus romeri*	Tibia	128	113

OMNH	627	*Cotylorhynchus romeri*	Tibia	130	95
OMNH	631	*Cotylorhynchus romeri*	Tibia	174	88
OMNH	655	*Cotylorhynchus romeri*	Ulna	218	N/A
OMNH	655	*Cotylorhynchus romeri*	Ulna	225	N/A
OMNH	655	*Cotylorhynchus romeri*	Ulna	220	135
OMNH	627	*Cotylorhynchus romeri*	Ulna	155	79
OMNH	631	*Cotylorhynchus romeri*	Ulna	203	79
FMNH	PR 272	*Cotylorhynchus romeri*	Ulna	208	117
MCZ	3386	*Ctenospondyles ninevahensis*	Humerus	145	63
FMNH	UC 1	*Dimetrdon incisivus*	Femur	223	104
FMNH	UC 1	*Dimetrdon incisivus*	Fibula	172	32+
FMNH	UC 1	*Dimetrdon incisivus*	Humerus	174	95
FMNH	UC 1	*Dimetrdon incisivus*	Radius	158	36?
FMNH	UC 1	*Dimetrdon incisivus*	Tibia	166	36+
FMNH	UC 1	*Dimetrdon incisivus*	Ulna	240	31?
FMNH	UC 1322	*Dimetrdon Loomisi*	Femur	187	44?
FMNH	UC 1322	*Dimetrdon Loomisi*	Femur	188	57?
FMNH	UC 1322	*Dimetrdon Loomisi*	Fibula	173	19+
FMNH	UC 1322	*Dimetrdon Loomisi*	Humerus	180	56?
FMNH	UC 1322	*Dimetrdon Loomisi*	Radius	156	36+
FMNH	UC 1322	*Dimetrdon Loomisi*	Tibia	166	34+
FMNH	UC 1322	*Dimetrdon Loomisi*	Ulna	172	24+
UMMP	22219	*Dimetrodon*	Femur	61	23
UMMP	22219	*Dimetrodon*	Femur	68	28
UMMP	22219	*Dimetrodon*	Femur	72	28
UMMP	22219	*Dimetrodon*	Femur	77	38
IPBSH	59	*Dimetrodon*	Femur	80	34
UMMP	22219	*Dimetrodon*	Femur	80	36
IPBSH	60	*Dimetrodon*	Femur	103	35
UMMP	38547	*Dimetrodon*	Femur	112	61
UMMP	22217	*Dimetrodon*	Femur	115	37
IPBSH	103	*Dimetrodon*	Femur	116	48
IPBSH	102	*Dimetrodon*	Femur	117	56
UMMP	22972	*Dimetrodon*	Femur	117	48
IPBSH	21	*Dimetrodon*	Femur	120	36
UMMP	22974	*Dimetrodon*	Femur	124	48*
IPBSH	61	*Dimetrodon*	Femur	126	45
UMMP	3392	*Dimetrodon*	Femur	132	52
UMMP	22973	*Dimetrodon*	Femur	135	45
UMMP	22976	*Dimetrodon*	Femur	140	58
UMMP	3393	*Dimetrodon*	Femur	144	57
YPM	6304	*Dimetrodon*	Femur	153.6	67

IPBSH	119	*Dimetrodon*	Femur	176	70
IPBSH	45	*Dimetrodon*	Femur	195	91
UMMP	22976	*Dimetrodon*	Femur	125+	45
IPBSH	99	*Dimetrodon*	Femur	50+	30
IPBSH	98	*Dimetrodon*	Femur	56+	27
IPBSH	96	*Dimetrodon*	Femur	81+	47
FMNH	UC 1306	*Dimetrodon*	Femur	16.3	25
FMNH	UC 586	*Dimetrodon*	Femur	31	13
FMNH	UC 1310	*Dimetrodon*	Femur	50	23
FMNH	UR 686	*Dimetrodon*	Femur	54	24
FMNH	UC 1309	*Dimetrodon*	Femur	55	23
FMNH	UC1294	*Dimetrodon*	Femur	60.3	26
IPBSH	105	*Dimetrodon*	Femur	80	48
MCZ	6420	*Dimetrodon*	Femur	80	37
FMNH	UC 55	*Dimetrodon*	Femur	85	33
FMNH	UC 1284	*Dimetrodon*	Femur	87	42
FMNH	UC 1282	*Dimetrodon*	Femur	88	44
FMNH	UC 57	*Dimetrodon*	Femur	88	34
FMNH	UC 1301	*Dimetrodon*	Femur	97	53
MCZ	2905?	*Dimetrodon*	Femur	103	52
MCZ	6336	*Dimetrodon*	Femur	108	50
FMNH	UC 1283	*Dimetrodon*	Femur	108	38
FMNH	UR 691	*Dimetrodon*	Femur	109	43
FMNH	UC 753	*Dimetrodon*	Femur	113	54
MCZ	6336	*Dimetrodon*	Femur	117	50
FMNH	UC 1153	*Dimetrodon*	Femur	130	52
MCZ	6465	*Dimetrodon*	Femur	154	80
MCZ	2878	*Dimetrodon*	Femur	170	80
MCZ	5979	*Dimetrodon*	Femur	176	72
FMNH	P12762	*Dimetrodon*	Femur	178	83
MCZ	1369	*Dimetrodon*	Femur	180	78
MCZ	6164	*Dimetrodon*	Femur	183	82
MCZ	6447	*Dimetrodon*	Femur	194	84
FMNH	UC 1174	*Dimetrodon*	Femur	196	84
MCZ	5979	*Dimetrodon*	Femur	197	87
MCZ	3261	*Dimetrodon*	Femur	225	106
FMNH	UC 49	*Dimetrodon*	Femur	225	94
MCZ	3201	*Dimetrodon*	Femur	230	98
MCZ	3261	*Dimetrodon*	Femur	240	100
MCZ	3261	*Dimetrodon*	Femur	250	125
MCZ	3261	*Dimetrodon*	Femur	255	134
MCZ	1737-3	*Dimetrodon*	Femur	270	111

IPBSH	41	*Dimetrodon*	Femur	69	27
IPBSH	8	*Dimetrodon*	Femur	180	96
UMMP	22985	*Dimetrodon*	Fibula	67	20
UMMP	22985	*Dimetrodon*	Fibula	76	21
UMMP	3375	*Dimetrodon*	Fibula	77	23
IPBSH	150	*Dimetrodon*	Fibula	99	23
UMMP	3376	*Dimetrodon*	Fibula	114	27
UMMP	23046	*Dimetrodon*	Fibula	120	27
FMNH	UC 1299	*Dimetrodon*	Fibula	63.2	19
FMNH	UC 1280	*Dimetrodon*	Fibula	84.5	24
FMNH	UC 780	*Dimetrodon*	Fibula	148	40
MCZ	1737-1	*Dimetrodon*	Fibula	149	54
OMNH	15078	*Dimetrodon*	Fibula	206	58
IPBSH	54	*Dimetrodon*	Fibula	37+	N/A
IPBSH	55	*Dimetrodon*	Fibula	47+	N/A
UMMP	22220	*Dimetrodon*	Humerus	51	18
UMMP	22220	*Dimetrodon*	Humerus	57	26
UMMP	22220	*Dimetrodon*	Humerus	60	27
UMMP	22220	*Dimetrodon*	Humerus	61	32
UMMP	22220	*Dimetrodon*	Humerus	63	27
UMMP	22220	*Dimetrodon*	Humerus	64	31
IPBSH	57	*Dimetrodon*	Humerus	64.3	35
UMMP	22220	*Dimetrodon*	Humerus	65	28
UMMP	22220	*Dimetrodon*	Humerus	69	34
UMMP	22220	*Dimetrodon*	Humerus	72	38
IPBSH	58	*Dimetrodon*	Humerus	73	25
UMMP	22236	*Dimetrodon*	Humerus	82	36
UMMP	22236	*Dimetrodon*	Humerus	94	32
UMMP	22236	*Dimetrodon*	Humerus	98	35
UMMP	22236	*Dimetrodon*	Humerus	104	39
UMMP	22236	*Dimetrodon*	Humerus	110	40
UMMP	22236	*Dimetrodon*	Humerus	113	39
UMMP	22236	*Dimetrodon*	Humerus	115	38
UMMP	3367	*Dimetrodon*	Humerus	116	39
UMMP	22236	*Dimetrodon*	Humerus	118	43
UMMP	3373	*Dimetrodon*	Humerus	119	43
UMMP	22236	*Dimetrodon*	Humerus	120	35
UMMP	67586	*Dimetrodon*	Humerus	120	49
UMMP	22236	*Dimetrodon*	Humerus	122	45
UMMP	22976	*Dimetrodon*	Humerus	122	50
UMMP	3360	*Dimetrodon*	Humerus	123	43
UMMP	67586	*Dimetrodon*	Humerus	124	52

UMMP	3359	*Dimetrodon*	Humerus	125	42
UMMP	22236	*Dimetrodon*	Humerus	126	47?
UMMP	22976	*Dimetrodon*	Humerus	126	46
UMMP	22236	*Dimetrodon*	Humerus	130	50
UMMP	22236	*Dimetrodon*	Humerus	131	46
UMMP	67586	*Dimetrodon*	Humerus	131	48
UMMP	22236	*Dimetrodon*	Humerus	132	47
UMMP	22236	*Dimetrodon*	Humerus	145	56
UMMP	3049	*Dimetrodon*	Humerus	170	100
UMMP	23056	*Dimetrodon*	Humerus	184	84
UMMP	67586	*Dimetrodon*	Humerus	110+	46
IPBSH	97	*Dimetrodon*	Humerus	26+	30
FMNH	UC 1300	*Dimetrodon*	Humerus	37.3	17
FMNH	UC 1293	*Dimetrodon*	Humerus	47.1	20
FMNH	UC 758	*Dimetrodon*	Humerus	50	23
FMNH	UC 1203	*Dimetrodon*	Humerus	54	24
FMNH	UC 758	*Dimetrodon*	Humerus	59	26
FMNH	UC 758	*Dimetrodon*	Humerus	65	31
FMNH	UC 758	*Dimetrodon*	Humerus	76	32
FMNH	UC 1305	*Dimetrodon*	Humerus	83	42
FMNH	UC 756	*Dimetrodon*	Humerus	89	48
FMNH	UC 756	*Dimetrodon*	Humerus	90	49
FMNH	UC 1304	*Dimetrodon*	Humerus	101	55
FMNH	UC 414	*Dimetrodon*	Humerus	112	48
MCZ	6154	*Dimetrodon*	Humerus	116	54
FMNH	UC 756	*Dimetrodon*	Humerus	131	53
MCZ	5964	*Dimetrodon*	Humerus	136	58
MCZ	2915	*Dimetrodon*	Humerus	160	68
MCZ	7074	*Dimetrodon*	Humerus	168	67
MCZ	5779	*Dimetrodon*	Humerus	177	84
MCZ	3222	*Dimetrodon*	Humerus	184	95
FMNH	P 12761	*Dimetrodon*	Humerus	190	72
OMNH	35201	*Dimetrodon*	Humerus	197	109
OMNH	1727	*Dimetrodon*	Humerus	204	104
OMNH	53542	*Dimetrodon*	Humerus	204	102
OMNH	1727	*Dimetrodon*	Humerus	209	103
IPBSH	110	*Dimetrodon*	Humerus	21+	27
UMMP	22978	*Dimetrodon*	Humerus	109	43
UMMP	22978	*Dimetrodon*	Humerus	95+	49
UMMP	22985	*Dimetrodon*	Radius	83	21
IPBSH	146	*Dimetrodon*	Radius	96	28
UMMP	23197	*Dimetrodon*	Radius	98	22

IPBSH	144	*Dimetrodon*	Radius	105	32
UMMP	3348	*Dimetrodon*	Radius	110	30
UMMP	3048	*Dimetrodon*	Radius	115	32
UMMP	3378	*Dimetrodon*	Radius	115	29
UMMP	23046	*Dimetrodon*	Radius	118	34
UMMP	3379	*Dimetrodon*	Radius	125	43
UMMP	23058	*Dimetrodon*	Radius	152	51
IPBSH	20	*Dimetrodon*	Radius	73+	37+
FMNH	UC 1292	*Dimetrodon*	Radius	50	23
FMNH	UC 1297	*Dimetrodon*	Radius	52	15
IPBSH	107	*Dimetrodon*	Radius	66	18
FMNH	UC 1298	*Dimetrodon*	Radius	67.5	17
FMNH	UC 1095	*Dimetrodon*	Radius	87	42
FMNH	UC 683	*Dimetrodon*	Radius	111	28
FMNH	UC 795	*Dimetrodon*	Radius	116	33
MCZ	No Number	*Dimetrodon*	Radius	137	50
FMNH	UC 599	*Dimetrodon*	Radius	143	37
MCZ	3222	*Dimetrodon*	Radius	148	54
OMNH	1727	*Dimetrodon*	Radius	168	62
OMNH	15078	*Dimetrodon*	Radius	185	60
IPBSH	147	*Dimetrodon*	Tibia	72	27
IPBSH	148	*Dimetrodon*	Tibia	72	25
IPBSH	151	*Dimetrodon*	Tibia	78	30
UMMP	22217	*Dimetrodon*	Tibia	80	23
IPBSH	149	*Dimetrodon*	Tibia	87	25
IPBSH	152	*Dimetrodon*	Tibia	87	32
UMMP	22217	*Dimetrodon*	Tibia	88	38
UMMP	3353	*Dimetrodon*	Tibia	89	31
UMMP	3365	*Dimetrodon*	Tibia	91	26
UMMP	3377	*Dimetrodon*	Tibia	104	32
IPBSH	145	*Dimetrodon*	Tibia	107	31
UMMP	23046	*Dimetrodon*	Tibia	115	34
UMMP	23057	*Dimetrodon*	Tibia	156	60
IPBSH	53	*Dimetrodon*	Tibia	137+	N/A
FMNH	UC 1302	*Dimetrodon*	Tibia	32.5	12
FMNH	UC 573	*Dimetrodon*	Tibia	40	15
FMNH	UR 686	*Dimetrodon*	Tibia	48	21
FMNH	UC 1296	*Dimetrodon*	Tibia	51	18
FMNH	UC 575	*Dimetrodon*	Tibia	53	22
FMNH	UC 758	*Dimetrodon*	Tibia	56	31
FMNH	UC 1303	*Dimetrodon*	Tibia	57.1	20
FMNH	UC 532	*Dimetrodon*	Tibia	58	18

FMNH	UC 756	*Dimetrodon*	Tibia	58	42
FMNH	UC 1295	*Dimetrodon*	Tibia	64.8	21
FMNH	UC 105	*Dimetrodon*	Tibia	66	25
FMNH	UC 111	*Dimetrodon*	Tibia	67	26
FMNH	UC 758	*Dimetrodon*	Tibia	72	31
FMNH	UC 135	*Dimetrodon*	Tibia	77	24
FMNH	UC 1279	*Dimetrodon*	Tibia	82	33
FMNH	UC 756	*Dimetrodon*	Tibia	82	38
FMNH	UC 522	*Dimetrodon*	Tibia	87	31
FMNH	UC 756	*Dimetrodon*	Tibia	88	47
FMNH	UC 756	*Dimetrodon*	Tibia	92	56
FMNH	UC 756	*Dimetrodon*	Tibia	92	50
OMNH	15047	*Dimetrodon*	Tibia	93	40
FMNH	UC 535	*Dimetrodon*	Tibia	98	33
FMNH	UC 524	*Dimetrodon*	Tibia	109	35
FMNH	UC 18	*Dimetrodon*	Tibia	133	53
IPBSH	18	*Dimetrodon*	Tibia	152	60
YPM	6301	*Dimetrodon*	Tibia	160	54
MCZ	1737-2	*Dimetrodon*	Tibia	190	73
OMNH	15078	*Dimetrodon*	Tibia	207	64
UMMP	22984	*Dimetrodon*	Ulna	101	20
UMMP	3369	*Dimetrodon*	Ulna	118	25
FMNH	UC 507	*Dimetrodon*	Ulna	107	30
FMNH	UC 683	*Dimetrodon*	Ulna	112	26
FMNH	UC 566	*Dimetrodon*	Ulna	171	38
OMNH	15078	*Dimetrodon*	Ulna	215	63
FMNH	UR 362	*Dimetrodon angelensis*	Ulna	285	78
MCZ	5110	*Dimetrodon booneorum*	Femur	82	38
MCZ	5985	*Dimetrodon booneorum*	Femur	90	49
MCZ	5354	*Dimetrodon booneorum*	Femur	94	39
MCZ	5110	*Dimetrodon booneorum*	Femur	99	56
MCZ	3176	*Dimetrodon booneorum*	Femur	100	42
MCZ	3176	*Dimetrodon booneorum*	Femur	100	49
MCZ	5110	*Dimetrodon booneorum*	Femur	100	43
MCZ	6084	*Dimetrodon booneorum*	Femur	106	58
MCZ	2914	*Dimetrodon booneorum*	Femur	118	50
FMNH	UC 875	*Dimetrodon booneorum*	Femur	118	63
MCZ	2914	*Dimetrodon booneorum*	Femur	125	52
MCZ	3226	*Dimetrodon booneorum*	Femur	126	50
MCZ	6087	*Dimetrodon booneorum*	Femur	126	57
MCZ	2860	*Dimetrodon booneorum*	Femur	127	55
MCZ	1312	*Dimetrodon booneorum*	Femur	130	72

MCZ	5617a	*Dimetrodon booneorum*	Femur	130	50
MCZ	5709	*Dimetrodon booneorum*	Femur	132	53
MCZ	6061	*Dimetrodon booneorum*	Femur	132	60
FMNH	UC 788	*Dimetrodon booneorum*	Femur	135.8	49
MCZ	8691	*Dimetrodon booneorum*	Femur	137	57
MCZ	1312	*Dimetrodon booneorum*	Femur	140	50
MCZ	5943	*Dimetrodon booneorum*	Femur	140	56
MCZ	6093	*Dimetrodon booneorum*	Femur	140	55
MCZ	8692	*Dimetrodon booneorum*	Femur	140	54
MCZ	5617	*Dimetrodon booneorum*	Femur	141	54
FMNH	UC 131	*Dimetrodon booneorum*	Femur	141	54
MCZ	5617	*Dimetrodon booneorum*	Femur	143	54
FMNH	UC 91	*Dimetrodon booneorum*	Femur	143	58
FMNH	UR 663	*Dimetrodon booneorum*	Femur	143	65
FMNH	UC 835	*Dimetrodon booneorum*	Femur	144	69
MCZ	5107	*Dimetrodon booneorum*	Femur	145	58
MCZ	5110	*Dimetrodon booneorum*	Femur	145	51
MCZ	5107	*Dimetrodon booneorum*	Femur	146	60
FMNH	UC 835	*Dimetrodon booneorum*	Femur	146	49
MCZ	8691	*Dimetrodon booneorum*	Femur	147	66
MCZ	1310	*Dimetrodon booneorum*	Femur	148	68
FMNH	UC 120	*Dimetrodon booneorum*	Femur	148	57
MCZ	5110	*Dimetrodon booneorum*	Femur	150	70
MCZ	5107	*Dimetrodon booneorum*	Femur	160	80?
MCZ	5107	*Dimetrodon booneorum*	Femur	160	64
FMNH	UC 1135	*Dimetrodon booneorum*	Femur	163	72
FMNH	UC 202	*Dimetrodon booneorum*	Femur	165	66
MCZ	7031	*Dimetrodon booneorum*	Femur	166	70
MCZ	5107	*Dimetrodon booneorum*	Femur	168	70
MCZ	1551	*Dimetrodon booneorum*	Femur	170	69
MCZ	2899	*Dimetrodon booneorum*	Femur	177	66
MCZ	3176	*Dimetrodon booneorum*	Fibula	105	40
FMNH	UC 68	*Dimetrodon booneorum*	Fibula	122	27
MCZ	5123	*Dimetrodon booneorum*	Fibula	131	42
MCZ	5123	*Dimetrodon booneorum*	Fibula	138	37
MCZ	5123	*Dimetrodon booneorum*	Fibula	152	40
FMNH	UC 821	*Dimetrodon booneorum*	Fibula	166	43
MCZ	7002	*Dimetrodon booneorum*	Humerus	71	33
MCZ	3176	*Dimetrodon booneorum*	Humerus	90	46
MCZ	3176	*Dimetrodon booneorum*	Humerus	95	40
MCZ	3176	*Dimetrodon booneorum*	Humerus	99	39
MCZ	6062	*Dimetrodon booneorum*	Humerus	112	44

FMNH	UC 75	*Dimetrodon booneorum*	Humerus	115	47
FMNH	UC 816	*Dimetrodon booneorum*	Humerus	115	45
FMNH	UC 816	*Dimetrodon booneorum*	Humerus	115	54
FMNH	UC 816	*Dimetrodon booneorum*	Humerus	116	47
MCZ	7003	*Dimetrodon booneorum*	Humerus	117	50
FMNH	UC 816	*Dimetrodon booneorum*	Humerus	117	51
MCZ	5423	*Dimetrodon booneorum*	Humerus	121	48
MCZ	5998	*Dimetrodon booneorum*	Humerus	121	45
MCZ	7033	*Dimetrodon booneorum*	Humerus	121	50
MCZ	5515	*Dimetrodon booneorum*	Humerus	122	51
FMNH	UC 816	*Dimetrodon booneorum*	Humerus	124	53
FMNH	UC 816	*Dimetrodon booneorum*	Humerus	125	58
MCZ	7004	*Dimetrodon booneorum*	Humerus	128	50
FMNH	UC 816	*Dimetrodon booneorum*	Humerus	130	57
FMNH	UC 247	*Dimetrodon booneorum*	Humerus	131	56
MCZ	6340	*Dimetrodon booneorum*	Humerus	134	55
MCZ	7035	*Dimetrodon booneorum*	Humerus	134	48
MCZ	1930	*Dimetrodon booneorum*	Humerus	135	58
MCZ	2888	*Dimetrodon booneorum*	Humerus	135	56
MCZ	1392	*Dimetrodon booneorum*	Humerus	137	60
MCZ	5043	*Dimetrodon booneorum*	Humerus	140	70
MCZ	1304	*Dimetrodon booneorum*	Humerus	141	60
MCZ	5022	*Dimetrodon booneorum*	Humerus	145	70
MCZ	5510	*Dimetrodon booneorum*	Humerus	149	63
MCZ	1537	*Dimetrodon booneorum*	Humerus	151	72
MCZ	2918	*Dimetrodon booneorum*	Humerus	151	63
FMNH	UC 844	*Dimetrodon booneorum*	Humerus	151	69
FMNH	UC 552	*Dimetrodon booneorum*	Humerus	154	53
MCZ	5043	*Dimetrodon booneorum*	Humerus	155	75
FMNH	UC 816	*Dimetrodon booneorum*	Humerus	158	79
MCZ	1537	*Dimetrodon booneorum*	Humerus	162	74
FMNH	UC 819	*Dimetrodon booneorum*	Radius	66.5	20
MCZ	3176	*Dimetrodon booneorum*	Radius	85	27
FMNH	UC 819	*Dimetrodon booneorum*	Radius	88	30
MCZ	3176	*Dimetrodon booneorum*	Radius	89	28
FMNH	UC 819	*Dimetrodon booneorum*	Radius	96	31
FMNH	UC 819	*Dimetrodon booneorum*	Radius	108	26
MCZ	1302	*Dimetrodon booneorum*	Radius	109	35
MCZ	5628	*Dimetrodon booneorum*	Radius	113	33
FMNH	UC 819	*Dimetrodon booneorum*	Radius	117	40
MCZ	5628	*Dimetrodon booneorum*	Radius	121	33
MCZ	5063	*Dimetrodon booneorum*	Radius	126	40

MCZ	No Number	*Dimetrodon booneorum*	Radius	128	40
MCZ	5628	*Dimetrodon booneorum*	Radius	131	43
FMNH	UC 819	*Dimetrodon booneorum*	Radius	147	54
FMNH	UC 819	*Dimetrodon booneorum*	Radius	154	52
MCZ	3176	*Dimetrodon booneorum*	Tibia	80	n/a
FMNH	UC 821	*Dimetrodon booneorum*	Tibia	104	35
FMNH	UC 126	*Dimetrodon booneorum*	Tibia	112	36
FMNH	UC 514	*Dimetrodon booneorum*	Tibia	112	44
FMNH	UC 61	*Dimetrodon booneorum*	Tibia	116	39
MCZ	5882	*Dimetrodon booneorum*	Tibia	123	41
MCZ	5452	*Dimetrodon booneorum*	Tibia	124	44
MCZ	5116	*Dimetrodon booneorum*	Tibia	125	44
MCZ	6212	*Dimetrodon booneorum*	Tibia	125	45
MCZ	5116	*Dimetrodon booneorum*	Tibia	129	50
MCZ	5116	*Dimetrodon booneorum*	Tibia	132	54
MCZ	5116	*Dimetrodon booneorum*	Tibia	134	52
MCZ	5116	*Dimetrodon booneorum*	Tibia	136	50
MCZ	5116	*Dimetrodon booneorum*	Tibia	146	52
FMNH	UC 819	*Dimetrodon booneorum*	Ulna	59	29
MCZ	8449	*Dimetrodon booneorum*	Ulna	77	40
MCZ	5724	*Dimetrodon booneorum*	Ulna	124	29
FMNH	UC 819	*Dimetrodon booneorum*	Ulna	125	33
FMNH	UC 821	*Dimetrodon booneorum*	Ulna	125	34
MCZ	3184	*Dimetrodon booneorum*	Ulna	137	31
MCZ	5369	*Dimetrodon booneorum*	Ulna	139	34
MCZ	5369	*Dimetrodon booneorum*	Ulna	144	42
MCZ	5052	*Dimetrodon booneorum*	Ulna	164	50
FMNH	UC 819	*Dimetrodon booneorum*	Ulna	166	48
MCZ	1319	*Dimetrodon booneorum*	Ulna	167	36
MCZ	5052	*Dimetrodon booneorum*	Ulna	171	47
MCZ	5052	*Dimetrodon booneorum*	Ulna	172	51
MCZ	5052	*Dimetrodon booneorum*	Ulna	176	56
MCZ	1917	*Dimetrodon crozier*	Fibula	92	24
MCZ	1917	*Dimetrodon crozier*	Fibula	93	23
MCZ	1917	*Dimetrodon crozier*	Humerus	106	40
MCZ	1917	*Dimetrodon crozier*	Humerus	107	40
MCZ	1917	*Dimetrodon crozier*	Radius	85	25
MCZ	1917	*Dimetrodon crozier*	Radius	85	25
MCZ	2872	*Dimetrodon dollovianus*	Femur	180	105
AMNH	4057	*Dimetrodon dollovianus*	Femur	213	92
AMNH	4064	*Dimetrodon dollovianus*	Femur	240	98
AMNH	4057	*Dimetrodon dollovianus*	Fibula	183	46

AMNH	4057	*Dimetrodon dollovianus*	Radius	170	59
FMNH	UC 1201	*Dimetrodon dollovianus*	Radius	184	54
AMNH	4057	*Dimetrodon dollovianus*	Tibia	182	58
AMNH	4057	*Dimetrodon dollovianus*	Tibia	186	62
AMNH	4057	*Dimetrodon dollovianus*	Ulna	214	58
FMNH	UC 1201	*Dimetrodon dollovianus*	Ulna	N/A	58
TMM	30966-291	*Dimetrodon giganhomogenes*	Femur	124	45
TMM	30966-201	*Dimetrodon giganhomogenes*	Femur	142	59
TMM	30966-270	*Dimetrodon giganhomogenes*	Femur	191	85
FMNH	UR 36	*Dimetrodon giganhomogenes*	Femur	203	84
TMM	30966-276	*Dimetrodon giganhomogenes*	Femur	210	91
TMM	30966-186	*Dimetrodon giganhomogenes*	Femur	219	108
MCZ	1283	*Dimetrodon giganhomogenes*	Femur	220	108
TMM	30966-49	*Dimetrodon giganhomogenes*	Femur	221	103
FMNH	UR 33	*Dimetrodon giganhomogenes*	Femur	230	91
FMNH	UR 208	*Dimetrodon giganhomogenes*	Femur	260	117
OMNH	15044	*Dimetrodon giganhomogenes*	Femur	81	38
MCZ	2898	*Dimetrodon giganhomogenes*	Fibula	153	40
MCZ	1283	*Dimetrodon giganhomogenes*	Fibula	210	45
FMNH	UC 1134	*Dimetrodon giganhomogenes*	Fibula	225	63
MCZ	1283	*Dimetrodon giganhomogenes*	Humerus	204	95
AMNH	4145	*Dimetrodon giganhomogenes*	Humerus	208	94
AMNH	4145	*Dimetrodon giganhomogenes*	Humerus	209	196
MCZ	1283	*Dimetrodon giganhomogenes*	Humerus	214	92
AMNH	4037A	*Dimetrodon giganhomogenes*	Humerus	218	102
AMNH	4145	*Dimetrodon giganhomogenes*	Radius	74	64
FMNH	UC 1134	*Dimetrodon giganhomogenes*	Radius	184	66
MCZ	1283	*Dimetrodon giganhomogenes*	Tibia	197	70
MCZ	1283	*Dimetrodon giganhomogenes*	Tibia	209	80
AMNH	4145	*Dimetrodon giganhomogenes*	Ulna	202	58
FMNH	UC 1134	*Dimetrodon giganhomogenes*	Ulna	213	62
UMMP	3410	*Dimetrodon gigas*	Femur	229	112
UMMP	10148	*Dimetrodon gigas*	Femur	239	114
YPM	3267	*Dimetrodon gigas*	Femur	270	40
OMNH	590	*Dimetrodon grandis*	Femur	215	80
AMNH	21117	*Dimetrodon grandis*	Femur	218	120
FMNH	UR 694	*Dimetrodon grandis*	Femur	219	106
AMNH	21095	*Dimetrodon grandis*	Femur	235	100
MCZ	1118	*Dimetrodon grandis*	Femur	240	123
MCZ	1969	*Dimetrodon grandis*	Femur	248	120
FMNH	UC 1002	*Dimetrodon grandis*	Femur	256	100
AMNH	21116	*Dimetrodon grandis*	Femur	262	136

AMNH	21122	*Dimetrodon grandis*	Femur	278	145
AMNH	21122	*Dimetrodon grandis*	Fibula	156	59
FMNH	UC 1002	*Dimetrodon grandis*	Fibula	199	59
AMNH	21235	*Dimetrodon grandis*	Fibula	210	51
FMNH	UC 1002	*Dimetrodon grandis*	Humerus	209	130
AMNH	21122	*Dimetrodon grandis*	Humerus	226	120
OMNH	590	*Dimetrodon grandis*	Humerus	235	120
AMNH	21116	*Dimetrodon grandis*	Humerus	239	104
AMNH	21116	*Dimetrodon grandis*	Humerus	240	114
FMNH	UC 1136	*Dimetrodon grandis*	Humerus	253	131
FMNH	UC 1131	*Dimetrodon grandis*	Tibia	182	87
AMNH	21122	*Dimetrodon grandis*	Tibia	191	76
AMNH	21254	*Dimetrodon grandis*	Tibia	194	91
FMNH	UC 1002	*Dimetrodon grandis*	Tibia	196	85
FMNH	UC 779	*Dimetrodon grandis*	Tibia	203	97
UMMP	22235	*Dimetrodon incisivus*	Femur	145	65
UMMP	22235	*Dimetrodon incisivus*	Femur	147	70
UMMP	22235	*Dimetrodon incisivus*	Femur	148	58
UMMP	22235	*Dimetrodon incisivus*	Femur	150	60
UMMP	22235	*Dimetrodon incisivus*	Femur	153	68
UMMP	55037	*Dimetrodon incisivus*	Femur	159	77
UMMP	22235	*Dimetrodon incisivus*	Femur	161	62
UMMP	3383	*Dimetrodon incisivus*	Femur	184	96
UMMP	55037	*Dimetrodon incisivus*	Femur	185	84
UMMP	3401	*Dimetrodon incisivus*	Femur	200	90
UMMP	3349	*Dimetrodon incisivus*	Fibula	152	57
UMMP	9767	*Dimetrodon incisivus*	Fibula	169	38
UMMP	55037	*Dimetrodon incisivus*	Fibula	170	40
MCZ	5732	*Dimetrodon incisivus*	Humerus	152	66
UMMP	9765	*Dimetrodon incisivus*	Humerus	156	76
MCZ	6905	*Dimetrodon incisivus*	Humerus	159	76
MCZ	1572	*Dimetrodon incisivus*	Humerus	160	82
UMMP	16148	*Dimetrodon incisivus*	Humerus	203	90
UMMP	16350	*Dimetrodon incisivus*	Radius	139	46
UMMP	10614	*Dimetrodon incisivus*	Radius	145	61+
UMMP	55037	*Dimetrodon incisivus*	Radius	157	57
UMMP	3390	*Dimetrodon incisivus*	Radius	164	43
UMMP	9766	*Dimetrodon incisivus*	Tibia	153	57
UMMP	3046	*Dimetrodon incisivus*	Tibia	154	58
UMMP	55037	*Dimetrodon incisivus*	Tibia	158	60
UMMP	16350	*Dimetrodon incisivus*	Ulna	197	55
UMMP	55037	*Dimetrodon incisivus*	Ulna	199	57

AMNH	24725	*Dimetrodon kempae*	Humerus	52	34
AMNH	24724	*Dimetrodon kempae*	Humerus	54	34
FMNH	UC 1139	*Dimetrodon kempae*	Humerus	121	48
MCZ	1361	*Dimetrodon kempae*	Humerus	130	47
MCZ	3227	*Dimetrodon limbatus*	Femur	122	58
MCZ	5619	*Dimetrodon limbatus*	Femur	130	62
MCZ	5665	*Dimetrodon limbatus*	Femur	146	66
MCZ	5619	*Dimetrodon limbatus*	Femur	152	63
MCZ	2867	*Dimetrodon limbatus*	Femur	158	78
MCZ	7008	*Dimetrodon limbatus*	Femur	167	80
AMNH	25750	*Dimetrodon limbatus*	Femur	168	133
MCZ	1315	*Dimetrodon limbatus*	Femur	169	71
MCZ	5665	*Dimetrodon limbatus*	Femur	170	85
MCZ	5691	*Dimetrodon limbatus*	Femur	170	79
MCZ	7008	*Dimetrodon limbatus*	Femur	171	84
FMNH	UC 857	*Dimetrodon limbatus*	Femur	172	81
MCZ	2863	*Dimetrodon limbatus*	Femur	178	75
MCZ	5106	*Dimetrodon limbatus*	Femur	185	100
FMNH	UR 671	*Dimetrodon limbatus*	Femur	185	77
MCZ	3311	*Dimetrodon limbatus*	Femur	186	84
MCZ	2937	*Dimetrodon limbatus*	Femur	187	81
MCZ	6003	*Dimetrodon limbatus*	Femur	187	82
MCZ	1108	*Dimetrodon limbatus*	Femur	188	80
FMNH	UC 787	*Dimetrodon limbatus*	Femur	188	77
MCZ	1726	*Dimetrodon limbatus*	Femur	190	~88
MCZ	5829	*Dimetrodon limbatus*	Femur	190	76
MCZ	6165	*Dimetrodon limbatus*	Femur	190	81
MCZ	6230	*Dimetrodon limbatus*	Femur	190	87
MCZ	5828	*Dimetrodon limbatus*	Femur	191	93
MCZ	3292	*Dimetrodon limbatus*	Femur	193	80
AMNH	4101	*Dimetrodon limbatus*	Femur	195	91
FMNH	UR 665	*Dimetrodon limbatus*	Femur	196	81
FMNH	UC 857	*Dimetrodon limbatus*	Femur	197	82
MCZ	3171	*Dimetrodon limbatus*	Femur	198	85
MCZ	1916	*Dimetrodon limbatus*	Femur	200	85
MCZ	3198	*Dimetrodon limbatus*	Femur	201	106
FMNH	UC 857	*Dimetrodon limbatus*	Femur	201	100
FMNH	UR 672	*Dimetrodon limbatus*	Femur	201	82
MCZ	3358	*Dimetrodon limbatus*	Femur	202	100
MCZ	1123	*Dimetrodon limbatus*	Femur	205	90
MCZ	2891	*Dimetrodon limbatus*	Femur	205	95
MCZ	5106	*Dimetrodon limbatus*	Femur	206	96

MCZ	6229	*Dimetrodon limbatus*	Femur	209	90
MCZ	6072	*Dimetrodon limbatus*	Femur	211	96
MCZ	2894	*Dimetrodon limbatus*	Femur	213	125
MCZ	1332	*Dimetrodon limbatus*	Femur	220	100
MCZ	2886	*Dimetrodon limbatus*	Femur	220	107
OMNH	TMM 30966-356	*Dimetrodon limbatus*	Femur	225	101
AMNH	4054	*Dimetrodon limbatus*	Femur	264	119
MCZ	6237	*Dimetrodon limbatus*	Femur	129	69
MCZ	6237	*Dimetrodon limbatus*	Femur	136	67
MCZ	5371	*Dimetrodon limbatus*	Fibula	130	40
DMNH	11905	*Dimetrodon limbatus*	Fibula	132.7	50
MCZ	6474	*Dimetrodon limbatus*	Fibula	137	33
MCZ	5981	*Dimetrodon limbatus*	Fibula	148	42
FMNH	UR 662	*Dimetrodon limbatus*	Fibula	165	48
MCZ	6099	*Dimetrodon limbatus*	Fibula	168	48
MCZ	5124	*Dimetrodon limbatus*	Fibula	170	50
MCZ	3426	*Dimetrodon limbatus*	Fibula	180	49
OMNH	TMM 30966-356	*Dimetrodon limbatus*	Fibula	184	51
MCZ	2936	*Dimetrodon limbatus*	Fibula	210	54
MCZ	5034	*Dimetrodon limbatus*	Humerus	42	19
MCZ	6544	*Dimetrodon limbatus*	Humerus	72	37
MCZ	5937	*Dimetrodon limbatus*	Humerus	94	53
DMNH	12149	*Dimetrodon limbatus*	Humerus	113.4	52
MCZ	5045	*Dimetrodon limbatus*	Humerus	138	67
MCZ	6097	*Dimetrodon limbatus*	Humerus	150	76
MCZ	1908	*Dimetrodon limbatus*	Humerus	152	69
MCZ	5040	*Dimetrodon limbatus*	Humerus	154	67
MCZ	5038	*Dimetrodon limbatus*	Humerus	163	97
FMNH	UC 843	*Dimetrodon limbatus*	Humerus	163	74
MCZ	5574	*Dimetrodon limbatus*	Humerus	165	90
MCZ	1395	*Dimetrodon limbatus*	Humerus	166	94
MCZ	3292	*Dimetrodon limbatus*	Humerus	166	84
MCZ	5039	*Dimetrodon limbatus*	Humerus	167	92
MCZ	1314	*Dimetrodon limbatus*	Humerus	168	87
MCZ	1338	*Dimetrodon limbatus*	Humerus	168	90
MCZ	5422	*Dimetrodon limbatus*	Humerus	169	76
MCZ	1123	*Dimetrodon limbatus*	Humerus	170	92
MCZ	2832	*Dimetrodon limbatus*	Humerus	170	80
MCZ	2913	*Dimetrodon limbatus*	Humerus	170	70
MCZ	1972	*Dimetrodon limbatus*	Humerus	171	85
FMNH	UC 841	*Dimetrodon limbatus*	Humerus	171	101

MCZ	5042	*Dimetrodon limbatus*	Humerus	172	80
MCZ	2832	*Dimetrodon limbatus*	Humerus	176	82
MCZ	5037	*Dimetrodon limbatus*	Humerus	178	84
MCZ	5836	*Dimetrodon limbatus*	Humerus	178	87
MCZ	5041	*Dimetrodon limbatus*	Humerus	180	105
FMNH	UC 1001	*Dimetrodon limbatus*	Humerus	182	97
FMNH	UC 1147	*Dimetrodon limbatus*	Humerus	183	94
MCZ	2875	*Dimetrodon limbatus*	Humerus	195	92
MCZ	2848	*Dimetrodon limbatus*	Humerus	197	89
MCZ	6160	*Dimetrodon limbatus*	Humerus	198	85
MCZ	3246	*Dimetrodon limbatus*	Humerus	200	95
OMNH	TMM 30966-356	*Dimetrodon limbatus*	Humerus	200	110
AMNH	4107	*Dimetrodon limbatus*	Humerus	212	103
MCZ	1123	*Dimetrodon limbatus*	Humerus	195+	95
IPBSH	27	*Dimetrodon limbatus ?*	Humerus	171	122
MCZ	5498	*Dimetrodon limbatus*	Radius	119	39
OMNH	TMM 30966-356	*Dimetrodon limbatus*	Radius	130	70
MCZ	5062	*Dimetrodon limbatus*	Radius	131	50
MCZ	6051	*Dimetrodon limbatus*	Radius	134	53
MCZ	2846	*Dimetrodon limbatus*	Radius	143	54
MCZ	6054	*Dimetrodon limbatus*	Radius	143	45
MCZ	6051	*Dimetrodon limbatus*	Radius	150	55
MCZ	5954	*Dimetrodon limbatus*	Radius	153	79
MCZ	1368	*Dimetrodon limbatus*	Radius	159	64
FMNH	UC 91	*Dimetrodon limbatus*	Radius	162	60
DMNH	11905	*Dimetrodon limbatus*	Radius	172	40
FMNH	UR 667	*Dimetrodon limbatus*	Tibia	133	44
FMNH	UC 69	*Dimetrodon limbatus*	Tibia	134	46
FMNH	UR 676	*Dimetrodon limbatus*	Tibia	140	45
FMNH	UR 666	*Dimetrodon limbatus*	Tibia	152	53
MCZ	5114	*Dimetrodon limbatus*	Tibia	153	64
OMNH	TMM 30966-356	*Dimetrodon limbatus*	Tibia	153	68
FMNH	UR 661	*Dimetrodon limbatus*	Tibia	154	58
MCZ	5371	*Dimetrodon limbatus*	Tibia	155	59
FMNH	UR 305	*Dimetrodon limbatus*	Tibia	159	66
MCZ	3183	*Dimetrodon limbatus*	Tibia	160	68
MCZ	5114	*Dimetrodon limbatus*	Tibia	160	60
DMNH	11905	*Dimetrodon limbatus*	Tibia	162	58
FMNH	UR 305	*Dimetrodon limbatus*	Tibia	164	63
MCZ	1334	*Dimetrodon limbatus*	Tibia	165	64

MCZ	5365	*Dimetrodon limbatus*	Tibia	165	58
MCZ	5114	*Dimetrodon limbatus*	Tibia	166	64
MCZ	2886	*Dimetrodon limbatus*	Tibia	183	90
AMNH	4123	*Dimetrodon limbatus*	Tibia	183	69
MCZ	1319	*Dimetrodon limbatus*	Ulna	170	52
FMNH	UC 1001	*Dimetrodon limbatus*	Ulna	178	62
MCZ	1113	*Dimetrodon limbatus*	Ulna	182	45
OMNH	TMM 30966-356	*Dimetrodon limbatus*	Ulna	183	60
MCZ	1123	*Dimetrodon limbatus*	Ulna	186	56
MCZ	2846	*Dimetrodon limbatus*	Ulna	195	57
MCZ	8180	*Dimetrodon limbatus*	Ulna	195	58
FMNH	UC 1001	*Dimetrodon limbatus*	Ulna	198	57
MCZ	1368	*Dimetrodon limbatus*	Ulna	204	56
MCZ	1445	*Dimetrodon limbatus*	Ulna	209	55
MCZ	1368	*Dimetrodon limbatus*	Ulna	213	59
AMNH	24581	*Dimetrodon loomisi*	Femur	103	59
AMNH	24581	*Dimetrodon loomisi*	Femur	110	46
FMNH	UR 693	*Dimetrodon loomisi*	Femur	176	76
AMNH	21242	*Dimetrodon loomisi*	Femur	184	86
AMNH	21177	*Dimetrodon loomisi*	Femur	188	89
MCZ	1341	*Dimetrodon loomisi*	Femur	192	82
FMNH	UC 776	*Dimetrodon loomisi*	Femur	193	78
FMNH	UC 147	*Dimetrodon loomisi*	Femur	194	98
AMNH	21222	*Dimetrodon loomisi*	Femur	196	88
AMNH	21176	*Dimetrodon loomisi*	Femur	197	98
AMNH	21227	*Dimetrodon loomisi*	Femur	197	105
FMNH	UC 1269	*Dimetrodon loomisi*	Femur	209	85
MCZ	2870	*Dimetrodon loomisi*	Femur	210	94
AMNH	21346	*Dimetrodon loomisi*	Fibula	140	58
FMNH	UC 147	*Dimetrodon loomisi*	Fibula	156	37
AMNH	21177	*Dimetrodon loomisi*	Fibula	164	37
AMNH	21222	*Dimetrodon loomisi*	Fibula	165	38
AMNH	21280	*Dimetrodon loomisi*	Fibula	171	38
AMNH	21176	*Dimetrodon loomisi*	Fibula	178	41
FMNH	UC 424	*Dimetrodon loomisi*	Fibula	179	42
FMNH	UC 424	*Dimetrodon loomisi*	Fibula	181	36
AMNH	21148	*Dimetrodon loomisi*	Humerus	160	55
AMNH	21346	*Dimetrodon loomisi*	Humerus	163	79
AMNH	21335	*Dimetrodon loomisi*	Humerus	169	98
AMNH	21045	*Dimetrodon loomisi*	Humerus	170	74
AMNH	21288	*Dimetrodon loomisi*	Humerus	170	76

FMNH	UC 1140	*Dimetrodon loomisi*	Humerus	174	81
AMNH	21293	*Dimetrodon loomisi*	Humerus	176	81
AMNH	21226	*Dimetrodon loomisi*	Humerus	178	74
AMNH	21334	*Dimetrodon loomisi*	Humerus	180	71
AMNH	21045	*Dimetrodon loomisi*	Humerus	183	48
AMNH	21222	*Dimetrodon loomisi*	Humerus	184	86
FMNH	UC 766	*Dimetrodon loomisi*	Humerus	186	77
AMNH	4148	*Dimetrodon loomisi*	Humerus	190	92
AMNH	21149	*Dimetrodon loomisi*	Humerus	190	44
FMNH	UC 421	*Dimetrodon loomisi*	Humerus	191	74
AMNH	21148	*Dimetrodon loomisi*	Humerus	200	111
FMNH	UC 771	*Dimetrodon loomisi*	Humerus	200	88
FMNH	UR 682	*Dimetrodon loomisi*	Humerus	206	97
AMNH	4612	*Dimetrodon loomisi*	Humerus	214	102
AMNH	4152	*Dimetrodon loomisi*	Humerus	215	86
YPM	1766	*Dimetrodon loomisi*	Humerus	175+	74+
AMNH	21293	*Dimetrodon loomisi*	Radius	152	47
FMNH	UC 766	*Dimetrodon loomisi*	Radius	154	54
FMNH	UC 585	*Dimetrodon loomisi*	Radius	155	39
AMNH	21293	*Dimetrodon loomisi*	Radius	156	49
AMNH	21226	*Dimetrodon loomisi*	Radius	161	44
AMNH	21255	*Dimetrodon loomisi*	Radius	161	49
AMNH	21226	*Dimetrodon loomisi*	Radius	163	50
FMNH	UC 149	*Dimetrodon loomisi*	Radius	163	48
AMNH	21334	*Dimetrodon loomisi*	Radius	164	49
AMNH	21288	*Dimetrodon loomisi*	Radius	168	51
FMNH	UC 428	*Dimetrodon loomisi*	Tibia	142	43
AMNH	21277	*Dimetrodon loomisi*	Tibia	144	69
AMNH	21346	*Dimetrodon loomisi*	Tibia	153	55
AMNH	21177	*Dimetrodon loomisi*	Tibia	155	67
FMNH	UC 147	*Dimetrodon loomisi*	Tibia	156	45
AMNH	21280	*Dimetrodon loomisi*	Tibia	162	50
AMNH	21276	*Dimetrodon loomisi*	Tibia	168	68
AMNH	21227	*Dimetrodon loomisi*	Tibia	179	74
AMNH	21338	*Dimetrodon loomisi*	Ulna	160	49
AMNH	21226	*Dimetrodon loomisi*	Ulna	178	39
AMNH	21293	*Dimetrodon loomisi*	Ulna	179	45
AMNH	21255	*Dimetrodon loomisi*	Ulna	184	48
AMNH	21293	*Dimetrodon loomisi*	Ulna	185	59
FMNH	UC 149	*Dimetrodon loomisi*	Ulna	191	51
FMNH	UC 584	*Dimetrodon loomisi*	Ulna	193	47
MCZ	1365	*Dimetrodon milleri*	Femur	145	59

MCZ	1365	*Dimetrodon milleri*	Femur	150	55
MCZ	1365	*Dimetrodon milleri*	Fibula	122	27
MCZ	1365	*Dimetrodon milleri*	Fibula	125	28
MCZ	1365	*Dimetrodon milleri*	Humerus	124	73
MCZ	3167	*Dimetrodon milleri*	Humerus	127	47
MCZ	1365	*Dimetrodon milleri*	Humerus	140	56
MCZ	3167	*Dimetrodon milleri*	Radius	111	32
MCZ	1365	*Dimetrodon milleri*	Radius	112	36
MCZ	1365	*Dimetrodon milleri*	Radius	117	34
MCZ	1365	*Dimetrodon milleri*	Tibia	110	40
MCZ	1365	*Dimetrodon milleri*	Tibia	113	40
MCZ	1365	*Dimetrodon milleri*	Ulna	142	30
MCZ	1365	*Dimetrodon milleri*	Ulna	154	35
MCZ	6217	*Dimetrodon natalis*	Femur	62	27
MCZ	6217	*Dimetrodon natalis*	Femur	63	28
MCZ	5097b	*Dimetrodon natalis*	Femur	64	27
IPBSH	42	*Dimetrodon natalis*	Femur	67	31
IPBSH	87	*Dimetrodon natalis*	Femur	67	27
MCZ	6060	*Dimetrodon natalis*	Femur	68	29
IPBSH	3	*Dimetrodon natalis*	Femur	69	25
MCZ	5097a	*Dimetrodon natalis*	Femur	71	28
MCZ	2839	*Dimetrodon natalis*	Femur	72	29
DMNH	13084	*Dimetrodon natalis*	Femur	72.2	30
MCZ	5572	*Dimetrodon natalis*	Femur	73	30
MCZ	5834	*Dimetrodon natalis*	Femur	73	33
MCZ	2839	*Dimetrodon natalis*	Femur	75	31
MCZ	1320	*Dimetrodon natalis*	Femur	77	30
MCZ	5097c	*Dimetrodon natalis*	Femur	77	27
MCZ	6184	*Dimetrodon natalis*	Femur	78	30
DMNH	19096	*Dimetrodon natalis*	Femur	78.2	42
IPBSH	1	*Dimetrodon natalis*	Femur	79	37
DMNH	14126	*Dimetrodon natalis*	Femur	83.2	35
MCZ	1328	*Dimetrodon natalis*	Femur	85	35
MCZ	6088	*Dimetrodon natalis*	Femur	85	41
MCZ	1324	*Dimetrodon natalis*	Femur	89	38
MCZ	3211	*Dimetrodon natalis*	Femur	95	39
MCZ	7021	*Dimetrodon natalis*	Femur	96	48
UMMP	22215	*Dimetrodon natalis*	Femur	96	37
FMNH	UC 76	*Dimetrodon natalis*	Femur	96	35
UMMP	22215	*Dimetrodon natalis*	Femur	97	36
IPBSH	19	*Dimetrodon natalis*	Femur	98	38
MCZ	5865	*Dimetrodon natalis*	Femur	98	34

MCZ	5865	*Dimetrodon natalis*	Femur	98	42
MCZ	7027	*Dimetrodon natalis*	Femur	99	34
MCZ	5616	*Dimetrodon natalis*	Femur	100	32
MCZ	5865	*Dimetrodon natalis*	Femur	100	36
MCZ	6085	*Dimetrodon natalis*	Femur	100	39
FMNH	UC 150	*Dimetrodon natalis*	Femur	100	37
UMMP	22215	*Dimetrodon natalis*	Femur	103	38
UMMP	22215	*Dimetrodon natalis*	Femur	103	47
MCZ	7022	*Dimetrodon natalis*	Femur	104	33
MCZ	1329	*Dimetrodon natalis*	Femur	105	48
MCZ	7024	*Dimetrodon natalis*	Femur	105	42
MCZ	8690	*Dimetrodon natalis*	Femur	105	36
UMMP	22224	*Dimetrodon natalis*	Femur	105	37
UMMP	22224	*Dimetrodon natalis*	Femur	105	35
MCZ	5865	*Dimetrodon natalis*	Femur	106	36
MCZ	7446	*Dimetrodon natalis*	Femur	106	55
MCZ	8689	*Dimetrodon natalis*	Femur	106	40
DMNH	17170	*Dimetrodon natalis*	Femur	106.3	40
IPBSH	6	*Dimetrodon natalis*	Femur	107	50
MCZ	5359	*Dimetrodon natalis*	Femur	107	40
IPBSH	31	*Dimetrodon natalis*	Femur	108	45
MCZ	5098	*Dimetrodon natalis*	Femur	109	37
DMNH	17935	*Dimetrodon natalis*	Femur	109.05	40
MCZ	5098	*Dimetrodon natalis*	Femur	112	43
MCZ	5098	*Dimetrodon natalis*	Femur	113	40
FMNH	UC 823	*Dimetrodon natalis*	Femur	113	46
FMNH	UC 823	*Dimetrodon natalis*	Femur	113	54
FMNH	UC 245	*Dimetrodon natalis*	Femur	114	36
UMMP	3399	*Dimetrodon natalis*	Femur	115	35
MCZ	5098	*Dimetrodon natalis*	Femur	115	35
MCZ	5865	*Dimetrodon natalis*	Femur	115	50
FMNH	UC 244	*Dimetrodon natalis*	Femur	115	39
UMMP	3391	*Dimetrodon natalis*	Femur	116	45
MCZ	5098	*Dimetrodon natalis*	Femur	116	40
FMNH	UC 243	*Dimetrodon natalis*	Femur	116	45
FMNH	UC 74	*Dimetrodon natalis*	Femur	116	37
MCZ	5098	*Dimetrodon natalis*	Femur	117	42
MCZ	5865	*Dimetrodon natalis*	Femur	117	37
MCZ	6086	*Dimetrodon natalis*	Femur	117	42
UMMP	22224	*Dimetrodon natalis*	Femur	118	47
MCZ	5098	*Dimetrodon natalis*	Femur	119	43
MCZ	7023	*Dimetrodon natalis*	Femur	120	41

FMNH	UC 58	*Dimetrodon natalis*	Femur	120	40
DMNH	11875	*Dimetrodon natalis*	Femur	120.06	42
IPBSH	37	*Dimetrodon natalis*	Femur	121	45
AMNH	dvp 4110	*Dimetrodon natalis*	Femur	121.1	46
MCZ	5865	*Dimetrodon natalis*	Femur	122	47
FMNH	UC 823	*Dimetrodon natalis*	Femur	122	45
FMNH	UC 823	*Dimetrodon natalis*	Femur	122	47
MCZ	7025	*Dimetrodon natalis*	Femur	123	45
MCZ	5865	*Dimetrodon natalis*	Femur	124	46
FMNH	UC 823	*Dimetrodon natalis*	Femur	124	50
UMMP	22224	*Dimetrodon natalis*	Femur	125	45
UMMP	22224	*Dimetrodon natalis*	Femur	125	44
MCZ	6033	*Dimetrodon natalis*	Femur	126	52
UMMP	22224	*Dimetrodon natalis*	Femur	126	45
FMNH	UC523	*Dimetrodon natalis*	Femur	126	46
IPBSH	35	*Dimetrodon natalis*	Femur	127	63
UMMP	3387	*Dimetrodon natalis*	Femur	127	46
UMMP	3389	*Dimetrodon natalis*	Femur	127	45
UMMP	22224	*Dimetrodon natalis*	Femur	127	46
UMMP	22224	*Dimetrodon natalis*	Femur	128	51
FMNH	UC 510	*Dimetrodon natalis*	Femur	129	46
UMMP	22224	*Dimetrodon natalis*	Femur	130	44
IPBSH	29	*Dimetrodon natalis*	Femur	131	45
IPBSH	40	*Dimetrodon natalis*	Femur	132	55
UMMP	22224	*Dimetrodon natalis*	Femur	132	48
UMMP	22224	*Dimetrodon natalis*	Femur	132	48
UMMP	3398	*Dimetrodon natalis*	Femur	133	45
UMMP	22224	*Dimetrodon natalis*	Femur	133	50
UMMP	22224	*Dimetrodon natalis*	Femur	135	50
IPBSH	2	*Dimetrodon natalis*	Femur	137	52
UMMP	22216	*Dimetrodon natalis*	Femur	114	37
IPBSH	104	*Dimetrodon natalis*	Fibula	29	20
MCZ	1327	*Dimetrodon natalis*	Fibula	68	18
MCZ	5125	*Dimetrodon natalis*	Fibula	83	20
DMNH	19097	*Dimetrodon natalis*	Fibula	84.4	34
UMMP	22232	*Dimetrodon natalis*	Fibula	85	20
MCZ	5639	*Dimetrodon natalis*	Fibula	86	18
UMMP	22232	*Dimetrodon natalis*	Fibula	86	19
UMMP	22232	*Dimetrodon natalis*	Fibula	91	21
UMMP	22225	*Dimetrodon natalis*	Fibula	97	23
UMMP	22225	*Dimetrodon natalis*	Fibula	100	22
MCZ	5125	*Dimetrodon natalis*	Fibula	101	21

MCZ	5125	*Dimetrodon natalis*	Fibula	101	20
MCZ	5129	*Dimetrodon natalis*	Fibula	101	21
MCZ	5125	*Dimetrodon natalis*	Fibula	102	22
UMMP	22225	*Dimetrodon natalis*	Fibula	104	23
MCZ	5125	*Dimetrodon natalis*	Fibula	106	22
MCZ	1300	*Dimetrodon natalis*	Fibula	108	27
MCZ	1303	*Dimetrodon natalis*	Fibula	108	27
MCZ	5125	*Dimetrodon natalis*	Fibula	108	25
UMMP	22225	*Dimetrodon natalis*	Fibula	108	23
UMMP	22225	*Dimetrodon natalis*	Fibula	108	22
MCZ	5131	*Dimetrodon natalis*	Fibula	109	31
UMMP	22225	*Dimetrodon natalis*	Fibula	109	25
FMNH	UC 822	*Dimetrodon natalis*	Fibula	110	31
UMMP	22225	*Dimetrodon natalis*	Fibula	114	28
IPBSH	93	*Dimetrodon natalis*	Fibula	115	28
IPBSH	13	*Dimetrodon natalis*	Humerus	57.8	28
IPBSH	25	*Dimetrodon natalis*	Humerus	58.1	27
IPBSH	49	*Dimetrodon natalis*	Humerus	60	30
FMNH	UC 818	*Dimetrodon natalis*	Humerus	62.5	31
IPBSH	11	*Dimetrodon natalis*	Humerus	63.3	29
MCZ	5936	*Dimetrodon natalis*	Humerus	65	30
MCZ	5936	*Dimetrodon natalis*	Humerus	65	26
MCZ	6217	*Dimetrodon natalis*	Humerus	65	33
MCZ	5593	*Dimetrodon natalis*	Humerus	66	26
FMNH	UC 818	*Dimetrodon natalis*	Humerus	66.2	30
DMNH	11999	*Dimetrodon natalis*	Humerus	68.9	35
IPBSH	14	*Dimetrodon natalis*	Humerus	69.8	33
AMNH	dvp 4110	*Dimetrodon natalis*	Humerus	80	38
IPBSH	22	*Dimetrodon natalis*	Humerus	81	42
AMNH	dvp 4110	*Dimetrodon natalis*	Humerus	81.1	40
AMNH	dvp 4110	*Dimetrodon natalis*	Humerus	81.1	34
IPBSH	5	*Dimetrodon natalis*	Humerus	82	40
FMNH	UC 837	*Dimetrodon natalis*	Humerus	88	32
FMNH	UC 90	*Dimetrodon natalis*	Humerus	88	33
MCZ	5031	*Dimetrodon natalis*	Humerus	89	32
MCZ	8706	*Dimetrodon natalis*	Humerus	89	30
FMNH	UC 818	*Dimetrodon natalis*	Humerus	89.8	34
IPBSH	95	*Dimetrodon natalis*	Humerus	90	31
MCZ	5595	*Dimetrodon natalis*	Humerus	91	34
MCZ	2847	*Dimetrodon natalis*	Humerus	94	33
MCZ	1325	*Dimetrodon natalis*	Humerus	95	30
MCZ	2838	*Dimetrodon natalis*	Humerus	95	37

DMNH	11910	*Dimetrodon natalis*	Humerus	97.5	32
MCZ	5596	*Dimetrodon natalis*	Humerus	101	38
MCZ	5864	*Dimetrodon natalis*	Humerus	103	31
MCZ	5718	*Dimetrodon natalis*	Humerus	104	43
FMNH	UC 79	*Dimetrodon natalis*	Humerus	105	41
MCZ	5864	*Dimetrodon natalis*	Humerus	106	36
MCZ	8705	*Dimetrodon natalis*	Humerus	106	38
FMNH	UC 538	*Dimetrodon natalis*	Humerus	106	38
MCZ	8710	*Dimetrodon natalis*	Humerus	107	37
FMNH	UC 549	*Dimetrodon natalis*	Humerus	111.5	47
MCZ	5948	*Dimetrodon natalis*	Humerus	112	37
MCZ	8708	*Dimetrodon natalis*	Humerus	112	36
DMNH	17670	*Dimetrodon natalis*	Humerus	112.2	40
MCZ	8707	*Dimetrodon natalis*	Humerus	113	48
MCZ	8709	*Dimetrodon natalis*	Humerus	113	39
IPBSH	33	*Dimetrodon natalis*	Humerus	113.5	54
IPBSH	92	*Dimetrodon natalis*	Humerus	116	40
FMNH	UC 802	*Dimetrodon natalis*	Humerus	116	53
FMNH	UC 531	*Dimetrodon natalis*	Humerus	118	50
IPBSH	4	*Dimetrodon natalis*	Humerus	120	42
FMNH	UC 802	*Dimetrodon natalis*	Humerus	120	51
FMNH	UC 802	*Dimetrodon natalis*	Humerus	121	58
FMNH	UC 802	*Dimetrodon natalis*	Humerus	121	49
MCZ	1937	*Dimetrodon natalis*	Humerus	122	45
UMMP	9744	*Dimetrodon natalis*	Humerus	123	48
FMNH	UC 682	*Dimetrodon natalis*	Humerus	123	46
FMNH	UC 802	*Dimetrodon natalis*	Humerus	124	57
FMNH	UC 856	*Dimetrodon natalis*	Humerus	124	47
IPBSH	47	*Dimetrodon natalis*	Humerus	125	43
FMNH	UC 248	*Dimetrodon natalis*	Humerus	125	60
UMMP	3052	*Dimetrodon natalis*	Humerus	126	53
MCZ	5948	*Dimetrodon natalis*	Humerus	128	45
FMNH	UC 802	*Dimetrodon natalis*	Humerus	128	58
IPBSH	34	*Dimetrodon natalis*	Humerus	131	55
UMMP	16343	*Dimetrodon natalis*	Humerus	132	51
MCZ	5603	*Dimetrodon natalis*	Humerus	134	52
FMNH	UC 545	*Dimetrodon natalis*	Humerus	134	50
FMNH	UC 802	*Dimetrodon natalis*	Humerus	134	53
MCZ	2837	*Dimetrodon natalis*	Humerus	135	56
FMNH	UC 802	*Dimetrodon natalis*	Humerus	135	54
MCZ	1367	*Dimetrodon natalis*	Humerus	144	70
IPBSH	10	*Dimetrodon natalis*	Radius	70	20

MCZ	2839	*Dimetrodon natalis*	Radius	71	15
MCZ	6895	*Dimetrodon natalis*	Radius	72	20
MCZ	5869	*Dimetrodon natalis*	Radius	86	25
MCZ	5869	*Dimetrodon natalis*	Radius	88	26
MCZ	5065	*Dimetrodon natalis*	Radius	89	23
MCZ	1476	*Dimetrodon natalis*	Radius	90	23
MCZ	5065	*Dimetrodon natalis*	Radius	91	25
MCZ	5065	*Dimetrodon natalis*	Radius	91	29
MCZ	5065	*Dimetrodon natalis*	Radius	91	24
MCZ	5065	*Dimetrodon natalis*	Radius	93	25
IPBSH	32	*Dimetrodon natalis*	Radius	94	33
FMNH	UC 518	*Dimetrodon natalis*	Radius	94	28
IPBSH	112	*Dimetrodon natalis*	Radius	96	23
UMMP	22230	*Dimetrodon natalis*	Radius	96	23
UMMP	22230	*Dimetrodon natalis*	Radius	97	26
MCZ	5065	*Dimetrodon natalis*	Radius	101	27
MCZ	5896	*Dimetrodon natalis*	Radius	101	27
UMMP	22230	*Dimetrodon natalis*	Radius	104	27
FMNH	UC 538	*Dimetrodon natalis*	Radius	104	31
FMNH	UR 92	*Dimetrodon natalis*	Radius	105	33
UMMP	22230	*Dimetrodon natalis*	Radius	106	30
IPBSH	91	*Dimetrodon natalis*	Radius	107	27
MCZ	5112	*Dimetrodon natalis*	Radius	107	29
IPBSH	24	*Dimetrodon natalis*	Radius	108	33
MCZ	5869	*Dimetrodon natalis*	Radius	109	28
UMMP	22230	*Dimetrodon natalis*	Radius	110	29
IPBSH	50	*Dimetrodon natalis*	Tibia	50	20
IPBSH	12	*Dimetrodon natalis*	Tibia	51	17
MCZ	5119	*Dimetrodon natalis*	Tibia	56	17
MCZ	5634	*Dimetrodon natalis*	Tibia	58	17
MCZ	2839	*Dimetrodon natalis*	Tibia	65	20
MCZ	2839	*Dimetrodon natalis*	Tibia	65	20
IPBSH	15	*Dimetrodon natalis*	Tibia	66	18
MCZ	5867	*Dimetrodon natalis*	Tibia	71	24
IPBSH	43	*Dimetrodon natalis*	Tibia	73	28
MCZ	5867	*Dimetrodon natalis*	Tibia	77	27
MCZ	1322	*Dimetrodon natalis*	Tibia	79	22
AMNH	dvp 4110	*Dimetrodon natalis*	Tibia	80	35
MCZ	5867	*Dimetrodon natalis*	Tibia	82	25
UMMP	22226	*Dimetrodon natalis*	Tibia	86	27
IPBSH	44	*Dimetrodon natalis*	Tibia	88	33
MCZ	5118	*Dimetrodon natalis*	Tibia	88	27

MCZ	6057	*Dimetrodon natalis*	Tibia	88	25
UMMP	22226	*Dimetrodon natalis*	Tibia	90	18
MCZ	5118	*Dimetrodon natalis*	Tibia	91	24
MCZ	5118	*Dimetrodon natalis*	Tibia	91	25
MCZ	5867	*Dimetrodon natalis*	Tibia	91	29
MCZ	5867	*Dimetrodon natalis*	Tibia	91	25
MCZ	5118	*Dimetrodon natalis*	Tibia	93	~30
MCZ	5634	*Dimetrodon natalis*	Tibia	93	23
MCZ	5867	*Dimetrodon natalis*	Tibia	93	31
MCZ	5118	*Dimetrodon natalis*	Tibia	94	30
MCZ	5118	*Dimetrodon natalis*	Tibia	95	25
MCZ	5363	*Dimetrodon natalis*	Tibia	95	25
MCZ	5867	*Dimetrodon natalis*	Tibia	95	32
FMNH	UC 822	*Dimetrodon natalis*	Tibia	95	30
UMMP	22226	*Dimetrodon natalis*	Tibia	96	32
UMMP	22226	*Dimetrodon natalis*	Tibia	96	31
MCZ	5118	*Dimetrodon natalis*	Tibia	97	38
MCZ	5362	*Dimetrodon natalis*	Tibia	97	30
MCZ	5867	*Dimetrodon natalis*	Tibia	99	38
IPBSH	30	*Dimetrodon natalis*	Tibia	100	33
MCZ	5362	*Dimetrodon natalis*	Tibia	100	35
MCZ	5118	*Dimetrodon natalis*	Tibia	101	35
MCZ	5118	*Dimetrodon natalis*	Tibia	101	30
MCZ	5118	*Dimetrodon natalis*	Tibia	101	28
MCZ	6198	*Dimetrodon natalis*	Tibia	101	32
MCZ	5065	*Dimetrodon natalis*	Tibia	103	31
UMMP	22226	*Dimetrodon natalis*	Tibia	103	32
MCZ	6198	*Dimetrodon natalis*	Tibia	104	38
IPBSH	39	*Dimetrodon natalis*	Tibia	105	43
MCZ	5405	*Dimetrodon natalis*	Tibia	105	35
FMNH	UC 513	*Dimetrodon natalis*	Tibia	106	32
MCZ	5939	*Dimetrodon natalis*	Tibia	107	39
FMNH	UC 822	*Dimetrodon natalis*	Tibia	107	36
UMMP	22226	*Dimetrodon natalis*	Tibia	110	37
UMMP	22226	*Dimetrodon natalis*	Tibia	110	29
FMNH	UC 1146	*Dimetrodon natalis*	Tibia	111	49
IPBSH	52	*Dimetrodon natalis*	Tibia	121	48
FMNH	UC 822	*Dimetrodon natalis*	Tibia	122	44
IPBSH	89	*Dimetrodon natalis*	Tibia	32+	19
IPBSH	94	*Dimetrodon natalis*	Tibia	37+	23
MCZ	1476	*Dimetrodon natalis*	Ulna	93	18
DMNH	12098	*Dimetrodon natalis*	Ulna	100.05	26

UMMP	22221	*Dimetrodon natalis*	Ulna	109	24
IPBSH	28	*Dimetrodon natalis*	Ulna	112	28
MCZ	5951	*Dimetrodon natalis*	Ulna	113	32
FMNH	UC 108	*Dimetrodon natalis*	Ulna	114	26
UMMP	22221	*Dimetrodon natalis*	Ulna	125	28
IPBSH	26	*Dimetrodon natalis*	Ulna	128	45
MCZ	5055	*Dimetrodon natalis*	Ulna	133	35
IPBSH	36	*Dimetrodon natalis*	Ulna	56+	20
IPBSH	41	*Dimetrodon*	Femur	69	27
IPBSH	8	*Dimetrodon*	Femur	180	96
IPBSH	110	*Dimetrodon*	Humerus	21+	27
IPBSH	55	*Dimetrodon*	Fibula	47+	N/A
AMNH	7003	*Edaphosaur boanerges*	Femur	163	68
MCZ	4323-1	*Edaphosaur boanerges*	Fibula	107.1	49
MCZ	4323-2	*Edaphosaur boanerges*	Fibula	117.6	49
AMNH	7003	*Edaphosaur boanerges*	Humerus	149	61
AMNH	7128	*Edaphosaur boanerges*	Humerus	166	79
AMNH	7003	*Edaphosaur boanerges*	Radius	76	36
AMNH	7003	*Edaphosaur boanerges*	Tibia	90	na
MCZ	4324-3	*Edaphosaur boanerges*	Tibia	98	46
MCZ	4324-2	*Edaphosaur boanerges*	Tibia	101.8	53
MCZ	4324-6	*Edaphosaur boanerges*	Tibia	103.6	54
MCZ	4324-5	*Edaphosaur boanerges*	Tibia	98.2	49
MCZ	4324-4	*Edaphosaur boanerges*	Tibia	98.3	49
MCZ	4324-1	*Edaphosaur boanerges*	Tibia	99.6	49
AMNH	7003	*Edaphosaur boanerges*	Ulna	123	61
MCZ	4319-2	*Edaphosaur boanerges*	Ulna	130	57
MCZ	4319-3	*Edaphosaur boanerges*	Ulna	118.7	43
MCZ	4319-1	*Edaphosaur boanerges*	Ulna	120.7	44
AMNH	21121	*Edaphosaur pogonias*	Femur	222	131
AMNH	21001	*Edaphosaur pogonias*	Ulna	192	64
IPBSH	84	*Edaphosaurus*	Femur	118	87
OMNH	1674	*Edaphosaurus*	Femur	170	70
UMMP	3021	*Edaphosaurus*	Femur	170	77
MCZ	6196	*Edaphosaurus*	Femur	195	88
OMNH	35176	*Edaphosaurus*	Femur	292	109
UMMP	25572	*Edaphosaurus*	Femur	104 +	54
OMNH	50252	*Edaphosaurus*	Fibula	75	47
OMNH	1674	*Edaphosaurus*	Fibula	105	40
AMNH	21005	*Edaphosaurus*	Humerus	198	82
OMNH	1674	*Edaphosaurus*	Humerus	150	70
MCZ	3306	*edaphosaurus*	Humerus	157	68

MCZ	3419	*Edaphosaurus*	Humerus	163	58
MCZ	3417	*Edaphosaurus*	Humerus	149	70
OMNH	1674	*Edaphosaurus*	Radius	95	37
MCZ	3417	*Edaphosaurus*	Radius	96	48
MCZ	1760	*Edaphosaurus*	Tibia	90	46
OMNH	1674	*Edaphosaurus*	Tibia	100	50
MCZ	1351	*Edaphosaurus*	Tibia	116.8	63
FMNH	UR 729	*Edaphosaurus*	Tibia	96	47
FMNH	UR 723	*Edaphosaurus*	Tibia	103	52
OMNH	1674	*Edaphosaurus*	Ulna	112	36
MCZ	1709	*Edaphosaurus*	Ulna	205	72
MCZ	1709	*Edaphosaurus*	Ulna	205	72
MCZ	4322	*Edaphosaurus boanerges*	Femur	117	55
MCZ	3166	*Edaphosaurus boanerges*	Femur	141	66
TMM	31255-20	*Edaphosaurus boanerges*	Femur	159	72
TMM	31255-20	*Edaphosaurus boanerges*	Femur	159	72
MCZ	1764/1531	*Edaphosaurus boanerges*	Femur	160	75
MCZ	4322	*Edaphosaurus boanerges*	Femur	163	68
AMNH	7003	*Edaphosaurus boanerges*	Femur	163	68
FMNH	UR 733	*Edaphosaurus boanerges*	Femur	164	74
MCZ	1755	*Edaphosaurus boanerges*	Femur	168	77
MCZ	4322	*Edaphosaurus boanerges*	Femur	168	73
YPM	14686	*Edaphosaurus boanerges*	Femur	170	64
MCZ	4322	*Edaphosaurus boanerges*	Femur	171	75
MCZ	4322	*Edaphosaurus boanerges*	Femur	174	84
MCZ	1755	*Edaphosaurus boanerges*	Femur	177	76
MCZ	4322	*Edaphosaurus boanerges*	Femur	177	78
TMM	31255-6.1	*Edaphosaurus boanerges*	Femur	180	76
MCZ	4863	*Edaphosaurus boanerges*	Femur	205	100
MCZ	1764/1531	*Edaphosaurus boanerges*	Fibula	83	27
MCZ	4319	*Edaphosaurus boanerges*	Humerus	99	39
MCZ	2855	*Edaphosaurus boanerges*	Humerus	100	40
MCZ	2906	*Edaphosaurus boanerges*	Humerus	104	40
MCZ	5021	*Edaphosaurus boanerges*	Humerus	109	52
MCZ	1762	*Edaphosaurus boanerges*	Humerus	142	61
MCZ	1764/1531	*Edaphosaurus boanerges*	Humerus	144	67
FMNH	UR 733	*Edaphosaurus boanerges*	Humerus	145	63
YPM	14686	*Edaphosaurus boanerges*	Humerus	148	62
AMNH	7003	*Edaphosaurus boanerges*	Humerus	149	61
MCZ	4318	*Edaphosaurus boanerges*	Humerus	151	74
YPM	14686	*Edaphosaurus boanerges*	Humerus	151	64
TMM	31255-70	*Edaphosaurus boanerges*	Humerus	151	61

MCZ	4318	*Edaphosaurus boanerges*	Humerus	156	63
YPM	14686	*Edaphosaurus boanerges*	Humerus	159	73
MCZ	1755	*Edaphosaurus boanerges*	Humerus	167	90?
TMM	31255-2	*Edaphosaurus boanerges*	Humerus	174	76+
TMM	31255-71	*Edaphosaurus boanerges*	Humerus	120+	60
AMNH	7003	*Edaphosaurus boanerges*	Radius	76	36
YPM	14686	*Edaphosaurus boanerges*	Radius	81.1	35
YPM	14686	*Edaphosaurus boanerges*	Radius	90	37
YPM	14686	*Edaphosaurus boanerges*	Radius	94	34
MCZ	1764/1531	*Edaphosaurus boanerges*	Radius	99	41
AMNH	7003	*Edaphosaurus boanerges*	Tibia	90	
MCZ	1764/1531	*Edaphosaurus boanerges*	Tibia	92	54
FMNH	UC 703	*Edaphosaurus boanerges*	Tibia	101	46
YPM	14686	*Edaphosaurus boanerges*	Tibia	101.7	47
MCZ	3421	*Edaphosaurus boanerges*	Tibia	110	59
DMNH	12075	*Edaphosaurus boanerges*	Tibia	102	40
YPM	14686	*Edaphosaurus boanerges*	Ulna	122	44
AMNH	7003	*Edaphosaurus boanerges*	Ulna	123	61
MCZ	1764/1531	*Edaphosaurus boanerges*	Ulna	123	47
YPM	14686	*Edaphosaurus boanerges*	Ulna	127	48
YPM	14686	*Edaphosaurus boanerges*	Ulna	127.3	41
UMMP	1164	*Edaphosaurus cruciger*	Femur	175	70
UMMP	1165	*Edaphosaurus cruciger*	Femur	206	97
UMMP	1163	*Edaphosaurus cruciger*	Humerus	180	76
UMMP	1166	*Edaphosaurus cruciger*	Radius	140	50
UMMP	1166	*Edaphosaurus cruciger*	Ulna	102	40
FMNH	UC 1099?	*Edaphosaurus pogonias*	Femur	124	68
MCZ	1652	*Edaphosaurus pogonias*	Fibula	162	64
FMNH	UC 239	*Edaphosaurus pogonias*	Humerus	187	91
MCZ	3421	*Edaphosaurus pogonias*	Tibia	110.2	58
MCZ	1754	*Edaphosaurus pogonias*	Tibia	139.5	85
MNHN	F.MCL-2	*Euromycter rutenus*	Radius	86	35
MNHN	1884-26	*Haptodus baylei*	Femur	55	8
MNHN	1884-26	*Haptodus baylei*	Humerus	53	11
MNHN	1884-26-3A	*Haptodus baylei*	Humerus	56	11
MNHN	1884-26-3A	*Haptodus baylei*	Radius	42	6
MNHN	1884-26-3A	*Haptodus baylei*	Tibia	40	5
MNHN	1884-26-3A	*Haptodus baylei*	Ulna	50+	5
MCZ	3415	*Lupeosaurus kayi*	Femur	228	118
Private	1	*Lupeosaurus kayi*	Femur	188	130
Private	2	*Lupeosaurus kayi*	Femur	200	136
MCZ	3414	*Lupeosaurus kayi ?*	Femur	235	129

MCZ	3412	*Lupeosaurus kayi ?*	Femur	239	114
AMNH	4006	*Lupeosaurus kayi*	Femur	256	156
AMNH	4006	*Lupeosaurus kayi*	Femur	263	138
MCZ	?1368	*Lupeosaurus kayi ?*	Humerus	213	109
UMMP	3445	*Lupeosaurus kayi*	Humerus	253	114
AMNH	21017	*Lupeosaurus kayi?*	Humerus	216	99
MCZ	3414	*Lupeosaurus kayi ?*	Tibia	150	97
AMNH	4006	*Lupeosaurus kayi*	Tibia	140	70
OMNH	52543	*Mycterosaurus*	Humerus	30	8
FMNH	UC 169	*Mycterosaurus longiceps*	Femur	62	32
AMNH	4796	*Nitosaurus jacksonum*	Femur	94	41
AMNH	4796	*Nitosaurus jacksonum*	Femur	98	38
UMMP	3432	*Ophiacodon*	Femur	61	?
UMMP	3366	*Ophiacodon*	Femur	71	38
UMMP	67587	*Ophiacodon*	Femur	72	42
UMMP	22212	*Ophiacodon*	Femur	73	39
UMMP	22212	*Ophiacodon*	Femur	74	40
UMMP	22212	*Ophiacodon*	Femur	75	41
IPBSH	46	*Ophiacodon*	Femur	78	37
UMMP	22212	*Ophiacodon*	Femur	78	50
UMMP	22212	*Ophiacodon*	Femur	78	37
UMMP	67587	*Ophiacodon*	Femur	79	41
UMMP	22212	*Ophiacodon*	Femur	82	52
MCZ	2928	*Ophiacodon*	Femur	129	59
AMNH	4155	*Ophiacodon*	Femur	155	
AMNH	4155	*Ophiacodon*	Femur	155	na
AMNH	4155	*Ophiacodon*	Femur	170	98
FMNH	UC 1586	*Ophiacodon*	Femur	185	112
AMNH	4155	*Ophiacodon*	Femur	170+	98
UMMP	22223	*Ophiacodon*	Fibula	72	21
UMMP	22223	*Ophiacodon*	Fibula	75	21
UMMP	22223	*Ophiacodon*	Fibula	81	23
UMMP	22223	*Ophiacodon*	Fibula	82	21
FMNH	UC 157	*Ophiacodon*	Fibula	87	33
UMMP	22231	*Ophiacodon*	Fibula	99	25
UMMP	22231	*Ophiacodon*	Fibula	101	26
UMMP	22228	*Ophiacodon*	Fibula	110	32
UMMP	22228	*Ophiacodon*	Fibula	111	33
UMMP	22228	*Ophiacodon*	Fibula	128	39
UMMP	3354	*Ophiacodon*	Humerus	57	31
UMMP	3354	*Ophiacodon*	Humerus	59	30
UMMP	3354	*Ophiacodon*	Humerus	61	31

FMNH	UC 512	*Ophiacodon*	Humerus	62	33
UMMP	3354	*Ophiacodon*	Humerus	65	32
UMMP	3354	*Ophiacodon*	Humerus	66	30
UMMP	9003	*Ophiacodon*	Humerus	70	40
IPBSH	88	*Ophiacodon*	Humerus	82	37
UMMP	3354	*Ophiacodon*	Humerus	86	37
FMNH	UC 157	*Ophiacodon*	Humerus	104	49
UMMP	22234	*Ophiacodon*	Humerus	125	55
FMNH	UC 1156	*Ophiacodon*	Humerus	131	70
UMMP	22234	*Ophiacodon*	Humerus	140	73
UMMP	22234	*Ophiacodon*	Humerus	142	56
UMMP	22234	*Ophiacodon*	Humerus	145	68
UMMP	22234	*Ophiacodon*	Humerus	148	57
UMMP	22234	*Ophiacodon*	Humerus	149	65
UMMP	22234	*Ophiacodon*	Humerus	152	65
AMNH	4155	*Ophiacodon*	Humerus	158	72
AMNH	4155	*Ophiacodon*	Humerus	158	72
UMMP	22234	*Ophiacodon*	Humerus	158	81
UMMP	22234	*Ophiacodon*	Humerus	160	71
UMMP	22234	*Ophiacodon*	Humerus	160	65
IPBSH	101	*Ophiacodon?*	Humerus	84+	41
AMNH	4155	*Ophiacodon*	Humerus	165	N/A
UMMP	22222	*Ophiacodon*	Radius	50	38
UMMP	22222	*Ophiacodon*	Radius	50	20
UMMP	22222	*Ophiacodon*	Radius	50	18
UMMP	22222	*Ophiacodon*	Radius	53	20
UMMP	22222	*Ophiacodon*	Radius	58	20
FMNH	UC 157	*Ophiacodon*	Radius	76	30
FMNH	WM 459	*Ophiacodon*	Radius	111	41
UMMP	3346	*Ophiacodon*	Radius	118	38
UMMP	3346	*Ophiacodon*	Radius	119	41
UMMP	3346	*Ophiacodon*	Radius	122	45
UMMP	22059	*Ophiacodon*	Tibia	63	27
UMMP	22059	*Ophiacodon*	Tibia	64	27
UMMP	22059	*Ophiacodon*	Tibia	65	25
UMMP	22059	*Ophiacodon*	Tibia	68	19
UMMP	22059	*Ophiacodon*	Tibia	70	28
UMMP	22059	*Ophiacodon*	Tibia	71	20
UMMP	22059	*Ophiacodon*	Tibia	72	26
UMMP	22059	*Ophiacodon*	Tibia	73	19
UMMP	3364	*Ophiacodon*	Tibia	82	31
UMMP	3352	*Ophiacodon*	Tibia	86	33

UMMP	22214	*Ophiacodon*	Tibia	114	41
UMMP	22214	*Ophiacodon*	Tibia	117	42
UMMP	22214	*Ophiacodon*	Tibia	121	44
UMMP	46130	*Ophiacodon*	Tibia	127	51
AMNH	4155	*Ophiacodon*	Tibia	145	61
AMNH	4155	*Ophiacodon*	Tibia	145	61
AMNH	4155	*Ophiacodon*	Tibia	155	56
AMNH	4155	*Ophiacodon*	Tibia	155	56
UMMP	21769	*Ophiacodon*	Ulna	98	25
UMMP	22231	*Ophiacodon*	Ulna	99	27
UMMP	21769	*Ophiacodon*	Ulna	102	22
UMMP	21769	*Ophiacodon*	Ulna	102	31
UMMP	21769	*Ophiacodon*	Ulna	110	27
UMMP	21769	*Ophiacodon*	Ulna	110	28
UMMP	21769	*Ophiacodon*	Ulna	123	28
UMMP	21774	*Ophiacodon*	Ulna	153	42
FMNH	UR 632	*Ophiacodon mirus*	Femur	82	47
FMNH	UC 240	*Ophiacodon mirus*	Femur	90	49
FMNH	UC 241	*Ophiacodon mirus*	Femur	102	52
FMNH	UC 241	*Ophiacodon mirus*	Femur	106	46
FMNH	UC 671	*Ophiacodon mirus*	Femur	117	62
FMNH	UR 631	*Ophiacodon mirus*	Femur	120	59
FMNH	UR 631	*Ophiacodon mirus*	Femur	120	61
FMNH	UC 672	*Ophiacodon mirus*	Femur	121	63
FMNH	UC 671	*Ophiacodon mirus*	Femur	122	63
MCZ	4856	*Ophiacodon mirus*	Femur	129	58
FMNH	UR 630	*Ophiacodon mirus*	Femur	130	69
MCZ	4856	*Ophiacodon mirus*	Femur	135	61
YPM	808	*Ophiacodon mirus*	Femur	136	18
FMNH	UC 671	*Ophiacodon mirus*	Fibula	98	30
FMNH	UC 671	*Ophiacodon mirus*	Fibula	105	31
YPM	808	*Ophiacodon mirus*	Fibula	119	10
OMNH	55229	*Ophiacodon mirus?*	Fibula	86	30
OMNH	55231	*Ophiacodon mirus?*	Fibula	92+	30
FMNH	UR 632	*Ophiacodon mirus*	Humerus	64	39
FMNH	UC 240	*Ophiacodon mirus*	Humerus	72	41
FMNH	UC 241	*Ophiacodon mirus*	Humerus	84	38
MCZ	6289	*Ophiacodon mirus*	Humerus	90	43
YPM	808	*Ophiacodon mirus*	Humerus	108	17
FMNH	UC 671	*Ophiacodon mirus*	Humerus	108	57
FMNH	UC 671	*Ophiacodon mirus*	Humerus	111	56
OMNH	55200	*Ophiacodon mirus?*	Humerus	99	55

OMNH	55204	*Ophiacodon mirus?*	Humerus	101	57
OMNH	55203	*Ophiacodon mirus?*	Humerus	112	60
FMNH	UC 671	*Ophiacodon mirus*	Radius	72	28
FMNH	UR 632	*Ophiacodon mirus*	Radius	72	31
FMNH	UC 671	*Ophiacodon mirus*	Radius	75	32
YPM	808	*Ophiacodon mirus*	Radius	78.5	8.5
OMNH	55210	*Ophiacodon mirus?*	Radius	69	36
OMNH	55211	*Ophiacodon mirus?*	Radius	71	40
FMNH	UC 671	*Ophiacodon mirus*	Tibia	94	43
FMNH	UC 671	*Ophiacodon mirus*	Tibia	99	39
FMNH	UR 631	*Ophiacodon mirus*	Tibia	105	37
MCZ	4915	*Ophiacodon mirus*	Tibia	110	45
YPM	808	*Ophiacodon mirus*	Tibia	118.2	15.5
FMNH	UC 241	*Ophiacodon mirus*	Ulna	77	28
FMNH	UC 241	*Ophiacodon mirus*	Ulna	78	25
YPM	808	*Ophiacodon mirus*	Ulna	86	11.2
FMNH	UC 671	*Ophiacodon mirus*	Ulna	100	34
FMNH	UC 671	*Ophiacodon mirus*	Ulna	102	40
YPM	2837	*Ophiacodon navajovicus*	Femur	78	45
YPM	2837	*Ophiacodon navajovicus*	Femur	78.3	45
YPM	2837	*Ophiacodon navajovicus*	Humerus	64	30
AMNH	4777	*Ophiacodon navajovicus*	Humerus	98	37
YPM	2837	*Ophiacodon navajovicus*	Radius	72.7	24
AMNH	4777	*Ophiacodon navajovicus*	Tibia	72	25
OMNH	35389	*Ophiacodon retroversus?*	Tibia	180	100
MCZ	1729	*Ophiacodon retroversus*	Femur	89	63
AMNH	21063	*Ophiacodon retroversus*	Femur	115	70
MCZ	4813	*Ophiacodon retroversus*	Femur	127	77
FMNH	UC 3	*Ophiacodon retroversus*	Femur	129	66
MCZ	4813	*Ophiacodon retroversus*	Femur	131	82
AMNH	4926	*Ophiacodon retroversus*	Femur	138	78
AMNH	24805	*Ophiacodon retroversus*	Femur	140	88
MCZ	1205	*Ophiacodon retroversus*	Femur	141	89
MCZ	1206	*Ophiacodon retroversus*	Femur	141	80
MCZ	1205	*Ophiacodon retroversus*	Femur	143	82
MCZ	1121	*Ophiacodon retroversus*	Femur	144	89
MCZ	3296	*Ophiacodon retroversus*	Femur	148	74
MCZ	1121	*Ophiacodon retroversus*	Femur	151	90
MCZ	1205	*Ophiacodon retroversus*	Femur	163	92
MCZ	1971	*Ophiacodon retroversus*	Femur	164	91
FMNH	UC 458	*Ophiacodon retroversus*	Femur	164	92
MCZ	4812	*Ophiacodon retroversus*	Femur	167	93

MCZ	1299	*Ophiacodon retroversus*	Femur	168	101
FMNH	UC 9	*Ophiacodon retroversus*	Femur	175	96
MCZ	3266	*Ophiacodon retroversus*	Femur	186	99
MCZ	1203	*Ophiacodon retroversus*	Femur	194	95
AMNH	24806	*Ophiacodon retroversus*	Femur	194	118
MCZ	1203	*Ophiacodon retroversus*	Femur	198	100
OMNH	35389	*Ophiacodon retroversus ?*	Femur	214	135
OMNH	35389	*Ophiacodon retroversus?*	Femur	221	145
MCZ	1298	*Ophiacodon retroversus*	Fibula	132	45
FMNH	UC 458	*Ophiacodon retroversus*	Fibula	144	35
AMNH	24804	*Ophiacodon retroversus*	Fibula	150	40
MCZ	5904	*Ophiacodon retroversus*	Fibula	160	45
MCZ	1435	*Ophiacodon retroversus*	Humerus	69	42
MCZ	5926	*Ophiacodon retroversus*	Humerus	77	40
MCZ	2819	*Ophiacodon retroversus*	Humerus	100	48
MCZ	4816	*Ophiacodon retroversus*	Humerus	122	63
MCZ	4816	*Ophiacodon retroversus*	Humerus	124	n/a
MCZ	1121	*Ophiacodon retroversus*	Humerus	127	78
DMNH	11859	*Ophiacodon retroversus*	Humerus	127.1	65
MCZ	1426	*Ophiacodon retroversus*	Humerus	130	70
FMNH	UC646	*Ophiacodon retroversus*	Humerus	135	66
MCZ	5661	*Ophiacodon retroversus*	Humerus	137	72
FMNH	UC 458	*Ophiacodon retroversus*	Humerus	140	75
MCZ	5958	*Ophiacodon retroversus*	Humerus	151	87
MCZ	1915	*Ophiacodon retroversus*	Humerus	157	75
MCZ	1486	*Ophiacodon retroversus*	Humerus	170	82
MCZ	1433	*Ophiacodon retroversus*	Radius	93	37
MCZ	1121	*Ophiacodon retroversus*	Radius	95	40
MCZ	1121	*Ophiacodon retroversus*	Radius	99	45
MCZ	4841	*Ophiacodon retroversus*	Radius	100	38
MCZ	1426	*Ophiacodon retroversus*	Radius	101	45
MCZ	5977	*Ophiacodon retroversus*	Radius	104	41
MCZ	1203	*Ophiacodon retroversus*	Radius	117	47
MCZ	1802	*Ophiacodon retroversus*	Tibia	119	55
MCZ	1443	*Ophiacodon retroversus*	Tibia	110	45
MCZ	1121	*Ophiacodon retroversus*	Tibia	124	51
FMNH	UC 458	*Ophiacodon retroversus*	Tibia	141	53
MCZ	1203	*Ophiacodon retroversus*	Tibia	152	64
MCZ	5374	*Ophiacodon retroversus*	Ulna	114	32
MCZ	1426	*Ophiacodon retroversus*	Ulna	124	45
FMNH	UC 458	*Ophiacodon retroversus*	Ulna	127	38
MCZ	1203	*Ophiacodon retroversus*	Ulna	163	48

FMNH	UC 249	*Ophiacodon uniformis*	Femur	73	38
MCZ	2818	*Ophiacodon uniformis*	Femur	75	51
MCZ	2831	*Ophiacodon uniformis*	Femur	75	53
MCZ	1292	*Ophiacodon uniformis*	Femur	76	45
MCZ	7077	*Ophiacodon uniformis*	Femur	76	44
MCZ	4905	*Ophiacodon uniformis*	Femur	77	41
MCZ	1291	*Ophiacodon uniformis*	Femur	79	45
MCZ	5895	*Ophiacodon uniformis*	Femur	81	42
FMNH	UC 548	*Ophiacodon uniformis*	Femur	81	48
MCZ	7077	*Ophiacodon uniformis*	Femur	82	58
MCZ	4905	*Ophiacodon uniformis*	Femur	85	43
MCZ	2825	*Ophiacodon uniformis*	Femur	92	54
FMNH	UC 547	*Ophiacodon uniformis*	Femur	92	55
MCZ	1295	*Ophiacodon uniformis*	Femur	93	57
MCZ	2822	*Ophiacodon uniformis*	Femur	94	57
MCZ	4905	*Ophiacodon uniformis*	Femur	97	62
FMNH	UC 130	*Ophiacodon uniformis*	Femur	106	55
DMNH	11861	*Ophiacodon uniformis*	Femur	107.2	43
MCZ	1366	*Ophiacodon uniformis*	Femur	116	66
DMNH	11985	*Ophiacodon uniformis*	Femur	118.2	55
MCZ	1366	*Ophiacodon uniformis*	Femur	119	62
DMNH	11862	*Ophiacodon uniformis*	Femur	120.3	48
MCZ	1366	*Ophiacodon uniformis*	Femur	123	60
MCZ	7077	*Ophiacodon uniformis*	Fibula	71	20
MCZ	6386	*Ophiacodon uniformis*	Fibula	74	22
MCZ	1366	*Ophiacodon uniformis*	Fibula	105	27
MCZ	1366	*Ophiacodon uniformis*	Fibula	115	30
FMNH	UC 143	*Ophiacodon uniformis*	Humerus	57	29
MCZ	6157	*Ophiacodon uniformis*	Humerus	59	31
MCZ	5026	*Ophiacodon uniformis*	Humerus	60	33
YPM	17800	*Ophiacodon uniformis*	Humerus	60.6	
MCZ	5958	*Ophiacodon uniformis*	Humerus	61	32
FMNH	UR 656	*Ophiacodon uniformis*	Humerus	63	49
MCZ	2926	*Ophiacodon uniformis*	Humerus	69	38
MCZ	2926	*Ophiacodon uniformis*	Humerus	69	39
MCZ	5047	*Ophiacodon uniformis*	Humerus	83	37
IPBSH	62	*Ophiacodon uniformis*	Humerus	82	37
MCZ	1366	*Ophiacodon uniformis*	Humerus	90	60
MCZ	1366	*Ophiacodon uniformis*	Humerus	95	65
MCZ	1366	*Ophiacodon uniformis*	Humerus	95	50
MCZ	5935	*Ophiacodon uniformis*	Humerus	95	48
MCZ	5517	*Ophiacodon uniformis*	Humerus	134	65

MCZ	5060	*Ophiacodon uniformis*	Radius	65	23
MCZ	1366	*Ophiacodon uniformis*	Radius	76	32
MCZ	7077	*Ophiacodon uniformis*	Tibia	67	30
MCZ	7077	*Ophiacodon uniformis*	Tibia	69	30
MCZ	4966	*Ophiacodon uniformis*	Tibia	72	27
MCZ	5404	*Ophiacodon uniformis*	Tibia	72	38
MCZ	4966	*Ophiacodon uniformis*	Tibia	76	33
MCZ	4966	*Ophiacodon uniformis*	Tibia	77	30
MCZ	5706	*Ophiacodon uniformis*	Tibia	77	32
MCZ	1297	*Ophiacodon uniformis*	Tibia	94	50
MCZ	5996	*Ophiacodon uniformis*	Tibia	95	40
MCZ	1366	*Ophiacodon uniformis*	Tibia	97	55
MCZ	1297	*Ophiacodon uniformis*	Tibia	104	40
MCZ	1366	*Ophiacodon uniformis*	Tibia	105	40
MCZ	1366	*Ophiacodon uniformis*	Ulna	96	27
MCZ	1366	*Ophiacodon uniformis*	Ulna	98	35
DMNH	11879	*Ophiacodon uniformis*	Ulna	113.5	45
OMNH	73694	Ophiacodontidae	Femur	109	41
OMNH	73698	Ophiacodontidae	Humerus	113	50
OMNH	73693	Ophiacodontidae	Tibia	94	43
UMMP	3361	*Poliosaurus?*	Femur	94	55
MNHN	F.MCL-1	*Ruthenosaurus russellorum*	Femur	225	130
MNHN	F.MCL-1	*Ruthenosaurus russellorum*	Humerus	245	130
MNHN	F.MCL-1	*Ruthenosaurus russellorum*	Radius	100+	58
MNHN	F.MCL-1	*Ruthenosaurus russellorum*	Tibia	137	86
MNHN	F.MCL-1	*Ruthenosaurus russellorum*	Ulna	150	72
MCZ	3150	*Ruthiromia elcobriensis*	Femur	116	52
MCZ	3150	*Ruthiromia elcobriensis*	Humerus	105	53
MCZ	3150	*Ruthiromia elcobriensis*	Tibia	82	40
FMNH	UC736	*Scoliomus puercencis*	Femur	144	56
FMNH	UC736	*Scoliomus puercencis*	Humerus	117	48
MCZ	8694	*Secodontosaurus*	Femur	99	37
MCZ	5355	*Secodontosaurus*	Femur	115	47
MCZ	5099	*Secodontosaurus*	Femur	123	45
MCZ	8697	*Secodontosaurus*	Femur	123	48
MCZ	5099	*Secodontosaurus*	Femur	125	49
MCZ	2871	*Secodontosaurus*	Femur	126	57
MCZ	8697	*Secodontosaurus*	Femur	126	46
MCZ	5099	*Secodontosaurus*	Femur	127	48
MCZ	8697	*Secodontosaurus*	Femur	128	47
MCZ	5099	*Secodontosaurus*	Femur	129	65
MCZ	5099	*Secodontosaurus*	Femur	130	45

MCZ	5099	*Secodontosaurus*	Femur	130	48
MCZ	8697	*Secodontosaurus*	Femur	130	48
MCZ	8697	*Secodontosaurus*	Femur	130	55
MCZ	5099e	*Secodontosaurus*	Femur	130	52
MCZ	5099	*Secodontosaurus*	Femur	131	47
MCZ	8697	*Secodontosaurus*	Femur	131	45
MCZ	5099	*Secodontosaurus*	Femur	132	46
MCZ	8697	*Secodontosaurus*	Femur	132	50
MCZ	5099a	*Secodontosaurus*	Femur	132	53
MCZ	8697	*Secodontosaurus*	Femur	134	55
MCZ	1326	*Secodontosaurus*	Femur	135	51
MCZ	8697	*Secodontosaurus*	Femur	135	52
MCZ	8697	*Secodontosaurus*	Femur	138	51
MCZ	5099	*Secodontosaurus*	Femur	141	52
MCZ	2944	*Secodontosaurus*	Femur	142	54
MCZ	3170	*Secodontosaurus*	Femur	146	60
MCZ	3170	*Secodontosaurus*	Femur	151	65
MCZ	8699	*Secodontosaurus*	Fibula	112	28
MCZ	8699	*Secodontosaurus*	Fibula	118	27
MCZ	8699	*Secodontosaurus*	Fibula	119	27
MCZ	1301	*Secodontosaurus*	Fibula	120	27
MCZ	8699	*Secodontosaurus*	Fibula	120	28
MCZ	5024	*Secodontosaurus*	Humerus	98	38
MCZ	5018	*Secodontosaurus*	Humerus	106	57
MCZ	5018a	*Secodontosaurus*	Humerus	118	45
MCZ	5018	*Secodontosaurus*	Humerus	119	46
MCZ	5019	*Secodontosaurus*	Humerus	119	43
MCZ	1308	*Secodontosaurus*	Humerus	120	48
MCZ	5018g	*Secodontosaurus*	Humerus	120	46
MCZ	5018	*Secodontosaurus*	Humerus	121	42
MCZ	5018	*Secodontosaurus*	Humerus	122	44
MCZ	7012	*Secodontosaurus*	Humerus	122	68
MCZ	5018e	*Secodontosaurus*	Humerus	122	44
MCZ	5019c	*Secodontosaurus*	Humerus	122	55
MCZ	5018	*Secodontosaurus*	Humerus	124	54
MCZ	5020	*Secodontosaurus*	Humerus	124	63
MCZ	3157	*Secodontosaurus*	Humerus	126	46
MCZ	5018f	*Secodontosaurus*	Humerus	128	45
MCZ	5019e	*Secodontosaurus*	Humerus	128	50
MCZ	5019d	*Secodontosaurus*	Humerus	130	53
MCZ	7013	*Secodontosaurus*	Humerus	131	55
MCZ	2944	*Secodontosaurus*	Humerus	132	50

MCZ	5020	*Secodontosaurus*	Humerus	132	63
MCZ	7066	*Secodontosaurus*	Humerus	135	50
MCZ	5020	*Secodontosaurus*	Humerus	136	54
MCZ	7014	*Secodontosaurus*	Humerus	137	59
MCZ	5019	*Secodontosaurus*	Humerus	139	52
MCZ	5064	*Secodontosaurus*	Radius	107	27
MCZ	5064	*Secodontosaurus*	Radius	107	33
MCZ	5064	*Secodontosaurus*	Radius	111	30
MCZ	5064	*Secodontosaurus*	Radius	114	37
MCZ	5064	*Secodontosaurus*	Radius	116	36
MCZ	5064	*Secodontosaurus*	Radius	116	33
MCZ	5941	*Secodontosaurus*	Radius	118	40
MCZ	8698	*Secodontosaurus*	Tibia	98	33
MCZ	8698	*Secodontosaurus*	Tibia	100	45
MCZ	8698	*Secodontosaurus*	Tibia	102	35
MCZ	8698	*Secodontosaurus*	Tibia	102	36
MCZ	8698	*Secodontosaurus*	Tibia	103	33
MCZ	8698	*Secodontosaurus*	Tibia	106	42
MCZ	8698	*Secodontosaurus*	Tibia	110	39
MCZ	8698	*Secodontosaurus*	Tibia	111	33
MCZ	6480	*Secodontosaurus*	Tibia	112	35
MCZ	8698	*Secodontosaurus*	Tibia	112	38
MCZ	8698	*Secodontosaurus*	Tibia	112	35
MCZ	5635	*Secodontosaurus*	Tibia	114	35
MCZ	8698	*Secodontosaurus*	Tibia	114	36
MCZ	5635	*Secodontosaurus*	Tibia	115	35
MCZ	8698	*Secodontosaurus*	Tibia	115	33
MCZ	8698	*Secodontosaurus*	Tibia	118	45
MCZ	5635	*Secodontosaurus*	Tibia	120	37
MCZ	1311	*Secodontosaurus*	Ulna	116	25
MCZ	5949	*Secodontosaurus*	Ulna	118	26
MCZ	5054	*Secodontosaurus*	Ulna	138	32
MCZ	1306	*Secodontosaurus*	Ulna	141	38
MCZ	7078	*Secodontosaurus*	Ulna	151	38
FMNH	UC 1100	*Secodontosaurus willistoni*	Femur	200	94
FMNH	UC 1218	*Sphenacodon*	Femur	137	71
MCZ	4917	*Sphenacodon*	Femur	183	82
MCZ	4906	*Sphenacodon*	Humerus	150	55
MCZ	4906	*Sphenacodon*	Humerus	176	78
MCZ	4916	*Sphenacodon*	Tibia	84	34
MCZ	4916	*Sphenacodon*	Tibia	90	30
MCZ	4916	*Sphenacodon*	Tibia	91	30

MCZ	7060	*Sphenacodon ferox*	Femur	98	48
FMNH	UC 35	*Sphenacodon ferox*	Femur	156	74
YPM	818	*Sphenacodon ferox*	Humerus	163	N/A
FMNH	UC 35	*Sphenacodon ferox*	Humerus	131	69
FMNH	UC 35	*Sphenacodon ferox*	Humerus	134	56
OMNH	73663	*Sphenacodontidae*	Femur	122	46
MNHN	AUT 588	*Stereorachis dominans*	Ulna	147	61
FMNH	UC 652	*Trichasaurus texensis*	Femur	121	56
FMNH	UC 652	*Trichasaurus texensis*	Humerus	108	55
FMNH	UC 652	*Trichasaurus texensis*	Ulna	86.8	36
FMNH	UC 955	*Varanops*	Femur	83	34
FMNH	UR 607	*Varanops*	Femur	83	35
FMNH	UR 608	*Varanops*	Femur	83	33
FMNH	UC 906	*Varanops*	Femur	84	45
FMNH	UC 985	*Varanops*	Femur	86	35
FMNH	UC 906	*Varanops*	Femur	87	42
FMNH	UC 915	*Varanops*	Femur	87	45
OMNH	73758	*Varanops*	Femur	88	37
FMNH	UC 920	*Varanops*	Femur	88	37
FMNH	UC 922	*Varanops*	Femur	88	47
FMNH	UC 943	*Varanops*	Femur	90	47
FMNH	UC 943	*Varanops*	Femur	90	45
FMNH	UC 936	*Varanops*	Femur	95	53
FMNH	UC 946	*Varanops*	Femur	97	36
FMNH	UC 934	*Varanops*	Femur	99	48
FMNH	UR 941	*Varanops*	Femur	100	26
FMNH	UC 944	*Varanops*	Humerus	68	34
FMNH	UR 695	*Varanops*	Humerus	70	33
FMNH	P 12841	*Varanops*	Humerus	71	25
FMNH	UC 940	*Varanops*	Humerus	72	37
FMNH	UC 978	*Varanops*	Humerus	79	36
FMNH	UC 955	*Varanops*	Tibia	61.8	22
FMNH	UC 936	*Varanops*	Tibia	73	32
FMNH	UC 942	*Varanops*	Tibia	82	36
FMNH	UR 348	*Varanops brevirostris*	Femur	80	33
FMNH	UR 348	*Varanops brevirostris*	Femur	84	30
FMNH	UR349	*Varanops brevirostris*	Femur	86	33
MCZ	1926	*Varanops brevirostris*	Femur	87	32
MCZ	1926	*Varanops brevirostris*	Femur	88	27
FMNH	UC 644	*Varanops brevirostris*	Femur	93	41
FMNH	UC 644	*Varanops brevirostris*	Femur	94	45
FMNH	UR 348	*Varanops brevirostris*	Fibula	69	18

MCZ	1926	*Varanops brevirostris*	Fibula	72	15
MCZ	1926	*Varanops brevirostris*	Fibula	72	16
FMNH	UC 644	*Varanops brevirostris*	Fibula	80	29
FMNH	UC 644	*Varanops brevirostris*	Fibula	82	29
MCZ	1926	*Varanops brevirostris*	Humerus	62	25
MCZ	1926	*Varanops brevirostris*	Humerus	69	27
FMNH	UC 644	*Varanops brevirostris*	Humerus	70	42
FMNH	UC 644	*Varanops brevirostris*	Humerus	72	31
FMNH	UC 644	*Varanops brevirostris*	Radius	52	25
FMNH	UC 644	*Varanops brevirostris*	Radius	56	21
MCZ	1926	*Varanops brevirostris*	Tibia	69	24
MCZ	1926	*Varanops brevirostris*	Tibia	71	24
FMNH	UC 644	*Varanops brevirostris*	Tibia	76	31
FMNH	UC 644	*Varanops brevirostris*	Tibia	78	28
FMNH	UC 644	*Varanops brevirostris*	Ulna	58	29
FMNH	UC 644	*Varanops brevirostris*	Ulna	60	28
OMNH	73750-C	*Varanopseidae*	Femur	49	17
OMNH	73354	*Varanopseidae*	Femur	50	17
OMNH	73750-B	*Varanopseidae*	Femur	51	18
OMNH	73750-A	*Varanopseidae*	Femur	57	22
OMNH	73355	*Varanopseidae*	Fibula	37	N/A
FMNH	UC 756	*Varanosaurus*	Femur	74	33
FMNH	WM 909	*Varanosaurus*	Femur	89	33
FMNH	WM 909	*Varanosaurus*	Femur	90	34
YPM	3269	*Varanosaurus*	Femur	104	46
YPM	3269	*Varanosaurus*	Fibula	61	26
YPM	3269	*Varanosaurus*	Humerus	84.7	40
FMNH	UC 1307	*Varanosaurus*	Tibia	58	26
FMNH	UC 1314	*Varanosaurus*	Tibia	62	27
FMNH	UC 758	*Varanosaurus*	Tibia	55	24
YPM	3269	*Varanosaurus*	Tibia	70.2	29
FMNH	UC 1281	*Varanosaurus*	Tibia	76	28
UMMP	22056	*Varanosaurus*	Ulna	46	18
UMMP	22056	*Varanosaurus*	Ulna	55	20
UMMP	22056	*Varanosaurus*	Ulna	57	20
FMNH	UC 1256	*Varanosaurus acutirostris*	Femur	89.5	32
MCZ	6373	*Varanosaurus wichitaensis*	Femur	63	28
MCZ	6377	*Varanosaurus wichitaensis*	Femur	64	31
MCZ	6373	*Varanosaurus wichitaensis*	Femur	71	28
MCZ	6373	*Varanosaurus wichitaensis*	Femur	75	31
UMMP	11655	*Varanosaurus wichitaensis*	Femur	75	30
UMMP	11655	*Varanosaurus wichitaensis*	Femur	75	30

MCZ	8162	*Varanosaurus wichitaensis?*	Femur	47	21

Appendix 4 (Chapter 2):
Consumptive samples of excavated and loaned material (L= longitudinal, T= transverse).

Specimen Number	Bone	Cut	Organism	Notes
IPBSH-142	Cartilage	T	Shark	RS2
IPBSH-130	Femur	L	*Dimetrodon*	LP-2, Distal
MSU	Femur	L	*Dimetrodon*	MSU-5B, Distal
IPBSH-99	Femur	T	*Dimetrodon*	SABCBB2010-76, Prox.
IPBSH-98	Femur	T	*Dimetrodon*	SABCBB2010-42, Prox.
IPBSH-132	Femur	L	*Dimetrodon*	LP-3, Prox.
MSU	Femur	L & T	*Dimetrodon*	MSU-5A, Prox.
IPBSH-103	Femur	T	*Dimetrodon*	53blk5B
IPBSH-102	Femur	T	*Dimetrodon*	53blk5A
IPBSH-65	Femur	T	*Archeria*	SABCBB2010-196
OMNH 00631	Femur	T	*Cotylorhynchus romeri*	
OMNH-01728	Femur	T	*Cotylorhynchus romeri*	C
IPBSH-77	Femur	T	*Diadectes*	A85, A27
IPBSH-96	Femur	T	*Dimetrodon*	SABCBB2010-176, Distal
IPBSH -59	Femur	T	*Dimetrodon*	SABCBB2010-185
IPBSH -60	Femur	T	*Dimetrodon*	SABCBB2011-41
IPBSH -61	Femur	T	*Dimetrodon*	SABCBB2010-156
IPBSH -45	Femur	T	*Dimetrodon*	SABCBB2011-3
IPBSH-119	Femur	T	*Dimetrodon*	LP-1, RSC
IPBSH-114	Femur	T	*Dimetrodon*	A96a, Prox.
TMM 30966-291	Femur	T	*Dimetrodon*	
IPBSH-105	Femur	T	*Dimetrodon*	SABCBB2010-108
OMNH-15044	Femur	T	*Dimetrodon giganhomogenes*	Core
TMM 30966-201	Femur	T	*Dimetrodon giganhomogenes*	
TMM 30966-49	Femur	T	*Dimetrodon giganhomogenes*	
HMNS-3-106R3	Femur	T	*Dimetrodon limbatus*	Oklahoma via Japan
MCZ VPRA-5106	Femur	T	*Dimetrodon limbatus*	
MCZ VPRA-7008	Femur	T	*Dimetrodon limbatus*	
IPBSH -42	Femur	T	*Dimetrodon natalis*	SABCBB2011-184
IPBSH -3	Femur	T	*Dimetrodon natalis*	SABCBB2010-10
IPBSH -1	Femur	T	*Dimetrodon natalis*	SABCBB2010- 184
IPBSH -19	Femur	L & T	*Dimetrodon natalis*	SABCBB2010-26,A,B
IPBSH -6	Femur	T	*Dimetrodon natalis*	SABCBB2010-11
IPBSH -31	Femur	T	*Dimetrodon natalis*	SABCBB2010-66
IPBSH -37	Femur	T	*Dimetrodon natalis*	SABCBB2010-79, serial
IPBSH -35	Femur	T	*Dimetrodon natalis*	SABCBB2010-76
IPBSH -29	Femur	T	*Dimetrodon natalis*	SABCBB2010-57

IPBSH -40	Femur	T	*Dimetrodon natalis*	SABCBB2011-1
IPBSH -2	Femur	L & T	*Dimetrodon natalis*	SABCBB2010-1
IPBSH-87	Femur	T	*Dimetrodon natalis*	102blk13A
IPBSH -8	Femur	T	*Dimetrodon ?*	SABCBB2010-124
IPBSH-84	Femur	T	*Edaphosaurus*	SABCBB2010-157
TMM 31255-6.1	Femur	T	*Edaphosaurus boanerges*	
TMM 31255-20	Femur	T	*Edaphosaurus boanerges*	
IPBSH-64	Femur	T	*Eryops*	SABCBB2011-29
IPBSH-78	Femur	T	*Eryops*	SABCBB2010-158
IPBSH-85	Femur	T	*Eryops*	RSC3-2013-17
MSU	Femur	T	*Eryops*	MSU-1, Prox.
IPBSH -56	Femur	T	*Eryops*	SABCBB2011-9
MCZ VPRA-3412A	Femur	T	*Lupeosaurus kayii*	1 mi East Geraldine BB
IPBSH -46	Femur	L & T	*Ophiacodon*	SABCBB2011-36
OMNH-55234	Femur	T	*Ophiacodon mirus*	Kissel and Lehman 2002
OMNH-35389	Femur	T	*Ophiacodon retroversus*	
MSU	Femur	T	*Ophiacodon uniformis*	MSU-3
OMNH-73694	Femur	T	*Ophiacodontidae*	
OMNH-01728	Femur	T	pelycosaur	D
IPBSH -51	Femur	T	Reptile	SABCBB2010-71, keel
OMNH-73663	Femur	T	Sphenacodontidae	Core
IPBSH-86	Femur	T	Unknown	17blk2b
OMNH 73750	Femur	T	Varanopidae	A
OMNH 73750	Femur	T	Varanopidae	B
OMNH 73750	Femur	T	Varanopidae	C
OMNH 73758	Femur	T	*Varanops brevirostris*	
OMNH 73554	Femur	T	Varanopseidae	
IPBSH-111	Femur	T	Unknown	SABCBB2011-27
IPBSH -21	Femur?	T	*Dimetrodon*	SABCBB2010-28
IPBSH -41	Femur?	T	*Dimetrodon?*	SABCBB2011-11
IPBSH-72	Fibula	T	Amphibian	SABCBB2010-83
IPBSH -54	Fibula	T	*Dimetrodon*	SABCBB2011-85, head
HMNS-3-107R3	Fibula	T	*Dimetrodon limbatus*	Oklahoma via Japan
IPBSH-139	Fibula	T	*Dimetrodon limbatus*	P26, head
IPBSH-93	Fibula	T	*Dimetrodon natalis*	144Blk19B
IPBSH-104	Fibula	T	*Dimetrodon natalis*	5blk1A
IPBSH -55	Fibula	T	*Dimetrodon?*	SABCBB2011-86, head
IPBSH-81	Fibula	T	*Eryops*	144blk10a, -19a
IPBSH-79	Humerus	T	*Amphibian*	SABCBB2010-82
IPBSH -38	Humerus	T	*Archeria*	SABCBB2010-85
IPBSH -48	Humerus	T	*Archeria*	SABCBB2011-56

IPBSH- 23	Humerus	T	*Archeria*	SABCBB2010-33
OMNH 00631	Humerus	T	*Cotylorhynchus romeri*	Core
OMNH-01728	Humerus	T	*Cotylorhynchus romeri*	A
OMNH-01728	Humerus	T	*Cotylorhynchus romeri*	B
IPBSH -57	Humerus	T	*Dimetrodon*	SABCBB2010-12
IPBSH -58	Humerus	T	*Dimetrodon*	SABCBB2011-68
IPBSH-97	Humerus	T	*Dimetrodon*	SABCBB2010-195
IPBSH-133	Humerus	L	*Dimetrodon*	LP-4, Distal
IPBSH-135	Humerus	T	*Dimetrodon*	LP-5, Prox.
MCZ VPRA-5022	Humerus	T	*Dimetrodon booneorum*	
MCZ VPRA-7002	Humerus	T	*Dimetrodon booneorum*	
MCZ VPRA-7004	Humerus	T	*Dimetrodon booneorum*	
OMNH-590	Humerus	T	*Dimetrodon grandis*	Core
IPBSH -27	Humerus	T	*Dimetrodon limbatus ?*	SABCBB2010-46
IPBSH -13	Humerus	T	*Dimetrodon natalis*	SABCBB2010-152
IPBSH -25	Humerus	L & T	*Dimetrodon natalis*	SABCBB2010-36
IPBSH -49	Humerus	T	*Dimetrodon natalis*	SABCBB2011-64
IPBSH -11	Humerus	T	*Dimetrodon natalis*	SABCBB2010-139
IPBSH -14	Humerus	L & T	*Dimetrodon natalis*	SABCBB2010-154
IPBSH -22	Humerus	T	*Dimetrodon natalis*	SABCBB2010-33
IPBSH -5	Humerus	T	*Dimetrodon natalis*	SABCBB2010-109
IPBSH- 33	Humerus	L & T	*Dimetrodon natalis*	SABCBB2010-68
IPBSH -4	Humerus	T	*Dimetrodon natalis*	SABCBB2010-107
IPBSH -34	Humerus	T	*Dimetrodon natalis*	SABCBB2010-72, Serial
IPBSH -47	Humerus	T	*Dimetrodon natalis*	SABCBB2011-49
IPBSH-95	Humerus	T	*Dimetrodon natalis*	17blk2A
IPBSH-92	Humerus	T	*Dimetrodon natalis*	120blk15B
IPBSH-110	Humerus	T	*Dimetrodon?*	SABCBB2011 (2010)-163
TMM 31255-2	Humerus	T	*Edaphosaurus boanerges*	
TMM 31255-71	Humerus	T	*Edaphosaurus boanerges*	
TMM 31255-70	Humerus	T	*Edaphosaurus boanerges*	
MCZ VPRA-1368	Humerus	T	*Lupeosaurus kayii*	2 mi South of Black Flats
OMNH 52543	Humerus	T	*Mycterosaurus longiceps*	
OMNH-55204	Humerus	T	*Ophiacodon mirus*	Semnole OK
MCZ VPRA-1486	Humerus	T	*Ophiacodon retroversus*	Brinkman 1988
MCZ VPRA-2819	Humerus	T	*Ophiacodon retroversus*	Brinkman 1988
MCZ VPRA-4816	Humerus	T	*Ophiacodon retroversus*	Brinkman 1988
MCZ VPRA-4816	Humerus	T	*Ophiacodon retroversus*	Brinkman 1988
MCZ VPRA-5926	Humerus	T	*Ophiacodon retroversus*	Brinkman 1988
IPBSH-62	Humerus	T	*Ophiacodon uniformis*	102blk13B
IPBSH-88	Humerus	T	*Ophiacodon uniformis*	102blk13B
IPBSH-101	Humerus	T	*Ophiacodon?*	SABCBB2011-88, Prox.

OMNH-73698	Humerus	T	Ophiacodontidae	
IPBSH-136	Humerus	L	Pelycosaur	LP-7, Prox.
MSU	Humerus	T	Pelycosaur	MSU-6, Prox.
IPBSH-63	Intercentrum	T	*Eryops*	Float
IPBSH-68	Long bone	T	Unknown	SABCBB2010-195B
IPBSH -7	Metatarsal	T	Amphibian	SABCBB2010-118
IPBSH -16	Metatarsal	T	Amphibian	SABCBB2010-172
IPBSH-113	Metatarsal	T	Reptile	A
IPBSH -17	Metatarsal	T	Reptile	SABCBB2010-173
IPBSH-141	Nrl. spine	T	*Ctenospondylus*	RS1a and RS1b
IPBSH-127	Nrl. spine	L & T	*Dimetrodon*	LP-17
IPBSH-128	Nrl. spine	T	*Dimetrodon*	LP-18
MSU	Nrl. spine	T	*Dimetrodon grandis*	MSU-4
MNG 10598	Nrl. spine	T	*Dimetrodon tuetonis*	Gotha, Germany- holotype
IPBSH-129	Nrl. spine	T	*Edaphosaurus*	LP-19
IPBSH-131	Nrl. spine	T	*Edaphosaurus*	LP-20
IPBSH-82	Nrl. spine	L	*Edaphosaurus*	Float, Serial
IPBSH-83	Nrl. spine	L	*Edaphosaurus*	Float, Serial
IPBSH-100	Nrl. spine	T	*Edaphosaurus*	SABCBB2011-87
IPBSH-118	Nrl. spine	T	*Edaphosaurus*	LBB-1 2013, Texas
CM 38029	Nrl. spine	T	*Platyhystrix rugosus*	20129, New mexico
IPBSH -9	Phalange	T	*Caseidae*	SABCBB2010-126
IPBSH-122	Phalange	T	*Eryops*	LP-12
IPBSH-115	Phalange	T	Reptile	B
IPBSH-116	Phalange	T	Reptile	C
IPBSH-117	Phalange	T	Reptile	D
IPBSH-66	Radius	T	Amphibian	SABCBB2010-183
IPBSH-71	Radius	T	Amphibian	SABCBB2010-194
IPBSH-70	Radius	T	Amphibian	ACBB2010-1
IPBSH-75	Radius	T	Amphibian	SABCBB2011-44
IPBSH-106	Radius	T	Amphibian	SABCBB2010-109B
MNG 10552	Radius	T	Caseidae	Gotha, Germany
IPBSH -20	Radius	T	*Dimetrodon*	SABCBB2010-27, Distal
IPBSH-107	Radius	T	*Dimetrodon*	SABCBB2010-24
IPBSH -10	Radius	T	*Dimetrodon natalis*	SABCBB2010-138
IPBSH -32	Radius	T	*Dimetrodon natalis*	SABCBB2010-67
IPBSH -24	Radius	T	*Dimetrodon natalis*	SABCBB2010-34
IPBSH-112	Radius	T	*Dimetrodon natalis*	78blk10A
IPBSH-91	Radius	T	*Dimetrodon natalis*	120blk15A
IPBSH-90	Radius	T	Pelycosaur	102blk13E, embryonic?
MNHN.F.MCL-1	Radius	L & T	*Ruthenosaurus russellorum*	France, holotype
MPUR-151	Rib	T	*Alierasaurus ronchii*	Sardinia, Italy

IPBSH-80	Rib	T	*Amphibian*	102blk13c
OMNH-627	Rib	T	*Cotylorhynchus romeri*	Head
OMNH-00627	Rib	T	*Cotylorhynchus romeri*	Head
IPBSH-69	Rib	T	*Eryops*	SABCBB2010-35
MNHN.F.MCL-1	Rib	L & T	*Ruthenosaurus russellorum*	France, holotype
IPBSH-67	Rib	T	Unknown	SABCBB2010-195A
HMNS A51-2	Skeleton	L	*Lysorophus*	Adult, Craddock BB
HMNS A51-9	Skeleton	L	*Lysorophus*	Juvenile, Craddock BB
IPBSH-120	Tarsal	T	*Pelycosaur*	LP-10
IPBSH-138	Tarsal	T	*Pelycosaur*	LP-9
IPBSH-121	Tarsal	T	*Pelycosaur*	LP-11
IPBSH -53	Tibia	T	*Dimetrodon*	SABCBB2011-84
IPBSH -18	Tibia	T	*Dimetrodon*	SABCBB2010-2
IPBSH -50	Tibia	T	*Dimetrodon natalis*	SABCBB2011-67
IPBSH -15	Tibia	T	*Dimetrodon natalis*	SABCBB2010-165
IPBSH -43	Tibia	T	*Dimetrodon natalis*	SABCBB2011-19
IPBSH -44	Tibia	T	*Dimetrodon natalis*	SABCBB2011-28
IPBSH -30	Tibia	T	*Dimetrodon natalis*	SABCBB2010-65
IPBSH -39	Tibia	T	*Dimetrodon natalis*	SABCBB2010-92
IPBSH -52	Tibia	T	*Dimetrodon natalis*	SABCBB2011-83
MCZ VPRA-3412B	Tibia	T	*Lupeosaurus kayii*	1 mi East Geraldine BB
HMNS-3-108R3	Tibia	T	*Dimetrodon limbatus*	Oklahoma via Japan
IPBSH-89	Tibia	T	*Dimetrodon natalis*	102blk13D, prox.
IPBSH-94	Tibia	T	*Dimetrodon natalis*	147blk22A, prox.
IPBSH-137	Tibia/Fibula	T	Pelycosaur	LP-8, Distal
IPBSH -12	Tibia?	T	*Dimetrodon natalis*	SABCBB2010-139x
IPBSH-76	Ulna	T	Amphibian	SABCBB2010-117
IPBSH-73	Ulna	T	Amphibian	SABCBB2010-103
IPBSH-74	Ulna	T	Amphibian	SABCBB2010-81
MNG 10552	Ulna	T	Caseidae	Gotha, Germany
OMNH-627	Ulna	T	*Cotylorhynchus romeri*	Core
MSU	Ulna	T	*Dimetrodon*	MSU-2
IPBSH -28	Ulna	L & T	*Dimetrodon natalis*	SABCBB2010-55
IPBSH -26	Ulna	T	*Dimetrodon natalis*	SABCBB2010-39
IPBSH -36	Ulna	T	*Dimetrodon natalis*	SABCBB2010-77, head
IPBSH-134	Ulna	T	*Edaphosaurus*	LP-4X, Prox.
IPBSH-108	Vertebrae	T	*Dimetrodon*	SABCBB2010-78
IPBSH-109	Vertebrae	T	*Dimetrodon*	SABCBB2010-84
IPBSH-123	Vertebrae	L	*Dimetrodon*	LP-13
IPBSH-124	Vertebrae	T	*Dimetrodon*	LP-14
IPBSH-125	Vertebrae	L	*Edaphosaurus*	LP-15, ACBBIII

IPBSH-126	Vertebrae	T	*Edaphosaurus*	LP-16, ACBBIII
IPBSH-140	Vertebrae	T	*Edaphosaurus*	P8
IPBSH-143	Vertebrae	T	Shark	RS3

Appendix 5 (Chapter 3):

BCBB sphenacodontid humeri and femora used to create scatter plots of the minimal diaphysis circumference plotted against length. Listing is in order of increasing length.

Specimen ID	Bone	Sphenacodontidae	Length (mm)	Circumference (mm)
MCZ- 5034	Humerus	D. limbatus	42	19
UMMP- 22220	Humerus	Dimetrodon sp.	51	18
UMMP- 22220	Humerus	Dimetrodon sp.	57	26
IPBSH-13	Humerus	D. natalis	57.8	28
IPBSH-25	Humerus	D. natalis	58.1	27
UMMP- 22220	Humerus	Dimetrodon sp.	60	27
IPBSH-49	Humerus	sphenacodontid	60	28
UMMP- 22220	Humerus	Dimetrodon sp.	61	32
FMNH-UC 818	Humerus	D. natalis	62.5	31
UMMP- 22220	Humerus	Dimetrodon sp.	63	27
IPBSH-11	Humerus	D. natalis	63.3	29
UMMP- 22220	Humerus	Dimetrodon sp.	64	31
IPBSH-57	Humerus	sphenacodontid	64.3	35
UMMP- 22220	Humerus	Dimetrodon sp.	65	28
FMNH-UC 818	Humerus	D. natalis	66.2	30
UMMP- 22220	Humerus	Dimetrodon sp.	69	34
IPBSH-14	Humerus	D. natalis	69.8	33
UMMP- 22220	Humerus	Dimetrodon sp.	72	38
IPBSH-58	Humerus	sphenacodontid	73	25
IPBSH-22	Humerus	D. natalis	81	42
UMMP- 22236	Humerus	Dimetrodon sp.	82	36

IPBSH-5	Humerus	D. natalis	82	40
FMNH-UC 837	Humerus	D. natalis	88	32
FMNH-UC 90	Humerus	D. natalis	88	33
FMNH-UC 818	Humerus	D. natalis	89.8	34
MCZ- 5937	Humerus	D. limbatus	94	53
UMMP- 22236	Humerus	Dimetrodon sp.	94	32
UMMP- 22978	Humerus	Dimetrodon sp.	95	49
MCZ- 5024	Humerus	secodontosaurus sp.	98	38
UMMP- 22236	Humerus	Dimetrodon sp.	98	35
UMMP- 22236	Humerus	Dimetrodon sp.	104	39
FMNH-UC 79	Humerus	D. natalis	105	41
UMMP- 22978	Humerus	Dimetrodon sp.	109	43
UMMP- 22236	Humerus	Dimetrodon sp.	110	40
UMMP- 67586	Humerus	Dimetrodon sp.	110	46
UMMP- 22236	Humerus	Dimetrodon sp.	113	39
IPBSH-33	Humerus	D. natalis	113.5	54
FMNH- UC 75	Humerus	D. booneorum	115	47
FMNH- UC 816	Humerus	D. booneorum	115	45
FMNH- UC 816	Humerus	D. booneorum	115	54
UMMP- 22236	Humerus	Dimetrodon sp.	115	38
FMNH-UC 802	Humerus	D. natalis	116	53
FMNH- UC 816	Humerus	D. booneorum	116	47
UMMP- 3367	Humerus	Dimetrodon sp.	116	39
MCZ- 7003	Humerus	D. booneorum	117	50
FMNH- UC 816	Humerus	D. booneorum	117	51
UMMP- 22236	Humerus	Dimetrodon sp.	118	43

MCZ- 5019	Humerus	secodontosaurus sp.	119	43
UMMP- 3373	Humerus	Dimetrodon sp.	119	43
MCZ- 1308	Humerus	secodontosaurus sp.	120	48
UMMP- 22236	Humerus	Dimetrodon sp.	120	35
UMMP- 67586	Humerus	Dimetrodon sp.	120	49
IPBSH-4	Humerus	D. natalis	120	42
FMNH-UC 802	Humerus	D. natalis	121	58
MCZ-7012	Humerus	secodontosaurus sp.	122	68
MCZ- 5019c	Humerus	secodontosaurus sp.	122	55
UMMP- 22236	Humerus	Dimetrodon sp.	122	45
UMMP- 22976	Humerus	Dimetrodon sp.	122	50
UMMP- 9744	Humerus	D. natalis	123	48
UMMP- 3360	Humerus	Dimetrodon sp.	123	43
MCZ- 5020	Humerus	secodontosaurus sp.	124	63
FMNH-UC 856	Humerus	D. natalis	124	47
FMNH-UC 802	Humerus	D. natalis	124	57
FMNH- UC 816	Humerus	D. booneorum	124	53
UMMP- 67586	Humerus	Dimetrodon sp.	124	52
FMNH-UC 248	Humerus	D. natalis	125	60
FMNH- UC 816	Humerus	D. booneorum	125	58
UMMP- 3359	Humerus	Dimetrodon sp.	125	42
IPBSH-47	Humerus	sphenacodontid	125	43
MCZ- 3157	Humerus	secodontosaurus sp.	126	46
UMMP- 22236	Humerus	Dimetrodon sp.	126	47
UMMP- 22976	Humerus	Dimetrodon sp.	126	46
MCZ- 5019e	Humerus	secodontosaurus sp.	128	50

MCZ- 7004	Humerus	D. booneorum	128	50
MCZ- 5019d	Humerus	secodontosaurus sp.	130	53
FMNH- UC 816	Humerus	D. booneorum	130	57
UMMP- 22236	Humerus	Dimetrodon sp.	130	50
MCZ- 7013	Humerus	secodontosaurus sp.	131	55
FMNH- UC 247	Humerus	D. booneorum	131	56
UMMP- 22236	Humerus	Dimetrodon sp.	131	46
UMMP- 67586	Humerus	Dimetrodon sp.	131	48
IPBSH-34	Humerus	sphenacodontid	131	55
MCZ- 5020	Humerus	secodontosaurus sp.	132	63
UMMP- 16343	Humerus	D. natalis	132	51
UMMP- 22236	Humerus	Dimetrodon sp.	132	47
FMNH-UC 802	Humerus	D. natalis	134	53
MCZ- 7066	Humerus	secodontosaurus sp.	135	50
MCZ- 1930	Humerus	D. booneorum	135	58
MCZ- 5020	Humerus	secodontosaurus sp.	136	54
MCZ- 7014	Humerus	secodontosaurus sp.	137	59
MCZ- 5045	Humerus	D. limbatus	138	67
MCZ- 5019	Humerus	secodontosaurus sp.	139	52
MCZ- 5043	Humerus	D. booneorum	140	70
MCZ- 5022	Humerus	D. booneorum	145	70
UMMP- 22236	Humerus	Dimetrodon sp.	145	56
UMMP- 55037	Humerus	D. limbatus	150	77
FMNH- UC 844	Humerus	D. booneorum	151	69
MCZ- 5040	Humerus	D. limbatus	154	67
MCZ- 5043	Humerus	D. booneorum	155	75

UMMP- 9765	Humerus	D. limbatus	156	76
FMNH- UC 816	Humerus	D. booneorum	158	79
MCZ- 5038	Humerus	D. limbatus	163	97
FMNH-UC 843	Humerus	D. limbatus	163	74
MCZ- 5039	Humerus	D. limbatus	167	92
MCZ- 1338	Humerus	D. limbatus	168	90
FMNH-UC 841	Humerus	D. limbatus	171	101
MCZ- 5042	Humerus	D. limbatus	172	80
MCZ- 5037	Humerus	D. limbatus	178	84
MCZ- 5041	Humerus	D. limbatus	180	105
FMNH- 22219	Femur	Dimetrodon sp.	60	23
MCZ- 5097b	Femur	Dimetrodon sp.	64	27
FMNH- 22219	Femur	Dimetrodon sp.	68	28
MCZ- 5097a	Femur	Dimetrodon sp.	71	28
FMNH- 22219	Femur	Dimetrodon sp.	72	28
MCZ- 5572	Femur	Dimetrodon sp.	73	30
MCZ- 1320	Femur	Dimetrodon sp.	77	30
MCZ- 5097c	Femur	Dimetrodon sp.	77	27
FMNH- 22219	Femur	Dimetrodon sp.	77	38
FMNH- 22219	Femur	Dimetrodon sp.	80	36
IPBSH-59	Femur	sphenacodontid	80	34
UMMP- UC 55	Femur	Dimetrodon sp.	85	33
UMMP- UC 57	Femur	Dimetrodon sp.	88	34
UMMP- UC 76	Femur	D. natalis	96	35
FMNH- 22215	Femur	D. natalis	96	37
FMNH- 22215	Femur	D. natalis	97	36

IPBSH-19	Femur	D. natalis	98	38
MCZ- 8694	Femur	Secodontosaurus sp.	99	37
UMMP- UC 150	Femur	D. natalis	100	37
FMNH- 22215	Femur	D. natalis	103	38
FMNH- 22215	Femur	D. natalis	103	47
IPBSH-60	Femur	sphenacodontid	103	35
MCZ- 8690	Femur	Dimetrodon sp.	105	36
FMNH- 22224	Femur	D. natalis	105	37
FMNH- 22224	Femur	D. natalis	105	35
MCZ- 8689	Femur	Dimetrodon sp.	106	40
IPBSH-6	Femur	D. natalis	107	50
IPBSH-31	Femur	D. natalis	108	45
MCZ- 5098	Femur	Dimetrodon sp.	109	37
MCZ- 5098	Femur	Dimetrodon sp.	112	43
FMNH- 38547	Femur	Dimetrodon sp.	112	61
MCZ- 5098	Femur	Dimetrodon sp.	113	40
UMMP- UC 823	Femur	D. natalis	113	46
UMMP- UC 823	Femur	D. natalis	113	54
UMMP- UC 245	Femur	D. natalis	114	36
MCZ- 5355	Femur	Secodontosaurus sp.	115	47
MCZ- 5098	Femur	Dimetrodon sp.	115	35
UMMP- UC 244	Femur	D. natalis	115	39
FMNH- 3399	Femur	D. natalis	115	35
MCZ- 5098	Femur	Dimetrodon sp.	116	40
UMMP- UC 243	Femur	D. natalis	116	45
UMMP- UC 74	Femur	D. natalis	116	37

FMNH- 3391	Femur	D. natalis	116	45
MCZ- 5098	Femur	Dimetrodon sp.	117	42
FMNH- 22972	Femur	Dimetrodon sp.	117	48
FMNH- 22224	Femur	D. natalis	118	47
UMMP- UC 875	Femur	D. booneorum	118	63
MCZ- 5098	Femur	Dimetrodon sp.	119	43
UMMP- UC 58	Femur	D. natalis	120	40
IPBSH-21	Femur	sphenacodontid	120	36
IPBSH-37	Femur	sphenacodontid	121	45
UMMP- UC 823	Femur	D. natalis	122	47
UMMP- UC 823	Femur	D. natalis	122	45
MCZ- 8697	Femur	Secodontosaurus sp.	123	48
MCZ- 5099	Femur	Secodontosaurus sp.	123	45
UMMP- UC 823	Femur	D. natalis	124	50
FMNH- 22974	Femur	Dimetrodon sp.	124	48
MCZ- 5099	Femur	Secodontosaurus sp.	125	49
FMNH- 22224	Femur	D. natalis	125	45
FMNH- 22224	Femur	D. natalis	125	44
FMNH- 22976	Femur	Dimetrodon sp.	125	45
MCZ- 2871	Femur	Secodontosaurus sp.	126	57
MCZ- 8697	Femur	Secodontosaurus sp.	126	46
FMNH- 22224	Femur	D. natalis	126	45
MCZ- 5099	Femur	Secodontosaurus sp.	127	48
FMNH- 22224	Femur	D. natalis	127	46
FMNH- 3389	Femur	D. natalis	127	45
FMNH- 3387	Femur	D. natalis	127	46

IPBSH-35	Femur	sphenacodontid	127	63
MCZ- 8697	Femur	Secodontosaurus sp.	128	47
FMNH- 22224	Femur	D. natalis	128	51
MCZ- 5099	Femur	Secodontosaurus sp.	129	65
MCZ- 5099e	Femur	Secodontosaurus sp.	130	52
MCZ- 8697	Femur	Secodontosaurus sp.	130	48
MCZ- 8697	Femur	Secodontosaurus sp.	130	55
MCZ- 5099	Femur	Secodontosaurus sp.	130	45
MCZ- 5099	Femur	Secodontosaurus sp.	130	48
FMNH- 22224	Femur	D. natalis	130	44
MCZ- 8697	Femur	Secodontosaurus sp.	131	45
MCZ- 5099	Femur	Secodontosaurus sp.	131	47
IPBSH-29	Femur	D. natalis	131	45
MCZ- 8697	Femur	Secodontosaurus sp.	132	50
MCZ- 5099	Femur	Secodontosaurus sp.	132	46
MCZ- 5099a	Femur	Secodontosaurus sp.	132	53
FMNH- 22224	Femur	D. natalis	132	48
FMNH- 22224	Femur	D. natalis	132	48
FMNH- 3392	Femur	Dimetrodon sp.	132	52
IPBSH-40	Femur	sphenacodontid	132	55
FMNH- 22224	Femur	D. natalis	133	50
FMNH- 3398	Femur	D. natalis	133	45
MCZ- 8697	Femur	Secodontosaurus sp.	134	55
MCZ- 1326	Femur	Secodontosaurus sp.	135	51
MCZ- 8697	Femur	Secodontosaurus sp.	135	52
FMNH- 22224	Femur	D. natalis	135	50

FMNH- 22973	Femur	Dimetrodon sp.	135	45
MCZ- 8691	Femur	D. booneorum	137	57
IPBSH-2	Femur	D. natalis	137	52
MCZ- 8697	Femur	Secodontosaurus sp.	138	51
MCZ- 5943	Femur	D. booneorum	140	56
FMNH- 22976	Femur	Dimetrodon sp.	140	58
MCZ- 5099	Femur	Secodontosaurus sp.	141	52
UMMP- UC 131	Femur	D. booneorum	141	54
UMMP- UC 91	Femur	D. booneorum	143	58
UMMP- UC 835	Femur	D. booneorum	144	69
FMNH- 3393	Femur	Dimetrodon sp.	144	57
FMNH- 22235	Femur	D. limbatus	145	65
MCZ- 5107	Femur	D. booneorum	145	58
MCZ- 5107	Femur	D. booneorum	146	60
UMMP- UC 835	Femur	D. booneorum	146	49
FMNH- 22235	Femur	D. limbatus	147	70
MCZ- 8691	Femur	D. booneorum	147	66
FMNH- 22235	Femur	D. limbatus	148	58
UMMP- UC 120	Femur	D. booneorum	148	57
FMNH- 22235	Femur	D. limbatus	150	60
FMNH- 22235	Femur	D. limbatus	153	68
MCZ- 5107	Femur	D. booneorum	160	80
MCZ- 5107	Femur	D. booneorum	160	64
FMNH- 22235	Femur	D. limbatus	161	62
UMMP- UC 1135	Femur	D. booneorum	163	72
MCZ- 7008	Femur	D. limbatus	167	80

MCZ- 5107	Femur	D. booneorum	168	70
MCZ- 7008	Femur	D. limbatus	171	84
UMMP- UC 857	Femur	D. limbatus	172	81
IPBSH-8	Femur	sphenacodontid	180	96
UMMP- 23056	Humerus	Dimetrodon sp.	184	84
FMNH- 3383	Femur	D. limbatus	184	96
MCZ- 5106	Femur	D. limbatus	185	100
FMNH- 55037	Femur	D. limbatus	185	84
IPBSH-45	Femur	sphenacodontid	195	91
UMMP- UC 857	Femur	D. limbatus	197	82
UMMP- UC 857	Femur	D. limbatus	201	100
MCZ- 5106	Femur	D. limbatus	206	96

Appendix 6 (Chapter 4):

The seven sampled *Ophiacodon* humeri used in this study, dorsal (top) and ventral (bottom) views, scale is 10 mm. A) MCZ-5926 (right) B) MCZ-2819 (left) C) MCZ-4816 (left) D) MCZ-4816 (right) E)MCZ-1486(right) F)IPBSH-62 (left) G)OMNH-73698 (right).

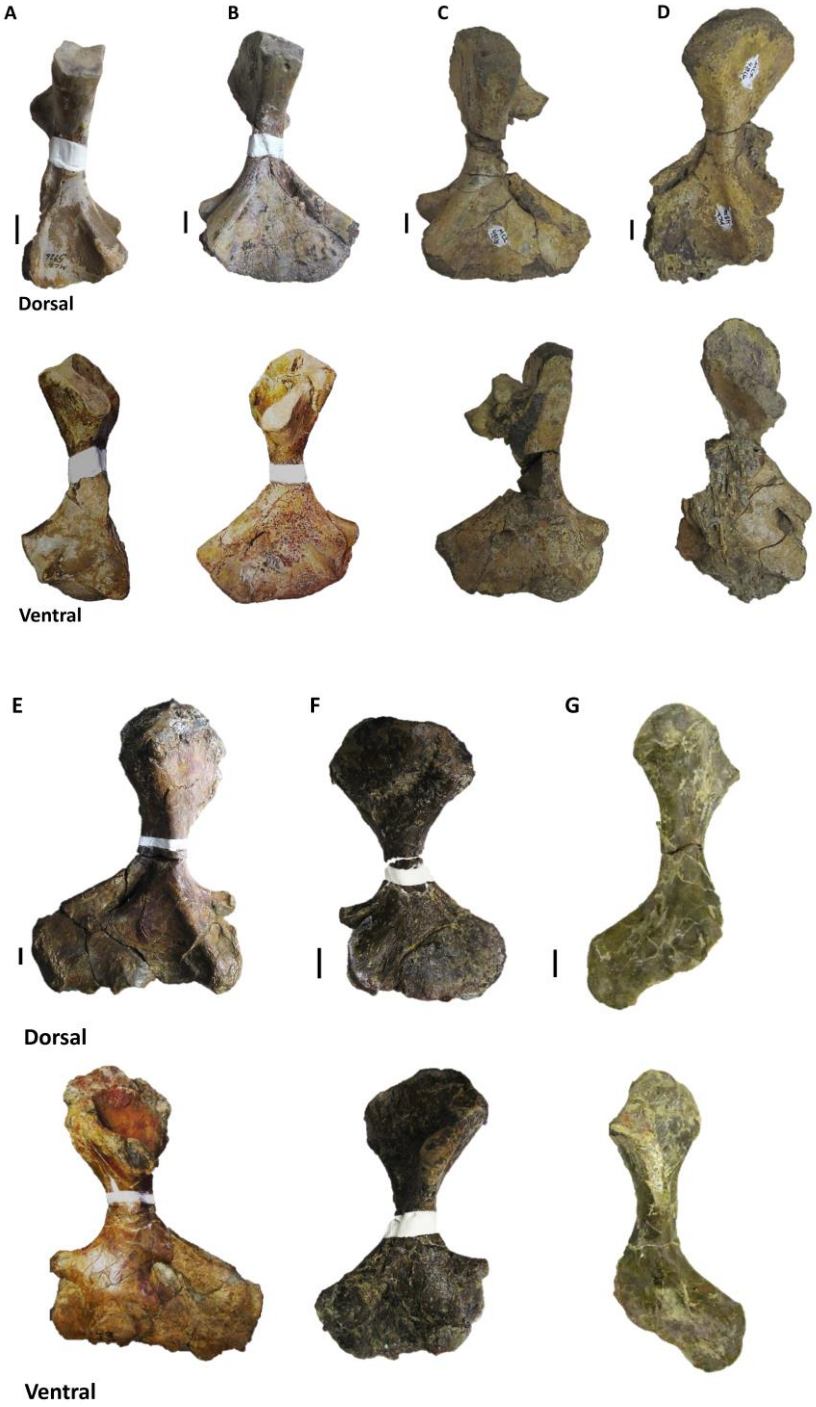

Appendix 7 (Chapter 4):
The four sampled *Ophiacodon* femora used in this study, dorsal (top) and ventral (bottom) views, scale is 10 mm. A) OMNH-55234 (right) B) OMNH-35389 (left) C) Uncataloged MSU specimen (right) D) IPBSH-46 (left).

Appendix 8 (Chapter 7):
Dorsal and ventral views of juvenile *Cotylorhynchus romeri* postcrania OMNH-01728: A) right humerus, B) left humerus, C) left femur, D) right femur

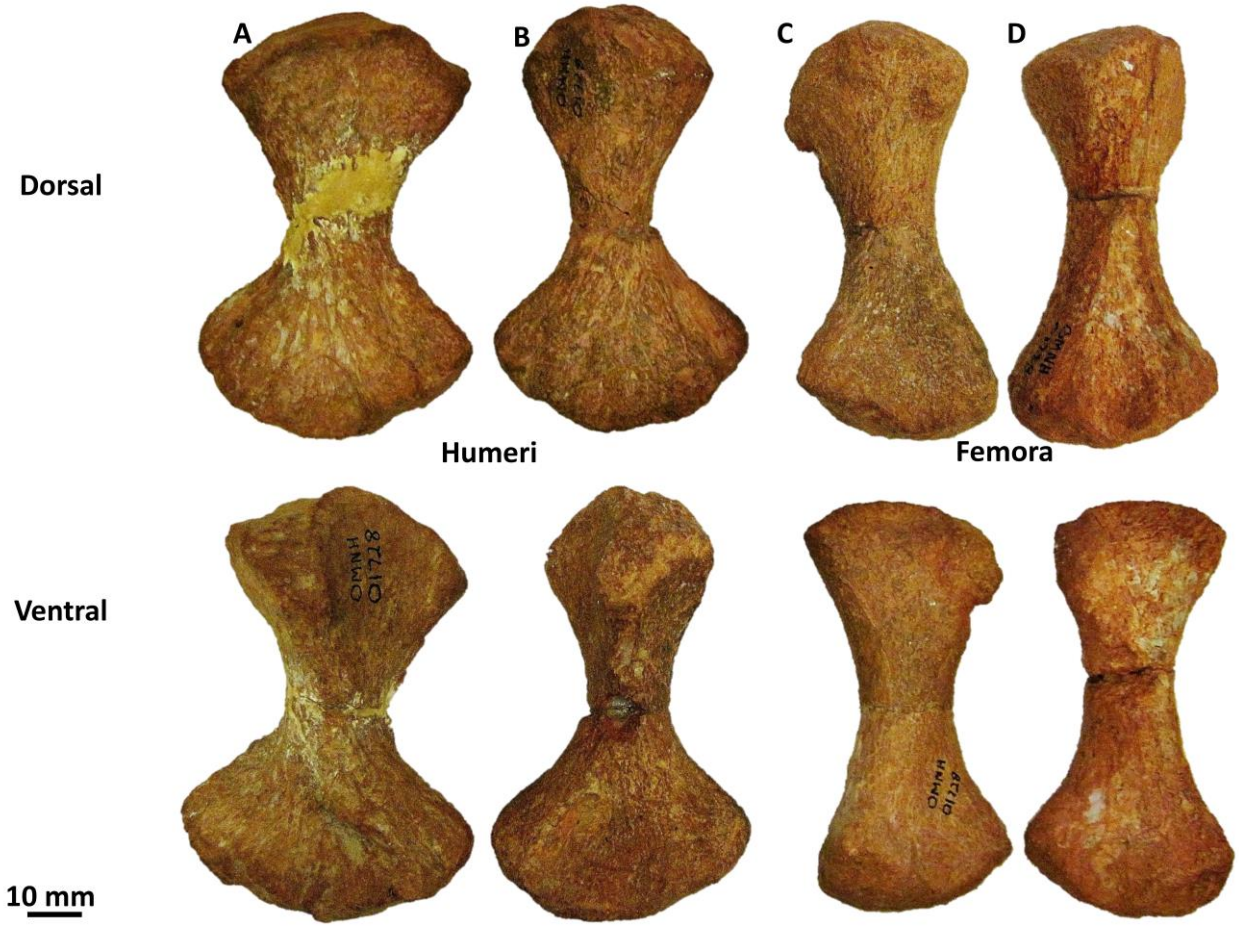

Appendix 9 (Chapter 7):

Corresponding transverse sections taken from the minimal diaphysis of the juvenile *Cotylorhynchus romeri* postcrania (OMNH-01728) shown in S.F. 1: A) right humerus, B) left humerus, C) left femur, D) right femur

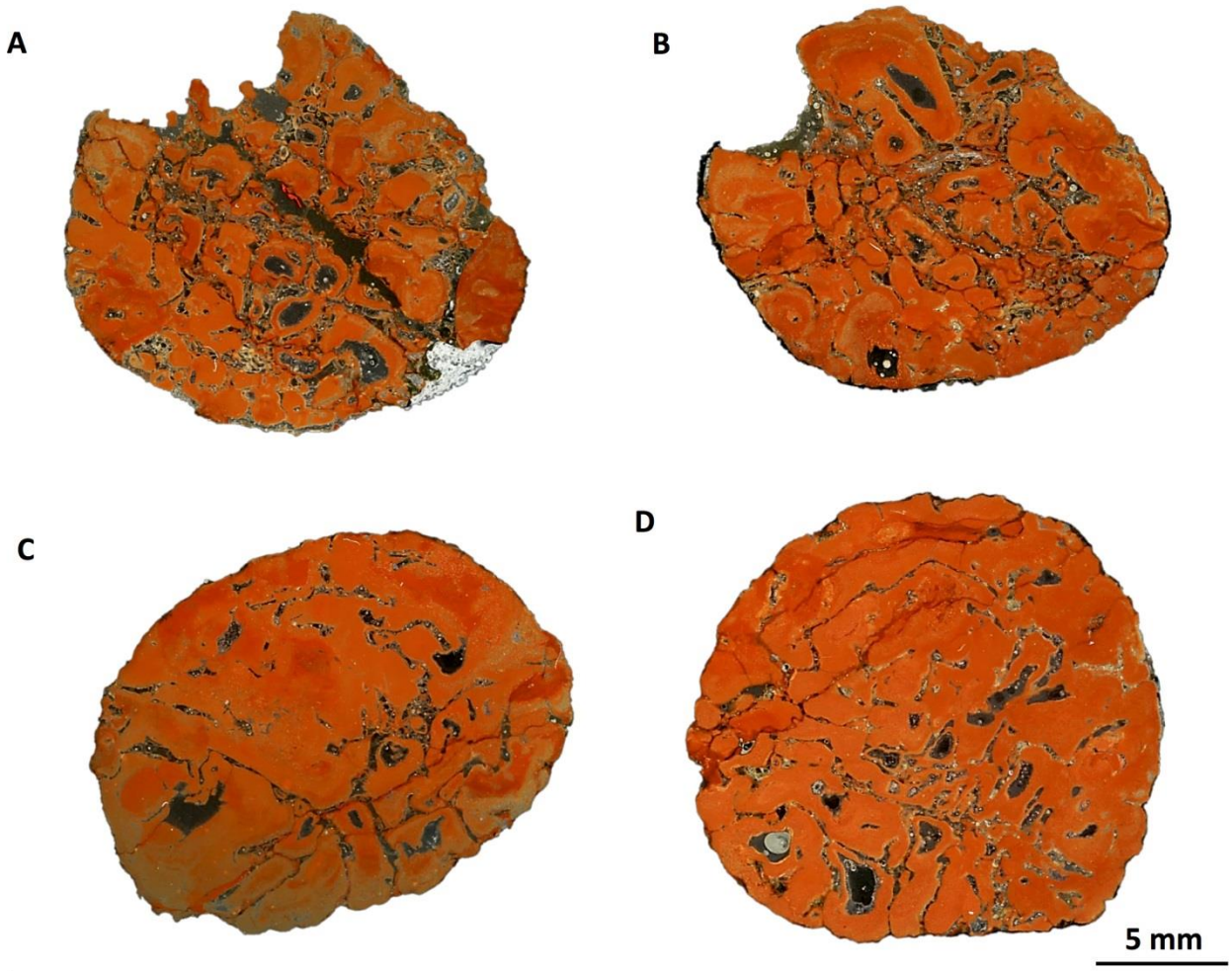

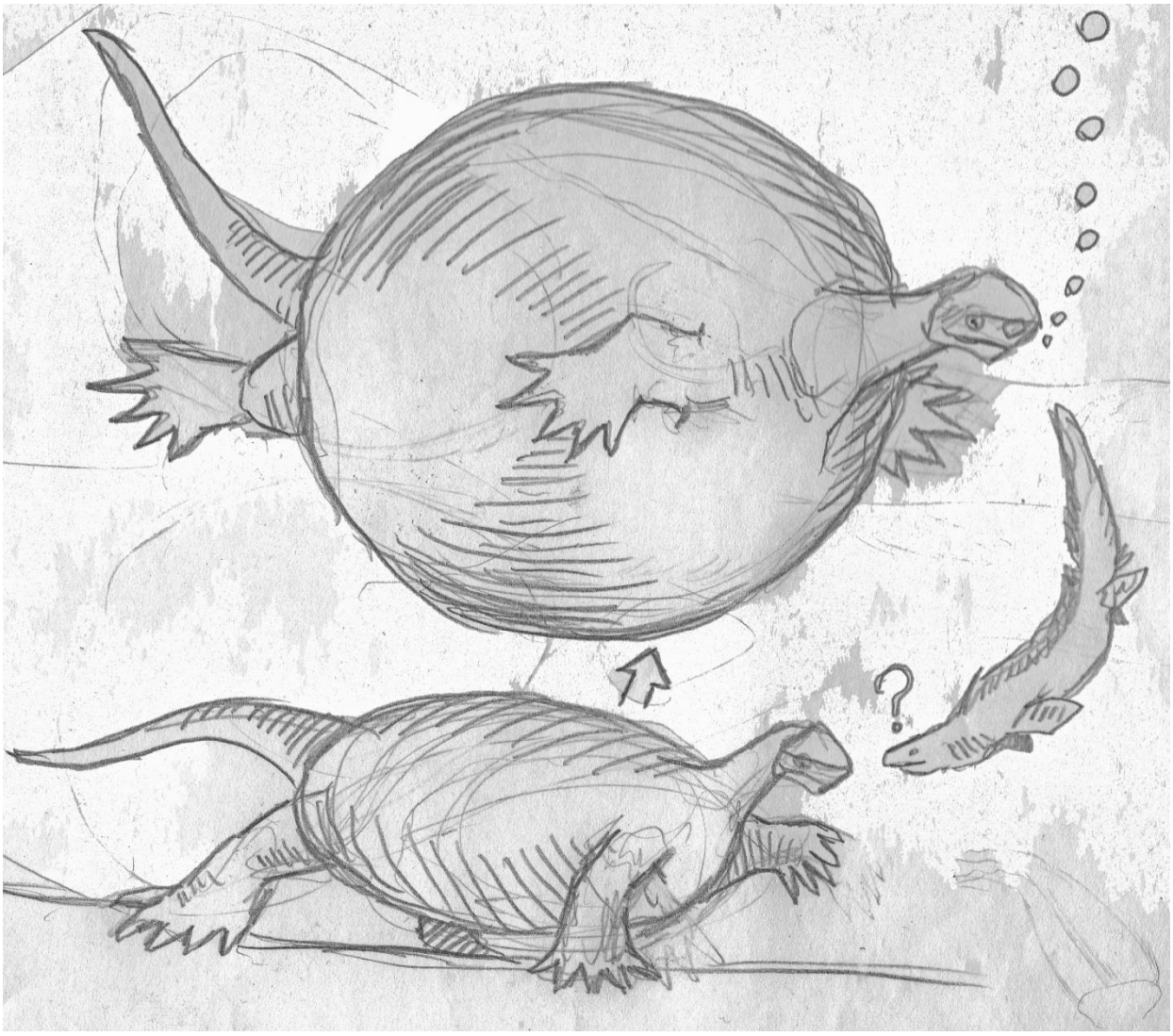

Robert Bakker's response to chapter 5